Transactions of the ASME

An Investigation of Cemented Tungsten Carbide as Bearing Material; Progress Report No. 2 . . . . . *J. S. Kozacka, H. A. Erickson, H. W. Highriter, and A. F. Gabriel* 1403

Thermal Lags in Flowing Incompressible Fluid Systems Containing Heat Capacitors . . . . . *J. W. Rizika* 1407

A Systematic and Rapid Procedure of Computing Approximate Characteristic Values Pertaining to Bare-Tube Crossflow Heat Exchangers . . . . . *F. J. Neugebauer* 1415

Validity of Time-Compensated Temperature Parameters for Correlating Creep and Creep-Rupture Data . . . . . *F. Garofalo, G. V. Smith, and B. W. Royle* 1423

Mechanical Properties at Elevated Temperatures of Ductile Cast Iron . . . . . *F. B. Foley* 1435

Structural Stability of Modified 12-Chromium Alloys . . . . . *W. C. Hagel and E. F. Beckc* 1439

Review of the Pitot Tube . . . . . *R. G. Folsom* 1447

Pulsation Errors in Manometer Gages . . . . . *T. J. Williams* 1461

A Practical Pulsation Threshold for Flowmeters . . . . . *V. P. Head* 1471

Effect of Range of Stress in Combined Bending and Torsion Fatigue Tests of 25S-T6 Aluminum Alloy . . . . . *W. N. Findley, W. I. Mitchell, and D. D. Strobbeck* 1481

The Influence of Shank Area on the Tensile Impact Strength of Bolts . . . . . *John Love, Jr., and O. A. Pringle* 1489

New Techniques in Metal-Cutting Research . . . . . *W. R. Backer and E. J. Krabacher* 1497

Heat Transfer to, and Temperature Distribution in, a Metal-Cutting Tool . . . . . *D. L. Rall and W. H. Giedt* 1507

An Analysis of the Orthogonal Boring Operation . . . . . *B. W. Shaffer* 1517

Report of the Investigation of the Turbine Wheel Fracture at Tanners Creek . . . . . *A. W. Rankin and B. R. Seguin* 1527

Investigation of Large Steam-Turbine Spindle Failure . . . . . *H. D. Emmert* 1547

Report of the Investigation of Two Generator Rotor Fractures . . . . . *C. Schabtach, E. L. Fogleman, A. W. Rankin, and D. H. Winne* 1567

Large Rotor Forgings for Turbines and Generators . . . . . *N. L. Mochel, R. E. Peterson, J. D. Conrad, and D. W. Gunther* 1585

Acceptance Guides for Ultrasonic Inspection of Large Rotor Forgings . . . . . *A. W. Rankin and C. D. Moriarty* 1603

Work of the Task Group on Brittle Failure of Steel Forgings . . . . . *A. O. Schaefer* 1623

TRANSACTIONS OF THE AMERICAN SOCIETY OF MECHANICAL ENGINEERS

VOLUME 78 OCTOBER 1956 NUMBER 7

Transactions

of The American Society of Mechanical Engineers

Published on the tenth of every month, except March, June, September, and December

OFFICERS OF THE SOCIETY:

J. W. Barker, *President*

Joseph L. Kopf, *Treasurer* — C. E. Davies, *Secretary*

Edgar J. Kates, *Asst. Treasurer*

COMMITTEE ON PUBLICATIONS:

Otto de Lorenzi, *Chairman*

W. E. Reaser — John de S. Coutinho

Kerr Atkinson — B. G. A. Skrotzki

R. A. Cederberg, H. N. Weinberg } *Junior Advisory Members*

George A. Stetson, *Editor Emeritus* — K. W. Clendinning, *Managing Editor* (Deceased, August 16, 1956)

J. J. Jaklitsch, Jr., *Acting Editor* — J. A. North, *Asst. Managing Editor*

REGIONAL ADVISORY BOARD OF THE PUBLICATIONS COMMITTEE:

Roy L. Parshall—I — H. M. Cather—V

A. D. Blake—II — C. R. Earle—VI

C. L. France—III — M. B. Hogan—VII

Francis C. Smith—IV — Linn Helander—VIII

Published monthly by The American Society of Mechanical Engineers. Publication office at 20th and Northampton Streets, Easton, Pa. The editorial department is located at the headquarters of the Society, 29 West Thirty-Ninth Street, New York 18, N. Y. Cable address, "Dynamic," New York. Price $1.50 a copy, $12.00 annually for Transactions and the *Journal of Applied Mechanics*; to members $1.00 a copy, $6.00 annually. Add $1.50 for postage to all countries outside the United States, Canada, and Pan-American Union. Changes of address must be received at Society headquarters seven weeks before they are to be effective on the mailing list. Please send old as well as new address. . . . By-Laws: The Society shall not be responsible for statements or opinions advanced in papers or . . . printed in its publications (B13, Par. 4). . . . Entered as second-class matter March 2, 1928, at the Post Office at Easton, Pa., under the Act of August 24, 1912. . . .Copyrighted, 1956, by The American Society of Mechanical Engineers. Reprints from this publication may be made on condition that full credit be given the Transactions of the ASME and the author, and that date of publication be stated.

An Investigation of Cemented Tungsten Carbide as Bearing Material

Progress Report No. 2

By J. S. KOZACKA,[1] H. A. ERICKSON,[2] H. W. HIGHRITER,[3] AND A. F. GABRIEL,[4] CHICAGO, ILL.

This paper is a continuation of Report No. 1 which was contributed by the Machine Design and Production Engineering Divisions and presented at the 1952 Annual Meeting.[5] The investigation is principally concerned with the effects of higher bearing pressures than previously used on bearing performance, the effect of bearing roughness surface on coefficient of friction, and the effects of speed on coefficient of friction under otherwise constant conditions. In these tests the same bearings were used as for tests reported previously. These bearings and journals were made of straight tungsten carbide with 6 per cent cobalt as the binder.

Method of Testing

TESTS were made in the Almen testing machine with the same setup previously reported. This was done in order to compare test results with earlier tests.[5] However, the machine and the instruments used were recalibrated so as to assure correctness of readings. A G-E load visualizer was used to determine electrical energy input. The speed was checked with a "strobotac."

Surface Finish of Test Bearings. Surface finish of the three bearings A, B, and C was checked before the tests and the results are given in Table 1.

TABLE 1 DIMENSIONS AND SURFACE FINISH OF THE TEST BEARINGS

Bearing	Diameter, in.	Surface finish, rms
A	0.31263	15–30
B	0.31265	10–20
C	0.31256	8– 9
Journals		
A	0.31254	20–65
B	0.31253	3–50
C	0.31252	8–10

Lubricants Used. For tests to determine friction losses at bearing pressures from 707.2 to 2652 psi, mineral oil of viscosity 60 SSU at 100 F with 10 per cent EP base added was used. This lubricant was designated previously as No. 4, and is so designated in this report. In tests to determine frictional losses at variable speed, constant bearing pressure 884 psi, and constant temperature 45 C, straight mineral oil of 60 SSU at 100 C designated as No. 1 lubricant, and the No. 4 lubricant having viscosity 87 SSU at 100 F were used. During tests, bearing and shaft were mounted in the reservoir filled with 20 cc of the lubricant. The temperature of oil was measured at the end of the bearing.

Friction Tests at Bearing Pressures 707.2 to 2652 Psi. Series of tests were run with bearings A, B, and C at constant speed of 2750 rpm using lubricant No. 4, varying the load from 707.2 to 2652 psi and allowing the temperature to rise up to 100 C, except where it was impossible to reach this temperature in a two-hour continuous-run period as was the case of bearing C which was considered a smooth bearing. Data, shown in Table 2, represent averages of several readings. For each test the machine was prepared by first running it under light load to a temperature of 35 C. This was the machine warm-up. Then the load was applied and when the temperature of about 45 C was reached, readings were taken every minute with each increase of load. During tests of bearing C, readings were taken less often. This was done in order to reach sufficient differential in temperature for readings.

Results of Tests

Fig. 1 shows curves of the coefficient of friction as a function of bearing pressure at constant speed 2750 rpm for bearing A, B, and C, using lubricant No. 4. These curves were plotted from data in Table 2. From data in Table 2 and curves in Fig. 1, it may be seen that the coefficient of friction at a constant speed of 2750 rpm remains about the same for the three bearings up to about 500 psi, when using oil No. 4 as the lubricant regardless of the bearing surface finish. As the load is increased the coefficient of friction of bearing A increases rather rapidly, and this increase is attributed to the breaking of the oil film by the irregularities in

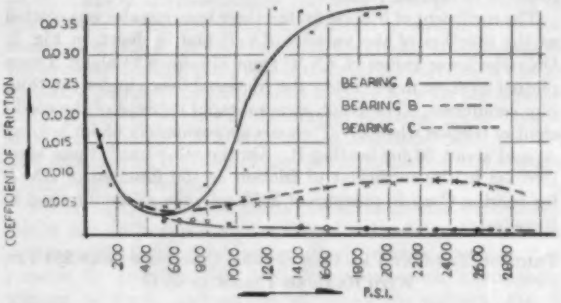

FIG. 1 COEFFICIENT OF FRICTION VERSUS BEARING PRESSURE AT CONSTANT SPEED OF 2750 RPM, VARIABLE TEMPERATURE, VARIABLE PRESSURE, 44.4 TO 2652 PSI, USING OIL NO. 4 AS LUBRICANT

[1] Professor of Mechanical Engineering and Director of Engineering Shop Laboratories, University of Illinois. Mem. ASME.

[2] Director of Engineering, D. A. Stuart Oil Company, Ltd. Mem. ASME.

[3] Vice-President and Technical Director, Vascoloy-Ramet Corporation.

[4] Vice-President, Acme Industrial and Acme Scientific Company.

[5] "An Investigation of Cemented Tungsten Carbide as Bearing Material," by J. S. Kozacka, H. A. Erickson, H. W. Highriter, and A. F. Gabriel, Trans. ASME, vol. 75, 1953, pp. 1203–1209.

Contributed by the Research Committee on Metal Processing and presented at a joint session of the Research Committee on Metal Processing and Production Engineering Division at the Fall Meeting, Milwaukee, Wis., September 8–10, 1954, of THE AMERICAN SOCIETY OF MECHANICAL ENGINEERS.

NOTE: Statements and opinions advanced in papers are to be understood as individual expressions of their authors and not those of the Society. Manuscript received at ASME Headquarters, June 2, 1954. Paper No. 54—F-3.

TABLE 2 TEST DATA FOR BEARINGS A, B, AND C, FROM TESTS AT 2750 RPM, BEARING PRESSURES 707.2 TO 2652 PSI, TEMPERATURE RANGE 45 TO 100 C OR TO PRESSURE 2652 PSI, USING OIL NO. 4 AS LUBRICANT

Pressure, psi	Bearing A			Bearing B			Bearing C		
	T, deg C	f	ZN/P	T, deg C	f	ZN/P	T, deg C	f	ZN/P
44.2	35.0	0.03220	1210.0	35.0	0.03165	1210.0	35.0	0.03120	1210.0
88.4	36.0	0.01610	585.0	35.5	0.01470	598.0	36.5	0.01675	576.0
176.8	37.0	0.00835	290.0	37.0	0.00800	283.0	38.0	0.00935	274.0
265.0	39.0	0.00617	176.0	38.5	0.00525	178.5	39.0	0.00620	176.0
354.0	40.5	0.00415	125.8	40.5	0.00413	126.0	40.0	0.00420	128.0
442.0	42.0	0.00332	98.5	42.5	0.00321	96.5	42.0	0.00298	98.5
530.0	44.0	0.00307	78.0	44.0	0.00417	78.0	44.0	0.00252	78.0
618.0	45.0	0.00340	63.2	45.5	0.00447	61.5	45.0	0.00212	63.2
707.2	50.0	0.00410	47.0	46.0	0.00400	52.4	45.0	0.00210	55.3
795.6	53.0	0.00800	38.3	46.0	0.00200	46.7	47.0	0.00187	46.9
884.0	56.0	0.01500	32.4	46.0	0.00230	42.0	48.0	0.00142	40.4
972.4	61.0	0.01300	26.3	48.0	0.00411	36.8	49.0	0.00129	35.1
1060.8	65.0	0.01060	21.7	49.0	0.00520	32.5	50.0	0.00129	31.2
1149.2	70.0	0.02780	17.9	50.0	0.00480	28.5	51.0	0.00124	28.2
1237.6	75.0	0.03750	15.0	52.0	0.00405	25.7	52.0	0.00115	26.0
1326.0	79.0	0.03900	13.1	53.0	0.00520	22.8	51.0	0.00113	24.5
1414.0	87.0	0.03700	10.7	56.0	0.00550	19.7	52.0	0.00112	22.2
1502.8	90.0	0.03320	9.3	58.0	0.00630	17.6	53.0	0.00100	20.9
1591.2	95.0	0.03360	8.1	60.0	0.00762	16.2	53.0	0.00105	19.7
1679.6	98.0	0.02710	7.3	63.0	0.00762	14.3	53.5	0.00068	18.0
1768.2	99.0	0.02750	6.8	66.0	0.00720	12.8	54.0	0.00065	16.8
1856.4	101.0	0.03610	6.4	68.0	0.00820	11.7	55.0	0.00082	15.7
1944.8	115.0	0.03620	4.9	69.0	0.00780	10.9	55.0	0.00075	15.0
2033.5	...	.....	....	70.0	0.00840	10.1	55.0	0.00070	14.3
2121.6	...	.....	....	70.0	0.00930	9.7	55.0	0.00072	13.7
2230.6	...	.....	....	71.0	0.00890	9.1	55.0	0.00069	13.2
2298.4	...	.....	....	74.0	0.00830	8.1	56.0	0.00069	12.4
2386.8	...	.....	....	72.0	0.00800	8.3	56.0	0.00060	12.0
2475.2	...	.....	....	74.0	0.00750	7.5	56.0	0.00060	11.5
2563.6	...	.....	....	75.0	0.00810	7.2	57.0	0.00060	10.9
2652.0	...	.....	....	75.0	0.00790	7.0	58.0	0.00053	10.2

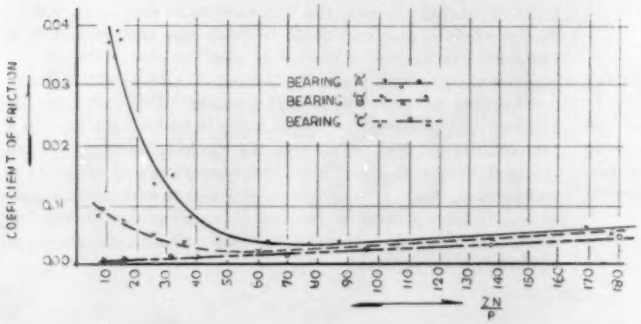

FIG. 2 COEFFICIENT OF FRICTION AS A FUNCTION OF OPERATING VARIABLE ZN/P AT CONSTANT SPEED OF 2750 RPM, VARIABLE TEMPERATURE, BEARING PRESSURES UP TO 2652 PSI, USING OIL NO. 4 AS LUBRICANT

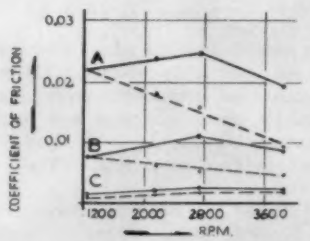

FIG. 3 COEFFICIENT OF FRICTION VERSUS SPEED AT CONSTANT PRESSURE OF 884 PSI FOR BEARINGS A, B, C; CONSTANT TEMPERATURE OF 45 C

the surface of this bearing. For B bearing, there is an increase in the coefficient of friction from approximately 500 psi as the load is increased. However, this increase is not as rapid as it is in the more roughly finished bearing A. Bearing C, being one of the smoothest of the three, shows, within the limits of this investigation a continuous drop in the coefficient of friction as a function of bearing pressure.

The coefficient of friction for the three bearings also was plotted as the function of the variable ZN/P and is shown in Fig. 2. Only the lower values of ZN/P from 176 down to about 5 were plotted to show more clearly the frictional losses under the thin-film conditions. The graph shows a rapid increase of the coefficient of friction when ZN/P equals approximately 65 for bearing A, and about 60 for bearing B. On the other hand, there is no increase in the coefficient of friction as the function of ZN/P for bearing C up to pressure of 2652 psi—the maximum used in these tests.

FRICTION TESTS AT VARIABLE SPEEDS, CONSTANT LOAD 884 PSI, WITH READING TAKEN AT 45 C

Series of tests were run with the three bearings at speeds 1250, 2140, 2750, and 3875 rpm to determine the effect of speed on the coefficient of friction for cemented tungsten-carbide bearings with shafts also made of the same grade of carbide, using oils Nos. 1 and 4 as lubricants. Data obtained in the tests are given in Table 3. From these data the coefficient of friction was plotted as the function of the journal speed. The curves for bearings A, B, and C are shown in Fig. 3.

From these data and from the graphs, Fig. 3, it is seen that within the limits of this investigation, with bearing pressure of 884 psi, taking readings at 45 C, the coefficient of friction increases at lower speeds for bearings A and B and then decreases from 2750 rpm, when oil No. 1 is used as the lubricant. For bearing C the values of coefficient of friction increase slightly up to 3875 rpm when oil No. 1 is used as the lubricant. When oil No. 4 is substituted as the lubricant the coefficient of friction decreases with the increase of speed for bearings A and B, and it remains reasonably constant for bearing C.

The data and the graphs indicate the beneficial effect of addition of the EP base to the mineral oil to be used as a lubricant for cemented tungsten-carbide bearings. The beneficial effect is more pronounced in relatively coarsely finished bearings, such as bearings A and B, and is less noticeable in more finely finished bearings such as bearing C. This effect in all probability is due to somewhat stronger film of the lubricant on which the shaft rotates in the bearing and therefore there is less metal-to-metal

TABLE 3 COEFFICIENT OF FRICTION AS A FUNCTION OF SPEED AT CONSTANT BEARING PRESSURE 884 PSI, FOR BEARINGS A, B, AND C, WITH READINGS TAKEN AT 45 C, USING LUBRICANTS NO. 1 AND NO. 4

Rpm	Lubricant No. 1			Lubricant No. 4		
	Bearing A	Bearing B	Bearing C	Bearing A	Bearing B	Bearing C
1250	0.0218	0.0075	0.00160	0.0218	0.0075	0.0014
2140	0.0236	0.0106	0.00180	0.0180	0.0062	0.0011
2750	0.0247	0.0110	0.00240	0.0160	0.0051	0.0022
3875	0.0192	0.0089	0.00213	0.0089	0.0046	0.0019

contact between the irregularities of the bearing and the shaft.

Time Required for the Bearings to Reach Temperature 50 C From 35 C at Constant Speed 2750 Rpm and Constant Pressure 1768 Psi

In the tests, it was observed that the temperature rise was rapid for relatively rough-finished bearings A and B, and slow for bearing C. For this reason it was decided to take readings of time required for the bearing to reach temperature 50 C from 35 C when room temperature was 23 C, at constant speed 2750 rpm and 1768 psi bearing pressure, using oil No. 4 as the lubricant. Volume of oil in the bearing reservoir was 22 cc in each case. Data obtained are given in Table 4. These data plotted surface of bearing finish versus time required to reach temperature 50 C from 35 C give Fig. 4. This graph indicates that the time required for the bearing to generate a certain amount of heat to increase the temperature of the oil bath in which the bearing is tested is a function of bearing finish.

TABLE 4 TIME IN MINUTES REQUIRED TO REACH TEMPERATURE 50 C FROM 35 C IN TESTS OF BEARINGS A, B, AND C UNDER CONSTANT LOAD 1768 PSI AT 2750 RPM USING 22 CC LUBRICANT NO. 4

Bearing	Average bearing surface roughness, rms	Average journal surface roughness, rms	Time to reach 50 C
A	22	42	2
B	15	27	10
C	8	10	37

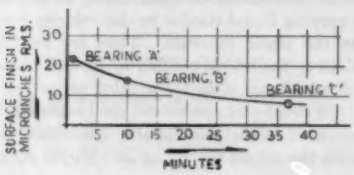

Fig. 4 Time in Minutes for Temperature to Rise From 35 C to 50 C at 1768 Psi and 2750 Rpm

Conclusions

Test data given in Table 2 and curves in Fig. 1 indicate that for bearings made of cemented tungsten carbide with journals also made of the same material, at constant speed of 2750 rpm, using oil No. 4 as the lubricant, the coefficient of friction is nearly the same for the three bearings up to a bearing pressure of 500 psi regardless of surface finish, provided that the surfaces are reasonably smooth. Above 500 psi bearing A develops frictional losses at an accelerated rate due primarily to some metal-to-metal contacts between the irregularities of the bearing and the journal. Bearing C which has a fine finished surface develops the smallest frictional losses and these are nearly constant up to the highest pressure used in the test. Bearing B having a rougher surface finish than bearing C develops higher frictional losses than bearing C but not as high as bearing A.

The coefficient of friction of the three bearings plotted as a function of the operating variable ZN/P shows a straight line for bearing C, while there is a reversal of the trend in the thin-film region for bearing A and B at approximate value of ZN/P equals 60. In the thick-film region, the friction lines almost coincide, and for practical reasons can be considered to be the same.

As shown in Fig. 1, tests on bearing A were discontinued when the temperature of 115 C or 239 F was reached as it was assumed that this temperature was too high for operation of the bearings, using oil No. 4 as the lubricant.

Tests of cemented tungsten-carbide bearings at constant pressure 884 psi at variable speeds, taking readings at 45 C, indicate within the limits of this investigation a decrease in coefficient of friction for bearings with rougher than 10 microinches of finish and approximately constant coefficient of friction for bearing 8 to 10 microinches of finish. Fig. 3 also indicates the beneficial effect of the EP base additive on bearing performance particularly for bearings with rougher finish.

Tests of cemented tungsten-carbide bearings to determine the time required for the bearing to develop enough heat to raise 22 cc of oil No. 4 as the lubricant from 35 C to 50 C at constant speed and constant pressure is inversely proportional to bearing roughness.

Discussion

E. M. Kipp.[6] The authors are to be congratulated for their contributions to a better understanding of the problems of friction and wear of bearing materials, particularly for the unorthodox combination which they have investigated. The use of bearing materials involving a shaft and journal of the same material is not common, and has been generally avoided because of the general rule that like materials are more apt to have poor bearing characteristics than are selected combinations of unlike materials.

We are somewhat concerned by the relatively wide spreads in the surface-finish values for the individual test specimens as presented in Table 1 of the paper. The spread in surface-finish data is such as to indicate a definite possibility that, for at least appreciable portions of the areas involved, the finishes of journals and bearings of the A-series could well have overlapped those of the B-series. It would be interesting to know whether the reported surface-finish values represent measurements made on an appreciable percentage of the total areas or whether they were confined to only a few such areas.

In the authors' discussion of the relationships between the effectiveness of extreme-pressure additives in the performance of the relatively coarsely finished bearings as compared to the smoother bearings, they suggest that the greater effectiveness of the extreme-pressure additives on the rougher surfaces is due to the lesser degree of metal-to-metal contact between the bearing and the shaft in the case of the rougher surfaces. It is implied that the "stronger" film of lubricant associated with the EP additives is more effective in preventing metal-to-metal contact in the rougher bearings.

We would like to suggest that a more fundamental explanation can be derived from the often-observed and well-known fact that as the surface finish of a bearing surface becomes smoother, it is possible to maintain full fluid lubrication with increasingly thinner oil films. Indeed, the curves of the authors' Fig. 2 clearly illustrate the shift of the minimum point in the ZN/P

[6] Chief, Lubricants Division, Aluminum Research Laboratories, Aluminum Company of America, New Kensington, Pa.

diagram to the left as the surface finishes of the bearing materials are made smoother. Therefore it is suggested that the existence of, or approach to, essentially full fluid lubrication in the bearings with the smoothest finish would tend to minimize the occurrence of unstable or boundary friction and hence would tend to minimize the effect of the extreme-pressure-type lubricants. The coarser bearing elements present conditions of boundary friction under which the extreme-pressure agents would be expected to be most noticeable in their effects.

The authors present valuable data to indicate that with suitable lubrication bearing elements of like materials and manufactured from hard materials such as cemented tungsten carbides may have attractive advantages. However, it would be interesting to know whether the authors have any data on the frictional properties of the cemented-tungsten-carbide bearing materials in the inadvertent or temporary absence of effective lubrication such as is bound to occur from time to time in most practical applications. This contingency, of course, is one of the reasons why most bearing assemblies involve the use of a softer material such as a babbit rubbing against a harder material. In the event of failure in such a case, more often than not only one of the bearing elements is damaged. We would be interested to know what would happen with the cemented-tungsten-carbide materials in such a case.

R. G. Moyer.[7] The authors are to be complimented on their pioneering work in the study of lubrication of cemented-tungsten-carbide bearings.

In the problem of lubrication of steel against steel, it has been theorized that sulphur, chlorine, and/or phosphorus in the EP lubricant react with the metal, under conditions of heavy loading, to produce films of sulphides, chlorides, and/or phosphides which preferentially rupture to protect the metal from damage. It is not easy to understand how the same theory may be applied to cemented tungsten-carbide bearings since the carbide is quite inert, but the authors indicate a substantial reduction in friction in some cases when EP base is added to the mineral oil. Is it possible that the EP additives react with the cobalt matrix in the cemented tungsten-carbide bearings or is the improvement due to the oiliness of the fatty material in the lubricant? If the former were true, one would expect eventual disintegration of the bearings. If the latter were true, equivalent performance might be expected from a mineral oil-fatty oil blend without EP additives.

Perhaps the authors have investigated a sufficient variety of lubricants to be in a position to advance a theory covering the action of EP lubricants on cemented-tungsten-carbide bearings.

[7] Group Leader, Research and Development Laboratories, The Pure Oil Company, Crystal, Lake, Ill. Mem. ASME.

Authors' Closure

The authors appreciate the effort and interest shown by Dr. Kipp and Mr. Moyer for their comments. We tend to narrow our field of vision as we become more engrossed with our own problem and it is through discussion that we again can attain the proper perspective to benefit the greatest number concerned.

Our problem began with the specific request for performance data on running similar materials as journal and bearing. It is true that dissimilar materials are usually selected for bearings; however, as mentioned, in the absence of specific data the experiment was carried out to determine some of the limitations involved.

Considerable time and effort were expended in the preparation of the bearing components, and values of surface finish are the results over appreciable areas. Perhaps the choice of the word "stronger" to explain the behavior of the EP additives was inadvertent. Some may say that there was full fluid lubrication, others a metallic sulphide and/or chloride having certain shear properties. We have tried to steer clear of these controversies. Fortunately we are able to use and take advantage of these desirable characteristics even though we are not able to explain precisely what takes place. In this connection it is difficult to believe that sufficient pressures are built up within a bearing, as has been described elsewhere, while both ends of the bearing itself are open and allow leakage. It is possible on the other hand that the pressure indications we observe may be due to the inertia effect of the moving liquid similar to the velocity pressure of air in respect to the static pressure. Thus far we have not attempted to destroy the bearing, either by lack of lubrication or by loading, until additional data for a third paper has been completed. In that event perhaps we can shed some light as to what happens because of lubrication failure or whether the EP additives react with the cobalt matrix as Mr. Moyer suggests.

Thermal Lags in Flowing Incompressible Fluid Systems Containing Heat Capacitors

By J. W. RIZIKA,[1] CAMBRIDGE, MASS.

The transient thermal conditions in problems involving flowing fluid systems in contact with heat capacitors are becoming increasingly important with the advent of modern control techniques. The temperature controlability of a flowing fluid system is a direct function of the transient thermal response of the fluid to a specific temperature input function. In a previous paper,[2] the author presented an analysis which considered the transient fluid temperatures in a system consisting of a compressible fluid flowing through a duct or in a heat exchanger. The case of a compressible fluid, with an exponential or step-function fluid temperature input, flowing through an insulated tube or pipe was analyzed in detail and examples were presented. The treatment of the transient conditions for a compressible fluid flowing through a heat exchanger was partially analyzed and the method of solution was demonstrated. The present paper consists of an extension of this work in which the transient conditions due to thermal lags in flowing incompressible fluid systems are analyzed. Both the case of an incompressible fluid, with a step-function temperature input, flowing through a circular tube or pipe and the case of an incompressible fluid flowing in a simple heat exchanger are examined in detail. An example which demonstrates the transient condition at the exit of a simple (condensing-steam/water) heat exchanger is presented also.

Nomenclature

The following nomenclature is used in the paper:

$A \equiv \dfrac{r_o h_o}{r_i h_i}$, dimensionless

$B \equiv \dfrac{\pi(r_o^2 - r_i^2)\rho_m c_m}{2\pi r_i h_i}$, hr

c_m = specific heat of duct material, Btu/lb deg F
c_f = specific heat of inner liquid, Btu/lb deg F

$C \equiv \dfrac{w_f c_f}{2\pi r_i h_i}$, ft

$D \equiv \dfrac{\pi r_i^2 \rho_f c_f}{2\pi r_i h_i}$, hr

f_1, f_2 = functions defined where utilized
F_1, F_2, F_3, F_4, F_5 = functions defined where utilized
F_a, F_b = arbitrary functions
G_1, G_2, G_3, G_4, G_5 = inverse functions of F_1, F_2, F_3, F_4, F_5, respectively, and defined where utilized
h_i = film coefficient of heat transfer between inner liquid and duct surface, Btu/hr sq ft deg F
h_o = film coefficient of heat transfer between outer medium and duct surface, Btu/hr sq ft deg F
$i = \sqrt{-1}$
$I_1 \equiv$ Bessel function of first kind
l = length of tube, ft
m = integer, dimensionless
p = Laplace transform variable, 1/hr
P = pressure, psf
q = rate of heat transfer, Btu/hr
r_i = inner radius of circular duct, ft
r_o = outer radius of circular duct, ft
R = gas constant in equation of state, ft/deg F
Re_f = inner liquid Reynolds number, dimensionless
S = heat-transfer area, sq ft
T_{fi} = inner liquid inlet temperature, $u(0, \theta)$, deg F
T_o = inner liquid and/or duct temperature at initial condition, $u(x, 0)$ and/or $y(x, 0)$, deg F
T_s = outer medium temperature, a constant, deg F
$\Delta T \equiv T_s - u(x, \infty)$, deg F
$\Delta T_1 = T_s - u(l, \infty)$, deg F
$\Delta T_2 = T_s - T_{fi}$, deg F

$\Delta T_m \equiv \dfrac{\Delta T_2 - \Delta T_1}{\ln\left(\dfrac{\Delta T_2}{\Delta T_1}\right)}$, log mean temperature, deg F

u = inner liquid temperature, deg F
U = over-all coefficient of heat transfer, Btu/hr sq ft deg F
$\mathbf{U}$ = Laplace transformation of inner liquid temperature, $\mathbf{U}(x, p) = \int_0^\infty e^{-p\theta} u(x, \theta) d\theta$
w_f = inner liquid flow rate, lb/hr
x = distance from duct inlet, ft
y = duct temperature, deg F
$\mathbf{Y}$ = Laplace transformation of duct temperature, $\mathbf{Y}(x, p) = \int_0^\infty e^{-p\theta} y(x, \theta) d\theta$
z = variable of integration, dimensionless

$\alpha \equiv \dfrac{AD + D + B}{2DB}$, 1/hr

$\beta \equiv \sqrt{\dfrac{A}{DB} - \left(\dfrac{AD + D + B}{2DB}\right)^2}$, 1/hr

θ = time, hr
κ_f = thermal conductivity of inner liquid, Btu/hr ft deg F

---

[1] Harvard University. Assoc. Mem. ASME.

[2] "Thermal Lags in Flowing Systems Containing Heat Capacitors," by J. W. Rizika, Trans. ASME, vol. 76, 1954, pp. 411–420.

Contributed by the Heat Transfer Division and presented at the Semi-Annual Meeting, Pittsburgh, Pa., June 20–24, 1954, of The American Society of Mechanical Engineers.

Note: Statements and opinions advanced in papers are to be understood as individual expressions of their authors and not those of the Society. Manuscript received at ASME Headquarters, June 23, 1954. Paper No. 54—SA-50.

κ_m = thermal conductivity of duct material, Btu/hr ft deg F
ρ_f = density of inner liquid, pcf
ρ_m = density of duct material, pcf
ω = variable of integration, dimensionless

Basic Analysis and Assumptions

Consider the system shown in Fig. 1. Let an incompressible

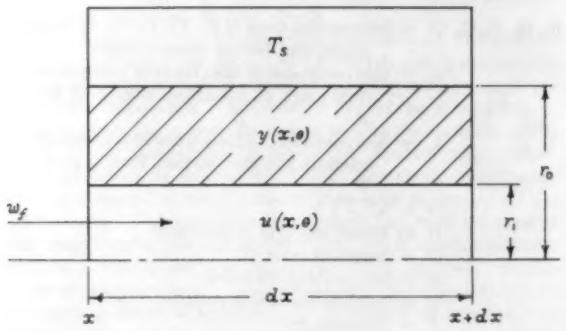

Fig. 1

fluid be flowing in a circular duct with a flow rate w_f; the temperature of this fluid at any longitudinal distance x, from the duct entrance and at any time θ, is $u(x, \theta)$. The temperature of the circular duct, which is also a heat capacitor, at any distance and any time is $y(x, \theta)$. The temperature of the medium outside the circular duct is assumed constant and equal to T_s. Such a system could physically represent a single tube of a condensing-vapor/liquid heat exchanger.

The following assumptions are made:

1 The heat flow and temperature distribution are functions of both time and axial distance from the duct inlet.

2 Both the inner radius and the outer radius of the duct are assumed constant.

3 The density and the specific heat are constant throughout the duct material.

4 The thermal conductivity of the duct material is constant (eventually to be assumed zero) in the axial direction; the thermal conductivity of the duct material is considered infinite in the radial direction.

5 There are no energy sources within the duct material itself.

6 The film coefficients of heat transfer between the fluid and duct material h are uniform and constant over the inner and outer duct surfaces for a constant fluid mass flow rate.

7 The specific heat of the inner fluid is assumed to be constant.

8 The heat transferred at any section due to the fluid thermal conductivity in the axial direction, within the fluid, is negligible compared to other heat transfers from the fluid at the same section.

Equating the sum of the thermal energies crossing the boundaries of an elemental section of the circular duct to the accumulation of energy within this elemental section, one obtains

$$2\pi r_i h_i(u - y) - 2\pi r_o h_o(y - T_s) + \pi(r_o^2 - r_i^2)\kappa_m \frac{\partial^2 y}{\partial x^2} = \pi(r_o^2 - r_i^2)\rho_m c_m \frac{\partial y}{\partial \theta} \quad [1]$$

Similarly, for an elemental section of fluid, one obtains

$$-2\pi r_i h_i(u - y) - w_f c_f \frac{\partial u}{\partial x} + \pi r_i^2 \kappa_f \frac{\partial^2 u}{\partial x^2} = \pi r_i^2 c_f \rho_f \frac{\partial u}{\partial \theta} \quad [2]$$

Neglecting the third terms in Equations [1] and [2] (note assumptions 4 and 8), and rearranging, the following are obtained

$$u = y + A(y - T_s) + B\frac{\partial y}{\partial \theta} \quad [1a]$$

$$y = u + C\frac{\partial u}{\partial x} + D\frac{\partial u}{\partial \theta} \quad [2a]$$

where

$$A \equiv \frac{r_o h_o}{r_i h_i}$$

$$B \equiv \frac{\pi(r_o^2 - r_i^2)\rho_m c_m}{2\pi r_i h_i}$$

$$C \equiv \frac{w_f c_f}{2\pi r_i h_i}$$

$$D \equiv \frac{\pi r_i^2 c_f \rho_f}{2\pi r_i h_i}$$

Now, defining the following Laplace transformations

$$\mathbf{U}(x, p) \equiv \int_0^\infty e^{-p\theta} u(x, \theta) d\theta \quad [3a]$$

$$\mathbf{Y}(x, p) \equiv \int_0^\infty e^{-p\theta} y(x, \theta) d\theta \quad [3b]$$

It can be seen that

$$\int_0^\infty e^{-p\theta}\frac{\partial y}{\partial \theta} d\theta = p\mathbf{Y} - y(x, 0) \quad [3c]$$

$$\int_0^\infty e^{-p\theta}\frac{\partial u}{\partial \theta} d\theta = p\mathbf{U} - u(x, 0) \quad [3d]$$

$$\int_0^\infty e^{-p\theta}\frac{\partial u}{\partial x} d\theta = \frac{\partial \mathbf{U}}{\partial x} \quad [3e]$$

$$\int_0^\infty e^{-p\theta} T_s d\theta = \frac{T_s}{p} \quad [3f]$$

Thus, by multiplying Equations [1a] and [2a] by $e^{-p\theta}d\theta$ and integrating between 0 and ∞

$$\mathbf{U} = [1 + A + Bp]\mathbf{Y} - \left[\frac{AT_s}{p} + By(x, 0)\right] \quad [1b]$$

$$\mathbf{Y} = C\frac{\partial \mathbf{U}}{\partial x} + [1 + Dp]\mathbf{U} - Du(x, 0) \quad [2b]$$

Solving Equation [1b] for $\mathbf{Y}$, substituting this expression into Equation [2b], and rearranging, the following differential equation is obtained

$$C\frac{\partial \mathbf{U}}{\partial x} + \left[1 + Dp - \frac{1}{1 + A + Bp}\right]\mathbf{U} - \left[Du(x, 0) + \frac{AT_s + By(x, 0)p}{(1 + A + Bp)p}\right] = 0 \quad [4]$$

The general solution to Equation [4] is

$$\mathbf{U} = e^{-f_1 x}\int_0^x e^{f_1 x} f_2 dx + e^{-f_1 x}\mathbf{U}(0, p) \quad [5]$$

where

$$f_1 \equiv \frac{1}{C}\left[1 + Dp - \frac{1}{1 + A + Bp}\right]$$

$$f_2 \equiv \frac{1}{C}\left[Du(x, 0) + \frac{AT_s + By(x, 0)p}{(1 + A + Bp)p}\right]$$

TABLE 2 FUNCTIONS AND INVERSIONS

	$F(p)$		$G(\theta)$	Reference Campbell and Foster[3] and limitations
F_1	$\frac{1}{p}$	G_1	1 (unit step function)	
F_2	$\exp\left[\frac{1}{\frac{CB}{x}\left(p+\frac{1}{B}\right)}\right]-1$	G_2	$\sqrt{\frac{x}{CB\theta}}\,e^{-\frac{\theta}{B}}I_1\left(2\sqrt{\frac{x\theta}{CB}}\right)$	654.2 $0<\theta$
F_3	$\frac{e^{-\frac{Dx}{C}p}-1}{p}$	G_3	-1	603 $0<\theta<\frac{Dx}{C}$
F_4	$\frac{e^{-\frac{Dx}{C}p}}{p}$	G_4	1	604 or 606.1 $\frac{Dx}{C}<\theta$
	F_aF_b		$\int_0^\theta F_a(z)F_b(\theta-z)dz$	

Once the boundary conditions are given explicitly, the specific solution to Equation [4] may be presented, the inverse transformation may be taken, and the final solution may thereby be obtained.

TABLE 1 BOUNDARY CONDITIONS

Mathematical	Physical
$y(x,0)=T_o$	Circular duct temperature is initially ($\theta=0$) at a uniform temperature, T_o.
$u(x,0)=T_o$	Inner fluid temperature is initially ($\theta=0$) at a uniform temperature, T_o.
$u(0,\theta)=T_{fi}$ or $\mathbf{U}(0,p)=\frac{T_{fi}}{p}$	The inner fluid temperature at entrance to the circular duct ($x=0$) is always ($\theta>0$) at the temperature T_{fi}.

Assuming the boundary conditions given in Table 1, the specific solution to Equation [5] may be shown to be

$$\mathbf{U}=\frac{(1+A+Bp)DT_op+AT_o+BT_op}{p[(1+Dp)(1+A+Bp)-1]}+\left(\frac{T_{fi}}{p}-\frac{(1+A+Bp)DT_op+AT_o+BT_op}{p[(1+Dp)(1+A+Bp)-1]}\right)e^{-\left[1+Dp-\frac{1}{1+A+Bp}\right]\frac{x}{C}} \quad \ldots\ldots[6]$$

For the case of a fluid flowing in an insulated circular duct or pipe, $A\to 0$. This specific solution can be directly obtained from Equation [6] and is

$$\mathbf{U}=\frac{T_o}{p}+\frac{(T_{fi}-T_o)}{p}e^{-\left[1+Dp-\frac{1}{1+Bp}\right]\frac{x}{C}} \quad \ldots\ldots[7]$$

Now, the inverse transformations may be taken and the final solutions can be obtained.

Incompressible Fluid Flowing in an Insulated Circular Duct

Let us now rewrite Equation [7] in the following forms and further examine its solution

$$\mathbf{U}=T_oF_1+(T_{fi}-T_o)e^{-\frac{x}{C}}(F_2+1)(F_3+F_1)\ldots.[7a]$$

$$\mathbf{U}=T_oF_1+(T_{fi}-T_o)e^{-\frac{x}{C}}(F_2+1)F_4\ldots\ldots.[7b]$$

where the foregoing functions and their inversions are expressed in Table 2.

The solutions to Equations [7a] and [7b] are

$$u(x,\theta)=T_oG_1(\theta)+(T_{fi}-T_o)e^{-\frac{x}{C}}\left[\int_0^\theta G_1(z)G_3(\theta-z)dz+\int_0^\theta G_3(z)G_1(\theta-z)dz+G_3(\theta)+G_1(\theta)\right]\ldots\ldots[8a]$$

when

$$0<\theta<\frac{Dx}{C}$$

$$u(x,\theta)=T_oG_1(\theta)+(T_{fi}-T_o)e^{-\frac{x}{C}}\left[\int_0^\theta G_2(z)G_4(\theta-z)dz+G_4(\theta)\right]\ldots\ldots[8b]$$

when

$$\frac{Dx}{C}<\theta$$

where Dx/C simply represents the time the fluid takes to reach point x from the entrance. These can be seen to reduce to (see Appendix 1)

$$u(x,\theta)=T_o\ldots\ldots\ldots\ldots\ldots\ldots[9a]$$

when

$$0<\theta<\frac{Dx}{C}$$

[3] "Fourier Integrals for Practical Applications," by G. A. Campbell and R. M. Foster, D. Van Nostrand Company, Inc., New York, N. Y., 1948.

TABLE 3 FUNCTIONS AND INVERSIONS

	$F(p)$		$G(\theta)$	Reference in Campbell and Foster[4] and limitations
F_1	$1/p$	G_1	1 (unit step function)	
F_2	$\exp\left[\frac{1}{\frac{CB}{x}\left(p+\frac{1+A}{B}\right)}\right]-1$	G_2	$\sqrt{\frac{x}{CB\theta}}\,e^{-\frac{(1+A)\theta}{B}}I_1\left(2\sqrt{\frac{x\theta}{CB}}\right)$	654.2 $0<\theta$
F_3	$\frac{e^{-\frac{Dx}{C}p}-1}{p}$	G_3	-1	603 $0<\theta<\frac{Dx}{C}$
F_4	$\frac{e^{-\frac{Dx}{C}p}}{p}$	G_4	1	604 or 606.1 $\frac{Dx}{C}<\theta$
F_5	$\frac{\frac{A}{DB}(T_s-T_0)}{\left[\left(p+\frac{AD+D+B}{2DB}\right)^2+\frac{A}{DB}-\left(\frac{AD+D+B}{2DB}\right)^2\right]}$	G_5	$\frac{\left[\frac{A}{DB}(T_s-T_0)e^{-\frac{AD+D+B}{2DB}\theta}\sin\left(\sqrt{\frac{A}{DB}-\left(\frac{AD+D+B}{2DB}\right)^2}\,\theta\right)\right]}{\sqrt{\frac{A}{DB}-\left(\frac{AD+D+B}{2DB}\right)^2}}$	448.1 $0<\theta$
	F_aF_b		$\int_0^\theta F_a(x)F_b(\theta-x)dx$	

$$u(x,\theta)=T_0+(T_{fi}-T_0)e^{-\frac{x}{C}}\left[1+\sum_{m=0}^{\infty}\frac{\left(\frac{x}{CB}\right)^{m+1}}{m!(m+1)!}\int_0^\theta e^{-\frac{x}{B}}x^m dx\right]\quad\ldots\ldots[9b]$$

when

$$\frac{Dx}{C}<\theta$$

Equations [9a] and [9b] are the final solutions for the transient fluid temperature at any section for an incompressible fluid flowing with a step-function fluid temperature input in an insulated circular duct.

A Condensing-Vapor/Liquid Heat Exchanger

Let us now return to the more general case of an incompressible fluid flowing in a circular duct, the medium surrounding the duct being maintained at a constant temperature. Such a case would physically correspond to a single tube of a simple heat exchanger such as a condensing-vapor/liquid heat exchanger.

Equation [6] can be rewritten in the following form

$$U=(T_0+F_4)F_1+(T_{fi}-T_0-F_4)e^{-\frac{x}{C}}(F_2+1)(F_3+F_1)\quad\ldots\ldots[10a]$$

$$U=(T_0+F_4)F_1+(T_{fi}-T_0-F_4)e^{-\frac{x}{C}}(F_2+1)F_4\quad\ldots\ldots[10b]$$

where the foregoing functions and their inversions are expressed in Table 3.[4]

[4] The functions in this table differ slightly from those presented in the earlier table in that these functions are more general.

The solutions to Equation [10a] and [10b] are

$$\begin{aligned}u(x,\theta)&=T_0G_1(\theta)+\int_0^\theta G_3(z)G_1(\theta-z)dz\\&+(T_{fi}-T_0)e^{-\frac{x}{C}}\left[\int_0^\theta G_2(z)G_3(\theta-z)dz\right.\\&\left.+\int_0^\theta G_2(z)G_1(\theta-z)dz+G_3(\theta)+G_1(\theta)\right]\\&-e^{-\frac{x}{C}}\left[\int_0^\theta G_3(z)\left\{\int_0^{\theta-z}G_2(\omega)G_3(\theta-z-\omega)d\omega\right\}dz\right.\\&+\int_0^\theta G_3(z)\left\{\int_0^{\theta-z}G_2(\omega)G_1(\theta-z-\omega)\,d\omega\right\}dz\\&\left.+\int_0^\theta G_3(z)G_2(\theta-z)dz+\int_0^\theta G_3(z)G_1(\theta-z)dz\right]\quad\ldots\ldots[11a]\end{aligned}$$

when

$$0<\theta<\frac{Dx}{C}$$

$$\begin{aligned}u(x,\theta)&=T_0G_1(\theta)+\int_0^\theta G_3(z)G_1(\theta-z)dz\\&+(T_{fi}-T_0)e^{-\frac{x}{C}}\left[\int_0^\theta G_2(z)G_4(\theta-z)dz+G_4(\theta)\right]\\&-e^{-\frac{x}{C}}\left[\int_0^\theta G_3(z)\left\{\int_0^{\theta-z}G_2(\omega)G_4(\theta-z-\omega)d\omega\right\}dz\right.\\&\left.+\int_0^\theta G_3(z)G_4(\theta-z)dz\right]\quad\ldots\ldots[11b]\end{aligned}$$

when $$\frac{Dx}{C} < \theta$$

These can be seen to reduce to (see Appendix 1)

$$u(x, \theta) = T_s - \frac{(T_s - T_o)e^{-\alpha\theta}}{\beta}[\alpha \sin(\beta\theta) + \beta \cos(\beta\theta)] \quad [12a]$$

when $$0 < \theta < \frac{Dx}{C}$$

and where

$$\alpha \equiv \frac{AD + D + B}{2DB}$$

$$\beta \equiv \sqrt{\frac{A}{DB} - \left(\frac{AD + D + B}{2DB}\right)^2}$$

$$u(x, \theta) = T_s - \frac{(T_s - T_o)e^{-\alpha\theta}}{\beta}[\alpha \sin(\beta\theta) + \beta \cos(\beta\theta)]$$

$$+ (T_{fi} - T_o)e^{-\frac{x}{C}}\left[1 + \sum_{m=0}^{\infty} \frac{\left(\frac{x}{CB}\right)^{m+1}}{m!(m+1)!} \int_0^{\theta} e^{-\frac{(1+A)z}{B}} z^m dz\right]$$

$$- (T_s - T_o)e^{-\frac{x}{C}}\left[1 - \frac{e^{-\alpha\theta}}{\beta}\{\alpha \sin(\beta\theta) + \beta \cos(\beta\theta)\}\right.$$

$$+ \frac{A}{DB\beta} \sum_{m=0}^{\infty} \frac{\left(\frac{x}{CB}\right)^{m+1}}{m!(m+1)!} \int_0^{\theta} e^{-\alpha z} \sin(\beta z)$$

$$\left.\left\{\int_0^{\theta - z} e^{-\frac{(1+A)\omega}{B}} \omega^m \, d\omega\right\} dz\right] \quad [12b]$$

when $$\frac{Dx}{C} < \theta$$

Equations [12a] and [12b] are the final solutions for the transient fluid temperature at any section for an incompressible fluid flowing, with a step-function fluid temperature input, in a circular duct, the medium surrounding the duct being maintained at a constant temperature.

Comparison of Steady-State Result of This Analysis for a Condensing-Vapor/Liquid Heat Exchanger to Steady-State Result Obtained in McAdams' "Heat Transmission"[5]

Let us now compare the steady-state result of this analysis for a condensing-vapor/liquid heat exchanger to the steady-state result obtained in McAdams' "Heat Transmission."[5] Consider this system to be a single tube in a heat exchanger of length l, in which a condensing vapor on the exterior section of the tube heats the liquid flowing through the tube. The steady-state temperature of the liquid leaving the heat exchanger can be obtained from Equation [12b] by letting $\theta \to \infty$. The mathematics, shown in Appendix 2, leads to the following result

$$\frac{T_s - u(l, \infty)}{T_s - T_{fi}} = e^{-\frac{l}{C}\left(\frac{A}{1+A}\right)} = e^{-\frac{2\pi l r_i h_i r_o h_o}{w_f c_f (r_i h_i + r_o h_o)}} \quad [13]$$

McAdams' approach to the problem is the following: Consider the situation as shown in Fig. 2. The thermal energy crossing

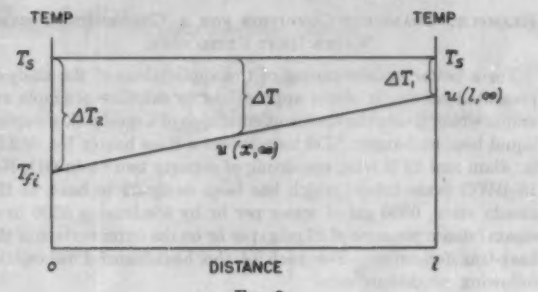

FIG. 2

the inside boundary of the tube is spent in raising the temperature of the liquid flowing through the tube and is equal to the product of the over-all heat-transfer coefficient times the surface area itmes the log mean temperature.[6] Thus

$$w_f c_f[u(l, \infty) - T_{fi}] = US\Delta T_m \quad [14]$$

where

$$\Delta T_m \equiv \frac{\Delta T_2 - \Delta T_1}{\ln \frac{\Delta T_2}{\Delta T_1}} = \frac{u(l, \infty) - T_{fi}}{\ln\left[\frac{T_s - T_{fi}}{T_s - u(l, \infty)}\right]}$$

or, rearranging

$$\frac{T_s - u(l, \infty)}{T_s - T_{fi}} = e^{-\frac{US}{w_f c_f}} \quad [14a]$$

The over-all heat transfer coefficient is defined[7]

$$US \equiv \frac{q}{\Delta T} \quad [15]$$

Considering a tube of the heat exchanger, with a film on either side of the tube

$$q = 2\pi r_i l h_i (y - u) = 2\pi r_o l h_o (T_s - y) \quad [16]$$

or

$$(y - u) = \frac{q}{2\pi l r_i h_i} \quad [16a]$$

$$(T_s - y) = \frac{q}{2\pi l r_o h_o} \quad [16b]$$

Adding Equations [16a] and [16b], one obtains

$$(T_s - u) = \Delta T = \frac{q(r_o h_o + r_i h_i)}{2\pi l r_i h_i r_o h_o} \quad [16c]$$

Comparing this equation with the definition of US, in Equation [15], one notes that

$$US = \frac{2\pi l r_i h_i r_o h_o}{(r_o h_o + r_i h_i)} \quad [17]$$

Now, substituting Equation [17] into Equation [14a], the following is obtained

$$\frac{T_s - u(l, \infty)}{T_s - T_{fi}} = e^{-\frac{2\pi l r_i h_i r_o h_o}{w_f c_f (r_o h_o + r_i h_i)}} \quad [18]$$

It can be seen immediately that this equation is identical to Equation [13], the result for the steady-state condition from the analysis presented in this paper.

[5] "Heat Transmission," by W. H. McAdams, McGraw-Hill Book Company, Inc., New York, N. Y., second edition, 1942.

[6] Ibid., p. 141ff.

[7] Ibid., p. 133ff.

Example: Transient Condition for a Condensing-Steam/Water Heat Exchanger

For a better understanding of the applications of the analysis presented herein, it seems appropriate to examine a simple example which treats the transient condition of a condensing-vapor/liquid heat exchanger. Let us consider a Ross heater No. 812 (8 in. diam and 12 ft long, consisting of seventy two $^5/_8$-in-OD, No. 18 BWG brass tubes) which has been designed to heat, in the steady state, 6300 gal of water per hr by condensing 5200 lb of steam (steam pressure of 10 psig) per hr on the outer surface of the heat-transfer tubes. For each of the heat-transfer tubes, the following conditions exist

$$w_f = \frac{6300(8.3)}{72} = 725 \text{ lb/hr}$$
$$l = 12 \text{ ft}$$
$$c_f = 1 \text{ Btu/lb deg F}$$
$$\rho_f = 62.4 \text{ pcf}$$
$$r_i = \frac{0.2635}{12} = 0.022 \text{ ft}$$
$$r_o = \frac{0.3125}{12} = 0.026 \text{ ft}$$
$$\pi(r_o^2 - r_i^2)\rho_m = 0.329 \text{ lb/ft}$$
$$c_m = 0.1 \text{ Btu/lb deg F}$$
$$\text{Re}_f = 8680$$

From McAdams[8]

$$h_i \simeq 600 \text{ Btu/hr sq ft deg F}$$
$$h_o \simeq 1500 \text{ Btu/hr sq ft deg F}$$

Thus
$$A = 2.95$$
$$B = 3.97 \times 10^{-4} \text{ hr}$$
$$C = 8.74 \text{ ft}$$
$$D = 1.145 \times 10^{-3} \text{ hr}$$
$$\alpha = 5.42 \times 10^3 \frac{1}{\text{hr}}$$
$$\beta = 4.77 \times 10^3 i \frac{1}{\text{hr}}$$
$$\frac{Dl}{C} = 1.57 \times 10^{-3} \text{ hr} = 5.65 \text{ sec}$$

Let us assume that the water valve is initially opened and equilibrium is reached so that both the water and tube material are at a constant temperature T_o throughout the length of the exchanger. Suddenly, at time $\theta = 0$, the steam is allowed to flow. Assume that the water entrance temperature $u(0\ \theta)$ has remained unchanged and is equal to T_o; this implies that $T_{fi} = T_o$. What is the water exit temperature $u(12, \theta)$ as a function of time?

Equation [12a] is applicable when $0 < \theta < 5.65$ sec; during this interval this equation can be seen to reduce to

$$\frac{T_s - u(12,\theta)}{T_s - T_o} = 0.210e^{-5.42\times10^3\theta}\,[5.42 \sinh (4.77 \times 10^3\theta) + 4.77 \cosh (4.77 \times 10^3\theta)] \ldots\ldots [12a']$$

The steady-state temperature of the water leaving the heat exchanger can be obtained directly from Equation [13]

$$\frac{T_s - u(12,\infty)}{T_s - T_o} = e^{-\frac{(12.0)(2.95)}{(8.74)(3.95)}} = 0.359 \ldots\ldots [13']$$

[8] "Heat Transmission," by W. H. McAdams, fig. 81, p. 179.

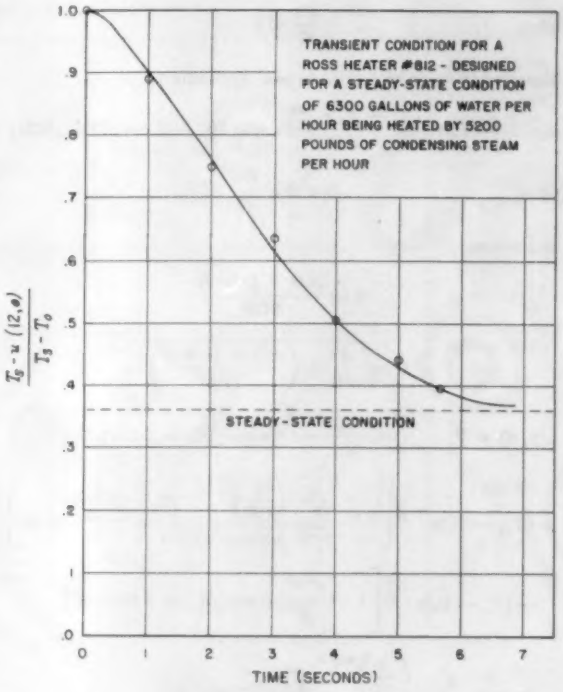

Fig. 3

These equations precipitate the result given in Table 4 (also shown in Fig. 3):

TABLE 4

θ (sec)	$\frac{T_s - u(12,\theta)}{T_s - T_o}$
0	1.000
1	0.888
2	0.750
3	0.635
4	0.504
5	0.440
5.65	0.395
∞	0.359

G. M. Dusinberre[9] outlines the numerical procedure for the solution of such problems. A comparison, by Dusinberre, of the analytical solution with the numerical solution for this problem shows the results given in Table 5.

TABLE 5 COMPARISON OF RESULTS

Time (sec)	Dimensionless temperature ratio — Analytical solution	Dimensionless temperature ratio — Numerical solution
0	1.000	1.000
1	0.888	0.916
2	0.750	0.761
3	0.635	0.639
∞	0.359	0.358

It can easily be seen, of course, that the steady-state exit water temperature is almost fully achieved by the end of the interval $0 < \theta < Dl/C$. This negated the necessity of utilizing the more complicated Equation [12b] for times greater than 5.65 sec and less than infinity. It should be pointed out that such a procedure

[9] "Calculation of Transient Temperatures in Pipes and Heat Exchangers by Numerical Methods," by G. M. Dusinberre, Trans. ASME, vol. 76, 1954, pp. 421–426.

is not always applicable and in many instances Equation [12b] must be utilized. When such instances arise, it is suggested that the reader utilize the curves in the author's previous paper[2] to simplify the necessary calculations.

Results and Summary

The transient conditions due to thermal lags in flowing incompressible fluid systems have been analyzed for two particular cases: (1) An incompressible fluid flowing, with a step-function temperature input, in an insulated circular duct or pipe, and (2) an incompressible fluid flowing, with a step-function temperature input, in a circular duct, the exterior of the duct being surrounded by a constant-temperature medium. The solutions for the fluid temperatures, as a function of both distance and time, are presented in Equations [9] and [12], respectively, for these cases.

The solution to the latter case is also applicable to the transient solution for a simple condensing-vapor/liquid heat exchanger. In the limit, as the time goes to infinity, the result has been shown to be identical to the result normally obtained from a steady-state heat-exchanger analysis. An example has been presented, which adequately demonstrates the method of application of this analysis to a practical heat-exchanger problem.

In conclusion, it should be pointed out that the solutions obtained in this paper consist of similar functions to those already tabulated by the author in a previous paper[2]; these tabulations greatly simplify the calculations necessary for a specific numerical answer.

Acknowledgment

The author would like to thank Prof. G. M. Dusinberre of the Pennsylvania State College, for his initial review of and suggestions concerning the subject material. The major portion of this work was financed by the Jackson and Moreland Company, Boston, Mass.

Appendix 1

The expressions appearing in Equations [8] and [11] are evaluated below

$$T_o G_1(\theta) = T_o \quad [19]$$

$$\int_0^\theta G_2(z)G_1(\theta - z)dz = (T_s - T_o)\left\{1 - \frac{e^{-\alpha\theta}}{\beta}\left[\alpha \sin(\beta\theta) + \beta\cos(\beta\theta)\right]\right\} \quad [20]$$

$$\int_0^\theta G_2(z)G_3(\theta - z)dz = -\int_0^\theta G_2(z)G_1(\theta - z)dz \quad [21]$$

$$G_3(\theta) = -G_1(\theta) \quad [22]$$

$$\int_0^\theta G_4(z)\left[\int_0^{\theta - z} G_2(\omega)G_3(\theta - z - \omega)\,d\omega\right]dz = -\int_0^\theta G_3(z)\left[\int_0^{\theta - z} G_2(\omega)G_1(\theta - z - \omega)\,d\omega\right]dz \quad [23]$$

$$\int_0^\theta G_3(z)G_3(\theta - z)dz = -\int_0^\theta G_3(z)G_1(\theta - z)dz \quad [24]$$

$$\int_0^\theta G_3(z)G_4(\theta - z)\,dz = \sum_{m=0}^{\infty}\frac{\left(\frac{x}{CB}\right)^{m+1}}{m!(m+1)!}\int_0^\theta e^{-\frac{(1+A)z}{B}} z^m dz \quad [25]$$

$$G_4(\theta) = 1 \quad [26]$$

$$\int_0^\theta G_3(z)\left[\int_0^{\theta - z} G_2(\omega)G_4(\theta - z - \omega)d\omega\right]dz = \frac{(T_s - T_o)A}{DB\beta}\sum_{m=0}^{\infty}\frac{\left(\frac{x}{CB}\right)^{m+1}}{m!(m+1)!}\int_0^\theta e^{-\alpha z}\sin(\beta z)\left[\int_0^{\theta - z} e^{-\frac{(1+A)\omega}{B}}\omega^m d\omega\right]dz \quad [27]$$

$$\int_0^\theta G_3(z)G_4(\theta - z)dz = (T_s - T_o)\left\{1 - \frac{e^{-\alpha\theta}}{\beta}\left[\alpha\sin(\beta\theta) + \beta\cos(\beta\theta)\right]\right\} \quad [28]$$

Appendix 2

Let us find the steady-state temperature at any section, from Equation [12b]. Rewriting this equation, letting $\theta \to \infty$

$$u(x, \infty) = T_s + (T_{fi} - T_o)e^{-\frac{x}{C}}\left[1 + \sum_{m=0}^{\infty}\frac{\left(\frac{x}{CB}\right)^{m+1}}{m!(m+1)!}\int_0^\infty e^{-\frac{(1+A)z}{B}} z^m dz\right] - (T_s - T_o)e^{-\frac{x}{C}}\left\{1 + \frac{A}{DB\beta}\sum_{m=0}^{\infty}\frac{\left(\frac{x}{CB}\right)^{m+1}}{m!(m+1)!}\int_0^\infty e^{-\alpha z}\sin(\beta z)\left[\int_0^\infty e^{-\frac{(1+A)\omega}{B}}\omega^m d\omega\right]dz\right\} \quad [12c]$$

But

$$\int_0^\infty e^{-\frac{(1+A)z}{B}} z^m\,dz = \frac{m!}{\left(\frac{1+A}{B}\right)^{m+1}} = \int_0^\infty e^{-\frac{(1+A)\omega}{B}}\omega^m d\omega$$

and

$$\sum_{m=0}^{\infty}\frac{\left[\frac{x}{C(1+A)}\right]^{m+1}}{(m+1)!} = e^{\frac{x}{C(1+A)}} - 1$$

Substituting these equations into Equation [12c]

$$u(x, \infty) = T_s + (T_{fi} - T_o)e^{-\frac{x}{C}\left(\frac{A}{1+A}\right)} - (T_s - T_o)e^{-\frac{x}{C}}\left[1 + \frac{A}{DB\beta}\left(e^{\frac{x}{C(1+A)}} - 1\right)\int_0^\infty e^{-\alpha z}\sin(\beta z)dz\right] \quad [12d]$$

But

$$\int_0^\infty e^{-\alpha z}\sin(\beta z)dz = \frac{\beta}{\alpha^2 + \beta^2} = \frac{DB\beta}{A}$$

Substituting this into Equation [12d], one obtains

$$u(x, \infty) = T_s + (T_{fi} - T_s)e^{-\frac{x}{C}\left(\frac{A}{1+A}\right)} \quad [12e]$$

or, if $x = l$

$$\frac{T_s - u(l, \infty)}{T_s - T_{fi}} = e^{-\frac{l}{C}\left(\frac{A}{1+A}\right)} \quad [13]$$

A Systematic and Rapid Procedure of Computing Approximate Characteristic Values Pertaining to Bare-Tube Crossflow Heat Exchangers

By F. J. NEUGEBAUER,[1] SCHENECTADY, N. Y.

This paper presents a systematic method of determining approximate characteristic values pertaining to crossflow heat exchangers of the bare-tube bundle type. Only the case of turbulent flow has been taken into consideration. The method described allows rapid computation of entire families of heat exchangers having the same requirements with regard to heat-transfer and pressure losses. The basic idea of this method is not confined to the aforementioned type of heat exchanger and flow pattern. The interested reader will immediately recognize that the method can be adapted to other configurations.[2]

Nomenclature

The following nomenclature is used in the paper:

A = area of heat-transfer surface, sq ft
a, b = constants used in heat-transfer formulas, dimensionless
c = specific heat of fluid, Btu/(lb)(deg F)
D = mean tube diameter, ft
g = acceleration of gravity = 4.17×10^8 ft/(hr)(hr)
h = surface heat-transfer coefficient, Btu/(hr)(sq ft)(deg F)
k = thermal conductivity of fluid, Btu/(hr)(sq ft)(deg F per ft)
L = length of tubes, ft
M = constant used in heat-transfer formulas, dimensionless
N = total number of tubes
N_T = number of tubes in each row transverse to stream
N_L = number of tube rows, longitudinal
N_{Pr} = Prandtl number, dimensionless $c\mu/k$
N_{Re} = Reynolds number, based on tube diameter D, dimensionless
p = absolute fluid pressure, average of inlet and outlet, lb force per sq ft
Δp = pressure loss, without entrance and exit losses, lb force per sq ft
q = rate of heat flow, Btu per hr
s_T = spacing between centers of tubes transverse to stream, ft
s_L = spacing between centers of tubes, longitudinal, ft
S = minimum cross-sectional area open for fluid flow, sq ft
t_1 = inlet temperature of fluid inside of the tubes, deg F
t_2 = discharge temperature of fluid inside of tubes, deg F
t_3 = inlet temperature of fluid outside of tubes, deg F
t_4 = discharge temperature of fluid outside of tubes, deg F
t_i = average temperature of fluid inside of tubes, deg F
t_o = average temperature of fluid outside of tubes, deg F
U = over-all heat-transfer coefficient, fluid to fluid, Btu/(hr)(sq ft)(deg F)
V = flow velocity, fph
w = mass flow rate, lb per hr
α = characteristic computation factor, ft^{-2}
β = characteristic computation factor, ft
γ = characteristic computation factor, ft
δ = characteristic computation factor, ft
ϵ = characteristic computation factor, dimensionless
Δt_{13} = $t_1 - t_3$, difference of inlet temperatures, deg F
Δt_e = effective difference between fluid temperatures, deg F
Δt_{12} = $t_1 - t_2$, change of fluid temperature inside of tubes, deg F
Δt_{43} = $t_4 - t_3$, change of fluid temperature outside of tubes, deg F
μ = viscosity of fluid, lb/(hr)(ft)
ρ = mass density of fluid, pcf

Subscript i refers to inside of tubes.
Subscript o refers to outside of tubes.

Introduction

It is the objective of research to reveal and describe the laws of nature, however intricate they may be. The engineer frequently must simplify the basic scientific picture to make it more useful for practical application.

Calculations, which render approximate results but at the same time allow a rapid survey over a wide range of conditions and assumptions, are important in the approach to an engineering problem. They serve as timesavers in that they confine the more detailed investigations to a smaller numerical range.

The preliminary computation of crossflow heat exchangers, the basic conception of which is illustrated in Figs. 1, 2, and 3, is a typical example of such a procedure.

Nature of Problem

Fig. 1 shows the temperature distribution in crossflow heat exchangers with the hotter fluid flowing either inside or outside of the tubes. Fig. 2 illustrates the arrangement of the tubes. A limitation of the longitudinal spacing ratio s_L/D has been established in order to make the following analysis simpler and clearer. This limitation guarantees that the flow velocity outside of the tubes reaches its highest value in the transverse openings between the tubes as explained in Fig. 3.

The total number of tubes is

$$N = N_T N_L \quad \text{[1]}$$

---

[1] Consulting Engineer, Thermal Systems, General Engineering Laboratory, General Electric Company. Mem. ASME.

[2] A contribution to the same problem has been published by Dr. W. Traupel (6). Numbers in parentheses refer to the Bibliography at the end of the paper.

Contributed by the Heat Transfer Division and presented at the Semi-Annual Meeting, Pittsburgh, Pa., June 20–24, 1954, of The American Society of Mechanical Engineers.

Note: Statements and opinions advanced in papers are to be understood as individual expressions of their authors and not those of the Society. Manuscript received at ASME Headquarters, April 1, 1954. Paper No. 54—SA-40.

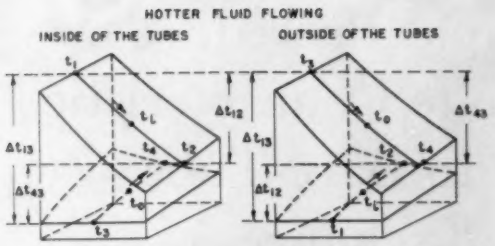

FIG. 1 TEMPERATURE DISTRIBUTION IN CROSSFLOW HEAT EXCHANGERS

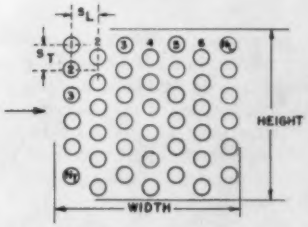

FIG. 2 ARRANGEMENT OF TUBES

The basic problem may be presented as follows: Known values are

Temperatures..... t_1, t_2, t_3
Absolute fluid pressures..... p_i, p_o
Mass densities..... ρ_i, ρ_o
Mass flows..... w_i, w_o
Specific heats of the fluids..... c_i, c_o
Permissible pressure losses..... Δp_i, Δp_o

The five unknowns D, L, s_T, N_T, and N_L are to be determined. The purpose of the analysis is to set up the required five simultaneous equations and to solve them without using a trial-and-error method.

THE DISCHARGE TEMPERATURE t_4

The cold fluid absorbs the heat which is removed from the hot fluid

$$w_i c_i \Delta t_{12} = w_o c_o \Delta t_{43} \quad [2]$$

$$t_4 = \frac{w_i c_i}{w_o c_o} \Delta t_{12} + t_2 \quad [3]$$

EFFECTIVE DIFFERENCE OF TEMPERATURE OF FLUIDS, Δt_e

The determination of the effective temperature difference is based upon Nusselt's investigation (1). From

$$\frac{\Delta t_{12}}{\Delta t_{13}} = \frac{t_1 - t_2}{t_1 - t_3} \quad [4]$$

and

$$\frac{\Delta t_{43}}{\Delta t_{13}} = \frac{t_4 - t_3}{t_1 - t_3} \quad [5]$$

The temperature ratio $\Delta t_e / \Delta t_{13}$ may be determined using Fig. 4. The effective temperature difference is

$$\Delta t_e = \left(\frac{\Delta t_e}{\Delta t_{13}} \right) \Delta t_{13} \quad [6]$$

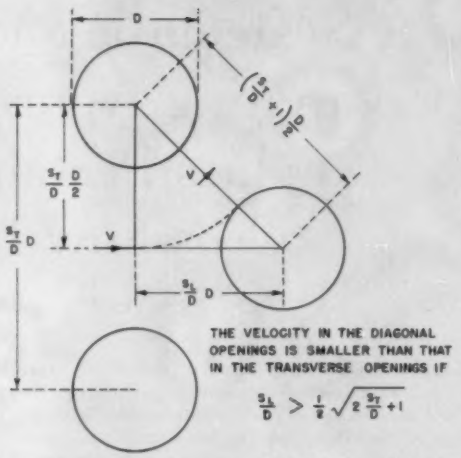
D
THE VELOCITY IN THE DIAGONAL OPENINGS IS SMALLER THAN THAT IN THE TRANSVERSE OPENINGS IF
$\frac{S_L}{D} > \frac{1}{2}\sqrt{2\frac{S_T}{D}+1}$

FIG. 3 LIMITATION ASSUMED FOR THE LONGITUDINAL SPACING s_L/D

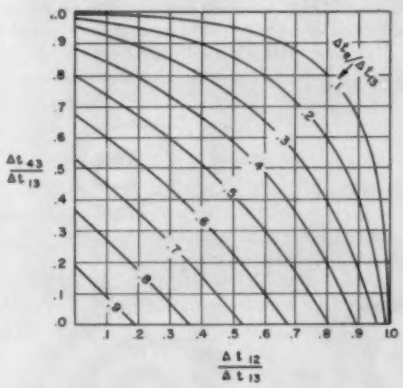
$\frac{\Delta t_{43}}{\Delta t_{13}}$
$\frac{\Delta t_{12}}{\Delta t_{13}}$
$\frac{\Delta t_e}{\Delta t_{13}}$
THIS DIAGRAM IS TAKEN FROM REFERENCE (5)
IT IS VALID FOR UNMIXED FLOW OF BOTH FLUIDS AND FOR CONSTANT HEAT-TRANSFER COEFFICIENT "U"
FOR OTHER CASES AND FOR VARIABLE "U" SEE REFERENCE (3) p. 146.

FIG. 4 MEAN EFFECTIVE TEMPERATURE DIFFERENCE IN CROSSFLOW HEAT EXCHANGERS

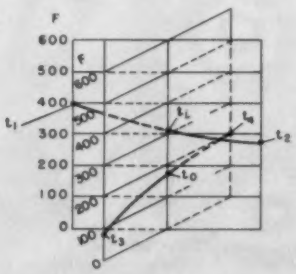

FIG. 5 ESTIMATE OF AVERAGE TEMPERATURES

ESTIMATING AVERAGE FLUID TEMPERATURES

The estimate of the average fluid temperatures t_i and t_o is made by sketching a three-dimensional plot as shown in Fig. 5. The average values of densities and viscosities used in Reynolds numbers are evaluated at the average temperatures t_i and t_o.

Reynolds Numbers

For either side of the heat exchanger, the Reynolds number may be written

$$N_{Re} = \frac{VD\rho}{\mu} \quad [7]$$

where

$$V = \frac{w}{\rho S} \quad [8]$$

so that

$$N_{Re} = \frac{wD}{\mu S} \quad [9]$$

The known limitations of the heat-transfer and pressure-drop formulas in addition to any special requirement for the particular job must be considered when selecting the Reynolds numbers. The influence of this selection on the dimensions of a heat exchanger will be discussed later.

Derivation of Five Simultaneous Equations

1 The flow area inside of the tubes is

$$S_i = \frac{\pi D^2}{4} N_L N_T \quad [10]$$

From Equations [9] and [10] we obtain the Reynolds number inside of the tubes

$$(N_{Re})_i = \frac{4w_i}{\pi D N_L N_T \mu_i} \quad [11]$$

From Equation [11] we define a quantity δ which provides the first of the simultaneous equations

$$\delta = N_L N_T D = \frac{4w_i}{\pi \mu_i (N_{Re})_i} \quad [12]$$

2 The smallest flow area outside of the tubes, as explained in Fig. 3, is

$$S_o = N_T(s_T - D)L \quad [13]$$

Combined with Equation [9]

$$(N_{Re})_o = \frac{w_o D}{N_T(s_T - D)L\mu_o} \quad [14]$$

From Equation [14] we define a quantity γ which provides the second simultaneous equation

$$\gamma = N_T L = \frac{w_o}{\left(\frac{s_T}{D} - 1\right)\mu_o (N_{Re})_o} \quad [15]$$

3 E. Hofmann (2), by consolidating the findings of several investigatore (2a), recommends M. Jakob's approximation for the pressure loss at the outer side of the tubes

$$\Delta p_o = N_L \frac{\rho_o V_o^2}{2g} \frac{1 + \frac{0.47}{\left(\frac{s_T}{D} - 1\right)^{1.08}}}{(N_{Re})_o^{0.16}} \quad [16]$$

The pressure loss inside of the tubes according to Blasius (4) is

$$\Delta p_i = 0.32 \frac{\rho_i V_i^2}{2g} \frac{L}{D} \frac{1}{(N_{Re})_i^{0.25}} \quad [17]$$

From Equations [16] and [17] we obtain

$$\frac{\Delta p_i}{\Delta p_o} = \frac{0.32 \rho_i V_i^2 L (N_{Re})_o^{0.16}}{N_L \rho_o V_o^2 D (N_{Re})_i^{0.25} \left[1 + \frac{0.47}{\left(\frac{s_T}{D} - 1\right)^{1.08}}\right]} \quad [18]$$

To get Equation [18] in a more useful form, we multiply it by

$$\left[\frac{(N_{Re})_i}{(N_{Re})_o} \frac{(N_{Re})_o}{(N_{Re})_i}\right]^2 = \left[\frac{(N_{Re})_i}{(N_{Re})_o} \frac{V_o \rho_o \mu_i}{V_i \rho_i \mu_o}\right]^2 = 1 \quad [19]$$

and substitute

$$\frac{V_o}{V_i} = \frac{\pi w_o \rho_i D N_L}{4 w_i \rho_o L \left(\frac{s_T}{D} - 1\right)} \quad [20]$$

Combining with Equations [8], [10], and [13] we obtain the third simultaneous equation which defines a quantity ϵ

$$\left.\begin{aligned} \epsilon &= \left[1 + \frac{0.47}{\left(\frac{s_T}{D} - 1\right)^{1.08}}\right]\left(\frac{s_T}{D} - 1\right) \\ &= 0.08\pi \frac{\Delta p_o}{\Delta p_i} \frac{w_o}{w_i} \frac{\rho_o}{\rho_i} \left(\frac{\mu_i}{\mu_o}\right)^2 \frac{(N_{Re})_i^{2.75}}{(N_{Re})_o^{2.84}} \end{aligned}\right\} \quad [21]$$

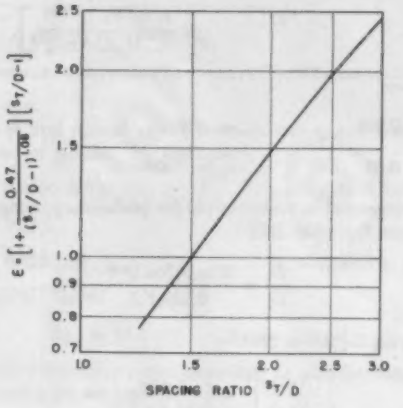
2.5
2.0
1.5
1.0
0.9
0.8
0.7
1.0
1.5
2.0
2.5
3.0
SPACING RATIO s_T/D
$\epsilon = \left[1 + \frac{0.47}{\left(\frac{s_T}{D} - 1\right)^{1.08}}\right]\left(\frac{s_T}{D} - 1\right)$
UNDER CERTAIN CONDITIONS, THE CALCULATION MAY NOT PROVIDE A PRACTICAL VALUE OF THE SPACING RATIO s_T/D. THE CHANGE IN ASSUMPTIONS THAT MUST BE MADE TO OBTAIN A REASONABLE SPACING RATIO CAN THEN EASILY BE DETERMINED FROM EQUATION [21]

Fig. 6 Factor ϵ Versus Spacing Ratio

The value of the spacing ratio s_T/D may be taken from Fig. 6 after the last term in Equation [21] has been evaluated.

4 Formulas for the heat-transfer coefficients inside and outside of tubes are presented by McAdams[3] in the form

$$h = M(N_{Pr})^a (N_{Re})^b \frac{k}{D} \quad [22]$$

This also may be written as

$$h_i = \frac{M_i (N_{Re})_i^{b_i} \mu_i c_i}{D (N_{Pr})_i^{1-a_i}} \quad [23]$$

for the inside of the tubes, and as

[3] Reference (3), pp. 168 and 22.

$$h_o = \frac{M_o(N_{Re})_o^{b_o}\mu_o c_o}{D(N_{Pr})_o^{1-a_o}} \quad [24]$$

for the outside of the tubes.

The thickness of the tube wall is so small in many cases that its heat-flow resistance as well as the difference between the inner and outer diameter and surface area can be neglected. With this assumption we obtain for the over-all heat-flow resistance

$$\frac{1}{U} = \frac{1}{h_i} + \frac{1}{h_o} = D\left[\frac{(N_{Pr})_i^{1-a_i}}{M_i\mu_i c_i(N_{Re})_i^{b_i}} + \frac{(N_{Pr})_o^{1-a_o}}{M_o\mu_o c_o(N_{Re})_o^{b_o}}\right] \quad [25]$$

The rate of heat flow is

$$q = AU\Delta t_o = w_i c_i \Delta t_{12} \quad [26]$$

The heat-transfer area is

$$A = \pi DLN_L N_T \quad [27]$$

Combining Equations [25], [26], and [27], we obtain the fourth simultaneous equation, which defines a quantity β

$$\beta = N_L N_T L = \frac{w_i \Delta t_{12}}{\pi \Delta t_o}\left[\frac{(N_{Pr})_i^{1-a_i}}{M_i\mu_i(N_{Re})_i^{b_i}} + \frac{c_i}{c_o}\frac{(N_{Pr})_o^{1-a_o}}{M_o\mu_o(N_{Re})_o^{b_o}}\right] \quad [28]$$

The values

$M_i = 0.023$	$a_i = 0.4$	$b_i = 0.8$
$M_o = 0.33$	$a_o = 0.333$	$b_o = 0.6$

are recommended in reference (3) for preliminary computations.

5 From Equation [17]

$$\frac{L}{D} = \frac{2\Delta p_i g(N_{Re})_i^{0.25}}{0.32\rho_i V_i^2} \quad [29]$$

Multiplying Equation [29] by

$$\left[\frac{(N_{Re})_i}{(N_{Re})_i}\right]^3 = \left[\frac{V_i D\rho_i}{\mu_i(N_{Re})_i}\right]^3 = 1 \quad [30]$$

we obtain the fifth simultaneous equation, which defines a quantity α

$$\alpha = \frac{L}{D^3} = \frac{g\Delta p_i \rho_i}{0.16\mu_i^2(N_{Re})_i^{1.75}} \quad [31]$$

Computing Heat-Exchanger Dimensions From Simultaneous Equations

The physical dimensions of the heat exchanger result immediately from the characteristic computation factors α, β, γ, δ, and ϵ:

Spacing ratio: Compute ϵ and read s_T/D from Fig. 6

Tube diameter

$$D = \left(\frac{\beta}{\alpha\delta}\right)^{0.5} \quad [32]$$

Length of tubes

$$L = \frac{\beta}{\delta}\left(\frac{\beta}{\alpha\delta}\right)^{0.5} = \frac{\beta}{\delta}D \quad [33]$$

Number of tubes in each row transverse to fluid flow

$$N_T = \frac{\gamma}{\frac{\beta}{\delta}\left(\frac{\beta}{\alpha\delta}\right)^{0.5}} = \frac{\gamma}{L} \quad [34]$$

Number of rows, longitudinal

$$N_L = \frac{\beta}{\gamma} \quad [35]$$

Area of heat-transfer surface

$$A = \pi\frac{\beta^{1.5}}{(\alpha\delta)^{0.5}} = \pi D\beta \quad [36]$$

The absence of s_L in Equation [16] indicates that the longitudinal spacing s_L can be freely chosen; the limitation established in Fig. 3 has to be borne in mind.

Survey of a Heat-Exchanger Family

In the first approach, heat-exchanger dimensions calculated in accordance with the described method may not be suitable for the job application or may involve manufacturing problems. An entire family of heat exchangers fulfilling the same requirements with regard to pressures, temperatures, flow rates, and pressure losses can be calculated rapidly and may provide a configuration with more suitable dimensions.

To compute a heat-exchanger family, the spacing ratio s_T/D is held constant and the Reynolds number inside of the tubes, $(N_{Re})_i$, is varied. Equation [21] shows that the ratio $(N_{Re})_i^{2.75}/(N_{Re})_o^{2.24}$ is constant under these conditions so that the Reynolds number outside of the tubes can be computed immediately. With both Reynolds numbers known, the dimensions of the heat exchangers can be determined as explained previously. The calculation is then repeated for other spacing ratios s_T/D.

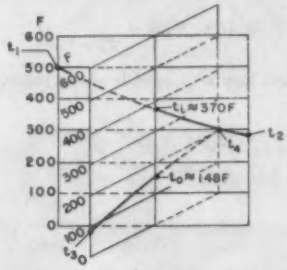

Fig. 7 Heat-Exchanger Family
(The known magnitude of the effective temperature difference, Δt_e, is helpful in estimating the curvature of the temperature curves.)

Fig. 7 shows a typical heat-exchanger family. An entire set of dimensions can be read after selecting a single dimension such as tube length or tube diameter.

Other Applications of Method

In many cases it is desirable to begin the computation by assuming physical dimensions such as tube diameter and tube length rather than assuming fixed pressure losses. The numerical example following shows that only one of the Reynolds numbers, $(N_{Re})_i$ or $(N_{Re})_o$, may be chosen freely if tube diameter and length are assumed. However, an additional variable such as spacing ratio s_T/D, tube number N_T or N_L, tube-number ratio N_T/N_L, one of the pressure losses Δp_i or Δp_o, or the pressure loss ratio $\Delta p_i/\Delta p_o$ may be selected.

The numerical example provided below illustrates a few of the

possible applications without fully exhausting the versatility of the method.

Summary

The purpose of the described procedure is to find approximate characteristic values in a convenient and timesaving way. Reference (3) may be consulted for the necessary final corrections. Special care must be taken if liquids of high viscosity are under consideration, or if the temperature difference between the two liquids is so large that the wall temperatures become significant, or if the figures involved do not fall between the following limitations which are dictated by the range of validity of pressure loss and heat-transfer formulas:

Reynolds number inside of the tubes	$(N_{Re})_i = 8000$ to 80,000
Reynolds number outside of the tubes	$(N_{Re})_o = 2000$ to 40,000
Spacing ratios	$s_T/D = 1.25$ to 3.0
	$s_L/D \geq 0.5[(2s_T/D) + 1]^{0.5}$
Prandtl number	$N_{Pr} \leq 20$
Number of tube rows	$N_L \geq 10$
Length diameter ratio	$L/D \geq 10$ in the case of gases
	$L/D \geq 2.5$ in the case of liquids

Numerical Examples

The following computation has been made with slide-rule accuracy.

Data and Evaluation Steps Which Are Fixed Throughout all Numerical Examples:

Hotter fluid flowing inside of the tubes

$t_1 = 500$ deg F $\quad t_2 = 270$ deg F $\quad t_i = 85$ deg F

$w_i = 16{,}200$ lb per hr $\quad w_o = 32{,}400$ lb per hr

$p_i = 9900$ lb per sq ft $\quad p_o = 2115$ lb per sq ft

$c_i = c_o$

$M_i = 0.023, \quad a_i = 0.4, \quad b_i = 0.8$

$M_o = 0.33, \quad a_o = 0.333, \quad b_o = 0.6$

Tables or graphs showing the viscosities, Prandtl numbers, and mass densities of the fluids in question.

1 t_4 from Equation [3]

$$t_4 = \frac{16{,}200}{32{,}400}(500 - 270) + 85 = 200 \text{ deg F}$$

2 $\Delta t_{12}/\Delta t_{13}$ and $\Delta t_{42}/\Delta t_{13}$ from Equations [4] and [5]

$$\Delta t_{12}/\Delta t_{13} = \frac{500 - 270}{500 - 85} = 0.555, \quad \Delta t_{42}/\Delta t_{13} = \frac{200 - 85}{500 - 85} = 0.277$$

3 $\Delta t_o/\Delta t_{13}$ from Fig. 4

$$\Delta t_o/\Delta t_{13} = 0.542$$

4 Δt_o from Equation [6]

$$\Delta t_o = 0.542\,(500 - 85) = 225 \text{ deg F}$$

5 In most cases it will be exact enough to estimate t_i and t_o as the arithmetic-mean temperatures of the streams. A sketch like Fig. 8 may be drawn if a closer estimate is desired

$$t_i = 270 \text{ deg F}, \quad t_o = 148 \text{ deg F}$$

6 The viscosities, Prandtl numbers, and mass densities at the

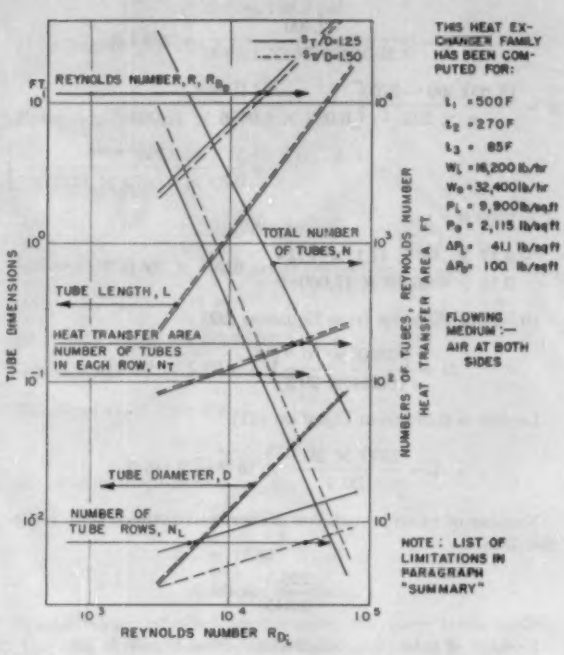
s_T/D=1.25
s_T/D=1.50
THIS HEAT EXCHANGER FAMILY HAS BEEN COMPUTED FOR:
t_1 = 500 F
t_2 = 270 F
t_3 = 85 F
W_i = 16,200 lb/hr
W_o = 32,400 lb/hr
P_i = 9,900 lb/sq ft
P_o = 2,115 lb/sq ft
ΔP_i = 41 lb/sq ft
ΔP_o = 100 lb/sq ft
FLOWING MEDIUM :— AIR AT BOTH SIDES
FT
REYNOLDS NUMBER, R, R_{D_o}
TOTAL NUMBER OF TUBES, N
TUBE LENGTH, L
HEAT TRANSFER AREA
NUMBER OF TUBES IN EACH ROW, N_T
TUBE DIAMETER, D
NUMBER OF TUBE ROWS, N_L
TUBE DIMENSIONS
NUMBERS OF TUBES, REYNOLDS NUMBER HEAT TRANSFER AREA FT
NOTE : LIST OF LIMITATIONS IN PARAGRAPH "SUMMARY"
REYNOLDS NUMBER R_{D_i}

Fig. 8 Estimate of Average Temperatures (Numerical Example)

pressures p_i and p_o and at the temperatures t_i and t_o are taken from tables or graphs; for example

$\mu_i = 0.0596$ lb/(hr)(ft) $\quad \mu_o = 0.0476$ lb/(hr)(ft)

$(N_{Pr})_i = 0.71 \quad (N_{Pr})_o = 0.71$

$\rho_i = 0.224$ pcf $\quad \rho_o = 0.0653$ lb per cu ft

Example 1. Given

$$\Delta p_i = 41.1 \text{ psf}, \quad \Delta p_o = 100 \text{ psf}$$

Reynolds numbers selected according to the directions given after Equation [9], for example

$$(N_{Re})_i = 17{,}000, \quad (N_{Re})_o = 12{,}000$$

Unknown: D, L, N_T, N_L, N, A

7 Factor ϵ from Equation [21]

$$\epsilon = \frac{0.08\pi \times 100 \times 32{,}400 \times 0.0653}{41.1 \times 16{,}200 \times 0.224}\left(\frac{0.0596}{0.0476}\right)^{3} \times \frac{17{,}000^{2.75}}{12{,}000^{2.84}} = 0.785$$

8 Spacing ratio s_T/D from Fig. 6

$$s_T/D = 1.25$$

The minimum longitudinal-spacing ratio according to Fig. 3 is

$$(s_L/D)_{min} = 0.5\,(2 \times 1.25 + 1)^{0.5} = 0.94$$

9 Factors δ, γ, β, and α from Equations [12], [15], [28], and [31]

$$\delta = \frac{4 \times 16{,}200}{\pi \times 0.0596 \times 17{,}000} = 20.3 \text{ ft}$$

$$\gamma = \frac{32{,}400}{0.25 \times 0.0476 \times 12{,}000} = 226.5 \text{ ft}$$

$$\beta = \frac{16{,}200(500-270)}{\pi \times 225}\left[\frac{0.71^{(1-0.4)}}{0.023 \times 0.0596 \times 17{,}000^{0.8}} + \frac{0.71^{(1-0.333)}}{0.33 \times 0.0476 \times 12{,}000^{0.6}}\right]$$

$$\beta = 2300 \text{ ft}$$

$$\alpha = \frac{4.17 \times 10^8 \times 41.1 \times 0.224}{0.16 \times 0.0596^2 \times 17{,}000^{1.75}} = 0.264 \times 10^6 \text{ ft}^{-2}$$

10 Tube diameter from Equation [32]

$$D = \left(\frac{2300 \times 10^{-6}}{0.264 \times 20.3}\right)^{0.5} = 20.7 \times 10^{-3} \text{ ft}$$

Length of tubes from Equation [33]

$$L = \frac{2300 \times 20.7}{20.3} \times 10^{-3} = 2.345 \text{ ft}$$

Number of tubes in each row transverse to stream from Equation [34]

$$N_T = \frac{226.5}{2.345} = 96.6$$

Number of tube rows, longitudinal, from Equation [35]

$$N_L = \frac{2300}{226.5} = 10.15$$

Total number of tubes from Equation [1]

$$N = 96.6 \times 10.15 = 980$$

Area of heat-transfer surface from Equation [36]

$$A = \pi \times 20.7 \times 10^{-3} \times 2300 = 149.2 \text{ sq ft}$$

Example 2. Given

$$\Delta p_i = 41.1 \text{ psf}, \qquad \Delta p_o = 100 \text{ psf}$$

Varied

$$(N_{Re})_i \text{ and } s_T/D$$

Aim: Graphical representation of the entire heat-exchanger family which fulfills the same pressure-drop requirements.

11 Keep s_T/D = const, for example, $s_T/D = 1.25$. Read ϵ = const = 0.785 from Fig. 6. Compute the ratio

$$(N_{Re})_o^{2.24}/(N_{Re})_i^{2.75}$$

from Equation [21]

$$\frac{(N_{Re})_o^{2.24}}{(N_{Re})_i^{2.75}} = \frac{0.08\pi \times 100 \times 32{,}400 \times 0.0653}{0.785 \times 41.1 \times 16{,}200 \times 0.224}\left(\frac{0.0596}{0.0476}\right)^2 = 0.89$$

Assume different values of $(N_{Re})_i$ and compute $(N_{Re})_o$ from the foregoing equation

$(N_{Re})_i$ =	3000	10,000	17,000	70,000
$(N_{Re})_o$ =	2205	7,200	12,000	48,000

12 Repeat steps 9 and 10 for these Reynolds numbers.

13 Repeat steps 11 and 12 for other spacing ratios s_T/D.

14 Plot the result in a graph like Fig. 7.

Examples with fixed assumptions of tube diameter D, and tube length L. From Equation [33] we find

$$\frac{\beta}{\delta} = \frac{L}{D} \qquad [37]$$

Combining with Equations [12] and [28]

$$(N_{Re})_o^{b_o} = \frac{\dfrac{c_i}{c_o}\dfrac{\mu_i}{\mu_o}\dfrac{(N_{Pr})_i^{1-a_i}}{M_o}(N_{Re})_i}{\dfrac{L}{D}\dfrac{4\Delta t_i}{\Delta t_{12}} - \dfrac{(N_{Pr})_i^{1-a_i}(N_{Re})_i^{1-b_i}}{M_i}} \qquad [38]$$

This equation reveals that only one of the Reynolds numbers can be freely chosen if L and D are fixed values.

For the following examples we assume

$$D = 20.8 \times 10^{-3} \text{ ft} \qquad L = 3 \text{ ft}$$

$$(N_{Re})_i = 25{,}900$$

15 Compute $(N_{Re})_o$ from Equation [38]

$$(N_{Re})_o = 11{,}000$$

16 Compute the factors δ, β, and α from Equations [12], [37], and [31]

$$\delta = 13.33 \text{ ft}, \quad \beta = 1930 \text{ ft}, \quad \alpha = \frac{L}{D^4} = 0.333 \times 10^6 \text{ sq ft}$$

17 Compute Δp_i from Equation [31]

$$\Delta p_i = 110 \text{ psf}$$

18 Compute the area of heat-transfer surface from Equation [36]

$$A = 126 \text{ sq ft}$$

19 Compute the total number of tubes

$$N = \frac{A}{\pi DL} = 643$$

Equations [15] and [21] are still available which gives us the freedom to make one additional assumption as shown in the following examples:

Example 3. Given

$$D = 20.8 \times 10^{-3} \text{ ft}, \qquad L = 3 \text{ ft}$$

Additional assumption

$$s_T/D = 1.3$$

Unknown

$$\Delta p_o, N_T, N_L$$

20 Read ϵ from Fig. 6

$$\epsilon = 0.82$$

21 Compute Δp_o from Δp_i and Equation [21]

$$\frac{\Delta p_o}{\Delta p_i} = 0.627$$

$$\Delta p_o = \frac{\Delta p_o}{\Delta p_i}\Delta p_i = 69 \text{ psf}$$

22 Compute γ from Equation [15]

$$\gamma = 206$$

23 Compute the numbers of tubes from Equations [34] and [35]

$$N_T = 68.8, \qquad N_L = 9.37$$

Example 4. Given

$$D = 20.8 \times 10^{-3} \text{ ft}, \qquad L = 3 \text{ ft}$$

Additional assumption

$$N_L = 15$$

Unknown

$$s_T/D,\ \Delta p_o,\ N_T$$

24 Combine Equations [12], [15], [34], [35], [37], and compute s_T/D

$$s_T/D = 1 + N_L \frac{\pi D w_0 \mu_i (N_{Re})_i}{4 L w_i \mu_o (N_{Re})_o} \qquad [39]$$

$$s_T/D = 1.48$$

25 Read ϵ from Fig. 6

$$\epsilon = 0.985$$

26 Repeat steps 21, 22, and 23

$$\frac{\Delta p_o}{\Delta p_i} = 0.755, \qquad \Delta p_o = 83 \text{ psf}$$

$$\gamma = 128.5$$

$$N_T = 42.9$$

Example 5. Given

$$D = 20.8 \times 10^{-3} \text{ ft}, \quad L = 3 \text{ ft}$$

Additional assumption

$$\frac{N_T}{N_L} = 1$$

Unknown

$$s_T/D,\ \Delta p_o,\ N_T,\ N_L$$

27 Combine Equations [34], [35], and [37] and compute γ

$$\frac{N_T}{N_L} = \frac{\gamma^2}{\beta L} = 1$$

$$\gamma = L \left(\frac{\delta}{D} \right)^{0.5}$$

$$\gamma = 76$$

28 Compute s_T/D from Equation [15]

$$s_T/D = 1.815$$

29 Read ϵ from Fig. 6

$$\epsilon = 1.29$$

30 Repeat step 21

$$\Delta p_o = 108.2 \text{ psf}$$

31 Compute N_T and N_L from Equation [34]

$$N_T = N_L = 25.4$$

Example 6. Given

$$D = 20.8 \times 10^{-3} \text{ ft}, \quad L = 3 \text{ ft}$$

Additional assumption

$$\Delta p_o / \Delta p_i = 1.5$$

Unknown

$$s_T/D,\ N_T,\ N_L$$

32 Compute ϵ from Equation [21]

$$\epsilon = 1.962$$

33 Read s_T/D from Fig. 6

$$s_T/D = 2.51$$

34 Repeat steps 22 and 23

$$\gamma = 41$$

$$N_T = 13.67 \quad N_L = 47$$

Acknowledgments

Special acknowledgment for discussing this paper is due to Dr. O. E. Baljé, Hydro Aire, Inc., Burbank, Calif., Mrs. F. F. Buckland, General Electric Company, Dr. J. B. Jones, Purdue University, Mr. E. L. Lustenader, General Electric Company, and Mr. R. H. Norris, General Electric Company.

BIBLIOGRAPHY

1 "Der Wärmeuebergang im Kreusstrom," by W. Nusselt, *Zeitschrift, VDI*, vol. 55, 1911, p. 2021.

2 "Wärmeuebergang und Druckverlust bei Querströmung durch, Rohrbündel," by E. Hofmann, *Zeitschrift, VDI*, vol. 84, 1940, p. 97.

2(a) "Experimental Investigation of the Influence of Tube Arrangement of Convection Heat Transfer and Flow Resistance in Cross Flow of Gases Over Tube Banks," by O. L. Pierson, Trans. ASME, vol. 59, 1937, Paper PRO—59-6.

"Experimental Investigation of the Effect of Equipment Size on Convection Heat Transfer and Flow Resistance in Cross Flow of Gases Over Tube Banks," by E. C. Huge, Trans. ASME, vol. 59, 1937, Paper PRO—59-7.

"Correlation and Utilization of New Data on Flow Resistance and Heat Transfer for Cross Flow of Gases Over Tube Banks," by E. D. Grimson, Trans. ASME, vol. 59, 1937, Paper PRO—59-8.

Discussion by M. Jakob of the preceding three papers, Trans. ASME, vol. 60, 1938, pp. 384–386.

"Der Strömungswiderstand eines Rohrbündels," by A. J. Ter Linden, *Wärme*, vol. 62, 1939, pp. 319–323.

3 "Heat Transmission," by W. H. McAdams, McGraw-Hill Book Company, Inc., New York, N. Y., and London, England, 1942.

4 "Das Aehnlichkeitagesetz bei Reibungsvorgängen in Flüssigkeiten," by H. Blasius, *Forschungs Arbeiten auf dem Ingenieurwesen*, heft 131, 1913, pp. 1–39.

5 "Mean Temperature Difference in Cross Flow," by D. M. Smith, *Engineering*, vol. 138, 1934, p. 479.

6 "The Dimensionless Theory of Heat Exchange Apparatus," by W. Traupel, *Sulzer Technical Review*, no. 1, 1944, p. 1.

Validity of Time-Compensated Temperature Parameters for Correlating Creep and Creep-Rupture Data

By F. GAROFALO,[1] G. V. SMITH,[2] and B. W. ROYLE[3]

Several time-compensated temperature parameters, which were proposed as dependent only on the initial stress, are discussed with relation to time of creep rupture and to minimum and average creep rates. The so-called master "curve" is discussed in terms of experimentally determined relationships. In checking the validity of the proposed parameters, using experimental results for several ferritic and austenitic steels, it is found that these parameters are not single-valued functions of the initial stress over wide ranges in stress, and the existence of a master curve for these parameters is doubtful.

Introduction

IN EVALUATING the strength of metals at elevated temperatures, long-time creep and creep-rupture tests at various temperatures and under various loads are necessary to simulate service life. Such tests are time-consuming and expensive. In recent years a number of semiempirical relations (1–6)[4] have been proposed for correlating the results of short and long-time tests at various loads and temperatures. By suggesting the existence under creep conditions of single-valued functions between creep load, minimum creep rate, or creep strain, and a creep-rate or time-compensated temperature parameter, procedures have been defined by which creep behavior under a variety of conditions may be predicted from limited test data. Similarly, several single-valued functions between creep-load and time-compensated temperature parameters have been proposed for predicting rupture time under various conditions of stress and temperature (1–6).

In a number of these proposals, attempts have been made to justify theoretically the specific parameter suggested. However, such efforts seem basically unrealistic since the stress, which is assumed constant, actually varies throughout the test, as creep and rupture tests are usually made—only the load or initial stress remains constant.

In all of the proposals, graphical methods resulting in so-called "master curves" have been relied upon to prove the validity of the suggested parameters, even though adequate, experimentally determined, empirical relations are available in a number of cases for a more rigorous analytical check. The latter approach has been seemingly ignored, and thus has led to an unjustified confidence on the part of a number of engineers in the validity of the parametric techniques.

From the practical viewpoint the parametric procedures, without question, provide valuable approximations, and are useful not only in summarizing many data in convenient form, but in furnishing reliable predictions. For the latter purpose, however, the procedures should be used with a full realization of the possible errors.

Time, Temperature, and Stress Relationships in Creep Rupture

The recent proposals (1–6) of empirical relations correlating time, temperature, and stress in creep-rupture may be summarized as follows:

Larson-Miller (1) proposed that

$$T(C + \log t) = \frac{\Delta H}{2.3R} = \alpha = F(\sigma) \quad [1]$$

Manson-Haferd (2) proposed that

$$\frac{T - T_a}{\log t - \log t_a} = \beta = F_1(\sigma) \quad [2]$$

and Dorn and associates (3–6) proposed that

$$t \exp\left[-\frac{\Delta H}{RT}\right] = \gamma = F_2(\sigma) \quad [3]$$

where

T = temperature in degrees Rankine, Fahrenheit, and Kelvin for relations [1], [2], and [3], respectively.
t = time for rupture
C, T_a, and $\log t_a$ = material constants
ΔH = activation energy
R = gas constant
σ = initial stress

Analogous expressions were proposed for secondary creep rate, as discussed in a later section.

Relation [1], though first developed empirically, was also derived (1) from the usual rate equation

$$r = A \exp\left[-\frac{\Delta H}{RT}\right] \quad [4]$$

where r is a rate (in this case creep rate), A is a constant, and ΔH, R, and T are as defined for Equation [1]. However, a number of unsound assumptions were made in its derivation.

Although it is not pointed out in reference (1), the authors assume for constant initial stress that

[1] Research Metallurgist, Fundamental Research Laboratory, U. S. Steel Corporation, Kearny, N. J.
[2] Bard Professor of Metallurgical Engineering, Cornell University, Ithaca, N. Y.
[3] American Steel and Wire Division, Cuyahoga Works, U. S. Steel Corporation, Cleveland, Ohio.
[4] Numbers in parentheses refer to the Bibliography at the end of the paper.

Contributed by the Joint ASTM-ASME Committee on Effect of Temperature on the Properties of Metals and presented at a joint session of the Joint ASTM-ASME Committee on Effect of Temperature on the Properties of Metals and Metals Engineering Division at the Diamond Jubilee Annual Meeting, Chicago, Ill., November 13–18, 1955, of The American Society of Mechanical Engineers.

Note: Statements and opinions advanced in papers are to be understood as individual expressions of their authors and not those of the Society. Manuscript received at ASME Headquarters, August 30, 1955. Paper No. 55—A-164.

$$r = \frac{A_1}{t} \quad [5]$$

Thus, by combining relations [4] and [5], relation [1] is obtained. Larson and Miller incorrectly state that $C = \log A$, whereas the true value of C is $\log A/A_1$. In addition, it is not mentioned that the assumption of relation [5] requires that if r is the average creep rate, the strain to rupture be constant and independent of temperature. This is not in agreement with experimental finding. Nor is relation [5] valid if r is the minimum creep rate. Of a more fundamental nature, however, is the implication in relation [1] that during creep the activation energy (ΔH) is a single-valued function of the initial stress.

Experimental proof of the variation of ΔH with stress during creep is essentially nonexistent; however, in relation [3] the authors assume that ΔH is independent of the stress (6), and offer limited experimental data in support thereof.

In relation [1] it is suggested that the time-compensated temperature parameter α depends only on the initial stress. Proof of the existence of this single-valued function has been limited to the showing of a so-called master curve where it is implied that if the computed values in a $\log \sigma$ versus α plot fall on a number of straight lines or on a smooth curve the function is valid. This procedure provides no proof at all, unless it can be shown that the computed values satisfy, over wide limits in σ, an analytically determined solution for the function $\alpha = F(\sigma)$. Moreover, the stress changes markedly throughout a constant load-rupture test, and it seems basically unsound to attempt to apply a fundamental rate equation such as relation [4].

It is possible, by making use of other experimentally determined relationships, to derive a solution for this function, $\alpha = F(\sigma)$. For steels, it is generally found that creep-rupture data at constant temperature result in a $\log \sigma$ versus $\log t$ plot of either one or two intersecting straight lines. No evidence of more than two intersecting straight lines has been found even for rupture times greater than 10^4 hr.[5] It is possible, therefore, to relate with some confidence the initial stress and the rupture time by the linear relation

$$\log \sigma = [k(T, \sigma)] \log t + \log [k_1(T, \sigma)] \quad [6]$$

where $k(T, \sigma)$ is the slope and $\log k_1(T, \tau)$ the intercept at $t = 1$. When two straight lines are found, $k(T, \sigma)$ and $\log k_1(T, \sigma)$ will have two different values, each applying within a specific range in σ. By combining relations [1] and [6] a solution for the function $\alpha = F(\sigma)$ becomes

$$\log \sigma = \left[\frac{k(T, \sigma)}{T}\right] \alpha + [\log k_1(T, \sigma) - k(T, \sigma)C] \quad [7]$$

From the conditions given in the foregoing, relation [7] at constant temperature describes one or two straight lines. Therefore the existence of a single-valued function, $\alpha = F(\sigma)$, requires that the computed values of $\log \sigma$ and α plotted as a master curve fall on one or two straight lines. This means of course that

$$\frac{k(T, \sigma)}{T} \text{ and } [\log k_1(T, \sigma) - k(T, \sigma)C]$$

are independent of temperature. The validity of the function $\alpha = F(\sigma)$ for the creep-rupture behavior in steels will be discussed in the following.

Relation [1] predicts that at constant stress $\log t$ varies linearly with $1/T$. Manson and Haferd (2), however, attempt to show that $\log t$ varies linearly with T. On the basis of their observation, they suggest that the slope of the straight line for each initial stress depends only on the stress. This is expressed in relation [2] where β is the slope and T_a and $\log t_a$ are constants determined from the point where all straight lines ($\log t$ versus T) meet.

It is possible again to find a solution for the single-valued function $\beta = F_1(\sigma)$ in a manner similar to the case for the function in relation [1]. By combining relations [2] and [6] it is found that

$$\log \sigma = \frac{1}{\beta} [k(T, \sigma)(T - T_a)] + [k(T, \sigma) \log t_a + \log k_1(T, \sigma)] \quad [8]$$

This equation is similar to relation [7] in that at constant temperature this relation describes one or two straight lines when plotting $\log \sigma$ against $1/\beta$. If the function $\beta = F_1(\sigma)$ exists, then, upon varying the temperature the quantities $[k(T, \sigma)(T - T_a)]$ and $[k(T, \sigma) \log t_a + \log k_1(T, \sigma)]$ remain constant and the master curve is described in the case of steels by one or two straight lines.

The time-compensated temperature parameter

$$\left[t \exp\left(-\frac{\Delta H}{RT}\right)\right]$$

of relation [3] was suggested initially as a means for correlating the entire creep curve for one material at various temperatures but at constant initial stress (3, 4). A single curve was found experimentally when plotting the creep strain against the foregoing parameter. It should be mentioned, however, that the experimental data presented in support were very limited. It was further proposed (5) that if this parameter correlates the entire creep curve for different temperatures, then it also must correlate the terminal points which constitute the points at rupture. This implies, however, that the strain to fracture remains constant with temperature, a condition which, as mentioned before, is not experimentally true.

The relationship between σ and γ in this case is found by substituting relation [3] in relation [6] or

$$\log \sigma = [k(T, \sigma)] \log \gamma + \frac{k(T, \sigma)}{T} \frac{\Delta H}{2.3R} + \log k_1(T, \sigma) \quad [9]$$

The characteristics of this relation are again similar to those of relation [7] and of course [8]. To satisfy the single-valued function $\gamma = F_2(\sigma)$, it is observed from relation [9] that the $\log \sigma$ versus $\log \gamma$ plot, or the master curve, should result in one or two intersecting straight lines. It should be mentioned here that in relation [3] and therefore [9] it is assumed that the activation energy, ΔH, remains constant with initial stress.[6]

In comparing relations [1], [2], and [3], gross contradictions are found, yet it has been reported that each has satisfactorily correlated test results (1–6). The fact is, however, that only limited correlations have been attempted and no real proof of the validity of the parameters has been presented.

Referring again to the foregoing relations, one finds that, at constant stress, relations [1] and [3] state that $\log t$ is a linear function of $1/T$, whereas relation [2] states that $\log t$ is a linear function of T. In plots of $\log t$ versus T, relation [1] states that one intercept, $\log t = -C$ and $T = \infty$, exists and the slope $(\Delta H)/(2.3R)$ varies with the stress, but relation [3] states that

[5] The claimed "proof" by Grant and Bucklin (10) of more than one break is not considered acceptable for reasons outlined in discussion to that paper by Smith and by Blickwede and Shahinian.

[6] It is proposed in reference (6) that ΔH, the activation energy during creep, is not affected by temperature, time under test, creep strain, stress, grain size, and substructures developed during creep, and is found to agree with the activation energy for self-diffusion. This proposal applies at temperatures where recovery effects are sufficiently rapid.

the intercept log γ varies with the stress but the slope $(\Delta H)/(2.3R)$ is constant.

Relation [2] states that slope β varies with the stress while the point (T_a, log t_a) is constant. However, at this point as well as at the point ($T = \infty$, log $t = -20$) for relation [1] the fracture time is constant and independent of the stress. Although this is of no consequence at $T = \infty$, there is a great deal of doubt about realizing such behavior at the point (T_a, log t_a), since in many cases T_a for steels falls within the usual range of test temperature in creep.

Creep Rate, Temperature, and Stress Relationships in Creep

In order to correlate minimum creep rate, temperature, and stress the function in relation [1] must necessarily be rewritten (1). The modified relation becomes

$$T(C - \log r) = \alpha' = F_3(\sigma) \quad \ldots\ldots\ldots\ldots [10]$$

where r is the minimum creep rate. Basically, this relation resembles relation [1] and since in our experience[7] the relationship between log σ and the logarithm of the minimum creep rate generally results, for steels, in one straight line for each temperature, the solution for the function, $\alpha' = F_3(\sigma)$, is basically similar to relation [7]. This solution becomes

$$\log \sigma = \left(-\frac{n}{T}\right)\alpha' + [nC + \log D] \quad \ldots\ldots [11]$$

where n is the slope of the straight lines in the log σ versus log r plot, and log D is the intercept at $r = 1$; that is, at a creep rate of 1 per cent per hr. It is seen from relation [11] that the existence of $\alpha' = F_3(\sigma)$ requires that the log σ versus α' plot result in one straight line; that is, the master curve should be a straight line. A similar analysis involving creep-rupture data is possible by substituting for r the average creep rate; that is, the total elongation divided by the rupture time.

Relation [2] also has been modified (2) for purposes of correlating minimum creep rates under different temperatures and stresses. A second modification has been proposed for predicting the correlation between the time for a constant creep strain, stress, and temperature. The results presented by the authors (2) indicate that the modified relation [2] does not satisfy a single-valued function. No further check of this relation, therefore, will be attempted here.

The parameter in relation [3] has been modified for correlating creep data up to the point of fracture. An attempt is made to show (3, 4) for constant initial stress that, upon plotting the logarithm of the creep strain ϵ against the logarithm of γ, a single curve which is not dependent on temperature is obtained. The function proposed is

$$t \exp\left(-\frac{\Delta H}{RT}\right) = \gamma = F(\epsilon) \quad \ldots\ldots\ldots\ldots [12]$$

The data presented to prove this relation have been extremely limited. Since no results of this nature are available for the steels to be discussed no further check of this function will be possible.

Validity of Time-Compensated Temperature Parameters

Creep-Rupture Parameters. The time-temperature parameters for creep rupture given in relations [1], [2], and [3] are amenable to experimental verification. Thus their validity can be determined readily by ascertaining whether or not these parameters are truly single-valued functions of the initial stress over an adequate range in stress. Creep and creep-rupture data (7, 8, 9) for a number of ferritic and stainless steels were employed in determining the validity of the time-compensated temperature parameters given in relations [1], [2], and [3]. The composition of the steels included in this study is given in Table 1.

[7] In a few instances we have observed a curvilinear relation. Other investigators have sometimes reported two straight lines.

TABLE 1 DESCRIPTION AND CHEMICAL COMPOSITION OF STEELS

Steel	Type	Weight Per Cent C	Mn	Si	Cr	Ni	Mo	Ti	Heat-treatment
19D	5 Cr-½ Mo-Ti..	0.05	0.40	0.31	5.19	...	0.51	0.55	1375 F-FC
G29	8 Cr-1 Mo.....	0.10	0.38	0.32	8.21	0.14	1.06	..	1700 F-FC
G43	304L.....	0.03	0.65	0.54	19.50	10.22	..	..	1900 F-WQ
O38	316L.....	0.03	1.50	0.34	17.46	10.70	2.20	..	2000 F-WQ
T37	316.....	0.08	1.63	0.37	17.76	12.47	2.55	..	2000 F-WQ

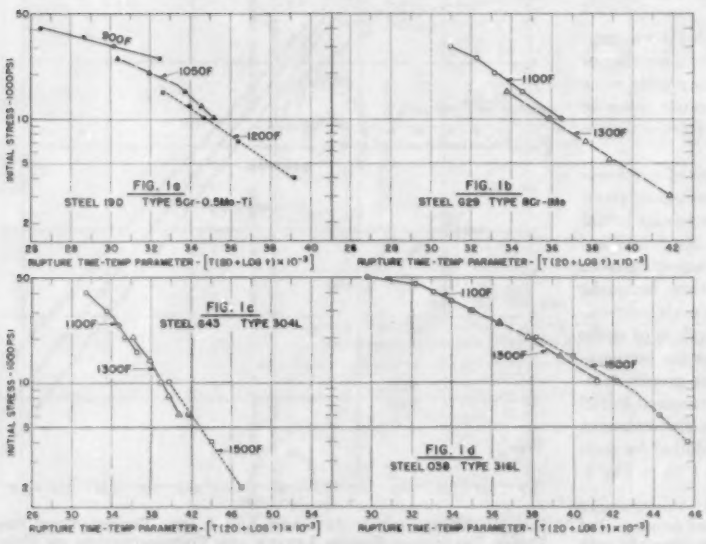

FIG. 1 VARIATION OF RUPTURE TIME-TEMPERATURE PARAMETER WITH INITIAL STRESS

The variation of the rupture time-temperature parameter $[T(20 + \log t)]$ (see relation [1]) with initial stress for the first four steels of Table 1 is shown in Fig. 1. For constant temperature, it may be observed from these results that relation [7], which predicts a linear relationship between the initial stress and the rupture time-temperature parameter, is satisfied for each steel. The finding of two straight lines at constant temperature indicates the existence of two intersecting straight lines in the log σ versus log t plot. In no case, however, do the results for all temperatures in Fig. 1 fall on one or two intersecting straight lines without introducing appreciable scatter. It must be concluded therefore that the single-valued function $\alpha = F(\sigma)$ does not apply even over a relatively

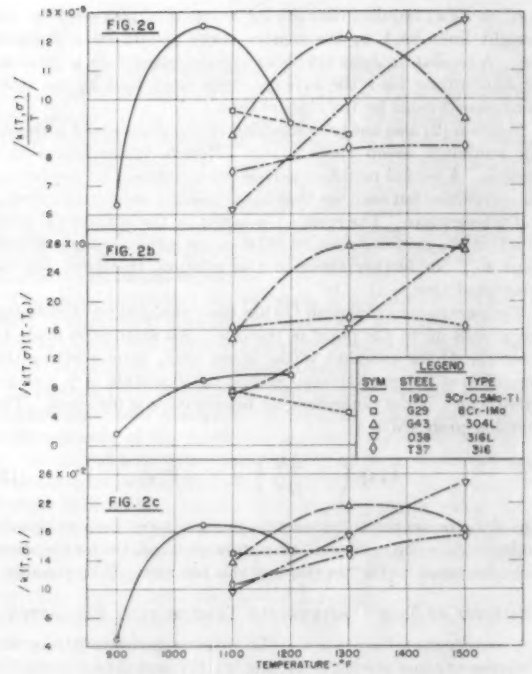

FIG. 2 VARIATION OF $\left|\frac{k(T,\sigma)}{T}\right|$, $|k(T,\sigma)\ (T - T_a)|$, AND $|k(T,\sigma)|$ WITH TEMPERATURE

(The existence of a master curve for each parameter discussed requires that these quantities remain constant with temperature.)

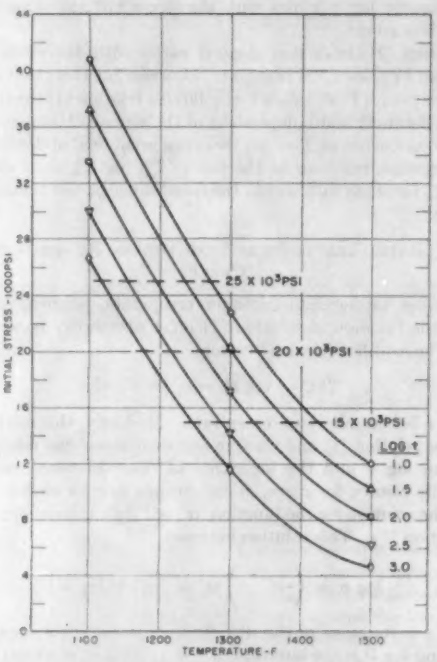

FIG. 3 RELATIONSHIP BETWEEN INITIAL STRESS AND TEMPERATURE FOR SEVERAL DIFFERENT RUPTURE TIMES, STEEL O38, TYPE 316L

limited range of temperature and that for these steels the parameter $[T(C + \log t)]$ is temperature-dependent for the entire stress range covered. As should be expected, the quantity

$$\frac{K(\sigma, T)}{T}$$

in relation [7] is not constant as temperature is varied, Fig. 2(*a*).[8]

The value of 20 taken as the constant in relation [1] was suggested by Larson and Miller as the best average for a number of alloys. Although another value for this constant may bring some of the curves in Fig. 1 closer to coincidence, this could never be exactly attained, since a change in C mainly shifts the curves horizontally.

For an adequate check of relation [2], the values of constants $\log t_a$ and T_a must be determined initially. These constants could be computed directly from data obtained under constant initial stress at various temperatures. However, since such data are usually not available, these constants must be computed from interpolated values (2). Stress values for constant time, including $\log t$ of 1.0, 1.5, 2.0, 2.5, and 3.0, were obtained for each temperature from expanded $\log \sigma$ versus $\log t$ plots. The values of stress for each constant rupture time were plotted against the temperature as shown for Steel O38 in Fig. 3. From these graphs, temperature values were determined at three levels of constant initial stress (25, 20, and 15 $\times$ 10^3 psi) for each of the five constant times. The values of time and temperature were plotted for each value of constant stress as shown again for Steel O38 in Fig. 4.

[8] In Fig. 2 the absolute value of the slopes is plotted. The existence of a single-valued function of each parameter discussed requires that the quantities plotted as ordinate in Fig. 2 remain constant with temperature.

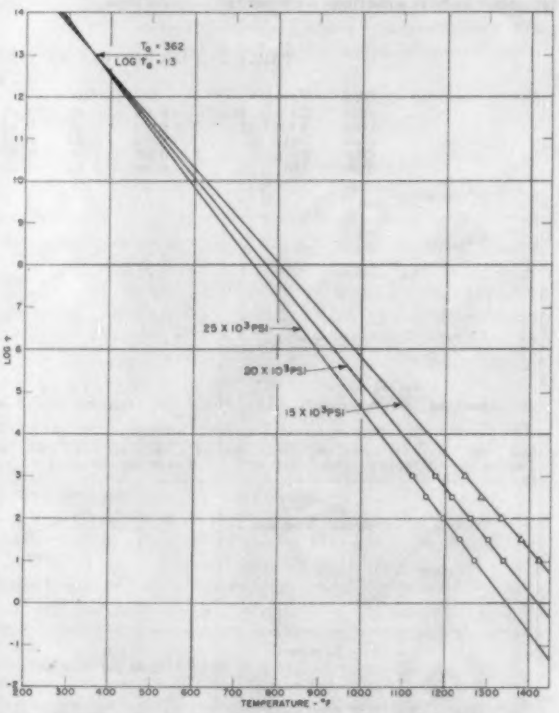

FIG. 4 RELATIONSHIP BETWEEN LOG t AND TEMPERATURE FOR THREE DIFFERENT STRESS LEVELS AND DETERMINATION OF CONSTANTS T_a AND LOG t_a, STEEL O38, TYPE 316L

TABLE 2 SUMMARY OF CONSTANTS LOG t_a AND T_a

Steel	Type	log t_a	T_a
19D.....	5 Cr-½ Mo-Ti	11.2	575
G29.....	8 Cr-1 Mo	−3.75	1595
G43.....	304L	15.5	15
O38.....	316L	13	362
T37.....	316	−10.8	2505

The computed values seem to fall on three straight lines which intersect at a common point. The co-ordinates of this point are equal to log t_a and T_a. The values of these constants for all steels mentioned in Table 1 are given in Table 2. These constants show large variations, even between such similar materials as steels O38 (Type 316L) and T37 (Type 316). Because of these wide variations it becomes impossible to compare a number of steels on a single plot. Moreover, the usefulness of the parameter for any one steel is limited by the large amount of data necessary for accurate evaluation of the constants. By means of the linear relation [8], it is possible to check the validity of the parameter in relation [2], using the computed values of log t_a and T_a. In the event that β depends only on the initial stress, relation [8] states, as mentioned previously, that the so-called master curve should be one or two intersecting straight lines when log σ is plotted against $1/\beta$.

Such plots for the steels examined are shown in Fig. 5. For each constant temperature and for each steel the points are found to lie on one or two straight lines, but the slopes of these lines are dependent on temperature. Thus all points for each steel do not lie on one or two straight lines, with the exception perhaps of steel G43 (Type 304L) in Fig. 5(*c*). It is not likely that the slope at the lower stress levels at 1100 F for this steel would change downward again to follow along the straight line for the 1300 F results because two straight lines are already observed for this steel at 1100 F. Thus it is suspected that additional tests at 1100 F at lower stresses would invalidate even for this steel the single-valued function, $\beta = F_1(\sigma)$. Furthermore, the quantity $k(T, \sigma)$ $(T - T_a)$ in relation [8] does not remain constant with temperature, Fig. 2(*b*). From the results in Figs. 2(*b*) and 5, it seems clear that the parameter

$$\frac{T - T_a}{\log t - \log t_a}$$

is not independent of temperature and the existence of a so-called master curve is precluded when a large enough range in initial stress is examined.

The function in relation [3] also can be checked experimentally. It may be observed from relation [9] that in order the single-valued function, $\gamma = F_2(\sigma)$, be satisfied, the quantity, $k(T, \sigma)$, that is, the slope of the straight lines in the log σ versus log t plot, must remain constant as temperature is varied. Computed values of $K(T, \sigma)$ for all steels, Fig. 2(*c*), indicate that this quantity varies with temperature, although the variation does not appear to be a systematic one. This limited check, however, indicates that relation [3] is not satisfied for the steels under consideration and the parameter

$$t \exp\left(-\frac{\Delta H}{RT}\right)$$

is not solely dependent on the initial stress over the range in stresses used here.

Creep Rate Versus Temperature Parameters. Relation [1] has been modified as shown in relation [10] for the purpose of correlating initial stress with minimum or average creep rate. The analytical relation between the initial stress and the proposed function α' is given by relation [11]. As mentioned previously, to satisfy the single-valued function of relation [10] it is required that as shown by relation [11] the log σ versus α' plot should result in one straight line irrespective of the test temperature. This applies to both the minimum and average creep rates.

The variation of the minimum creep rate versus temperature parameter with the initial stress for the first four steels given in Table 1 is shown in Fig. 6. It is observed that for all steels a separate straight line is observed for each temperature, indicating the nonexistence of a so-called master curve. Changing the constant C from 20 in Fig. 6(*a*) to 44 in Fig. 6(*b*) brings about only a displacement of the straight lines. This is not surprising since according to relation [11] the slopes of the straight lines in Fig. 6(*a*) should not be affected a great deal upon changing the value of C. The effect on the intercept is greater and results in a lateral displacement of the straight lines.

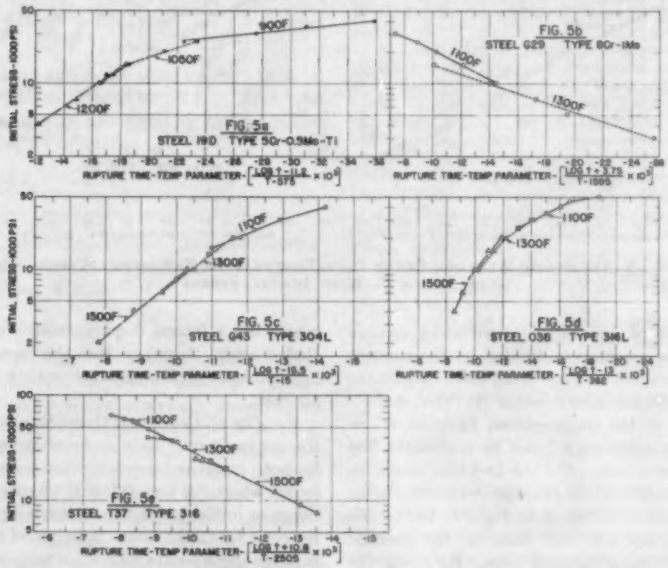

FIG. 5 VARIATION OF LINEAR RUPTURE TIME-TEMPERATURE PARAMETER WITH INITIAL STRESS

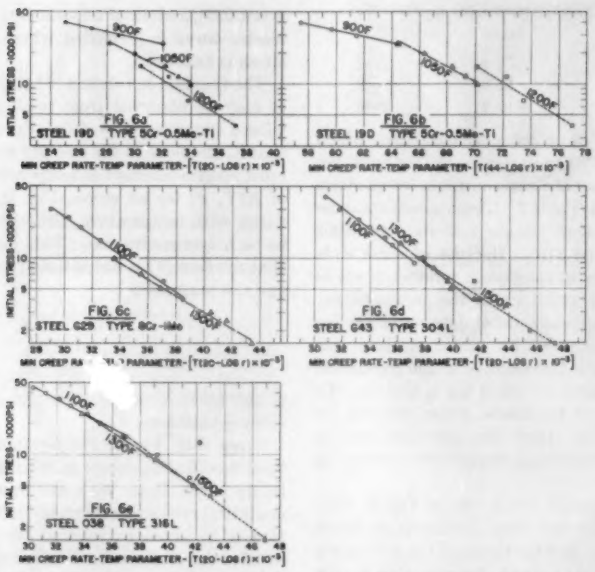

FIG. 6 VARIATION OF MINIMUM CREEP RATE-TEMPERATURE PARAMETER WITH INITIAL STRESS

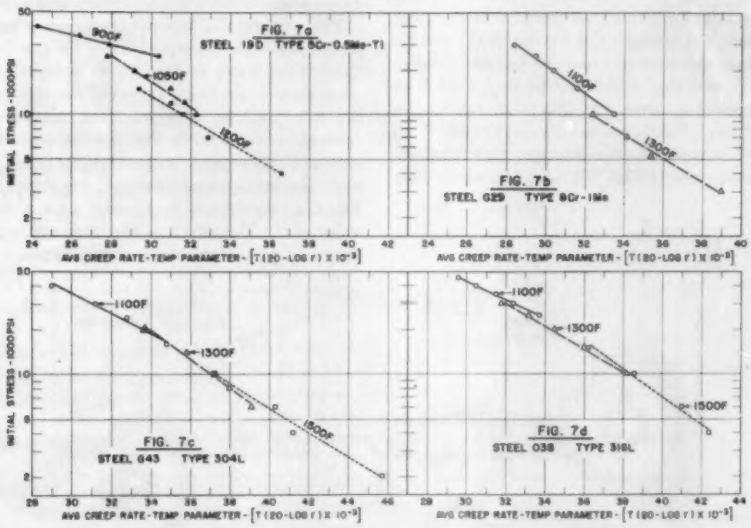
FIG. 7a
STEEL 19D TYPE 5Cr-0.5Mo-Ti
FIG. 7b
STEEL 629 TYPE 9Cr-1Mo
FIG. 7c
STEEL 643 TYPE 304L
FIG. 7d
STEEL 038 TYPE 316L
INITIAL STRESS - 1000 PSI
AVG CREEP RATE-TEMP PARAMETER - [T(20 - LOG r) × 10⁻³]

FIG. 7 VARIATION OF AVERAGE CREEP RATE-TEMPERATURE PARAMETER, USING A VALUE OF 20 FOR C, WITH INITIAL STRESS

In checking the validity of relation [10] for correlating average creep rates, that is, the total elongation divided by the rupture time, the quantity r becomes the average creep rate. Again, as mentioned previously, it is found from relation [11] that the existence of a master curve or the single-valued function $\alpha' = F_3(\sigma)$ requires that the log σ versus α' plot be a straight line irrespective of testing temperatures. For the first four steels included in Table 1 the parameter α' for average creep rate, using $C = 20$, is plotted against the initial stress in Fig. 7. As was observed for the minimum creep rate, the data for the average creep rate again fall on a series of straight lines. By using different values of C, ranging from 29 to 47, as in Fig. 8, it is found as before that the slopes of the straight lines are not affected very much, but a lateral displacement is observed. It must be concluded again, therefore, that the parameter $T(C - \log r)$ is not independent of temperature within the range of stresses examined.

Validity of Creep and Creep-Rupture Parameters Within Small Ranges in Stress. As may be observed from Figs. 1, 5, 6, and 7, for both creep and creep-rupture parameters, many instances are found where for two different temperatures and within a limited range in initial stress the computed points lie on adjacent or intersecting straight lines. A common straight line could be drawn through these points with little scatter. Thus it would seem that in these cases, relations [1] and [2] apply within limited ranges in initial stress. However, the scatter observed could be misleading

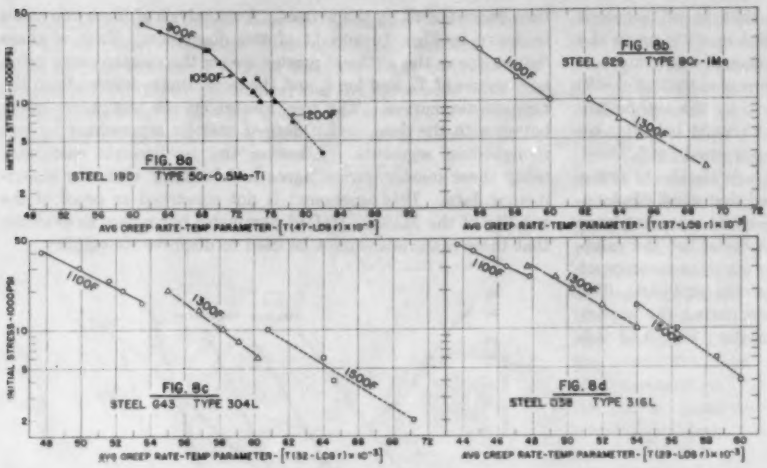

FIG. 8 VARIATION OF AVERAGE CREEP RATE-TEMPERATURE PARAMETER, USING DIFFERENT VALUES FOR C, WITH INITIAL STRESS

ing in terms of rupture time or creep rate. An indication of the importance of the observed scatter may be had by determining at any one temperature the change in $\log t$ or $\log r$ for any range in the parameter at a constant stress level. Thus, differentiating relation [1] for constant temperature, one obtains

$$d \log t = \frac{d\alpha}{T} \quad \ldots\ldots\ldots\ldots\ldots\ldots [13]$$

For the data examined, α is of the order of 20 T. Also, it can be determined readily from Fig. 1 that a range of $d\alpha/T = 0.5$ is not unusual. It follows therefore that even within a limited range in stress, relation [1] may lead to large errors when dealing with rupture times beyond 10^3 hr. A similar analysis applies in the case of creep rates less than 10^{-3} sec^{-1} where α' is of the order of 30 T.

Upon differentiating relation [2] at constant temperature it is found that

$$d \log t = \left(\frac{\log t_a - \log t}{\beta}\right) d\beta \quad \ldots\ldots\ldots\ldots [14]$$

In this case, however, the error in interpolating rupture times is not excessive unless rupture times beyond about 3×10^3 hr are encountered. This is estimated by assuming, for the steels discussed here, a value of 0.2 for

$$\left(\frac{\log t_a - \log t}{\beta}\right)$$

and a range in β of about 1.3 at constant stress. Errors of several factors may be encountered under these conditions for rupture times in excess of approximately 3×10^3 hr.

SUMMARY

In this paper the use of three different time-compensated temperature parameters in correlating creep-rupture results is discussed, and it is shown that the existence of a single-valued time-temperature function or the existence of a master curve relating rupture stress to these parameters is doubtful. A similar but shorter analysis of the creep problem leads to the same conclusion. In the light of these observations it is believed that an entirely new and more fundamental experimental approach is necessary to provide information which may indicate correlations between creep and creep-rupture properties determined under various conditions of initial stress and temperature. Such tests should include determination of the reproducibility of the experimental measurements so that the significance of any observed correlation can be established.

Whereas the results reported herein disprove the strict validity of the various parameters that have been suggested, it should not be concluded that parameter techniques are without value. In fact, they furnish an excellent means of summarizing many data in convenient form for purposes of comparison and, when judiciously used, yield valuable predictions. However, they should be used for this latter purpose only with a realization of the magnitude of the possible errors.

BIBLIOGRAPHY

1 "A Time-Temperature Relationship for Rupture and Creep Stresses," by F. R. Larson and J. Miller, Trans. ASME, vol. 74, 1952, pp. 765–771.

2 "A Linear Time-Temperature Relation for Extrapolation of Creep and Stress-Rupture Data," by S. S. Manson and A. M. Haferd, NACA TN 2890, March, 1953.

3 "Creep Correlations in Alpha Solid Solutions of Aluminum," by O. D. Sherby and J. E. Dorn, Trans. AIME, vol. 194, 1952, p. 959.

4 "Some Observations on Correlations Between the Creep Behavior and the Resulting Structures in Alpha Solid Solutions," by O. D. Sherby and J. E. Dorn, Trans. AIME, vol. 197, 1953, p. 324.

5 "Correlations of Rupture Data for Metals at Elevated Temperatures," by R. L. Orr, O. D. Sherby, and J. E. Dorn, Trans. ASM, vol. 46, 1954, p. 113.

6 "Effect of Cold Work on the High-Temperature Properties of Dilute Aluminum Alloys," by R. E. Frenkel, O. D. Sherby, and J. E. Dorn, Trans. ASM, vol. 47, 1955, p. 632.

7 "Creep and Rupture of Several Chromium-Nickel Austenitic Stainless Steels," by G. V. Smith, E. J. Dulis, and E. G. Houston, Trans. ASM, vol. 42, 1950, p. 935.

8 "Creep and Rupture of Chromium-Nickel Austenitic Stainless Steels," by E. J. Dulis, G. V. Smith, and E. G. Houston, Trans. ASM, vol. 45, 1953, p. 42.

9 "Creep and Creep-Rupture of Some Ferritic Steels Containing 5 Per Cent to 17 Per Cent Chromium," by E. J. Dulis and G. V. Smith, Proceedings of the ASTM, vol. 53, 1953, p. 627.

10 "On the Extrapolation of Short-Time Stress-Rupture Data," by N. J. Grant and A. G. Bucklin, Trans. ASM, vol. 42, 1950, p. 720.

Discussion

S. S. MANSON[9] AND W. F. BROWN, JR.[9] The writers regret to state that they do not agree with the authors either on the criterion used for checking the validity of time-temperature parameters nor with their conclusions. In addition, the writers wish to point out several technical inaccuracies.

[9] NACA, Lewis Flight Propulsion Laboratory, Cleveland, Ohio.

In the Introduction the authors state that in all previous evaluations "master curves" have been relied upon to prove the validity of the proposed parameter even though adequate empirical relations are available for a more rigorous analytical check. The adequate empirical relations referred to by the authors are presumably based on representation of isothermal behavior by two intersecting straight lines. The approach used by Manson and Haferd in the authors' reference (2) was decidedly not a reliance on master curves. It was recognized that small displacements of data points from the master curve could represent large errors in rupture time. The criterion used to establish the validity of the correlation was to use the master curve to reconstruct isothermal curves on a conventional log σ versus log t plot. The time errors were then seen directly by comparing the experimental data points with the calculated curves. Fig. 9 of this

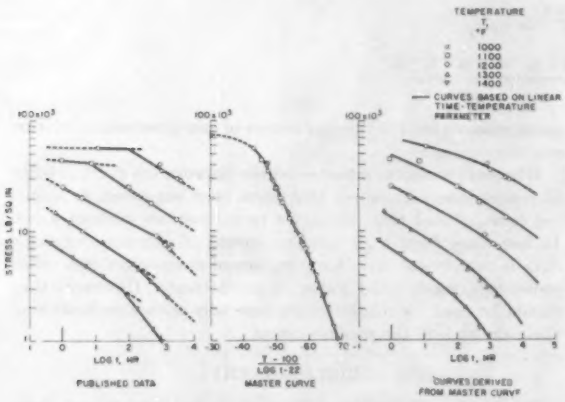

FIG. 9 ANALYSIS OF DM STEEL USING THE LINEAR PARAMETER

(Reference, Manson and Haferd.)

discussion illustrates the approach for DM steel. Each isothermal, it will be noted, was represented by the publisher ("Timken Digest for High Temperature Steels") by two straight-line segments. The master curve is shown in the center of the figure. By assigning fixed values of temperature, the master curve was then used to reconstruct isothermals, as shown at the right in Fig. 9. The true measure of the extent of "correlation" is now seen as the deviations between the solid curves and the data points. These deviations are well within the limits of data scatter. The writers have analyzed suitable data for over 50 materials in the same manner as shown for DM steel.

Fig. 9 also serves to point out that the original stress-rupture data are equally well represented by a family of continuous curves as by a family in which each member consists of two straight lines. Although it has been common practice to draw isothermal stress-rupture curves as straight-line segments, this property has no basic significance. It is the writers' belief—and convincing arguments could be brought to bear on this point—that the best representation of isothermals is not by straight lines. However, the pertinent point here is that the criterion of straightness cannot be used as the critical test of the validity of time-temperature parameters.

The authors would have presented a better case for the Manson-Haferd parameter if they had made proper selection of T_a and log t_a for all their alloys. Of the five materials analyzed in this paper, the poorest correlations obtained by the authors are for steels G29 and T37. For both materials, they have selected negative values of log t_a. Negative values of log t_a have never been encountered by the writers. A reanalysis of these two steels is shown in Figs. 10 and 11 of this discussion. Each of these figures shows the authors' master curve, the master curve using new values of T_a and log t_a and the isothermals derived from the new master curves. The new master curves now agree much better with the data, and if desired may be represented by two straight-line segments. Likewise the isothermals calculated using these master curves agree satisfactorily with the experimental data. This agreement is not construed as proof of the validity of the Manson-Haferd parameter but rather as evidence that these materials cannot be used to disprove its validity.

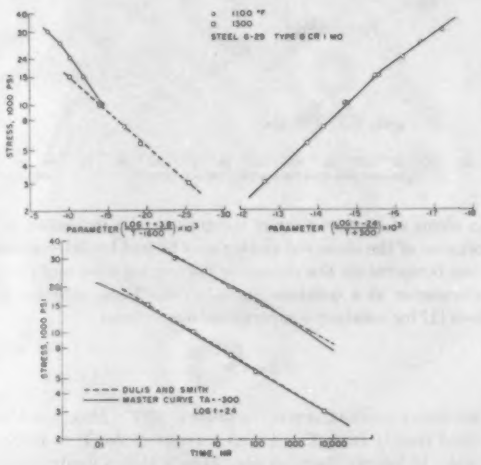

FIG. 10 ANALYSIS OF G29 STEEL USING IMPROVED VALUES OF THE LINEAR PARAMETER CONSTANTS

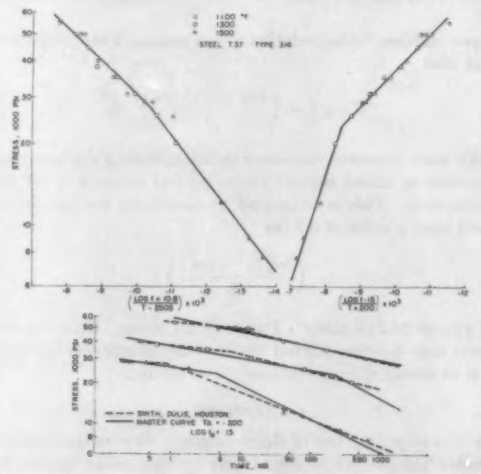

FIG. 11 ANALYSIS OF T37 STEEL USING IMPROVED VALUES OF THE LINEAR PARAMETER CONSTANTS

Convincing proof of validity of the Manson-Haferd parameter requires consideration of materials for which a large number of isothermal data is available (as presented in the authors' reference 2). However, preferably the analysis should make use of constant nominal-stress data. Such data directly check the assumptions inherent in the parameter. A series of critical constant stress

experiments on five materials[10] were not mentioned by the authors. Fig. 12 of this discussion illustrates the constant stress results for DM steel.[11] The solid lines represent correlation of the data by the linear parameter, and the agreement with the data points is seen to be very good. An attempt to correlate the data by other parameters, such as those of Larson-Miller

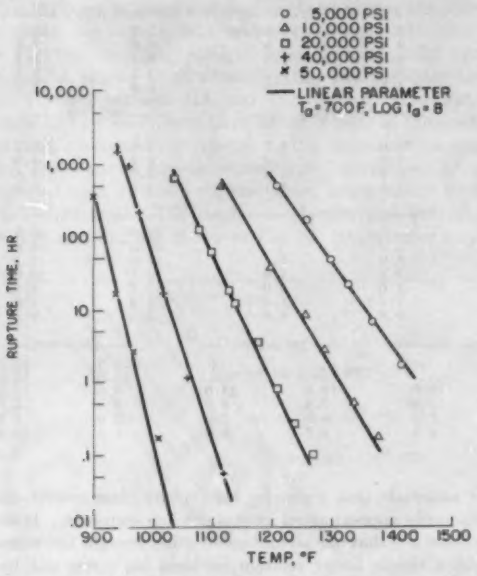

FIG. 12 CRITICAL CONSTANT NOMINAL STRESS DATA ON DM STEEL AND CORRELATION BY THE LINEAR PARAMETER

(Reference, Manson and Brown.)

and Dorn, led to considerable discrepancies. These critical tests may, in some measure, satisfy the need indicated by the authors in their Summary for a more fundamental experimental approach which may indicate correlations between creep-rupture properties, initial stress, and temperature.

The authors have attempted to provide some guidance to the reader as to the quantitative error in rupture time involved in each of the parameters. As already pointed out, their selection of values of T_a and $\log t_a$ were not such as to produce the best correlation; however even using their analysis of errors, it is difficult to accept their conclusion. For

$$\frac{\log t_a - \log t}{\beta} = 0.2$$

and for a range in β of 1.3, as assumed by the authors, Equation [14] of the paper leads to the conclusion that the ratio between the experimental rupture time and the rupture time as indicated by the master curve is 1.8, independent of the rupture time (that is, it is no greater at times in excess of 3×10^3 hr than in any other time range). It is thus difficult to see how the authors conclude that errors of several orders of magnitude are involved at times in excess of 3×10^3 hours.

The authors throw doubt on the validity of the Manson-Haferd parameter by stating that a material would not exhibit stress-dependent rupture properties at the point (T_a, $\log t_a$). In reference (2) of the paper the following is carefully pointed out: "The point (T_a, $\log t_a$) is not considered to have physical significance; it is considered only to be the point of convergence of the tangents to the curves of $\log t$ against T in the time range from approximately 10 to 10,000 hr. Since there is relatively little curvature in this time range, the tangents represent a good approximation to the experimental curves, but no conclusions can be drawn about the linearity in longer time ranges." In the vicinity of $\log t_a$ the rupture time for all materials investigated is well over 1000 years. In the reference[10] the possibility of curvature of constant stress lines even within the experimental time range is also considered, and a general method of data correlation is suggested when such curvature is noted. Manson and Haferd (2) and Manson and Brown[10] also recognize the possibilities of anomalous behaviors in certain ranges of the variables. Thus, for example, it is pointed out[11] that the linear parameter may not be applicable where major metallurgical transformations take place. Likewise,[12] it is pointed out that 16-13-3 steel shows unusual curvature in a very limited temperature range. Very few such anomalies have been found for the materials, times, and temperature investigated. To define the limitations of the parameter we are presently investigating various materials over very wide ranges of stress and temperature.

The authors state that the usefulness of the Manson-Haferd parameter is limited by the large number of data necessary to evaluate the material constants. In our experience not more than 30 tests having an average duration of about 50 hr will establish the entire master curve for a given material. This represents 1500 hr of test time, about the same amount of time as is necessary to establish a single isothermal between 0.1 and 1000 hr by direct testing.

The authors in the body of their paper certainly paint a very dark picture of the validity of the various parameters. Their conclusion is in rather surprising contrast and emphasizes that, when judiciously used, the parameters yield valuable predictions. Some clarification would appear necessary as the "judicious use" of these parameters.

J. MILLER.[13] The authors have analyzed the parameter $T(C + \log t)$ and two other time-temperature parameters for correlating creep and rupture data. As a result of their analysis, they conclude that the validity of these parameters over wide ranges of variables is doubtful.

The paper is correct in implying that significant errors can result from injudicious use of time-temperature parameters. We agree that the relation expressed by the parameter $T(C + \log t)$ is not precise over large ranges of variables. In other words, 10,000-hr data cannot be predicted from 10-hr data in all cases with high accuracy.

However, by proper use of this parameter, extremely valuable predictions can be made. As an illustration, in the accompanying Table 3, 10,000-hr rupture data reported in the U. S. Steel Bulletin on "Steels for Elevated Temperature Service" are compared with predicted values. The predicted values were obtained by plotting the 1000-hr strength as a function of $T(20 + \log t)$ and reading the 10,000-hr points from the resulting "master curves." In most cases the two values agree within experimental error although in some cases the difference is somewhat larger than normal experimental scatter.

To obtain these data by the conventional method of extrapolating a log-log plot, a minimum of four or five specimens and

[10] "Time-Temperature-Stress Relations for the Correlation and Extrapolation of Stress-Rupture Data," by S. S. Manson and W. F. Brown, Jr., Proceedings of the ASTM, vol. 53, 1953, p. 693.

[11] The DM steel reported in Fig. 12 is of somewhat different composition from that of Fig. 9 and consequently the stress-rupture properties of these two heats are different.

[12] Reference (2) of paper, p. 6.

[13] Thomson Laboratory, Small Aircraft Engine Department, General Electric Company, West Lynn, Mass.

TABLE 3 U. S. STEEL 10,000-HR RUPTURE DATA

(For each steel the first column is the 10,000-hr rupture strength reported by U. S. Steel in 1000 psi. The second column is the 10,000-hr rupture strength predicted by the parameter $T(20 + \log t)$ from the 1000-hr strength reported by U. S. Steel.)

Temp, deg F	Carbon		½Mo		⅛Cr-½Mo		1Cr-½Mo	
900	...	...	33.0	31.0	53.0	48.0	...	...
1000	6.8	7.2	14.5	14.0	32.5	26.0	24.0	22.0
1100	3.6	3.6	5.4	6.0	14.5	10.0	8.0	8.2
1200	1.0	1.8	2.6	2.7	4.2	3.4	...	...
1300	0.8	0.9	1.2	1.2	1.0	0.9	...	...
	2Cr-½Mo		2¼Cr-1Mo		3Cr-½Mo-1½Si		5Cr-½Mo	
1000	15.7	16.0	19.0	18.0	15.4	13.5	13.7	13.6
1100	9.7	8.6	11.2	10.4	7.4	7.8	8.0	7.8
1200	4.5	4.2	6.2	5.1	4.8	4.6	4.5	4.1
1300	...	...	...	...	3.0	2.7	2.2	2.1
1400	...	...	...	...	1.7	1.5	1.0	1.0
	5Cr-½Mo-1½Si		5Cr-½Mo-Ti		7Cr-½Mo		9Cr-1Mo	
1000	13.2	12.5	14.0	14.0	...	...	...	...
1100	7.0	7.1	7.0	7.0	11.0	8.7	14.6	10.3
1200	3.6	4.0	3.6	3.5	4.6	4.2	6.2	4.9
1300	2.1	2.4	...	...	2.2	2.3	2.6	2.5
1400	1.2	1.3	...	...	1.1	1.1	1.0	1.3
	12Cr		17Cr		27Cr		18Cr-8Ni	
900	26.0	25.0	24.0	22.0	...	...	38.0	40.0
1000	13.0	12.5	13.5	11.7	...	...	27.0	26.0
1100	...	...	6.5	6.2	3.0	4.4	17.0	16.5
1200	...	...	...	...	2.2	3.0	9.7	10.0
1300	...	...	...	...	1.6	2.0	5.7	6.5
1400	...	...	...	...	1.1	1.3	3.9	4.0
1500	...	...	...	...	0.8	0.8	2.5	2.8

	18Cr-8Ni-Ti		18Cr-8Ni-Cb		18Cr-8Ni-Mo		25Cr-12Ni		25Cr-20Ni	
1000	...	...	...	...	...	...	...	...	24.0	25.0
1100	16.0	19.7	22.0	22.0	...	...	...	...	15.0	16.0
1200	9.8	11.5	11.0	13.0	18.2	19.0	15.0	14.0	8.5	9.6
1300	6.9	7.0	4.6	8.0	12.0	12.5	7.8	8.6	4.9	5.7
1400	3.6	4.0	...	...	6.9	7.4	4.3	5.0	3.0	3.7
1500	...	...	...	...	3.4	4.3	2.7	3.0	1.8	2.5

about 4000 hr of testing time would be required for each material and temperature. In this example, the parameter method would therefore effect a saving of four to one in time.

It has been our experience in examining data on all types of alloys ranging from aluminum and magnesium to nickel and cobalt base that the parameter method will give more accurate results for equivalent testing times or that equivalent accuracy can be obtained with shorter times as compared with the log-log extrapolation method.

Authors' Closure

The discussions of Messrs. Manson and Brown and Mr. Miller are particularly welcome because of the association of these discussers with the procedures considered in the paper.

The initial point raised by Messrs. Manson and Brown, indicating that the validity of the linear parameter was investigated beyond the establishment of a master curve, is somewhat misleading. For example, the master curve for Steel DM in Fig. 9 shows that in only very few instances is more than one experimental point available at any stress level. The calculation of the log-stress log-rupture time curves from the master curve therefore depends entirely on interpolation. Reducing this procedure to its simplest form, it amounts to the calculation of a segment of a master curve from each of a number of isothermal log-stress log-rupture time curves and then reverting back and recalculating the same isothermal log-stress log-rupture time curves from each individual segment. It would seem that verification of the linear parametric procedure should be based on extensive extrapolations in both time and temperature. Our results clearly show that extrapolation over wide, but practical, limits in time and temperature leads to serious errors for the steels included in this paper.

The statement in the second point asserting that the criterion of straightness cannot be used in testing the validity of time-temperature parameters is, per se, meaningless without substantiation. It is commonly accepted for steels as well as many other materials that log-stress log-rupture time results can be satisfactorily approximated by straight line segments. It should be pointed out that one advantage of using straight line segments is that a simple linear relation between log stress and by log rupture time can be easily obtained. Because creep and rupture at elevated temperatures are extremely complex phenomena, relationships between stress and rupture time cannot as yet be derived from purely fundamental concepts. Under such conditions as these it is generally accepted that empirical relations giving good agreement be employed. It should be pointed out, after all, that the parametric relation proposed by Manson and Haferd is empirical in nature.

It is stated by Messrs. Manson and Brown, in the third point raised, that proper selection of T_a and $\log t_a$ were not made for steels G29 and T37. The procedure employed in determining the constants for these two steels was exactly the same as that employed for the other three steels and is completely discussed in the paper. It is regrettable, however, that Messrs. Manson and Brown did not describe briefly the procedure employed by them in obtaining the new constants which reduced the scatter somewhat in the master curves in Figs. 10 and 11 for these two steels. This point is somewhat disturbing because it seems that a great deal of experience is necessary to determine the proper material constants. Yet, according to Messrs. Manson and Brown in their closure to the discussion of their paper[18] they state, "The selection of a point of intersection has not been found to be critical or to require great experience." To pursue this point further, it may be observed from relation [8] in this paper that the slopes and intercepts of the line segments within the master curve depend on T_a and $\log t_a$. It would seem then that if one could in some way determine the proper combination of T_a and $\log t_a$ this should result in the least scatter in the master curve. The procedure for obtaining the optimum combination of the material constants is as yet obscure. This statement is made because, according to Manson and Haferd, the success of the linear parametric procedure for purposes of

extrapolation depends on the proper combination of T_a and log t_a rather than on the individual value of these constants. They even go so far as to suggest that a single value of T_a be used for all materials. This suggestion, of course, cannot be taken seriously because for the two different heats of steel DM discussed by Messrs. Manson and Brown, the computed values of T_a differ a great deal.

In a paper by Manson and Succop,[14] test results are presented in a plot of log rupture time against the temperature that indicate that the resulting straight lines are essentially parallel. The results employed in obtaining the straight lines include rupture times between 0.3 and 1819 hours. However, Mr. Manson and his co-workers have stated in each of their publications that because of divergence in the region of low rupture times, the material constants should be determined from experimental data in which rupture times below about 30 hours should be omitted. The results of Manson and Succop have been replotted and are shown in Fig. 13, but in order to retain

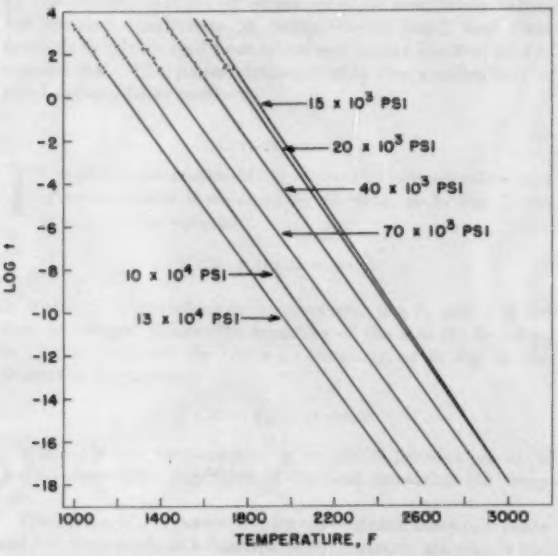

FIG. 13 RELATIONSHIP BETWEEN THE LOGARITHM OF THE RUPTURE TIME AND TEMPERATURE FOR VARIOUS CONSTANT INITIAL STRESSES (After Manson and Succop.)

sufficient experimental points, only data in which the rupture time was below 12 hours rather than 30 hours was omitted. One set of experimental points for a stress of 5000 psi was omitted entirely because only three experimental points remained. The results in Fig. 13 show that the straight lines converge at a negative value of log t_a and further point to the fact that negative values of log t_a are encountered in materials other than steels. Since, as pointed out by Manson and Haferd, the experimental points in plots of log t against temperature are only approximately linear between 10 and 10,000 hours, the straight lines, which converge at the point (T_a, log t_a) are constructed as tangents to the experimental curves. Thus the location of the convergence, that is, whether log t_a is positive or negative, depends on the type divergence from linearity of the experimental curves.

[14] "Stress Rupture Properties of Inconel 700 and Correlation on the Basis of Several Time-Temperature Parameters," by S. S. Manson and G. Succop, presented at ASTM meeting, June 30, 1955.

The results of Manson and Brown and Manson and Succop indicate that there is no set pattern to the type of divergence which may occur.

The fourth point raised by Messrs. Manson and Brown concerns the error encountered with the linear parameter within small ranges in stress for rupture times greater than 3×10^3 hours. The error encountered is of the order of several factors, as stated in the paper, and not of several orders of magnitude as stated in the preprint of this paper.

The next point raised by Messrs. Manson and Brown is of some importance because it throws some light onto some limitations of the linear parametric procedure. If the point (T_a, log t_a) is not significant stresswise for values of T_a within the creep range of temperatures, it follows that the experimental log t-temperature curves diverge from linearity at low values of rupture times. For some materials this divergence is found to occur appreciably below 1000 hours. It is then reasonable to state that for all materials which are investigated, the point of divergence should be established with certainty before attempting extrapolations. Mr. Manson and his co-workers have stated that little divergence from linearity is found for the log t-temperature curves in the approximate range between 10 and 10,000 hours. However, of all of the results published by Mr. Manson and his co-workers, the experimental results seem to seldom exceed 3000 hours. It would seem that the implication that the linear parameter can be used for extrapolations to 10,000 hours from short time results is not substantiated and requires more extensive proof. Any further light thrown on this point by the investigation now being conducted by Messrs. Manson and Brown will be received with interest.

The next point relating the necessary amount of testing to establish the material constants has in the past been of some concern to Messrs. Manson and Haferd. They have suggested that a single value of T_a be used for all materials to reduce the amount of testing. Of greater importance is the fact, however, that the establishment of the so-called master curve gives very little indication of the limits within which extrapolations can be attempted, for example, the limitation imposed by divergence in the long t-temperature plot. To define these limitations for each new material more than 30 tests are indicated.

Concerning the final point raised by Messrs. Manson and Brown, it must be re-emphasized that the purpose of the present paper is to point out various limitations of the parametric procedures as well as to indicate some of the inconsistencies which exist among the parameters proposed. Our findings show that over practical ranges in stress or temperature, parametric procedures encounter serious limitations for purposes of extrapolation. For example, the use of the linear parameter for purposes of extrapolation, even over small ranges in stress and over a range of only several hundred degrees in temperature, results for the steels investigated in this paper to errors in rupture time of several factors of magnitude when rupture times greater than 3×10^3 hours are encountered. That parametric procedures have limitations is substantiated by the statement of Messrs. Manson and Brown in the authors' closure of their paper.[10] They state, "The authors wish to emphasize that they feel none of the parameters so far presented, including their own, can truly represent the basic behavior of a complex alloy (such as a low-alloy steel) over extremely wide ranges of both time and temperature. It must be realized that the conception of a correlating parameter in the relatively simple forms thus far proposed is at best a tool which can permit the shortening of stress rupture testing times in ranges of practical application."

One application in which parametric procedures have been

found particularly useful has been the summarizing of creep-rupture results for purposes of comparison. Thus, for example, the Larsen-Miller parameter has been used to determine the approximate merits for high-temperature application of various alloys by comparing the master curves on a single plot. Such a procedure can also be used to determine the optimum heat-treatment for individual alloys. In using such procedures, there should be no attempt, however, to use such comparisons for predicting behavior over large ranges in time, stress, or temperature from limited results.

The authors agree with Mr. Miller that from a practical viewpoint, proper usage of parametric procedures as stated in the foregoing leads to useful approximate predictions. If the use of parametric procedures decreases the testing time, and, of course, this may depend on the approximate predictions desired, this fact is of importance from the practical viewpoint.

Mechanical Properties at Elevated Temperatures of Ductile Cast Iron

By F. B. FOLEY,[1] NEW YORK, N. Y.

Interest in the elevated-temperature properties of the relatively new engineering metal, ductile cast iron, has prompted the gathering together of data (1 to 5)[2] on the subject and the correlation of them on a uniform basis. In correlating the values obtained by the several laboratories on different melts of somewhat different compositions, use is made of the equation applied originally in the evaluation of effects of time and temperature in the tempering of steel and later adapted by Larson and Miller (6) to the determination of stress rupture and creep values for various conditions of temperature, load, and time from data which had been obtained under limited sets of conditions. The paper demonstrates the application of the Larson-Miller method.

Introduction

IN applying the Larson-Miller method to stress-rupture data a master curve is obtained by plotting, as in Fig. 1, the product of the equation

$$T\,(20 + \log t) = \text{const}$$

in which T is the absolute temperature, deg F, and t is the time to rupture, against the logarithm of the load (in lb per sq in.) which produced the rupture. Similarly, as in Fig. 2, the product of the equation

$$T\,(20 - \log t) = \text{const}$$

in which t is now the minimum creep rate in per cent per hr, is plotted against the logarithm of the load producing the creep rate.

The Larson-Miller parameters for conventional times to rupture and for creep rates, as a function of temperature, are readily obtained by substituting in the equation selected rupture times, or creep rates, along with corresponding temperatures and thus obtaining the appropriate Larson-Miller parameter values for plotting against the temperatures. For convenience, such plottings have been placed in the upper portion of Figs. 1 and 2.

In using these figures, to obtain the stress for a given creep rate and temperature or for fracture for a given time and temperature, one first finds the correct constant for the specific temperature from the upper plotting and then, by following its value down into the lower portion of the figure, the corresponding stress may be derived. For example, the stress for a 10,000-hr rupture life at 900 F is desired: Using the upper portion of Fig. 1 the value for 900 F and 10,000-hr life is found to be 32.64. By following this ordinate down to its intersection with the master curve in the lower portion of the figure one finds a corresponding stress of 8700 psi.

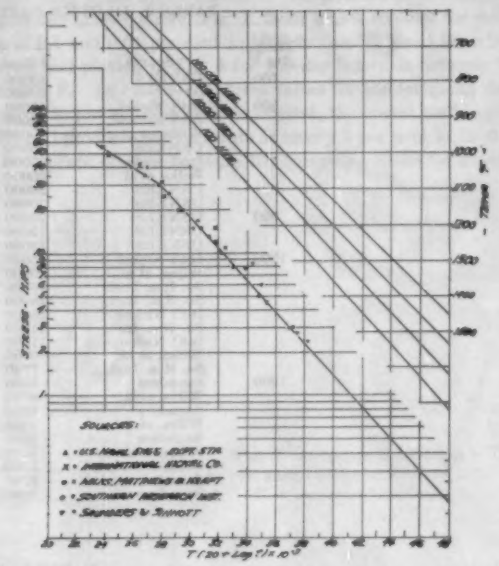

FIG. 1 MASTER STRESS-RUPTURE CURVE—DUCTILE CAST IRON

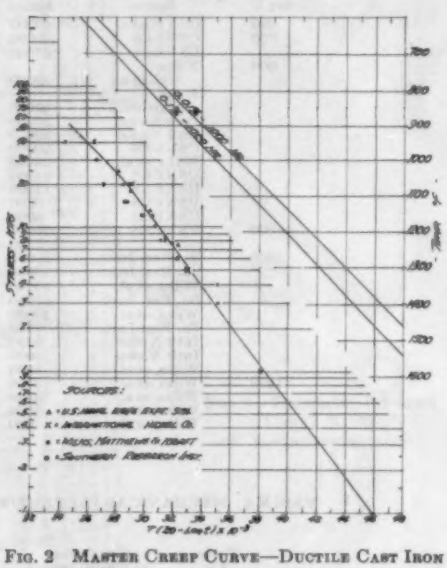

FIG. 2 MASTER CREEP CURVE—DUCTILE CAST IRON

[1] Consulting Metallurgist, The International Nickel Company.

[2] Numbers in parentheses refer to the Bibliography at the end of the paper.

Contributed by the Joint ASTM-ASME Committee on Effect of Temperature on Properties of Metals and presented at a joint session of the Joint ASTM-ASME Committee on Effect of Temperature on the Properties of Metals and Metals Engineering Division at the Diamond Jubilee Annual Meeting, Chicago, Ill., November 13–18, 1955, of THE AMERICAN SOCIETY OF MECHANICAL ENGINEERS.

NOTE: Statements and opinions advanced in papers are to be understood as individual expressions of their authors and not those of the Society. Manuscript received at ASME Headquarters, September 2, 1955. Paper No. 55—A-204.

TABLE 1 COMPOSITIONS OF FERRITIC DUCTILE IRONS

Source	TC	Mn	Si	P	S	Ni	Cu	Mg
U.S.N. Eng'g Exp. Sta.	3.47	0.42	2.49	...	...	0.55	0.30	0.048
International Nickel Co.	3.57	0.78	2.51	0.087	...	1.18	0.58	0.07
Wilks, Matthews & Kraft	3.64	0.46	2.66	0.032	0.014	0.66	..	0.076
Southern Research Inst.	3.56	0.53	2.67	0.11	0.021	0.04	0.04	0.08
Saunders & Sinnott[a]	3.33	0.50	2.28	0.05	0.01	1.12	..	...

[a] Pearlitic.

TABLE 2 DUCTILE CAST-IRON STRESS-TO-RUPTURE DATA

Temp, deg F	Source	Stress, psi — Actual	Stress, psi — Computed	Fracture time, hr — Actual	Fracture time, hr — Computed	Larson-Miller Parameter
700	USNEES	48000		16		24.59
		40000	34000	1842	280	26.99
800	Int'l Nickel	55000		0.1		23.94
	Int'l Nickel	44000		10.6		26.48
	Wilks, et al.	40000		4.1		25.97
	USNEES	35000		19		26.81
	Int'l Nickel	33000	28200	190.4	60	28.07
	Wilks, et al.	30000	30000	127.8	125	27.85
	USNEES	26000	25200	432	380	28.52
	USNEES	20000	20100	2471	2800	29.47
900	USNEES	20000		39		29.36
	USNEES	17000	15500	277	150	30.52
	USNEES	13000	12600	1155	1000	31.36
1000	Int'l Nickel	25000		0.2		28.18
	Wilks, et al.	20000		1.0		29.20
	So. Res. Inst.	15000		4.5		30.15
	So. Res. Inst.	15000		10.5		30.69
	Int'l Nickel	15000		45.4		31.62
	So. Res. Inst.	11950		57.3		31.77
	Int'l Nickel	11000	9400	184.2	80	32.50
	Wilks, et al.	10000	10300	98	133	32.10
	So. Res. Inst.	7740	6800	1363	620	33.77
1200	Saunders	8500		5.2		34.39
	Wilks, et al.	8000		0.64		32.88
	Saunders	6000		13.7		35.09
	Wilks, et al.	5000		10.1		34.86
	Saunders	4500		22.6		35.44
	Wilks, et al.	3000	3200	170	180	36.90
	Saunders	3000	2750	284.4	180	37.26
	Saunders	2700	2590	404.8	340	37.53
	Saunders	2400	2090	1272	620	38.35

TABLE 3 DUCTILE CAST IRON

Temp, deg F	Source	Creep data, stress, psi — Actual	Creep data, stress, psi — Computed	Creep rate, % per hr — Actual	Creep rate, % per hr — Computed	Larson-Miller Parameter
600	Int'l Nickel	40000		0.00001		26.50
700	USNEES	40000	42000	0.0046	0.0044	25.92
	USNEES	25000	23200	0.000052	0.000092	28.17
800	Wilks, Matthews	40000		3.7		24.48
	Wilks, Matthews	30000		0.078		26.60
	Int'l Nickel	20000	18300	0.0009	0.0015	29.04
	Int'l Nickel	20000	18100	0.0008	0.0015	29.11
	USNEES	20000	21100	0.0023	0.0015	28.53
	Wilks, et al.	18000	18500	0.0009	0.00078	29.04
	USNEES	14000	13500	0.00014	0.00016	30.05
	USNEES	12000	11800	0.00006	0.000068	30.52
	USNEES	8500	8700	0.00001	0.00001	31.50
	USNEES	8000	8800	0.000011		31.45
900	USNEES	13000	12000	0.0041	0.0062	30.45
		7500	10000	0.00148	0.00033	32.41
1000	So. Res. Inst.	20000			27.0	27.11
	So. Res. Inst.	15000			2.6	28.59
	Wilks, et al.	15000			2.2	28.70
	So. Res. Inst.	11950			0.4	29.78
	Wilks, et al.	10000			0.093	30.70
	So. Res. Inst.	7740			0.013	31.95
	Int'l Nickel	6000	6500	0.0064	0.0042	32.40
	Int'l Nickel	5000	5200	0.00207	0.0017	33.11
	Wilks, et al.	4000	2800	0.0001	0.00056	35.04
1200	Wilks, et al.	8000		18.0		31.11
	Wilks, et al.	5000		1.14		33.10
	Wilks, et al.	3000		0.074		35.08
	Wilks, et al.	1000	1080	0.001	0.0007	38.18

TABLE 4 MECHANICAL PROPERTIES AT ELEVATED TEMPERATURES OF DUCTILE CAST IRON

Temp, deg F	Short-time tensile, psi — TS	Short-time tensile, psi — YS	Stress, psi to rupture, hr — 1000	Stress, psi to rupture, hr — 10000	Stress, psi to rupture, hr — 100000	Stress, psi for creep rate (% per 1000 hr) — 0.1%	Stress, psi for creep rate (% per 1000 hr) — 0.01%
70	65300	46000					
700	55800	35400	36000	30000	24000	25100	19000
800	48600	34100	23000	17000	12300	12800	8700
900	40000	29000	13000	9100	6400	6000	3900
1000	29750	24000	7100	4900	3350	2800	1800
1100	19000	17500	3900	2620	1760	1350	...
1200	10800	10400	2190	1450	920	...	...

The determinations used in this summary were obtained from ferritic ductile irons of the compositions given in Table 1. Excepting the Saunders and Sinnott iron, all the materials were practically completely graphitized and presented a ferritic structure with a tensile strength at room temperature of about 65,000 psi. The Saunders and Sinnott metal was pearlitic with a room-temperature tensile strength of 75,000 psi.

Stress-Rupture Results

The data used in deriving the stress-to-rupture values are given in Table 2 and are plotted in the master stress-rupture curve in Fig. 1, from which the values in Table 4 have been derived and, in turn, plotted in Fig. 3. The computed stress for the actual fracture time and the computed fracture time for the actual stresses, derived from Fig. 2, have been entered in the appropriate columns of Table 2 showing acceptable agreement between the actual and the computed values.

Creep Results

The use of the Larson-Miller method of deriving stress-rupture values has gained rather wide acceptance, and values so obtained are verified by comparison with actual test results. The use of this method for deriving creep values is not on so firm a footing but it has been used, nevertheless, in this summary with quite as consistent agreement with actual results as in the case of stress-rupture tests. The extrapolated values may therefore be considered only a fair approximation. Data in Table 3 were used to plot the master curve, Fig. 2, from which stresses for creep-rate of 0.1 and 0.01 per cent in 1000 hr (see Table 4) have been derived and plotted in Fig. 4 for 100-deg intervals between 700 and 1200 F. At 1200 F the stress values for the foregoing creep rates are so low as to be of little interest, the lowest load applied (1000 psi) producing a creep rate of nearly 1 per cent in 1000 hr. As in the case of stress rupture the computed stress for actually

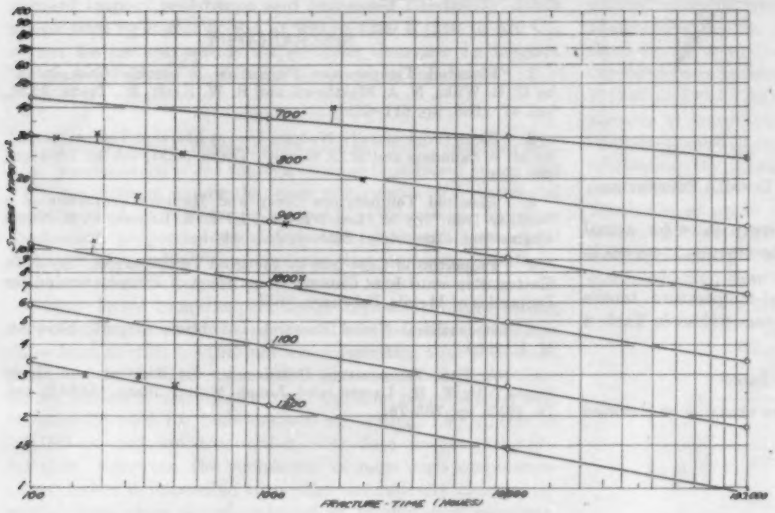

Fig. 3 Ductile Cast-Iron Stress-Rupture Values
(X = experimental values.)

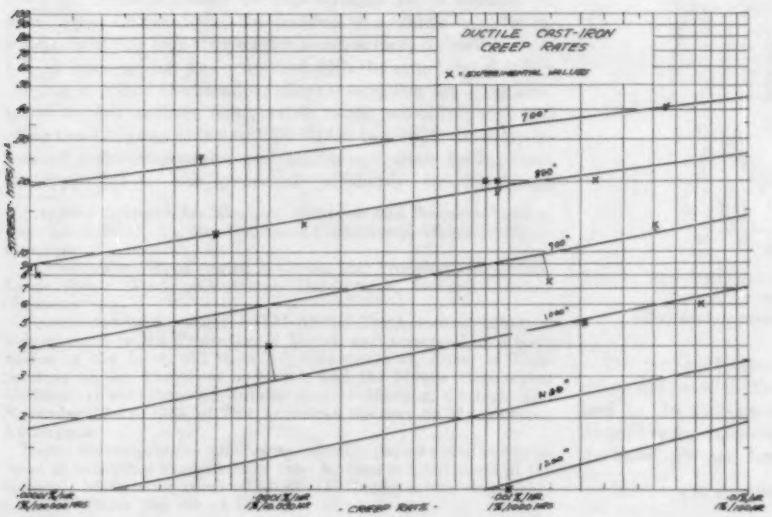

Fig. 4 Ductile Cast-Iron Creep Rates
(X = experimental values.)

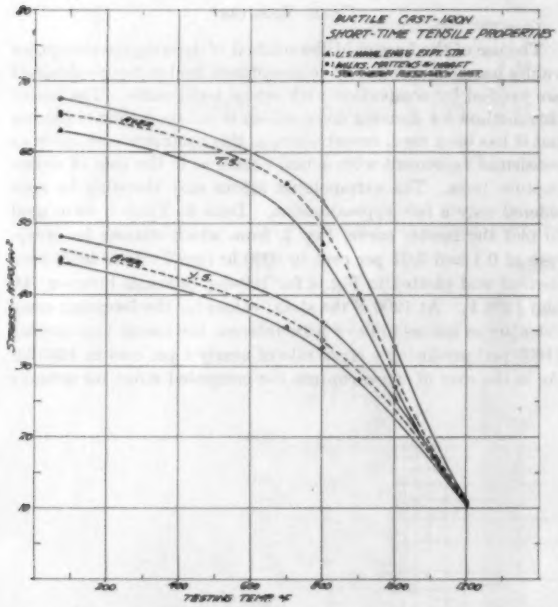

FIG. 5 DUCTILE CAST-IRON SHORT-TIME TENSILE PROPERTIES

observed creep rates and the computed creep rates for actual applied stresses have been derived from the creep-rate curves in Fig. 4 and entered in Table 3.

The few available short-time elevated-temperature tensile values have been plotted in Fig. 5 and average values in Table 4 have been derived.

PEARLITIC DUCTILE CAST IRON

The pearlite of ductile cast iron becomes unstable at elevated temperatures, the carbide phase decomposing to form graphite and ferrite. Wilks, et al. (1), suggest that the pearlite of ductile iron is stable at 800 F but graphitizes gradually at 1000 F and completely in a matter of less than 100 to 200 hr at 1200 F. The result of this graphitization is to cause the elevated-temperature properties of the pearlitic iron to decrease gradually at temperatures above incandescence and ultimately to become the same as those of completely ferritic ductile iron.

SUMMARY

The elevated-temperature properties of ferritic ductile cast iron for 100-deg intervals from 700 to 1200 F are summarized in Table 4, in which the values, other than those for short-time tensile tests, have been computed by means of the Larson-Miller equation. These are quite close approximations of values to be expected from wholly ferritic ductile iron. The presence of combined carbon will tend to increase these values, particularly in the low-temperature range, so that from this point of view they are minimum values.

BIBLIOGRAPHY

1 "Elevated Temperature Properties of Ductile Cast Irons," by C. R. Wilks, N. A. Matthews, and R. W. Kraft, Jr., Trans. ASM, vol. 47, 1955, pp. 611–631.

2 "Some Properties of a Nodular Iron at Elevated Temperatures," by M. S. Saunders and M. J. Sinnott, Trans. ASM, vol. 45, 1953, pp. 362–376.

3 "Elevated Temperature Creep and Rupture Properties of a Nodular Iron," by W. Lee Williams, E. E. S. Report, U. S. Naval Engineering Experiment Station, July, 1954.

4 "Properties of Cast Iron at Elevated Temperatures," by J. R. Kattus, Report to Joint Committee on Effect of Temperature on the Properties of Metals, February, 1955.

5 International Nickel Research Laboratory Report, Bayonne, N. J., 1955.

6 "A Time-Temperature Relationship for Rupture and Creep Stress," by F. R. Larson and James Miller, Trans. ASME, vol. 74, 1952, pp. 765–781.

Structural Stability of Modified 12-Chromium Alloys

By W. C. HAGEL[1] and E. F. BECHT,[2] SCHENECTADY, N. Y.

In addition to possessing an attractive combination of mechanical properties for turbine applications, certain modified 12-chromium alloys were found to be structurally stable after long-time static aging and service exposure at high temperatures. However, two precipitation reactions have been observed to occur unpredictably in 12 Cr-Co-W-V alloy. The precipitating phases have been identified, and their effects upon mechanical properties are reported. After about 200 hr at 800 to 950 F (445 to 510 C), precipitation of chromium-rich ferrite causes decreased impact resistance and increased hardness; after about 6000 hr under stress at 950 to 1200 F (510 to 650 C), sigma formation causes an extreme decrease in impact resistance and no significant increase in hardness.

Introduction

THE stringent requirements placed upon long-life low-maintenance prime movers, such as land-based steam and gas turbines, require that some components be designed and manufactured of high-temperature alloys possessing optimum mechanical properties combined with maximum structural stability. Depending upon exposure time, temperature, stress, and the variations thereof, property and structural changes not observed during room-temperature or high-temperature testing may occur unpredictably in service. These long-life applications differ from aircraft gas turbines where operating time is so short that it is possible to base a complete laboratory testing procedure on the full life of a component. In the time range beyond that customarily used for high-temperature testing, i.e., 10,000 to 100,000 hr, complete structural-stability data are not easily obtainable; moreover, the complexity of most high-temperature alloys makes it impossible to predict theoretically changes resulting from phase transformations or precipitation reactions. Since metallurgists can expect little respite from the pressing need of turbine engineers for high-strength alloys suitable for even higher temperatures, the problem of avoiding harmful instabilities during long-time service becomes more difficult.

This investigation was concerned with the structural stability of some modified 12-chromium alloys undergoing extended service as turbine buckets, bolts, valve stems, wheel forgings, and other small forgings at 900 to 1200 F (480 to 650 C). A compilation of room-temperature and high-temperature testing data for these alloys was presented previously by Newhouse, Seguin, and Lape (1).[3] However, at that time there was no knowledge of the precipitation reactions which have since been detected in the 12 Cr-Co-W-V alloy. By combining the observed results of long-time service exposure with recent metallurgical research, it is now possible for the authors to explain many heretofore anomalous changes in the properties and structure of turbine components.

Alloy Modifications

The combination of high corrosion resistance, hardenability, internal damping, and structural stability found in the straight 12-chromium alloys, AISI Types 403 and 410, has popularized them for many turbine applications since the year 1914. Yet, the rapid decrease in creep and rupture strength at 1000 to 1100 F (540 to 590 C) has limited their use in highly stressed components to lower temperatures; as turbine operating temperatures increased through this range for higher thermodynamic efficiencies, the straight 12-chromium alloys consequently became inadequate. By replotting the rupture-strength data of Newhouse, et al., as shown in Fig. 1, alloy modifications can be seen to cause a rewarding increase in rupture strength at temperatures up to about 1200 F. In 12 Cr-Cb alloy, rupture strength is increased only below 1100 F.

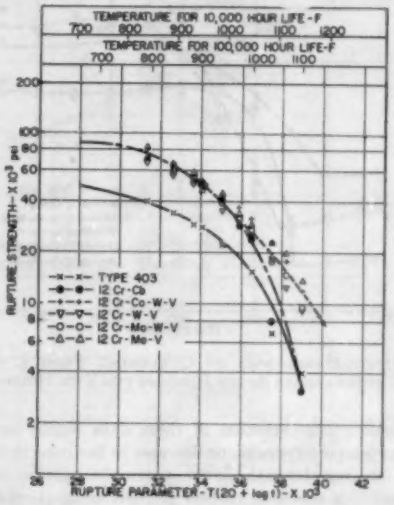

FIG. 1 RUPTURE STRENGTH AT 0.2 PER CENT TOTAL STRAIN VERSUS THE RUPTURE PARAMETER $T(20 + \log t)$
(Temperature scales are given for 10,000 and 100,000-hr life.)

The preferred composition ranges for modified 12-chromium alloys are listed in Table 1. Alloy modifications are characterized by the addition of various carbide formers, e.g., tungsten, molybdenum, vanadium, and columbium, for improved tempering resistance and ferrite strengthening; carbon content is in-

[1] Applied Research Metallurgist, Materials and Processes Laboratory, Large Steam Turbine-Generator Department, General Electric Company.

[2] Development Metallurgist, Materials and Processes Laboratory, Large Steam Turbine-Generator Department, General Electric Company.

Contributed by the Joint ASTM-ASME Committee on Effect of Temperature on the Properties of Metals and presented at a joint session of the Joint ASTM-ASME Committee on Effect of Temperature on the Properties of Metals and the Metals Engineering Division, at the Diamond Jubilee Annual Meeting, Chicago, Ill., November 13–18, 1955, of THE AMERICAN SOCIETY OF MECHANICAL ENGINEERS.

NOTE: Statements and opinions advanced in papers are to be understood as individual expressions of their authors and not those of the Society. Manuscript received at ASME Headquarters, September 7, 1955. Paper No. 55—A-173.

[3] Numbers in parentheses refer to the Bibliography at the end of the paper.

TABLE 1 PREFERRED COMPOSITION RANGES FOR MODIFIED 12-CHROMIUM ALLOYS

Alloy designation		Weight per cent alloy											
		C	Cr	Mn	Ni	Co	W	Mo	V	Cb	Si	S	P
Type 403	Max	0.13	13.00	0.80	0.50						0.50	0.03	0.03
	Min	0.06	11.50	0.25									
12 Cr-Cb	Max	0.18	13.00	0.60	0.50					0.45	0.50	0.03	0.04
	Min	0.13	11.50	0.40						0.35			
12 Cr-Co-W-V	Max	0.22	13.00	1.50	0.50	5.50	3.50	0.15	0.27		0.60	0.025	0.025
	Min	0.17	11.50	1.00		4.50	2.50		0.19		0.30		
12 Cr-W-V	Max	0.32	13.00	1.50	0.50		2.75		0.26		0.60	0.025	0.025
	Min	0.27	11.50	1.00			2.25		0.18		0.30		
12 Cr-Mo-W-V	Max	0.23	14.00	1.00	1.00		1.25	1.25	0.50		1.00	0.03	0.04
	Min	0.18	12.00		0.50		0.75	0.75	0.20				
12 Cr-Mo-V	Max	0.35	12.00	1.25	0.50			3.00	0.30		0.50	0.03	0.03
	Min	0.25	11.00	0.95				2.50	0.20				

creased accordingly. Carbide-forming elements are also ferrite stabilizers, and detrimental amounts of ferrite are avoided by adding austenite stabilizers such as manganese, nickel, and cobalt. Chromium contents of 12 to 13 per cent require delicate composition balancing, because small alloy additions can completely change fully martensitic stainless steels to partially ferritic stainless steels.

Heat-Treatment

The response to heat-treatment of modified 12-chromium alloys is similar to that reported in detail by Rickett, et al. (2) for Types 403 and 410. Most commercial austenitizing treatments consist of holding modified alloys for 1 hr at 1750 to 2100 F (955 to 1150 C), followed by air cooling or oil quenching. During a laboratory study of austenitizing reactions, as-tempered specimens were heated for 2 hr at 100 deg F intervals from 1300 to 2300 F (705 to 1260 C). The resulting specimen hardnesses after water quenching give an indication of alloy austenitizing characteristics as shown in Fig. 2.

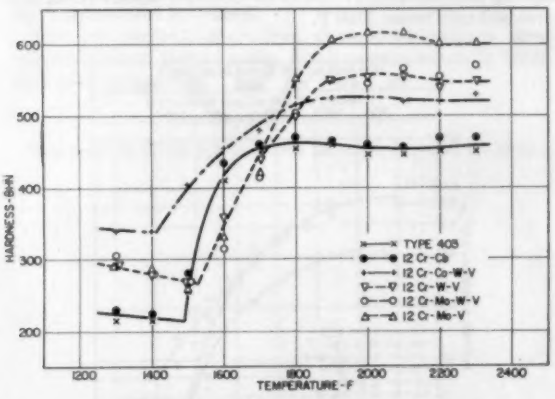

Fig. 2 Alloy Hardnesses on Quenching From a Series of Temperatures After Holding for Two Hours

A structural interpretation of these data would be that, on heating, as-tempered specimens decrease in hardness until austenite starts forming above the lower A_1 temperature for each alloy. As the carbides dissolve, carbon content in austenite solution (or martensite on quenching) increases until the maximum amount of carbon hardening can be attained. This closely corresponds with microstructural observations showing complete carbide solubility at some upper A_1 temperature. The hardness level of quenched specimens is mainly dependent upon per cent carbon in resulting martensite, although a slight decrease in hardness at still higher temperatures can be attributed to austenite grain growth and delta-ferrite formation.

The lower A_1 temperature is fairly constant at 1500 F (815 C) for all alloys; the upper A_1 temperature is about 1750 F (955 C) for Type 403 and 12 Cr-Cb, 1800 F (980 C) for 12 Cr-Co-W-V, 1900 F (1040 C) for 12 Cr-Mo-W-V, and 2000 F (1095 C) for 12 Cr-W-V and 12 Cr-Mo-V alloys. The 12 Cr-W-V and 12 Cr-Mo-V alloys used in this investigation contain some ferrite at all temperatures. Delta ferrite appears at about 2100 F in Type 403, 12 Cr-Cb, and 12 Cr-Mo-W-V alloys, whereas the 12 Cr-Co-W-V alloy is completely austenitic, at least up to 2300 F. Large differences in the austenitizing characteristics and carbide stability of these alloys are caused by small compositional variations.

Martensitic alloys are commercially tempered at 1100 to 1250 F (595 to 675 C) for such time as will give them the desired balance of properties. Tempering at lower temperatures causes low impact resistance, and other mechanical properties suffer on tempering above 1250 F. Figs. 3 to 6 summarize the mechanical properties of Types 403, 12 Cr-Co-W-V, 12 Cr-W-V, and 12 Cr-Mo-W-V alloys after tempering for times of 3 to 100 hr. The rupture or tempering parameter $P = T\ (C + \log t)$ is frequently employed for time-temperature considerations, where T equals absolute temperature in degrees Rankine, t is time in hours, and C is a constant (usually 20 or sometimes 25 for rupture) selected to show less data scatter.

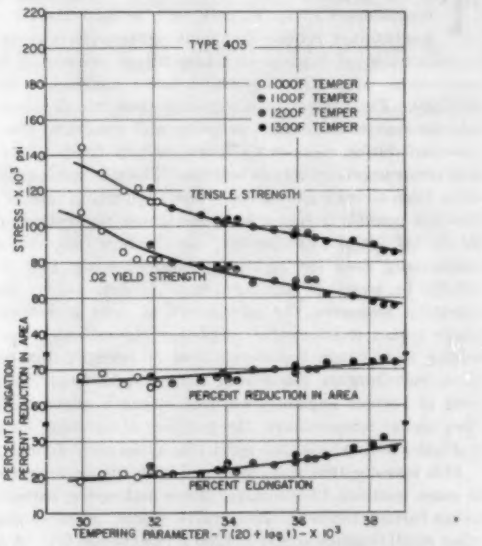

Fig. 3 Room-Temperature Mechanical Properties Versus the Tempering Parameter $T(20 + \text{Log } t)$ for Type 403 Alloy

A striking feature of Figs. 3 to 6 is the increased tempering resistance exhibited by alloy modifications in comparison with Type 403 alloy. Modified 12-chromium alloys, as normally heat-treated, will possess higher room-temperature tensile strength and lower ductility and impact resistance than Type 403 alloy. No evidence has been found for the occurrence of secondary hardening caused by retained-austenite transformation or carbide precipitation; these alloys apparently are not subject to temper brittleness, since cooling rate following tempering is unimportant. Incidental to these data, the relation that tensile strength in lb per sq in. equals 485 times the Brinell hardness holds well for modified 12-chromium alloys, as evidenced by the probability plot of Fig. 7. Therefore exposure data are

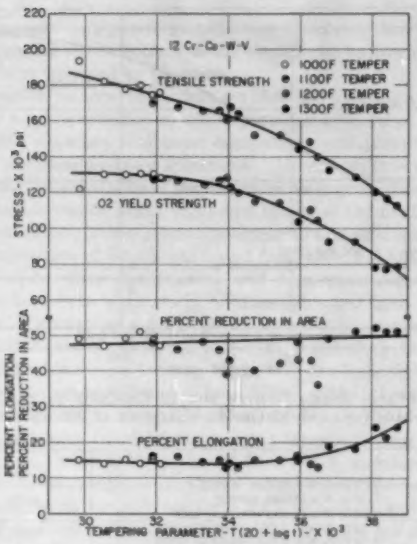

FIG. 4 ROOM-TEMPERATURE MECHANICAL PROPERTIES VERSUS THE TEMPERING PARAMETER $T(20 + \text{LOG } t)$ FOR 12 CR-CO-W-V ALLOY

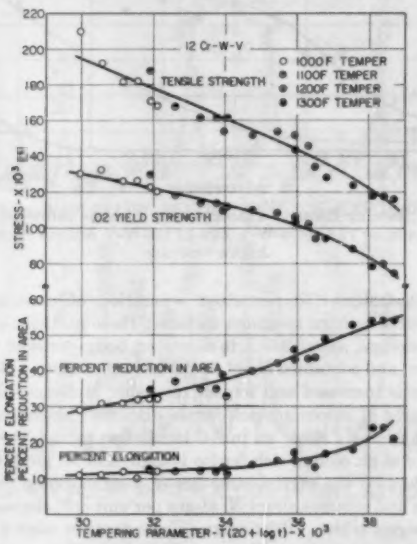

FIG. 5 ROOM-TEMPERATURE MECHANICAL PROPERTIES VERSUS THE TEMPERING PARAMETER $T(20 + \text{LOG } t)$ FOR 12 CR-W-V ALLOY

usually given in hardness units as a measure of room-temperature mechanical properties.

LONG-TIME EXPOSURE DATA

Although testing is rarely continued beyond 10,000 hr, constant-stress creep data sometimes give corroborating, but not conclusive, evidence of structural instabilities. In Fig. 8 one can note an abrupt change of slope after about 6000 hr at 1050 F (565 C) which will later be shown to be caused by sigma precipitation under stress in 12 Cr-Co-W-V alloy. Contrastingly, the more stable 12 Cr-W-V alloy exhibits continuous creep behavior under the same conditions. Unless carefully collected at constant temperature, constant-stress creep data are not completely reliable; the possibilities always exist that structural instabilities appear after extremely long times or that they cause no observable effect upon specimen elongation.

Stability data can be simply obtained by taking hardness tests

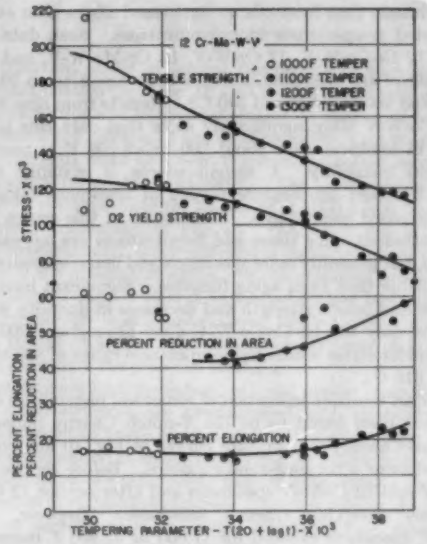

FIG. 6 ROOM-TEMPERATURE MECHANICAL PROPERTIES VERSUS THE TEMPERING PARAMETER $T(20 + \text{LOG } t)$ FOR 12 CR-MO-W-V ALLOY

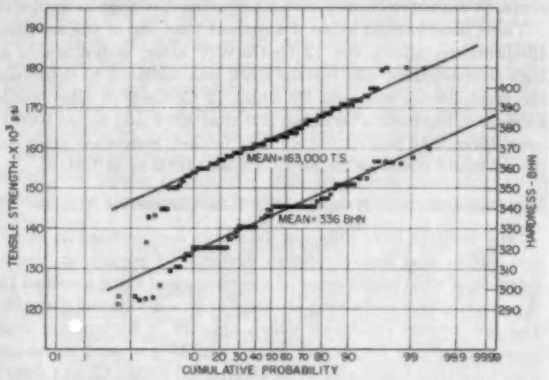

FIG. 7 PROBABILITY PLOT SHOWING RELATIONSHIP BETWEEN TENSILE STRENGTH AND BRINELL HARDNESS IN MODIFIED 12-CHROMIUM ALLOYS

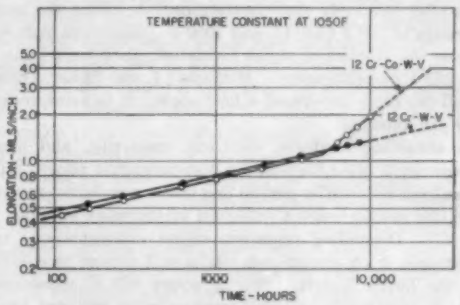

FIG. 8 CONSTANT-STRESS (10,000 PSI) CREEP DATA AT 1050 F FOR 12 CR-CO-W-V AND 12 CR-W-V ALLOYS

at logarithmic time intervals on unstressed alloys after exposure to elevated temperatures in aging furnaces. Such data for 12 Cr-Cb, 12 Cr-Co-W-V, 12 Cr-W-V, 12 Cr-Mo-W-V, and 12 Cr-Mo-V alloys are presented in Fig. 9 after aging up to 10,000 hr at 900 and 1000 F (480 and 540 C). Results from nine heats of 12 Cr-Co-W-V alloy significantly show that only this alloy increases in hardness after about 200 hr at 900 F as result of a structural instability. A second source of stability data is offered by room-temperature testing of specimens taken from service-exposed components. The nature of this source is such that continuous aging times and temperatures are not easily obtainable, but generally more specimens and longer-exposure times are available than from aging furnaces. Significant increases in hardness and tensile strength and decreases in ductility were observed in only the 12 Cr-Co-W-V alloy after about 200 hr exposure under stress within the temperature range of 800 to 950 F (425 to 510 C).

The most sensitive indication of structural instabilities in these alloys has been found to be the V-notch Charpy impact test; the impact energy-temperature curves of Fig. 10 are typical of alloy behavior after long-time exposure. Before service 12 Cr-Co-W-V and 12 Cr-W-V specimens and after service 12 Cr-W-V specimens show high impact resistance. However, 12 Cr-Co-W-V specimens exposed for 17,000 hr at 900 F increased in hardness with decreased impact resistance; 12 Cr-Co-W-V specimens exposed for 17,000 hr at 1000 F showed an extreme decrease in impact resistance with no significant change in hardness.

These observations made it apparent that one of the modified 12-chromium alloys, the 12 Cr-Co-W-V alloy, is not stable at high temperatures, and further work was initiated to determine the precipitation reactions by which 12 Cr-Co-W-V alloy would increase in hardness after about 200 hr at 900 F and not at 1000 F, even though it has extremely low impact resistance after exposure under stress for longer than about 6000 hr at 1000 F.

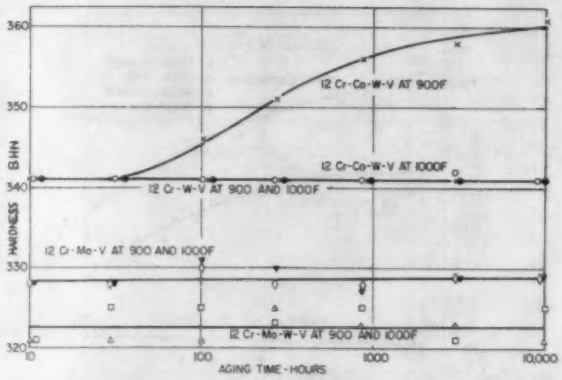

FIG. 9 STATIC AGING CURVES FOR 12 CR-CO-W-V, 12 CR-W-V, 12 CR-MO-W-V, AND 12 CR-MO-V ALLOYS AT 900 AND 1000 F

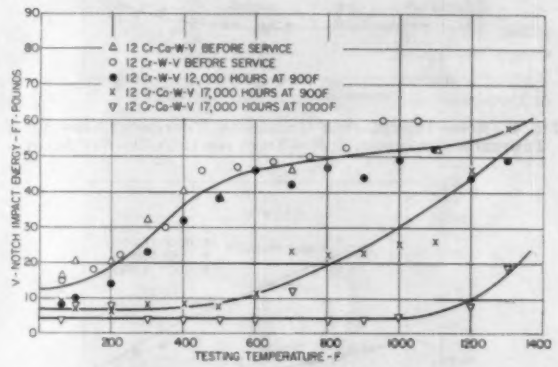

FIG. 10 IMPACT ENERGY-TEMPERATURE CURVES SHOWING IMPACT RESISTANCE OF 12 CR-CO-W-V AND 12 CR-W-V ALLOYS BEFORE AND AFTER SERVICE

PRECIPITATION REACTIONS IN IRON-CHROMIUM ALLOYS

Only recently have sufficient data been accumulated on simple iron-carbon and iron-chromium systems to permit an understanding of what might occur on tempering and aging modified 12-chromium alloys containing as many as nine additional elements. The low impact resistance which appears in high-purity iron-chromium alloys containing more than 15 per cent chromium after long-time heating between about 1050 F (565 C) and 1380 F (750 C) is well understood; it is caused by excessive precipitation of the hard brittle sigma phase. Another form of instability, usually termed 885 F (475 C) embrittlement, occurs in the same alloys after relatively short heating periods within the temperature range of 700 F (370 C) and 1050 F. Although high stresses increase the kinetics of sigma formation, they have little effect upon 885 F embrittlement. Williams (3) and Fisher, Dulis, and Carroll (4) have uncovered a new approach in interpreting the latter phenomenon.

On obtaining hardness, electrical resistivity, and magnetic measurements upon high-purity iron-chromium alloys, Williams rationalized his data by postulating that a miscibility gap is present in this system below a eutectoid temperature of about 970 F (520 C). Depending upon chromium concentration, various percentages of chromium-rich ferrite will coexist in equilibrium with the ferrite matrix. Shortly above 970 F, chromium-rich ferrite is metastable and will eventually be replaced by sigma phase; at still higher temperatures only sigma can appear. Addition of manganese and silicon is thought to expand the solubility limits and decrease the temperatures at which these reactions occur. By means of electron microscopy and diffraction, Fisher, Dulis, and Carroll observed the formation of chromium-rich ferrite to accompany 885 F embrittlement. Their extraction-replica technique (5) permitted separation of chromium-rich ferrite particles from specimen surfaces; these particles appeared to be spherical, about 200 Å in diameter, body-centered cubic in structure, and contained about 85 per cent chromium. Specimen hardness is increased and impact resistance is decreased by the high degree of chromium-rich ferrite dispersion accompanied by internal strains. After an initial incubation period, the nucleation rate of chromium-rich ferrite is high, and its growth rate is low. Because the crystal structure of a sigma-phase nucleus is complex and requires about 30 atoms per unit cell, the nucleation rate of sigma is low. Brittle sigma phase does not cause a noticeable hardness increase until it occupies about 15 per cent of the base alloy; in 12 Cr-Co-W-V specimens less than 10 per cent sigma was found to form. Neither precipitation reaction is normally expected in alloys containing only 12 per cent chromium.

X-RAY PHASE IDENTIFICATION

To investigate whether modified 12-chromium alloys show the same precipitation reactions seen in high-purity alloys, an extensive phase-identification program was undertaken. Since both carbides and sigma are noble relative to ferrite, they can be separated by electrolytic extraction. A service-exposed specimen is used as the anode, and a copper strip is used as the cathode. Both electrodes are immersed in 10 per cent hydrochloric acid, and a current of about 1.0 amp is passed through the electrolyte under a d-c potential of 1.0 volt for 15 hr. The ferrite matrix

and chromium-rich ferrite particles are dissolved; the carbides and sigma fall to the bottom of the electrolytic bath where they can be later collected by filtration.

Diffraction patterns of residues are obtained by using a General Electric x-ray spectrometer, which provides a record of relative intensities, dispenses with most calculations, and permits a convenient powdered form for specimens. Identification is made by comparison with patterns of pure carbides and sigma phases. No other carbide except $M_{23}C_6$ was found in any of the modified 12-chromium alloys; this is present in tempered and aged specimens. The composition of $M_{23}C_6$ was found from chemical analyses to depend upon alloy composition and heat-treatment. Sigma patterns have been observed in residues extracted from some 12 Cr-Co-W-V specimens exposed under stress at temperatures between 950 F (510 C) and 1200 F (650 C) for 6000 to 32,000 hr; chemical analyses show that the sigma is of the basic FeCr type. No sigma has yet been found to form in any of the other modified 12-chromium alloys under the same conditions. Static aging experiments have failed to cause sigma formation long after it appears; i.e., over 6000 hr, in 12 Cr-Co-W-V specimens held under stress at aging temperatures. Representative x-ray diffraction patterns for residues from 12 Cr-Co-W-V and 12 Cr-Mo-W-V specimens after long-time service exposure are shown in Fig. 11.

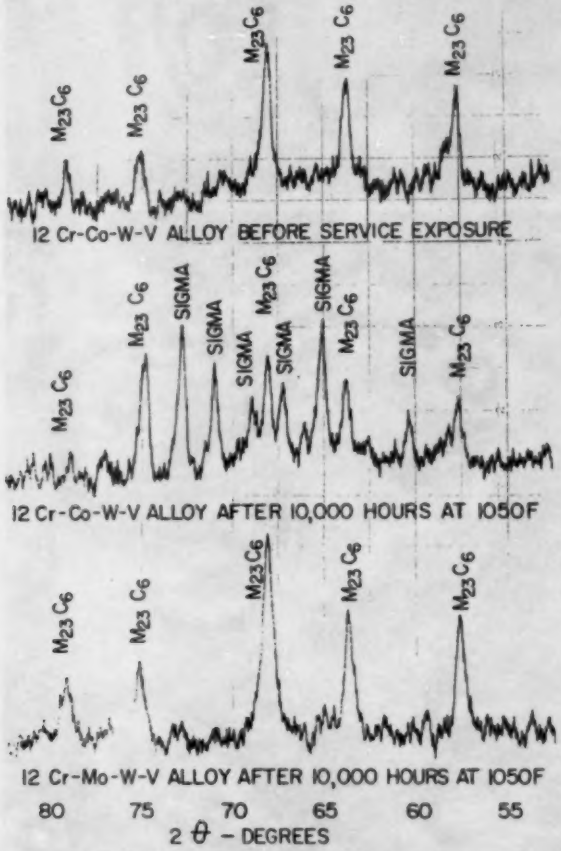

FIG. 11 X-RAY DIFFRACTION PATTERNS OF RESIDUES ELECTROLYTICALLY EXTRACTED FROM 12 CR-CO-W-V AND 12 CR-MO-W-V ALLOYS

(The 2 θ positions result from chromium Kα radiation where wave length λ equals 2.28962 Å.)

ELECTRON MICROSCOPY

The resolving power of optical microscopy is inadequate for phase identification in those 12 Cr-Co-W-V specimens showing etchant darkening and hardness increases on holding at temperatures below 950 F. Figs. 12 and 13 show electron micrographs at 60,000 diameters of 12 Cr-Co-W-V specimens before service and after exposure for 40,000 hr at 900 F. The blocky sigma in a 12 Cr-Co-W-V specimen held for 22,000 hr at 1000 F can be seen in the electron micrograph of Fig. 14. Whenever this phase appears microscopically, x-ray diffraction patterns show positive evidence of the presence of sigma. Widmanstätten precipitation of fine platelets (about 1000 Å in diameter) has been observed within the free ferrite of an overalloyed 12 Cr-Mo-W-V specimen after 22,000 hr at 1000 F, but diffraction patterns of extracted residues show only the presence of $M_{23}C_6$.

To obtain such high resolution, original plastic replicas of the etched metal structure are preshadowed with chromium in a high vacuum at an angle of 15 deg. A thin amorphous carbon film is then deposited at an angle of 90 deg, and the original plastic is dissolved to leave a thin carbon backing supporting a shadowed reproduction of surface irregularities. High points on the original replica (or depressions in the metal structure) have more chromium and are therefore darker in the electron micrographs. All electron micrographs are printed as negatives of optical micrographs. The electron micrograph of an embrittled specimen (Fig. 13) shows an array of spherical holes in the matrix, represented by black dots on shadowing, which are about 250 Å in diameter. These holes are apparently caused by etchant attack upon low-chromium regions immediately adjacent to chromium-rich ferrite particles. Few, if any, spherical holes can be seen in electron micrographs of before-service and retempered specimens.

On etching embrittled specimens with Vilella's reagent through the original plastic replica, it is possible to free from the ferrite matrix those chromium-rich ferrite particles which are embedded in the plastic. Fig. 15(*a*) is an electron micrograph of an extraction replica showing large tempered carbides and very fine chromium-rich ferrite particles present in the same specimen used for Fig. 13. An electron-diffraction pattern obtained from beam transmission through the afore-mentioned extraction replica, Fig. 15(*b*), discloses a network of reflections from carbide single crystals and a crystalline ring pattern from fine chromium-rich ferrite particles. With body-centered cubic lattices, there are characteristic reflections for only even values of $(h^2 + k^2 + l^2)$; the h, k, l indexes of the rings seen in Fig. 15(*b*) are (110), (200), (211), and so on. X-ray diffraction of the etched surfaces of embrittled specimens shows just a slight broadening of the original body-centered cubic ferrite lines, which may be a strain effect. Distinguishing between lattice parameters of chromium-poor ferrite and chromium-rich ferrite is also below the sensitivity of electron diffraction. Conclusive evidence then depends upon determining the magnetic properties of the fine residue seen in Fig. 15(*a*), since chromium-rich ferrite is paramagnetic.

The critical experiment performed for identification of chromium-rich ferrite in extraction replicas was to hang, with a thin cotton thread, a copper grid covered with plastic for simple replication, a grid carrying the extraction replica for Fig. 15(*a*), and a grid covered with plastic plus high-purity iron particles of less mass than extracted particles within a cored magnetic field. Only the grid carrying iron was attracted to the magnetic core; the extraction replica was unaffected by high magnetic-field strengths.

DISCUSSION

Except for the addition of more components, precipitation reactions in 12 Cr-Co-W-V alloy are similar to those occurring in

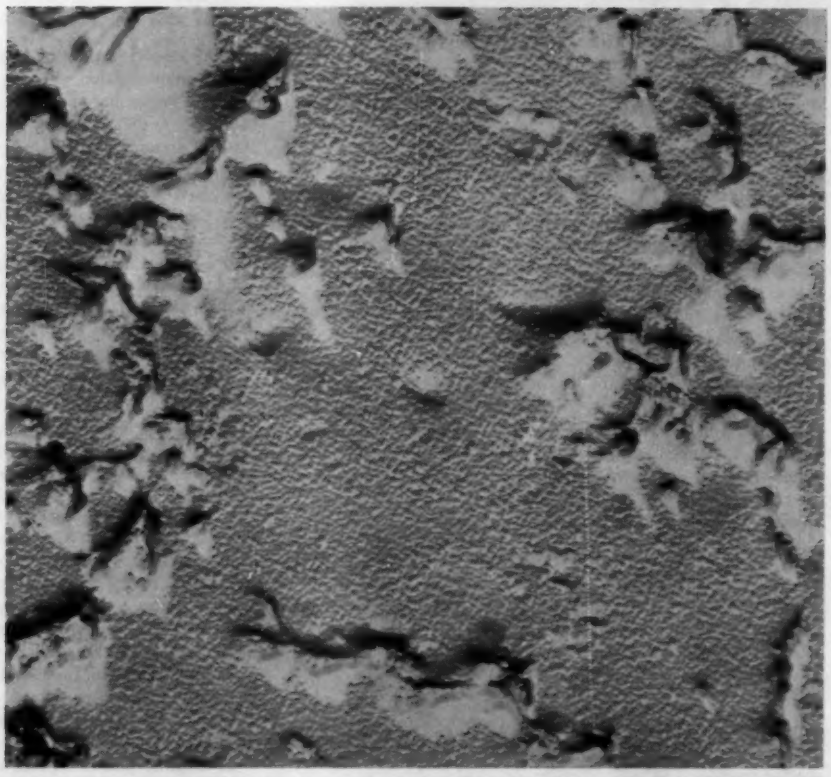

FIG. 12 ELECTRON MICROGRAPH AT 60,000× OF 12 CR-CO-W-V ALLOY BEFORE SERVICE
(Replica was chromium shadowed at 15 deg.)

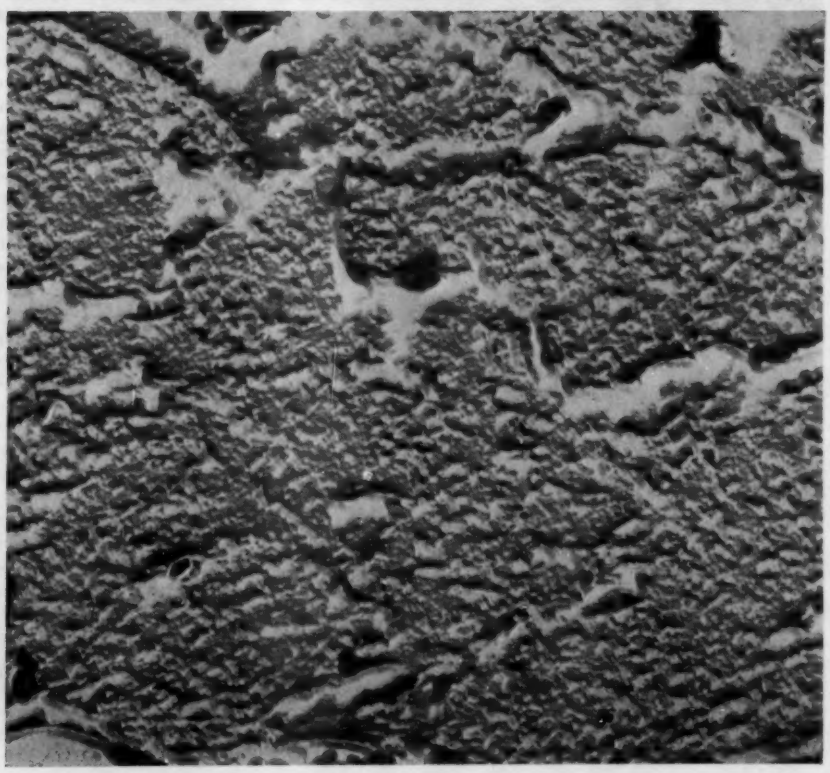

FIG. 13 ELECTRON MICROGRAPH AT 60,000× OF 12 CR-CO-W-V ALLOY AFTER EXPOSURE FOR 40,000 HR AT 900 F

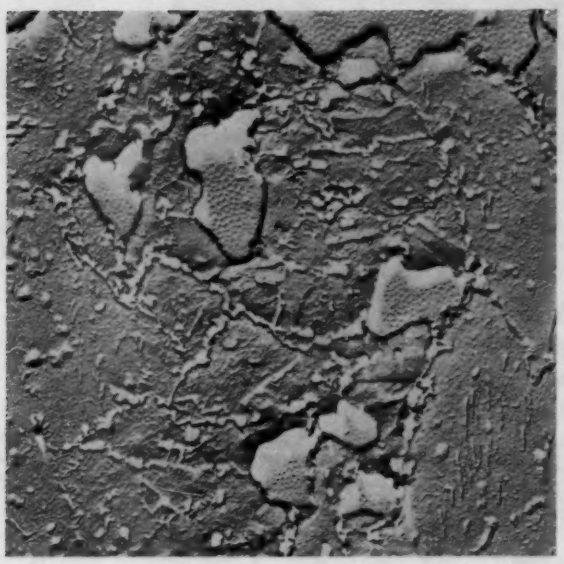

FIG. 14 ELECTRON MICROGRAPH AT 10,000× OF 12 CR-CO-W-V ALLOY AFTER EXPOSURE FOR 22,000 HR AT 1000 F SHOWING APPEARANCE OF BLOCKY SIGMA

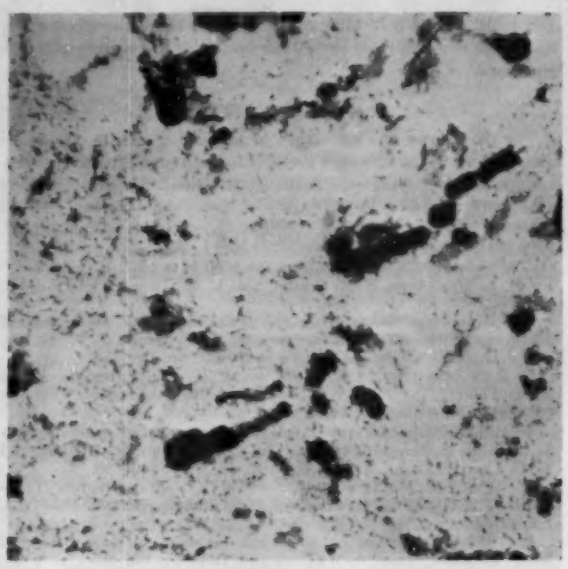

FIG. 15(a) ELECTRON MICROGRAPH AT 30,000× OF EXTRACTION REPLICA SHOWING TEMPERED CARBIDES AND FINE CHROMIUM-RICH FERRITE PARTICLES

high-purity iron-chromium alloys. The effects upon mechanical properties have been observed, and the precipitation phases have been identified. Of course, variations in temperature, alloy segregation, and stress always cause some uncertainty in predicting the exact structural stability of service-exposed components. To date, there has been no evidence of any precipitation reactions in other modified 12-chromium alloys.

It is generally known (6) that chromium, manganese, tungsten, and molybdenum are alloy elements which increase the thermodynamic feasibility and rate of sigma and chromium-rich ferrite formation; some investigators report that cobalt increases the rate of sigma formation. In the ferritic matrix of 12 Cr-Co-W-V alloy, the chromium, manganese, and tungsten content has been chemically analyzed and has been found to be higher than in other modified 12-chromium alloys. A slight decrease in chromium content should increase structural stability without sacrificing mechanical properties. The presence of cobalt may catalytically influence precipitation-reaction rates as a function of its electronic properties; in addition, cobalt may decrease carbide stability so that chromium can diffuse to adjacent regions in increased concentration. The presence of these elements displaces equilibrium solubility limits to lower chromium contents and temperatures, thus explaining the surprising observation of precipitation reactions in 12 Cr-Co-W-V alloy and not the others.

CONCLUSIONS

1 The temperature at which austenite first appears on heating modified 12-chromium alloys is fairly constant at 1500 F; the $M_{23}C_6$ carbides dissolve on further heating at about 1750 F for Type 403 and 12 Cr-Cb, 1800 F for 12 Cr-Co-W-V, 1900 F for 12 Cr-Mo-W-V, and 2000 F for 12 Cr-W-V and 12 Cr-Mo-V alloys.

2 As a result of increased carbide stability, modified 12-chromium alloys exhibit high rupture strength and tempering resistance in comparison to Type 403 alloy.

3 Static-aging tests show that only 12 Cr-Co-W-V alloy significantly increases in hardness after about 200 hr at 900 F; no hardness increase appears after static aging for 10,000 hr at 1000 F.

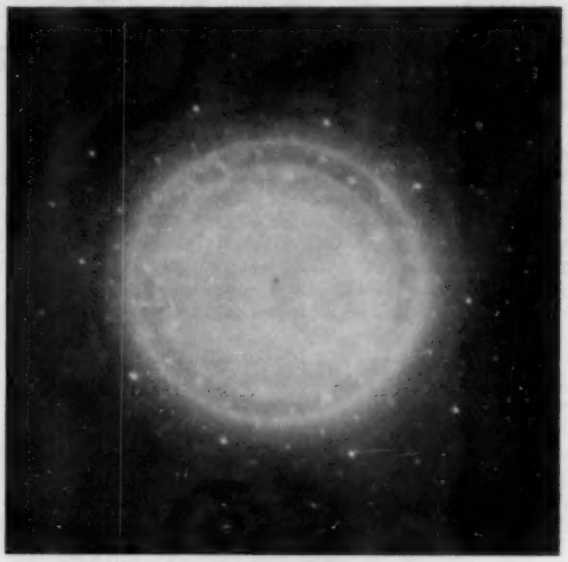

FIG. 15(b) ELECTRON DIFFRACTION PATTERN OF REPLICA IN FIG. 15(a)

4 However, 12 Cr-Co-W-V specimens decrease in impact resistance after exposure under stress for longer than about 6000 hr at 950 to 1200 F; sigma patterns have been observed in residues extracted from these specimens.

5 Electron micrographs and diffraction patterns show the presence of ferrite particles on extraction replicas from 12 Cr-Co-W-V specimens aged for relatively short times between 800 and 950 F; the paramagnetic properties of these extracts indicate high chromium content.

6 Of the modified 12-chromium alloys studied, the higher chromium, manganese, and tungsten content of the ferritic ma-

trix in 12 Cr-Co-W-V alloy and a possible catalytic effect of cobalt upon reaction rates causes susceptibility to two precipitation reactions.

Acknowledgment

For permission and assistance in publishing results of this investigation, the authors are grateful to the Large Steam Turbine-Generator Department, Turbine Division, General Electric Company.

BIBLIOGRAPHY

1 "Some 12-Chromium Alloys for 1000 F to 1200 F Operation," by D. L. Newhouse, B. R. Seguin, and E. M. Lape, Trans. ASME, vol. 76, 1954, pp. 1107–1122.

2 "Isothermal Transformation, Hardening and Tempering of 12-Chromium Steel," by R. L. Rickett, W. F. White, C. S. Walton, and J. C. Butler, Trans. ASM, vol. 44, 1952, pp. 138–175.

3 "An Investigation Into the Aging of Iron-Chromium Alloys Around 500 C," by R. O. Williams, Doctorate Dissertation, Carnegie Institute of Technology, 1955.

4 "Identification of the Precipitate Accompanying 885 F Embrittlement in Chromium Steels," by R. M. Fisher, E. J. Dulis, and K. G. Carroll, Trans. AIME, vol. 197, 1953, pp. 690–695.

5 "Electron Microstructure by the Extraction-Replica Technique," by R. M. Fisher, ASTM Special Publication No. 155, 1953, pp. 49–64.

6 "885 F Embrittlement in Stainless Steels," by A. J. Lena and M. F. Hawkes, Trans. AIME, vol. 200, 1954, pp. 607–615.

Discussion

D. L. Newhouse.[4] The authors are to be complimented for their identification of two different embrittling reactions with overlapping and only slightly differing symptoms. The fact that these reactions were observed only in the 12 Cr-Co-W-V material of the six alloys described is of considerable interest.

The subtle nature of the reactions and their effects described in this paper illustrate very well the problems facing the metallurgist in the development of materials for long-time, high-temperature service. In the case of 12 Cr-Co-W-V alloy, the "885 embrittlement" reaction could be produced by relatively short-time laboratory aging tests, but its effects are rather readily obscured by testing variables and the reaction is most noticeable at aging temperatures below those of usual interest and testing for this alloy. The sigma-phase precipitation apparently occurs only after very much longer exposure at 1000 F or above, and under conditions of stress. Both reactions may vary in their intensity and effect on ductility with normal variations in chemical composition, and perhaps also with heat-treatment or hardness level.

It seems apparent that, to obtain reasonable assurance of freedom from deterioration of properties in long-time high-temperature service, long-time exposure tests must be run duplicating as closely as is feasible actual operating conditions, and that material exposed to long-time aging must be most critically examined for clues to such changes. As the authors point out, long-time creep tests can sometimes furnish such information, but generally offer very little material for after-creep evaluation of possible embrittlement.

To obtain such information on currently used and possible new high-temperature materials, the company with which the authors and the writer are associated has had in progress for some time, long-time aging tests directed toward revealing metallurgical changes which may occur and their effect on properties.

[4] Supervisor, Forging Development, Materials and Processes Laboratory, Large Steam Turbine-Generator Department, General Electric Company, Schenectady, N. Y.

Review of the Pitot Tube

By R. G. FOLSOM,[1] ANN ARBOR, MICH.

This paper is an attempt to bring together the important information regarding Pitot tubes and their use; to summarize the available data on the application of various types of impact and velocity probes for the guidance of engineers and research workers; and to aid them in the design of flow instruments for specific applications.

Introduction

MODERN engineering practice and research frequently require the measurement of a fluid velocity (both magnitude and direction) at a given point in a flow field. Tubes of various sizes and ingenious shapes have been constructed and calibrated for a large number of conditions. Although many valuable data appear scattered throughout the technical literature, there appears to be a dearth of articles providing a summary of pertinent information for the designer and user of such equipment. This paper is an attempt to summarize most of the available material about such tubes. It will have achieved its objective if this paper eliminates the necessity of some user wasting time in the development or calibration of an unsatisfactory velocity-measuring probe.

Apparently, the first description of a tube used to measure pressures for velocity determinations was by Henri Pitot in 1732 (1)[2] and tubes for this purpose have frequently been named after him. He described a tube to meet a practical problem; namely, the determination of whether the fluid velocities in a river were higher near the bottom than they were near the surface. The name "Pitot tube" has been applied to two general classifications of instruments, the first being a tube that measures the impact or total pressures only, and the second a combined tube that measures both the impact and the static pressures with a single primary instrument. Darcy mentioned improvements to the instrument in 1854 (2, 3). Airey (15) and Guy (16) give a reasonable summary of the history and status of information about the tubes up to about 1910.

As late as the period from 1900 to 1915, lengthy discussions were held about the fundamental form of the basic equation that applied to Pitot tube measurements. The two forms were

$$V = \sqrt{2gh}$$

and

$$V = \sqrt{gh}$$

Typical of the discussions of the period are the papers by White (4, 5) and Gregory (6, 9). Conclusive articles were presented by Rowse (17), Moody (18), and Groat (19). Attention during the 1920's was devoted principally to a study of the various shapes of tubes for special conditions and to an investigation of some of the limitations in the use of the tubes. The rapidly growing field of aeronautics presented a fruitful area for application of velocity-measuring probes. Also, the general progress of fluid mechanics required more information about the internal mechanism of the flow system, with the result that more emphasis was placed on determining velocity distributions in a wide variety of circumstances.

During the 1930's there was a revived interest in studying the fundamentals of the Pitot tube and other velocity-measuring tubes as applied to water measurements for quantity rate-flow determinations. The papers by Hubbard (60), Cole (45, 46, 59), and Allen and Hooper (39) are examples of this interest.

Since the late 1930's there has been widespread application of velocity-measuring tubes to compressible fluids, incompressible fluids at sub and supersonic velocities, multiphase fluids, viscous and turbulent-flow phenomena, boundary-layer investigations (basic to heat transfer and fluid friction), fluids passing through cascade systems as in turbomachinery, air speed of airplanes, rockets, upper-atmosphere investigations, and other scientific and engineering problems. This widespread usage developed from a demand for more fundamental information about fluid flow in order to understand the mechanisms involved and to be able to evaluate predictions based on theoretical considerations. A wide range of engineering and scientific literature contributes to our present knowledge about velocity probes.

Although the ASME Power Test Codes for Hydraulic Prime Movers (77) and the Special Research Committee on Fluid Meters (34) describe velocity-measuring tubes of various kinds, the information regarding the variables involved in their application is largely missing. Books devoted to flow measurement, like Ower (41), Addison (68), and Linford (78), although including some design and application details, provide inadequate discussions of velocity-measuring probes for the normal use of the engineer.

A Pitot tube or similar velocity-measuring device consists essentially of three parts; namely, the head or instrument section, the pressure-connecting lines between the head and the pressure-indicating device, and the indicating device. The discussions of this presentation will be limited to the head or instrument section. It is recognized that the connecting lines and the pressure-measuring device are important elements of the system, but in many respects they are adequately treated elsewhere (111). Although the matter of measurements in pulsating flow is of extreme importance in many applications, this subject will not receive more than a scant mention in this paper since the effect of pulsations cannot be adequately treated without a detailed consideration of the flow in connecting pressure lines and the dynamic characteristics of the pressure-measuring device.

A large variety of geometrical shapes are possible and actually have been used. This complicates the problem when one attempts to analyze and correlate available data for presentation in summarized but adequate form. Any suitable opening in a reasonable geometrical shape will provide a pressure approaching closely the total or impact pressure. Also, any difference in pressure between two pressure openings can be calibrated in terms of velocity or, if the tube is installed in a pipe line, against the rate of flow. This paper attempts to correlate similar phenomena

---

[1] Professor of Mechanical Engineering and Director of the Engineering Research Institute, University of Michigan. Mem. ASME.

[2] Numbers in parentheses refer to the Bibliography at the end of the paper.

Contributed by the Research Committee on Fluid Meters and presented at the Diamond Jubilee Annual Meeting, Chicago, Ill., November 13–18, 1955, of The American Society of Mechanical Engineers.

Note: Statements and opinions advanced in papers are to be understood as individual expressions of their authors and not those of the Society. Manuscript received at ASME Headquarters, November 14, 1955. This paper was not preprinted.

associated with probes, giving references to guide the reader to specific calibration information.

Flow Systems

Many flow situations approach closely a one-dimensional flow system. Wind-tunnel and water-tunnel throat sections are designed for constant velocity outside the boundary layer, i.e., a one-dimensional flow system. Usually, the direction is known, due to the location of the solid boundaries, and the problem is to determine the magnitude of velocity. For this simple flow system Pitot or Pitot-static tubes are suitable instruments for velocity-distribution determinations. The following definitions will be used:

(*a*) *Pitot Tube.* A cylindrical tube with an open end pointed upstream, used in measuring impact pressure.

(*b*) *Pitot-Static Tube.* A parallel or coaxial combination of a Pitot and a static tube. The difference between the impact pressure and the static pressure is a function of the velocity of flow past the tube.

Bernoulli's equation is applied most frequently on the basis of the average velocity, which corresponds to the assumption of one-dimensional flow across the cross section considered. Frequently, in practice, two-dimensional flow considerations more nearly approach actual conditions; i.e., the real velocity distribution in pipe flow when symmetrical about the pipe axis. When the magnitude of the kinetic-energy term becomes important, the velocity distribution must be known in order to evaluate α in the equation

$$\text{Kinetic energy (ft-lb/lb)} = (\alpha V_a^2)/2g$$

when the velocity distribution is symmetrical with respect to the pipe axis

$$\frac{\alpha V_a^2}{2g} = \frac{\int_0^R 2\pi r \frac{w}{g}\frac{u^3}{2} dr}{\int_0^R 2\pi r w u dr}$$

and

$$\alpha = \frac{\int_0^A V^3 dA}{AV_a^3}$$

where

A = area of cross section of flow
V = average velocity for area dA
V_a = average velocity for area A
r = radius to center of area dA
R = inside radius of pipe
u = velocity at radius r
$Q = AV_a$ = quantity rate flow through area A

The problem of velocity-measuring probes for two-dimensional flow is complicated because it becomes necessary to measure pressures in velocity gradients and frequently the direction of flow is unknown. In general, a two-dimensional probe measures an average magnitude and direction of velocity in a small area rather than at a point in a two-dimensional flow field. An example of a typical instrument is a circular cylinder with two or three pressure-tap holes which is placed with its axis perpendicular to the plane of symmetry of the flow.

In turbomachinery, process equipment, and other cases, it is desirable to know the magnitude and direction of the velocity at any point within the flow system. A probe with a spherical (36) or claw head containing five pressure taps forms a suitable instrument for such measurement.

Tube Shape

Impact Total Pressure. The results obtained by a large number of investigators have demonstrated that, if the shape of the Pitot head is one in which a stagnation point exists in the flow system, the full impact pressure is measured at a tap located at the stagnation point. It should be pointed out that this conclusion applies only to a uniform-velocity flow field such as that obtained in a wind tunnel or at the center-line position in a pipe, where the velocity gradients with respect to the radius are small and thus the flow approaches one of uniform velocity in the vicinity of the tube. It is conceivable that the full impact pressure would not be measured in the case where the flow about the tube head is changed due to mutual interference effects between the tube and a solid boundary or the tube and a liquid-free surface. The influence of impact-tube size in a uniform-velocity stream was checked by Zahm (31), using a $^1/_8$-in-diam square-ended tube against a 5-in-diameter pipe as well as a $^1/_8$-in. glass tube against a 0.01-in-ID hypodermic needle. Both checks gave the same impact pressure within instrumentation tolerances. The ability of Pitot tubes to determine the true impact pressure for a wide range of geometrical shapes has been recognized for a long time, a typical statement in this respect being given by Zahm (8) in 1903: "Almost any size and form of nozzle will convey the impact perfectly, providing it squarely face the wind."

The most common type of Pitot tube has the head mounted on

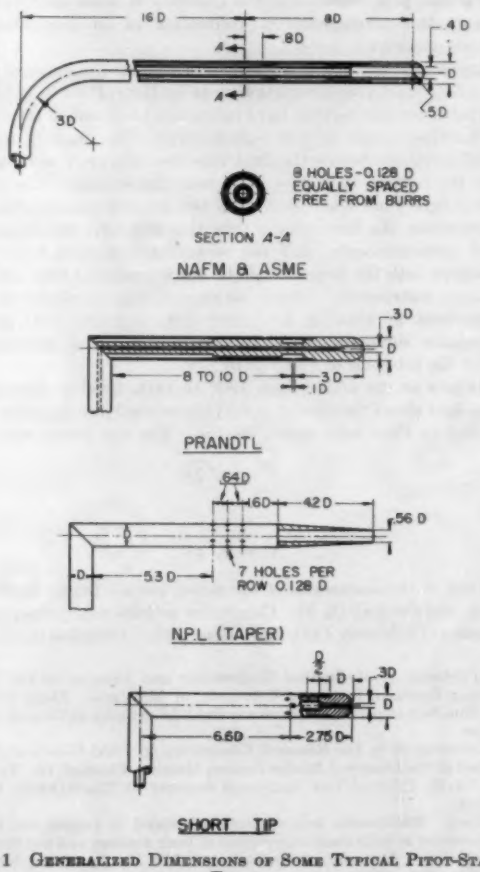

Fig. 1 Generalized Dimensions of Some Typical Pitot-Static Tubes

a support stem. The axis of symmetry of the head is parallel to the direction of the velocity and perpendicular to the axis of its stem. The head may have an impact-pressure tap, one or more static-pressure taps, or both impact and static taps in the same head, the latter forming a Pitot-static tube. The generalized dimensions of some typical Pitot-static tubes are given in Fig. 1.

A wide variety of head-tip shapes have been investigated, a general classification being presented in Fig. 2. It should be noted that only two examples of possible combinations of basic types are given. It is necessary to consider the addition of a miscellaneous group classification in order to cover many shapes investigated for special purposes, such as the wedge or cone for static-pressure determinations in supersonic flow.

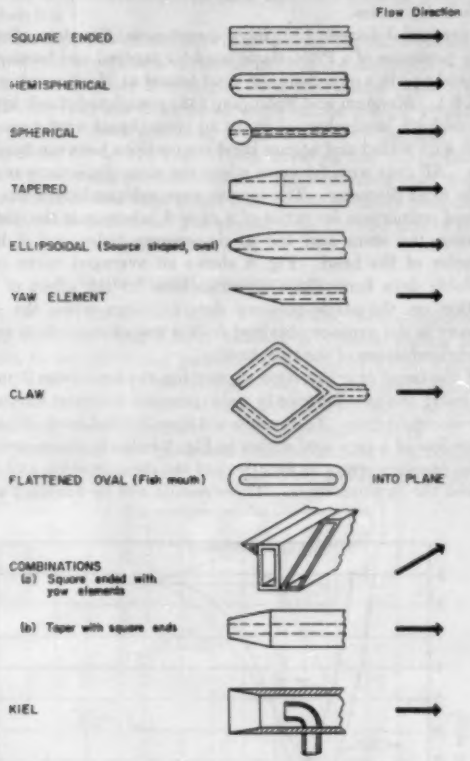

FIG. 2 TYPICAL HEAD SHAPES FOR PITOT TUBES

Typical of experiments relating to the magnitude of the impact pressure measured by Pitot heads of different shapes is the work of Merriam and Spaulding (48) and Ower and Johansen (30). Cole, in the discussion of Hubbard's work (60), presents a series of tests for tubes in a pipe. Merriam and Spaulding have investigated the effect of the size of the pressure tap with respect to the diameter of the Pitot head in the case of a hemispherical tip within the range of $0.2 < d/D < 0.74$ and found that the size of the hole has no effect on the magnitude of the impact pressure measured at zero yaw. On the other hand, to obtain the true impact pressure, the problem of alignment in yaw of the Pitot head is much more critical in the case of the smaller pressure-tap sizes.

Another common type of tube is formed by installing pressure taps at suitable locations in a tube of uniform cross section placed with its axis perpendicular to the direction of the flow field. The tube may project into the fluid stream from one boundary or it may pass through the fluid stream with the pressure taps located near the middle portion. The tubes projecting into the stream have been designated as cantilevered Pitot cylinder (114), cylindrical impact tube (43), and heavy-duty Cole Pitometer (77). The common head shapes are square-ended, hemispherical, ellipsoidal (oval shaped), and spherical when the tube does not span the flow. The cross-section shape is circular or of some type of streamlined section. In the event the tube passes through the flow field, the probe is known as a transverse tube. In the usual case, the cross section is circular. This type of tube has been designated a transverse Pitot tube (57), Pitot cylinder (69), Collins tube (57), and streamlined Pitot-tube bar (117).

Static Pressure. In some cases of flow in pipes it is possible to obtain a suitable measurement of the static pressure from a piezometer installed in the pipe wall. Allen and Hooper (39) investigated types of construction and magnitudes of errors of such pipe-piezometer installations for the determination of static pressure. Within the range of tests in a 12-in-diam pipe with average water velocities up to 7.3 fps, variations in the size of piezometer hole from $^1/_{16}$ to $^{27}/_{32}$-in diameter have no effect. A true square-edged hole without edge burrs, flush with the inside pipe wall, and with a depth of constant cross section for at least two diameters, provides an accurate piezometer when there are no fluid swirls or crossflow. A slight rounding (radius of curvature less than one fourth of hole diameter) does not change the reading of the piezometer and is easier to produce than a sharp edge without burrs. Errors due to a variety of poor constructions were found to be expressible in terms of a constant percentage of local velocity head existing at the orifice for each type of piezometer. Comparison of readings from piezometers installed downstream from a 90-deg elbow will provide some information about effects of crossflow and swirls on static-pressure measurements. Angus (56) has made such tests and showed pressure variations up to almost one velocity head. The general pattern of pressure variations remained unchanged over the velocity range of his tests from 5.3 to 17.3 fps.

When a Pitot tube is used in a pipe and the static pressure is determined by a pipe-wall piezometer, the pressure distribution about the Pitot tube stem may affect the piezometer pressure. Hubbard (60) presents data from a 12-in-diam pipe for the magnitude of the pressure and resulting velocity error for various distances of piezometer ahead of the Pitot tube stem and at different positions around the pipe circumference when the stem extends to the middle of the pipe. For example, if the pipe-wall piezometer were situated 45 deg from the plane of the Pitot stem axis, the piezometer should be placed about 3.7 stem diameters ahead of the stem center line to obtain a static-pressure measurement with no error. At 90 deg, the distance becomes 7 diameters. Within the limits of the tests which extend to 180 deg and distances of 12 diameters, an over or underdetermination of velocity magnitude may be made, depending on the relative positions existing for a given arrangement.

When the head of a Pitot tube extends into the region of the plane of a pipe-wall piezometer, the pressure measured by the piezometer tends to be low due to the reduced cross section of flow. For the case of a head-projected area of 0.47 per cent of pipe cross-section area and located at pipe center line, Hubbard (60) found the pressure reduction to correspond to the "venturi effect" calculated on the basis of average velocities when the tip was five or more tip diameters ahead of the plane of the wall piezometer.

With a Pitot-static tube, the magnitude of the pressure sensed at the static-pressure tap may be a function of the shape of the tip and the distance from the tip to the plane of the holes. If the tube head is a body of revolution, potential flow calculations will

provide the approximate pressure distribution. For most real tubes, an experimental calibration is necessary to achieve desired accuracy. Static-pressure distributions on tube heads have been made by several investigators.

Fig. 3 shows the difference in indicated and free-stream static pressures as per cent of dynamic heads for hemispherical tips as found by Ower and Johansen (30) in a closed-throat wind tunnel at Ma < 0.1. Their data on tapered tips showed a similar pressure pattern. Merriam and Spaulding (48) obtained similar results for a wide range of Pitot-static tube tips and static-pressure locations, demonstrating the wide applications possible for the design curves of Figs. 3 and 4. Experimental data by Krause

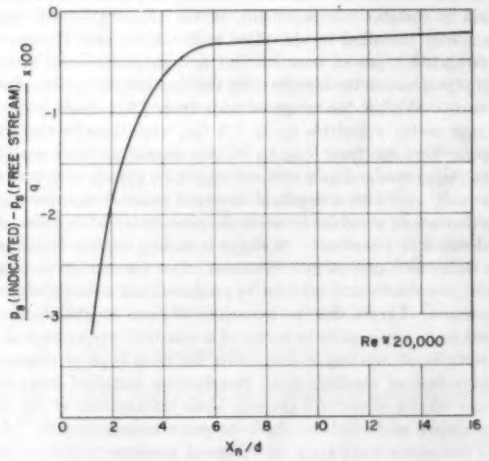

FIG. 3 INDICATED STATIC PRESSURE ALONG TUBE BODY WITH HEMISPHERICAL TIP
(x_n = diameters from base of nose along tube body. Ower and Johansen, reference 30.)

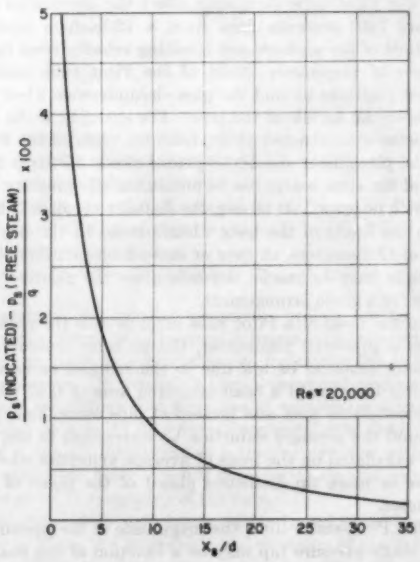

FIG. 4 INFLUENCE OF STEM POSITION ON OBSERVED STATIC PRESSURE (x_s = ▼ stem distance aft of static holes. Ower and Johansen, reference 30.)

(89) for a hemispherical tip show that the reading at the static-pressure taps located from 3 to 7 tube diameters from the tip is unchanged through a velocity range up to Ma = 0.6. At Ma = 0.9, a change in static-pressure coefficient developed.

The Pitot-static tube must have a support to hold the head in position. Generally the support takes the form of a continuation of the head tube by means of a right angle or a 90-deg bend with reasonable radius to form a stem perpendicular to the head. Any object placed in a stream will influence the static pressure upstream from the object. The approximate magnitude can be obtained from potential-flow calculations such as carried out by Zahm (33) and others. For real fluids and unsymmetrical flows about the head and stem it is desirable to measure the differences in static pressure as the position of the stem with respect to the static holes varies.

Ower and Johansen (30) have investigated the stem effect on static pressures of a Pitot-static head for tapered and hemispherical head tips in a closed-throat wind tunnel at Mach numbers less than 0.1. Merriam and Spaulding (48) completed check investigations for a hemispherical tip in an open-throat wind tunnel for tubes with round and square bend connections between head and stem. All data were for cases where the stem diameter was equal to the head diameter. The results were independent of the type of bend connection for ratios of $x_s/d > 4$, where x_s is the distance between the stem and the static-pressure holes and d is the diameter of the head. Fig. 4 shows an averaged curve of the available data from these investigations for the effect of stem position on the static-pressure determination when the static pressure is the average obtained from a row of static taps around the circumference of the tube head.

In the usual case the stem supporting the head joins it on one side only; thus a difference in static pressure will exist around the tube circumference. Test results obtained by Hubbard (60) at the center line of a pipe and shown in Fig. 5 indicate the magnitudes of the pressure errors as functions of the stem location and angle around the circumference. These results will be modified as the

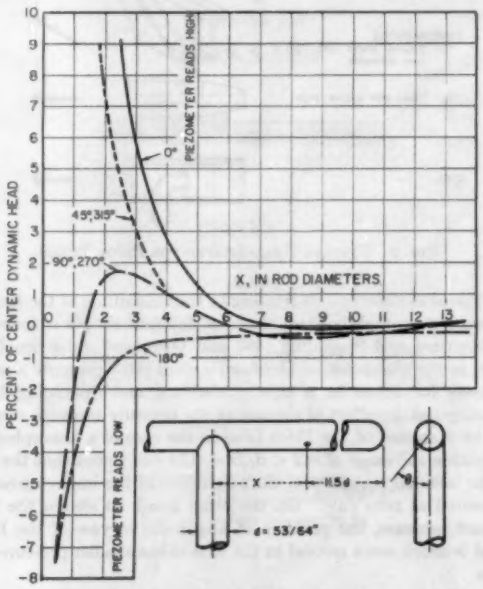

FIG. 5 EFFECT OF STEM LOCATION ON READING FROM STATIC-PRESSURE PIEZOMETER IN PITOT-STATIC TUBE WITH HEMISPHERICAL HEAD; HUBBARD (60)

tube head is displaced from its position at the pipe center line, but magnitudes of variations are not known.

Krause (89) has investigated the stem effects and mutual interference for static-pressure tubes in a rake when used in an open jet. He calls attention to the low registration of a static-pressure sensing device when used in an open jet of limited diameter as compared to an infinite stream. He found the stem effect to be a function of the ratio of stem diameter to jet diameter and of the Mach number in the range 0.3 to 0.9 for the values of $5 < x_s/d_s < 10$, where d_s is the diameter of the stem. He found a change of less than 1 per cent for $2 \times 10^4 < \mathrm{Re} < 9 \times 10^4$. For correct static-pressure measurements for tubes used in a rake, the centerline distance between heads should be greater than 6 head diameters. Greater distances are required if the Mach number becomes larger than 0.6.

Consideration of the difficulties in measuring the static pressure would lead one to expect a variation in pressure distribution determined for a cylinder if different sized piezometer holes were used. Hemke (32) has determined some values using a circular cylinder of 1 in. diam spanning a 6-in-diam open jet with air velocities from 30 to 175 fps. Tests covering the range from 0.008 to 0.25-in-diam piezometer holes demonstrated that hole diameters must be less than about 0.06 in. for accurate pressure-distribution measurements. The pressures on the rear side of the cylinder were independent of hole size.

Fluid-Flow Characteristics

Owing to the requirements of a particular flow-measuring situation, there has been a large amount of interest among investigators in the pitch and yaw characteristics of Pitot, Pitot-static, and other velocity-measuring tubes. An extensive literature provides excellent empirical data over a wide range of flow conditions and tube geometries. Characteristic curves for a typical hemispherical-tip Pitot-static tube as obtained by Merriam and Spaulding (48) appear in Fig. 6. [See Ower and Johansen (30), Hodkinson (66), Markowski and Moffatt (71), Gracey, et al. (86, 87, 95), Russell, et al. (90), and Schulze, et al (99).] These characteristic curves are a function of the geometry of the tube and must be determined for each tube over the expected operating range.

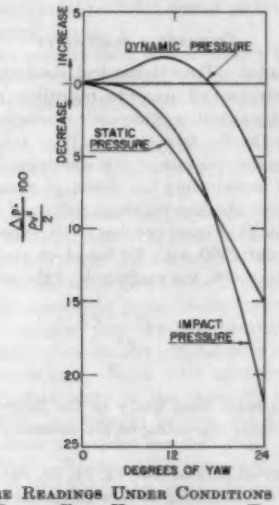

Fig. 6 Pressure Readings Under Conditions of Yaw for a Prandtl Pitot-Static Tube-Hemispherical Tip; Merriam and Spaulding (48)

Investigations, development, and testing of turbomachines such as steam and gas turbines, axial and radial air compressors, and centrifugal pumps require reliable flow-surveying instruments. Flow characteristics of greatest concern include total pressure, static pressure, velocity direction and magnitude, and temperature. Although extremely important, temperature probes are considered to be beyond the scope of this paper. Meyer and Benedict (100) present a brief summary on performance and design characteristics of claw, cylindrical (cantilevered Pitot), spherical, disk averaging, and rake probes. Markowski and Moffatt (71) give corresponding material on micro-Pitot-static, Kiel, cylindrical, and three-dimensional cylindrical probes. Schulze, Ashby, and Erwin (99) compare the performance of several probes for this service and find high-sensitivity yaw indication with simple yaw-element probes when the angle of slant is between 30 and 60 deg relative to the tube axis, maximum directional sensitivity for the claw-type probes when the included angle between the two yaw-element tubes is 120 deg, and that several miscellaneous combination probes will provide suitable information.

Velocity Gradient. Limited experiments (55) have demonstrated that when a tube is used in a two-dimensional velocity field, the effective center of the total pressure of a square-ended circular impact tube is displaced from the geometric center toward the region of higher velocity. The experiments covered the range of $0.35 < d/D < 0.75$ and

$$0.1 < \frac{\frac{D}{\rho V^2} d \left(\frac{\rho V}{2}\right)^2}{\frac{2}{dx}} < 1.2$$

with the results being expressed in $\delta/D = 0.131 + 0.82d/D$, where d = internal diameter, D = external diameter, δ = displacement of effective center of total pressure, and x = co-ordinate transverse to velocity. The air velocities were low and provided essentially incompressible flow conditions. Data were obtained in the wake of an airfoil where the tube was free from wall mutual interference and also in the boundary layer of a model airship hull where mutual interference existed. Results of these tests have been applied generally to other tubes of different nose shape due to the lack of specific data regarding those shapes.

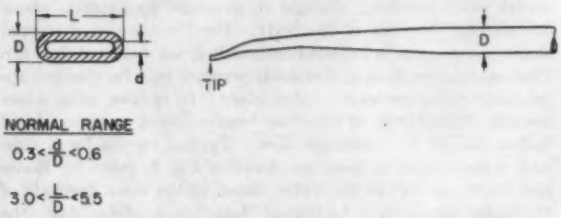

Fig. 7 Impact Tube for Boundary-Layer Measurements

Impact tubes with square-ended flattened oval sections (fish mouth), Fig. 7, have been used for boundary-layer velocity-distribution measurements in order to reduce the displacement effect (88, 97, 107). Livesey (109) states, without presenting the supporting experimental evidence, that for incompressible flow, the displacement error is a function of the solidity of the cross section of the probe tip and the aspect ratio of that tip. Livesey recommends a displacement correction of $0.15 < \delta/D < 0.18$. On the basis of boundary-layer measurements O'Donnell (106) shows that measurements are subject to tube interference if $D/\lambda > 0.22$, where λ is laminar boundary-layer thickness. Livesey also points out that there is no consistent indication of a displacement error in compressible sub or supersonic flow.

Blue and Low (102) made laminar boundary-layer velocity

measurements under identical conditions with a series of flattened oval impact tubes. The thickness ratios varied by $0.20 < d/D < 0.72$, the aspect ratio by $2.5 < L/D < 16.6$, and the solidity correspondingly. These tests made in air with $2 < \text{Ma} < 3$ were in the range of no low Reynolds number effects. The results determined with each probe showed that the variations of measured boundary-layer momentum thickness were of greater magnitude than could be explained by correcting for the effective center-line displacement (55) on the basis of presently available data.

Turbulence. Turbulence in the fluid stream may have a decided effect on the flow in a system, such as changing the boundary-layer characteristics, including the separation point (if one exists) (112), and producing a pressure reading on a Pitot-static higher than the true mean pressure. On the basis of the theory of isotropic turbulence, Goldstein (53) obtains the expressions for the pressures as

$$\text{Total head} = p + \frac{\rho q^2}{2} + \frac{\overline{\rho(q')^2}}{2}$$

$$\text{Static pressure} = p_s + \frac{\overline{\rho(q')^2}}{6}$$

where q is the resultant mean velocity and q' the resultant turbulent velocity. Flow in pipes does not exhibit isotropic turbulence, and Fage (54) calculated on the basis of turbulence measurements (42)

$$\text{Static pressure} = p_s + \frac{\overline{\rho(q')^2}}{4}$$

[See Grossman (101) and Laufer (103) for additional pipe-turbulence data.]

For the usual degree of turbulence at sections in pipes of fully developed velocity distribution, the turbulence errors are small and tend to equalize in the velocity determination (49). For higher degrees of turbulence it is possible for the turbulence errors to reach appreciable magnitudes in terms of the dynamic pressure (83).

Cavitation. When the local pressure in the vicinity of a body submerged in flowing liquid is reduced sufficiently, cavitation occurs, with resulting changes in pressure distribution about downstream portions of the body. For Pitot tubes of normal shape, no changes in impact-head reading are expected, but if a Pitot-static tube is used, the static pressure may be changed appreciably when cavitation takes place. In studies using water tunnels, a large body of data has been collected on symmetrical bodies subject to cavitation flow. Typical results for a tube with a hemispherical head are shown in Fig. 8, taken by Rouse and McNown (72) in the water tunnel of the Iowa Institute of Hydraulic Research. Additional data are available from the work of the David W. Taylor Model Basin, California Institute of Technology, and Pennsylvania State University.

Multiphase Fluids. If condensation takes place when a condensable vapor exists in the fluid, the velocity and temperature downstream from the condensation region will differ from corresponding properties in the undisturbed air (67). Care must be used in the interpretation of measurements obtained under such conditions. Pearcey (92) made experimental studies in wind tunnels with water vapor in the air and a Mach number range of 0.5 to 0.8 and found that condensation caused a loss in total head which depended on supersaturation phenomena.

Modified impact tubes may be used to determine impact pressures in two-phase fluid streams. Examples would be the gas-velocity measurement when liquid or fine solid particles are involved in the stream. Difficulties arise because of plugging and reading changes due to the influence of the momentum exchange between gas and particles upstream and within the instrument. The tendency to plug can be reduced by venting the tube at the rear through a nozzle having an area of about 5 per cent of the inlet area. Dussourd and Shapiro (115) have theoretically and experimentally studied the momentum-exchange effects on pressures for a deceleration probe with static taps located in the inside wall of the probe head. Good correlation of theory and experiments was shown to exist in the overpressure recorded with the tube. Practical calibration data are available in the original articles.

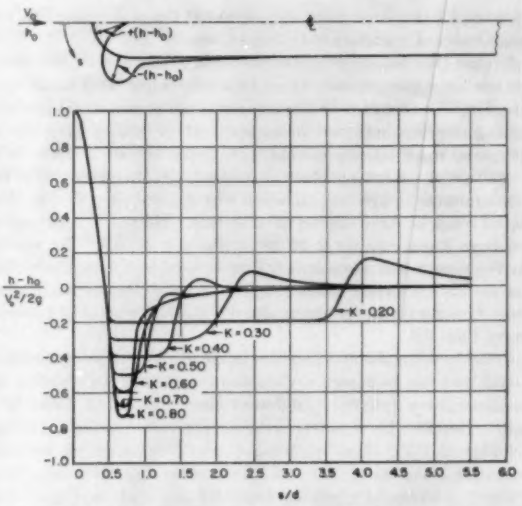

FIG. 8 EFFECT OF CAVITATION UPON PRESSURE DISTRIBUTION ON A CYLINDRICAL BODY WITH A HEMISPHERICAL HEAD ($K = [h_0 - h_v]/[V_0^2/2g]$, where h_v = vapor-pressure head, d = diameter of cylindrical body. Rouse and McNown, reference 72.)

DYNAMICAL SIMILARITY

Reynolds Number. True dynamical similarity requires geometrical similarity in all respects regarding probe and flow-system boundaries as well as kinematic similarity. If dynamical similarity exists for the flow about a Pitot tube, the Reynolds number becomes the measure of this condition, i.e., Re = const. A wide range of experiments has shown no change in Pitot tube pressure-coefficient characteristics at values of Re greater than about 500 and for Pitot-static probes (NPL type) at values of Re greater than about 2300 with Re based on probe-head external diameter. At $\text{Re} < 500$, the magnitude of the pressure coefficient

$$C_i = \frac{p_i - p_\infty}{\frac{\rho V_\infty^2}{2}}$$

is increasingly greater than unity as the Reynolds number decreases, actual values depending on the geometry of the probe and impact opening.

Theoretical investigations (50, 73, 74, 79, 96) have been made for the purpose of calculating the low Reynolds number effects on the impact-tube pressure coefficient in incompressible fluids. One procedure has been to integrate the momentum equation along the upstream stagnation streamline from the stagnation point to the free stream for specified velocity variations in the vicinity of the stagnation streamline. Approximate velocity distributions at appropriate Reynolds numbers have been based on Stokes, Oseen, and potential flow with boundary-layer considerations. The geometrical shapes have included spheres, cylinders, and prolate

TABLE 1 THEORETICAL PRESSURE COEFFICIENTS FOR IMPACT TUBES WITH DIFFERENT SHAPES OF PROBE HEADS

Flow	Stokes	Ossen	Low Re
Approximate Re range	(Re < 0.1)	(0.1 < Re < 5)	(10 < Re < 100)
Cylinder		$\left(1 + \frac{4}{\mathrm{Re}}\right)^{c}$	$\left(1 + \frac{4}{\mathrm{Re}}\right)^{a}$ $\left(1 + \frac{4}{\mathrm{Re} + 0.457\sqrt{\mathrm{Re}}}\right)^{c}$
Sphere	$1 + \frac{3}{\mathrm{Re}}$ [a]		$\left(1 + \frac{6}{\mathrm{Re}}\right)^{a}$ $\left(1 + \frac{6}{\mathrm{Re} + 0.455\sqrt{\mathrm{Re}}}\right)^{c}$ $\left(1 + \frac{6}{\mathrm{Re} + 0.457\sqrt{\mathrm{Re}}}\right)^{b}$
Prolate spheroid	$\left(1 + \frac{3}{\mathrm{Re}}\left[\left(1 + \frac{\epsilon^2}{10} + \frac{109}{1400}\epsilon^4 \ldots\right)\right]\right)^{c}$	$1 + \frac{D}{\mathrm{Re}}\left(1 + \frac{D\mathrm{Re}}{8}\right)^{c}$	
Source shape			$\left(1 + \frac{8}{\mathrm{Re}}\right)^{c}$

where $D = f(\epsilon)$, ϵ = eccentricity of ellipsoid

NOTE: Re based on outside radius perpendicular to flow.

[a] Homann (50).
[b] Chambré (73) and Chambré and Smith (79).
[c] Ipsen (96).

spheroids. The results in terms of the pressure coefficients are given in Table 1.

Impact tubes have been calibrated by several different means to ascertain empirical magnitudes of the viscosity effects. The usual calibration methods are the following:

(*a*) The rotating-arm equipment where the results are subject to corrections for the fluid-swirl velocity induced by the probe under test and the determination of static pressure.

(*b*) The center-line velocity (maximum) determination in fully developed viscous flow in a circular conduit, the rate of flow through the known cross-sectional area of pipe being determined by other calibrating means.

(*c*) The known velocity field, where velocity at location of impact tube is known from other calibrating means such as wind-tunnel or water-tunnel nozzles or the float method.

Table 2 lists the important available calibration tests, and Fig. 9 presents the work in terms of curves omitting the experimental points. MacMillan (108) shows a smaller spread in these curves if Re is based on internal tube diameter.

The calibration work shows that the impact-pressure coefficient rises rapidly at lower Reynolds numbers, even reaching a magnitude of 2 at Reynolds numbers in the order of 4, the actual magnitude depending on the shape of the tip. Pressure coefficients for spherical and source-shaped probe heads depart from unity at larger Reynolds numbers and reach higher values at given low Reynolds numbers than do straight tubes with square-cut or sharpened upstream ends. Some tests have shown pressure coefficients of less than unity in the Reynolds number range of about 100 to 6000; however, in general, the more reliable tests have tended to show no values less than unity.

Supersonic Flow. Wilson (110) investigated the Reynolds number effects on static-pressure measurements in a supersonic flow field for a cone-cylinder type of static probe. The tube head was formed by a 15-deg total included-angle cone with the static holes located about 13 tube outside diameters downstream from the base of the cone. At Mach numbers of 4.13, 4.67, and 6.39 the probe diameter and static-hole diameter had no effect on static-pressure readings for Re > 3.500 (based on tube OD). There was a trend (not established) for the static pressure to increase at Re below this magnitude.

In the special application of measurement under rarefied-gas-dynamics conditions at low Reynolds numbers with Mach numbers below or above unity, slip-flow phenomena may become important. Lin and Schaaf (84) have developed theoretical values for these conditions, and Sherman (91) includes tests on supersonic flows at low Reynolds numbers, but does not reach the region where slip flow (molecular mean free path same magnitude as characteristic length of flow system) becomes important. Sherman (91) calibrated spherical, source-shaped, and sharpened upstream-end probes throughout a limited range of Mach numbers. The results show characteristics which are similar but take place

TABLE 2 IMPACT-PRESSURE CALIBRATIONS

Ref.	Head shape	d/D	Re range (VD/μ)
50	Sphere	...	2–80
	Cylinder	...	2–120
91	Square, sharp	1.0	4–400
	Source shape	0.20	4–400
104	Square, blunt	0.74	2–8000
108	Square, blunt	0.06	25–2200
28	Square	...	9–55
14	Square	...	40–1300
38*	N.P.L. Std	...	3–4000
	Hemispherical	0.155	3–3000

d = tube hole diameter
D = outside tube diameter

* Data for Pitot-static tube.

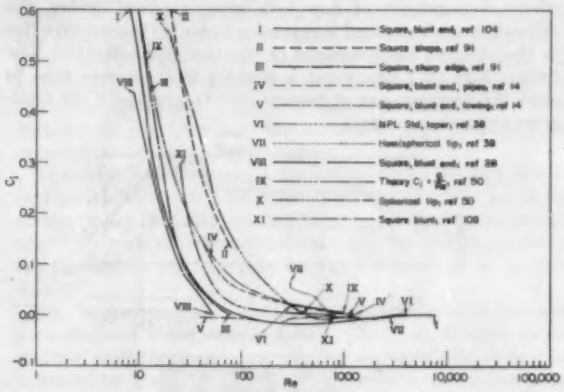

FIG. 9 FAIRED CURVES OF PRESSURE COEFFICIENTS AT LOW REYNOLDS NUMBERS

at different free-stream Reynolds numbers, as compared with subsonic data, the impact-pressure coefficient being a function of probe shape and Reynolds number, with only a trend indicated for change with Mach number.

Mutual Interference. When pressure-measuring tubes are placed in the vicinity of a fluid boundary, the tube calibrations made without such boundaries usually cannot be applied directly. Information about special flow boundaries is very limited and only a few cases are available. Some data for static-pressure differences with Pitot-static tubes approaching pipe walls are discussed in the sections on the tubes concerned. Comparisons of hot-wire and impact tube with known static pressure for velocity measurement in the boundary layer have shown good correlation as long as the tube diameter is small enough. Care must be exercised when making measurements in the flow passages of turbomachines for the purpose of interpreting the instrument readings obtained.

Free Surface. At times it becomes desirable to use a Pitot probe near the free surface of a liquid. There is a mutual interference in fluid flow between a tube and a solid wall. It would be expected that a Pitot tube measuring a velocity near a free surface would have a mutual interference effect with that surface. This phenomenon does not appear to have been investigated, either on an experimental or a theoretical basis. Parkin, Perry, and Wu (113), in checking the velocity distribution in a free-surface water tunnel, indicate that discrepancies in the uniform velocity distribution found near the free surface were not significant, since they felt that the Prandtl probe near the surface did not read correctly. They indicate "so far as the writers know, calibration data for a Prandtl probe near the surface are not available."

Applications

Shielded Total-Pressure Tube. In the determination of the total pressure, it is frequently important to use instruments insensitive to yaw and pitch angles. Although it is possible to correct for effects of angularity of flow with many types of probes, the calibration work required is expensive and often inconclusive due to the different characteristics of the test and calibration flow fields. Kiel (47) introduced a shielded total-pressure tube to meet the requirements of insensitivity to angularity for total-pressure measurements.

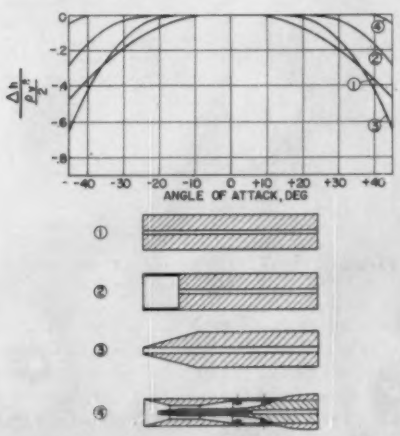

Fig. 10 Total-Pressure Tubes at Large Angles of Yaw; Gracey, et al. (87)

Gracey, Letko, and Russell (87) investigated thirty-nine total-pressure tubes over an angle-of-attack range of ±45 deg at Ma < 0.3. A few typical results are given in Fig. 10. Russell, Gracey, Letko, and Fournier (90) extended the observations to six Kiel-type tubes for the range $0.26 < Ma < 0.95$, demonstrating the greater insensitivity of a curved entry (Fig. 11) compared to a straight conical entry (Fig. 10–4). Typical characteristics for Mach number effects are shown in Fig. 11, taken from Gracey, Pearson, and Russell (95), who investigated a typical shielded total-pressure tube through the transonic region. Gracey, Coletti, and Russell (86) used twenty tubes selected from the thirty-nine (87) previously tested to determine Mach number effects in the supersonic region up to Ma = 2.4. The Kiel-type probe was the only tube to show a decrease in range of insensitivity as Mach numbers increased. Markowski and Moffatt (71) call attention to the miniaturization of the Kiel tube for use in turbomachinery work without appreciable change in the yaw-insensitive range, resulting in the shape shown in Fig. 12.

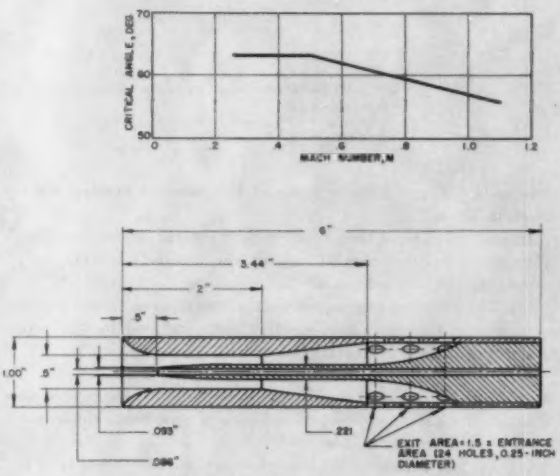

Fig. 11 Yaw Performance of a Typical Shielded Total-Pressure Tube at Various Mach Numbers

(Critical angle is angle of attack of tube head where total-pressure error reaches a value of 1 per cent of impact pressure. Gracey, et al, reference 95.)

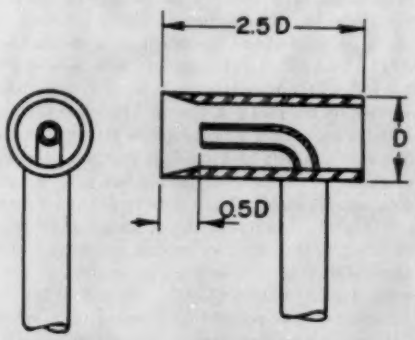

Fig. 12 Typical Miniature Shielded Impact Tube; Markowski and Moffatt (71)

Cantilevered Pitot Tubes. Tubes of circular or other constant cross-sectional shape that are inserted into a pipe with an impact-pressure tap faced into the stream are classed as cantilevered Pitot tubes or cylinders. A static-pressure tap or a downstream tap may be included in the tube, or an independent piezometer

may be used for static-pressure determination. Standard tips include hemispherical, square-ended, and ellipsoidal shapes with one, two, or three holes in a transverse plane located at various distances from the tip. Fig. 13 shows the magnitude of variations in impact pressure to be expected for different tap locations for hemispherical and ellipsoidal tips. Numachi and Hutizawa (58) present data for square-ended cylinders with approximately the same coefficients for $Z \geq 2D$.

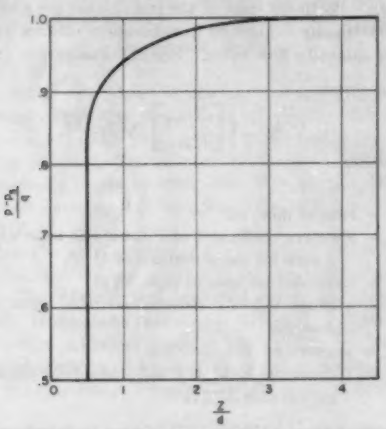

FIG. 13 PITOT-CYLINDER IMPACT COEFFICIENT $(p - p_s)/q$ AS A FUNCTION OF PIEZOMETER DISTANCE FROM THE TIP (Z/D) FOR HEMI AND ELLIPSOIDAL TIPS
(Data from Silberman, reference 69, and Winternitz, reference 114.)

Cantilevered Pitot tubes are valuable for measuring impact pressure and for determining the direction of velocity in two-dimensional flow, the latter determination being independent of position of holes with respect to pipe walls. The directional properties are satisfactory also when the flows are inclined to the cylinder axis.

The total pressure measured with cantilevered Pitot tubes appears to have constant coefficients for Re greater than about 4×10^3 [see Numachi (43), Kasai (51), Kito (52), Numachi and Hutizawa (58), and Winternitz (114)]. This result appears to hold for hemispherical, square-end, and ellipsoidal heads with holes 0.5 diameter or more from the tip.

The pressure distribution about the cylinder at the transverse plane of the taps is similar to the pressure distribution about a cylinder of infinite length. The distribution is a function of Re and the position of the taps with respect to the pipe walls. Winternitz (114) shows that pressures vary for angles greater than 40 deg as the taps approach the pipe walls. The "critical angle," where the true static pressure is indicated, reduces from 0.5 to 1 deg for a Re increase of from 10 to 15×10^3. The piezometer hole size compared to tube diameter is important.

Silberman (69) and Winternitz (114) provide information on the total-pressure-coefficient changes on a cantilevered Pitot cylinder when the flow is inclined to the axis of the tube. Within angles of pitch of ± 20 deg, the coefficients are lower when the tip is pointing downstream than when pointing upstream at a given inclination. A cosine square law gives coefficients within about 3 per cent of experimental values for the range considered. Meyer and Benedict (100) show that there is some variation in coefficients in inclined flow for tubes with a range of from 1 to 3 diameters distance from a square tip to the plane of the static-pressure holes. Markowski and Moffatt (71) describe a cantilevered tube with four holes, one being on the hemispherical portion of the head in the same plane parallel to the head axis and containing the center hole of the normal three-hole tube. With the calibration curves which they give, it is possible to determine velocities in three dimensions with this tube.

Winternitz (114) calibrated cantilevered Pitot cylinders in a towing tank and in the throat of a wind tunnel. On the basis of agreement of experimental results, it can be inferred that turbulence effects were insignificant within the range $1000 < \text{Re} < 12{,}000$ and the variations in turbulence of still water and the wind-tunnel throat. On the other hand, turbulence affects the point of separation of flow from the periphery of the cylinder and changes the pressure distribution for angles greater than the angle of separation. Meyer and Benedict (100) give limited data on the effect of turbulence produced by a screen on the static-pressure calibration of a tube with a tap at 40 deg from the flow direction.

Winternitz (114) used a three-hole cantilevered Pitot tube to measure static pressure in the throat of a circular closed-throat wind tunnel. The Pitot diameter was 0.311 in. and the tunnel throat 7.5 in. Using the wind-tunnel piezometer as a standard static pressure, the measured static-pressure difference from the standard varied from +10 to −10 per cent of the velocity head at the tunnel center line, with the measured value being high near the wall where the tube was inserted.

Cole Pitometer. This instrument, in its various forms, has been used for many years and is specified in the ASME fluid meters report (34) and in its Power Test Codes for Hydraulic Prime Movers (77). Many articles have appeared in the technical literature, so that reasonably complete information is available for normal applications (7, 10, 11, 12, 23, 24, 45, 46, 59).

Transverse Tube. One type of transverse Pitot tube is a straight circular tube of uniform diameter with one or more pressure taps for the determination of the dynamic head in a stream of fluid. When used in a pipe line, the tube passes through stuffing boxes in opposite pipe walls and is free to slide and rotate to place pressure taps at desired locations in the pipe. One form of this instrument is the Collins tube of $^5/_{16}$ in. diam with two pressure holes of 0.116 in. diam placed 180 deg apart and offset by a distance of $^7/_{16}$ in. Calibration data are presented by Christiansen and French (57) and by Cornwell (62), the latter being more complete. For two-hole instruments similar to the Collins tube, the tube coefficient is less than unity since the downstream pressure is less than static, and a blocking correction (function of tube diameter or pipe diameter) and an over-all pipe coefficient are necessary to determine flow in a pipe.

The inside pipe contours at the stuffing boxes are very important for a transverse tube. The type illustrated in the fluid-meters report (34) may produce large errors, and recommendations have been made to have the gland welded to the outside of the pipe and let the tube pass through a simple hole in the pipe wall (57).

Fig. 14 shows measurements made with a transverse tube and a cantilevered Pitot tube in a 6-in. pipe with 20-diam unobstructed straight pipe upstream. For the same rate of flow as indicated by a calibrated orifice, all curves compare the pressure indicated with the pressure from a standard piezometer placed in the side of the pipe. The shape of the static-pressure curve illustrates the difficulties in the interpretation of such measurements.

Many pressure distributions about circular cylinders crossing a uniform flow field have been reported in the literature. Fig. 15 shows typical pressure distributions at Reynolds numbers above and below the critical Reynolds number range (Reynolds numbers through which the drag coefficient decreases rapidly from about 1.2 to 0.3) determined in air at Mach number of about 0.06. Tests have demonstrated that the potential-flow solution provides information closely approximating actual conditions on the forepart of the cylinder. The departure of theory from experiment

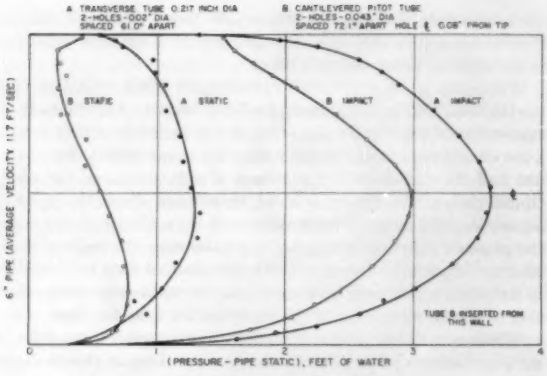
A TRANSVERSE TUBE 0.217 INCH DIA
2-HOLES-.002" DIA
SPACED 61.0" APART
B CANTILEVERED PITOT TUBE
2-HOLES-0.043" DIA
SPACED 72.1" APART HOLE ℄ 0.05" FROM TIP
B STATIC
A STATIC
B IMPACT
A IMPACT
TUBE B INSERTED FROM THIS WALL
6" PIPE (AVERAGE VELOCITY 11.7 FT/SEC)
(PRESSURE - PIPE STATIC), FEET OF WATER

FIG. 14 IMPACT AND STATIC-PRESSURE INDICATIONS ACROSS A PIPE WITH AVERAGE VELOCITY OF WATER OF 11.7 FPS FOR A TRANSVERSE TUBE AND A CANTILEVERED PITOT TUBE; JUE, REFERENCE (61)

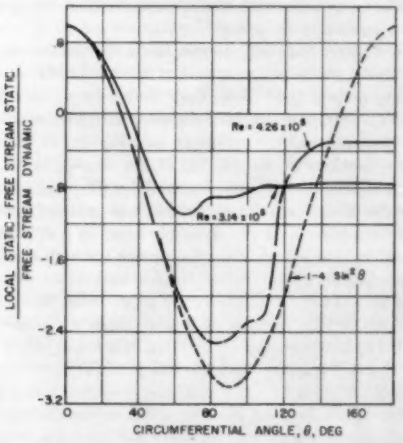

FIG. 15 TYPICAL PRESSURE DISTRIBUTIONS ABOUT A LONG CIRCULAR CYLINDER IN A UNIFORM FLOW FIELD; GOWEN AND PERKINS, REFERENCE (98)

depends on the establishment of the adverse pressure gradient associated with boundary-layer separation. This separation takes place at larger angles as the Reynolds number increases. Gowen and Perkins (98) have shown that Reynolds number effects on pressure distribution were negligible at Mach numbers above unity to the limit of their tests, i.e., Ma = 2.9.

Short-Head Tubs. The dimensions of the short-head tube given in Fig. 1 were selected from the design data of Figs. 3 and 4 to give a velocity coefficient of unity. This procedure was verified by the work of Merriam and Spaulding (48). The square corner between the head and the stem was to allow measurements to positions one-half tube diameter from the pipe wall.

Comparative calibrations in a 3-ft-square closed wind tunnel on five Pitot-static tubes (Prandtl 3/8 in., ASHVE 1/4 in., ASHVE 5/16 in., NAFM 1/4 in., and short-head 1/2 in.) showed no significant variation in tube-velocity coefficient (all test coefficients within ±0.2 per cent of standard Prandtl tube). The wind tunnel was checked for constant velocity in magnitude and direction and constant static pressure in the region occupied by the tubes under test. The air velocity varied from 50 to 100 fps.

In an effort to evaluate the velocity-gradient errors and the wall effects when using a Pitot-static tube for quantity rate-flow measurements of water in a pipe, Page (81) made velocity measurements in 4, 6, and 8-in. pipes with 1/8-in. and 1/2-in-diam short-head tubes. Pertinent data of the installation are given in Table 3. Volumetrically calibrated free-discharge orifices were used to determine quantity flow rates. The calibration was expressed in terms of

$$Q = C_e A \left[\frac{U'_{avg}}{U_{max}}\right] \sqrt{2g\Delta h_{\text{℄}}}$$

where

Q = rate of flow, cfs
C_e = effective coefficient of Pitot-static tube when used in a pipe for measurement of Q
A = cross-section area of pipe, sq ft
U'_{avg} = average velocity determined from Pitot tube traverse, fps
U_{max} = center-line velocity, fps
$\Delta h_{\text{℄}}$ = differential head of Pitot-static tube when placed at pipe center line, ft

If the method of equal areas (34) is used to determine U'_{avg} and the Pitot-static-tube velocity coefficient is assumed to be unity, the U'_{avg} determined will be greater than the true average velocity in the pipe. Assuming that the velocity distribution will follow the equation

$$1 - r/R = \left[\frac{U}{U_{\text{℄}}}\right]^n$$

where U is the velocity at any radius r, Page (81) has computed the error in indicated average velocity. The results are given in Table 4. His experimental results may be expressed in terms of

$$C_e = [1.00 - fL/2D - 1.7(d/D)^2]/(1 + m/100)$$

where $fL/2D$ is the correction for pressure gradient between head tip and plane of static-pressure holes, $1.7(d/D)^2$ is correction for blocking, velocity gradient, and wall effects, and $(1 + m/100)$ is correction for error due to taking a finite number of traverse positions to obtain U'_{avg}. Almost all experimental points are within ±0.5 per cent of the value given by the equation.

Since the impact-pressure tap and the static-pressure tap are

TABLE 4 CALCULATED RESULTS OVER INDICATION OF AVERAGE VELOCITY WHEN USING STANDARD PROCEDURE FOR METHOD OF EQUAL AREAS AND A ONE-SEVENTH POWER-LAW VELOCITY DISTRIBUTION; PAGE (81)

Number in equal areas in traverse	Average indicated velocity (U'_{avg}) too large by per cent
2	2.27
4	1.40
6	0.91
8	0.67
10	0.53
20	0.25

TABLE 3 DATA ON TEST EQUIPMENT OF PAGE (81)

Nominal pipe size, in.	L/D straight upstream	L/D straight downstream	f pipe-friction factor	Re range × 10^{-6}	(ϵ/d) mean	1/8-in-diam tube, d/D	1/2-in-diam tube, d/D
4	138	61	0.0218	2.0–3.0	0.0015	0.062	0.125
6	104	29	0.0253	3.0–4.5	0.0028	0.042	0.083
8	77	23	0.0188	3.5–5.1	0.0008	0.031	0.062

frequently at different transverse planes in the pipe, a reduction in static pressure will occur due to the pressure gradient in the pipe. The magnitude of reduction on tube velocity coefficient can be approximated by the quantity $f(L/2D)$, where f is the friction factor in the expression

$$h_f = f \frac{L}{D} \frac{V^2}{2g}$$

L is the axial distance between impact and static-pressure taps, and D is the diameter of the pipe. If for orders of magnitude, we consider $f = 0.02$, then the per cent reduction in tube velocity coefficient will be $1/D$.

When a Pitot-static head is placed on the center line of the pipe, the venturi effect of the volume occupied by the tube head will produce a reduction in measured static head, while the impact head is constant. The effective tube velocity coefficient will be less than unity by the amount of $(d/D)^2$; e.g., at (d/D) of 0.1 the coefficient becomes 0.99 and for (d/D) of 0.2 the coefficient becomes 0.96.

If the head is at a position other than the center line, it is probable that the venturi effect will be the same if a sufficient number and size of static holes are used around the circumference of the head. If the static taps are not adequate, it is possible that the reduction in measured static pressure might be different due to mutual interference on flow produced between the Pitot-static head and the pipe wall. No experimental data on this point are known.

The ratio U_{avg}/U_{max}, where $Q = AU_{avg}$, is known as the pipe factor (PF), a quantity that is a function of Re, pipe roughness, and the degree of establishment of fully developed velocity distribution; i.e., sufficient upstream straight pipe so that velocity transverse is the same at downstream points and the test traverse section. The relative roughness ϵ/D is determined from Moody's pipe-friction charts (65) by measuring pipe-friction factor and Reynolds number. Through application of the mixing-length theory of turbulence to data from Moody's pipe-friction charts, Fig. 16 can be obtained (49, 76, 82). If Re and ϵ/D are known,

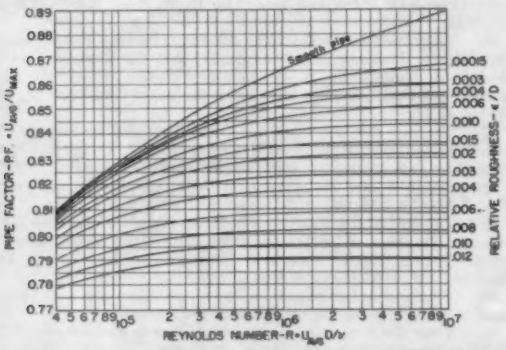

FIG. 16 PIPE FACTORS FOR TURBULENT FLOW WITH A STABILIZED VELOCITY DISTRIBUTION; SCHUBAUER AND DRYDEN (49), FOLSOM AND IVERSEN (76)

the pipe factor can be determined from Fig. 16, and it is only necessary to measure the center-line velocity and use

$$Q = C_s A(\mathrm{PF}) V_{\mathbb{C}}$$

where $C_s = 1.00 - fL/2D - (d/D)^2$ if straight pipe sections allow fully developed velocity distributions to form.

To investigate static-pressure determination with a Pitot-static tube, a piezometer tap was installed in a 6-in. pipe, 7.1 in. upstream from the hole in the pipe for the tube stem. This distance was chosen on the basis of data from Hubbard (60) to insure that the piezometer reading is independent of the tube position. The indicated static pressure was determined at several radii using short-head tubes of two different sizes. The data were corrected for pipe friction between the piezometer tap and plane of static taps in the tube and results expressed in terms of per cent of velocity head and shown in Fig. 17. The calculated difference for head-blocking effect at the center line is 1.0 per cent, while the curves show about 1.4 per cent of velocity head. Examination of Fig. 17 reveals characteristics of indicated static pressure when measured with a Pitot-static tube. The mutual interference between the tube head and stem and the pipe wall produces the observed distortions for the geometry investigated.

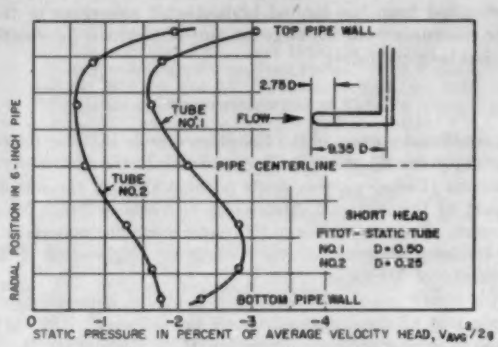

FIG. 17 STATIC-PRESSURE MEASUREMENTS IN WATER FLOW WITH SHORT-HEAD PITOT-STATIC TUBES OF DIFFERENT SIZE IN A 6-IN. PIPE; FERGUSON (70)

Three-Dimensional Flow. The measurement of magnitude and direction of velocity at a point in a fluid is accomplished frequently with a probe providing five readings. One form of this type of probe is a sphere having a central hole and four holes distributed equally around the sphere and spaced at the same angular distance from the center hole (36, 40, 80, 116). From experimental calibrations and pressures measured at the five holes, the velocity in a three-dimensional flow may be determined. Similar results may be obtained from a claw-type probe having the corresponding five pressure determinations. An understanding of the probe performance results from considerations of pressure distributions about a sphere when it is placed in a uniform flow field. The claw probe depends on indications of impact pressure by a square-ended tube when a yaw deflection of velocity with respect to the tube axis exists. Some mutual interference between adjacent tubes of the claw makes calibration under operating conditions desirable.

Special Purpose Probes. In designing probes for special purposes, the general considerations are modified to meet the particular requirements. For example, Bentzel (44) developed a probe with a pressure indicator to measure very low velocities in hydraulic models of civil-engineering applications. Several manufacturing firms have compiled design and performance data for specific applications of Pitot tubes of various forms (118, 120–127). Summaries of particular interest have been made for the field of turbojet-engine investigations into flow characteristics in compressors and turbines (119). Considerable information on special-purpose probes appears in the technical literature, but space limitations prevent an adequate presentation in this paper.

SUMMARY

Many forms of Pitot and Pitot-static tubes have been calibrated and used for a wide variety of applications. Several of the

more common forms of probes are described, and their pressure performance is discussed in detail for normal and for a few special flow conditions.

Experimental calibrations for a Pitot-static tube with a short tip, especially designed for measurements of quantity rate of flow of liquids in pipes, demonstrate the suitability of the probe. Necessary corrections to probe calibrations in a large cross-section uniform flow field for use in pipes are developed, presumably to account for effects of velocity gradients and mutual interference of flow between the pipe wall and the probe.

Quantitative information, presented in the form of curves, provides readily available data for designers and users to determine desirable forms for given applications and to interpret pressure measurements made with specific probes. Additional data may be obtained from the limited bibliographic references or from other references from the large amount of technical information that has been published.

Acknowledgments

A significant portion of the literature search and the preliminary experimental work, both conducted at the University of California (Berkeley), was made possible through the financial support of the National Association of Vertical Pump Manufacturers. The preparation of this paper was aided materially by the Industry Program of the College of Engineering of The University of Michigan.

In a review paper of this type it is almost impossible to be certain that all significant references are included. The author wishes to express appreciation to Mr. H. S. Bean of the Bureau of Standards, for calling attention to the original suggestion of Dr. Sanford A. Moss for calibrating a flow nozzle with an impact tube. This work was presented to the ASME in 1916 (128) and the procedure with refinements used to calibrate flow nozzles (129). The method has the advantage of simple and inexpensive equipment.

BIBLIOGRAPHY

1 "Description d'une machine pour mesurer la vîtesse des eaux courantes et le sillage des vaisseaux," by H. Pitot, Mémoires, Académie des Sciences, Paris, France, 1732, pp. 363–376.

2 "Mémoires sur le mouvement de l'eau dans les tuyaux," by H. Darcy, Comptes Rendus, Académie des Sciences, Paris, France, vol. 38, 1854, p. 407. Discussion by Messrs. Poncelet, Combes, and Morin, ibid., pp. 1109–1121.

3 "Relative à quelques modifications à introduire dans le tube Pitot," by H. Darcy, *Annales des Ponts et Chaussées*, ser. 3, vol. 1858, 1st part, pp. 351–359.

4 "Water Measurements in Connection With a Test of a Centrifugal Pump at Jourdan Avenue Drainage Station, New Orleans, La.," by W. M. White, *J. Assn. Engrg. Socs.*, vol. 25, no. 4, 1900, pp. 167–171.

5 "The Pitot Tube: Its Formula," by W. M. White, *J. Assn. Engrg. Socs.*, vol. 27, no. 2, 1901, pp. 34–77.

6 "Tests of Centrifugal Pumps," by W. B. Gregory, Trans. ASME, vol. 22, 1901, pp. 262–274.

7 "Discussion on Flow of Water in Pipes," by E. S. Cole, Trans. ASCE, vol. 47, 1902, pp. 197–369. Discussion of "Experiments at Detroit, Mich., on the Effect of Curvature Upon the Flow of Water in Pipes," by G. S. Williams, C. W. Hubbell, and G. H. Fenkell, ibid., pp. 1–197.

8 "Measurement of Air Velocity and Pressure," by A. F. Zahm, *Physical Review*, vol. 17, 1903, pp. 410–423.

9 "The Pitot Tube," by W. B. Gregory, Trans. ASME, vol. 25, 1904, pp. 184–212.

10 "The Pitometer and Its Uses," by E. M. Blake, *New Engl. Water Works Assn. J.*, vol. 20, 1906, pp. 152–162.

11 "The Pitometer," by J. D. Underwood, Proc. Engrs. Soc. West. Penn., vol. 22, 1906, pp. 445–458.

12 "The Pitometer and Water Works Losses," by E. S. Cole, Proc. Amer. Water Works Assn., 1907, pp. 136–156.

13 "The Pitometer," by E. S. Cole, *J. Franklin Inst.*, vol. 164, 1907, pp. 425–441.

14 "On the Value of the Pitot Constant," by J. D. Fry and A. M. Tyndall, *Phil. Mag.*, ser. 6, vol. 21, 1911, pp. 348–366.

15 "Notes on the Pitot Tube," by J. Airey, *Engrg. News*, vol. 69, 1913, pp. 782–783.

16 "Origin and Theory of the Pitot Tube," by A. E. Guy, *Engrg. News*, vol. 69, 1913, pp. 1172–1175.

17 "Pitot Tubes for Gas Measurement," by W. C. Rowse, Trans. ASME, vol. 35, 1913, pp. 633–691.

18 "Measurement of the Velocity of Flowing Water," by L. F. Moody, Proc. Engrs. Soc. West. Penn., vol. 30, 1914, pp. 280–323.

19 "Pitot-Tube Formulas," by B. F. Groat, Proc. Engrs. Soc. West. Penn., vol. 30, 1914, pp. 324–381.

20 "Investigation of the Direction and Velocity of Flow in the Neighbourhood of the Tail Plane of B.E. 2," by E. F. Relf, Gt. Brit., ACA, R and M 156, pt. 4, 1914, 4 p. + 4 figs.

21 "The Pitot Tube and Other Anemometers for Aeroplanes," by W. H. Herschel, NACA TR 2, pt. 1, 1915, 24 p.

22 "The Theory of Pitot and Venturi Tubes," by E. Buckingham, NACA TR 2, pt. 2, 1915, 10 p.

23 "Graphic Recorder for Cole Pitometer," by E. S. Cole, *Engrg. News*, vol. 73, 1915, p. 875.

24 "Rerating a Pitometer," by C. G. Gillespie, *Engrg. Rec.*, vol. 72, 1915, p. 144. Also in *Engrg. and Contracting*, vol. 43, 1915, p. 275.

25 "The Design of a Sensitive Yawmeter," by J. R. Pannell and R. Jones, Gt. Brit., ACA, R and M 445, 1918, 6 p. + 4 pl.

26 "Altitude Effect on Air Speed Indicators," by M. D. Hersey, F. L. Hunt, and H. N. Eaton, NACA TR 110, 1920, 27 p.

27 "The Altitude Effect on Airspeed Indicators—II," by H. N. Eaton and W. A. MacNair, NACA TR 156, 1922, 44 p.

28 "On the Use of Very Small Pitot-Tubes for Measuring Wind Velocity," by M. Barker, Proceedings of the Royal Society of London, England, series A, vol. 101, 1922, pp. 435–445.

29 "A Direction and Velocity Meter for Use in Wind Tunnel Work" by T. Lavender, Gt. Brit., ACA, R and M 844, 1923, 2 p. + 2 pl.

30 "The Design of Pitot-Static Tubes," by E. Ower and F. C. Johansen, Gt. Brit., ARC, R and M 981, 1925, 12 p. + 11 p. of figs.

31 "Pressure of Air on Coming to Rest From Various Speeds," by A. F. Zahm, NACA TR 247, 1926, 7 p.

32 "Influence of the Orifice on Measured Pressures," by P. E. Hemke, NACA TN 250, 1926, 7 p. + 8 p. of figs.

33 "Flow and Drag Formulas for Simple Quadrics," by A. F. Zahm, NACA TR 253, 1926, 23 p.

34 "Fluid Meters: Their Theory and Application," ASME, Special Research Committee on Fluid Meters, pt. 1, 1927 (4th ed. 1937); pt. 2, 1931; pt. 3, 1933.

35 "Differential Pressures on a Pitot-Venturi and a Pitot-Static Nozzle Over 360° Pitch and Yaw," by R. M. Bear, NACA TR 264, 1927, 9 p.

36 "Improved Instrument for the Simultaneous Determination of the Static Pressure, the Magnitude, and the Direction of the Velocity of Fluids," by B. G. Van der Hegge Zijnen, K. Akad. Wetensch., Amsterdam, Proc., Sec. of Sciences, vol. 32, 1929, pp. 658–668.

37 "Einfluss der Zähigkeit bei Geschwindigkeitsmessungen mit Staudruck Multiplikatoren," by H. Peters, *Zeitsch. Flugt. und Motorluftschiffahrt*, vol. 22, no. 11, 1931, pp. 321–323. Translation: "Effect of Viscosity in Speed Measurements With Double-Throat Venturi Tubes," NACA TM 633, 1931, 5 p. + 2 p. of figs.

38 "On the Determination of the Pitot-Static Tube Factor at Low Reynolds Numbers, With Special Reference to the Measurement of Low Air Speeds," by E. Ower and F. C. Johansen, Gt. Brit., ARC, R and M 1437, 1931, 28 p. + 9 p. of figs.

39 "Piezometer Investigation," by C. M. Allen and L. J. Hooper, Trans. ASME, vol. 54, Paper Hyd-7-8, 1932.

40 "Über die Messung von Geschwindigkeit und Druck in einer dreidimensionalen Strömung," by F. Krisam, *Zeitsch. Flugt. und Motorluftschiffahrt*, vol. 23, 1932, pp. 369–373. Translation: "Speed and Pressure Recording in Three-Dimensional Flow," NACA TM 688, 1932, 13 p. + 3 pl.

41 "The Measurement of Air Flow," by E. Ower, second edition, rev. and enl., Chapman and Hall, Ltd., London, 1933, viii, 243 p. Chap. III, "Design of Pitot and Static Tubes" (pp. 16–35). Chap. V, "Measurements of Flow and Resistance With Pitot-Static Tubes" (pp. 56–71).

42 "Statistical Measurements of Turbulence in the Flow of Air Through a Pipe," by H. C. H. Townend, Proceedings of the Royal Society of London, England, series A, vol. 145, 1934, pp. 180–211.

43 "Über zylindrische Staurohre zur Messung von Geschwindigkeit, Richtung und statischem Druck der Wasserströmungen," by F. Numachi, pts. 1 and 2, Tôhoku Imp. Univ., Sendai, Japan, Technology Rep., vol. 11, 1934, pp. 307–364. For pt. 3 see reference 58.

44 "New Velocity-Measuring Device Developed in Waterways Laboratory," by C. E. Bentzel, *Engrg. News-Rec.*, vol. 112, 1934, pp. 508–509.

45 "The Pitot Tube in Current Practice," by E. S. Cole, *Civil Engr.*, vol. 5, 1935, pp. 220–222.

46 "Pitot Tube Practice," by E. S. Cole, Trans. ASME, vol. 57, Paper Hyd-7-8, 1935.

47 "Gesamtdruckgerät mit grosser Unempfindlichkeit gegen Schräganströmung," by G. Kiel, *Luftfahrtforschung*, vol. 12, 1935, pp. 75–79. Translation: "Total-Head Meter With Small Sensitivity to Yaw," NACA TM 775, 1935, 6 p. + 3 p. of figs.

48 "Comparative Tests of Pitot-Static Tubes," by K. G. Merriam and E. R. Spaulding, NACA TN 546, 1935, 46 p. + 14 p. of figs.

49 "The Effect of Turbulence on the Drag of Flat Plates," by G. B. Schubauer and H. L. Dryden, NACA TR 546, 1935, 7 p.

50 "Der Einfluss grosser Zähigkeit bei Strömung um den Zylinder und um die Kugel," by F. Homann, *Zeitsch. für angew. Math. und Mech.*, vol. 16, 1936, pp. 153–164. Translation: "The Effect of High Viscosity on the Flow Around a Cylinder and Around a Sphere," Univ. of Calif., Berkeley, Inst. of Engrg. Res., Rep. HE-150-88, 1931, 16 + 7 p. Translation also published as: NACA TM 1334, 1952, 29 p.

51 "On the Exit Velocity and Slip Coefficient of Flow at the Outlet of the Centrifugal Pump Impeller, With Some References to the Characteristics of the Pump," by T. Kasai, Kyushu Imp. Univ., Fukuoka, Japan, Faculty of Engrg., Memoirs, vol. 8, no. 1, 1936, 89 p.

52 "Experimental Study on a Propeller Pump," by S. Kito, *Tokyo Imp. Univ., Faculty of Engrg., Journal*, vol. 20, no. 12, 1936, pp. 283–384 + 30 pl.

53 "A Note on Measurement of Total Head and Static Pressure in a Turbulent Stream," by S. Goldstein, Proceedings of the Royal Society of London, England, series A, vol. 155, 1936, pp. 570–575.

54 "On the Static Pressure in Fully-Developed Turbulent Flow," by A. Fage, Proceedings of the Royal Society of London, England, series A, vol. 155, 1936, pp. 576–596.

55 "The Behaviour of a Pitot Tube in a Transverse Total-Pressure Gradient," by A. D. Young and J. N. Maas, Gt. Brit., ARC, R and M 1770, 1936, 16 p.

56 "Errors in Pressure Readings Due to Wrong Gauge Connections," by R. W. Angus, *J. Amer. Water Works Assn.*, vol. 29, 1937, pp. 458–468.

57 "Characteristics of Transverse Pitot Tubes," by J. E. Christiansen and O. C. French, *Agric. Engrg.*, vol. 18, 1937, pp. 21–24.

58 "Über zylindrische Staurohre zur Messung von Geschwindigkeit, Richtung und statischem Druck der Wasserströmungen," by F. Numachi and S. Hutizawa, pt. 3, Tôhoku Imp. Univ., Sendai, Japan, Technology Rep., vol. 12, 1938, pp. 543–559. For pts. 1 and 2 see reference (43).

59 "Pitot Tubes in Large Pipes," by Edward S. Cole and E. Shaw Cole, Trans. ASME, vol. 61, 1939, pp. 465–473.

60 "Investigation of Errors of Pitot Tubes," by C. W. Hubbard, Trans. ASME, vol. 61, 1939, pp. 477–492.

61 "Investigations in a Horizontal 6-Inch Pipe With Transverse Impact Tubes," by L. S. Jue, Special Graduate Student Report, Univ. of Calif., Berkeley, 1939.

62 "Measurement of Water in Pipe Lines With Transverse Pitot Tubes," by W. A. Cornwell, MS thesis, Univ. of Calif., Berkeley, 1940.

63 "The Effect of Compressibility on Static Heads," by C. N. H. Lock, A. E. Knowler, and H. H. Pearcey, Gt. Brit., ARC, R and M 2386 (Jan., 1943; Publ. 1950), 13 p.

64 "Application of Pitometer to Water Distribution Systems," by E. S. Cole, *New Engl. Water Works Assn. J.*, vol. 58, 1944, pp. 74–83.

65 "Friction Factors for Pipe Flow," by L. F. Moody, Trans. ASME, vol. 66, 1944, pp. 671–684.

66 "The Impact Tube," by B. Hodkinson, Proceedings of the Instn. Mech. Engrs., vol. 151, 1944, pp. 257–263.

67 "Pitot Pressures in Moist Air," by G. I. Taylor, Gt. Brit., ARC, R and M 2248, 1945, 5 p.

68 "Hydraulic Measurements: A Manual for Engineers," by H. Addison, John Wiley and Sons, Inc., New York, N. Y., 1946. Chap. 5, "Measurement of Velocity" (pp. 81–89).

69 "The Pitot Cylinder," by E. Silberman, Univ. of Minn., St. Anthony Falls Hydraulic Lab. Circular No. 2, 1947, 18 p.

70 "Pitot Tube Calibration Tests," by C. K. Ferguson, Special Graduate Student Report, Univ. of Calif., Berkeley, 1948, 12 + 34 p.

71 "Instrumentation for the Development of Aircraft Power Plane Components Involving Fluid Flow," by S. J. Markowski and E. M. Moffatt, Quart. Trans. SAE, vol. 2, 1948, pp. 104–116.

72 "Cavitation and Pressure Distribution, Head Forms at Zero Angle of Yaw," by H. Rouse and J. S. McNown, State Univ. of Iowa, Stud. Engrg. Bull. 32, 1948, 70 p.

73 "The Theory of the Impact Tube in a Viscous Compressible Gas," by P. L. Chambré, Univ. of Calif., Berkeley, Inst. of Engrg. Res., Rep. HE-150-50, 1948, 6 + 5 p.

74 "Wind-Tunnel Testing Problems in Superaerodynamics," by Hsue-Shen Tsien, *J. Aero. Sci.*, vol. 15, 1948, pp. 573–580.

75 "The Theory of the Impact Tube at Low Pressures," by P. L. Chambré and S. A. Schaaf, *J. Aero. Sci.*, vol. 15, 1948, pp. 735–737.

76 "Pipe Factors for Quantity Rate Flow Measurements With Pitot Tubes," by R. G. Folsom and H. W. Iversen, ASME Advance Paper 48—A-35, 1948, 18 p. Abstracted in *Mechanical Engineering*, vol. 70, 1948, pp. 1019–1020.

77 "Hydraulic Prime Movers," ASME Power Test Codes, 18-1949, ASME, 1949, 29 p. Sections on Pitot Tube Traverse and Cole Pitometer Methods.

78 "Flow Measurement and Meters," by A. Linford, E. and F. N. Spon, London, England, 1949, 95 p.

79 "The Impact Tube in a Viscous Compressible Gas," by P. L. Chambré and H. R. Smith, Univ. of Calif., Berkeley, Heat Transfer and Fluid Mechanics Inst. Publ., June 1949, pp. 271–278.

80 "Flow Around Bends in an Open Flume," by A. Shukry, Proc. ASCE, vol. 75, 1949, pp. 713–741. Discussion, ibid., pp. 1391–1396.

81 "Performance Characteristics of Pitot Tubes in Water Pipes," by W. A. Page, MS thesis, Univ. of Calif., Berkeley, 1949.

82 "Quelques caractéristiques de l'écoulement en conduite d'un intérêt pratique," by L. F. Moody, *Houille Blanche*, vol. 5, 1950, pp. 315–325.

83 "Impact Tube Measurements in Isothermal Air Jets," by J. F. Taylor and E. W. Comings, Proc. Midwestern Conference on Fluid Dynamics, 1950, pp. 204–215.

84 "The Effect of Slip on Flow Near a Stagnation Point and in a Boundary Layer," by T. C. Lin and S. A. Schaaf, Univ. of Calif., Berkeley, Inst. of Engrg. Res., Rep. HE-150-76, 1950. Also: NACA TN 2568, 1951, 28 p.

85 "The Three-Quarter Radius Pitot Tube Flow Meter," by J. H. Preston, *Engr.*, vol. 190, 1950, pp. 400–402.

86 "Wind-Tunnel Investigation of a Number of Total-Pressure Tubes at High Angles of Attack—Supersonic Speeds," by W. Gracey, D. E. Coletti, and W. R. Russell, NACA TN 2261, 1951, 48 p.

87 "Wind-Tunnel Investigation of a Number of Total-Pressure Tubes at High Angles of Attack—Subsonic Speeds," by W. Gracey, W. Letko, and W. R. Russell, NACA TN 2331, 1951, 69 p.

88 "On Reflection of Shock Waves From Boundary Layers," by H. W. Liepmann, A. Roshko, and S. Dhawan, NACA TN 2334, 1951, 100 p.

89 "Effects of Pressure-Rake Design Parameters on Static-Pressure Measurement for Rakes Used in Subsonic Free Jets," by L. N. Krause, NACA TN 2520, 1951, 20 p.

90 "Wind-Tunnel Investigation of Six Shielded Total-Pressure Tubes at High Angles of Attack—Subsonic Speeds," by W. R. Russell, W. Gracey, W. Letko, and P. Fournier, NACA TN 2530, 1951, 25 p.

91 "New Experiments on Impact Pressure Interpretation in Supersonic and Subsonic Rarefied Airstreams," by F. S. Sherman, Univ. of Calif., Berkeley, Inst. of Engrg. Res., Rep. HE-150-99, 1951, 30 + 46 p.

Also: NACA TN 2995, 1953, 30 + 40 p.

92 "The Effect of the Condensation of Atmospheric Water Vapour on Total Head and Other Measurements in the N.P.L. High Speed Tunnels," by H. H. Pearcey, Gt. Brit., ARC, R and M 2249, 1951, pp. 1–35.

93 "The Pitot-Venturi Flow Element," by H. W. Stoll, Trans. ASME, vol. 73, 1951, pp. 963–969.

94 "Small Pitot Tubes With Fast Pressure Response Time," by W. S. Bradfield and G. E. Yale, Univ. of Minn., Rosemount Res. Cent. Condensed in *J. Aero. Sci.*, vol. 18, 1951, pp. 697–698.

95 "Wind-Tunnel Investigation of a Shielded Total-Pressure Tube at Transonic Speeds," by W. Gracey, A. O. Pearson, and W. R. Russell, NACA RM L51K19, 1952, 8 p.

96 "Viscosity Correction to Impact Pressure on Prolate Spheroid," by D. C. Ipsen, Univ. of Calif., Berkeley, Inst. of Engrg. Res., Rep. HE-150-89, 1952, 15 + 3 p.

97 "Direct Measurements of Skin Friction," by S. Dhawan, NACA TN 2567, 1952, 60 p.

"The Effect of High Viscosity on the Flow Around a Cylinder and Around a Sphere," by F. Homann, NACA TM 1334, 1952, 29 p. Translation of reference 50.

98 "Drag of Circular Cylinders for a Wide Range of Reynolds Numbers and Mach Numbers," by F. E. Gowen and E. W. Perkins, NACA RM A52C20, 1952, 26 p.

99 "Several Combination Probes for Surveying Static and Total

Pressure and Flow Direction," by W. M. Schulze, G. C. Ashby, Jr., and J. R. Erwin, NACA TN 2830, 1952, 64 p.

100 "Instrumentation for Axial-Flow-Compressor Research," by C. A. Meyer and R. P. Benedict, Trans. ASME, vol. 74, 1952, pp. 1327–1336.

101 "Measurement of Turbulent Velocity Fluctuations by Method of Electromagnetic Induction," by L. M. Grossman and A. F. Charwat, *Rev. Sci. Instruments*, vol. 23, 1952, pp. 741–747.

102 "Factors Affecting Laminar Boundary Layer Measurements in a Supersonic Stream," by R. E. Blue and G. M. Low, NACA TN 2891, 1953, 49 p.

103 "The Structure of Turbulence in Fully Developed Pipe Flow," by J. Laufer, NACA TN 2954, 1953, 55 p.

104 "Influence of Viscous Effects on Impact Tubes," by C. W. Hurd, K. P. Chesky, and A. H. Shapiro, *Journal of Applied Mechanics*, Trans. ASME, vol. 75, 1953, pp. 253–256.

105 "Pitot-Venturi Flow Element Water Service Report," by H. W. Stoll, Trans. ASME, vol. 75, 1953, pp. 969–974.

106 "Experimental Investigation at a Mach Number of 2.41 of Average Skin-Friction Coefficients and Velocity Profiles for Laminar and Turbulent Boundary Layers and an Assessment of Probe Effects," by R. M. O'Donnell, NACA TN 3122, 1954, 38 p.

107 "Experimental Velocity Profiles for Adiabatic Supersonic Flow of Air in a Tube," by J. Kaye, G. A. Brown, and J. J. Dieckmann, M.I.T. Report. Condensed in *J. Aero. Sci.*, vol. 21, 1954, p. 203.

108 "Viscous Effects on Pitot Tubes at Low Speeds," by F. A. MacMillan, Engrg. Lab., Cambridge (Aeronautical Research Council, Fluid Motion Sub-Committee), Report F.M. 2081, 1954, 8 p.

109 "Design of Total Pressure Probes for Minimum Interference With Measured Flow," by J. L. Livesey, *J. Aero. Sci.*, vol. 21, 1954, p. 641.

110 "An Experimental Investigation of Reynolds Number Effects on Supersonic Static Probes," by L. N. Wilson, Univ. of Toronto, UTIA TN-3, 1954, xii, 24 p.

111 "Pressure Probe Response in Fluctuating Flow," by R. E. Kronauer and H. P. Grant, Proc., 2nd U.S. National Congress of Applied Mechanics, 1954, pp. 763–769.

112 "Boundary Layer Theory," by H. Schlichting, tr. by J. Kestin, McGraw-Hill Book Co., Inc., New York, N. Y., 1955, xx, 535 p.

113 "Pressure Distribution on a Hydrofoil Running Near the Water Surface," by B. R. Parkin, B. Perry, and T. Y. Wu, C.I.T., Hydrodynamics Lab., Report No. 47-2, 1955, vi, 38 p.

114 "Cantilevered Pitot Cylinder," by F. A. L. Winternitz, *The Engineer*, vol. 199, 1955, pp. 729–732.

115 "A Deceleration Probe for Measuring Stagnation Pressure and Velocity of a Particle-Laden Gas Stream," by J. L. Dussourd and A. H. Shapiro, M.I.T., Dept. Mech. Engrg., Gas Turbine Lab., Report DIC 5-6985, based on ScD thesis, 1955.

116 "A Three-Dimensional Spherical Pitot Probe," by J. C. Lee and J. E. Ash, Trans. ASME, vol. 78, 1956, pp. 603–608.

117 "Streamlined Pitot-Tube Bar for Measuring Water Flow in Large Pipe," by F. Numachi, H. Murai, and S. Abe, Trans. ASME, vol. 78, 1956, pp. 1079–1089.

118 "Instructions for Installing and Operating Indicating Flow Meters, Type T, With Flow Nozzles, Pitot Tubes and Orifice Tubes (Instructions 86512A)," second edition, General Electric Company, Schenectady, N. Y., 1925, 19 p. + 11 fold. diagrams in pocket.

119 "Design Manual for Air and Gas Flow Measurement Probes, Volume I—Pressure," by C. B. Haughton, Jr., and E. P. Newborg, General Electric Co., Aircraft Gas Turbine Engineering Div., West Lynn, Mass., Bul. R51GT41, Sept. 1951, various pagination. Index and Corrections to this bulletin, issued by authors Dec., 1951, Bul. DF51GT379.

120 "Calibration and Use of the Spherical Search Tube," by B. S. Kudravets, Westinghouse Report AGT-338.

121 "The Averaging Pressure Probe," by H. Gladston, Westinghouse Report AGT-477.

122 "The Effect of Hole Geometry on the Total Pressure Recovery of Cylindrical Pressure Probes," by F. A. Gagliardi and G. A. Cederborg, Westinghouse Report AGT-1088.

123 "A Note on the Accuracy of the Averaging Pressure Probe," by F. F. Ehrich, Westinghouse Report AGT-1157.

124 "The Directional Pressure Probe-Claw Type," by R. P. Benedict, Westinghouse Report AGT-1196.

125 "The Directional Pressure Probe-Cylindrical Type," by R. P. Benedict and W. E. Gunson, Westinghouse Report AGT-1210.

126 "The Development of the Disc Probe," by W. N. Gilmer, Westinghouse Report AGT-1295.

127 "The Cylindrical Pressure Probe Accuracy as Affected by Angle of Attack, Mach Number, and Hole Geometry," by E. F. Hammond, Westinghouse Report AGT-781.

128 "The Impact Tube," S. A. Moss, Trans. ASME, vol. 38, 1916, p. 761.

129 "Discharge Coefficients of Square-Edged Orifices for Measuring the Flow of Air," by H. S. Bean, E. Buckingham, and P. S. Murphy, *NBS Journal Res.*, vol. 2, March, 1929, p. 561.

Discussion

WALTON FORSTALL.[3] This is a valuable summary of present knowledge concerning the Pitot tube. It is most helpful to have so much information brought together in one place, a service for which the author will have the sincere, though often unspoken, thanks of many workers in fluid mechanics. The paper, in addition, is suggestive of further work that should be done.

The writer is curious about some of the implications of Fig. 14. If the velocity profile is symmetrical, one would expect a symmetrical curve from the transverse tube and, indeed, the "A Impact" curve seems reasonably symmetrical. One would now expect that the "B Impact" readings would be slightly less than the A Impact values due to the difference in velocities which should result from the difference in areas blocked. However, the maximum pressure difference that can be attributed to blocking is only about 9 per cent (when the B tube is barely inserted) and decreases rapidly. The B curve should approach the A curve more and more closely as the cantilevered probe approaches the far side of the pipe. Since it does not, some essential difference in the behavior of the measuring device is indicated, perhaps attributable to the presence or absence of a free end.

The author states that the shape of the static-pressure curve illustrates the difficulties in the interpretation of such measurements. Indeed it does, but perhaps there is an opportunity here for someone to explore the matter further. It may be that by some additional work the mystery could be uncovered.

T. W. HEAD.[4] My comments consist of two questions. First, how much straight pipe is required ahead of an instrument station to assure uniform flow? Are the correction data in the paper applicable to air flow at low Reynolds numbers?

AUTHOR'S CLOSURE

Mr. Forstall has been most generous in his general comments on the paper. His discussion points out the apparent difference in mutual interference between the flow about the transverse tube and pipe walls and the cantilevered tube and the pipe walls as shown by Fig. 14, impact pressure curves. Due to the difference in free end conditions, the author does not agree that curves A and B should necessarily approach each other as the pressure holes approach the far side of the pipe. No satisfactory explanation can be made for the experimental static-pressure curves at this time.

Mr. Head raises a very practical question which is most difficult to answer briefly since the velocity distribution at the instrument station is a function of the upstream pipe as well as the geometry of the piping system upstream of the straight section if insufficient straight pipe is used. Some idea of the order of magnitude of required straight lengths is presented in reference (76) for various upstream pipe fittings, a typical example being about 40 diameters for a single 90-degree elbow. The author has seen measurable changes in velocity distributions as far downstream from a single elbow as 125 diameters.

With regard to Mr. Head's second question, it should be noted that usually the compressibility of air may be neglected at low Reynolds numbers. Experiments at low Reynolds numbers reported in Fig. 9 include data for air and liquids indicating that correction data are applicable to both fluids.

A recent article of interest is:

130 "Investigation of the Time Response and Outgassing Effects of Pressure Probes in Free Molecule Flow," by E. L. Harris, Univ. of Toronto, UTIA TN-6, 1955, 14 p.

---

[3] Assistant Dean, Carnegie Institute of Technology, Pittsburgh, Pa. Mem. ASME.

[4] Research Engineer, Caterpillar Tractor Company, Peoria, Ill.

Pulsation Errors in Manometer Gages

By T. J. WILLIAMS,[1] SWANSEA, WALES

It is known that manometer gages of conventional design are subject to errors when the gas-pressure differential is pulsating. In this paper, various factors contributing to the production of such errors are analyzed and the requirements for their elimination established. A differential manometer capable of indicating the true time-mean of a pulsating head is described.

Introduction

MANY instruments are available for measuring a steady gas-pressure differential with a high degree of accuracy. Little information is available, however, for designing a manometer capable of indicating accurately the time mean of a periodic pulsating pressure drop. Such pulsating conditions are encountered by a manometer employed for measuring the head across a pressure-inferential meter installed in a duct leading to or from a reciprocating engine or compressor where the damping capacity between the meter and the source of pulsation is inadequate.

With pressure-inferential meters of the "square-law" type, such as the orifice-plate meter, in which the head is proportional to the square of the flow velocity, the manometer is required to measure the time-mean of the square root of the instantaneous pressure drop across the meter element. Although an attempt to construct a manometer for this specific purpose was made by Bailey (1),[2] in general it has been assumed that any type of damped manometer will give a reading approximating the time-mean of the instantaneous pressure differential. In the great majority of such cases it may be shown that the metering device will then read incorrectly owing to the velocity fluctuations (2). It has been found in practice, however, that the observed errors are often far greater than those which could be attributed to velocity fluctuations alone (3).

In the case of viscous flowmeters (4) the head across the metering element is directly proportional to the gas velocity, and with pulsating flows, the manometer is required to indicate the true time-mean of the pressure differential over the cycle. In an investigation conducted by Kastner and the present author (5), large errors were noted when conventional manometers were used to determine the head across the metering element, although these manometers were perfectly satisfactory with steady flows.

Wave Action in the Manometer Connecting Leads

In order to locate a manometer in a position convenient to the observer, or in order to prevent the transmission of mechanical vibrations to the gage, it is often necessary to use connecting leads of some length between the manometer and the source of pressure fluctuation. These pressure fluctuations will initiate a series of waves which will be propagated along the leads toward the manometer. The form of the pressure pattern at the manometer will, in general, differ in form from the original pattern at the source due to (*a*) variations in propagation velocity with pulse pressure; (*b*) wave attenuation due to gas viscosity and wall friction; and (*c*) wave reflection at both ends of the connecting leads. It will be shown later that the manometer reading is often dependent on the form of the pulsation pattern; hence the connecting leads can have an important influence on the indicated head.

Propagation Velocity. Neglecting the effects of wave attenuation, it has been demonstrated by Earnshaw (6) that the velocity of propagation c along the connecting leads of a nonshock-fronted wave point at an absolute pressure P propagated into stationary air at an absolute pressure P_0 is given by

$$c = a_0 \left[6 \left(\frac{P}{P_0} \right)^{1/7} - 5 \right] \quad \text{.....[1]}$$

where a_0 is the acoustic velocity in the undisturbed air, the value of the adiabatic index being taken as 1.4. Since $c > a_0$ when $P > P_0$, there is a tendency in pressure pulses for the wave crest to overtake the leading portion of the pulse, an air wave point at a pressure of 1 in. of mercury gage, for example, having a propagation velocity 3 per cent greater than the acoustic velocity in atmospheric air. The type of pulse distortion expected for a single sinusoidal pulse is shown in Fig. 1, the tendency being for wave fronts with positive pressure gradients to become shock-fronted when the leads are of sufficient length.

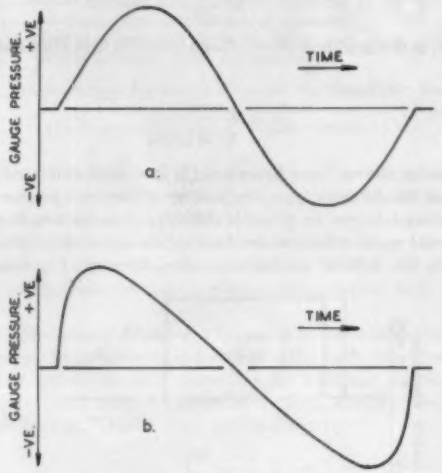

Fig. 1 Pulse Distortion Due to Variation in Propagation Velocity With Pressure
(*a*, Pulse at source. *b*, Pulse at a point along connecting lead.)

Wave Attenuation. The wall roughness and the gas viscosity will result in a retardation of the gas-particle velocity in the manometer connecting leads. Where the inner surface of the tubing used is comparatively rough and the pulse amplitude sufficiently large, the flow resistance will be proportional to V^n, where V is the gas velocity and n an index having a value between 1 and 2. The solution of the resulting flow equations would be very complex, and it is therefore proposed to deal only with the case where the flow is laminar in character. With $^1/_4$-in. smooth-

[1] University Lecturer in Engineering, University College of Swansea, Engineering Department, Singleton Park.

[2] Numbers in parentheses refer to the Bibliography at the end of the paper.

Contributed by the Research Committee on Fluid Meters and presented at the Diamond Jubilee Annual Meeting, Chicago, Ill., November 13–18, 1955, of The American Society of Mechanical Engineers.

Note: Statements and opinions advanced in papers are to be understood as individual expressions of their authors and not those of the Society. Manuscript received at ASME Headquarters, January 4, 1955. Condensed from Paper No. 55—A-92.

bore metal tubes, for example, it would be expected that this would be the case with air providing the pulsation amplitude did not exceed about ± 7 in. of water.

With the conditions for laminar flow satisfied and neglecting the effect of frictional heating and heat transference across the tube walls, Euler's equations of flow become

$$-\frac{\partial p}{\partial x} - Rw = \frac{\rho_0}{g}\frac{\partial w}{\partial t} \quad \ldots\ldots [2]$$

$$\frac{1}{\gamma P_0}\frac{\partial p}{\partial t} = -\frac{\partial w}{\partial x} \quad \ldots\ldots [3]$$

where P_0 and ρ_0 refer to the absolute pressure and density, respectively, of the undisturbed gas; R is the frictional resistance per unit area, length, and velocity; and w is the mean velocity across the section in the direction of the length x of the connecting lead. These partial differential equations are of the same form as those applying in the case of certain electrical transmission-line problems and can be solved by means of an appropriate Laplace transform (7). If the variable gage pressure p_i at the source can be expressed as a function of the time t, $p_i = f(t)$, say, and if $p_i = 0$ when $t = 0$, then the pressure p_x at a distance x along the connecting lead will be given by

$$p_x = f\left(t - \frac{x}{a_0}\right)e^{-kx} + kx\int_x^{a_0 t} f\left(t - \frac{z}{a_0}\right)e^{-kz}\frac{I_1(k\sqrt{z^2 - x^2})}{\sqrt{z^2 - x^2}}\,dz \quad \ldots [4]$$

when

$$t > \frac{x}{a_0}$$

where I_1 is the modified Bessel function of the first kind and order 1; and

$$k = \frac{R}{\sqrt{2P_0 g\gamma\rho_0}}$$

It can be shown from Equation [4] that the attenuated pulsation is of the diffusive type, the passage of the main portion of the pulse being followed by a tail of diffusive pressure resulting from the partial wave reflection due to the flow resistance. Shown in Fig. 2 is the type of attenuated pulse expected at a distance x

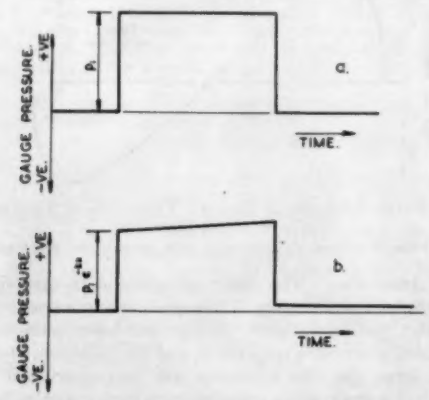

FIG. 2 DISTORTION OF "RECTANGULAR" PRESSURE PULSE DUE TO WAVE ATTENUATION

(a, Pulse at source. b, Pulse at a point distance x along connecting lead, flow resistance being assumed directly proportional to particle velocity.)

along an infinitely long lead when the original pulsation is rectangular in form, the initial pulse amplitude being p_i.

Wave Reflection. Wave reflection will occur at both ends of the connecting leads. At the connection to the source of pressure pulsation, the reflection generally will be of the "open-end" type assuming that the volume of the chamber or the cross-sectional area of the duct is sufficiently large to insure that the pressure there is unaffected by the inflows and outflows of gas in the connecting leads. Therefore pressure pulses will be reflected as rarefactions and vice versa, the incident absolute pressure P_i of a wave point and the corresponding reflected absolute pressure P_r, being related for air by the equation[3]

$$\left(\frac{P_r}{P}\right)^{1/\gamma} = 2 - \left(\frac{P_i}{P}\right)^{1/\gamma} \quad \ldots\ldots [5]$$

where P is the absolute pressure in the chamber or duct, the connection being assumed to be "bell-mouthed." For waves of small amplitude this equation reduces to $P_r = 2P - P_i$.

At the manometer end of the connecting leads, the amplitude of the reflected pulse will be dependent upon the air volume V in the manometer above the liquid column. On equating the air flow into this volume[3] to the rate of increase of mass in the volume, the following equation is obtained

$$5\,a_0 S\left[\left(\frac{P_i}{P_0}\right)^{1/\gamma} - \left(\frac{P_r}{P_0}\right)^{1/\gamma}\right] = \frac{V}{\gamma P_2}\frac{dP_2}{dt} \quad \ldots\ldots [6]$$

where P_2 is the absolute instantaneous pressure in the manometer volume, P_0 the absolute pressure of the undisturbed air, and S the effective area of the lead connection at the manometer. Assuming that the net pressure at the manometer end of the connecting lead is equal to the pressure P_2, then it can be shown that Equation [6] can be rewritten as

$$7\,a_0 S\left[2\left(\frac{P_i}{P_0}\right)^{1/\gamma} - \left(\frac{P_2}{P_0}\right)^{1/\gamma} - 1\right] = \frac{V}{P_2}\frac{dP_2}{dt} \quad \ldots\ldots [7]$$

and for waves of small amplitude this equation becomes

$$\frac{V}{a_0 S}\frac{dp_2}{dt} + p_2 = 2\,p_i \quad \ldots\ldots [8]$$

where p_2 and p_i are the corresponding gage pressures in the manometer capacity and of the incident wave point, respectively. The solution of this differential equation is

$$p_2 = \frac{2a_0 S}{V}e^{-\left(\frac{a_0 S}{V}\right)t}\int p_i\, e^{\left(\frac{a_0 S}{V}\right)t}\,dt + Ce^{-\left(\frac{a_0 S}{V}\right)t} \quad \ldots [9]$$

When the pressure pulsation is periodic, after allowing sufficient time for the pressure patterns to stabilize, the term

$$Ce^{-\left(\frac{a_0 S}{V}\right)t}$$

can be neglected, the reflected wave gage pressure p_r being obtained from

$$p_r = p_2 - p_i \quad \ldots\ldots [10]$$

It should be noted that the effective area S of the lead connection at the manometer will not generally be the same for inflows and outflows.

In the case of a U-tube manometer in which the tube bore is equal to that of the connecting lead, assuming that the surface oscillation of the liquid column is small, then for small pulse amplitudes, the gage pressure p_2 at the liquid surface will be twice that of the incident pulse p_i.

[3] See reference (8), p. 286.

The pressure pattern of the incident wave arriving at the manometer will, of course, be that resulting from the superimposition of periodic pulsations, originating at the main duct or capacity, which have traversed the length of the leads 1, 3, 5, ... times with reflection at the ends of the connecting tube. An analytical determination of the mean manometer pressure P_2 after the stabilization of the pressure patterns would therefore be a matter of some complexity, particularly as attenuation effects would have to be taken into account.

Capacities and Restrictions in the Manometer Leads

While it is possible to reduce considerably the pulsation amplitude at the manometer liquid surface by inserting either an orifice-type restriction or a capacity, or both, into the manometer leads or forming part of the manometer itself, the following treatment shows that such devices contribute to the production of errors in the manometer reading. The effect of wave action in the connecting leads is neglected, the manometer capacity being assumed to be connected directly to the source of pulsation through an orifice.

Manometer Pressure Gradient. Assuming that the flow through the orifice is proportional to the square root of the pressure difference across it, then by equating the instantaneous air-mass flow through the orifice to the rate of increase of mass in the capacity, the following approximate expression for the manometer pressure gradient is obtained for adiabatic conditions and moderate amplitudes

$$\frac{dp_2}{dt} = \pm K\sqrt{\pm (p_1 - p_2)} \quad \ldots\ldots [11]$$

where

$$K = \frac{a_0 S}{V}\sqrt{\frac{14}{5}P_0}$$

a_0 = acoustic velocity
S = effective area of orifice
V = volume
p_1 = instantaneous gage pressure at source
p_2 = instantaneous gage pressure in manometer capacity
P_0 = mean absolute pressure

the upper signs being taken when $p_1 > p_2$.

Manometer Pressure Time Lag. If the pressure in the main duct or chamber were to change suddenly from zero gage pressure to a gage pressure p_1', there would be a time lag T before the pressure in the manometer capacity attained the pressure at the source. On integrating Equation [11] we obtain

$$\sqrt{p_1'} - \sqrt{(p_1' - p_2)} = \frac{K}{2}t \quad \ldots\ldots [12]$$

The total time lag is given by

$$T = \frac{2}{K}\sqrt{p_1'} \quad \ldots\ldots [13]$$

Constant Gradient Pulsation. If the pressure pattern at the source consists of a series of constant-pressure gradients

$$\frac{dp_1}{dt} = m \text{ (say)} \quad \ldots\ldots [14]$$

then writing

$$z^2 = \pm (p_1 - p_2) \quad \ldots\ldots [15]$$

and differentiating with respect to t

$$2z\frac{dz}{dt} = \pm\frac{dp_1}{dt} \mp \frac{dp_2}{dt}$$

$$= \pm m - Kz \quad \ldots\ldots [16]$$

from Equations [14] and [11]. Integrating this equation and taking $t = 0$ when $p_1 = p_2$

$$t = -\frac{2}{K}\sqrt{\pm (p_1 - p_2)}$$

$$\mp \frac{2m}{K}\log_e\left[\frac{\pm m - K\sqrt{\pm (p_1 - p_2)}}{\pm m}\right] \quad \ldots\ldots [17]$$

the upper sign being taken in each case when $p_1 > p_2$. Fig. 3 shows the type of manometer-response curves expected for both positive and negative constant-pressure gradients at the source of

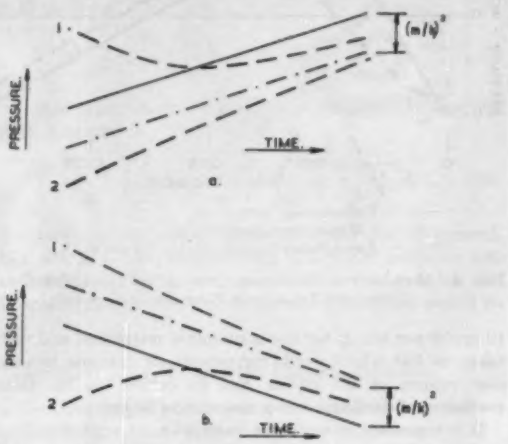

——— Pressure at source, p_1
– – – – Pressure in manometer capacity, p_2
— . —Asymptote to manometer pressure
1 Initial pressure above asymptote
2 Initial pressure below asymptote

Fig. 3 Manometer Response Curves to Constant Pressure Gradients at Source
(a, Positive gradient. b, Negative gradient.)

pulsation. It will be noted that in either case the manometer pressure tends toward an asymptote parallel to the pressure line p_1, but displaced vertically from it at a distance $(m/K)^2$. The asymptote is below the pressure line when the gradient m is positive, and above when m is negative. Where the pressure line sp_1 and p_2 cross, the manometer pressure gradient is, of course, zero.

Mean Manometer Pressure. In order to determine the mean pressure at the manometer in relation to the mean pressure at the source of pulsation, it is necessary to calculate the areas of the loops of the manometer pressure curve p_2, above or below the pressure lines p_1. These areas will be given by

$$A = \int_0^t (p_2 - p_1)\,dt \quad \ldots\ldots [18]$$

the area being positive when the loop is above the pressure line p_1. On substituting for $(p_2 - p_1)$ and dt in terms of z from Equations [15] and [16], respectively, the foregoing integral can be rewritten as

$$A = \int_0^z \frac{\mp 2z^2\,dz}{\pm m - Kz}$$

$$= \mp\frac{2}{K}\left[\frac{z^3}{3} \pm \frac{m}{K}z^2 + \left(\frac{m}{K}\right)^2 z \pm \left(\frac{m}{K}\right)^3 \log_e\left(\frac{\pm m - Kz}{\pm m}\right)\right]$$

$$\ldots [19]$$

the upper sign being taken in each case when $p_1 > p_2$, and the area being determined from the point at which the curves p_1 and p_2 cross.

Example. To determine the mean manometer pressure corresponding to the source pressure pattern shown in Fig. 4, the pulsation amplitude being ±1 in. Hg with a positive gradient three times as great as the negative and a pulsation frequency of

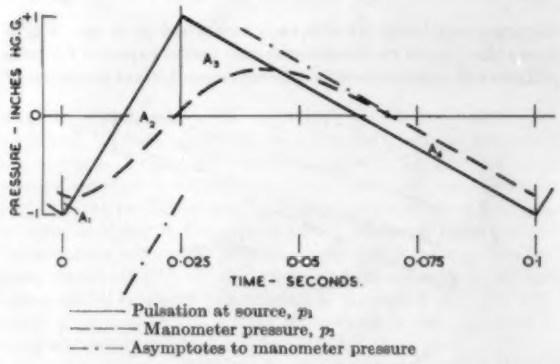

FIG. 4 MANOMETER RESPONSE CURVES TO CONSTANT GRADIENT PRESSURE PULSATION PATTERN; (K = 480)

10 cycles per sec, K for the manometer restriction and volume is taken as 480, which would correspond, for example, to a manometer volume of 6.5 cu in. and an orifice $^1/_{16}$ in. diam, the coefficient of discharge being assumed to be unity.

It is necessary to assume a value of p_2 at a given point in the cycle and, taking this as a starting point, determine the subsequent manometer pressure curves p_2 by means of Equation [17]. Unless the assumed value of p_2 is repeated at the end of a cyclic period, the starting value will have to be readjusted, and the manometer response curve redrawn until cyclic repetition is achieved. The curve obtained in this way is shown in Fig. 4, and the values of the loop areas A_1, A_2, A_3, and A_4 calculated by means of Equation [19] are +2.1, —127, —69.5, and +84.5 in. Hg sec × 10^{-4} units, respectively. The mean manometer pressure is, therefore, —0.11 in. Hg gage as compared with the zero mean gage value of the pressure at the source.

Small Values of K. Where the orifice restriction is of small diameter, and/or the manometer volume is large, cyclical variations in manometer pressure can be neglected. By equating the air inflow into the manometer volumes to the outflow over the cycle, the following integral is obtained

$$\int_0^T \pm \sqrt{\pm (p_1 - p_2)}\, dt = 0 \quad \ldots\ldots\ldots [20]$$

the upper signs being taken when $p_1 > p_2$, T being the period of the pulsation.

In the case of a pulsation pattern in which the gage pressure is p_1' for $1/n$th of the pulsation period, and zero for the remainder, from Equation [20] it can be shown that

(Mean manometer gage pressure)

$$= \frac{n}{1 + (n-1)^2} \text{(mean gage pressure at source)} \quad \ldots [21]$$

Thus if $n = 4$, the mean gage pressure would be underestimated by 60 per cent.

VISCOUS RESISTORS IN MANOMETER LEADS

If viscous resisting elements were inserted into the manometer leads, the rate of mass flow W through the resistors corresponding to a pressure differential Δp would be given by an equation of the form

$$W = \frac{K}{\nu} \Delta p \quad \ldots\ldots\ldots [22]$$

where ν is the kinematic viscosity of the air or gas, and K a constant for the element, providing Δp did not exceed a value corresponding to that which gave the critical Reynolds number for the gas flow through the elements. With the resistor inserted near to the source of pulsation, on equating the mass inflow and outflow over a cycle as before, and neglecting wave action in the leads

$$\int_0^T \frac{1}{\nu} (p_1 - p_2)\, dt = 0 \quad \ldots\ldots\ldots [23]$$

p_1 and p_2 corresponding to the source and manometer gage pressures, respectively. Where changes of kinematic viscosity during the cycle can be neglected, then

$$\frac{1}{T} \int_0^T p_1\, dt = \frac{1}{T} \int_0^T p_2\, dt \quad \ldots\ldots\ldots [24]$$

and the mean manometer gage pressure is equal to the mean pressure at the source. Where long connecting leads are necessary, the resistance of the viscous elements should be high in order to eliminate wave action in the leads between the resistors and the manometer, the pressure p_2 then being assumed constant over the cycle.

When the amplitude of the pressure pulsations at the source are comparatively large, errors can arise due to variations in kinematic viscosity. In the case of high resistance "viscous plugs" and an air pressure pattern in which the pressure is +5 in. Hg gage for half the pulsation period, and —5 in. Hg for the remaining half, the mean manometer pressure p_2 would be about 0.4 in. Hg gage as compared with the true gage value of zero, adiabatic conditions being assumed.

The effectiveness of felt pads as viscous damping devices, as suggested by Alcock (2, 4, 9), is rather doubtful except in the case of very small pressure pulsation amplitudes. The investigation of Fleming and Binder (9) into the flow of air through plugs of cotton wool and steel wool, respectively, showed that these materials exhibited linear flow characteristics for very small flows only.

MANOMETER LIQUID DAMPING

Viscous Damping. In the simple manometer shown diagrammatically in Fig. 5, and consisting of two cylindrical tubes A and B of equal cross-sectional area S connected at their bases by a length l of tubing C of area s, the liquid column surfaces are subjected to a periodic pressure differential Δp such that the mean head indicated by the manometer is H. It will be assumed that the whole mass of the liquid column, of mean height h, in either cylinder moves with the same velocity at any instant, and that the resistance to the liquid flow is confined to the connecting tube and is viscous.

The kinetic energy of the liquid is, in gravitational units

$$\frac{\rho}{2g} S \left(\frac{dx}{dt}\right)^2 \left[2h + l\frac{S}{s}\right]$$

where x is the surface displacement. The potential energy relative to the mean level is

$$\rho S x [H + x]$$

and the rate of energy dissipation due to viscous resistance in the connecting tube

$$\frac{8\mu\pi l}{g}\left(\frac{S}{s}\right)^2\left(\frac{dx}{dt}\right)^2$$

By equating the rate of change of total energy (kinetic and potential) of the liquid to the difference between the rate of doing work by the pressure differential and the rate of energy dissipation in the connecting tube due to viscosity, the following differential equation is obtained

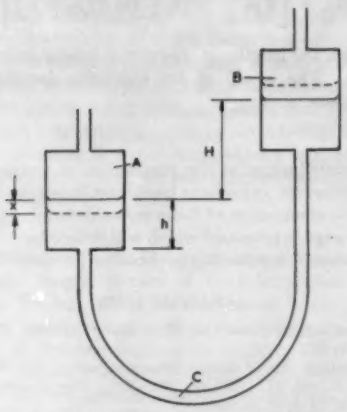

FIG. 5 DIAGRAM OF SIMPLE MANOMETER

$$C_2\frac{d^2x}{dt^2} + C_1\frac{dx}{dt} + C_0 x = \frac{\Delta p}{\rho} - H \quad [25]$$

where

$$C_2 = \frac{1}{g}\left[2h + l\frac{S}{s}\right]$$

$$C_1 = \frac{8\nu\pi Sl}{gs^2}$$

$$C_0 = 2$$

Aperiodic Damping. The condition necessary for complete damping of the natural oscillations (aperiodic damping) is

$$C_1^2 > 4\,C_0C_2$$

If $2h$ can be neglected in comparison with $l(S/s)$, then for a manometer containing water at 60 F this condition can be written as

$$l\frac{S}{s^2} > 2.7 \times 10^9$$

the dimensions being in feet.

Maximum Surface Oscillation. Given the maximum allowable surface oscillation x_{max}, and the frequency and amplitude of the pulsating pressure drop, which is assumed to vary sinusoidally, the necessary amount of damping can be determined[4]

Manometer Reading With Viscous and Nonviscous Damping

(*a*) *Viscous Damping.* The mean pressure difference across the manometer is

$$\frac{1}{T}\int_0^T \Delta p\ dt$$

T being the period of the pulsating pressure differential. On integrating Equation [25] with respect to t

$$H = \frac{1}{\rho T}\int_0^T \Delta p\ dt \quad [26]$$

after the manometer has had sufficient time to reach a steady reading. The mean indicated head therefore corresponds to the true mean pressure difference.

(*b*) *Nonviscous Damping.* If it were attempted to damp the liquid oscillation by means of an orifice or restriction in the connecting tube, then the resistance to motion would be proportional to (velocity)^n, n being an index having a value between 1 and 2. The differential equation for the liquid oscillation would then be of the form

$$C_2\frac{d^2x}{dt^2} \pm C_1\left(\frac{dx}{dt}\right)^n + C_0x = \frac{\Delta p}{\rho} - H \quad [27]$$

the upper sign being chosen when dx/dt is positive. Integrating this equation results in

$$H = \frac{1}{\rho T}\int_0^T \Delta p\ dt - \frac{C_1}{T}\int_0^T \pm\left(\frac{dx}{dt}\right)^n dt \quad [28]$$

Thus a manometer damped in this way would not, in general, indicate the true mean pressure head unless the pulsation was symmetrical in form, as in the case of a sinusoidal pressure differential where the second term on the right-hand side would be zero.

ELIMINATION OF MANOMETER PULSATION ERRORS

From the foregoing, it would appear that manometer pulsation errors can arise from one or more of the following sources:

1 Wave action and attenuation in the manometer connecting leads resulting in distortion at the manometer of the original pressure-pulsation pattern.

2 Volumes included in the manometer connections or forming part of the manometer itself. Errors occur whether the volumes are symmetrical on either side of the manometer liquid column or not.

3 Restrictions or throttles in the manometer leads.

4 Nonviscous damping of the manometer liquid oscillation.

Although the inclusion of "viscous" damping elements in the connecting leads should ideally eliminate errors resulting from pressure pulsations of moderate amplitudes, the use of short pads of felt or similar material can result in a partial improvement only in manometer accuracy.

It is concluded that a manometer gage must satisfy the following requirements if pressure-pulsation errors are to be eliminated:

1 The length of the "gas" filled leads from the source of pressure to the manometer liquid surface to be as short as possible, and the cross section of the leads to be uniform.

2 Damping to be confined to the manometer liquid or liquids and to be viscous in nature.

A type of manometer which satisfies these requirements is shown diagrammatically in Fig. 6, and has been used successfully in conjunction with viscous flowmeters subjected to flow pulsations (5). This is a two-liquid manometer in which the menisci of the upper liquid 1 are exposed to the pressure or pressure differential to be measured. These menisci are maintained at a constant level for all heads measured, the length of tubing A and B, of cross-sectional area S, above the liquid columns being very short, usually less than $^1/_2$ in. The menisci separating the two liquids are contained in two glass tubes of cross-sectional area s, one tube C being fixed in height but of adjustable inclination, while the other D is attached to an adjustable vernier height gage. To obtain a reading with this gage, the vernier slide is adjusted so as to maintain the meniscus in the inclined tube at a

[4] See, for example, Thomson (10), pp. 64–65.

definite position as determined by means of a small microscope F fitted with cross wires. To ensure an identical form of the menisci at each reading, it is essential that all adjustments of the vernier are either in an upward or downward direction when determining the head, the direction chosen being such as to produce

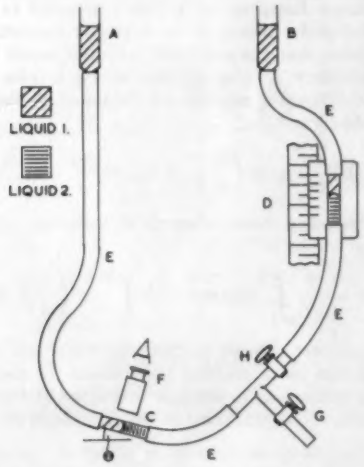

FIG. 6 DIAGRAM OF TWO-LIQUID DIFFERENTIAL MANOMETER

a meniscus concave to the darker liquid at the inclined tube. The tubing E must be chemically clean to maintain a clear meniscus, polyvinyl-chloride tubing being suitable as it is both clean and translucent, thus enabling the presence of any trapped gas to be detected easily. The wall rigidity of this tubing is also advantageous as it tends to maintain a reasonably constant cross section when bent.

In filling the gage with liquids, the heavier liquid 2 is first introduced through the T-connection G, liquid 1 being then poured into each leg from above with the connecting cock H closed. This prevents any mixing of the two liquids.

The choice of liquids is dependent upon the maximum heads to be measured. For heads of a few inches of water, oil can form the upper liquid 1, and water the lower. For larger heads, mercury should be used for liquid 2. The indicated head in each case will be

$$\frac{(\rho_2 - \rho_1)}{\rho_w} H \text{ in. of water}$$

where ρ_1, ρ_2, and ρ_w are the densities of liquid 1, liquid 2, and water, respectively, H being the vernier deflection from the zero differential position. A temperature correction must be applied because of the varying densities.

Gage Sensitivity. Gage sensitivity is defined as the ratio of the deflection Δx of the meniscus in the inclined tube, to the corresponding change in head ΔH, and can be shown to be

$$\frac{\Delta x}{\Delta H} = \frac{\rho_w}{(1 + \sin\theta)(\rho_2 - \rho_1) + 2\frac{s}{S}\rho_1} \quad \ldots\ldots [29]$$

Therefore sensitivity can be increased by (*a*) decreasing the angle of inclination θ; (*b*) increasing the area ratio S/s; (*c*) choosing liquids 1 and 2 with more equal densities.

Gage Damping. With this manometer gage, the value of the constants in the differential Equation [25] are

$$C_2 = \frac{\rho_2 l_2 + \rho_1 l_1}{g}$$

$$C_1 = \frac{8\pi}{g}\frac{(\mu_2 l_2 + \mu_1 l_1)}{s}$$

$$C_0 = \left[2\rho_1\frac{s}{S} + (1 + \sin\theta)(\rho_2 - \rho_1)\right]$$

l_1 and l_2 being the lengths of connecting tubing corresponding to each liquid. The condition for aperiodic damping is $C_1^2 > 4\,C_0C_2$ as before.

CONCLUSION

Factors contributing to the production of pressure-pulsation errors in manometer gages have been established, and the requirements for the elimination of these errors determined. A form of manometer gage is proposed which will determine accurately the true time-mean of a pulsating pressure or pressure differential.

BIBLIOGRAPHY

1 "Pulsating Air Flow," by N. P. Bailey, Trans. ASME, vol. 56 1934, pp. 781–786.

2 "Pulsating Air Velocity Measurement," by N. P. Bailey, Trans. ASME, vol. 61, 1939, pp. 301–308. See also contribution to the discussion by J. F. Alcock.

3 "Development in the Measuring of Pulsating Flows With Inferential-Head Meters," by S. R. Beitler, E. J. Lindahl, and H. B. McNichols, Trans. ASME, vol. 65, 1943, pp. 353–356.

4 "Improvements in or Relating to Fluid Flow Meters," by H. F. Ricardo and J. F. Alcock, British Patent Specification No. 473, 139, 1937.

5 "Pulsating Flow Measurement by Viscous Meters With Particular Reference to the Air Supply of Internal Combustion Engines," by L. J. Kastner and T. J. Williams, Proceedings of The Institution of Mechanical Engineers, vol. 169, no. 26, 1955.

6 "On the Mathematical Theory of Sound," by S. Earnshaw, Philosophical Trans. of the Royal Society of London, vol. 195, 1860, pp. 133–148.

7 "Operational Methods in Applied Mathematics," by H. S. Carshaw and J. C. Jaeger, Oxford University Press, London, England, second edition, 1947, pp. 184–209.

8 "Wave Action Following Sudden Release of Compressed Gas From a Cylinder," by F. K. Bannister and G. F. Mucklow, Proceedings of The Institution of Mechanical Engineers, vol. 159, 1948, pp. 269–287.

9 "Study of Linear-Resistance Flowmeters," by F. W. Fleming and R. C. Binder, Trans. ASME, vol. 73, 1951, pp. 621–624. See also contribution to discussion by J. F. Alcock.

10 "Mechanical Vibrations," by W. T. Thomson, Allen and Unwin, London, England, 1950, pp. 64–65.

Discussion

E. G. CHILTON.[5] An inferential flow-measuring device generally can be divided into two distinct parts: The primary meter such as an orifice, nozzle, etc., which produces a signal which is some function of the flow rate and other variables of the flow; and the secondary system which translates the signal into a reading such as the difference between two legs on a manometer. It is with this secondary system that the author has concerned himself in this paper. Even this system can generally be divided into two parts, namely, the lead lines from the primary system to the recording element, and the recording element itself. What the author has to say regarding the behavior of the lead lines is applicable to a large number of secondary recorders and therefore of great general importance. He has pointed out that the lead lines themselves may introduce appreciable errors in the transmission

[5] Supervisor, Shell Development Company, Emeryville, Calif. Mem. ASME.

of the signal and thereby confirms results previously found by such American investigators as Taback[6] or Iberall.[7]

Unfortunately, it is the primary system which is of greatest concern today in cases of pulsating flow. Contrary to the author's remarks in the introduction to his paper, an inferential flowmeter does not necessarily follow the square law that it does under steady-state conditions. This has been convincingly demonstrated by many investigators,[8] and many of the large errors under velocity fluctuations of which the author talks may not be altogether due to errors in the secondary system but to the fact that the primary system does not follow the square law.

It might be mentioned in this connection that the American Gas Association is sponsoring a large-scale investigation into the errors due to pulsating flow and is considering separately and together both the primary and the secondary measuring systems of inferential meters.

ERNEST FREUDMAN.[9] The Development and Research Laboratory, Industrial Power Division of the International Harvester Company has for some time been interested in the problem of pulsating-flow measurement, with special reference to the air consumption of internal-combustion engines. We have constructed two "viscous flowmeters" which, when used in conjunction with an "electric micromanometer," have given good results on supercharged engines. With naturally aspirated engines, however, we have found that the connecting leads, as well as the manometer itself, have a profound effect on the air-flow measurement, see Figs. 7 and 8 of this discussion.

Consequently, we were greatly pleased in reading within the past few months the present paper as well as another paper on the subject by Professors Kastner and Williams.[10]

We have built a manometer similar to the one shown in Fig. 6 of the paper but unfortunately we have not been able to obtain results as excellent as those shown in his fig. 11.[10] A typical curve obtained with our manometer is shown in Fig. 9. In connection with the manometer development work we would like to make the following comments:

1 With reference to the manometer shown in Fig. 5 of the paper, does the author feel the assumption stating that the damping is confined to the connecting tube will bear experimental corroboration?

2 Equation [29] of the paper is an expression for the sensitivity of the manometer in Fig. 6, i.e.

$$\frac{\Delta x}{\Delta H} = \frac{\rho_w}{(1 + \sin\theta)(\rho_2 - \rho_1) + 2\frac{s}{S}\rho_1}$$

This equation may be written in a more general form as

$$\frac{\Delta x}{\Delta H} = \frac{\rho_w}{\left(\frac{s}{s_1} + \sin\theta\right)(\rho_2 - \rho_1) + 2\frac{s}{S}\rho_1}$$

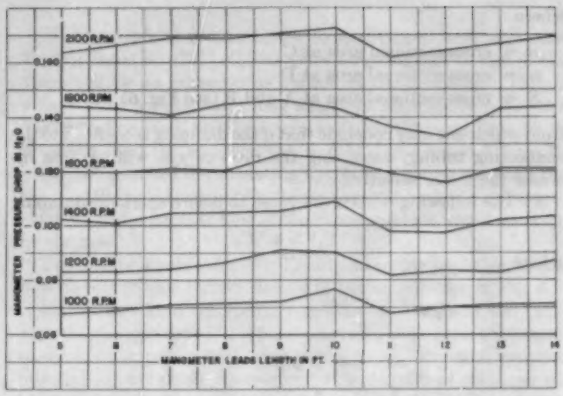

FIG. 7 MANOMETER PRESSURE DROP VERSUS LEAD LENGTH (WITH COTTON PLUGS)

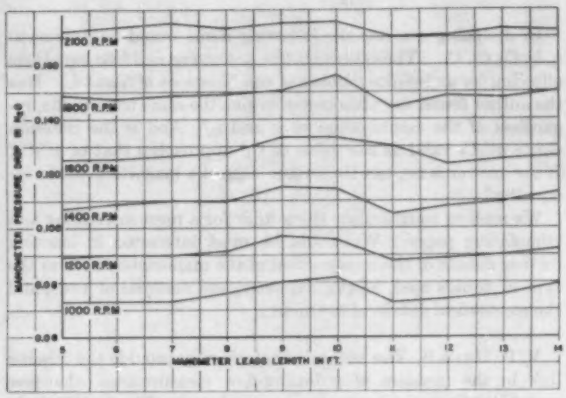

FIG. 8 MANOMETER PRESSURE DROP VERSUS LEAD LENGTH (WITHOUT COTTON PLUGS)

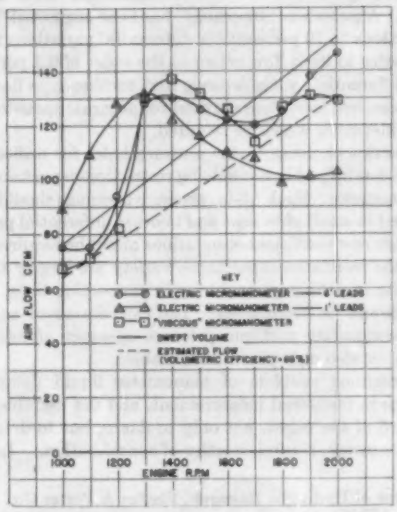

FIG. 9 AIR-FLOW MEASUREMENTS WITH VARIOUS MANOMETERS ON THE IHD 264 ENGINE

[6] "Response of Pressure Measuring Systems to Oscillating Pressures," by I. Taback, NACA TN 1819, February, 1949.

[7] "Attenuation of Oscillatory Pressures in Instrument Lines," by A. S. Iberall, Trans. ASME, vol. 72, 1950, pp. 689–695.

[8] "Pulsating-Flow Measurement—A Literature Survey," by A. K. Oppenheim and E. G. Chilton, Trans. ASME, vol. 77, 1955, pp. 231–248.

[9] Test Engineer, Industrial Power Engineering Department, Development and Research Laboratory, International Harvester Company, Melrose Park, Ill.

[10] See reference (5) of the Bibliography of the paper.

where

s = cross-sectional area at C
s_1 = cross-sectional area at D
S = cross-sectional area at A and B (see Fig. 6)

from which one may conclude that if the damping is confined to the connecting tubing, decreasing the ratio of s/s_1 will likewise increase the meter sensitivity.

3 The following criteria are given to insure aperiodic damping

$$C_1^2 > 4C_2C_0$$

where

$$C_2 = \frac{\rho_2 l_2 + \rho_1 l_1}{g}$$

$$C_1 = \frac{8\pi}{g} \cdot \frac{\mu_2 l_2 + \mu_1 l_1}{s}$$

$$C_0 = \left[2\rho_1 \frac{s}{S} + (1 + \sin\theta)(\rho_2 - \rho_1) \right]$$

In designing a meter the following items would be unknown: l_1, l_2, C_0, C_1, C_2. Thus there are five unknowns and four equations allowing for an infinite number of combinations of l_1 and l_2. Has the author found the manometer to give the same true results, regardless of the combination of l_1 and l_2? And is the criterion $C_1^2 > 4C_2C_0$ valid as the value of C_1^2 approaches that of $4C_2C_0$? If the answer is no, can the author suggest a magnitude of the inequality?

We wish to congratulate the author for a most interesting and stimulating paper. We would be most interested in learning further details of the construction of the manometer, such as the type of liquids used, length, diameter, and material of leads, and the mechanical details of the meter.

V. P. Head.[11] The author's analysis may provide the missing link in the problem of pulsating-flow measurement whenever variable-differential flowmeters are employed. The ASME Fluid Meters Research Committee has attempted to reduce the complex phenomena of flow pulsation to a first approximation suitable for establishing a border line between significant and insignificant pulsation. A pulsation "threshold" has been suggested[12] limiting flow variations to 10 per cent (or differential variations to 20 per cent) in order to limit flow errors to the order of 0.1 per cent for variable-differential, variable-area, and turbine-type flowmeters. It was recognized that separate rules for accurate measurement of average differential would be required.

The practice of using $^1/_2$-in. pressure holes for orifice taps in large pipes has helped in minimizing restriction-capacitance errors at the manometer. Such $^1/_2$-in. pressure openings should perhaps be extended to small pipe sizes and to other differential producers, even though new coefficient correlations might be required. Large errors of the resistance-capacitance variety are largely the result of attempts at deliberate snubbing in connecting lines, and this practice should be condemned. The capacitance of an annular chamber connecting multiple pressure openings of nozzles and venturi tubes also may prove undesirable.

The remaining problem of manometer liquid damping still looms large in industrial measurement, and the usefulness of the tube, Fig. 5 of the paper, not only to damp, but to decrease the natural frequency, is often worthy of consideration. In a $^1/_2$-in-bore water manometer, a $^1/_8$-in-diam tube some 30 in. long would cause overdamping. The same manometer with mercury would have a damping of only 20 per cent of critical, but the natural frequency would be reduced to only 0.2 cycle per sec (cps), and the response to 20 per cent fluctuations at 1 cps or more would be utterly negligible. Use of much larger well and range-tube diameters in industrial flowmeters make it possible to achieve in combination much higher damping and much lower frequencies with such a tube, which could perhaps be coiled in a flat spiral within the mercury well for thermal protection. Smaller bore damping tubes might be feasible, but a limit would be imposed by the tendency of mercury to rupture when entering or leaving very small restrictions.

Further study and tests are, of course, required, but the author's work certainly seems to open the door to a more adequate solution than the adjustable mercury snubbers so frequently responsible for excessive pulsation error, today.

Author's Closure

The author would like to thank Messrs. Chilton, Freudman, and Head for their interesting contributions to the discussion of the paper.

While the author would agree with Mr. Chilton that the orifice plate or nozzle flowmeter does not of necessity follow the steady-flow square law when the flow being metered is pulsating in character, manometer errors can, nevertheless, greatly exceed all errors associated with the primary element. The possible magnitude of the manometer error was very apparent during the course of the viscous meter investigation (5) referred to in the introduction to the paper. With this type of flowmeter, there are no primary element errors, yet errors of over 100 per cent were frequently noted when using conventional manometers with no damping devices in the connecting leads. Even when felt damping pads were inserted into these leads errors of over 12 per cent were observed.

Further examples of manometer errors are to be found in the results presented by Mr. Freudman in Figs. 7 and 8. It is of interest to note in Fig. 7 that the cotton pads have not rendered the leads aperiodic. This is probably due to the flow resistance of the pads being too small. It was disappointing to read that the two-liquid manometer constructed at the Development and Research Laboratory, Industrial Power Division of the International Harvester Company, had not given reliable results when used in conjunction with a viscous flowmeter. The IHD 264 engine referred to in the caption of Fig. 9 was a four-cylinder engine, bore 4 in., stroke $5^1/_4$ in., the viscous meter being connected to the intake manifold by a 30-in. length of 3-in. bore rubber hose. The author had been able to meter accurately the air flow to a single-cylinder four-stroke engine by means of a viscous meter and a two-liquid manometer of the type shown in Fig. 6, no damping being needed in the induction system. Pulsation conditions at the meter referred to by Mr. Freudman were far less severe, and as a result of further correspondence on this matter, the author had suggested that the source of the errors may be in the viscous element used, since it appeared that the mean value of the flow Reynolds number was rather high within the speed range considered.

In reply to further comments made by Mr. Freudman, the assumption that damping is confined to the connecting tube of the manometer shown in Fig. 5 would bear experimental verification providing that the area ratio, S/s, were sufficiently large. The suggestion that the sensitivity of the manometer of Fig. 6 could be further increased by enlarging the cross-sectional area of tube D is a valuable one, and well worth incorporating in the manometer design.

In deciding the manometer dimensions to insure aperiodic damping, having chosen the liquids to be used in the gage, four

---

[11] Director of Hydraulic Research, Fischer & Porter Co., Hatboro, Pa., Mem. ASME.

[12] "A Practical Pulsation Threshold for Flowmeters," by V. P. Head, published in this issue, pp. 1471–1479.

unknowns remain: l_1, l_2, S, and s. If C_1^2 were much larger than $4C_2C_0$, the gage would be overdamped, sluggish, and difficult to operate. It is therefore better to make C_1^2 approximately equal to $4C_2C_0$, since when $C_1^2 = 4C_2C_0$, critical damping results, and the manometer would attain the equilibrium position in the shortest period of time while still insuring complete damping of the natural vibrations. With critical damping, the maximum amplitude x_{max} of the meniscus oscillation in tube C when the manometer is exposed to a sinusoidal pressure differential of amplitude Δp_{max} is [13]

$$x_{max} = \frac{\Delta p_{max}}{C_0 + C_2\omega}$$

where ω is the frequency of the pressure differential in radians per second.

[13] See, for example, Thomson (10), pp 64-65.

Having made C_0 small in order to insure maximum gage sensitivity (Equation [29]), C_2 has to be large enough to insure that there will be no excessive oscillation of the meniscus. This involves using a sufficiently long length of manometer tube (E in Fig. 6). The cross-sectional area s of this tube can then be determined from the equation $C_1^2 = 4C_2C_0$, and hence S from the area ratio assumed in calculating C_0. It is of course essential that the flow Reynolds number for the manometer liquid be sufficiently small to insure laminar flow in the tubes and this would generally be the case.

The author would refer Mr. Freudman to the paper on viscous flow meters (5) for further details of the manometer of Fig. 6.

Mr. Head's kind comments regarding the value of the paper were much appreciated, and his remarks regarding the application of some of the points dealt with in the paper to various practical installations were most interesting. It is hoped that the paper will be of some assistance to those interested in the design of flowmeters for pulsating streams.

A Practical Pulsation Threshold for Flowmeters

By V. P. HEAD,[1] HATBORO, PA.

Pulsation intensity Γ is defined as the ratio of extreme flow variation to average flow. An intensity $\Gamma = 0.1$ is recommended as a practical pulsation threshold below which the performance of all types of flowmeters will differ negligibly from the mathematical ideal of steady flow. An equation suitable for estimating the error range at various intensities is presented, and the problems of correlation of attenuator performance and meter response are considered.

Nomenclature

The following nomenclature is used in the paper:

- a_0 = approach area or any conduit area
- a_1, a_2 = phase angles of sinusoidal components of any flow wave shape
- b = frequency-response coefficient unless used as an exponent
- d = denotes differentiation
- D = size criterion, a length
- F = drag force on variable-area meter float
- f_p = pulsation factor $\equiv q_i/\bar{q}$
- g = acceleration of gravity
- K = flow coefficient in steady flow
- m = exponent of ΔP or F in transitional or compressible flow equation
- N = motion rate in turbine-type flowmeter
- n = exponent determined by meter type and kind of flow
- ΔP = differential pressure across variable-differential meter
- q = volume flow rate based on ρ_0
- r, s = exponents relating K and Y to ΔP or F
- t = time measured from start of period where $q = \bar{q}$
- T = pulsation period $= 2\pi/\omega$
- V = section velocity $= q/a_0$
- V_s = velocity of sound propagation as a fluid property
- w = mass-flow rate
- X = generalization of time-dominant quantity in a flowmeter equation, such as ΔP, F, or N
- $\dot{y}$ = velocity of response motion of flowmeter secondary mass
- $\ddot{y}$ = acceleration of such response motion
- $\ddot{y}_0$ = peak value of oscillating $\ddot{y}$
- Y = expansion factor

a, b, c as exponents are defined by X units = (mass)^a (length)^b-(time)^c

- $(^-)$ = bar denotes time average over period T
- $(\ )_{max}$, $(\ )_{min}$ = denote maximum and minimum instantaneous values
- $(\ )_i$ = denotes indicated value
- α = wave-shape coefficient
- β = diameter ratio of variable-differential flowmeter
- γ = half amplitude of any sinusoidal component of flow
- Γ = full-flow amplitude relative to average flow
- ρ_0 = average observed fluid density
- ω = radian frequency of pulsation

Introduction

The complexity of flowmeter correction for the effects of pulsation has been emphasized by a number of recent articles (1, 2, 3).[2] On the other hand, true steady flow is an ideal that can never be realized. Engineers who refer to official publications of nations and technical societies are unable to determine the borderline between serious and negligible intensity or to estimate the associated flowmeter error. Trivial low-frequency fluctuations of two or three per cent of the average flow value are erroneously blamed for errors of other origin, and high-frequency fluctuations throughout the audio range, capable of producing errors of many per cent, often pass unnoticed. No basis for the engineering design of adequate but economical attenuation equipment can be established until a pulsation threshold of some intensity greater than zero is named. In order of urgency expressed by flowmeter engineers in power test laboratories and process industries, official answers are needed for the following questions:

1 When is pulsation serious?
2 What is the likely magnitude of a pulsation error?
3 How can pulsation effects be eliminated?
4 What types of flowmeter are least affected?
5 How can accurate corrections be made?

The objective of this paper is to propose for official publication the answers to the first two of these questions, based on long familiar elementary principles of incompressible one-dimensional flow theory. A secondary objective is to offer some speculative suggestions on the remaining three.

Pulsation Defined

Pulsation is a periodic fluctuation in the flow passing a cross section of a conduit. Pulsation may exist whether flow is laminar or turbulent, compressible or incompressible. Flow fluctuations at 1 cycle per hr and 10,000 cycles per sec (cps) are potential sources of equal flow error if wave shape and percentage variations in flow are the same. Because the curve of flow rate versus time may be far from sinusoidal, the difference between maximum and minimum flow is a convenient definition of amplitude. A given amplitude of flow variation does not determine the potential error. Amplitude must be divided by the average flow rate in order to define the seriousness of a pulsation. Pulsation intensity Γ, is therefore defined as

[1] Director of Hydraulic Research, Fischer & Porter Company. Mem. ASME.

Contributed by the Research Committee on Fluid Meters and presented at the Diamond Jubilee Annual Meeting, Chicago, Ill., November 13–18, 1955, of The American Society of Mechanical Engineers.

Note: Statements and opinions advanced in papers are to be understood as individual expressions of their authors and not those of the Society. Manuscript received at ASME Headquarters, October 5, 1955. Paper No. 55—A-188.

[2] Numbers in parentheses refer to the Bibliography at the end of the paper.

$$\Gamma = \frac{V_{max} - V_{min}}{\bar{V}} = \frac{q_{max} - q_{min}}{\bar{q}} = \frac{w_{max} - w_{min}}{\bar{w}} \quad \ldots [1]$$

where w is mass flow rate, q is volume rate (expressed at the observed average density if compressible), and V is pipe velocity based on q and pipe area.

Pulsation Threshold

An intensity threshold must be based on the sensitivity of all types of flowmeter which may fail to follow the variations in flow. It must be sufficiently low that the tolerances of flow-measurement accuracy associated with codified primary elements need not be increased. It must be just as acceptable in laboratory work where flowmeters are calibrated or where basic coefficients are established as it is in the most casual flow observation with industrial equipment. With such rigorous requirements the acceptable intensity is surprisingly large. A value of $\Gamma = 0.1$, that is, a peak-to-peak variation of 10 per cent of the average flow, will meet these requirements regardless of flowmeter type and response characteristics, and regardless of the kind of flow (laminar, turbulent, liquid, gas) or of the frequency or wave shape. The average deviation of flowmeter readings from the mathematical ideal for steady flow will be only 0.125 per cent at this intensity for the most extreme wave shape, in spite of deliberate damping to prevent paint-brush chart records at low frequency, or inability of the fastest secondary to respond at high.

Jorissen has shown that the two-sigma tolerance on research correlations of orifice coefficients has been in the order of ±0.3 per cent (4). Even if these data were completely free of pulsation effects, this tolerance would only increase to ±0.325 per cent for such a pulsation intensity. The direction of pulsation error in variable-head, variable-area, and turbine flowmeters is such as to produce a higher reading than would be the case if flow were steady. It appears likely that actual flowmeter coefficients are lower by about 0.1 per cent than would be the case if the ideal of steady flow were achievable in the laboratory. Actual pulsation errors in flow measurement at Γ restricted to 0.1 and below will therefore be plus or minus a few hundredths of a per cent and random.

That an intensity of flow fluctuation of almost 10 per cent may have existed in most laboratories where basic flowmeter data have been obtained may seem surprising until it is remembered that all sound waves are propagated by oscillatory velocity of the sound-carrying medium. It is significant to note that in the audio range hums and valve whistle may constitute significant sources of pulsation not always recognized as such. The largest and most elusive flow-measurement errors in liquid-fuel handling in the author's experience have been traced to the scream of high-pressure aircraft pumps, not previously identified as "pulsation" at all. The pulsation problem ceases to exist at frequencies above about 100,000 cps. No low-frequency limit can be named. Serious error due to excessive snubbing of a recording manometer to suppress 40 per cent pen fluctuations of 1 cycle per hr has been observed. The practical low-frequency limit is that at which the slowest flowmeter follows the flow variation faithfully.

Magnitude of Error

The magnitude of error likely to be caused by pulsation may be calculated readily from idealized one-dimensional incompressible flow theory. We define a pulsation factor f_p as the ratio of indicated average flow q_i to actual average $\bar{q}$. The approximate pulsation factor for a number of flow-measurement situations is

$$f_p \equiv \frac{q_i}{\bar{q}} = (1 + \alpha b \Gamma^2)^n \quad \ldots [2]$$

Except as discussed under Frequency Effects the factor b is unity for any nonfollowing meter. Values of n depend on meter type and kind of flow. For variable-differential and variable-area flowmeters in incompressible flow, $n = 0.5$ when flow is turbulent and zero when flow is purely viscous; in the transition region or the compressible flow region, where q is proportional to Δp^m or F^m (see section entitled Derivation), the exponent n is closely approximated by $n = 1 - m$. In critical flow (sonic velocity in the throat of a flow nozzle), where mass rate is proportional to upstream pressure in a region of negligible approach velocity, $n = 0$. For turbine or propeller or positive-displacement meters, $n =$ unity.

Values of the wave-shape coefficient α are: For sinusoidal variation of flow about the average, $\alpha = 1/8$; for a "sawtooth" wave, $\alpha = 1/12$; for any rectangular wave where the maximum flow persists for a fraction x of the period T, and minimum flow persists for the remaining fraction $(1 - x)$ of the period, $\alpha = x(1-x)$. The highest known value of α is that for a symmetrical rectangular wave where $x = 0.5$ and $\alpha = 0.25$.

Derivation

Equation [2] has been synthesized from the pulsation theory of one-dimensional incompressible flow for a number of flowmeter types where meter response is assumed nil, and where the possibility of flow reversal during any significant fraction of a period is ruled out. Use of such simplification is common (1–3).

If the manometer reading on a variable-differential meter is constant and equal to the true time average of ΔP, it is readily shown that q_i, the indicated flow (calculated from steady assumptions), will be greater than the true average flow $\bar{q}$ by the factor

$$f_p = \frac{q_i}{\bar{q}} = \overline{(q/\bar{q})^2}^{0.5} \quad \ldots [3]$$

If the float in a variable-area flowmeter is damped with a dashpot until response is nil, the float force F oscillates as a result of flow fluctuation about the average value, and since q is proportional to $\sqrt{F}$, the same result for turbulent incompressible flow is found as for the variable-differential meter

$$f_p = \overline{(q/\bar{q})^2}^{0.5} \quad \ldots [3a]$$

If the rotor of a turbine meter is so high in angular inertia that it flywheels at constant speed, the instantaneous torque is proportional to $q(q - q_i)$ while the average torque is zero, which leads to

$$f_p = \overline{(q/\bar{q})^2} \quad \ldots [4]$$

Thus the mean-square relative flow, $\overline{(q/\bar{q})^2}$, is found with either the exponent $n = 0.5$ for the nozzle, orifice, venturi, pitot-static tube, or any device employing a measured differential as shown by Equation [3], or for the rotameter, vane meter, orifice-and-plug meter, or any device employing a force F balanced by fluid drag as shown by the identical Equation [3a], or with the exponent $n = 1$ for the turbine, propeller, or positive-displacement meter or any fluid-driven device with a motion rate output, as shown by Equation [4]. Pulsation factors for all these meters are then given by

$$f_p = \overline{(q/\bar{q})^2}^n \quad \ldots [5]$$

with $n = 0.5$ or 1, for turbulent incompressible flow. We are led to inquire whether other values of n may have meaning. In incompressible viscous flow it is known that the coefficient K of variable-differential and variable-area meters becomes directly proportional to $\sqrt{\Delta P}$ or $\sqrt{F}$, so that q is proportional to ΔP or

F and the same idealized flow analysis leads to $f_P = 1$, which of course could be obtained by raising the mean-square relative flow to the zero power or letting $n = 0$ in Equation [5]. In compressible flow in nozzles at sonic throat velocity, the mass rate is proportional to upstream pressure if approach velocity is negligible, and the actual and apparent time averages are equal so that again $f_P = 1$ or $n = 0$. In the transition region between turbulent and viscous flow, the flow coefficient K varies with ΔP^r where r ranges from 0 to 0.5. Similarly in compressible flow, the expansion factor Y varies with ΔP^s. If r and s be assumed constant for small pulsation amplitudes, q is proportional to $KY\ \Delta P^{0.5}$ or to ΔP^m where $m = 0.5 + r + s$, and the previous idealized analysis procedure leads to

$$f_P \cong \overline{(q/\bar{q})^{1/m}}^m \quad [6]$$

The value of n can then be calculated from

$$\overline{(q/\bar{q})^{1/m}}^m = \overline{(q/\bar{q})^2}^n \quad [7]$$

Equation [7] has various solutions dependent on both pulsation amplitude and wave shape. For any rectangular wave (spike, symmetrical, or dip) in which $q_{min} = 0$, an exact solution of Equation [7] is found to be

$$n = 1 - m \quad [8]$$

For all other wave shapes and all smaller amplitudes (q_{min} greater than zero), values of n slightly lower than Equation [8] are found, so that the approximations of [8] for most real wave shapes offset the approximations of Equation [6] incurred by the assumptions of constant r and s. The net error of these offsetting approximations is trivial beside the experimental tolerances given in the section entitled Tests and Tolerances.

Estimation of pulsation effects for all cases considered is thus found to rest upon evaluation of the mean-square relative flow $\overline{(q/\bar{q})^2}$, for use in Equation [5]. Mathematically, this time average is

$$\overline{(q/\bar{q})^2} = \frac{1}{T}\int_0^T (q/\bar{q})^2 dt \quad [9]$$

where T is the period of the pulsation. Any wave shape whatever may be mathematically generalized by the infinite series

$$\frac{q}{\bar{q}} = 1 + \gamma_1 \sin(\omega t + a_1) + \gamma_2 \sin(2\omega t + a_2) + \ldots$$

where γ_1 is the maximum deviation of the fundamental component from zero, γ_2 that of the first harmonic, etc., and ω is the radian frequency. The constant phase angles a_1, a_2, etc., drop out in integration. Substitution in Equation [9] and integration from 0 to 2π yields

$$\overline{(q/\bar{q})^2} = 1 + \alpha\Gamma^2 \quad [10]$$

where α is a function of wave shape only and where Γ is the difference between the highest and lowest values of $q/\bar{q}$. Putting Equation [10] into [5] we have

$$f_P = (1 + \alpha\Gamma^2)^n \quad [11]$$

Numerical values of α given earlier for simple wave shapes are readily calculated from integrations indicated by Equation [9].

It is well known that when any flowmeter can follow the fluctuations of a low-frequency pulsation perfectly, the average value of indicated flow q_i is equal to the true average flow. Thus, in principle, values of f_P may range from 1.000 up to values from Equation [11]. The factor b, dominated largely by frequency response and ranging from zero to unity, is introduced into Equation [11] to obtain the recommended Equation [2], and for estimating the worst likely errors when the frequency response of a meter is unknown, $b = 1$ should be assumed.

Tests and Tolerances

Fig. 1 shows test points gleaned from the literature and from the files of the author. None of these data included measured values of Γ or wave shape.

Triangle test points show water tests of a 1-in. rotameter in

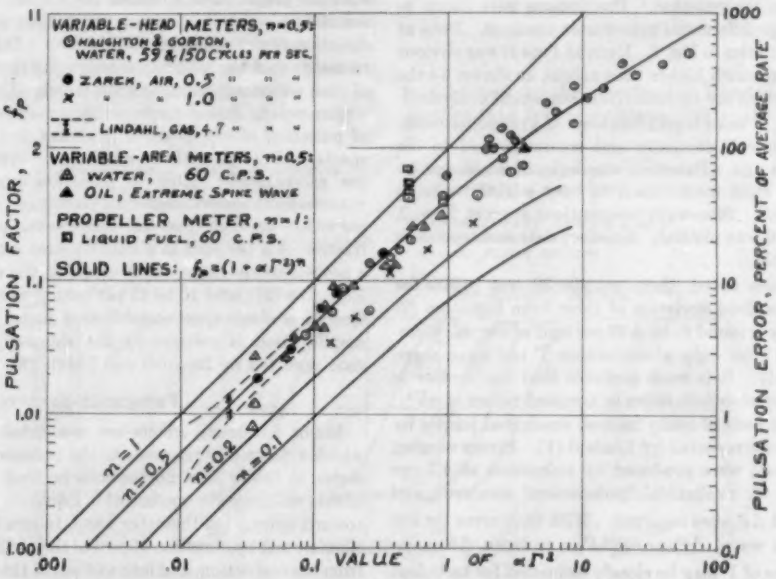

Fig. 1 Experimental and Theoretical Pulsation Error

the laboratory of the author's company in 1948. A diaphragm on a tee was vibrated at 60 cps. Sine wave was assumed, and flow variations were calculated from diaphragm amplitude, frequency, and area. A 200-in. run of pipe was ahead of the diaphragm. The meter was immediately downstream, with only a short nipple at the outlet. This setup assured that practically all pulsation would travel downstream, because of the high inertia of water in the long upstream pipe. A bucket and stop watch gave the steady and pulsating flow data, accurate to about 1 per cent, and the three lowest points ($\alpha\Gamma^2$ approximately 0.035) in Fig. 1 are excluded from statistical analysis for this reason.

The black triangle point was from a 1949 field report on a rotameter at the discharge of an adjustable-stroke single-cylinder positive-displacement oil pump. Rectangular spike, with $x = 0.21$, and $q_{min} = 0$, was inferred from the pump setting, whence $\Gamma = 1/0.21 = 4.76$, $\alpha = 0.21(1 - 0.21) = 0.166$, so $\alpha\Gamma^2$ is inferred to be 3.76. The pulsation factor of 2 was based on the statement that the meter read "twice the actual flow." No other data at such extreme wave shape are available to the author's knowledge. Frequency was not reported.

The circle test points were obtained from axial vibration of a 1-in. orifice run at 59 and 150 cps reported by Haughton and Gorton (5). We may assume that the water in the long run would remain at uniform velocity while pipe and orifice vibrate together. Thus the change in relative velocity of water and pipe was calculated from $2\pi f$ times the peak-to-peak displacement of the pipe, assuming sinusoidal vibration. Dividing by the flow velocity through the pipe area gave Γ, with α assumed $1/4$. Since the orifice ratio β was only 0.25, deviation from these assumptions resulting from forces of the orifice plate on the bulk of water in the meter run should be at a maximum, but since the results fall close to the line $n = 0.5$, this procedure should be valid for the estimation of pulsation error due to axial pipe vibration at any larger β. Points above $f_p = 2$ are excluded from statistical analysis because intensity was so high as to assure flow reversal for a significant fraction of each cycle.

Zarek (6) reported compressible flow data with air in a 2-in. orifice run using a large piston "pulsator" on a tee. We can only guess Γ from piston area, displacement, and frequency, because of compressibility in the pulsator. Precautions were taken to assure correct average differential manometer readings. Data at 0.5 cps are the black circles in Fig. 1. Even at 1 cps it was obvious that calculated Γ was much higher than actual, as shown by the "cross" test points which are excluded from statistical analysis.

The squares in Fig. 1 show liquid fuel tests of a propeller meter conducted by an aircraft company and communicated to the author several years ago. Pulsation was induced at 60 cps by oscillating a valve stem from closed to very slightly open in series with the meter. Sine-wave assumptions suggest $\Gamma = 2$, $\alpha = 1/8$, or $\alpha\Gamma^2 = 0.5$ as plotted. No other data corresponding to $n = 1$ are available.

With the exclusions noted, there remain 39 test points for analysis, and the standard deviation of these from Equation [2] with b assumed unity is found to be ± 22 per cent of the pulsation-error value ($f_p - 1$), for data where neither Γ nor wave shape was observed directly. It is more probable that the scatter is caused by ± 22 per cent uncertainties in assumed values of $\alpha\Gamma^2$.

Compressible-flow tests of many meters, conducted jointly by ASME and AGA, were reported by Lindahl (1). Errors ranging from 5 per cent down were produced by pulsations at 4.7 cps from a compressor. A mechanical "pulsometer" was used, and values of ΔP_{max} and $\overline{\Delta P}$ were reported. With little error for low amplitude near sine wave, $\Delta P_{max} - \Delta P_{min}$ is twice $\Delta P_{max} - \overline{\Delta P}$, and small values of Γ may be closely estimated for turbulent flow from

$$\Gamma \cong \frac{1}{2} \frac{\Delta P_{max} - \Delta P_{min}}{\overline{\Delta P}} \quad [12]$$

The arrowheads and dashed lines of Fig. 1 show the estimated scatter of 95 per cent of these data, and the approximate standard deviation is ± 11 per cent of the Equation [2] values of $f_p - 1$ except at intensities so low that pulsation effects are lost in normal testing.

Thus, still disregarding deviations of α from the assumed sine-wave value, direct observation of a quantity functionally related to Γ was enough to cut the deviations from Equation [2] in half. It is probable that considerable further reduction will result from more adequate pulsation instrumentation before any consistent error attributable to the assumptions used in deriving this equation can be detected experimentally. A major objective of further investigation should be the development of such instrumentation. Some progress in this direction has been reported by Hardway (7).

In experimental work, oscilloscopic observation of the output of piezoelectric or strain-gage differential transducers across any restriction, or hot-wire anemometers with grilles of wires across a pipe section, emf meters, and many other fast-response devices may be used. It is important that oscilloscopes should reveal both steady and varying flow, since evaluation of experimental Γ and α depend not on fluctuations of the flow variable about a mean but on deviations of the variable from the zero flow level. The requirements for such instrumentation are (*a*) data sufficient to relate flow to an experimental exponent of the signal (proportionality constants and drift are unimportant) and (*b*) adequate frequency response.

When a conduit is divided so as to permit metering only part of the total flow and inferring the total by the assumption of proportionality or by any other relationship established by calculation or calibration, serious deviations from Equation [2] may occur. It is likely that an approach or outlet value of pulsation intensity Γ below the threshold may be highly amplified in one of the branches and attenuated in the other, with the fluctuations in each branch out of phase with upstream and downstream fluctuations. The amplified intensity may affect not only the accuracy of the flowmeter in registering the flow in its branch, but also the proportions in which the stream divides. Such effects sometimes produce errors in total flow which are opposite in direction to the normal pulsation error. It is therefore necessary to assure that the intensity is below the threshold in each branch of such an arrangement, and not merely at an upstream or downstream point. Judicious proportions may permit the cancellation of pulsation effects between branches, but this requires highly specialized design without which shunt-type meter installations are exceptionally liable to pulsation error. The author has witnessed incompressible-flow tests in which aircraft-pump pulsation or high test-cell noise level produced errors of a fraction of a per cent in a variable-area meter, 2 to 3 per cent in a propeller-type meter (both errors in the direction indicated by Equation [2]), and 10 to 15 per cent errors in the opposite direction in a shunt-type variable-area meter installation. Similar amplification is evident in the shunt-type turbine flowmeter data reported by Dowdell and Liddle (8).

Frequency Effects

Major frequency effects are associated with the manner in which a flowmeter responds to the pulsation. Failure of a flowmeter to follow flow fluctuations because of viscous or inertial effects will force the coefficient b, Equation [2], upward from zero toward unity. On the other hand, failure to follow flow fluctuations caused by diversion of part of the oscillating-flow component from the restriction, and into and out of the spaces created by partial response in the secondary, leads to a local reduction in Γ at

the restriction. A meter response of only 10 or 15 per cent of the actual flow variation may result, with much more easily observable indication of the desired average flow rate, with negligible deviations of b from zero and negligible error. If a very large-bore manometer and pressure lines and taps were employed with a very small orifice meter, small motions of the manometer fluid could reduce flow variation in the orifice. A similar effect is inherent in float type-variable area flowmeters of all sizes, because the float and the flow restriction move together, and the oscillating volume rate represented by the product of float oscillatory velocity and tube area is subtracted from incoming and outgoing pulsation amplitude to reduce the local intensity of pulsation at the vena contracta. The dynamic equation for instantaneous flow rate with periodic small-amplitude float motion is, in the absence of viscous damping

$$q = q_i \sqrt{1 + \frac{\ddot{y}}{g}} + a_0 \dot{y} \quad \ldots\ldots [13]$$

where $\ddot{y}$ is instantaneous acceleration and $\dot{y}$ is instantaneous velocity of the float, and a_0 is the tube area at float level. At frequencies where $\ddot{y}$ is a significant fraction of the acceleration of gravity g, variations in q_i and a_0 may be neglected. Dr. Ing. Verhagen of the Delft Institute of Technology, Delft, Holland, has made available to the author the results of his dynamic-response experiments with $^1/_8$-in. rotameters with excellent confirmation of Equation [13]. Since the term $a_0\dot{y}$ represents a portion of the flow variation never felt at the restricted vena contracta, the local effective value of intensity Γ' associated with sinusoidal float motion in turbulent flow depends on maximum acceleration $\ddot{y}_0$

$$\Gamma' = \sqrt{1 + \frac{\ddot{y}_0}{g}} - \sqrt{1 - \frac{\ddot{y}_0}{g}} \quad \ldots\ldots [14]$$

and the pulsation factor becomes

$$f_p = \sqrt{1 + \frac{1}{8}\Gamma'^2} \quad \ldots\ldots [15]$$

As long as deliberate dashpot damping of the float motion is avoided, pulsations of known frequency which produce small but measurable float amplitude will produce errors whose magnitude can be estimated closely from Equation [15] without the necessity for additional instrumentation. The incoming intensity may be calculated by graphical summation of the out-of-phase terms of Equation [13] to yield values of Γ and b. Curves 4 and 5, Fig. 2, have been so calculated for average rotameters using two float materials, and the lower portion of curve 4, indicating negligible pulsation error up to several cycles per second in spite of high pipe-line intensity Γ, is confirmed by Verhagen's response data.

The actual shapes of the frequency-response curves for other meter types is not known, and the other curves of Fig. 2 serve to indicate only the frequencies at which pulsation errors may become significant. It is not proposed that numerical values of b significantly different from either zero or unity should be used for error calculation purposes. The entire object of introducing b into Equation [2] is to permit investigators to present experimental results in graphical form as shown in Fig. 2. No report on the performance of a particular meter type in pulsating flow can be meaningful without such a curve or equivalent data from which the frequency limit can be estimated.

It is believed that at very high frequencies the effects of pulsation are smaller than would be inferred from the idealized theory. Oscillatory inertial terms for motion of significant masses of the flowing fluid may produce apparent flow variations greater than actual and associated with the Strouhal number (3). Wave length determined from the pulsation frequency and the velocity of sound in the flowing fluid will approach the dimensions of flowmeters at very high frequencies and produce a similar effect. There is considerable speculation and some mathematical and experimental evidence to suggest that the interaction of pulsation intensity with Reynolds-number and acoustic-ratio effects will cause some deviations from the simple theory on which Equation [2] is based. High-frequency pulsations are attenuated by the actions of viscosity, compressibility, and reflection so that significant values of Γ measured a short distance from a meter are attenuated before reaching the primary element. While supporting data are not available, all these effects should combine to cause experimental values of the coefficient b to droop rapidly at frequencies above the audio range, regardless of type of flowmeter, as suggested by curve 7, Fig. 2.

Dimensional analysis suggests that a frequency parameter Φ of the form

$$\Phi = \frac{\omega X^{1/c}}{2\pi D \left(\frac{3a+b}{c}\right) \rho_0^{a/c}} \quad \ldots\ldots [16]$$

may be used for the experimental correlation of b to better advantage than frequency alone. Here $\omega/2\pi$ is the frequency of

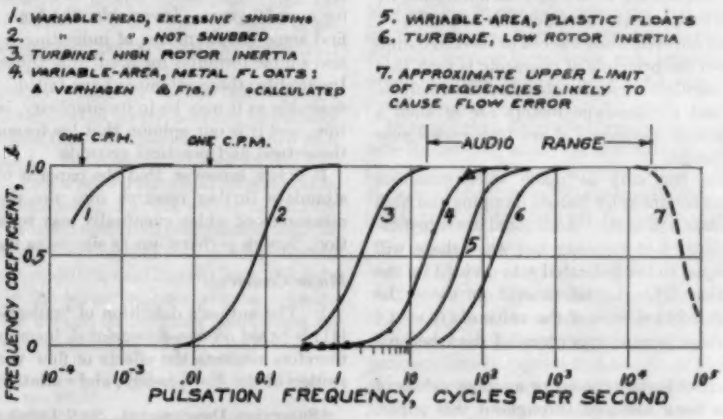

FIG. 2 FREQUENCY-COEFFICIENT TRENDS

each sinusoidal component (suggesting that pure sinusoidal flow oscillation should be approximated in tests for such correlation purposes), D is a meter size dimension, ρ_0 is the density of the flowing fluid (average observed if compressible), and X is that quantity of mechanics most descriptive of the particular meter type and containing time in its mass-length-time units. The values of a, b, c, in the exponents are determined from X which has units of $(\text{mass})^a\,(\text{length})^b\,(\text{time})^c$, where c is always a negative integer. For the variable-differential meter, X represents ΔP; for the variable-area meter, X is the float force F; for the turbine meter, X is the rotational speed N, etc. The parameter Φ combines a generalized form of Strouhal number with flow coefficient to eliminate these unknowns from the parameter. The coefficient b will also depend on $D\omega/2\pi V_s$ where V_s is the propagation velocity of sound in the fluid, and on average observed Reynolds number and acoustic ratio, and of course on the design geometry of the flowmeter.

It is well known that high frequencies are more easily attenuated than low. A need exists for standardized presentation of the performance of "desurgers" or "silencers" or other types of attenuating equipment. We may define an attenuation factor as the ratio of intensity of the pulsation at the connection farthest from the disturbance to the intensity at the opposite connection. A plot of this factor against frequency will give the performance of a particular attenuator with a particular fluid. Pure sinusoidal flow variation about the average should be approximated for such tests. A more general usefulness of results for geometrically similar attenuators of size D, handling fluids whose propagation velocity of sound V_s is known, can be achieved by plotting the attenuation factor against $D\omega/2\pi V_s$. The factor will range from near zero (excellent attenuation) at very high frequency to near unity (no effective attenuation) at low.

Conclusions and Recommendations

1 It has been shown that, from the viewpoint of accurate measurement of average flow, pulsation is potentially significant only when the intensity Γ is greater than 0.1. This value of Γ is recommended as a practical pulsation threshold for official publication, acceptable for the most exacting accuracy requirements.

2 Pulsation-error magnitude has been shown to depend primarily on pulsation intensity and wave shape in a manner readily calculable from Equation [2] when b is assumed unity, and secondarily, on frequency-response characteristics of the flowmeter.

3 Flow-measurement errors are best eliminated by the use of pulsation-attenuation equipment selected to reduce Γ to the threshold value. When this is impossible because of large attenuator size needed for low frequencies, errors may be minimized by selecting a high-response instrument, for which b is negligible.

4 Flowmeters are least affected when viscous or inertial damping is minimized and when the principle of operation is such that a large part of the flow oscillation can be absorbed by small response. Variable-area and turbine-type meters are of such a character, but this advantage disappears above frequencies near the low end of the audio range.

5 Accurate corrections can only be made when pulsation effects are forced to the maximum as by viscous damping and high inertia to force the coefficient b to unity. Additional instrumentation for accurate determination of intensity and wave shape will be required. Then $\bar{q}$ is equal to the indicated rate divided by the pulsation factor, Equation [2]. A "tolerance," or twice the standard deviation (4) of ± 20 per cent of the value of $(f_p - 1)$, must be assumed until more precise experimental data become available.

6 Proper measurement of instantaneous or average values of secondary quantities has been assumed throughout this paper. Secondary sources of pulsation error, particularly troublesome in variable-differential meters, are associated with nonsymmetrical damping and capacity in differential manometer lines. To a much smaller extent similar errors in measurement of absolute pressure may affect the accuracy of gas measurement with any type flowmeter. No flow-pulsation threshold can assure elimination of such errors, but the art of proper measurement of these secondary quantities is quite well developed. Excellent bibliographies will be found in references (1–3).

Acknowledgment

The author is deeply indebted to Mr. R. E. Gorton of Pratt & Whitney, East Hartford, Conn., for his literature survey leading to many of the data of Fig. 1; to Dr. Verhagen of the Delft Institute of Technology, Delft, Holland, for his variable-area meter response data; to Messrs. H. Hochreiter and D. Evans of Fischer & Porter Company, for their mathematical assistance, and to Messrs. Howard Bean, E. G. Chilton, and Profs. S. R. Beitler, E. J. Lindahl, A. K. Oppenheim, N. A. Hall, and E. E. Ambrosius, of the ASME Research Committee on Fluids Meters and its Pulsation Research Subcommittee, for their cautious scrutiny, guidance, and encouragement in the progress of this work.

BIBLIOGRAPHY

1 "Pulsation and Its Effect on Flowmeters," by E. J. Lindahl, Trans. ASME, vol. 68, 1946, pp. 883–894.

2 "Orifice and Flow Coefficients in Pulsating Flow," by N. A. Hall, Trans. ASME, vol. 74, 1952, pp. 925–929.

3 "Pulsating Flow Measurement—A Literature Survey," by A. K. Oppenheim and E. G. Chilton, Trans. ASME, vol. 77, 1955, pp. 231–248.

4 "On the Evaluation of the Accuracy of the Coefficient of Discharge in the Basic Flow-Measurement Equation," by A. L. Jorissen, Trans. ASME, vol. 75, 1953, pp. 1323–1326.

5 "Effect of Mechanical Vibration on the Water Flow Through a 1/4-Inch Sharp-Edged Concentric ASME Orifice in a 1-Inch Pipe," by C. B. Haughton, Jr., and R. E. Gorton, ASME Paper No. 54—A-113.

6 "Metering Pulsating Flow," by J. M. Zarek, *Engineering*, vol. 179, January 7, 1955, pp. 17–19.

7 "A Method for Correcting Orifice Meter Measurements for Flow Pulsations," by E. V. Hardway, Jr., *Instruments*, vol. 24, 1951, p. 763.

8 "Measurement of Pulsating Flow With Propeller and Turbine-Type Meters," by R. B. Dowdell and A. H. Liddle, Trans. ASME, vol. 75, 1953, pp. 961–968.

Discussion

E. G. Chilton.[1] The measurement of pulsating flow by conventional flowmeters, such as orifices, nozzles, variable-area, or propeller meters has been the subject of discussion and research for over 50 years. Invariably, the hope of engineers has been to find some simple means of indicating the severity of pulsations and simple formulas for predicting the ensuing flowmeter error. Invariably, these attempts have failed. The author's approach, desirable as it may be in its simplicity, is unfortunately no exception, and it is our opinion that his formulas are unacceptable on theoretical and practical grounds.

It is felt, however, that the paper is of value in that it should stimulate further research into the problem of pulsating-flow measurement which eventually may result in an acceptable solution, though perhaps not as simple as the author proposes.

Major Comments

1 The author's definition of "pulsation intensity" (Equation [1]) is based on one-dimensional, incompressible-flow theory. It therefore neglects the effects of flow variations within the cross section of the flow passage, and variations in density. There are

[1] Supervisor Development, Shell Development Company, Emeryville, Calif. Mem. ASME.

to date no test results to show where and when these variations can be neglected.

2 A criterion such as the pulsation intensity must be amenable to easy measurement if it is to be useful. No simple instrument exists to measure Γ. One must resort to such apparatus as hot-wire anemometers with rapid response and take measurements throughout the cross section. This was realized as early as 1918 when attempts were begun to correlate not velocity but pressure-pulsation measurements with metering errors.

3 For variable-differential meters (orifices, nozzles, etc.), the magnitude of the metering error (Equation [2]) is based on the assumption that the orifices (or nozzles) behave in pulsating flow as they do in steady flow. It has been shown repeatedly (for instance, reference 2 of the paper) that this is not true and that it is a good assumption only for small-amplitude and low-frequency pulsations. Where this assumption is adequate remains to be shown by experiments.

4 The sine-wave expansion for $q/\bar{q}$ (between Equations [9] and [10]) does not represent "any wave shape whatever" but only certain restricted shapes.

5 Even if one were to grant the assumption discussed in item 3, that the flowmeter behaves as if in steady flow, integrating of a Fourier series expansion does not yield Equation [10], so that the proposed Equation [2] has no theoretical foundation.

Minor Comments

1 Regarding the flow-pulsation amplitude due to sound waves, the author states that "average face-to-face conversation (about 50 db) propagated down the length of a pipe conveying atmospheric air at an average flow velocity of 10 fps, will constitute a pulsation intensity close to $\Gamma = 0.1$ in. Reference to any textbook on acoustics[4] shows that Γ is more nearly 0.00001 under these conditions.

2 Regarding the test points, Fig. 1, the writer took the liberty of checking Lindahl's pulsometer data, corresponding to the dotted line. To judge from the original paper (author's reference 1), the experimental points do not lie on the curve $n = 0.5$, but near the line for $n = 0.1$. This is for an error of about 1 per cent.

In conclusion, the writer submits that the proposed pulsation threshold is not a practical device, and that the proposed equation for pulsation-error magnitude is applicable only in very limited circumstances, the range of which has not been explored yet.

MARTIN GOLAND.[5] This paper is an interesting contribution to a difficult and long-standing engineering problem. While the writer takes exception to several of the recommendations advanced by the author, this does not detract from the virtue of his effort to formulate some simple (and perhaps partially successful) rules for the treatment of the pulsating-flow question.

These remarks are directed primarily toward the author's treatment of the variable-differential meter, and are specifically concerned with the suggestion that his methods be accepted as a tentative industrial standard. For reasons outlined in this discussion, the writer believes such a procedure would be premature.

As a first point, it should be noted that the author has subtly introduced a rather significant change, from the practical point of view, in the entire manner of observing and evaluating pulsation conditions at a meter. Particularly in field installations, the data conventionally available to the meter engineer are the pressure pulsations at the meter; the author, on the other hand, bases his entire approach on the velocity pulsations. True, with considerable practical difficulty and at some expense, instrumentation can be provided to measure the pulsation velocities at meters. Since, however, there is certainly a unique relationship between pressure and velocity, the author's approach only has practical merit if we believe it impractical to arrive at an understanding of the entire flow mechanism; i.e., at the interrelationships existing between flow and tap pressures. If this mechanism were known, evaluations of pulsation errors could be based on the pressure observations directly.

As an illustration of the difference in point of view, notice that the author claims no pulsation errors will exist if a high-response *velocity*-measuring instrument is used. This is, of course, a truism for the question at hand. However, note that a pulsation error will exist even if a high-response *pressure*-measuring instrument is employed. It is precisely here that the crux of the practical problem lies: How does one interpret pulsation errors from an examination of the differential-pressure records? The author gives no clue to the answer to this question.

The author may counter the foregoing criticism by stating that one can go from instantaneous pressure to instantaneous velocity, based on the argument that velocity is approximately proportional to the instantaneous square-root of the pressure; this is the *quasi-steady* flow assumption. Unfortunately, rather simple theoretical arguments suffice to show that this cannot be the case. A quite simple visualization of the incompressible flow through a venturi shows that the instantaneous differential pressure is given by an equation of the form

$$\Delta P(t) = K_1 V^2 + K_2(dV/dt) \quad [17]$$

where $\Delta P(t)$ is the instantaneous pressure *differential*, V the instantaneous velocity, t the time, and K_1 and K_2 are constants. For an orifice meter, since the "shape" of the effective venturi is continually changing during the pulsations, the form of the equation equivalent to Equation [17] is even more complex, and theoretically elusive.

For simple harmonic pulsations, note that Equation [17] takes the form

$$\Delta P(t) = K_1 V^2 + K_3 v \quad [18]$$

where v is the magnitude of the pulsating-flow component, and where K_3 is now a parameter whose value depends directly on the value of the Strouhal number based on the mean flow.

In most cases of pulsating flow it is found that the second terms in these equations, which represent the unsteady-flow effects, cannot be neglected within the confines of practical metering accuracies. This emphasizes the importance of arriving at a suitable working hypothesis regarding the over-all flow mechanism, for the purpose of guiding practical decisions of meter accuracy. Without such an hypothesis, only empirical observations are possible and these, to date, have not proved adequate for the problem.

In conclusion, the writer would like to point out that his Institute is currently studying this same problem under the sponsorship of the American Gas Association. By means of a carefully co-ordinated program of analytical and experimental trials, it is hoped that further light can be thrown on this important question.

AUTHOR'S CLOSURE

The position of both discussers is necessarily far removed from that of the author as a result of differences in objective. Both discussers are intimately associated with a long-range research program which appears to have as its goal a means for applying accurate corrections under conditions where the effects of pulsation on flowmeter accuracy are severe. They overlook the fact that most flowmeter engineers have never been given a practical

[4] "Sonics," by T. F. Hunter and R. H. Bolt, John Wiley and Sons, Inc., New York, N. Y., 1955, pp. 48–53.

[5] Vice-President, Southwest Research Institute, San Antonio, Texas. Mem. ASME.

answer in an official publication to the far less exacting question, "when is pulsation sufficiently intense to demand concern?"

We take Dr. Chilton's comments in order:

Major Comment 1: Equation [1] is based on no theory whatever but merely on the normal engineering meaning of volume rate and pipe velocity as compared with mass rate. Equation [2] is based on incompressible one-dimensional flow theory as clearly stated in the Derivation section. All the data of Fig. 1 show that variations from these assumptions have negligible influence for the purpose of this paper. The burden of proof seems to the author to fall on those who continue to maintain the importance of such variations in the absence of experimental evidence. Even the theoretical evidence points to the fact that errors may run less than, but never more than, the Equation [2] values. That is, the value of b may be less than unity, not greater.

Major Comment 2: The author must cite conclusion 5 of the paper, and can only concur that no simple universal instrument for measuring Γ (or α for that matter) to an ultimately desirable degree of accuracy *for correction purposes* is at present available. Nevertheless, it has been shown that meager knowledge often permits estimation of α and Γ from known causes of pulsation with sufficient accuracy to calculate error by Equation [2] with an experimental standard deviation of ± 22 per cent, and that in one case of compressible flow, instrumentation specifically for determining intensity but still ignoring wave shape cut the scatter in half. For the author's purpose of establishing a practical pulsation threshold, a tolerance of ± 100 per cent of the calculated error would have been acceptable. Further progress is evidenced by the work of Hardway (7) and of Li (9),[6] and intensity measurement at ever-increasing frequency is gradually resulting. Widespread understanding of just what is to be measured, namely, α and Γ or the product $\alpha\Gamma^2$, will accelerate such development.

It is futile to hope that line pressure variation can be used for intensity determination. The instrumentation is certainly not "simple" and experts can make intensity estimates only by guessing the combination of local and convection accelerations in every pipe fitting of a particular installation from reservoir to pressure tap. Such estimates are crude, as emphasized by Daily, et al. (10). The author has observed increases in line pressure pulsation as a result of steps which satisfactorily decreased flow pulsation.

Major Comment 3: Dr. Chilton cites purely theoretical mathematical analyses, written in symbolic form and having no means for evaluation, to support his contention. Dr. Hall quite properly included the *mathematical possibility* that loss terms might vary under transient conditions (2). The experiments of Daily, et al. (10) confirm that such loss variations may affect the measurement of *instantaneous rate* during transients to a significant degree when pipe taps are employed with variable differential producers, owing to the importance of the loss terms in the recovery zone. Their data also show that the effect on *average rate* determination is trivial for pipe taps and virtually nonexistent for every other flowmeter under discussion here. It is again the author's contention that the experimental evidence of Fig. 1 speaks for itself and that experimental evidence to the contrary must be found before this comment can be entertained.

Major Comment 4: In the original preprint of the paper the phase angles a_1, a_2, . . . were omitted in the sine series between Equations [9] and [10]. The pure sine series would cover those periodic functions known in mathematics as "odd" functions. A pure cosine series includes all "even functions." The general Fourier series includes both sine and cosine terms and is equally well represented by the sine series with the arbitrary phase angles included. This representation has the advantage that γ_1, γ_2, etc., represent peak amplitudes of each frequency present rather than pairs of out-of-phase components of each frequency whose sine and cosine term are determined by an artificial "zero" time. The step from Equation [9] to Equation [10] can be demonstrated with equal validity for an odd function, an even function, or the more general Fourier series. Even a stepwise integration of any scribbled curve of flow versus time over a period T in n steps of Δt such that $n\Delta t$ is equal to the period T leads to a form which approaches Equation [10] as the number of steps, n, approaches infinity. The wave shape coefficient α is independent of the intensity Γ, and Equation [10] stands, in the absence of actual flow reversal.

Major Comment 5: Equation [9] does not call for the "integrating of a Fourier series expansion," but for the integration of the *square* of such an expansion. This is covered by the so-called Parseval relation found in Churchill (11) and many other mathematics texts. Rearranged in the author's nomenclature for the problem at hand, the Parseval relation is Equation [10]. The only wave shapes that can be excluded are those violating the Dirichlet Conditions, described by Sokolnikoff (12) and others, namely, such fanciful "wave shapes" as might be deemed to have an infinite number of maxima and minima within a single period, or to exhibit flow variations from minus infinity to plus infinity, and the like. Such violations will void the applicability of the Fourier series, of the Parseval relation, and hence of Equation [10], but are never found in pipelines. It cannot be supposed that Dr. Chilton is seriously invoking such mythical wave shapes to condemn Equation [10], and the author can only repeat that Equation [10] results from the integration of Equation [9] for any wave shape whatever.

Minor Comment 1: The author is grateful to Dr. Chilton for catching an arithmetical blunder which appeared in the preprint. This has been corrected in the present text. It is a relief to know that the sound level must be some 80 db higher than "average face to face conservation" to produce $\Gamma = 0.1$ when air velocity is ten feet per second.

Minor Comment 2: The statement in this comment is incorrect. Some 95 per cent of the data on which the Lindahl correlation line is based fall between $f_p = 1.010$ and 1.014, for an average of 1.012 ± 0.002 (or approximately ± 20 per cent of the calculated error). The correlation line shows a peak differential 43 per cent above the average. If differential varied sinusoidally, the minimum should be 43 per cent below the average, and the approximate Equation [12] yields $\Gamma = 0.86/2 = 0.43$. The value of $\alpha = 1/3$ leads to $\alpha\Gamma^2 = 0.023$. Hence the arrowheads of Fig. 1. Thus the Lindahl article (1) precisely supports the expected exponent $n = 0.5$.

It is regrettable that the author's attempt to condemn the use of oscillating line pressure or oscillating differential as a means of defining pulsation, and to insist instead on defining flow pulsation as a periodic variation in flow itself, should appear "subtle" to Dr. Goland. He would appear to favor clinging to "the data conventionally available to the meter engineer . . . the pressure pulsations at the meter." However, we are grateful to Dr. Goland for proceeding on his own to demonstrate by means of his Equations [17] and [18] why it is that pressure pulsation *cannot* be a fundamental basis for defining flow pulsation and attendant flowmeter error, and why the author's Equation [12], while reasonable in gas handling, must be used with caution when fluid density and pulsation frequency are both high. Nevertheless, within the scope of the author's purpose, it must be emphasized that use of the approximate Equation [12], and ignoring the inertia of throats or pipes full of liquid between taps, which is responsible for the $K\omega$ term of Dr. Goland's Equation [18], will always be conservative. That is, actual flowmeter error must be less, and never more, than the quasisteady value. Consequently it appears that the answer to Dr. Goland's question, "How does one interpret pulsation errors from an examination of the differential records?" is of importance only to those who are bent upon discovering a

[6] Additional references will be found at the end of the closure.

method of applying significant corrections for pulsation rather than simply knowing when pulsation is significant and taking action to suppress it. For this latter purpose, Equation [12] is adequate. For the former, if correction methods based on differential fluctuation are to be achieved as a result of the program at Southwest Research Institute or any other, some experimental correlation of actual Γ deviations from quasisteady assumptions will be required as a function of Φ. When the X of the author's Equation [16] is defined as ΔP, we obtain

$$\Phi = \frac{D\omega/2\pi}{\sqrt{(\Delta P/\rho_0)}}$$

a dimensionless parameter equivalent in purpose and utility to the Strouhal number, but more uniquely suitable for the correlation of any ΔP device as a pulsation detector. Of course any such program will require a maximum cost for a minimum usefulness if attempted in connection with just any pair of taps the meter engineer happens to have available for any venturi, nozzle, or orifice at any β, because each and every flowmeter geometry, Reynolds number, and acoustic ratio would require a separate correlation line. It appears to the author that maximum utility of research results can be achieved with a minimum of cost and time by building a pulsation probe with geometry and pipe immersion frozen, preferably with piezoelectric or other transducer built into the probe to eliminate pressure connection lines, and with impact and static openings so close together that the liquid column acceleration influence associated with Φ can be minimized. All this, of course, merely serves to emphasize the fact that a fluctuating ΔP must be of a sort that is a good measure of *flow* pulsation, and that flow variation itself has been the real measure of pulsation errors all the time.

It may be helpful to the reader to point out that the two terms on the right of Dr. Goland's equations are not arithmetically additive, but rather add in the fashion of waves 90 deg out-of-phase, so that the mass-acceleration may be surprisingly large before the Φ influence becomes appreciable.

Far more serious than the Strouhal number (or Φ) effects have been those external manometer errors peculiar to differential-type flowmeters. A significant contribution to the analysis of such errors has been made by Williams (13).

Finally, with regard to the unnumbered commentary of Dr. Chilton and Dr. Goland: If the author had made a fantastic claim to have transmuted the dross of these 50 years into the purest gold of a valid system of measuring pulsating flow accurately, the labels "failure," "not practical," and "premature" would be well deserved. Such a valid system cannot be arrived at without major development and exhaustive test. However, there are some who doubt that this Utopia will ever dawn, and others who, while waiting, must utilize available knowledge to determine whether existing pulsations do, or do not, demand suppression. Many flowmeter engineers and technicians cannot afford to retain experts to guess these answers for them. Every engineer who has been close to a flow laboratory knows that perfectly steady flow is nonexistent. When he also reads that he must *eliminate* pulsation he can only conclude that accurate flow measurement is impossible. It was to correct this inconsistency that the author accepted this project. The tolerances found experimentally were much better than he had dared hope, and verify Hardway's findings (7) that we *can* use one-dimensional incompressible theory to correct for pulsations when the correction is as high as 5 per cent if only we develop our instrumentation. More important, we most certainly can quiet the fears of the pessimist and disrupt the false equanimity of the excessive optimist by publishing what is known, not by maintaining official silence during the infinite time required to arrive at the perfect answer.

ADDITIONAL REFERENCES

9 "New Schemes for Pulsating Flow Measurement With Head-type Meters," by Yao Tsu Li, ASME Paper No. 55—SA-79.

10 "Resistance Coefficients for Accelerated and Decelerated Flows Through Smooth Tubes and Orifices," by J. W. Daily, W. L. Hankey, Jr., R. W. Olive, and J. M. Jordaan, Jr., Trans. ASME, vol. 78, 1956, pp. 1071–1077.

11 "Fourier Series and Boundary Value Problems," by Ruel V. Churchill, first edition, p. 86, McGraw-Hill Publishing Company, New York, N. Y., and London, England, 1941.

12 "Higher Mathematics for Engineers and Physicists," by I. S. and E. S. Sokolnikoff, second edition, p. 65, McGraw-Hill Publishing Company, New York, N. Y., and London, England, 1941.

13 "Pulsation Errors in Manometer Gages," by T. J. Williams, published in this issue, pp. 1461–1469.

Effect of Range of Stress in Combined Bending and Torsion Fatigue Tests of 25S-T6 Aluminum Alloy

By W. N. FINDLEY,[1] W. I. MITCHELL,[2] and D. D. STROHBECK[3]

Fatigue-test data under bending, torsion, and combined bending and torsion are presented for mean stresses from zero to values which caused substantial yielding. The mean normal stresses in the bending and the torsion tests were corrected for the effect of the nonlinear distribution of stress resulting from yielding. The effect of stress relaxation at high mean stresses was investigated. The applicability of several theories of failure are compared with these test data. The influence of anisotropy, mechanism of crack formation, mean stress, and maximum stress are discussed.

Introduction

THE results of fatigue tests of 25S-T6 aluminum alloy under combined bending and torsion have been presented in another paper (1)[4] and compared with various theories of failure for completely reversed loading. In the present paper these data have been extended to include the additional variable "range-of-stress" and its effect under different combinations of bending and torsion.

The term range-of-stress is used here in the broadest sense, as employed by Smith (2); for example, to describe in a general way relationship between the maximum and minimum stress in a cycle of stress. A complete description of a sinusoidal cycle of stress requires a set of two algebraic quantities, such as maximum and minimum stress, alternating stress amplitude and mean stress, and so on.

Previous work on the effect of range of stress was outlined in a paper (3) by one of the authors on the effect of range of stress on the fatigue behavior of 76S-T61 aluminum alloy.

Material, Apparatus, and Procedure

Material. The material, material processing, chemical analysis, metallurgical analysis, specimens, and their preparation were described in the previous paper (1).

Apparatus. The machines used in the fatigue tests were Krouse plate fatigue machines which were modified as previously described (4) so that bending, torsion, or combinations of the two could be applied to the specimen.

Procedure. The machine was adjusted to zero mean stress. Then the alternating stress amplitude indicated by the spring dynamometer was applied by crank adjustment. The mean stress was then adjusted until the desired maximum and minimum stresses were indicated by the spring dynamometer as the crank was turned over by hand. In cases where the maximum stress was quite large, adjustment was continued over a few cycles until the maximum and minimum loads appeared stable. The stress values employed were nominal stresses determined from the ordinary formulas.

Additional static tests were conducted in bending and torsion on fatigue specimens in the fatigue machines to obtain information regarding the Bauschinger effect. The load was applied by turning the crank by hand. Deflection and angle-of-twist measurements were effected by suitable mountings of dial gages.

Supplementary tests indicated the extent of stress relaxation. For these tests the connecting rod of the machine was held in a fixed position and the desired initial stress rapidly applied to the specimen by driving the mean-stress adjustment with a speed wrench. The dynamometer was then read at intervals to determine the change in the applied bending or twisting moment, due to the relaxation phenomenon.

Fatigue Tests

Fatigue tests were conducted at five different states of stress produced by pure bending, three combinations of bending and torsion, and pure torsion. At each of these five states of stress, tests were conducted at five different values of nominal mean stress. The *S-N* diagrams are shown in Fig. 1. The curves for all diagrams were drawn on separate sheets by inspection before being combined as shown. The criterion of failure employed a reduction of stiffness to $^7/_8$ of its initial value (4).

The measure used for the state of stress was the state of stress number n, where n is the least direction cosine of the state of stress vector $\overline{S}$ as described in a previous paper (5)

$$n = \sigma_3/S$$

where σ_3 is the smallest principal stress and the state-of-stress vector is the vector sum of the three principal stresses.

As the mean stress increased the *S-N* diagrams exhibited a more pronounced curvature, particularly in bending.

None of the curves exhibited a true endurance limit, but the observed change in slope of these curves indicates the possible existence of an endurance limit at a larger number of cycles at high mean stresses in bending. However, it should be pointed out that at least part of the apparent curvature at high mean stresses (particularly at the lower number of cycles) is due to yielding. Because yielding is more pronounced in these cases, and the alternating stress is not affected by yielding, the actual mean stress (maximum — alternating) will be reduced to a greater extent at the lower number of cycles. In effect, this means that the *S-N* diagrams of Fig. 1 have variable mean stresses.

In order to determine more accurately the actual stresses existing in the specimens where yielding occurred, plasticity

[1] Professor of Engineering, Brown University, Providence, R. I.; formerly Research Associate Professor, University of Illinois, Urbana, Ill.

[2] Research Engineer, Boeing Aircraft Corporation, Seattle, Wash.; formerly, Instructor, University of Illinois, Urbana, Ill. Assoc. Mem. ASME.

[3] Aberdeen Proving Ground, Ordnance Corps, U. S. Army; formerly, Research Assistant, University of Illinois, Urbana, Ill.

[4] Numbers in parentheses refer to the Bibliography at the end of the paper.

Contributed by the Machine Design Division and presented at a joint session with the Metals Engineering Division at the Diamond Jubilee Annual Meeting, Chicago, Ill., November 13–18, 1955, of The American Society of Mechanical Engineers.

Note: Statements and opinions advanced in papers are to be understood as individual expressions of their authors and not those of the Society. Manuscript received at ASME Headquarters, August 5, 1955. Paper No. 55—A-68.

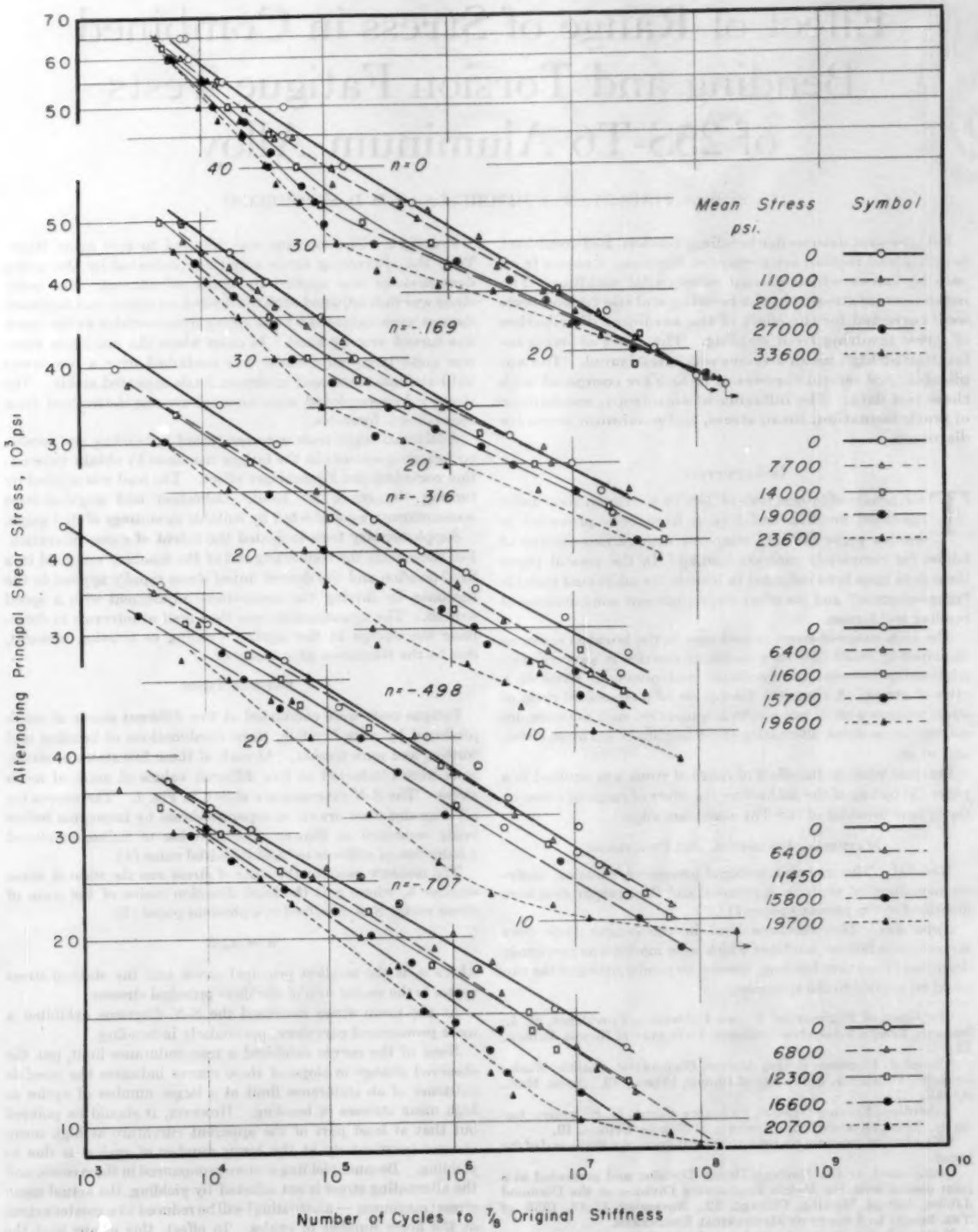

FIG. 1 *S-N* DIAGRAMS FOR COMBINED BENDING AND TORSION FATIGUE

theory was employed requiring the static tests described in the following section.

Static Tests

Average stress-strain curves for three tests each in tension, compression, and torsion are shown in Fig. 5 of reference (1) and several static properties measured from these tests are presented in Table 2 of the same reference. Also shown in reference (1) are the first two cycles of completely reversed alternating stress (Fig. 6, Part 1) together with two additional stress cycles (Fig. 6, Part 2) recorded after the same specimen was subjected to 250 cycles of dynamic stressing (as in a fatigue test) of the same nominal stress amplitude used in the static test of Fig. 6, Part 1 of reference (1).

As the corrections for yielding applied to the bending and torsion tests were based on the assumption that the unloading stress-strain diagrams were linear, it was necessary to establish whether or not the stress ranges which were corrected encountered the Bauschinger effect. Static bending tests at maximum nominal stresses of 60,000 and 80,000 psi (flexural stress) were conducted in order to establish at what stress level the unloading deflection curve departed from linearity for different maximum flexural stresses. The stress levels obtained from the foregoing tests together with the negative proportional limit provided a means of determining approximately which fatigue-strength ranges were not influenced by the Bauschinger effect. For the same purpose, similar tests were conducted in torsion.

Since relaxation of stresses might occur in specimens subjected to high mean stresses, relaxation tests were performed to evaluate this effect. Results obtained from relaxation tests in torsion are shown in Fig. 2. To supplement the static relaxation data

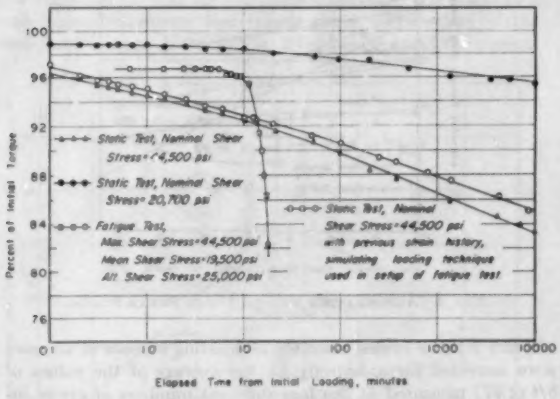

Fig. 2 Torsional Relaxation Curves for 25S-T Aluminum Alloy at Constant Deflection

a fatigue test was conducted in torsion at a high mean stress, during which the maximum load was checked periodically. The maximum nominal stress (mean + alternating) for this test was selected as 44,500 psi to represent the largest maximum shear stress employed in the fatigue tests. A mean stress of 19,500 psi was utilized with an alternating stress of 25,000 psi. To facilitate correlation of this dynamic relaxation test with the static data, the initial stress settings in the static tests were selected to correspond to the maximum and mean stresses used in the fatigue test.

The technique employed in setting up a fatigue test involved turning the crank of the machine over several times by hand for purpose of adjusting the load to the desired range. In order to determine the effect of this prestraining on the relaxation phenomenon, one of the static relaxation specimens was given a prestrain history simulating that of a fatigue test. The results of these tests are plotted in Fig. 2.

From the curve representing the fatigue test it was observed that only the first 5 min of these tests were important to the relaxation problem at this stress level as the abrupt decrease in torque at about 5 min was due to fatigue damage.

In the fatigue test, the torque decreased approximately 3.5 per cent in less than 1 min and then appeared to be stable until the fatigue crack initiated. Results are shown in Fig. 2.

During the first five minutes the relaxation from the initial stress of 20,700 psi was approximately 1.5 per cent for the constant deflection test, while the relaxation from the initial stress of 44,500 psi was about 6.5 per cent. The prestrain imposed on the specimen tested at an initial stress of 44,500 psi appeared to have a negligible effect on the relaxation phenomena during the the first five minutes.

Evaluation of Fatigue Stresses

Corrections for Yielding. Inasmuch as the object of this investigation was to determine the effect of the mean stress, it seemed desirable to extend the range of mean stress to as large values as possible and then to correct the nominal mean stresses for yielding.

In instances in which the maximum stress (mean + alternating) of the cycle was above the proportional limit, the actual maximum stress was less than the nominal maximum stress calculated from elastic formula. Thus the mean stress also was lower by an equal amount since the mean stress was equal to the maximum stress minus the alternating stress and the latter was not influenced by yielding unless the Bauschinger effect was encountered on unloading.

The static tests described in the preceding section provided information concerning the influence of the Bauschinger effect. No mean stresses have been reported as "corrected for yielding" in instances where significant Bauschinger effect existed.

For completely reversed stress cycles above the proportional limit, the nominal alternating stress was previously shown (1) to be very nearly equal to the correct value after the yielding of the first few cycles was complete.

Instead of correcting the mean stresses for each individual specimen, the fatigue strength was measured from all *S-N* diagrams at 10^4, 10^5, 10^6, and 2×10^7 cycles and the subsequent corrections were based on these values.

The correction employed in bending was a semigraphical procedure based on an extension of the Herbert equation by Morkovin and Sidebottom (6). The analysis was based on relationships applicable only when the stress-strain relation was the same in tension and compression. Although it was observed that this condition was not accurately fulfilled for this material (see Fig. 5 of reference 1), it has been shown (7) that a difference of 20 per cent in the yield strengths in tension and compression of steel will result in less than a 2 per cent error in the computed stresses if the average (of tension and compression) stress-strain diagrams is employed. Inasmuch as the average stress-strain diagram was employed in the present analysis, and the observed deviation in the tension-compression yield strength was less than 15 per cent (see Table 2 of reference 1), it follows that the error introduced by using the average of the tension and compression tests was probably less than 2 per cent.

In addition, errors were also introduced due to several simplifications from actual material behavior (3).

The graphical technique employed in the correction for torsional stresses was that outlined by Nadai (8) for determining the shearing stress at the surface of a specimen of a circular cross

section having a nonlinear stress-strain relation and subjected to pure torsion. It should be observed that the same limitations apply to this correction procedure as apply to the bending procedure except that no error is introduced due to the differences observed in the tension-compression stress-strain diagrams.

Effect of Relaxation. The results of the relaxation tests in torsion shown in Fig. 2 provide a means of evaluating the effect of the relaxation phenomenon on the reported fatigue stresses. Torsion tests were selected for this study because there was more material subjected to high stress in the torsion tests than in the bending tests so that the torsion tests were more sensitive to relaxation.

Inasmuch as these tests were conducted at stresses representing the largest stress amplitudes employed in the fatigue tests, it may be assumed that the results also represent the largest amount of relaxation encountered in the fatigue tests. The relation between the nominal and actual stresses in the relaxation tests is not known. However, examination of studies of stress distribution in beams which creep (9, 10, 11) suggests that the per cent decrease in the actual maximum stress in the specimen may not differ greatly from the per cent decrease in the nominal stress (or the torque). That is, the shape of the stress distribution in the member may not change greatly during relaxation.

In view of the foregoing discussion and the observed 3.5 per cent decrease of maximum torque during the dynamic test it seems probable that the magnitude of the reduction in the mean stress (and also the maximum stress) did not exceed 4 per cent in any of the fatigue tests as a consequence of relaxation.

Compared to the approximately 25 per cent reduction in mean stresses resulting from yielding at high stesses a correction for relaxation is a second-order correction and no attempt has been made to correct these tests for this effect.

The alternating stresses in the fatigue tests were probably not affected by stress relaxation since the amplitude remained constant and the elastic modulus and linearity of the stress-strain curve on rapid unloading above the Bauschinger effect remained the same.

Effect of Mean Stress

Nominal Value of Mean Principal Shear Stress. In describing the fatigue strength at different states of stress various quantities have been suggested such as principal shear stress, principal stress, octahedral shear stress, principal strain, energy of distortion, etc. The greatest principal shear stress was selected in the present analysis of the effect of mean stress because of the physical significance of this quantity as discussed in reference (1), and because this theory (corrected for anisotropy)[8] best described the fatigue strength at different states of stress for zero mean stress, as shown previously (1).

Fig. 3 shows the effect on the fatigue strength (corrected for anisotropy) of the nominal value of the mean stress for all five states of stress investigated. The stresses shown for both alternating and mean values are the greatest principal shear stress.

For each state of stress at each number of cycles to failure there was a decrease in the fatigue strength, with increase in the mean stress. The average slope of the five curves at each number of cycles decreased as the number of cycles increased. This suggests that the maximum stress may be of more significance in the description of the effect of range of stress in this material than the mean stress.

No particular significance should be attached to the greater spread of the curves at 10^4 cycles over that occurring at 10^5, 10^6, and 2×10^7 cycles, since the alternating stresses in all cases were corrected for anisotropy by the average of the values of b/t (1.67) measured at the four different numbers of cycles instead of the individual values. The values of b/t were 1.748, 1.651, 1.642, and 1.640 at 10^4, 10^5, 10^6, and 2×10^7 cycles, respectively.

[8] This correction employs the observed ratio of the bending fatigue strength to the torsion fatigue strength (b/t) and is described in reference (3).

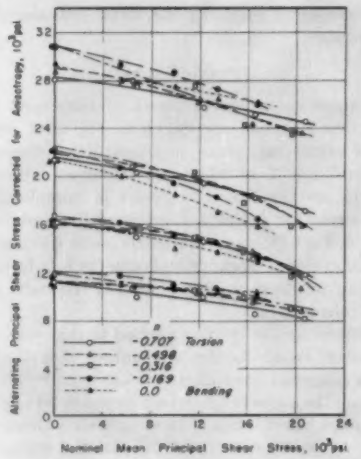

Fig. 3 Alternating Versus Mean Stress for Combined Bending and Torsion

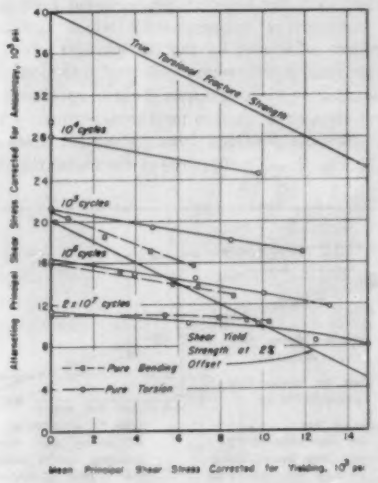
True Torsional Fracture Strength
10⁴ cycles
10⁵ cycles
10⁶ cycles
2 × 10⁷ cycles
Shear Yield Strength at 2% Offset
Pure Bending
Pure Torsion
Alternating Principal Shear Stress Corrected for Anisotropy, 10³ psi
Mean Principal Shear Stress Corrected for Yielding, 10³ psi

Fig. 4 Alternating Versus Mean Shear Stress

Mean Value of Principal Shear Stress Corrected for Yielding. Fig. 4 shows the effect of mean stress on the fatigue strength when the mean stress was corrected for the effect of yielding. Only two of the five states of stress (bending and torsion) are shown since methods of correcting for yielding under combined bending and torsion were not available. In both pure bending and pure torsion the fatigue strength decreased nearly linearly with increasing mean stress and decreased more rapidly than indicated by the nominal stresses.

At 10^4 cycles only the two values of mean stress shown for torsion and the one for bending were considered reliably corrected by the procedure employed. The intermediate values of mean stress were influenced by the Bauschinger effect.

For pure bending, an increase of mean stress appeared to have a greater effect on the fatigue strength at the lower number of cycles than at the higher number of cycles. This tendency was not exhibited by the curves for pure torsion.

The differences in the appearances of these curves is in agreement with observations made in a previous paper (3). In this paper it was suggested that fatigue failure initiated as a shear crack, and the propagation of this crack underwent a transition from shear to tension after a certain number of cycles depending on the state of stress and magnitude of alternating and mean stress. In pure torsion the propagation was mostly by shear and the major effect of an increase in the mean (or maximum) stress was to change the structure of the material, particularly if yielding resulted.

When the mean (or maximum) stress in bending was increased, there was also an increase in the normal component of stress acting on the plane of maximum shear stress. This normal stress (when tensile) apparently lowers the fatigue strength and accelerates the rate of crack propagation. This may account for the more pronounced decrease in the fatigue strengths with increase in mean stress at high alternating stresses in bending.

The data in torsion (corrected for yielding) agreed fairly well with the modified Goodman line, expressed by the relation

$$\tau_a/\tau_R + \tau_m/\tau_{ult} = 1$$

where τ_a is the fatigue strength at a given mean stress, τ_m is the mean stress, corrected for yielding, τ_R is the fatigue strength for completely reversed stresses, and τ_{ult} is the static modulus of rupture in torsion, and all stresses are principal shear stresses.

Alternating Versus Maximum Stress

Since general yielding probably affects fatigue strength it has been suggested (3) that the maximum stress of a cycle might be a more logical parameter than mean stress. The effect of the maximum stress is shown in Fig. 5 for bending and for torsion.

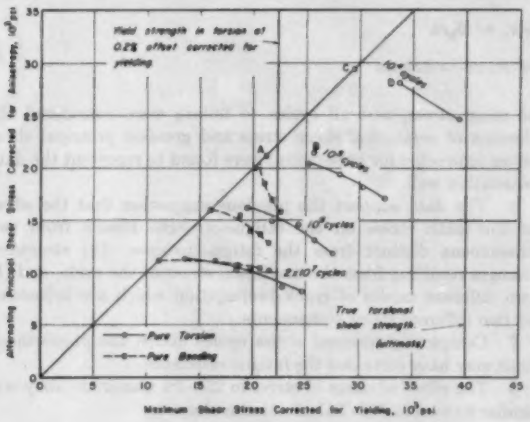

Fig. 5 Alternating Versus Maximum Shear Stress

The yield strength and ultimate strength are also shown. In this figure the region above the diagonal line is unavailable for testing by the methods employed since the maximum stress could never be less than the alternating stress.

It was observed that the fatigue strength decreased somewhat with increase in maximum stress for torsion tests and also for bending tests at low alternating stresses. At high alternating stresses the fatigue strength in bending decreased markedly with increase in maximum stress.

The curves in both bending and torsion at 10^6 cycles have higher fatigue strengths for completely reversed cycles (points A and B, Fig. 5) than indicated by the general trend. The specimens tested at these stresses entered the yield region on both extremes of the cycle. With the exception of points C and D, Fig. 5, the tests resulting in points A and B are the only ones shown which encountered the Bauschinger effect. These tests were discussed in reference (1) and were shown to have been subjected to approximately the stresses indicated.

The observed deviation of points A and B from the trend of the data at 10^6 cycles may result from one of the following possibilities: (a) Strain-hardening may occur on reverse yielding of the material resulting in increased fatigue resistance, (b) the corrections for yielding applied to tests at other values of mean stress may have indicated lower stresses than actually occurred, (c) scatter resulting from the statistical nature of fatigue.

The first of these possibilities might be worthy of further investigation. Two groups of specimens might be tested at a stress equal to the proportional limit, one group previously having been subjected to completely reversed cycles of stress well above the proportional limit until the resulting hysteresis loop disappeared, and the other group having no previous strain history. If the first group had a substantially larger number of cycles to failure than the second, the first possibility would be validated.

State of Stress at Different Mean Stresses

In the previous paper (1) the merits of six different theories of failure relative to their agreement with the test data were compared for completely reversed stress cycles. The two theories (principal shear stress corrected for anisotropy and octahedral shear stress), which were in best agreement with the test data at zero mean stress, have also been investigated at two different values of mean stress.

By use of the equations for these two theories as given in Table 2 of reference (5), the values corresponding to the fatigue strength at the following values of mean stress were computed for 10^4, 10^5, 10^6, and 2×10^7 cycles: 8000 and 16,000 psi for the principal shear-stress theory and 7000 and 14,000 psi mean stress for the octahedral shear-stress theory.

These values were plotted as a function of the state of stress number n for each theory as shown in Fig. 6. The value of b/t used in the correction for anisotropy was the average (1.67) of the values of b/t obtained from the fatigue strengths at each of the foregoing numbers of cycles for completely reversed stress cycles.

On a diagram of the type of Fig. 6 exact agreement with the theory would be represented by straight horizontal lines. A logarithmic ordinate was used in all of these diagrams because the per cent change in a quantity is represented by the same linear distance on a logarithmic scale, regardless of the magnitude of the quantity. Thus logarithmic diagrams permit direct comparison (between various curves) of the relative deviation of the test values from the theory. A scale is inset on the diagram to aid in evaluation of the degree of correspondence between theory and experiment.

An examination of these diagrams indicated that the octahedral shear-stress theory was in slightly better agreement with the test data than the principal shear-stress theory corrected for anisotropy. The difference, however, was very small. The agreement for both theories at the two mean stresses was less satisfactory than at zero mean stress (see Fig. 7 of reference 1).

Comparison With 76S-T61 Aluminum Alloy

A comparison with the previous data (3) on 76S-T61 aluminum alloy revealed the following: The S-N diagrams of the 76S-T61

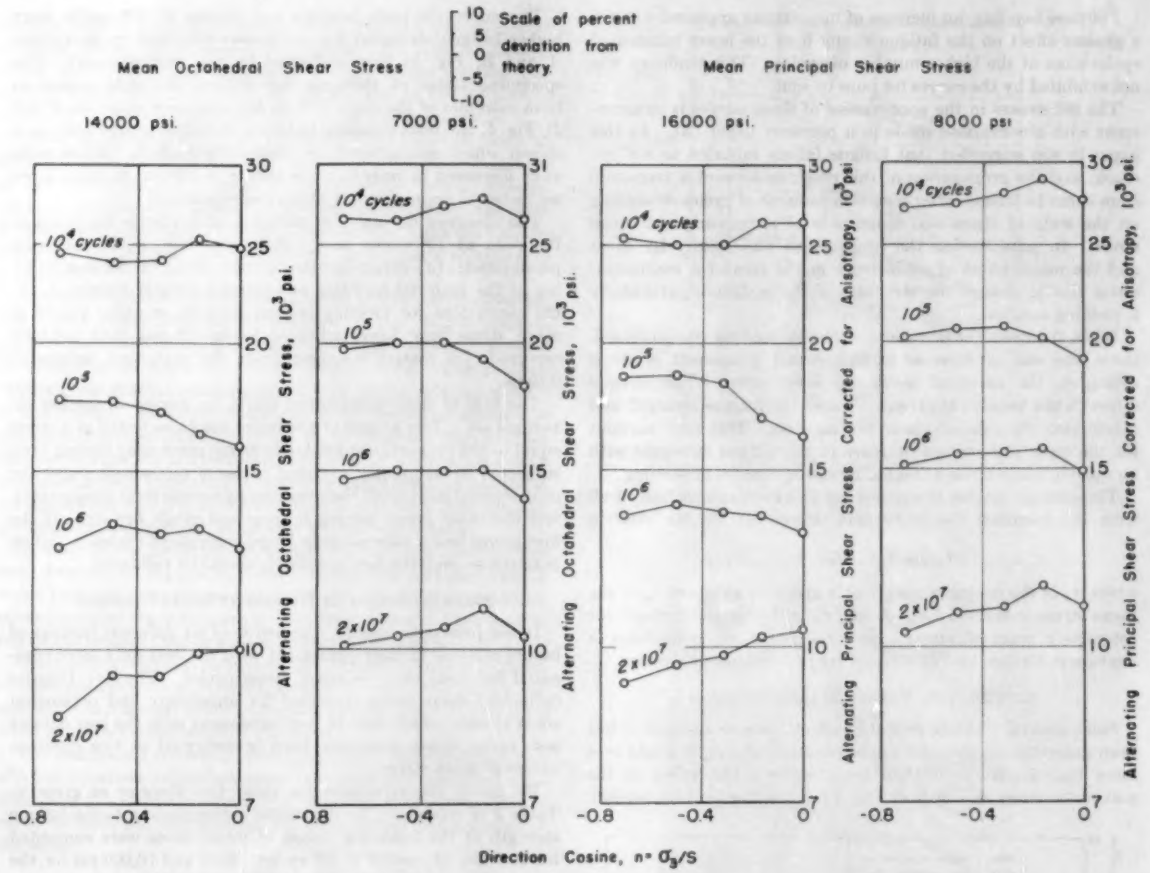

FIG. 6 THEORIES VERSUS STATE-OF-STRESS

alloy exhibited a knee in the curve, like an endurance limit, at high mean stresses. The 25S-T6 alloy exhibited only a tendency toward a knee in the *S-N* diagram for data of high mean stresses, particularly in bending.

The appearance of the alternating versus mean stress diagrams were similar.

The principal shear-stress theory corrected for anisotropy most closely represented all the data for 76S-T61 aluminum alloy and represented all the data for the 25S-T6 almost equally as well as the octahedral shear-stress theory.

CONCLUSIONS

1 An increase in the mean principal shear stress of the stress cycle caused a decrease in the fatigue strength for all states of combined stress studied.

2 The data in torsion were in fair agreement with the modified Goodman line when the mean stress was corrected for yielding.

3 In those states of stress produced by bending or having large bending-stress components, there was a decrease in the influence of mean stress as the number of cycles to failure increased.

4 A correction for possible anisotropy of the material appeared to be applicable to the alternating stresses but not to the mean stresses.

5 When the data for all states of combined stress, all values of mean stress, and all cycles to failure were considered the theories of octahedral shear stress and greatest principal shear stress (corrected for anisotropy) were found to represent the data reasonably well.

6 The data support the previous suggestion that the effect of the mean stress on the fatigue-strength results from two phenomena distinct from the fatigue process; (*a*) structural changes resulting from the maximum stress of the cycle, and (*b*) two different modes of crack propagation which are influenced by two different stress components.

7 Completely reversed stress cycles above the proportional limit may have increased the fatigue resistance.

8 The effect of range of stress in 25S-T6 aluminum alloy was similar to that in 76S-T61 aluminum alloy.

ACKNOWLEDGMENT

The project described was conducted as part of the work of the Engineering Experiment Station in the Department of Theoretical and Applied Mechanics of the University of Illinois. The authors are grateful to the following agencies for financial support of portions of the project: Hamilton Standard Division of United Aircraft, the Research Board of the Graduate School of the University of Illinois, and the Office of Ordnance Research, U. S. Army.

The authors are greatly indebted to the following for assistance

in various phases of the project: A. H. Rosenberg and W. F. Wendt.

The authors wish especially to acknowledge the assistance of D. E. Martin in the analysis of data and preparation of this manuscript.

BIBLIOGRAPHY

1 "Combined Bending and Torsion Fatigue Tests of 25S-T Aluminum Alloy," by W. N. Findley, W. I. Mitchell, and D. E. Martin, Proceedings of the Second National Congress of Applied Mechanics, June 14–18, 1954, pp. 585–593.

2 "The Effect of Range of Stress on the Fatigue Strength of Metals," by J. O. Smith, University of Illinois Engineering Experiment Station Bulletin No. 334, Urbana, Ill., February, 1942.

3 "Effect of Range of Stress on Fatigue of 76S-T61 Aluminum Alloy Under Combined Stresses Which Produce Yielding," by W. N. Findley, *Journal of Applied Mechanics*, Trans. ASME, vol. 75, 1953, pp. 365–374. See also "Combined Stress Fatigue Strength of 76S-T61 Aluminum Alloy With Superimposed Mean Stresses and Corrections for Yielding," by W. N. Findley, NACA Tech. Note 2924, May, 1953.

4 "Two Machines for Combined Bending and Torsion Fatigue," by W. N. Findley and W. I. Mitchell, Proceedings of the Society for Experimental Stress Analysis, vol. 11, no. 1, 1953, pp. 203–212.

5 "Fatigue of 76S-T61 Aluminum Alloy Under Combined Bending and Torsion," by W. N. Findley, Proceedings of the American Society for Testing Materials, vol. 52, 1952, pp. 818–832.

6 "The Effect of Non-Uniform Distribution of Stress on the Yield Strength of Steel," by D. Morkovin and O. M. Sidebottom, University of Illinois Engineering Experiment Station Bulletin No. 372, December, 1947.

7 "Inelastic Behavior of Ductile Members Under Dead Loading," by M. E. Clark, H. T. Corten, and O. M. Sidebottom, University of Illinois Engineering Experiment Station Bulletin No. 426, October, 1954.

8 "Theory of Flow and Fracture of Solids," by A. Nadai, Engineering Societies Monographs, McGraw-Hill Book Company, Inc., New York, N. Y., second edition, vol. 1, 1950, p. 349.

9 "Bending of Beams With Creep," by E. P. Popov, *Journal of Applied Physics*, vol. 20, 1949, pp. 251–256.

10 "Prediction of Creep-Deflection and Stress Distribution in Beams From Creep in Tension," by W. N. Findley and J. J. Pocsatek, *Journal of Applied Mechanics*, Trans. ASME, vol. 77, 1955, pp. 165–171.

11 "Prediction of Creep in Bending From Tension Creep Data When Creep Coefficients Are Unequal," by W. N. Findley, J. J. Pocsatek, and P. N. Mathur, Interim Report No. 3, Picatinny Arsenal Contract No. DA-11-022-ORD-401, February, 1954.

NOTE: A review of the past work on the effect of range of stress in fatigue may be found in reference (3).

The Influence of Shank Area on the Tensile Impact Strength of Bolts

By JOHN LOVE, JR.,[1] and O. A. PRINGLE[2]

The effect of reduction of shank cross-sectional area on the tensile impact strength of 5/16, 3/8, and 7/16-in. steel bolts was investigated experimentally. Low-carbon 3/8-in. bolts with rolled threads absorbed maximum impact energy when the ratio of shank area to thread-root area was equal to 1.23. Heat-treated medium-carbon 3/8-in. bolts absorbed maximum impact energy when the ratio of shank area to thread-root area was equal to 1.17 for shanks reduced by drilling or 1.12 for shanks reduced by turning. Results for other sizes were similar. It was concluded that for maximum energy absorption the shank area should approximately equal the mean or tensile-stress area of the threads, with minor corrections to compensate for work hardening due to thread rolling or surface oxidation resulting from heat-treatment.

Introduction

In order to withstand impact loads it is often more important that a machine element be capable of absorbing a given amount of strain energy rather than merely resisting a certain applied force, and for this reason the impact strength of a part is frequently measured by the energy required to produce fracture under impact. It has been pointed out many times that the impact strength of a bolt or similar threaded fastener may be increased by reducing the cross-sectional area of its shank (1 to 4).[3]

In a conventional bolt loaded in tension the stress in the shank is less than the stress in the threaded section, because the shank cross-sectional area is greater than the cross-sectional area at the threads. A reduction in shank area would increase the shank stress, the shank elongation, and the total strain energy absorbed by the bolt. Maximum impact strength should be obtained with the bolt proportioned for equal stresses in the shank and threaded section. Further reduction in shank area would then decrease the impact resistance of the bolt. Therefore the ideal bolt for shock-loading would seem to be one of uniform strength throughout. In attempting to design such a threaded part, past practice has been to reduce the shank area to a value equal to or slightly less than the thread-root area. A shank area equal to 0.9 times the root area has been frequently recommended. This practice was based on two assumptions, i.e., (*a*) that the thread-root area was a sufficiently accurate measure of the static strength of the threaded section; and (*b*) that stress concentration at the root of the threads weakened the threaded section during impact. Lately it has become customary to use the so-called mean or tensile-stress area as a more accurate measure of the static strength of the threaded section. This is a circular area computed from the mean of the pitch and minor diameters, and is a convenient approximation to the true area of a cross section through the threads. It would seem reasonable in the future to correlate recommended shank areas with stress areas rather than root areas. However, the magnitude of the stress-concentration effect in the threads during impact and the extent to which such an effect should be considered in proportioning the shank for maximum impact strength have been uncertain up to the present time. Thus, although it is well known that the impact strength of a bolt may be increased by reducing its shank, there is no conclusive evidence to show exactly what the size of the reduced shank should be.

Considerable increase in fatigue strength of bolts has been obtained by reducing the shank area (4, 5). However, the proportioning of a bolt for single impact by the use of data from fatigue tests or even repeated impact tests may be misleading, since the purpose served by the reduced shank may not be the same in the two cases. In fatigue, the reduced shank may relieve stress concentration at the last thread; also the increased bolt elasticity in comparison with the elasticity of the clamped parts may result in a smaller fraction of the repeated external load being transferred to the bolt. The effect of notches under fatigue conditions is not necessarily the same as under impact conditions. In the case of fatigue, the notch effect definitely and greatly reduces the endurance limit; therefore the area of the smooth shank can be reduced by a large amount without becoming weaker than the threaded section. In the case of impact, the primary effect of notches may be to promote the transition from the ductile to the brittle type of fracture; however, the brittle ultimate strength may not be substantially lower than the ductile ultimate strength.

The transition from ductile to brittle-type fracture is a factor of importance to be considered in any situation involving impact. This phenomenon is exhibited by several metals, including the ferritic steels, which normally behave in a ductile manner, but which may be made to fracture in a brittle fashion with greatly reduced energy absorption under certain conditions. The most important conditions which tend to bring about this transition are low temperatures, high strain rates, and triaxiality of stresses due to notches (6, 7). The Charpy impact specimen is an example of a notch effect severe enough to raise the transition temperature of certain steels into the range of room temperatures. However, the transition temperatures of notched tensile impact specimens tested in pendulum-type machines have usually been well below room temperature. In specifying bolt proportions for maximum impact strength, a distinction should be made as to the type of fracture expected, since optimum bolt proportions for ductile behavior might not prove suitable for brittle behavior.

Although the energy required to produce fracture is often used as a measure of impact strength, the properties of elastic limit and ultimate strength under impact must also be given due consideration. These properties are usually higher than their corresponding static values (8). It would be desirable for a bolt to absorb the energy of an impact load without the stress exceeding the elastic limit; consequently, its elastic limit and elastic resili-

[1] Supervisor, Requisition Engineering, Distribution Assemblies Department, General Electric Company, Cincinnati, Ohio. Assoc. Mem. ASME.

[2] Assistant Professor of Mechanical Engineering, University of Missouri, Columbia, Mo. Assoc. Mem. ASME.

[3] Numbers in parentheses refer to Bibliography at end of paper.

Contributed by the Machine Design Division and presented at a joint session with the Metals Engineering Division at the Diamond Jubilee Annual Meeting, Chicago, Ill., November 13–18, 1955, of The American Society of Mechanical Engineers.

Note: Statements and opinions advanced in papers are to be understood as individual expressions of their authors and not those of the Society. Manuscript received at ASME Headquarters, August 5, 1955. Paper No. 55—A-77.

ence should be high. On the other hand, in applications where actual fracture from an unduly high shock load would have serious consequences, the energy required for rupture would have great practical significance. In any event, reducing the shank area would increase both the elastic resilience and the energy required for rupture.

Experimental investigations of bolted joints or threaded specimens under tensile impact loads have not been numerous. Of historical interest are Sweet's drop tests on several $1^1/_4$-in. wrought-iron bolts with shanks reduced to the thread-root area (2). Whittemore, Nusbaum, and Seaquist made comparative static and tensile impact tests on threaded specimens of various sizes, materials, and thread forms, and also discussed the results of several other investigations (9). Moore reported the results of some impact tests on National Fine and Aero threads (10). Forkois, Conrad, and Vigness made shock tests on low-carbon steel bolts with full shanks and shanks reduced to the thread-root area (11).

In summary, there has been much uncertainty regarding the exact value of shank area which should be specified to enable a bolt to absorb the maximum possible amount of impact energy. Reducing the shank area to equal to, or slightly less than, the thread-root area has effected improvement in energy absorption in some instances, but all of the potential improvement may not have been realized. The purpose of the investigation described in this paper was to obtain specific experimental data concerning the effect of shank area on the room-temperature impact strength of some common bolt types, and if possible to determine optimum shank areas corresponding to maximum impact-energy absorption.

Experimental Equipment

The bolts tested were $^5/_{16}$-in-18, $^3/_8$-in-16, and $^7/_{16}$-in-14 UNC-2A × 3-in. hexagon head-cap screws used with regular and heavy semifinished hexagon nuts. Also tested were $^3/_8$-in-24 UNF-2A × 3-in. hexagon head-cap screws used with finished hexagon thick nuts. All items conformed to ASA B1.1–1949 and ASA B18.2–1952. These sizes were best suited to the capacity of the testing machine available. They were purchased in two materials, namely, 1018 steel, cold-headed with rolled threads; and 1038 steel, quenched and tempered to an average tensile strength of 130,000 psi. For the sake of brevity, the 1018 cold-headed bolts with rolled threads will subsequently be referred to as cold-forged bolts. The 1038 bolts were also cold-headed with rolled threads; however, work-hardening effects had been removed by the heat-treatment. The material of the nuts was 1108 steel. Dimensions of a random sample of the bolts were measured to verify that they were within standard tolerances. Average measured values were used in subsequent calculations, although differences between these and nominal dimensions were small. [A typical cap screw and nut as purchased are shown in Fig. 11(A).]

In the course of the investigation it became desirable to determine the effect of variables such as work hardening and heat-treatment by preparing some of the specimens in the following material conditions, in addition to the as-purchased conditions: 1018 bolts strain recrystallized at 1225–1250 F, 1018 bolts fully annealed from 1650–1675 F, and 1038 bolts fully annealed from 1550–1575 F.

As would be expected, there was considerable scatter in much of the impact data that were obtained. To secure reasonably reliable results, it was necessary to test many bolts. The number of specimens used to obtain some of the results may be noted by inspecting the appropriate curves, on which each plotted point represents a fractured bolt. Similar quantities of bolts were used in cases where the results are stated but no curves are shown. A total of 1215 bolts was tested.

Reduction of a bolt-shank area was accomplished by either drilling an axial hole through the shank, or by turning down the shank outside diameter. In either case the bolt was held in a standard collet in an engine lathe during the machining operation. Fig. 11(B) shows a drilled bolt which was sectioned to show the location of the hole. Fig. 11(C) shows a typical bolt with a shank reduced by turning.

The bolts were held in the testing machine by the fixture shown diagrammatically in Fig. 1. The two blocks of the fixture acted as the clamped parts of the bolted joint. Identical procedures were used in cleaning, lubricating, assembling, and tightening each bolt in the fixture in order to obtain consistent values of coefficient of friction. In some of the tests bolt elongations were measured with a micrometer, in which case both ends of the bolt were ground flat and parallel. The striking surfaces of the fixture were positioned so that the shock load on the bolt was axial. Fig. 2 shows the fixture installed in the pendulum of the testing machine.

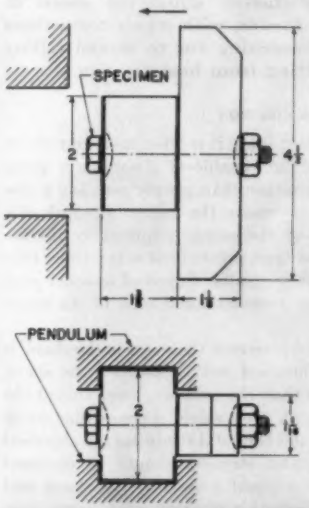

Fig. 1 Diagram of Specimen Load Fixture

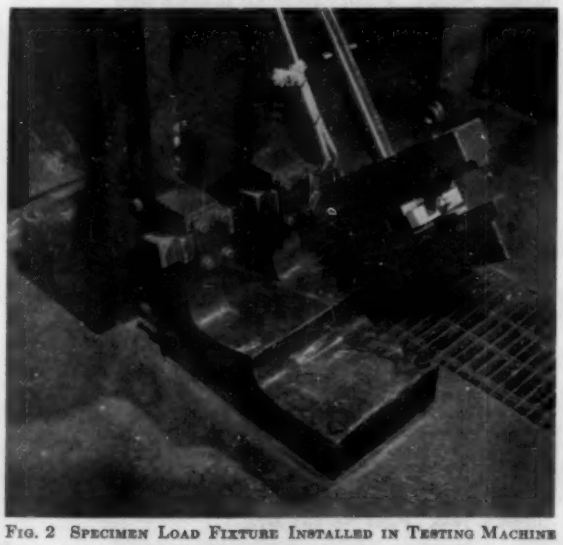

Fig. 2 Specimen Load Fixture Installed in Testing Machine

The testing machine was a Tinius Olsen pendulum-type universal impact testing machine with a capacity of 348 ft-lb and a striking velocity of 16.4 fps. When the pendulum was dropped, the two blocks of the fixture were pulled apart, thus fracturing the bolt. The energy absorbed during fracture was recorded from the backswing of the pendulum, and could be read to the nearest ft-lb. All tests were made at room temperature.

Test Procedure and Results

A number of bolts were tested in a preliminary series in order to check the functioning of the testing machine and fixture. During the first tests regular semifinished nuts were used with the UNC bolts; however, failure occasionally occurred by stripping the threads of the nut. Heavy semifinished nuts were substituted and used for the remainder of the tests. No failure of the heavy nuts occurred.

It was desired to tighten the bolts in the fixture to simulate an actual bolted joint; therefore a series of tests was made to determine the effect, if any, of tightening torque on the impact strength of the joint. The $^3/_8$-in. UNC bolts with full shanks were used in as-purchased, strain-recrystallized, and annealed conditions. Various tightening torques were applied, ranging in value from zero to those which caused failure during tightening. After tightening a bolt, its elongation was measured, and the impact strength of the joint determined. Test results are shown in Fig. 3 for two of the material conditions. The resemblance of the elongation curves to stress-strain diagrams indicated that fairly consistent values of coefficient of friction had been obtained during tightening, and it was assumed that the straight-line portions of the elongation curves corresponded to initial tightening stresses below the elastic limit. For all materials the scatter band of impact energy appeared to be independent of tightening torque as long as the tightening stress was less than the elastic limit. However, there was a definite decrease in impact strength for tightening stresses above the elastic limit. This drop in impact strength at high tightening stresses is well illustrated by the data for the 1018 strain-recrystallized bolts of Fig. 3, and it can be seen by comparing the energy and elongation curves that the drop begins when the tightening stress exceeds the elastic limit. The results obtained from the other material conditions were similar, with the possible exception of those for the 1018 cold-forged bolts. As shown in Fig. 3, there was very little reduction in impact strength noticeable for these bolts at tightening stresses above the elastic limit. Probably a very slight reduction in impact strength was concealed by the scatter in the data.

Since impact strength was independent of tightening torque for initial stresses below the elastic limit, conservative values of tightening torque were selected and used in the subsequent tests. Minor variations in coefficient of friction during tightening then had no effect on the impact strength.

The tests to determine the effect of shank area on the energy required for fracture were begun. At first, the tests were made on bolts in the as-purchased conditions; later bolts in the strain-recrystallized and annealed states were tested to assist in explaining the results. Various shank areas were obtained by drilling or turning down the shanks. The bolts were tightened in the fixture and tested to determine the impact energy required for fracture. Typical results are shown in Figs. 4 to 9, in which the impact strength of each bolt is plotted against the ratio of its shank area to its thread-root area. Bolts with full shanks plot at the extreme right end of each curve. For the curves shown, the length of the reduced section of shank was $1^3/_8$ in. for the drilled bolts and 1 in. for the turned bolts. The shorter reduced length of the turned bolts was necessary because some of the original shank length was required to support the bolts in the collet during machining. The length of threaded section exposed under the nut was $^1/_2$ in.

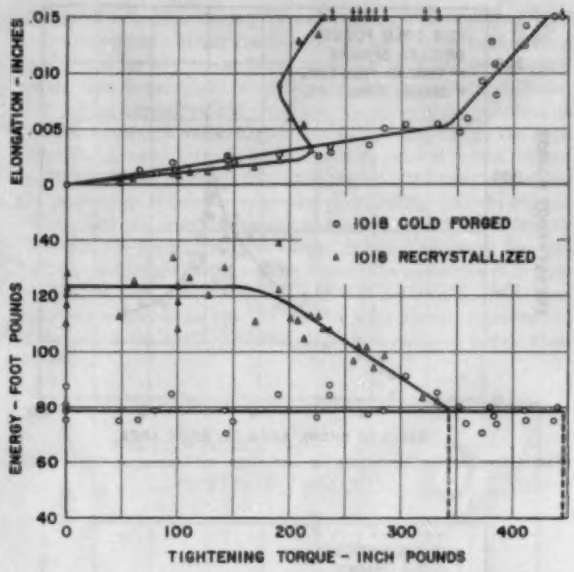

Fig. 3 Effect of Tightening Torque on Bolt Elongation and Impact Strength

The results show that there was an optimum shank area for each bolt material, and that large increases in energy absorption were obtained by reducing shank areas to these optimum values. Furthermore, the optimum ratios were considerably removed from the ratios of 0.9 or 1.0 which have been recommended in the past. Table 1 lists the optimum ratios for all of the bolts tested in the as-purchased material condition.

TABLE 1 OPTIMUM RATIOS OF SHANK TO ROOT AREA AND SHANK TO STRESS AREA

	Root-area ratio	Stress-area ratio
1038 Quenched and Tempered Bolts		
1 $^5/_{16}$ in. UNC drilled	1.16	1.01
2 $^5/_{16}$ in. UNC turned	1.13	0.98
3 $^3/_8$ in. UNC drilled	1.17	1.03
4 $^3/_8$ in. UNC turned	1.12	0.98
5 $^3/_8$ in. UNF drilled	1.10	1.02
6 $^3/_8$ in. UNF turned	1.06	0.98
7 $^7/_{16}$ in. UNC drilled	1.18	1.04
8 $^7/_{16}$ in. UNC turned	1.11	0.98
1018 Cold-Forged Bolts		
1 $^5/_{16}$ in. UNC drilled	1.25	1.09
2 $^5/_{16}$ in. UNC turned	1.25	1.09
3 $^3/_8$ in. UNC drilled	1.23	1.08
4 $^3/_8$ in. UNC turned	1.23	1.08
5 $^7/_{16}$ in. UNC drilled	1.26	1.11
6 $^7/_{16}$ in. UNC turned	1.26	1.11

The results presented in Table 1 may be summarized as follows: The optimum shank areas for the 1038 heat-treated bolts were slightly greater than the stress areas if the shanks were reduced by drilling or slightly less than the stress areas if the shanks were reduced by turning; the optimum shank areas for the 1018 cold-forged bolts were all considerably greater than the stress areas, and the same values were obtained regardless of whether the shanks had been reduced by drilling or turning.

The symbols used as plotted points in Figs. 4 to 9 distinguish between shank fractures and thread fractures. When the shank-to-root-area ratio was less than the optimum ratio, fracture usually occurred in the shank. When the shank-to-root-area ratio was greater than the optimum ratio, fracture usually occurred in the threads. Thus a bolt with the optimum shank area had a

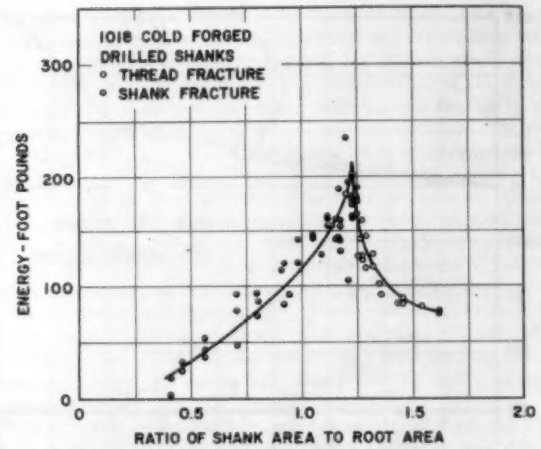

FIG. 4 EFFECT OF REDUCING SHANK AREA BY DRILLING, 1018 3/8-IN. UNC COLD-FORGED BOLTS

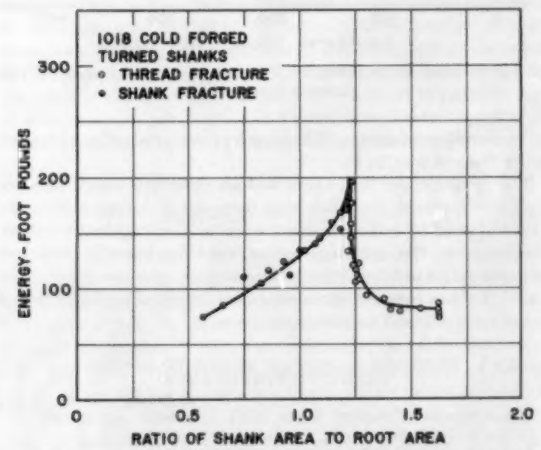

FIG. 5 EFFECT OF REDUCING SHANK AREA BY TURNING, 1018 3/8-IN. UNC COLD-FORGED BOLTS

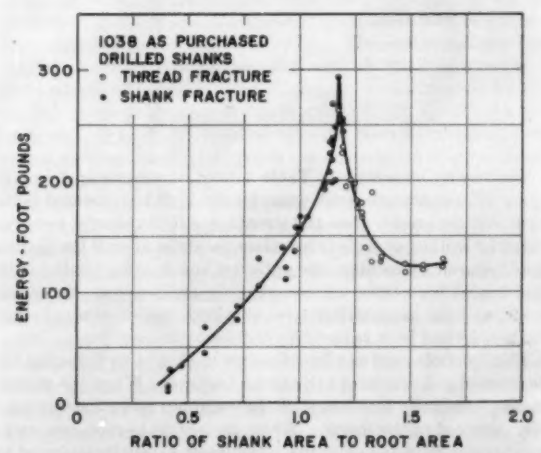

FIG. 6 EFFECT OF REDUCING SHANK AREA BY DRILLING, 1038 3/8-IN. UNC QUENCHED-AND-TEMPERED BOLTS

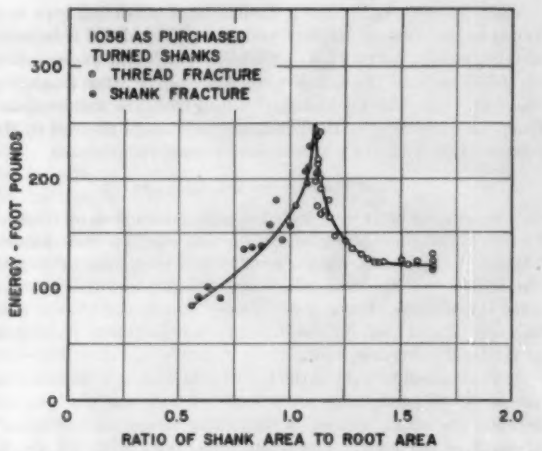

FIG. 7 EFFECT OF REDUCING SHANK AREA BY TURNING, 1038 3/8-IN UNC QUENCHED-AND-TEMPERED BOLTS

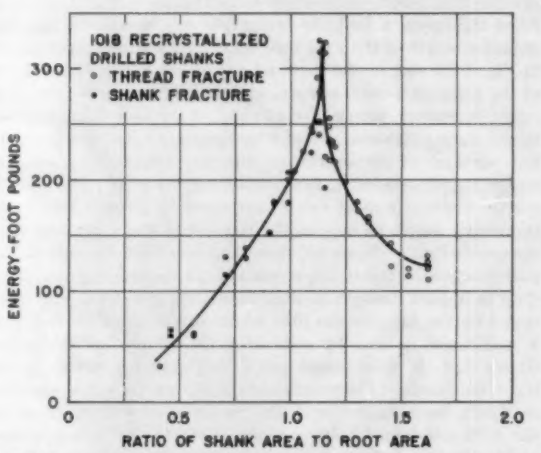

FIG. 8 EFFECT OF REDUCING SHANK AREA BY DRILLING, 1018 3/8-IN. UNC STRAIN-RECRYSTALLIZED BOLTS

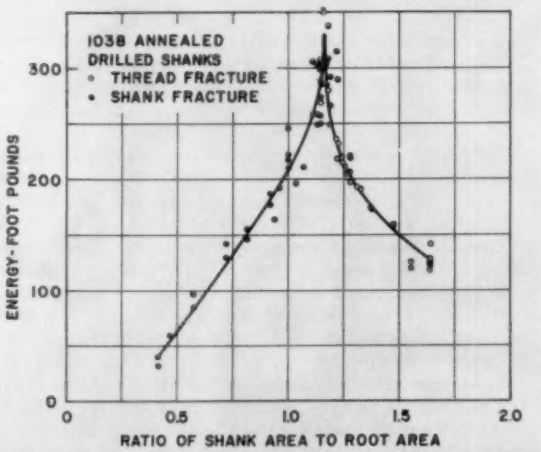

FIG. 9 EFFECT OF REDUCING SHANK AREA BY DRILLING, 1038 3/8-IN. UNC ANNEALED BOLTS

shank and threaded section of equal strength. The optimum shank-area to stress-area ratios of some of the bolts were only very slightly less than unity; the remainder were above unity. The stress area is a reasonably accurate measure of the static strength of the threads; therefore there was no evidence of a reduction in ultimate strength under impact due to stress concentration in the threads.

It is not surprising that the optimum shank areas for the 1038 quenched-and-tempered bolts should depend upon the method used in reducing the shank. In a drilled bolt the load is carried by the outer layers of the original shank material; in a turned bolt the load is carried by the core of the original shank. Core properties could differ from case properties for many reasons, such as, segregation, decarburization, shallow hardening, work-hardened layers, plating, scale, etc. Metallographic examination of sample heat-treated bolts revealed uniform cross sections except for slight decarburization extending the width of several grains near the surface and a thin layer of surface scale. It is believed that the different optimum shank areas for drilled bolts and turned bolts may be attributed to the effect of this scale plus the slight decarburization. This may be explained by referring to the optimum ratios grouped for comparison in Table 2. The 1038 bolts had been quenched and tempered by the manufacturer and were covered with the normal amount of scale. (Bolts from two different manufacturers gave identical results.) Drilling the shank removed no scale, thus the original scale was included in the calculated shank and thread areas. Turning the shank removed the shank scale, thus this scale was no longer included in the calculated shank area. For equal strengths, an area including scale would of necessity be slightly larger than an area not including scale; consequently, different optimum ratios would be obtained. The same effect is in evidence for the 1038 bolts of Table 2 which were annealed. During annealing, the surfaces of previously drilled holes were oxidized, resulting in a slight loss of effective cross section. Consequently, the optimum ratio of the bolts drilled before annealing was higher than that of the bolts drilled after annealing.

TABLE 2 EFFECT OF HEAT-TREATMENT ON OPTIMUM RATIOS OF $^3/_8$-IN. UNC 1038 BOLTS

Bolt description	Root-area ratio	Stress-area ratio
1 Quenched and tempered, then drilled	1.17	1.03
2 Quenched and tempered, then turned	1.12	0.98
3 Drilled, then annealed	1.17	1.03
4 Annealed, then drilled	1.15	1.01

The higher optimum ratios obtained for the 1018 cold-forged bolts indicated that the threaded sections of these bolts were unusually strong in comparison with their shanks. This was undoubtedly due to work hardening of the threaded section during the thread-rolling operation. As shown in Table 3 and Figs. 4 and 8, a strain-recrystallization heat-treatment removed this effect, lowering the optimum ratio from 1.23 to 1.15. A full anneal had little additional effect, except that the more severe surface oxidation resulted in a higher optimum ratio when the bolts were drilled before heat-treatment rather than after. Referring to Table 1, it will be noticed that the optimum ratios for the $^5/_{16}$ and $^7/_{16}$-in. cold-forged bolts were higher than the ratio for the $^3/_8$-in. cold-forged bolts. Although the smaller $^5/_{16}$-in. thread received somewhat less plastic deformation during thread rolling, the work-hardened region occupied a larger fraction of the total cross section than in the case of the $^3/_8$-in. bolts, resulting in a higher optimum ratio. The larger $^7/_{16}$-in. threads received more plastic deformation during thread rolling than the $^3/_8$-in. threads, resulting in increased strength and a higher optimum ratio. Thus the optimum shank areas for cold-forged bolts in general would depend on the amount of plastic deformation required to form the threads, the percentage of total cross section occupied by the cold-worked region, and the work-hardening characteristics of the material. Although the transition from thread fracture to shank fracture for the cold-forged bolts occurred near the optimum ratio, inspection of Figs. 4 and 5 will reveal that maximum energy was absorbed when shank fracture rather than thread fracture occurred, since the work-hardened threads were more brittle than the shank.

TABLE 3 EFFECT OF HEAT-TREATMENT ON OPTIMUM RATIOS OF $^3/_8$-IN. UNC 1018 BOLTS

Bolt description	Root-area ratio	Stress-area ratio
1 Cold-forged, then drilled	1.23	1.08
2 Cold-forged, then turned	1.23	1.08
3 Drilled, then strain-recrystallized	1.15	1.01
4 Drilled, then annealed	1.17	1.03
5 Annealed, then drilled	1.13	0.99

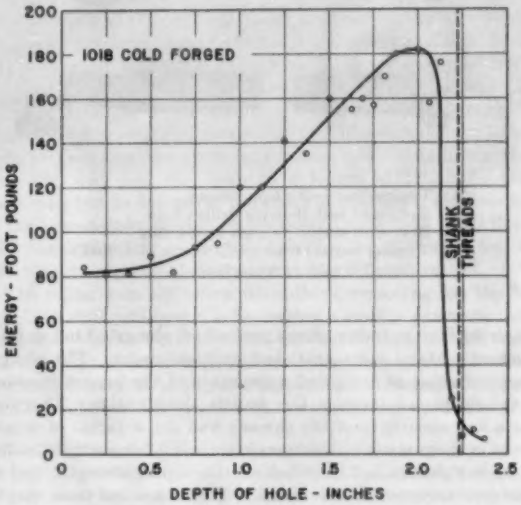

FIG. 10 EFFECT OF LENGTH OF REDUCED SECTION OF SHANK, 1018 $^3/_8$-IN. UNC COLD-FORGED BOLTS DRILLED

It was anticipated that the impact strength would increase as the length of reduced section of shank increased. A series of tests was made in which the depth of drilled hole and length of turned section were varied. Fig. 10 shows typical results for $^3/_8$-in. cold-forged bolts drilled for optimum shank areas. For shanks reduced by drilling, the bottom of the hole should not approach too close to the threaded section; otherwise the hole will weaken the cross section near the first thread. For the sizes tested, a safe distance to maintain between the bottom of the hole and the first thread was $^1/_4$ in. The exposed length of threaded section between the nut and bolt head serves the same purpose as the reduced shank and affects the energy absorption in the same manner. Although longer reduced shanks or exposed threaded sections increased the energy absorption, the optimum shank areas were independent of these lengths as long as the lengths were about 1 diam or more.

The general appearance of impact fractures was similar for all of the bolt materials. Substantial elongation and necking occurred at all of the fractures. A typical impact fracture in the shank of a drilled 1018 cold-forged bolt is shown in Fig. 11(D). Fig. 12 shows several 1038 quenched and tempered bolts. Fig. 12(B) is a typical impact thread fracture and may be compared with the static thread fracture of Fig. 12(A). Fig. 12(C) shows a typical impact fracture in a reduced shank and Fig. 12(D) shows

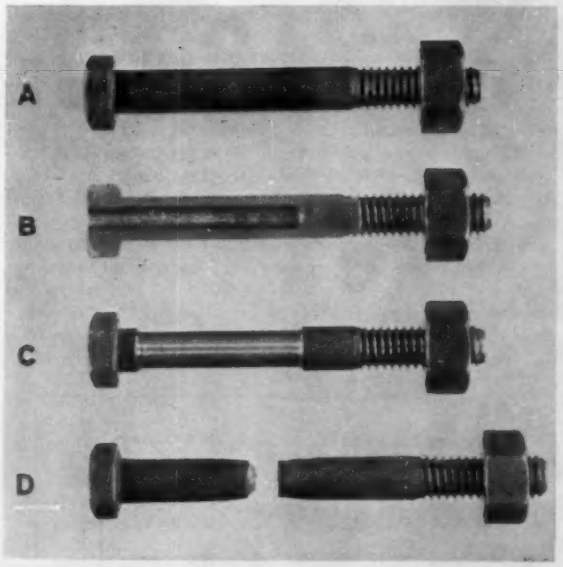

(A) Typical test bolt as purchased
(B) Sectioned bolt showing drilled hole
(C) Bolt with shank reduced by turning
(D) Typical impact fracture in shank of drilled bolt

FIG. 11 TEST BOLTS

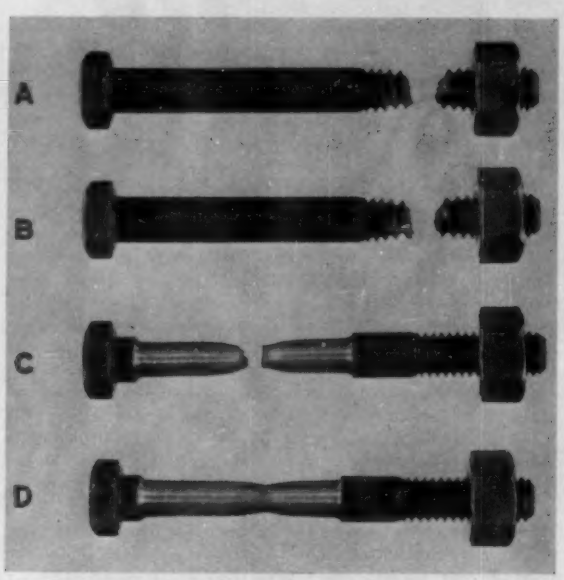

(A) Typical static thread fracture
(B) Typical impact fracture in threads of bolt with full shank
(C) Typical impact fracture of bolt with shank turned down to thread-root area
(D) Bolt with optimum shank area which did not fracture under impact

FIG. 12 QUENCHED-AND-TEMPERED BOLTS

a bolt with an optimum shank area which elongated but did not fracture. Many bolts exhibited multiple necks. The elongation, reduction of area, and appearance of the impact fractures definitely placed them in the ductile classification. Therefore the notch sensitivity of the threads was not a factor of importance in these tests. Variations in surface finish and fillet radius of turned shanks had no effect on the impact strength, and no fractures occurred at the fillets. The transition from ductile to brittle failure would be expected only if the temperature were lowered, the striking velocity increased, or some other less important factor varied sufficiently.

Bolts have been manufactured in the past by rolling threads directly upon a shank of uniform diameter, the shank diameter being slightly greater than the pitch diameter of the resulting threads. The shank-to-root-area ratio of such bolts would be greater than any of the optimum ratios in Table 1; hence additional shank reduction would be necessary in order to obtain maximum impact strength.

The use of spring washers as a means of increasing impact strength of bolts has been frequently discussed. Certain considerations in the proper design of such spring washers are clarified by the results of this investigation. If the spring washer is to be used to its fullest capacity in absorbing energy at all loads up to actual bolt fracture, it should be proportioned to undergo plastic deformation in unison with the bolt itself. In other words the spring washer should in effect serve as an additional length of reduced bolt shank. If loaded in tension and made of the same material as the bolt, its cross-sectional area should be equal to the optimum shank area. However, a compact and practical spring washer probably would be loaded in bending, and would not necessarily be made of the same material of the bolt. In this case the proper matching of washer to bolt might be a problem requiring experimental work similar to that of determining optimum shank areas. A simple elastic resilience calculation will show that a spring washer of reasonable size stressed below its elastic limit at loads corresponding to bolt ultimate strength would offer negligible assistance in absorbing sufficient energy to prevent bolt fracture. Such a spring washer would act only as an additional length of full-size bolt shank. On the other hand, a spring washer stressed to the same degree as a reduced shank and occupying a similar volume would absorb a comparable amount of energy.

Since it could be deduced from the results that the ultimate strength during impact was not reduced by stress concentration in the threads, there would appear to be no incentive to attempt to change the stress distribution by modification of the nut. It is possible, however, that a nut might be proportioned to do double duty by also serving as a spring washer.

Gaskets have negligible effect on the impact energy required to fracture a bolt. Although gasket rigidity may determine the extent to which the external load is transferred to the bolt at stresses below the elastic limit, the energy absorbed at these stresses is very small compared with the total fracture energy. A thick gasket may appear to increase the energy required for fracture; however, this is due to the increase in length of the exposed threaded section, which has the same effect as increasing the length of the reduced shank.

CONCLUSIONS

In summary, the room-temperature fractures of small and medium-sized steel bolts under single impact loads were of the ductile rather than brittle type; stress concentration, if present, had negligible effect in reducing the ultimate strength during impact. Substantial increases in energy required for fracture were obtained by reducing the shanks to the correct cross-sectional areas. The optimum shank areas for heat-treated steel bolts were approximately 2 per cent less than the corresponding tensile-stress areas if the oxidized shank surfaces were removed by turning, or approximately 2 per cent more than the

corresponding tensile-stress areas if the shanks were drilled and the oxidized shank surfaces retained. Because of work hardening, the optimum shank areas were higher for steel bolts with rolled threads not subsequently heat-treated, being from 8 to 11 per cent greater than the corresponding tensile-stress areas.

The utility of the foregoing information is well illustrated by the three bolts (B), (C), and (D) of Fig. 12. These bolts were subjected to identical impact loads of 255 ft-lb. Bolt (B), which had a full shank, fractured in the threads. The shank of bolt (C) had been turned down to the thread-root area; this reduction was excessive, and the bolt fractured in the shank. Bolt (D) had a shank of optimum cross section, and although considerably elongated, did not fracture. This information does not assist the designer in determining the size of bolt required for a certain application. However, once the size has been determined by previously used and possibly empirical methods, the designer will be able to specify superior bolt proportions in cases where the joint must primarily absorb a given amount of energy. Experience gained as a result of using such bolt proportions in service should eventually lead in many cases to revised procedures for selecting bolt sizes and to greater economy in design.

BIBLIOGRAPHY

1 "Die Vorzüge der Dehnschraube," by A. Thum and F. Debus, *Zeitschrift des Vereines deutscher Ingenieure*, vol. 79, 1935, pp. 917–919.

2 "Machine Design," by A. W. Smith and G. H. Marx, John Wiley & Sons, Inc., New York, N. Y., fourth edition, 1915, pp. 156–158.

3 "Design of Machine Elements," by V. M. Faires, The Macmillan Company, New York, N. Y., third edition, 1955, p. 126.

4 "On the Strength of Highly Stressed Dynamically Loaded Bolts and Studs," by J. O. Almen, *Journal of the Society of Automotive Engineers*, vol. 52, 1944, pp.151–158.

5 "Effect of Screw Threads on Fatigue," by S. M. Arnold, *Mechanical Engineering*, vol. 65, 1943, pp. 497–505.

6 "Fundamentals of Brittle Behavior in Metals," by E. Orowan, Symposium on Fatigue and Fracture of Metals, The Technology Press, Massachusetts Institute of Technology, Cambridge, Mass., 1952, pp. 139–167.

7 "The Velocity Aspect of Tension-Impact Testing," by W. H. Hoppman, Proceedings of the American Society for Testing Materials, vol. 47, 1947, pp. 533–543.

8 "Measurement of Dynamic Stress and Strain in Tensile Test Specimens," by R. O. Fehr and E. R. Parker, Proceedings of the Society for Experimental Stress Analysis, vol. 1, no. 1, 1943, pp. 76–82.

9 "Impact and Static Tensile Properties of Bolts," by H. L. Whittemore, G. W. Nusbaum, and E. O. Seaquist, *Journal of Research*, National Bureau of Standards, vol. 14, 1935, pp. 139–188.

10 "Strength of Screw Threads Under Tensile, Fatigue, and Impact Loads," by R. R. Moore, *Product Engineering*, vol. 10, 1939, pp. 475–479.

11 "Properties of Bolts Under Shock Loading," by H. M. Forkois, R. W. Conrad, and I. Vigness, Proceedings of the Society for Experimental Stress Analysis, vol. 10, no. 1, 1952, pp. 165–178.

Discussion

V. L. Doughtie.[4] The authors are to be commended for their extensive tests and excellent presentation of the results. Apparently, they have considered the many factors involved in the strength of bolts. A discussion of this paper could be given in two words, well done.

As indicated by the title, the purpose of the experiments was to determine the proper shank area of a bolt for impact loads; but other factors affecting the strength of a bolt were determined and discussed. Nut thickness, tightening torque, length of reduced area, heat-treating, use of spring washers, notch sensitivity, surface finish and fillet radius of the turned-down shank, nut modification, and gasket thickness are some of the factors considered. The tests show that the ratio of the shank area to the root area should be slightly above unity instead of unity or below as previously considered to be good practice. It is also clearly brought out that bolt size, material, and heat-treatment influence this ratio.

It should be observed that in most cases, the ratio of the shank area to the stress area is about unity. The Unified Thread Standards give values of the stress area and not root areas. Would it not be desirable to discontinue the use of root area?

The authors state: "In fatigue, the reduced shank may relieve stress concentration at the last thread." Perhaps, it is a question of definition of the last thread. The first threads in a nut carry most of the load.

It is surprising that the scatter of the results is not greater than it is. Several years ago, the writer tested in pure tension hundreds of bolts as purchased and found a much larger variation in failure loads.

The length of the reduced shank for the curves shown was $1^{3}/_{8}$ in. for the drilled shank and 1 in. for the turned shank. Fig. 10 of the paper indicates that a length of hole of approximately 2 in. absorbs the maximum energy. The authors state: The optimum shank areas for maximum energy absorption were independent of the length of reduced section of shank as long as the length was at least one diameter or more. If this is interpreted correctly, why drill the holes to a length of $1^{3}/_{8}$ in.? Also, were tests run to determine the effect of the length and location of the turned-down section on the energy absorbed? Is it likely that the drilled hole in the bolt head for the 1038 steel had an effect on the rigidity of the head causing different ratios?

The writer does not follow the authors' reasoning for the $^{3}/_{8}$-in. UNC 1018 cold-forged bolts having a smaller optimum ratio than the $^{5}/_{16}$-in. UNC and $^{7}/_{16}$-in. UNC bolts of the same material. It seems that if this reasoning were correct the ratio would decrease with an increase in bolt size. It is hoped that the authors will extend their research to cover larger-sized bolts.

W. C. Stewart.[5] The authors present some very new, interesting, and useful information with respect to the design of bolts. Of particular interest is the conclusion that the proper shank area of the bolt for maximum energy absorption (quenched and tempered bolts) is close to the so-called "tensile stress area." This area, in recent years, has become adopted as the conventional area for computing tensile strength of threaded sections since it is more representative than the root area. The present impact tests tend to confirm this assumption.

It would have been helpful if the authors had added another series of tests comparing optimum reduced-shank bolts with bolts threaded to the head (no shank, or only a very short shoulder). Presumably, the threaded-to-head bolts would also give optimum energy absorption. If this assumption proved true, it would have a practical significance since threaded-to-head bolts could be manufactured more economically than waisted or drilled bolts.

The authors observed that bolts tightened beyond their elastic limit suffer a loss of energy absorption. From this it might be concluded that it is bad practice to tighten the bolt above its elastic limit. Experience, however, indicates that this is not bad practice and there are other good reasons for so tightening in many applications. The authors' observations are no doubt true for the test arrangement used. The bolts were stretched almost to the breaking point and could stand very little further deformation (energy absorption). In this test setup all of the energy input to the joint was forced into the bolt. Therefore the bolt fails with little energy absorption. In an actual joint this situation generally does not hold.

[4] Professor, Department of Mechanical Engineering, University of Texas, Austin, Texas. Fellow ASME.

[5] Technical Adviser, Industrial Fasteners Institute, Cleveland, Ohio. Mem. ASME.

In practice the energy input can be absorbed either by the bolt or by the structure or by both. The bolt alone is not forced to absorb all of the energy. In such a joint the bolt may not break even though large amounts of energy are supplied, the energy being absorbed by the surrounding material. In other words, the high bolt tension deflects the energy and forces the structure to take the impact. The structure should be designed to take this energy anyway, unless the bolt is looked upon as a "safety valve" protecting an underdesigned fragile structure.

Authors' Closure

The authors wish to thank Professor Doughtie and Mr. Stewart for their interest in the paper and their valuable comments.

Although the results presented in the paper do emphasize the usefulness of the stress area in bolt strength calculations, it should be noted that cold-forged bolts present a somewhat exceptional case. These bolts were stronger than their stress areas would indicate, since their optimum shank areas were substantially greater than the corresponding stress areas. The increase in strength was undoubtedly due to work hardening during thread rolling, and the magnitude of the increase would depend upon such factors as bolt material, amount of plastic deformation required to form the thread, depth of the work-hardened layer, and previous work hardening due to the operation of reducing the diameter of the threaded section prior to thread rolling. In view of the many variables involved, it is not surprising that different optimum ratios were obtained for different sizes of cold-forged bolts. Furthermore, it will be difficult to accurately predict either the optimum shank areas or strengths of cold-forged bolts in general unless specific test data are available.

Both the area and the length of the reduced shank had an effect upon the energy absorption of a given bolt. For constant length of reduced shank, maximum energy absorption was obtained with a certain critical or optimum shank area. For constant shank area, the energy absorbed during fracture increased as the length of reduced shank increased. The optimum shank area for a given material condition remained constant regardless of the length of reduced shank. However, the above relationship was not investigated thoroughly for extremely short lengths of reduced shank, since little gain in energy absorption would be realized by such modification. Consequently, it was stated in the paper that the optimum ratios presented should be considered to apply only to reduced shank lengths of approximately one nominal bolt diameter or more. It should also be stated that some variation in the optimum ratios might result if the thickness of clamped parts were reduced until almost no threads were exposed under the nut.

The length of exposed threaded section between the nut and the bolt head acted in effect as an additional length of reduced shank, and energy absorption was increased by increasing the length of exposed threads. It would therefore seem reasonable to conclude that a bolt threaded to the head would offer maximum or near maximum energy absorption. However, cold-forged bolts might prove to be an important exception. Inspection of Figs. 4 and 5 shows that maximum energy was absorbed by cold-forged bolts with optimum shank areas when shank fracture rather than thread fracture occurred, since the shanks were less brittle than the work-hardened threads. A fracture occurring in a cold-forged bolt threaded to the head would of necessity be located in the threads, with a consequent loss in energy absorption. Thus the ideal cold-forged bolt for shock loading should have a minimum length of threaded section and a maximum length of smooth reduced shank. Furthermore, the shank area should be slightly less than the optimum area in order to guarantee that energy absorption will be concentrated in the ductile shank.

It was pointed out in the paper that one advantage of a reduced shank under repeated loading may be a reduction in stress concentration at the last thread. The term "last thread" was intended to specify the location at the juncture between the shank and the threads. Other likely locations for fatigue fracture would be the juncture between the shank and the head, and the thread adjacent to the face of the nut.

The authors agree that the observed decrease in fracture energy at initial tightening stresses above the elastic limit should not necessarily be interpreted as indicating that such high tightening stresses are always detrimental. Tightening a bolt above the elastic limit produces plastic deformation and work hardening, with resulting increase in elastic limit and decrease in ductility. Because of the increased elastic limit, the ability of the bolt to absorb energy at stresses below the elastic limit would thus actually be improved by high tightening stresses. No doubt in the majority of applications a properly selected bolt would not be stressed above the elastic limit by the external load; also, the surrounding structure would normally absorb a large fraction of the energy of a shock load. However, the decreased ductility of the bolt due to high tightening stresses would be cause for consideration if large and unpredictable overloads were anticipated in structures designed with low factors of safety.

FIG. 1 PARTIAL VIEW OF THE RADIOISOTOPE LABORATORY

New Techniques in Metal-Cutting Research

BY W. R. BACKER[1] AND E. J. KRABACHER,[1] CINCINNATI, OHIO

Information on newly developed research techniques for studying the metal-cutting process is presented in this paper. Tool-wear and grinding-wheel-wear measurement methods are discussed, and techniques for research into the mechanism of those wear processes are described. New equipment for studies of the mechanics of machining processes, including force measurements and chip-formation analysis, is also described. Representative data are presented to show how research utilizing these techniques contributes to the knowledge of machining principles.

INTRODUCTION

ADVANCES in any science are dependent on new research techniques that improve the precision or speed of measurements. The trend in the field of metal-cutting research is toward more fundamental investigations of the machining process. This trend requires more refined measurements in broader fields of technology, and co-ordination of the work of the engineer with that of the scientist. Research techniques must be devised to keep pace with these developments, and to provide experimental verification of cutting theories. Examples of methods and instruments developed in the authors' laboratory are described in the paper.

MEASUREMENT OF WEAR IN METAL CUTTING

In the machining of metals on a production basis, the nature and rate of wear of the cutting tool are of very significant importance to the economics of the operation. Evaluation of the performance of a cutting fluid, the effectiveness of different cutting-tool geometries, and the relative machinability of work materials are based primarily upon the nature and rate of tool wear. Thus research techniques for studying the nature and rate of wear are of great interest to investigators working in the field of metal cutting.

Radioisotopes, used as radioactive tracers, provide an excellent tool with which to measure and study the process of tool wear. They have been used routinely in our laboratory for several years to evaluate the performance of cutting fluids and the relative machinability of various work materials (1).[2] Fig. 1 presents a general view of a portion of the radioisotope laboratory at the authors' company. From left to right may be seen a radiochemical fume hood, two storage vaults, and the lathe setup on which the radioactive tool-wear studies are conducted.

The technique for the measurement of tool wear involves the use of a radioactive cutting tool for the rapid determination of the "instantaneous" rate of tool wear. A small clamped-in type of tool bit, which has been irradiated by neutron bombardment in a nuclear reactor, is used in a turning operation on a lathe. In the lathe setup, as shown in Fig. 1, metal is turned off the end of a tubular workpiece with either a straight turning tool which produces chips under orthogonal cutting conditions, or with a form tool when either cutting fluids or work materials are to be evaluated under rather severe cutting conditions. A wide variety of tool materials and geometries may be utilized in this test method.

It has been established that under normal conditions of tool wear upward of 90 per cent of the tool material worn away during the cutting operation adheres to the chips. Thus the amount of tool wear may be conveniently determined with a geiger counter

[1] Senior Research Engineer, The Cincinnati Milling Machine Company. Assoc. Mem. ASME.

Contributed by the Research Committee on Metal Processing and presented at the Diamond Jubilee Annual Meeting, Chicago, Ill., November 13–18, 1955, of THE AMERICAN SOCIETY OF MECHANICAL ENGINEERS.

NOTE: Statements and opinions advanced in papers are to be understood as individual expressions of their authors and not those of the Society. Manuscript received at ASME Headquarters, September 15, 1955. This paper was not preprinted.

[2] Numbers in parentheses refer to the Bibliography at the end of the paper.

by measuring the radioactivity of the chip sample, since this is a direct measure of the amount of radioactive tool material present thereon. If this measurement is expressed in terms of counts per minute per gram of chips, we then have an indication of the instantaneous rate of tool wear. Because we can measure the instantaneous rate of wear, it is possible to evaluate the relative performance of cutting variables. In the evaluation of cutting fluids, for example, we cut alternately with one fluid and then the other, under otherwise identical conditions. The relative radioactivity of the respective chip samples gives a direct measure of the relative rates of tool wear obtained with each of the cutting fluids. The relative machinability of work materials may be measured in like manner by alternating the work materials rather than the cutting fluids. It is obvious that tool wear also may be evaluated readily as a function of numerous other variables which exist in metal cutting. The routine evaluation of cutting fluids or of the machinability of various work materials requires a test cut of 15 to 30-sec duration, depending on the specific cutting conditions, to produce a sufficiently large sample of approximately 50 grams of chips. This compares with a cutting time of possibly an hour and many pounds of work material as is required with the conventional tool life-testing method. In addition to the tremendous savings in time and material, there is the opportunity to run a sufficient number of tests under given conditions so that the data may be evaluated statistically; this enhances the reliability of the data.

The application of radioisotopes to the fundamental study of tool wear affords a means of actually tracing the tool-wear particles, and of studying their origin, nature, and distribution. The ability to study qualitatively the distribution and nature of wear particles on the chip is graphically illustrated in Fig. 2. Here is presented a photomacrograph (*a*) and an autoradiograph (*b*) of the same chip segment which was a typical chip machined with a radioactive tool. The autoradiograph was prepared by placing the side of the chip which contacted the face of the tool during formation in contact with a piece of photographic film for a given period of exposure. This autoradiograph, which clearly delineates the chip, was produced entirely by the radiation coming from the tiny particles of radioactive tool material (wear products) adhering to the chip. It presents a true qualitative picture of the distribution of tool-face wear particles on this particular segment of chip. A comparison made with the photomacrograph indicates clearly that the distribution and concentration of wear particles on the chip occur on areas which exhibit conditions of high friction and the existence of considerable built-up edge. Studies of this nature contribute to a clearer understanding of the process of tool wear.

A quantitative study of the origin and distribution of the wear particles is readily made by measuring the beta radiation emanating from these particles with a geiger counter or some other suitable means, to determine the quantity of tool material worn from the face and the flank of the tool. Those wear particles which adhere to one side of the chip represent the tool material worn from the face of the tool while those which adhere to the opposite side of the chip are indicative of the flank wear. Since the beta radiation from the tool material is not capable of penetrating the chip, it is a simple matter to measure first the quantity of wear particles on one side of the chip and then the other.

Test apparatus and instrumentation have been designed and are now being built to provide a means for extending the use of radioactive cutting tools to a study of the milling process. This apparatus will provide facilities for both face milling and peripheral milling under varying conditions of tool geometry. These test facilities will be utilized in a fundamental study of the milling process.

An analysis of the foregoing techniques indicates that radioisotopes, in this case in the form of a radioactive cutting tool, offer a means for studying the mechanism of tool wear which has heretofore been beyond our grasp.

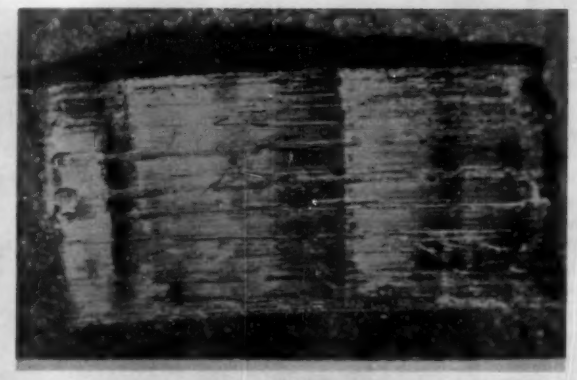

(*a*)

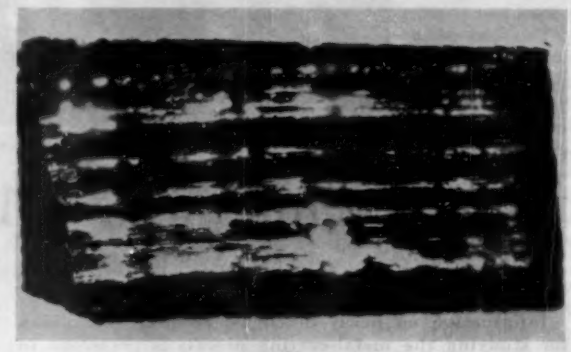

(*b*)

FIG. 2 TYPICAL CHIP CUT WITH RADIOACTIVE TOOL

(*a*, Photomacrograph of chip; *b*, autoradiograph of same chip.)

GRINDING-WHEEL WEAR

Although the rate of wear of a grinding wheel is about a million times the wear rate of a cutting tool, the actual amount of wheel material removed is still quite small, and the wear is spread around the entire circumference of the wheel. The technique for measuring grinding-wheel wear is to determine the changes in wheel radius resulting from incremental workpiece material removal. Knowing the change in wheel radius, plus the wheel diameter and face width, the volume of wheel worn away can be computed. Except with small grinding wheels, the measurement of wear by direct diameter readings is unsatisfactory because the wear is too small a portion of the total dimension. However, if a reference surface can be established at or near the outside of the wheel, the difference between the average level of the worn surface and the reference surface can be measured with reasonable accuracy.

Fig. 3 shows an electric-resistance strain-gage transducer designed for grinding-wheel wear measurements. The transducer is simply a cantilever beam with strain gages at its root and a contactor at its free end; the beam is mounted at a slight angle to provide clearance for the gage, its leads, and their insulation. The mechanical design provides the required sensitivity with a low enough spring constant to prevent excessive pressure loading on the wheel. The sensitivity of the transducer circuit

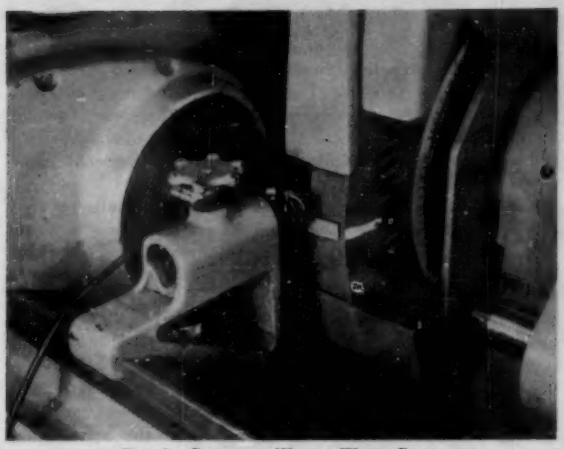

FIG. 3 GRINDING-WHEEL WEAR GAGE
(Note ceramic block used as reference surface.)

is about 0.05 volt output per volt excitation per in. deflection, and the spring constant is 135 lb per in. The contactor is a hardened steel ball with a small flat; the fine details of a wheel profile obtained with a finer stylus did not prove useful for data interpretation in preliminary tests. The effect of the friction force acting through the small moment arm arising from the contactor overhang and the angle of the beam is negligible. Calibration is accomplished on a surface plate using precision gage blocks.

The grinding-wheel wear test begins with grinding the first increment of workpiece volume under the desired set of conditions. The wheel is stopped and the transducer is mounted on the grinder table. The contactor is traversed across the face of the wheel and the reference surface, and this profiling is repeated at four points around the wheel; it was found that the number of points taken could be limited to four during preliminary tests. Subsequent increments of the workpiece may now be ground away, with profile charts being obtained after each run. The data are taken from the charts, averaged, and used to compute the volume of wheel worn away after each step.

The reference surface can be an unused part of the wheel face, a dressed-down portion of the wheel, or a separate surface attached to the wheel. Reference surfaces not integral with the wheel lead to errors as a result of motions and deflections in the spindle and its mounts when the wheel is stopped. The chart in Fig. 4(*a*) was obtained during a plunge-grinding operation on a cylindrical universal grinding machine. The workpiece was $^1/_2$ in. wide and the wheel face was 1 in. The unused portion of the wheel face becomes the reference surface, and each small division on the chart corresponds to a radial wheel wear of 50 microinches. A chart obtained from the setup of Fig. 3 is shown in Fig. 4(*b*); the sensitivity is now 100 microinches per small division. Here, a small ceramic tile block has been cemented to the grinding wheel for use as the reference surface. After dressing the wheel, the ceramic block is dressed about 0.002 in. below the wheel face. A zero reading is taken, and subsequent wear is found by the change in the step height on the chart. The use of a separate block allows full use of the wheel face for grinding, and the original step is made large enough so that the pickfeed will not cause interference during the entire run.

Originally, the profile charts were analyzed with a planimeter to obtain a true average wear reading. It was found that reducing the response of the recorder averaged the charts well enough electrically so that the readings could be taken by eye with the help of a straight edge. The profiling method allows the analysis

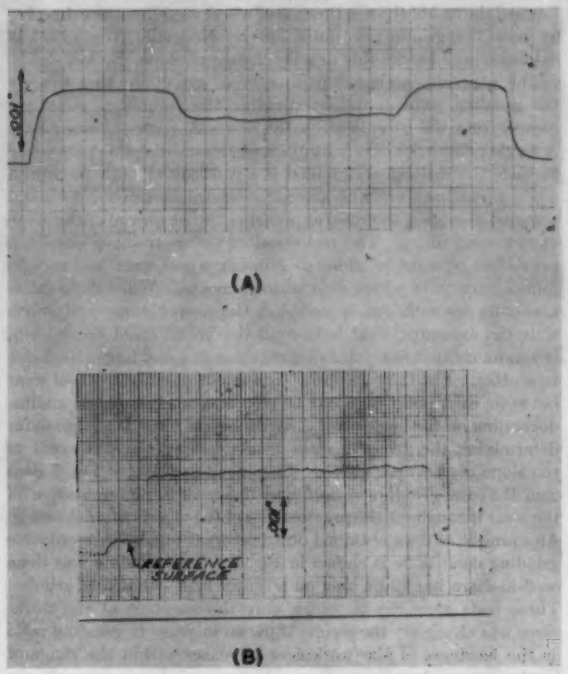

FIG. 4 GRINDING-WHEEL WEAR CHARTS
(*A*, Plunge grinding $^1/_2$-in-wide workpiece on 1-in-wide wheel; *B*, traverse grinding using ceramic-block reference surface.)

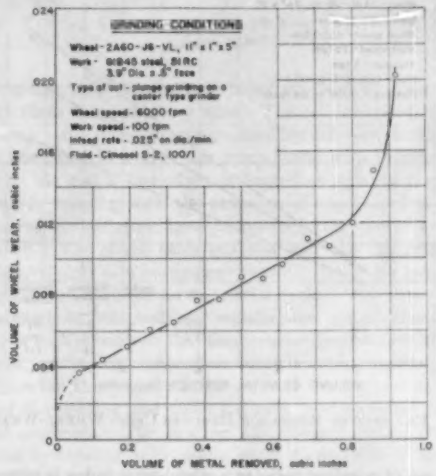

FIG. 5 TYPICAL GRINDING-WHEEL WEAR CURVE

of corner breakdown, and the general method enables the user to locate hard or soft spots on the wheel or other irregularities in the wheel-wear pattern.

A curve of wheel wear, by volume, versus volume of metal removed from the workpiece is shown in Fig. 5. When the wheel first contacts the workpiece, there is rapid breakdown of the fine sharp points left from the dressing; this initial breakdown may be considered instantaneous for practical purposes. Throughout the next portion of the process the wear rate is essentially constant although more scatter appears in the data with time.

Toward the end of the run the rate of wheel wear increases sharply; by now the grinding is quite noisy. Normally, the wheel is redressed well before this drastic change of slope.

The generally accepted parameter of grinding-wheel wear is the grinding ratio, found by dividing the volume of metal removed from the workpiece by the volume of wheel worn away. A single point of datum is insufficient to establish this parameter because the ratio thus obtained is a function of both the initial wheel breakdown and the amount of metal removed. As metal removal increases, the ratio approaches the reciprocal of the slope of the wear curve. The reciprocal of the wear-curve slope has proved to be a useful index of grinding-wheel wear and can be found from three wheel-wear measurements. While three measurements are sufficient to establish the proper slope and affirm that the measured wear is beyond the initial rapid breakdown, it was found that five points are required to avoid large errors due to scatter. For the measuring equipment described, wheel wear between each point of about 50–100 microinches on the radius, depending on the location of the reference surface, is adequate for determining the grinding ratio as defined by the reciprocal of the slope of the wear curve. Tests such as those of Fig. 5 confirm that the grinding ratio found this way is representative of the wear throughout the practical life of the wheel before dressing. An example of data obtained on wheel wear under representative grinding conditions is shown in Fig. 6. The grinding was done on 3-in-diam bar 12-in. long on a center-type cylindrical grinder. Three tests were run in which only the hardness of the workpiece was changed; the results show an increase in grinding ratio as the hardness of the workpiece increases within the range of hardnesses used.

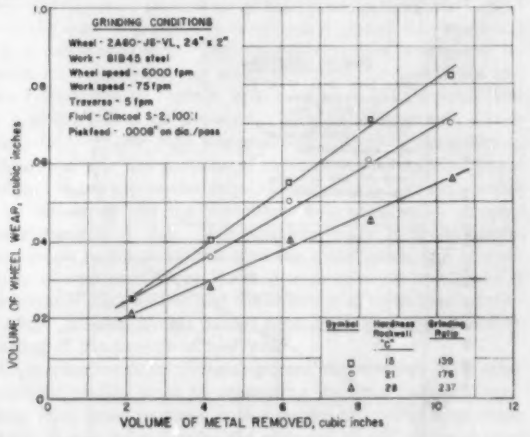
GRINDING CONDITIONS
Wheel - 2A60-J8-VL, 24" x 2"
Work - 8B45 steel
Wheel speed - 6000 fpm
Work speed - 75 fpm
Traverse - 5 fpm
Fluid - Cimcool 5-2, 100:1
Pickfeed - .0008" on dia./pass
Symbol
Hardness Rockwell "C"
Grinding Ratio
VOLUME OF WHEEL WEAR, cubic inches
VOLUME OF METAL REMOVED, cubic inches

FIG. 6 EXAMPLE OF RESEARCH RESULTS USING WHEEL-WEAR GAGE

The use of grinding ratio as a wheel-wear index is comparable to the use of counts per minute per gram of chips as an index of tool wear in the technique described previously for wear measurements in cutting using radioactive tracers. A complete wear curve of a cutting tool is similar in shape to Fig. 5; there is initial wearing in, then steady wear for the useful life of the tool. The instantaneous rate of tool wear found by absolute measurements using radioactive cutting tools is thus directly comparable to the grinding ratio. Actually, most tests with radioactive tools are conducted to find relative tool-wear rates between cuts made with different conditions; this would correspond to evaluating grinding variables in terms of ratios of grinding ratios.

WEAR-MECHANISM STUDIES

To complement the measurements of tool wear and the distribution of wear particles, work is needed on the basic mechanism of the wear process. Together, these studies are aimed at providing a basis for inventive work on inhibiting wear to extend the life of mating surfaces. Although the wear of cutting tools and grinding wheels is of direct interest, the fundamental work applies to other frictional processes as well.

Current literature shows a growing interest in diffusion as a factor in tool wear. Notable examples are the papers of Trent (2), and Trigger and Chao (3). The theories proposed to explain the role of diffusion in tool wear generally point to the attrition of interfacial alloys formed by diffusion across the tool-work (or chip) interface of various elements making up the materials used. The physical parameter of this interfacial diffusion that is significant in this work is the diffusion coefficient. For each mating pair of materials, the diffusion coefficient of each element depends on the prevailing temperature. Laboratory tests for finding pertinent diffusion coefficients and the relationship between diffusion and wear are in progress.

Information on diffusion and samples for determination of diffusion coefficients are obtained by clamping $^1/_2$-in. sq blocks of tool and workpiece materials together with a finely lapped and cleaned interface. The samples are heated in vacuo and held at a given temperature level for a specified time. They are furnace-cooled and the softer of the pair is cut away approaching the interface. The new surface is lapped smooth and parallel to the interface within 20 microinches. Successive lapping and x-ray examination of the surfaces follow; a special precision lapping machine allows accurate removal of about 0.0001 in. at a time, and a total zone of about 0.001 in. is analyzed. X-ray diffraction and x-ray fluorescence are both employed so that general structure as well as the concentration of the element studied are obtained. From a series of these tests at steps of temperature and time, the appropriate diffusion coefficients can be obtained.

The interfaces of the samples used are also examined in cross section by optical and electron microscopy to observe the nature of the diffusion. The samples, upon removal from the vacuum furnace, are ground or electrospark-machined across the interface and the surface is prepared for metallographic examination. The existence and nature of the diffusion and the interfacial alloys is revealed by this method, lending validity to the theory of the role of diffusion in tool wear.

Fig. 7(*a*) is an example of an interface between cemented carbide and 1020 steel; an interfacial alloy of iron-tungsten carbides results. A second example is shown in Fig. 7(*b*); this time a titanium alloy and a cemented carbide are combined and considerable diffusion is evident. The effect of this diffusion on tool wear will depend on the direction of the diffusion of certain elements and the physical properties of the interfacial alloys formed.

The tool-chip interface temperature is of prime interest in studies of tool-wear mechanism, both for its strong influence on diffusion and for its effect on the physical properties of the mating materials. It is also of interest, of course, in connection with research on cutting fluids and cutting mechanics. The report of Schallbroch, Schaumann, and Wallichs (4) on the relationship between temperature and tool life aroused considerable interest in the metal-cutting research field, and extensive experimental work with tool-work thermocouples followed, notably the work of Trigger (5, 6). Research techniques with tool-work thermocouples have been developed to avoid such problems as the loss of electrical continuity through the spindle bearings at high speeds and the spurious readings when carbide tips are backed with steel. However, one of the major complexities of the method, suitable rapid and accurate calibration, has remained. Reliable

(a)

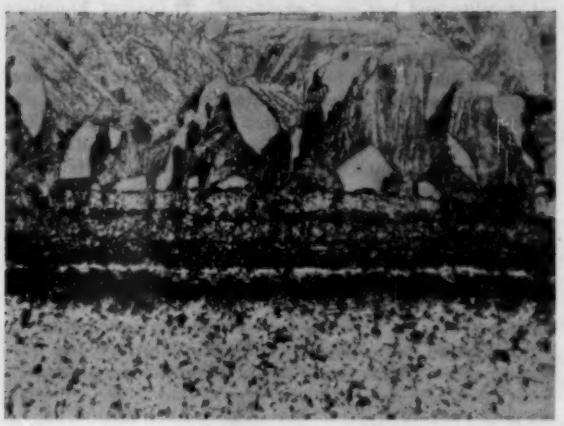

(b)

	(a)	(b)
Tool material (bottom)	78B carbide	78B carbide
Work material (top)	1020 steel	150A titanium
Temperature	2000 F	2000 F
Time at temperature	10	15

FIG. 7 DIFFUSION ZONE BETWEEN TOOL-WORK MATERIALS (×500)

readings call for calibration of each tool with each workpiece lot, so that large numbers of calibration curves are needed for any program on thermal measurements in machining.

A method for the rapid calibration of tool-work or other thermocouples has been developed to simplify the setup involved and to speed the test run. The essentials of such a calibration test are to heat the couple simultaneously with a known reference couple, keeping the temperatures of the two at the same level throughout the test; running the test in a short time; and obtaining an accurate record of the thermoelectric potentials throughout the run. These requirements are met in the setup shown in Fig. 8. The reference couple is placed in a small bead of silver which rests in a dished cup in a strip of nichrome; the cup is produced on a Brinell hardness tester. The thermocouple to be calibrated is simply placed to touch the silver with a light pressure. The thermocouple leads are attached to an X-Y recorder; the recorder in this instance is a variable-range instrument able to accommodate any thermoelectric combination expected. The silver is heated by passing a large current through

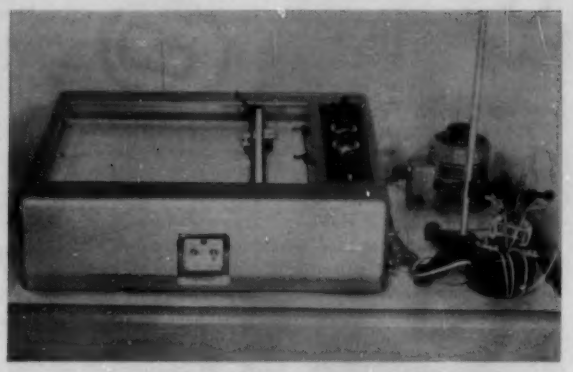

FIG. 8 SETUP FOR THERMOCOUPLE CALIBRATION

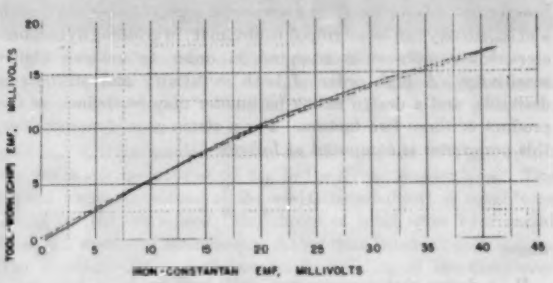

Reference couple	Iron-constantan
Tool-work couple	K7 carbide-81B45 steel
Cold junction	72 F

FIG. 9 TYPICAL CALIBRATION CHART FOR TOOL-WORK THERMOCOUPLE

the nichrome strip, the current being supplied by a simple coil through three turns of heavy wire. The coil is excited by a 110-volt Variac; different voltages are used for different heating rates.

The test procedure with this setup starts with turning on the power to the coil. The silver is heated at a fairly rapid rate, adjusted in keeping with the response of the recorder. When the desired temperature level is reached, the power switch is turned off. The silver cools quickly, and the full calibration chart is available as a permanent record. In actual use, only a few seconds are required for the entire cycle. The silver bead is small enough to heat and cool rapidly, and silver's thermal diffusivity is high enough so that temperature gradients in the bead are small. A typical calibration chart is shown in Fig. 9; the cycle time for this chart was 25 sec and the reasonable coincidence of the heating and cooling curves shows absence of large thermal gradients. The heating and cooling curves could be separated by fanning or dropping water on one side of the silver bead. If air currents are present, the apparatus can be placed in a covered container. The method is quite foolproof as well as fast, and represents a great convenience compared to calibrations involving furnace, torch, or lead-pot heat sources.

FORCE MEASUREMENTS

The measurement of cutting forces is an essential technique in studies of machining mechanics. Force measurements have been made by indirect methods involving power consumption, and by direct readings from mechanical, hydraulic, and electromechanical dynamometers. For research purposes, force dynamometers have won general acceptance, and those employing modern transducers such as the linear variable differential transformer

and the wire electric-resistance strain gage have been notably successful (7). Several strain-gage tool dynamometers are in use in the authors' laboratory; their construction and performance are of interest in connection with their use as tools in investigations of the cutting process.

The two primary requisites of a tool dynamometer are mechanical rigidity and a combination of high sensitivity and stiffness. Secondary specifications are thermal stability, absence of cross sensitivity between force components, compactness, protection of gages from fluids or chips, and a number of minor considerations. Assuming that the secondary specifications are satisfactorily met, the design rating of a dynamometer can be established in terms of sensitivity, stiffness, and natural frequency. It is desirable to set up a parameter for rating transducer designs in terms of these properties.

The sensitivity of an electromechanical force dynamometer can be expressed in units of volts output per volt excitation per lb force. Stiffness is indicated by the spring constant of the instrument. In turning dynamometers, high stiffness is required and sensitivity can be sacrificed to obtain it; in grinding dynamometers, lower stiffness is accepted in order to achieve higher sensitivity. A high order of both sensitivity and stiffness is desirable, and a design rating parameter may be defined as the product of these two factors. For a strain-gage dynamometer, this parameter is computed as follows

$$D = \frac{N}{4} G \frac{\epsilon}{\delta} \quad [1]$$

where

D = design rating parameter, volts/volt/in.
N = number of active legs in electrical bridge
G = gage factor of strain gage
ϵ = strain at gage
δ = deflection of dynamometer when strain at gage is ϵ, in.

The first two terms of this parameter are concerned with the bridge circuit and the choice of strain gage; the last, the ratio of strain to deflection, with the mechanical design of the dynamometer. A relative design rating, or design efficiency, can be determined by comparison of any cutting dynamometer to an ideal transducer. Theoretically, the ideal strain-gage tool dynamometer is one employing direct tension and compression strips for gage mounting, the strip length equaling the grid length of the gage, and with provision for four active legs in the electrical bridge circuit. For such a unit, the design parameter is

$$D_i = \frac{G}{l} \quad [2]$$

where

D_i = ideal design rating parameter, volts/volt/in.
l = length of grid of strain gage, in.

The proposed relative rating, or design efficiency, is

$$E = \frac{D}{D_i} \times 100 \quad [3]$$

where E = per cent efficiency of design.

The ideal design parameter of Equation [2] is a function of the gage characteristics only; since gage selection is often influenced by the secondary considerations in dynamometer design, Equation [3] allows evaluation of the design relative to the maximum performance that could have been obtained with the chosen gage. Actual design efficiencies are considerably less than 100 per cent because of necessary sacrifices to meet other specifications; the greatest influences are requirements of good mechanical stability and low cross sensitivity. The use of Equations [1] and [3], plus the natural frequency of the dynamometer, comprise a convenient way of comparing instrument designs.

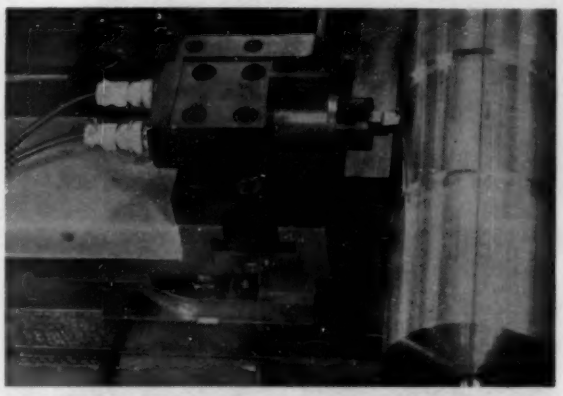

FIG. 10 STRAIN-GAGE TURNING DYNAMOMETER

Fig. 10 shows a two-force component-turning dynamometer designed for use in fundamental studies of cutting. The performance figures for this instrument are given in Table 1. The dynamometer is of cantilever design and is made of alloy steel. The free end provides a square hole and set screws for holding a $^5/_8$-in. $\times$ $^5/_8$-in., or smaller, tool bit. Behind this section is a specially machined portion for the gages, covered with a fluid shield sealed with rubber O-rings. The overhang of the instrument ends immediately behind the gage section. Holes are provided in the body for bolting the instrument securely to any suitable fixture. Leads are brought out through drilled holes to connector plugs, and a small hole is also provided through the entire block to the tool-insert space so that thermocouple leads or other connections are easily made and protected from chips.

TABLE 1 DYNAMOMETER PERFORMANCE FIGURES

Dynamometer	D Design parameter, volts/volt/in.	E Design efficiency, per cent	Cross sensitivity, per cent	Natural frequency, cps
Turning dynamometer	2.3	29	0.2	3500
Grinding dynamometer				
(a) Tangential force	1.6	12	1.5	1000
(b) Resultant force	2.1	15	1.5	1100
Table dynamometer				
(a) Vertical force	1.2	5	1	[a]
(b) Horizontal force	0.5	2	1	[a]

[a] Natural frequency depends on weight of workpiece.

A schematic diagram of the gaged portion of the turning dynamometer is shown in Fig. 11. The salient features of the configuration used are as follows:

1 The gaged strips are located some distance from the neutral axis for maximum moment of inertia of the cross section.

2 The high strain required for good sensitivity is restricted to a very small total volume of metal for good design efficiency.

3 Four active bridge legs are available for each force component, each strip being "used twice."

4 The thin web where the gages are mounted is only as long as the grid length of the gage.

5 Gages used in measuring one component are on the neutral axis of the other component for minimum cross sensitivity.

6 Torque sensitivity is low because of the direction of gage alignment and the high polar moment of inertia.

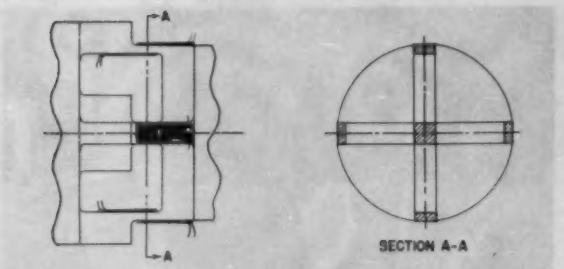

FIG. 11 SCHEMATIC VIEW OF DYNAMOMETRIC SENSING ELEMENT

7 The "center post" is a negligible contribution to the inertia so the gage webs transmit most of the bending moment. However, the relatively large area of the center post takes the shear load, provides mechanical stability, and makes the section insensitive to loads in the direction of the dynamometer axis.

8 The symmetrical geometry tends to eliminate thermal drift in the bridge circuit.

A mathematical analysis of a dynamometer employing this special configuration reveals that optimum design is obtained when the gage web is at its maximum distance from the neutral axis, in keeping with the required level of sensitivity and a reasonable web thickness that can be machined and not buckle. The overhang beyond the gages should be small; this is also desirable for obtaining high natural frequency. The use of a material with low elastic modulus and low density will improve the design by giving higher natural frequency and greater stability for a given sensitivity and design efficiency. In designing the turning dynamometer, the desired sensitivity and range was chosen to be 1 lb/mm pen deflection using a Sanborn Series 60 recorder, and 0–1000 lb, respectively. Next, reasonable gage-web dimensions were picked in keeping with manufacturing facilities. Finally, the optimum design equations were used to complete the configuration, except that steel was chosen over a low elastic-modulus metal like aluminum, sacrificing efficiency for strength, better linearity, and greater wear resistance.

A modification of the sensing element just described was incorporated in the design of the cylindrical grinding dynamometer shown in Fig. 12. The grinding process under study is a plunge-grinding operation on a 4-in-diam workpiece with a $^1/_2$-in. face. Two components describe the force system acting during this process, simplifying fundamental studies. The workpiece is large enough so that removal of 0.100 in. from the diameter during infeeding (the amount required for a grinding ratio determination) does not change the diameter significantly for the usual accuracies involved.

The dynamometer is again of the cantilever type, but the sensitivity requirements of 0.1 lb/mm on the Sanborn Series 60 recorder for the tangential force necessitated the use of an aluminum-alloy sensing element to maintain good mechanical stability. At the fixed end, the aluminum beam is bolted to a fixture which provides a flange with holes for retaining or removing the fixture from the headstock spindle nose, and a taper for actual alignment and drive. The central part of the beam, where the sensing elements are located, is covered with a shield sealed at each end with O-rings. The free end supports a workpiece-holding fixture.

The tangential force is sensed by a torque unit located at the center of the workpiece. This location insures that there will be no bending moment on the torque unit, even though further insurance against cross sensitivity is provided in the alignment of the gages and their placement in the bridge circuit. The torque

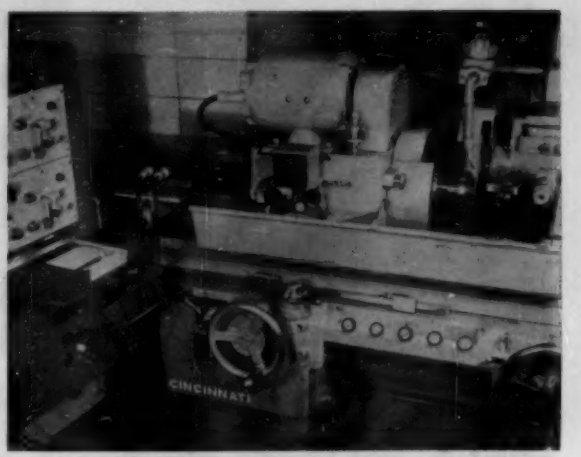

FIG. 12 CYLINDRICAL GRINDING DYNAMOMETER SETUP
(From left to right: Recorder, slip-ring assembly, grinder headstock, dynamometer, wheel-wear gage.)

unit has a cross section similar to the diagram of Fig. 11, but the gages are mounted at 45 deg to the dynamometer axis. The second force component measured is the resultant or total force acting on the workpiece; the choice of total force over radial force is a matter of convenience rather than inherent desirability. The resultant force produces simple bending of the cantilever beam and is thus easily measured, while the radial force is measured easily only from a stationary point with attendant problems of friction, loss of rigidity, and incomplete transmission of force through the gaged section. The sensing element for the resultant force follows the configuration of Fig. 11 except that gaging webs are provided in only one axis. This leaves a solid rectangular area along the other axis which is quite torque resistant and reduces possible cross sensitivity. Past experience had shown that the resultant force could be expected to be twice the tangential force, so only half the sensitivity was provided and greater stiffness achieved. Performance figures for this dynamometer are included in Table 1.

The electrical connections for this instrument are made by bringing the leads through a hole in the taper in the mounting flange, thence through the hollow headstock spindle to a set of slip rings in back of the headstock. The slip rings consist of a sealed multiple-cup mercury-pool arrangement which has been satisfactory in the relatively low workspeed range used in cylindrical grinding.

Fig. 13 shows a chart obtained during a typical cut with the grinding dynamometer. The resultant force acts sinusoidally on its sensing element because of the workpiece rotation, and the tare weight of the dynamometer and workpiece must be subtracted from the full amplitude to get the actual reading. The workpiece rotational speed can be thought of as a carrier for the force signal, and the response of the dynamometer to force fluctuation depends on the workspeed.

In addition to the two dynamometers described here, the laboratory also has other dynamometric devices, including a three force-component table dynamometer with a torque-sensitive subbase. This dynamometer is a purchased unit, and is capable of measuring forces in machining processes like milling and drilling. The approximate performance figures are given in Table 1; the severe problems of stability and cross sensitivity required some sacrifice of design efficiency in this instrument.

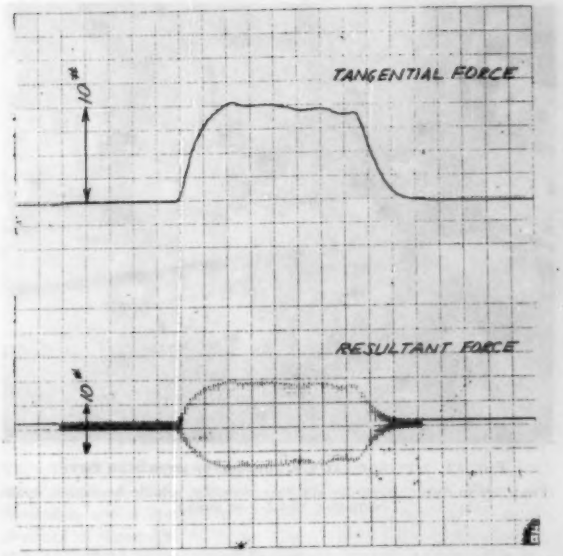

FIG. 13 TYPICAL FORCE RECORDING USING GRINDING DYNAMOMETER

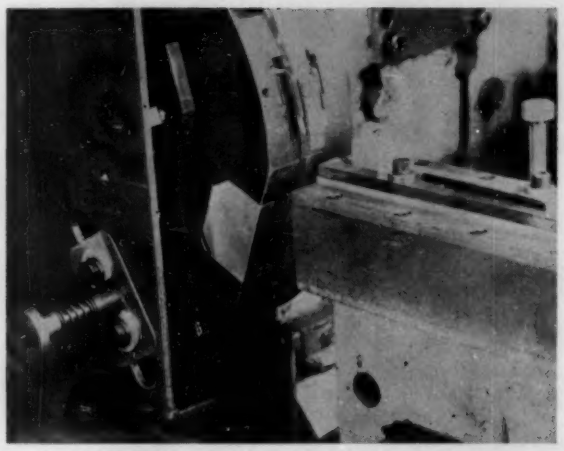

FIG. 14 MECHANISM FOR GRINDING-CHIP-FORMATION STUDIES

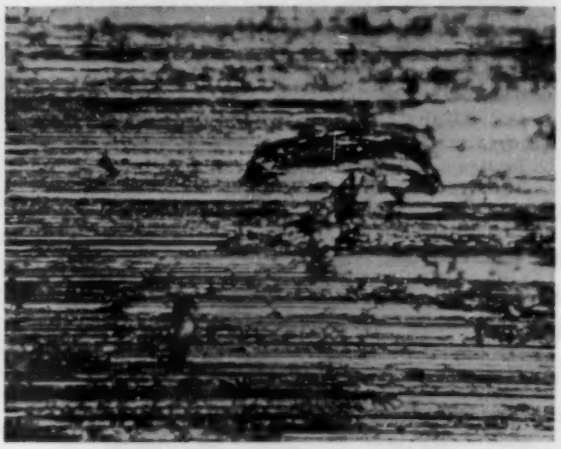

FIG. 15 SURFACE OF WORKPIECE FROM APPARATUS OF FIG. 14

CHIP-FORMATION STUDIES

Numerous investigators have made contributions to the literature in the field of chip formation in metal cutting. Very little information is available, however, on chip formation in grinding. A technique for studying chip formation in grinding is needed to supplement the studies made with the grinding dynamometer, as presented earlier. A technique has been developed which makes possible the study of grinding chips during the process of formation. This is accomplished by "instantaneously" accelerating the workpiece to the speed of the grinding wheel, thus freezing the grinding action.

The test apparatus is presented in Fig. 14. It consists essentially of four components; 1, the wheel mount, which supports the grinding-wheel segment, the spring fingers which pick up the workpiece, and the latch and trip mechanisms which operate the spring fingers; 2, the trip plunger which triggers the mechanism at the desired moment; 3, the retractable workpiece holder which supports the specially designed workpiece during grinding; and 4, the special variable infeed drive unit (not shown in Fig. 14) which makes possible a wide range of positive infeed rates.

The theory of operation of the apparatus is as follows: Initially the spring fingers are retracted and latched below the outer surface of the grinding-wheel segment to permit grinding. The workpiece is placed in the work holder and the infeed mechanism started. At the desired instant during grinding the mechanism is triggered, permitting the spring fingers to pick the workpiece out of the work holder, $^3/_4$ of a revolution later. The workpiece is almost instantaneously accelerated to grinding-wheel speed and is held against the wheel segment by the spring fingers and revolves with it until the wheel mount is stopped. At the instant the workpiece is snatched from the fixture, the latter retracts so as to be out of the way of the revolving assembly. After accelerating the workpiece from rest up to grinding-wheel speed almost instantaneously, and obtaining grinding chips in the process of formation, the next problem is the removal of the workpiece without breaking off the minute partially formed chips. This is done by providing another position on the latch which will permit the spring-finger arms to move out further, allowing the newly ground surface to be pushed away from the grinding-wheel segment.

The ground surfaces obtained by this technique show many partially formed chips. A typical example is shown in Fig. 15. The grinding chips of interest are oriented with respect to a reference point, and the grinding specimen is then mounted and sectioned to permit a study of the desired section through the chip-work contact area. An example of the chip formation found using this technique is shown in Fig. 16. Similar methods for chip-formation studies in cutting also have been developed.

The high-speed movie camera presents an additional technique for studying chip formation. Movies taken at 7500 frames per sec permit us to follow closely what happens as a chip is formed at conventional machining speeds. One second of cutting time is expanded to 8 min of projecting time at these high camera speeds. Fig. 17 shows a sequence of frames taken at 7500 frames per sec through a microscope. The field size covered by these movie frames is 0.030 × 0.050 in. The material being machined was titanium Ti 150A; the cutting speed was 100 fpm. Here we may observe very clearly the phenomena of the fluctuating shear angle which results in the sawtoothlike chip often obtained when

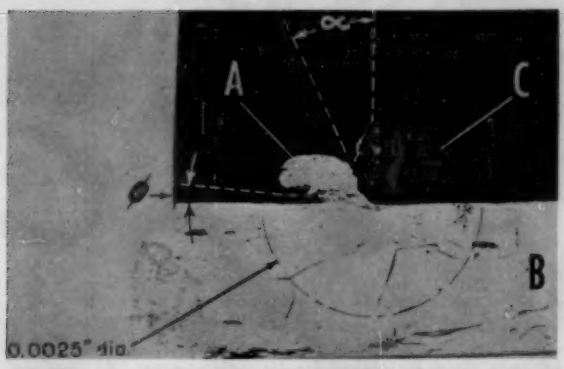

A, Chip
B, Workpiece
C, Grinding grit
ϕ, Approximate shear-zone angle
α, Approximate grit rake angle

FIG. 16 EXAMPLE OF CHIP FORMED DURING GRINDING

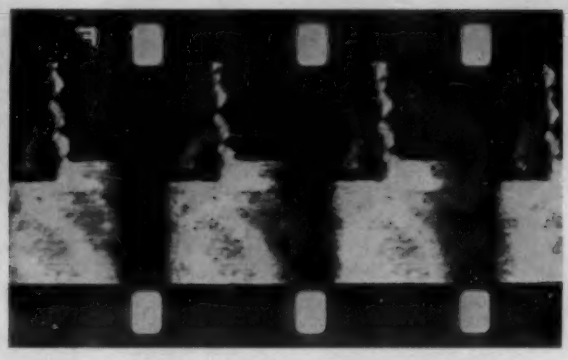

FIG. 17 STRIP FROM MOVIE OF CUTTING TITANIUM (Camera speed: 7500 frames/sec.)

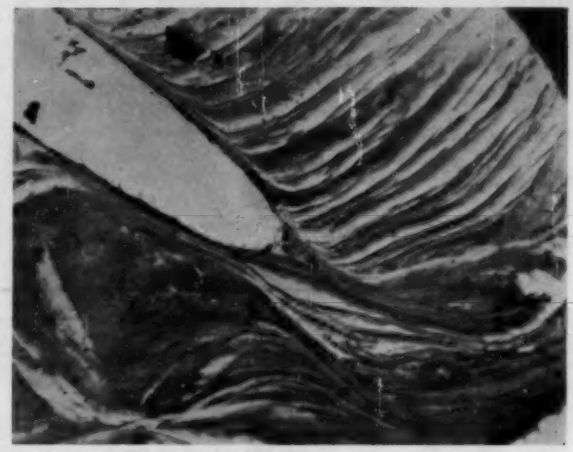

FIG. 18 ELECTRON-MICROGRAPH OF SECTION OF TITANIUM CHIP (×7500)

machining titanium. Pictures such as these have contributed to a better understanding of the basic machining characteristics of titanium (8).

Other techniques which are proving quite useful in the field of metal-cutting research are electron microscopy and analog computation. The electron microscope has been particularly useful in the studies made of chip formation and diffusion, because of the high magnification and degree of resolution obtainable. The electron-micrograph presented as an example in Fig. 18 shows the root area of one of the sawteeth existing on the titanium chip presented in Fig. 17, showing the local deformation in the chip in detail.

The analog computer, an instrument useful in the solution of physical problems which may be described mathematically, is useful, for example, in the study of tool vibrations. With proper auxiliary equipment the analog computer may be used to handle nonlinear functions which would not be susceptible of solution by classical means.

Research techniques such as those presented in this paper can contribute significantly to the advancement of the metal-cutting technology. As metal-cutting research progresses in the future, techniques such as these will call for further refinement and will be supplemented by still newer methods.

ACKNOWLEDGMENTS

The authors would like to express their appreciation to Mr. Hans Ernst, Director of Research, Dr. M. E. Merchant, Assistant Director of Research, and the members of the Metal Cutting and Physical Research Department of The Cincinnati Milling Machine Company for their contributions to the work described in this paper. The work on diffusion being done by Mr. Harry W. Young, and his help, plus that of Mr. George M. Hain on the thermocouple calibration, Mr. Edward B. Barnes on the electron microscopy, and Mr. Clarence Mehl on the grinding chip-formation studies, is especially appreciated. Credit for the preparation of the manuscript belongs to Miss Sue Hannaford and Mrs. Loreta Gill.

BIBLIOGRAPHY

1 "Radioactive Cutting Tools for Rapid Tool-Life Testing," by M. E. Merchant, H. Ernst, and E. J. Krabacher, Trans. ASME, vol. 75, 1953, pp. 549–559.

2 "Some Factors Affecting Wear on Cemented Carbide Tools," by E. M. Trent, Proceedings of The Institution of Mechanical Engineers, London, England, vol. 166, 1952, pp. 64–74.

3 "The Mechanism of Crater Wear of Cemented Carbide Tools," by K. J. Trigger and B. T. Chao, Trans. ASME, vol. 78, 1956, pp. 1119–1126.

4 "Testing for Machinability by Measuring Cutting Temperature and Tool Wear," by H. Schallbroch, H. Schaumann, and R. Wallichs, Vorträge der Hauptversammlung 1938 der Deutschen Gesellschaft für Metallkunde, VDI, Berlin, 1938.

5 "Progress Report No. 1 on Tool-Chip Interface Temperatures," by K. J. Trigger, Trans. ASME, vol. 70, 1948, pp. 91–98.

6 "Progress Report No. 2 on Tool-Chip Interface Temperatures," by K. J. Trigger, Trans. ASME, vol. 71, 1949, pp. 163–174.

7 "Machine Tool Dynamometers—A Current Appraisal," by N. H. Cook, E. G. Loewen, and M. C. Shaw, *American Machinist*, vol. 98, May 10, 1954, p. 125.

8 "Titanium Is Unorthodox When Machined," by M. E. Merchant, E. J. Krabacher, H. W. Young, and J. H. Miller, *American Machinist*, vol. 98, July 5, 1955, pp. 118–121.

Heat Transfer to, and Temperature Distribution in, a Metal-Cutting Tool

By D. L. RALL[1] and W. H. GIEDT[2]

An analytical and experimental investigation of heat transfer to, and the resulting temperature distribution in, a metal-cutting tool during orthogonal cutting is described. A rectangular parallelepiped-shaped tool is postulated and a product solution developed for the temperature distribution under the conditions of a continuous uniform release of heat over the tool-chip contact area and heat loss from each side arbitrarily specified. To test the validity of this solution two high-speed lathe tools with 0-deg and 15-deg back-rake angles were uniquely instrumented with thermocouples located in the tool bodies at selected distances from the cutting edges. Representative temperature records obtained during dry orthogonal cutting of SAE 1020 steel with these tools are presented. Extrapolation of temperature measurements to the center of the tool-chip contact area gave values for the average tool-chip interface temperatures which agree quite closely with results of other investigators. Average heat rates to the tools are determined and the applicability of the product solution is discussed.

Nomenclature

The following nomenclature is used in the paper:

A = tool-chip contact area, sq ft
a, b, c = dimensions of rectangular parallelepiped, ft
C = specific heat, Btu/lb deg F
d = length of tool-chip contact, ft
$2g$ = width of tool-chip contact, ft
h = combined surface convection-radiation coefficient, Btu/hr sq ft deg F
k = average thermal conductivity, Btu/hr ft deg F
$q = Q\rho CA$ = heat rate, Btu/hr, or Btu/min
Q = source strength (deg F ft³/hr) if point heat source; (deg F ft/hr) if finite-area heat source
r = radial distance from center of tool-chip contact area, in.
SFPM = cutting speed, surface feet/minute
t = temperature, deg F
x, y, z = co-ordinates of any point within tool, ft
x', y', z' = co-ordinates of point at which point heat source is being released, ft
α = average thermal diffusivity, sq ft/hr
$\lambda_l, \lambda_m, \lambda_n$ = solutions to transcendental equation, 1/ft
ρ = density, pcf
τ = time, hr or min
μ = variable of integration, hr

Introduction

Most of the energy input during the metal-cutting process appears as heat which is transferred to the chip, the workpiece, and to the cutting tool. The resulting thermal effects are of primary importance in that they influence the mode of deformation, the final metallurgical state of the machined surface, and the rate of tool wear. Hence considerable effort, both experimental and theoretical, has been devoted to the investigation of the various phenomena.

Although only a small proportion of the energy necessary for cutting is transferred to the tool, tool temperatures have long been of interest because of their known influence on tool life. The Herbert-Gottwein thermocouple technique has been used extensively for measuring tool-chip interface temperatures. Reports of recent results as well as references to earlier investigations can be found in references (1–3).[3] Other methods such as the use of thermosensitive colors (4) and radiation techniques (5) have been employed for the same purpose but with limited success. However, little attention has been devoted to the measurement of the temperature field within a tool, probably primarily because of the instrumentation problem. The only approach seems to be by the use of very small thermocouples located at appropriate points within the tool body. Such a study was conducted in the carbide insert of a lathe tool by Axer (6). He made measurements to within 0.008 in. of the tool-chip contact area from which isotherms were plotted. He did not estimate tool-chip interface temperatures, indicating plans to use a refined technique for this purpose.

Analytical approaches to the determination of cutting-tool temperatures have in general employed graphical or numerical solutions. In 1943 Pahlitzsch and Helmerdig (7) used a finite-difference method to calculate the temperature distributions resulting from a given cutting-edge temperature and the assumption of both a point and linear source of heat at the cutting edge. The tool was treated as a quarter section of an infinite cylinder. Axer (6) indicates trying these approximations to predict his experimental results. His only comment is that they were applicable only for greater distances from the cutting edge. In 1951 Trigger and Chao (8) made an analytical evaluation of the tool-chip-interface temperature. This involved consideration of the chip shear process and approximation of the tool as an infinite solid. The method used has since been refined by these same authors (9) and others (10, 11).

A different approach to the prediction of the temperatures in a cutting tool is suggested (12) by the formation of a product of three one-dimensional slab solutions to which appropriate boundary conditions are applied. It was noted that the product of

[1] Research Engineer, Research Division of Detroit Controls Corporation, Redwood City, Calif. Assoc. Mem. ASME.

[2] Assistant Professor of Mechanical Engineering, University of California, Berkeley, Calif. Assoc. Mem. ASME.

Contributed by the Research Committee on Metal Processing and presented at the Diamond Jubilee Annual Meeting, Chicago, Ill., November 13–18, 1955, of The American Society of Mechanical Engineers.

Note: Statements and opinions advanced in papers are to be understood as individual expressions of their authors and not those of the Society. Manuscript received at ASME Headquarters, April 12, 1955. Paper No. 55—A-217.

[3] Numbers in parentheses refer to the Bibliography at the end of the paper.

expressions for the temperature distributions in three slabs, due to arbitrarily located instantaneous plane heat sources, could be integrated with respect to time and area. By specification of appropriate limits for the integrations, a solution could be obtained for the temperature distribution in a parallelepiped-shaped tool under the conditions of uniform continuous heat release over the tool-chip contact area and with arbitrary specification of the heat loss from any side. It was the objective of the study described herein to test the validity of this solution with actual temperature measurements in cutting tools.

Product Solution for the Temperature Distribution in a Cutting Tool

The system for which a solution is desired can be approximated satisfactorily by a parallelepiped as shown in Fig. 1. Here the

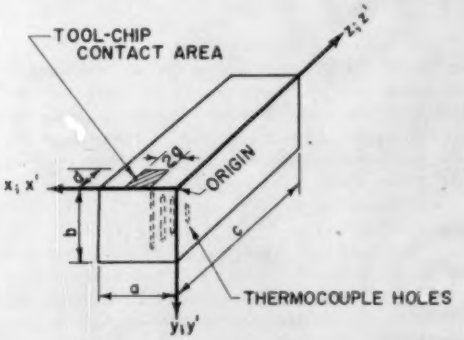

Fig. 1 Tool Geometry and Co-Ordinate System

x-axis coincides with the tool cutting edge and the crosshatched area of dimensions d and $2g$ indicates the area of contact between chip and tool. Heat energy resulting from the cutting process enters the tool through this area, from which it flows through the tool body, and is transferred to the surroundings and toolholder.

A procedure for developing a solution for such a system is indicated in reference (12). The solution is given for the temperature distribution in an infinite slab resulting from the instantaneous liberation of energy at a plane source located on or within its boundaries. All cases of zero temperature, radiation, or no heat flow at either surface can be provided for by proper selection of constants. By forming the product of this solution for three different slabs of thickness dimensions equal to the three dimensions of a rectangular parallelepiped, an expression is obtained which describes the temperature distribution in such a parallelepiped, losing heat to the surroundings as specified, when heated by a given amount of energy released instantaneously at an arbitrarily selected point on or within its bounding surface. The instantaneous point source is now specified to be on and within the tool-chip contact area; integration first over the tool-chip contact area and then with respect to time gives the desired solution.

The slab solution for an instantaneous unit source at x', on which the final solution is based, can be expressed as

$$t = \sum_{l=1}^{\infty} \frac{2(k^2\lambda_l^2 + h_2^2)\,(k\lambda_l \cos \lambda_l x + h_1 \sin \lambda_l x)}{(k\lambda_l \cos \lambda_l x' + h_1 \sin \lambda_l x')} \cdot \frac{e^{-\alpha\lambda_l^2\tau}}{(k^2\lambda_l^2 + h_1^2)\,[a(k^2\lambda_l^2 + h_2^2) + kh_2] + kh_1(k^2\lambda_l^2 + h_2^2)} \quad \ldots [1]$$

where a is the slab thickness, h_1 and h_2 are the heat-transfer coefficients at the two surfaces, k the thermal conductivity, α the diffusivity, τ the time, and

$$\tan \lambda_l a = \frac{\lambda_l k(h_1 + h_2)}{k^2\lambda_l^2 - h_1 h_2} \quad \ldots [2]$$

If h_1 and h_2 are both zero, a term, $1/a$ must be added to Equation [1].

A solution was formed by taking the product of Equation [1] appropriately applied to the three directions and integrating as just described. This was investigated by setting h_1 and h_2 = 2 Btu/hr sq ft deg F (a reasonable value for free convection and radiation) on all surfaces. Comparison of results with measured values indicated that heat flow to the toolholder must be of such proportions as to make the losses from the other sides negligible.

A second solution was therefore formed in which the heat-transfer coefficients on all tool faces except for $z = c$ were set equal to zero. With these boundary conditions the product of the three slab solutions integrated with respect to time and the tool-chip contact area is the following

$$\frac{t}{Q} = \sum_{l=1}^{\infty}\sum_{m=1}^{\infty}\sum_{n=1}^{\infty} \frac{16(k^2\lambda_n^2 + h_c^2)\,(\cos \lambda_l x \cos \lambda_l a/2 \sin \lambda_l g)\,(\cos \lambda_m y)(\cos \lambda_n z \sin \lambda_n d)}{ab\alpha\lambda_l\lambda_n(\lambda_l^2 + \lambda_m^2 + \lambda_n^2)\,[c(k^2\lambda_n^2 + h_c^2) + kh_c]} \times (1 - e^{-\alpha(\lambda_l^2 + \lambda_m^2 + \lambda_n^2)\tau})$$

$$+ \sum_{l=1}^{\infty}\sum_{n=1}^{\infty} \frac{8(k^2\lambda_n^2 + h_c^2)\,(\cos \lambda_l x \cos \lambda_l a/2 \sin \lambda_l g)\,(\cos \lambda_n z \sin \lambda_n d)}{ab\alpha\,\lambda_l\lambda_n(\lambda_l^2 + \lambda_n^2)\,[c(k^2\lambda_n^2 + h_c^2) + kh_c]} \times (1 - e^{-\alpha(\lambda_l^2 + \lambda_n^2)\tau})$$

$$+ \sum_{m=1}^{\infty}\sum_{n=1}^{\infty} \frac{8g(k^2\lambda_n^2 + h_c^2)\,(\cos \lambda_m y)\,(\cos \lambda_n z \sin \lambda_n d)}{ab\alpha\lambda_n(\lambda_m^2 + \lambda_n^2)\,[c(k^2\lambda_n^2 + h_c^2) + kh_c]} \times (1 - e^{-\alpha(\lambda_m^2 + \lambda_n^2)\tau})$$

$$+ \sum_{n=1}^{\infty} \frac{4g(k^2\lambda_n^2 + h_c^2)\,(\cos \lambda_n z \sin \lambda_n d)}{ab\alpha\lambda_n^2\,[c(k^2\lambda_n^2 + h_c^2) + kh_c]}\,(1 - e^{-\alpha\lambda_n^2\tau}) \quad \ldots [3]$$

This equation will be discussed later in connection with measured results.

Experimental Equipment and Test Procedure

Construction of Test Tools. To obtain the type of tool-chip contact desired, orthogonal cutting tests were planned. Two experimental lathe tools were machined from $^3/_8 \times {}^3/_8$-in. annealed high-speed steel bar stock of the following composition: Carbon, 0.83 per cent; chromium, 4.15 per cent; vanadium, 1.90 per cent; tungsten, 6.40 per cent; and molybdenum, 5.00 per cent. This alloy was chosen because of relatively good machinability, which was of prime importance for drilling the small thermocouple holes. A rake angle of 15 deg was provided on one tool and 0 deg on the other. Both had a 5-deg end-clearance angle.

Holes for inserting a thermocouple lead were drilled into the bottom along the center line of a tool, as shown in Fig. 1. The first three holes were about $^3/_{64}$ in. apart, starting from the front edge of the tool, and the fourth hole approximately $^5/_{16}$ in. from the front edge. Each hole was drilled to such a depth that its bottom lay approximately on a 45-deg plane from the top surface of the tool. These holes were first drilled to within $^1/_{16}$ in. of their full depth with a No. 75 (0.021-in.) twist drill, and then finished with a No. 80 (0.0135-in.) twist drill. Precise location of the bottom of each hole was accomplished by x-ray photographs and depth-micrometer measurements. To prevent scaling of these holes and decarburizing during heat-treating, the tools were heated to 2200 F in molten boric acid and then quenched in an air blast.

Thermocouple junctions were formed with nickel wire 0.010-in. diam and the tool body. To insure that these junctions were located at the bottoms of the holes in the tools the following procedure was used: The nickel wires were prepared by rolling 6-in. lengths between two ground plate-glass slabs to polish and work-harden the surfaces. They were then washed in benzene and the outside surface oxidized by placing them in a low-temperature flame (wires held around 1400 to 1500 F) for 1 hr. This oxide provided a thin but strong dielectric coat which insulated the wire from the sides of the hole. The oxidized end of the wire was polished to a slight point to insure good electrical contact with the base of the hole in the tool. It was then placed in a pin vise and held against the bottom of the hole, while an electric current from a bank of condensers was discharged through the wire and tool. This provided a discharge-welded thermocouple junction at the bottom of the hole. The wire was then further supported in the hole by filling the remaining annulus with a low-melting ceramic (a No. 022 Seger cone mixed with ceramic gum). This ceramic was fused during tempering of the tool at 1100 F.[4]

The tools were mounted in holders as shown in Fig. 2. Calibration of the thermocouple junctions was accomplished by placing the entire unit in a furnace.

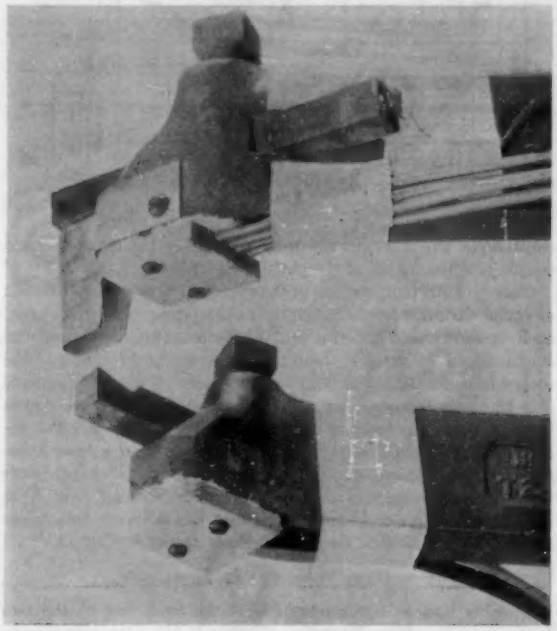

FIG. 2 (*Top*) TOOL M-2-4 0 DEG B. R. WITH T.C. WIRE GUARD; (*Bottom*) TOOL M-2-2 15 DEG B. R. T.C. WIRE GUARD REMOVED

Cutting Specimens. These were machined from $2^1/_2$-in-diam hot-rolled SAE 1020 steel (100 Bhn). The outside diameters were selected to give maximum surface speeds of 60, 80, and 100 fpm, for the spindle speeds available on the test lathe. The inside was bored out to give a wall thickness of 0.110 in.

Test Procedure. A Leeds and Northrup "Speed-O-Max" single-channel, self-balancing recording potentiometer with one second full-scale deflection was used to measure the temperatures in the tools during cutting. A cutting time of two minutes was used for each recording since at the end of this period steady-state conditions were indicated. The same feed [0.0025 in. per revolution (ipr)] and depth of cut (0.110 in.) were used for the three surface speeds. Since only one recording channel was available, it was necessary to allow the entire system to cool between runs. The width of the observable tool-chip contact area was measured with a toolmaker's microscope.

[4] At the time of this investigation Axer's work (6) was not known to the authors. His technique was to use small two-wire thermocouples soldered to the bottom of spark-drilled 0.020-in-diam holes.

TEMPERATURE MEASUREMENTS

Representative records of the transient temperatures indicated by the four thermocouples in each tool at the three cutting speeds are shown in Figs. 3 through 6. These will be noted to be actually composites of individual records of each thermocouple.

The most interesting comparison between the two tools is at the No. 1 thermocouple locations. Large temperature fluctuations of high frequency occur in the 15-deg back-rake-angle tool (designated M-2-2), while in the 0-deg tool the temperature rise is relatively steady. These fluctuations apparently are caused by intermittent contact of the chip with the tool. Reference to the curves at the other three thermocouple locations indicates rather rapid damping of the temperature variations near the tip. It is observed, however, that high frequency and amplitude temperature changes near the tip mean similar variations, which likely influence tool life, are occurring at the tool-chip interface.

A second point of interest is the apparent increase in the rate of temperature rise which was observed when the change from a discontinuous to a continuous chip occurred. This is most marked in Fig. 5. The increase in the rate of rise is of course due to increased heat transfer resulting from improved contact between the chip and tool. It is also significant to note the magnitude of the tool temperature before the chip becomes

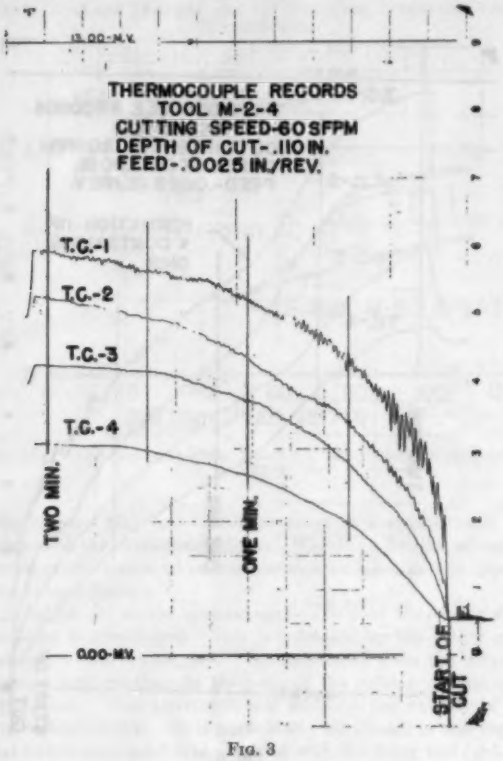

FIG. 3

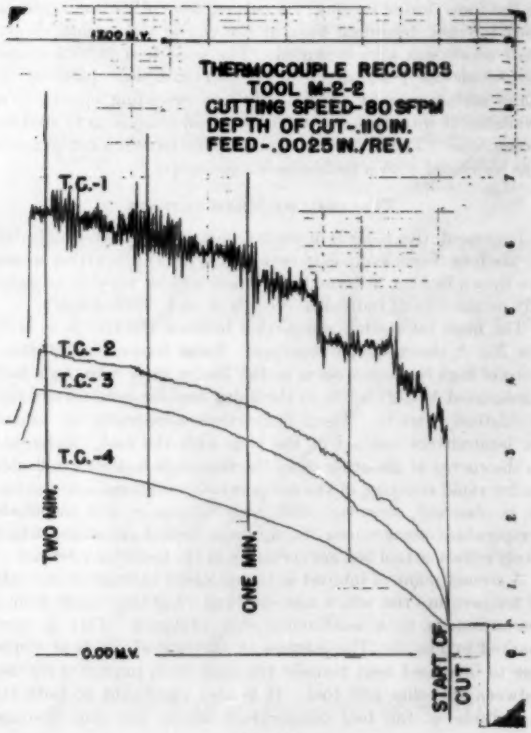

FIG. 4

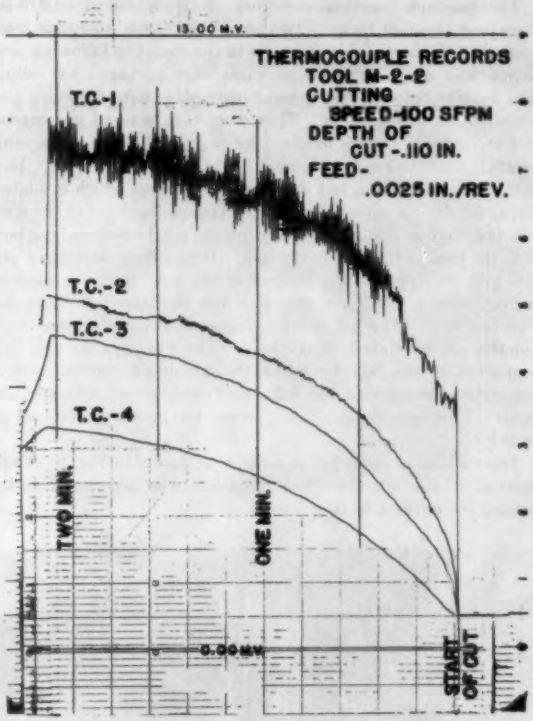

FIG. 6

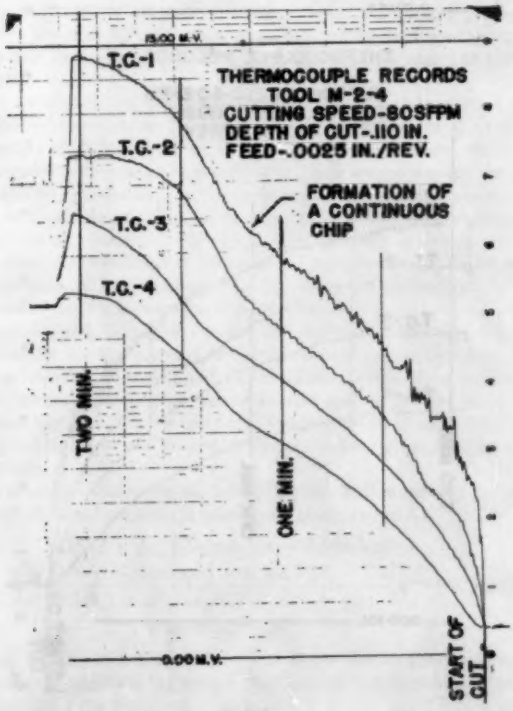

FIG. 5

continuous, which was of the order of 550 F at the No. 1 thermocouple position for all of the cutting speeds used.

Curves of the temperature in the two cutting tools as a function of radial distance from the center of the chip-tool contact area, such as shown in Fig. 7 for 80 SFPM, were prepared from the original data. Extrapolation of these curves to the center of the tool-chip contact area provided an estimate of the average tool-chip interface temperature. These estimated temperatures have been plotted as a function of cutting speed in Fig. 8. The results at the end of 2 min of cutting with the 15-deg back-rake-angle tool can be compared with those of previous investigators (3). That agreement within 10 per cent was found (Fig. 8) is considered quite satisfactory in view of the different techniques employed and possible minor variations in test conditions.

Heat Flow to the Tools

Turning now to a consideration of the heat flow to the two tools, it is seen from Equation [3] that if the heat rate is constant (i.e., Q = const), it can be calculated by substitution of an experimental temperature along with the appropriate co-ordinates and time at which this temperature is measured. Before this can be done, however, it is necessary to select applicable values of the constants involved. For k an average value of 13 Btu/hr ft deg F will be used, based on data from reference (13) and an average tool temperature of 400 F. This gives a value of 0.26 sq. ft/hr for α. Extrapolation of the measured temperatures toward the toolholder indicated that an effective heat-transfer coefficient h_e = 1000 Btu/hr sq ft deg F or greater would be necessary to account for heat flow to the holder. Although this did not appear to be a sufficiently accurate determination, subsequent investigation showed that use of values of from 1000 to infinity for h_e had almost negligible influence on the results.

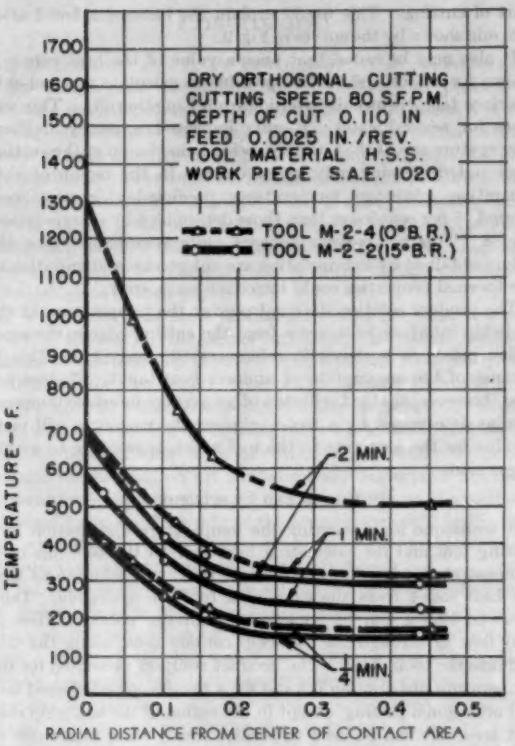

FIG. 7 TEMPERATURE VERSUS RADIAL DISTANCE FROM CENTER OF TOOL-CHIP CONTACT AREA

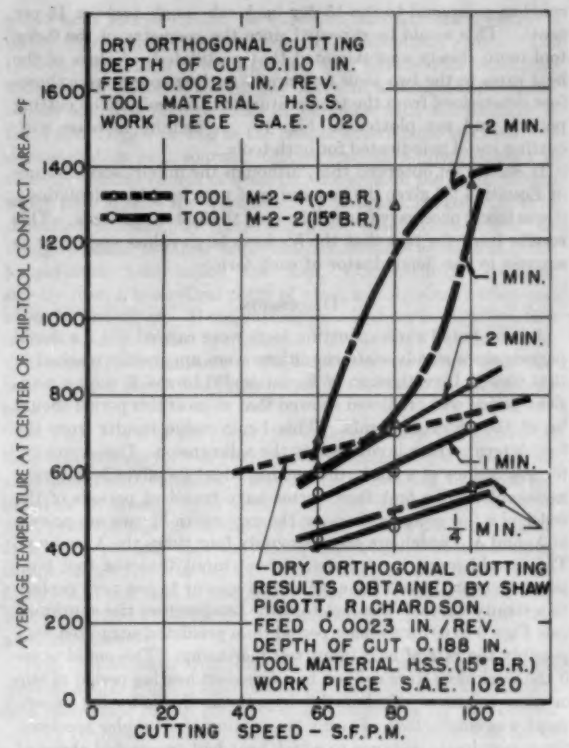

FIG. 8 AVERAGE TEMPERATURE AT TOOL-CHIP INTERFACE VERSUS CUTTING SPEED

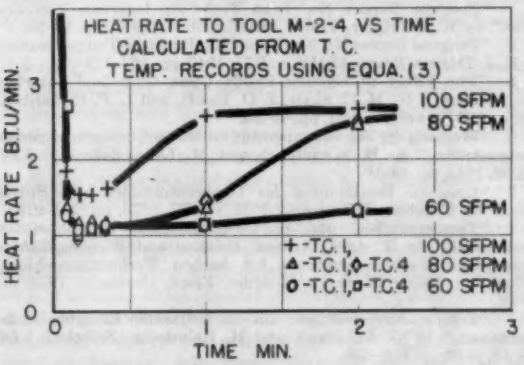
HEAT RATE TO TOOL M-2-4 VS TIME
CALCULATED FROM T.C.
TEMP. RECORDS USING EQUA. (3)
100 SFPM
80 SFPM
60 SFPM
+ - T.C. 1, 100 SFPM
Δ - T.C. 1, ◇ - T.C. 4 80 SFPM
○ - T.C. 1, □ - T.C. 4 60 SFPM
HEAT RATE BTU/MIN.
TIME MIN.

FIG. 9 HEAT RATE TO TOOL M-2-4 VERSUS TIME CALCULATED FROM T.C. TEMPERATURE RECORDS USING EQUATION [3]

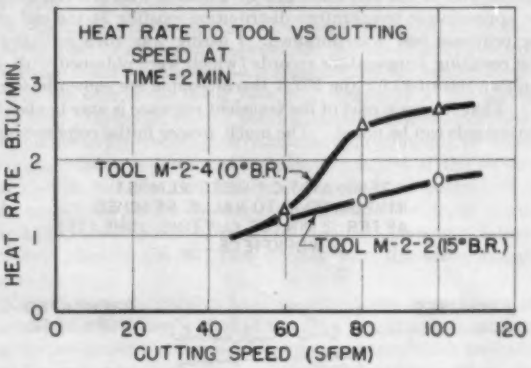

FIG. 10 HEAT RATE TO TOOL VERSUS CUTTING SPEED AT TIME = 2 MIN

In view of this, calculations were carried out considering h_c as infinite and c equal to the distance from the tool cutting edge to the front of the holder (0.75 in.). This is equivalent to saying that the tool temperature drops to ambient at the toolholder.

Evaluation of the heat rate to the tool by use of these values and the observed temperatures in Equation [3] yielded results of the type shown in Fig. 9 (for the 0-deg back-rake-angle tool). It is quite apparent that the heat rate to the tool was not constant with time. Although Equation [3] is not strictly applicable in this case, the trend indicated by the curves of Fig. 9 is physically reasonable. The flow to the cold tool would be initially very high and should decrease to a steady value dependent on the cutting conditions. Whether a definite minimum occurs or not seems to be associated with whether the type of chip formed changes.

Equation [3] should become applicable after the steady-state condition is established. This is indicated by the rather good agreement between the heat rates calculated from the different thermocouple readings as the ends of the cutting periods were approached. This agreement also supports the validity of the production solution. It is particularly significant in this regard that better agreement was obtained with the 0-deg tool (±5 per

cent) as compared to the 15-deg back-rake-angle tool (± 15 per cent). This would be expected since the geometry of the 0-deg tool more closely approximated that postulated. Values of the heat rates to the two tools for various cutting speeds were therefore determined from the temperatures at the ends of the cutting periods and are plotted in Fig. 10. A definite increase with cutting speed is indicated for both tools.

It should be observed that, although the infinite series nature of Equation [3] gives the impression of very lengthy calculations, it was found necessary to consider only the first three terms. This results from the fact that the λ's have large values and occur as squares in the denominator of each term.

Discussion

As was noted earlier, cutting tests were carried out for 2-min periods since steady-state conditions were apparently reached in that time. Investigation of Equation [3] to see if such a transient period was predicted showed that at most this period should be of the order of 1 min. This 1-min value results from the fourth term, which involves only the z-dimension. Consequently, for low values of z (near the cutting edge) its effect is not very noticeable. The first three terms have transient periods of the order of a few seconds (because the exponential terms are powers of λ_1 and λ_m, which are approximately four times the λ_n values). This would mean for a constant heat input that the tool temperature near the cutting edge should appear to rise very rapidly to a steady value. The fact that the temperature rise continued (see Figs. 3 to 6) for a longer period than predicted suggested that possibly the rate of heat input was increasing. This could occur if the workpiece were subject to a transient heating period of two or more minutes. To test this hypothesis the following experiment was conducted: During the cutting of a tubular specimen the approximate distance to which heat had penetrated ahead of the cutting location was determined after steady conditions (between two and three minutes) were indicated. For the next test the end of the specimen was first heated with a torch until the approximate temperature distribution existing at the end of the previous test was obtained. Cutting was then initiated. The resulting temperature records (which were obtained with a Sanborn recorder) for the No. 1 thermocouple are shown in Fig. 11. That the main part of the transient response is over in about two seconds can be noted. The much greater initial response for

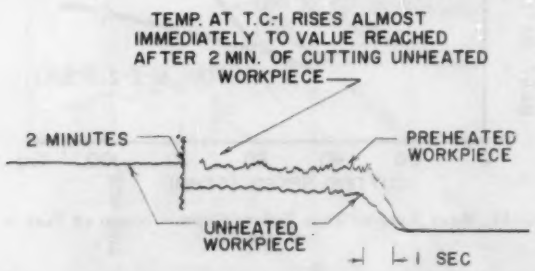

Fig. 11 Thermocouple Records During Cutting of Unheated and Preheated Workpiece—T.C. No. 1 Tool M-2-2, 80 SFPM

the preheated condition indicates a higher initial heat rate, which was not reached in the normal unheated test until after about two minutes of cutting. Thus it is concluded that a transient period does occur in the type of workpiece used, and that as a result the heat input to the tool increases for some time after the start of cutting. This would explain the increasing trend after 0.25 min shown by the curves in Fig. 9.

It also may be noted that once a value of the heat rate q is known for a tool it should be possible to calculate the tool-chip interface temperature distribution from Equation [3]. This was done for several cases. Results indicated a nearly uniform temperature across the interface, being a maximum at the cutting edge and decreasing only a few degrees in the region of chip separation. Average temperatures predicted this way were around 15 per cent lower than those determined by extrapolation, Fig. 8. This comparison appears quite reasonable since the values obtained by extrapolation are not precise and variation of the thermal properties could introduce some error.

The product solution does not predict the temperature at the tool-chip interface to increase from the cutting edge to the separation point, as is shown in references (9) and (11). This is because of the assumption of uniform heat input. It does appear, however, that substitution of an average interface temperature as determined by a tool-workpiece thermocouple will yield a value for the heat rate to the tool which is accurate to within 15 per cent.

Summary and Conclusions

A technique for measuring the temperature distribution in a cutting tool and for calculating heat flow to the tool has been demonstrated. Results substantiate previous assumptions that the heat losses from the sides of a tool are negligible. Temperature effects can be considered from the point of view of heat flow in through the tool-chip contact area, along the tool and into the toolholder. The product solution presented for the temperature distribution is valid for a parallelepiped-shaped tool and orthogonal cutting, except in the region of the tool-chip contact area. It can be used to predict steady-state heat rates to tools within ±15 per cent.

BIBLIOGRAPHY

1 "Progress Report No. 1 on Tool-Chip Interface Temperatures," by K. J. Trigger, Trans. ASME, vol. 70, 1948, pp. 91–98.

2 "Progress Report No. 2 on Tool-Chip Interface Temperatures," by K. J. Trigger, Trans. ASME, vol. 71, 1949, pp. 163–174.

3 "The Effect of Cutting Fluids Upon Chip-Tool Interface Temperatures," by M. C. Shaw, J. D. Pigott, and L. P. Richardson, Trans. ASME, vol. 73, 1951, pp. 49–56.

4 "Messung der Schnittemperatur mittel temperaturanzeigender Farbenstriche," by H. Schallbroch and M. Lang, *Zeitschrift VDI*, vol. 87, 1943, pp. 15–19.

5 "Über die Bestimmung des Temperaturfeldes beim Spanablauf," by F. Schwerd, *Zeitschrift VDI*, vol. 77, 1933, pp. 211–216.

6 "Temperaturfeld und electro-Chemischer Verschliess am Drehmessel," by H. Axer, *Aufand, Leistung und Wirtschaftlichkeit Neuzeitlicher Werkzeugmaschinen*, 6th Aachen Werkzeugmaschinenkolloquium, Leiter, H. Opitz, Girardet, Essen, Germany, 1953, pp. 23–26.

7 "Temperaturverhältnisse am den Schneiden spanabhebender Werkzeuge," by G. Pahlitzsch and H. Helmerdig, *Zeitschrift VDI*, vol. 87, 1943, pp. 691–698.

8 "An Analytical Evaluation of Metal-Cutting Temperatures," by K. J. Trigger and B. T. Chao, Trans. ASME, vol. 73, 1951, pp. 57–68.

9 "Temperature Distribution at the Tool-Chip Interface in Metal Cutting," by B. T. Chao and K. J. Trigger, Trans. ASME, vol. 77, 1955, pp. 1107–1119.

10 "On the Analysis of Cutting-Tool Temperatures," by E. G. Loewen and M. C. Shaw, Trans. ASME, vol. 76, 1954, pp. 217–231.

11 "A Theoretical Investigation of the Temperature Distribution in the Metal Cutting Process," by A. C. Rapier, British *Journal of Applied Physics*, vol. 5, 1954, pp. 400–405.

12 "Conduction of Heat in Solids," by H. S. Carslaw and J. C. Jaeger, Oxford University Press, London, England, 1950, p. 298.

13 "The Thermal Conductivity of Tool Steels," by D. Hattori, *Journal of the Iron and Steel Institute* (British), vol. 129, 1934, p. 299.

Discussion

A. O. Schmidt[5] and B. F. Turkovich.[6] The determination of the temperature distribution inside a solid with prescribed boundary conditions has been, in a majority of the cases, a problem of considerable difficulty. Although the mathematical theory of heat conduction supplies the analytical methods, the experimental verification of the results seldom can be achieved in a sufficiently satisfactory manner. One of many eminently complex cases is the problem the authors proposed to solve. They are commended for their effort and ingenuity, but, as usual, there are a few questions to be raised in order to clarify certain statements and conclusions in their paper.

It is apparent from their bibliography that the authors have surveyed almost all the important analytical works on the problem of the tool-chip interface temperature. This list could be divided into two parts: One, which consists of works primarily concerned with the tool-chip interface temperature, and the other, with the problem of the temperature field in the tool itself. From the point of view of metal cutting, the tool-face temperature and its distribution are fundamentally important, and the temperature field in the tool is contingent. However, if a method is devised based on the study of the temperature field inside the tool, which would elucidate the problem of the tool-face temperature, then such an attempt is definitely welcome.

A list of cases could be made in which the temperature distribution inside a solid is known fairly accurately, but the exact conditions on the boundaries are only a matter of intelligent supposition. Although this fact could be attributed probably to the intrinsic inaccuracy of the measurements when extraneous devices are introduced within the solid, a comparison of mathematical solutions with different but congruent boundary conditions would show that, in the cases of complex transient state combined with the peculiar material properties and geometry, it is rather difficult to determine to which mathematical solution the measurements comply if the points of the instrument application are not within the very neighborhood of one of the boundaries.

Referring now particularly to the tool temperatures, it becomes clear that a method in the study primarily of the tool-temperature distribution also should permit the determination of the conditions on the boundaries more or less accurately, i.e., the average distribution of temperature and heat inputs, and provides an indication where the probable extreme may be located. This is a rather ambitious requirement but hardly less mandatory if a comparison of data with other methods of solution is desirable because almost all methods devised up to date lack more or less the generality of argument, creating an exasperating series of divergent opinions which impedes the formation of a reliable body of data upon which further research activity could be based advantageously. Every one actively interested in metal-cutting research is, however, fully aware that the problem is an extremely difficult one and it is with the spirit of hoping for the best solution yet to come that the following discussion is presented.

When the tool closely resembles a parallelepiped, the analytical approach for evaluation of temperatures based on the method of product solutions seems to be a convenient one. Although infinite series arise in the solution, making the numerical work rather tedious, it is perhaps the most straightforward method available. Since the distribution of the heat input over the chip-tool interface is still a problem which needs further research, although the investigations by Chao and Trigger (authors' reference 9) point conclusively that the assumption of a uniform plane heat source cannot be expected, the authors assumed a uniformly distributed source, probably for simplicity's sake. The boundary condition of such a state, used jointly with other conditions well justified, necessarily leads to a temperature distribution which is diametrically at variance with the findings of Chao and Trigger as well as the results known from the theory of sliding-contact heat sources. Moreover, the authors neglect to consider another source of heat, i.e., the area on the flank of tool which rubs against the workpiece. This area enlarges with time providing a constantly increasing plane heat source which, although initially of minor importance, influences considerably the temperature field inside the tool. Consequently, speaking strictly from a theoretical point of view, a truly steady state can never be arrived at. If the cutting time is short in duration, this influence can probably be neglected. However, if the flank wear approaches the magnitude of the chip thickness before deformation (feed per revolution), it is doubtful whether it can be ignored safely.

In Figs. 3 to 6 of the paper, the diagrams show the millivolts-time relationship for the thermocouples indicating a leveling off after 2-min cutting time. It would be interesting to know the behavior of these graphs after prolonged cutting, i.e., 5 to 10 min, since the tool life should not be very low at the speeds used. It is quite possible that the strong temperature fluctuations in thermocouple No. 1 in the tool M-2-2 could be attributed to the influence of this heat source rather than to the intermittent contact of the chip with the tool. The built-up edge also could play an important role.

It is unfortunate that the paper lacks additional information about cutting conditions such as chip-thickness ratio and magnitude of the contact area. Isotherms for one or two cutting conditions also would increase the informative value of the paper. Since the authors already have used rake angles of 0 and 15 deg it will be of interest to see their temperature records extended to include also rake angles in the negative range. A tool with 5-deg negative back-rake angle and a 5-deg end clearance could be made to have exactly the geometry postulated and consequently a better agreement between the calculated and measured quantities could be obtained, as is suggested by the smaller deviation in the case of the 0-deg rake tool compared to the 15-deg rake tool. However, at this point it should be mentioned that the thermocouple records shown indicate approximately the same trend in relation to time and temperature as one of the writers was able to measure with a thermocouple located underneath a thin carbide tip, when turning magnesium.[7] The depth of cut was 0.125 in., feed 0.005, 0.010, and 0.015 ipr. Thus chip formation took place on the tool face directly over the thermocouple point.

Several research workers have measured the temperature at the tool-chip interface. Most of the data were obtained employing the tool-workpiece thermocouple arrangement which basically supplies only some sort of an average temperature value on the tool-chip interface. Although this method is essentially different from the authors' approach, it is noted that almost all reports on temperatures obtained by tool-workpiece thermocouples indicate that steady temperature readings prevail after a very short cutting time, substantially shorter than that indicated by the authors. Time lag observed at thermocouple No. 1 is not due entirely to conduction, the authors state, since it took about 2 min to reach a steady state instead of the 1-min lag predicted by Equation [3]. It also appears that the temperature rise is rather rapid near the cutting edge and should reach a steady state in a very short time. However, the authors note that the transient

[5] Research Engineer, Charge of Metal Cutting, Kearney & Trecker Corporation, Milwaukee, Wis. Mem. ASME.

[6] Kearney & Trecker Corporation, Milwaukee, Wis.

[7] "Metal Cutting Temperatures and Tool Wear," by A. O. Schmidt, *The Tool Engineer*, vol. 24, August, 1952, pp. 33–35.

period is more than twice that predicted from Equation [3] and suggest the possibility of increasing rate of heat input, as a result of the fact that the workpiece experiences a transient heating period of 2 to 3 min. When the workpiece is preheated, the steady condition is reached substantially sooner. To what temperature was the workpiece preheated?

This is a rather puzzling phenomenon. Considering that the feed at which the cutting was performed was only 0.0025 ipr, a time of 2 to 3 min seems a rather long transient period to establish the stationary state in the workpiece ahead of the shear zone. Is this the authors' implication? A substantial amount of energy can be released into the workpiece by rubbing of the flank which at fine feeds has much influence on temperature gradients. It would certainly help us to arrive at an explanation if other, coarser feeds also were considered. A twofold benefit could have been achieved: (1) The geometrical relationship would be improved (e.g., distance of the first thermocouple to the cutting edge versus chip thickness and magnitude of area of contact) and (2) the influence of feed could be clearly appreciated. Unless additional information is forwarded, the data shown in Figs. 7 and 8 of the paper should be viewed with a skepticism which not even apparent concordance with other investigators' data could mitigate.

Reluctantly we have to revert the whole problem to the conclusion that so far no successful indirect method to arrive at the tool temperature has been devised. However, anyone who has attempted to measure tool-tip temperatures can appreciate the thermocouple technique used here and the work that has gone into this investigation. Let us hope that the authors will continue to present additional experimental findings in the near future and thus will help to validate and augment the important tool-temperature data available today.

B. W. SHAFFER.[9] Have the authors considered the possibility of expanding each of the infinite series found in Equation [3] with the retention of but one or two terms in each case, and then collecting the resulting expression in a compact manner? The revised expression may not only look simpler but should give results which are not too different from the more exact equation because, as the authors point out, the series converges very rapidly.

K. J. TRIGGER[8] AND B. T. CHAO.[10] The authors are to be congratulated on the interesting experimental approach to the study of the tool-chip interface temperatures. Their technique, like that employed by Axer, opens additional avenues for further investigation.

There are, however, some aspects of the paper which need further discussion. The writers submit the following comments as constructive criticism in the hope of contributing to the value of the paper.

The assumption of a uniform heat-flux distribution at the tool-chip interface leads to the anomalous situation of an incompatible temperature distribution at the tool-chip interface when calculated from the point of view of the moving chip and that determined from the point of view of the tool. The authors' reference (9) contains a procedure for the quantitative evaluation of both the heat-flux distribution and the corresponding compatible tool-chip interface temperature distribution.

Metallurgical evidence of the interface temperature distribution can be seen in Fig. 12 of this discussion which shows a sectioned HSS tool after cutting under the conditions shown. The indicated (average) interface temperature was about 1060 deg F. Fig. 12 (*a*) shows the crater with some adhered work material. Fig. 12 (*b*) shows the same section after additional etching in a somewhat stronger solution. The darkening in the crater region is caused by a more rapid etching rate which is due to the additional tempering of the high-speed steel as a consequence of heating by the sliding chip. The nonuniformity of the temperature distribution along the path of contact is indicated by the varying depth of the heat-affected zone. The temperature distribution appears to be nearly symmetrical with respect to the center of the crater and the temperature at the cutting edge is clearly less than that at other points of contact. Indeed, the temperature there appears to be considerably lower than that at the point of departure of the chip from the tool. The geometrical shape of the crater conforms to the temperature distribution at the interface.

In view of these findings the writers cannot agree with the statement: "Results indicated a nearly uniform temperature across the interface, being a maximum at the cutting edge and decreasing only a few degrees in the region of chip separation."

The authors have acknowledged that the difference between

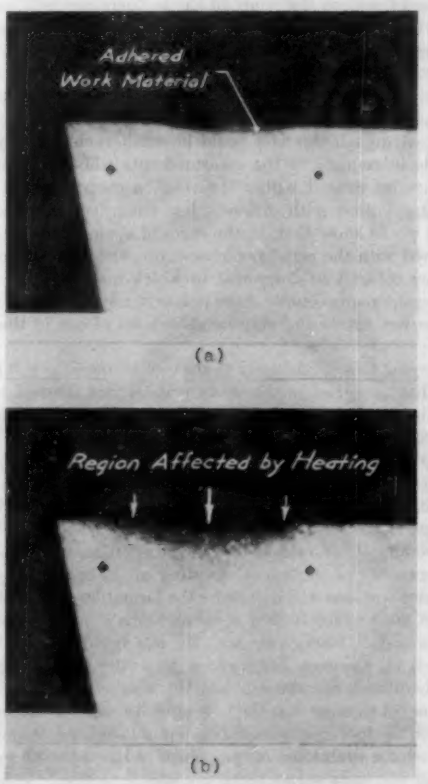

Work material:	AISI 4142 steel, annealed, 212 Bhn
Tool material:	18-4-1 HSS
Cutting speed:	V_s = 132 fpm
Depth of cut:	w_1 = 0.100 in.
Feed:	f_1 = 0.00979 ipr
Cutting time:	1.20 min

FIG. 12 SECTION OF CRATER SURFACE OF A HIGH-SPEED-STEEL TOOL SHOWING (a) ADHERED WORK MATERIAL, AND (b) REGION OF STRUCTURAL CHANGE DUE TO HEATING BY SLIDING CHIP

[8] Associate Professor of Mechanical Engineering, New York University, New York, N. Y. Assoc. Mem. ASME.

[9] Professor of Mechanical Engineering, University of Illinois, Urbana, Ill., Mem. ASME.

[10] Professor of Mechanical Engineering, University of Illinois, Urbana, Ill.

their temperature distribution and that presented by the writers (reference 9 of the paper) is due to the assumption of a uniform heat-flux distribution. The writers have found that both the heat flux and temperature distribution across the interface are invariably nonuniform.

It would appear for the 0-deg back-rake angle, Fig. 8 of the paper, that extrapolation to the center of the tool-chip contact area leads to excessive temperatures there.

Research by the writers, using the tool-work thermocouple technique, has revealed that high-speed steel tools become temperature sensitive at indicated (average) interface temperatures around 1050 F and that the indicated value is some 1250 F at failure.

If as shown in Fig. 8 the temperatures were to rise to 1400 F under the cutting conditions shown, tool failure would ensue quickly. This has not been the experience in machining 1020 steel (100 Bhn) at 100 fpm with the light feed and at the rake angle indicated.

It is hoped that the authors will pursue their study and perhaps compare their results with those determined directly from the measured temperature distribution using Axer's successive grinding technique.

Authors' Closure

The authors sincerely appreciate the interesting and constructive discussions of this paper. The observations and comments offered are well founded, pointing up definite need for additional study of this problem. The following information is submitted in answer to the several questions raised.

The suggestion that the temperature fluctuations noted in the experimental measurement of Figs. 3 to 6 might be attributable to the heat input on the flank of the tool does not seem likely, since, as already pointed out, these fluctuations disappear when a change from a discontinuous to a continuous chip takes place (see Fig. 5).

The reason for the difference between the findings of other investigators and the results presented in this paper regarding the duration of the transient heating period is due to the difference in workpiece geometry. For the tests described herein, orthogonal cutting of a hollow tubular specimen was used, as compared to a large solid cylindrical workpiece employed by others. A solid workpiece will act as a heat sink immediately behind the plane of cutting, and any heat which is conducted into the workpiece as a result of the cutting process can easily be absorbed by the large thermal capacity of the specimen. Thus the temperature of the specimen remains substantially constant, and the duration of the transient period is of the order of seconds. However, with orthogonal cutting of a tubular specimen, there is only a thin walled section through which the heat can be conducted away from the cutting plane and the thermal capacity is relatively low. Hence the energy entering the workpiece causes a gradual rise in temperature of the workpiece. Since this transient heating of the workpiece is, however, much slower than the simple heating of the tool, a much longer transient period is indicated by the tool temperature records.

The details of the simple experiment conducted to verify the foregoing explanation were as follows: First, after cutting of an initially unheated workpiece for two minutes, the distance from the cutting edge which could be safely touched by hand was determined (about 9 inches from the cutting edge). Next, a similar workpiece was preheated by playing an acetylene flame on its end while rotating it until the temperature at a distance of about 9 inches from the end began to rise. Cutting was then initiated and the tool temperature recorded. The results of these two tests are presented in Fig. 11.

The possibility of developing a compact closed expression for the temperature based on a limited number of terms from Equation [3], as suggested by Professor Shaffer, has been given some attention. This effort has not as yet, however, yielded a result that can be recommended in place of Equation [3].

The value of 1250 F obtained by Professors Trigger and Chao for the average interface temperature at which high-speed steel tools would fail was of considerable interest. The peak value estimated for the average interface temperature by the authors was 1300 F (see Fig. 7) for the zero-degree back-rake angle tool. It was at this temperature that failure of the tool actually occurred. In view of the close agreement between these two temperatures, it would appear that the upper curve in Fig. 8 should be drawn through the two points shown and should level off to a maximum around 1300 F.

To investigate further the heat-rate distribution along the tool-chip contact area (0.110 inch $\times$ 0.050 inch), a linear variation was considered, i.e., $Q = A + Bz'$ was assumed in Equation [3] where A and B are constants. A solution for this case is possible and evaluation of the constants A and B can be accomplished if the temperature at two points is known. The calculations for one of the tests using this assumed distribution were carried out. The results indicated that the heat rate increased from the cutting edge to the point of chip separation. The heat flow at the cutting edge was positive; that is, into the tool, and the increase over the chip contact length was about 15 per cent of the value at the cutting edge. The average value agreed very closely with that previously determined for an assumed uniform heat rate.

In contrast to this, Chao and Trigger (9) found a negative heat flow at the cutting edge and a much larger gradient in the direction of chip travel. It is recognized, however, that the heat-rate distribution found by Chao and Trigger differs significantly from linearity near the cutting edge and chip separation point. In addition, cutting speeds were quite different so that a comparison may not be proper. It was also noted that in our tests, rubbing of the tool flank against the workpiece occurred over an area of one third to one half of the tool-chip contact area. Possible heat flow in through this area would tend to indicate a higher heat rate near the cutting edge of the tool-chip contact area.

It is felt that the observation of Dr. Schmidt and Mr. Turkovitch, that a truly steady state never occurs, merits emphasis in connection with the heat rate and temperature distributions along the tool-chip contact area. In reviewing the results of this investigation, it appears quite likely that tool wear, particularly in the case of the zero-degree back-rake angle tool, during the course of the tests influenced the results. Unfortunately, the temperature measurements were neither close enough to th ecutting edge nor sufficiently close to point values to resolve this question. Although very small thermocouples were used further refinement is necessary.

An Analysis of the Orthogonal Boring Operation[1]

By BERNARD W. SHAFFER,[2] NEW YORK, N. Y.

The shear line, during the orthogonal boring operation, was found to be a circular arc extending from the tip of the tool and separating the uncut workpiece from the newly formed chip. Its orientation with respect to the cutting tool was prescribed in this paper, by the condition that the element within the chip, at the base of the tool, did not exceed the yield point of the material as the cutting force was transferred from the tool to the shear line. Under these conditions, a shear-angle relationship, an expression for machining force, and an expression for the chip-thickness ratio were derived for orthogonal boring. It was found, by examining these equations, that as the internal radius of the workpiece increases, the shear angle increases and the machining force decreases, whenever a given depth of cut is taken under identical machining conditions. At the same time, the chip-thickness ratio increases for small friction angles, and decreases for large friction angles. As the internal radius of the workpiece increases, the analytical expressions approach the corresponding equations found for the orthogonal planing operation.

Introduction

DURING a machining operation, continuous chips may be formed by a simple shearing action between the uncut workpiece, and the newly formed chip. The shearing process between these two regions takes place all along a single line of demarcation which is clearly visible on photomicrographs taken of specimens obtained during metal cutting (1, 2).[3] It is our intention to analyze, in this paper, the orthogonal boring operation when a continuous chip is formed by this process.

In orthogonal boring, the face of the cutting tool is assumed plane, and meets the noncutting surface in a straight line which is parallel to the longitudinal axis of the workpiece. The surface of the newly formed chip is also parallel to this line.

For reasons outlined in previous papers on metal cutting (3, 4) a machining operation in which continuous chips are formed may be analyzed as a plane-strain problem of a nonwork-hardening material in which elastic regions may be treated as rigid bodies. The uncut workpiece and newly formed chip, therefore, will be treated as rigid regions separated by the shear line.

The tool, during the boring operation, is held against the inside of the workpiece, and either the tool or the workpiece rotates at a constant angular velocity ω. For purposes of analysis, the tool will be held stationary, while the workpiece rotates about its center line at the relative angular velocity of these members.

As this relative rotation takes place, the tool is fed into the workpiece at a uniform rate, enabling it continuously to take a constant depth of cut. The combined effect of rotation and translation results in the machining of a helical surface on the inside of the workpiece. Because the depth of cut is relatively small, however, the difference between the actual helical surface and equivalent circular surface drawn tangent to the helix, at the point of the tool, is negligible in the neighborhood of the tool. Since we will be concerned only with this region, in the analysis to follow, it is permissible for any instant under consideration to replace the actual helical surface by an equivalent circular surface.

Geometry of the Shear Line

In order to identify the regions referred to in the introduction, a section was taken through the tool, chip, and workpiece, perpendicular to the longitudinal axis of the system, which is shown in Fig. 1. The section illustrated there was not drawn to scale,

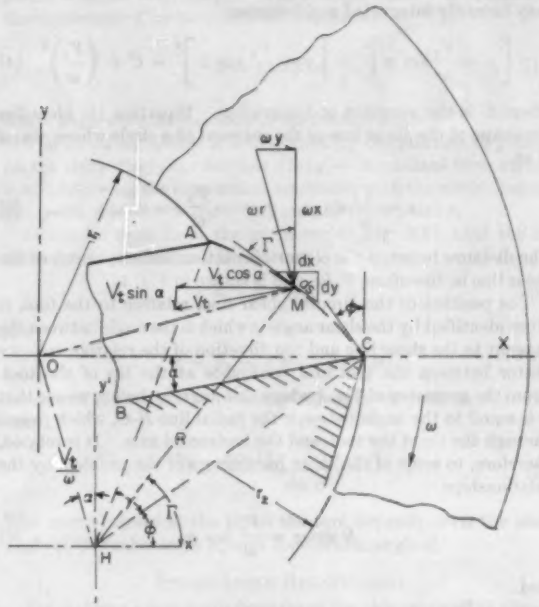

Fig. 1 Velocity Considerations for an Arbitrary Point on the Shear Line

thereby enabling us to exaggerate the regions of interest. Point O is the projection of the longitudinal axis; line B-C is the cutting face of the tool whose rake angle is α. The uncut workpiece, whose internal radius is r_1, is shown to the right, while the newly formed chip is shown to the left of the shear line A-C.

Each particle within the uncut workpiece and the newly formed chip move with rigid body motion. Two such particles are located at an arbitrary point M on the shear line. One of these particles

[1] The results presented in this paper were obtained in the course of research sponsored by the Office of Ordnance Research, Department of the Army (Ordnance Corps), under Contract No. DA-30-069-ORD-1135, with New York University. It was presented at the Fourth Symposium on Plasticity, Brown University, Providence, R. I., September 1–3, 1953.

[2] Associate Professor of Mechanical Engineering, New York University, University Heights. Assoc. Mem. ASME.

[3] Numbers in parentheses refer to the Bibliography at the end of the paper.

Contributed by the Research Committee on Metal Processing and presented at the Diamond Jubilee Annual Meeting, Chicago, Ill., November 13–18, 1955, of The American Society of Mechanical Engineers.

Note: Statements and opinions advanced in papers are to be understood as individual expressions of their authors and not those of the Society. Manuscript received at ASME Headquarters, August 5, 1955. Paper No. 55—A-67.

belongs to the uncut workpiece and rotates about the center O. Its velocity has been represented by the vector ωr perpendicular to the line O-M. The other belongs to the newly formed chip, moves as a rigid body along the face of the tool, and is represented by the velocity vector V_t.

Since plastic flow takes place along the shear line, the tangential components of these vectors are not equal to each other. In fact, each particle within the workpiece slips, with respect to the adjoining particle within the chip, toward the point of the tool. The vector components taken perpendicular to the shear line, however, are equal to each other, because there are no voids in the material during the cutting process.

The shape of the shear line permits continuity of the normal velocity components all along its surface. We may express continuity, at an arbitrary point on the shear line, by the equation

$$\omega x \sin \Gamma - \omega y \cos \Gamma = V_t \sin \alpha \sin \Gamma + V_t \cos \alpha \cos \Gamma \quad [1]$$

which is written in terms of the Cartesian co-ordinate system originating at point O and passing through the tip of the tool r_2 inches away. The angle Γ is the angle between the vertical axis and the tangent to the shear line. It may be written in terms of the arc length ds by the relationships

$$\cos \Gamma = dy/ds, \quad \sin \Gamma = -dx/ds \quad [2]$$

By eliminating Γ from these equations, we find that the resulting differential equation

$$\omega x\, dx + \omega y\, dy = V_t \sin \alpha\, dx - V_t \cos \alpha\, dy \quad [3]$$

may be easily integrated and becomes

$$\left[x - \frac{V_t}{\omega} \sin \alpha\right]^2 + \left[y + \frac{V_t}{\omega} \cos \alpha\right]^2 = C + \left(\frac{V_t}{\omega}\right)^2 \quad [4]$$

where C is the constant of integration. Equation [4] identifies the shape of the shear line as the segment of a circle whose center is at

$$x = \frac{V_t}{\omega} \sin \alpha, \quad y = -\frac{V_t}{\omega} \cos \alpha \quad [5]$$

The distance between the center of rotation and the center of the shear line is, therefore, V_t/ω, and is shown in Fig. 1.

The position of the circular shear line, relative to the tool, is often identified by the shear angle φ which is the angle between the tangent to the shear line and the direction of the relative velocity vector between the tool and workpiece at the tip of the tool. From the geometry of Fig. 1 where this angle is shown, we see that φ is equal to the angle between the radial line H-C, which passes through the tip of the tool, and the horizontal axis. It is related, therefore, to some of the other parameters of the problem by the relationships

$$R \sin \varphi = \frac{V_t}{\omega} \cos \alpha \quad [6]$$

and

$$R \cos \varphi = r_2 - \frac{V_t}{\omega} \sin \alpha \quad [7]$$

These equations show that the distance from the center of the workpiece to the center of curvature of the shear line, V_t/ω, is given by the expression

$$\frac{V_t}{\omega} = r_2 \frac{\sin \varphi}{\cos (\varphi - \alpha)} \quad [8]$$

while the radius of the shear line R is given by the expression

$$R = r_2 \frac{\cos \alpha}{\cos (\varphi - \alpha)} \quad [9]$$

The radius of the shear line is directly proportional to r_2 and increases as the radius of the workpiece increases.

Extreme positions of the radial lines, from the center of curvature to points on the shear line, are γ radians apart. The one extreme, H-A, is $\pi/2 - \gamma - \varphi + \alpha$ radians from O-H, while the other extreme, H-C, is $\pi/2 - \varphi + \alpha$ from this same line. In view of this, the law of cosines may be written

$$\left(\frac{V_t}{\omega}\right)^2 + R^2 = r_1^2 - 2\left(\frac{V_t}{\omega}\right) R \sin (\alpha - \varphi - \gamma) \quad [10]$$

for triangle O-H-A and may be written

$$\left(\frac{V_t}{\omega}\right)^2 + R^2 = r_2^2 - 2\left(\frac{V_t}{\omega}\right) R \sin (\alpha - \varphi) \quad [11]$$

for triangle O-H-C. By equating the right-hand sides of these expressions, and introducing the results of Equations [8] and [9], we find that

$$\sin (\alpha - \varphi - \gamma) = \sin (\alpha - \varphi) - \left[1 - \left(\frac{r_1}{r_2}\right)^2\right] \frac{\cos^2 (\varphi - \alpha)}{2 \sin \varphi \cos \alpha} \quad [12]$$

This expression will serve to define the angle γ that will appear in the analysis to follow.

We have just seen that the numerical value of the radius of the shear line R, as well as the angles which denote the extreme positions of this radius, depend on the numerical value of the shear angle φ. Since this angle is not given by velocity considerations, but may be given by stress considerations, we will study the stresses involved in the problem.

Stress Distribution Along the Shear Line

When a particle is in the uncut region its stresses are elastic. As it approaches the shear line, these stresses remain elastic and their magnitudes increase until their maximum value is reached on the shear line. Yielding then takes place, and the particle becomes part of the chip. As it moves with the chip, the stress on each element decreases until it finally becomes stress-free. It is then carried along the face of the tool by the particles behind it.

On the shear line the stress components satisfy the yield condition. For plane strain the yield condition, as expressed by Mises and Tresca, reduces to the same form (5)

$$\left(\frac{\sigma_x - \sigma_y}{2}\right)^2 + \tau^2 = k^2 \quad [13]$$

where σ_x and σ_y are the normal stresses and τ is the shear stress on an element in the region; k is the maximum shear stress of the material. If these stress components, σ_x, σ_y, and τ, are plotted on a plane whose axis represents the normal and shear stress, and if a Mohr's-circle diagram (6) is drawn on this plane, yielding will occur, according to Equation [13], whenever the radius of the Mohr's-circle diagram is equal to k.

Since yielding occurs all along the shear line, it is the direction of maximum shear stress. Furthermore, because of the direction of relative slippage between the chip and uncut material described in the last section, the shear stress on the chip is toward the tip of the tool.

Associated with this shear stress is the normal stress p, which is compressive because the tool is pressed into the workpiece. Its magnitude may vary along the shear line subject to the restrictions imposed upon it by the equation of equilibrium.

The equation of equilibrium can be obtained by studying Fig.

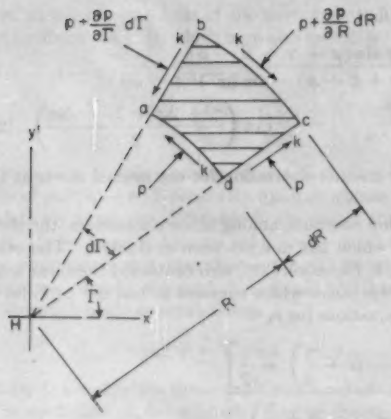

FIG. 2 TYPICAL ELEMENT ON THE SHEAR LINE

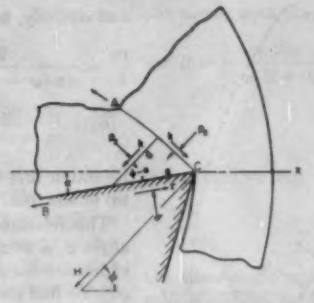

FIG. 3(a) ENLARGED VIEW OF ELEMENT IN THE CHIP AT THE BASE OF THE TOOL

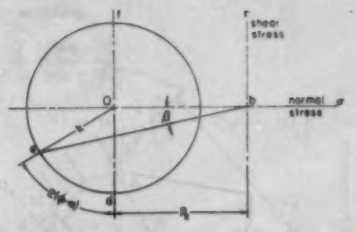

FIG. 3(b) THE CORRESPONDING MOHR'S-CIRCLE DIAGRAM

2 where a typical element is shown on the shear line. The shear stress on this element has attained its maximum value k. The associated normal stress may vary in the tangential and radial directions. From the equilibrium of forces, in the tangential direction, we find that the normal stress p satisfies the relationship

$$k\,dR\,d\Gamma + 2k\,dR\,\sin\frac{d\Gamma}{2} + \frac{\partial p}{\partial \Gamma}\,d\Gamma\,dR\,\cos\frac{d\Gamma}{2} = 0 \quad [14]$$

By introducing the small-angle relationships

$$\sin\frac{d\Gamma}{2} = \frac{d\Gamma}{2}, \quad \cos\frac{d\Gamma}{2} = 1 \quad [15]$$

the equilibrium equation reduces to

$$p + 2k\Gamma = \text{const} \quad [16]$$

along the shear line. If we call p_2 the normal stress at the tip of the tool, where the angle Γ is equal to the shear angle φ, Equation [16] may be written

$$p + 2k\Gamma = p_2 + 2k\varphi \quad [17]$$

The terms p_2 and φ will be evaluated later.

We see, therefore, that whereas the shear stress is constant, and equal to the maximum attainable value along the shear line, the associated normal stress varies with the arc length of this line.

NORMAL STRESS AT THE TIP OF THE SHEAR LINE

It has been shown (3, 4) that the solution to the machining problem is given by that configuration which results in a minimum tool force, and at the same time yields a satisfactory stress distribution within the chip. For most practical machining operations, this requirement is met by determining the position of the shear line for which the yield condition is satisfied at the most highly stressed point within the chip.

Since the tool force is transferred from the chip-tool interface through the chip to the shear line, the area between these surfaces is subject to very high stresses. Nevertheless, because some elastic unloading takes place, most of the region is not stressed up to the yield point. This may not hold true, however, for the element at the very tip of the tool. The unloading probably does not reach this element and, therefore, it remains the most highly stressed point within the chip.

In view of this, let us examine the stresses acting on the element at the very tip of the tool shown enlarged in Fig. 3(*a*). The element, as we see, is bounded on one side by the shear line and on the other by the tool surface. Surface f is on the shear line, and is subjected to the normal stress p_2, and the shear stress k. These stresses have also been depicted as the co-ordinates of point f on the corresponding Mohr's-circle diagram, shown in Fig. 3(*b*).

Surface e, on the other hand, is on the tool-chip interface. It is subject to the stress components σ and τ which are induced by the applied tool force. These stresses are depicted by the co-ordinates of point e, shown in the lower portion of the circle diagram of Fig. 3(*b*). Even though its position around the circle may change, for different coefficients of friction, point e will always be located in the lower half of the circle because of the sign convention associated with the diagram (6). The stresses σ and τ are related to the coefficient of friction μ by the expression

$$\mu = \tan\beta = \frac{\tau}{\sigma} \quad [18]$$

hence angle o-b-e corresponds to the friction angle β.

The stress on surface d is described by the position of point d on the circle diagram. Surface d is $(\varphi - \alpha)$ radians from surface e, and following the convention associated with the circle diagram (6), point d is shown $2(\varphi - \alpha)$ radians from point e.

It can be seen, from the geometry of Fig. 3(*b*), that the co-ordinates of point e may be written

$$\tau = k\cos 2(\varphi - \alpha) \quad [19]$$

and

$$\sigma = p_2 + k\sin 2(\varphi - \alpha) \quad [20]$$

In view of Equation [18], we may solve for the ratio p_2/k, to find that

$$\frac{p_2}{k} = \frac{\cos(2\varphi - 2\alpha + \beta)}{\sin\beta} \quad [21]$$

The normal stress at the tip of the tool depends upon the shear angle φ, the rake angle α, and the friction angle β.

SHEAR-ANGLE RELATIONSHIP

Fig. 4 shows a free-body diagram of the chip, with all the forces that are acting on it. The normal stress p and shear stress k are shown along the shear line. At the tool interface, the resultant tool force F is shown, as well as its components F_x and F_y taken parallel and perpendicular to the line joining the center of rotation to the tip of the tool. Since these are the only forces acting on the chip, and the chip is in equilibrium, the forces F_x and F_y are equal to the resultant of the force distribution along the shear line in the corresponding directions.

To find expressions for these tool forces, let us resolve the forces which act on a typical point M on the shear line, namely, $p\,ds$ and

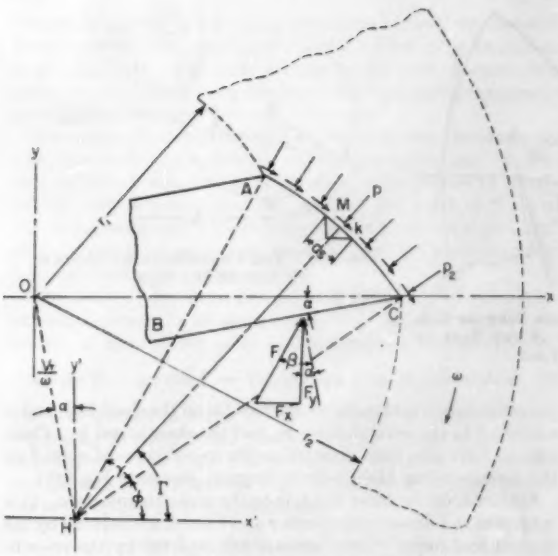

FIG. 4 FREE-BODY DIAGRAM OF THE CHIP

kds, into the components

$$dF_y = (p \sin \Gamma + k \cos \Gamma)ds \quad [22a]$$

$$dF_x = (p \cos \Gamma - k \sin \Gamma)ds \quad [22b]$$

and integrate along the shear line. Since the arc length, whose radius R is given by Equation [9]

$$ds = r_2 \frac{\cos \alpha}{\cos (\varphi - \alpha)} d\Gamma \quad [23]$$

and the normal stress p, given by Equation [17], are functions of Γ, the differential equations may be integrated from φ to $\varphi + \gamma$, to cover the entire shear line. The corresponding force components are then found to be

$$\frac{\cos (\varphi - \alpha)}{kr_2 \cos \alpha} F_y = -\left(\frac{p_2}{k} - 2\gamma\right) \cos (\varphi + \gamma) - \sin (\varphi + \gamma) + \frac{p_2}{k} \cos \varphi + \sin \varphi \quad [24a]$$

$$\frac{\cos (\varphi - \alpha)}{kr_2 \cos \alpha} F_x = \left(\frac{p_2}{k} - 2\gamma\right) \sin (\varphi + \gamma) - \cos (\varphi + \gamma) - \frac{p_2}{k} \sin \varphi + \cos \varphi \quad [24b]$$

If there were no friction, the resultant tool force F would be normal to the surface of contact between the tool and the chip. With friction, however, the resultant is inclined β radians to the normal, where β is the friction angle. The force components, therefore, shown in Fig. 4, are related to each other by the expression

$$F_x = F_y \tan (\beta - \alpha) \quad [25]$$

According to Equation [24], each of these force components contains the term p_2/k. By making the appropriate substitution, we can solve

$$\frac{p_2}{k} [\sin (\varphi + \gamma + \beta - \alpha) - \sin (\varphi + \beta - \alpha)] = 2\gamma \sin (\varphi + \gamma + \beta - \alpha) + \cos (\varphi + \gamma + \beta - \alpha) - \cos (\varphi + \beta - \alpha) \quad [26]$$

and simplify, to find

$$\frac{p_2}{k} = \frac{2\gamma \sin (\varphi + \gamma + \beta - \alpha)}{\sin (\varphi + \gamma + \beta - \alpha) - \sin (\varphi + \beta - \alpha)} - \tan \left(\frac{\gamma + 2\varphi + 2\beta - 2\alpha}{2}\right) \quad [27]$$

Equation [27] is another expression for the normal stress at the tip of the tool.

This relationship contains, among other parameters, the shear angle φ, a term which has not yet been evaluated. The other expression for p_2/k, Equation [21], also contained the shear angle φ. To find an expression which contains φ, but not p_2/k, let us equate the two equations for p_2/k

$$\frac{\gamma \sin \left[\left(\varphi + \beta - \alpha + \frac{\gamma}{2}\right) + \frac{\gamma}{2}\right]}{\sin \frac{\gamma}{2} \cos \left(\varphi + \beta - \alpha + \frac{\gamma}{2}\right)} - \tan \left(\varphi + \beta - \alpha + \frac{\gamma}{2}\right) = \frac{\cos [(2\varphi - 2\alpha) + \beta]}{\sin \beta} \quad [28]$$

and expand the terms shown above in squared brackets

$$\left(\frac{\gamma}{\tan \frac{\gamma}{2}} - 1\right) \tan \left[\left(\varphi - \alpha + \frac{\gamma}{2}\right) + \beta\right] - \frac{\cos 2(\varphi - \alpha)}{\tan \beta} = -\gamma - \sin 2(\varphi - \alpha) \quad [29]$$

This manipulation proves useful, because if we now expand the term shown in the foregoing in squared brackets, our equality may be written

$$A \tan^2 \beta + B \tan \beta + C = 0 \quad [30]$$

where

$$A = \frac{\gamma}{\tan \frac{\gamma}{2}} - 1 - [\gamma + \sin 2(\varphi - \alpha)] \tan \left(\varphi - \alpha + \frac{\gamma}{2}\right) \quad [31a]$$

$$B = \gamma + \sin 2(\varphi - \alpha) + \left[\frac{\gamma}{\tan \frac{\gamma}{2}} - 1 + \cos 2(\varphi - \alpha)\right] \tan \left(\varphi - \alpha + \frac{\gamma}{2}\right) \quad [31b]$$

$$C = -\cos 2(\varphi - \alpha) \quad [31c]$$

The solution to this quadratic equation

$$\tan \beta = \frac{-B \pm \sqrt{B^2 - 4AC}}{2A} \quad [32]$$

is the shear-angle relationship for orthogonal boring.

Mathematically speaking, it is correct to place both signs in front of the square root. Additional study has shown, however, that the positive sign should be used whenever $(\varphi - \alpha)$ is positive, and the negative sign should be used whenever $(\varphi - \alpha)$ is negative. For only then is the resulting solution feasible from a physical point of view.

The shear-angle relationship, Equations [31] and [32], may be simplified, whenever applicable, by introducing a small angle approximation for those trigonometric functions which involve the angle γ.

It will be recalled that γ is the angle between the normals

drawn at the extreme ends of the curved shear line. It was defined by Equation [12], which may also be written

$$\sin(\alpha - \varphi - \gamma) - \sin(\alpha - \varphi) = -\frac{(r_2 - r_1)(r_2 + r_1)}{2r_2^2}\frac{\cos^2(\varphi - \alpha)}{\sin\varphi\cos\alpha} \quad [33]$$

An inspection of this equation shows that whenever the initial depth of cut $(r_2 - r_1)$ is relatively small or whenever the radius r_2 is relatively large, the difference in the sin of the two angles is small. Under these conditions, which may occur in many of the more common boring operations, the difference in the angles themselves, namely, the angle γ, is small, and it is permissible to use the small-angle approximation

$$\cos\gamma = 1, \quad \sin\gamma = \gamma \quad [34]$$

in order to simplify the shear-angle relationship.

The coefficient A, for example, may be shortened by first expanding the tan of the sum of two angles, introducing the small-angle approximation

$$A\left[1 - \frac{\gamma}{2}\tan(\varphi - \alpha)\right] = 1 - \sin 2(\varphi - \alpha)\tan(\varphi - \alpha) - \frac{\gamma}{2}[3\tan(\varphi - \alpha) + \sin 2(\varphi - \alpha)] \quad [35]$$

and then multiplying the right and left-hand side by $1 + (\gamma/2)\tan(\varphi - \alpha)$, so that it reads

$$A = \cos 2(\varphi - \alpha) - 2\gamma\tan(\varphi - \alpha) \quad [36]$$

after dropping all higher-ordered terms. Likewise, the coefficient B may be shortened by rewriting Equation [31b] in the form

$$B = \frac{2\sin 2(\varphi - \alpha) + \gamma[1 + \cos 2(\varphi - \alpha)]}{1 - \frac{\gamma}{2}\tan(\varphi - \alpha)} \quad [37]$$

before multiplying the numerator and denominator by the expression $1 + (\gamma/2)\tan(\varphi - \alpha)$ in order to obtain

$$B = 2\gamma + 2\sin 2(\varphi - \alpha) \quad [38]$$

where again, the higher-ordered terms have been dropped.

When these shortened coefficients are introduced into Equation [32] the shear-angle relationship becomes, after dropping higher-ordered terms, simply

$$\tan\beta = \frac{-\gamma - \sin 2(\varphi - \alpha) \pm \sqrt{1 + 2\gamma\tan(\varphi - \alpha)}}{\cos 2(\varphi - \alpha) - 2\gamma\tan(\varphi - \alpha)} \quad [39a]$$

where, according to Equation [12]

$$\gamma = \left[1 - \left(\frac{r_1}{r_2}\right)^2\right]\frac{\cos(\varphi - \alpha)}{2\sin\varphi\cos\alpha} \quad [39b]$$

This expression for the shear-angle relationship applies only when the depth of cut is small enough or the internal radius of the workpiece is large enough to permit the use of the small-angle approximation for γ. Here, too, the positive sign should be used whenever $(\varphi - \alpha)$ is positive, whereas the negative sign should be used whenever $(\varphi - \alpha)$ is negative.

When γ is zero, Equation [39] with the positive sign[4] in front of the square root, may be written

$$\tan\beta = \frac{-\sin 2(\varphi - \alpha) + \sin\pi/2}{\cos 2(\varphi - \alpha) + \cos\pi/2} = \tan\frac{1}{2}\left[\frac{\pi}{2} - 2(\varphi - \alpha)\right] \quad [40]$$

from which we find

$$\varphi = \frac{\pi}{4} + \alpha - \beta \quad [41]$$

the shear-angle relationship for the limiting case. This is the same equation, derived independently, in references (3, 4). Certainly, this was to be expected. For as γ approaches zero, because the internal radius becomes infinitely large, the curved shear line becomes a straight line, and the configuration approaches that found for the planer or shaper operation.

Calculation of the Machining Force

In order to help visualize the relationship between the cutting force F_y and some of the independent parameters, the ratio F_y/kt_1, where t_1 is the initial depth of cut, will be plotted against the friction angle β for various physical configurations that may be encountered in practice. It is convenient in making such a study to rewrite the expression for the cutting force, previously given as Equation [24a], in the form

$$\frac{\cos(\varphi - \alpha)}{\cos\alpha}\left(1 - \frac{r_1}{r_2}\right)\frac{F_y}{kt_1} = -\left[\frac{p_2}{k} - 2\gamma\right]\cos(\varphi + \gamma) - \sin(\varphi + \gamma) + \frac{p_2}{k}\cos\varphi + \sin\varphi \quad [42]$$

so that we can solve directly for the required ratio.

Two sets of curves will be presented in this study. In the first set the effect of a change in the rake angle will be considered for a constant ratio r_2/r_1 of 1.10; whereas in the second set, the effect of changes in r_2/r_1 will be considered for a constant rake angle of 10 deg. These curves will be plotted against the friction angle β. In preparing these curves, it has been found more convenient to select an arbitrary value for φ and evaluate the corresponding friction angle rather than to choose the angle β directly, because of the form of the shear-angle relationship.

To complete one set of calculations, it is necessary to fix the ratio r_2/r_1, the rake angle α, and the shear angle φ. The angle γ is found by substituting these parameters into Equation [12] and the corresponding friction angle β is found by substituting the appropriate quantities into Equations [31] and [32]. Finally, the ratio F_y/kt_1 is obtained by introducing all the information into Equations [21] and [42].

The results of this type of calculation for a range in rake angle from —10 to +30 deg is shown in Fig. 5. An auxiliary scale was added to the abscissa in order to enable easy conversion from the friction angle to a more familiar term; namely, the coefficient of friction. It can be seen that the machining force increases with friction and decreases with increased rake angle.

The increase in machining force with friction continues until a critical value of friction is reached. Before this happens, frictional slip takes place along the tool surface and the shear stress on the element at the base of the tool, given by Equation [19], is less than k, the maximum shear stress of the chip material. At this critical value, however, the angle φ is equal to α and the shear stress τ is equal to k. The corresponding friction angle is, of course, still given by Equation [32], but the coefficients expressed in Equation [31] now simp'y read

[4] In view of the resulting shear-angle relationship, written $\varphi - \alpha = \pi/4 - \beta$ and the fact that β is always less than or equal to $\pi/4$ (see references 3, 4), $(\varphi - \alpha)$ is always positive for the limiting case.

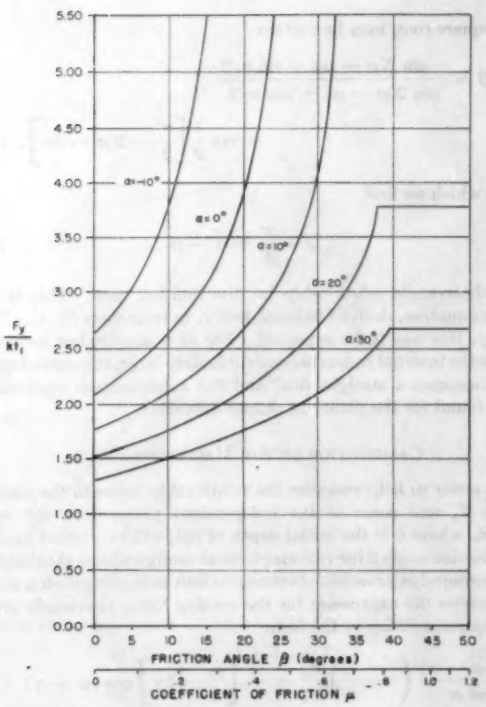

FIG. 5 MACHINING FORCE AS A FUNCTION OF FRICTION. $r_2/r_1 = 1.10$

$$A = \frac{2\gamma}{\tan \gamma} - 1, \quad B = 2\gamma, \quad C = 1 \ldots\ldots\ldots [43]$$

Beyond the critical value, shear flow takes place along the face of the tool and the machining force remains constant.

In Fig. 6 the effect of changes in the ratio r_2/r_1 was considered for a constant rake angle α equal to 10 deg. The steps taken to prepare these curves were similar to those previously described, with the exception of the one marked $r_2/r_1 = 1.00$. This curve represents the limit of the solution in which the curved shear line becomes a straight line. That problem, the planing operation, has already been studied (3, 4) and it was found that

$$\frac{F_y}{kt_1} = 1 + \cot\left(\frac{\pi}{4} - \beta + \alpha\right) \ldots\ldots\ldots [44]$$

Instead of seeking the limit of the equations previously derived Equation [44] may be used directly.

It can be seen in Fig. 6 that the machining force increases with friction and also increases as the ratio r_2/r_1 increases. If we think of this ratio as $1 + t_1/r_1$, where t_1 is the depth of cut, Fig. 6 shows that the machining force decreases as the internal radius of the workpiece increases.

In the computations described earlier in this section, numerical relationships were obtained between the shear angle φ and the friction angle β, for various rake angles and ratios of r_2/r_1. These results are of interest and have been reproduced in the next two figures.

Fig. 7 shows the effect on the shear angle of varying the rake angle from —10 deg to +30 deg while keeping the ratio r_2/r_1 const. It can be seen that the shear angle increases with an increase in rake angle and in general decreases with friction. For the larger rake angles this decrease continues until the critical

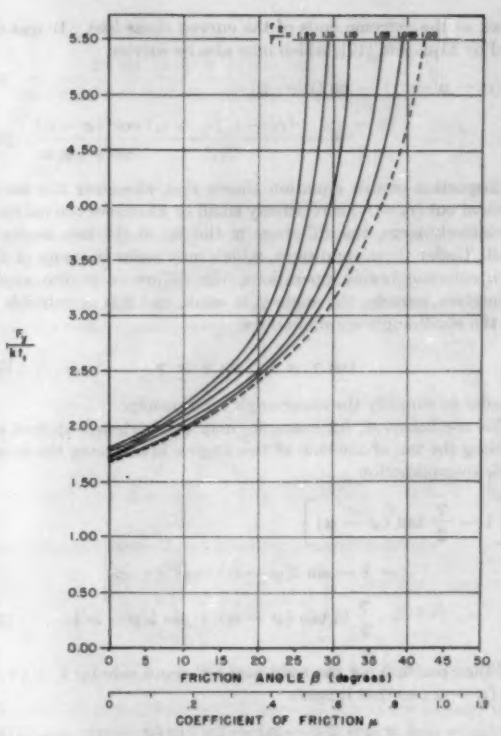

FIG. 6 MACHINING FORCE AS A FUNCTION OF FRICTION, RAKE ANGLE $\alpha = 10$ DEG

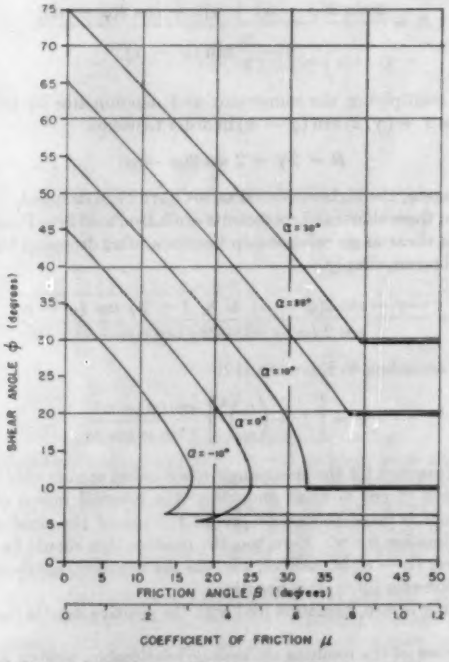

FIG. 7 SHEAR ANGLE AS A FUNCTION OF FRICTION, $r_2/r_1 = 1.10$

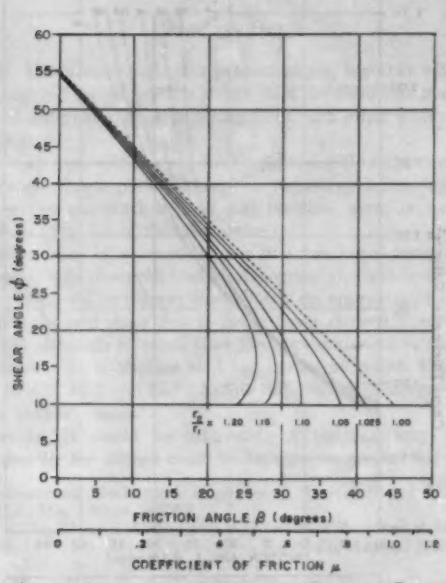

FIG. 8 SHEAR ANGLE AS A FUNCTION OF FRICTION, RAKE ANGLE α = 10 DEG

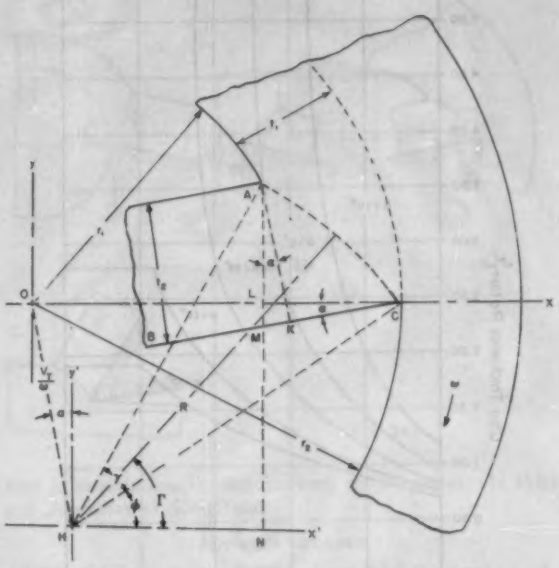

FIG. 9 CONSTRUCTION LINES TO DETERMINE CHIP-THICKNESS RATIO

friction angle is reached, at which point frictional slip, along the tool, changes to shear flow. Above these critical values no change in shear angle takes place and the results correspond to the ones shown in Fig. 5 for these same values of friction. For small or negative rake angles it appears that there can be two different shear angles for a given friction angle. At least the equations obtained in this paper show that such a result is possible if the solution is extended over the entire range of variables. It is felt, however, that this is not the case. In fact, because the corresponding force associated with the solution in this "unstable" range is extremely high, it is more than likely that a built-up nose (3) is formed. Consequently, the solution being presented here is no longer applicable within the range under discussion. Analysis of this phenomenon is beyond the scope of this paper but will be considered in a future publication.

Fig. 8 shows the effect on the shear angle of varying the ratio r_2/r_1 while keeping the rake angle constant. It can be seen that the shear angle increases as r_2/r_1 decreases. Here, too, we meet the unstable condition which implies that for a given friction angle we may have two different shear angles. It is felt that in practice this may not be the case, for the built-up nose probably would appear within this range.

THE CHIP-THICKNESS RATIO

The chip-thickness ratio is defined as the ratio between the final thickness of chip and initial depth of cut. It may be evaluated by studying the geometry of Fig. 9.

From point A, the intersection of the upper surface of the chip and the inner radius of the workpiece, drop a perpendicular to the face of the tool at point K, and one to the x'-axis at point N. These lines are α radians apart.

According to the geometry of Fig. 9, the final chip thickness

$$t_2 = (AL + LM)\cos\alpha \quad \ldots\ldots\ldots\ldots [45]$$

where

$$AL = R\sin(\varphi + \gamma) - \frac{V_t}{\omega}\cos\alpha \quad \ldots\ldots\ldots [46]$$

and

$$LM = \left\{r_2 - \left[\frac{V_t}{\omega}\sin\alpha + R\cos(\varphi + \gamma)\right]\right\}\tan\alpha \quad \ldots [47]$$

so that

$$t_2 = R\sin(\varphi + \gamma - \alpha) - \frac{V_t}{\omega} + r_2\sin\alpha \quad \ldots\ldots [48]$$

By introducing Equations [8] and [9], however, t_2 may be rewritten to read

$$t_2 = \frac{r_2\cos\alpha}{\cos(\varphi - \alpha)}[\sin(\varphi + \gamma - \alpha) - \sin(\varphi - \alpha)] \quad \ldots [49]$$

and, in view of Equation [12], the chip-thickness ratio may be written

$$\frac{t_2}{t_1} = \left[1 + \frac{r_1}{r_2}\right]\frac{\cos(\varphi - \alpha)}{2\sin\varphi} \quad \ldots\ldots\ldots [50]$$

where t_1 is the initial depth of cut, equal to $(r_2 - r_1)$.

In order to see how some of the parameters, encountered in the machining problem, affect the chip-thickness ratio, it has been plotted against friction for various physical configurations encountered in practice. In Fig. 10, where such a set of curves is shown, the ratio r_2/r_1 is kept constant at 1.10 while the rake angle is permitted to vary from —10 deg to +30 deg. As we can see, the chip-thickness ratio increases with friction and also increases as the rake angle decreases. The increase with friction continues until shear flow along the tool takes place and then remains constant.

In Fig. 11, where another set of curves show the relationship between t_2/t_1 and β, the rake angle is kept constant while the ratio r_2/r_1 varies from 1.00 to 1.20. Again, the case when r_2/r_1 is equal to 1.00 was taken directly from references (3, 4) to be

$$\frac{t_2}{t_1} = \frac{\cos(\pi/4 - \beta)}{\sin(\pi/4 - \beta + \alpha)} \quad \ldots\ldots\ldots\ldots [51]$$

It can be seen in Fig. 11 that for small values of friction the chip-thickness ratio decreases as r_2/r_1 increases; while for large values of friction the chip-thickness ratio increases as r_2/r_1 increases.

In the analysis just considered, each particle, within the uncut

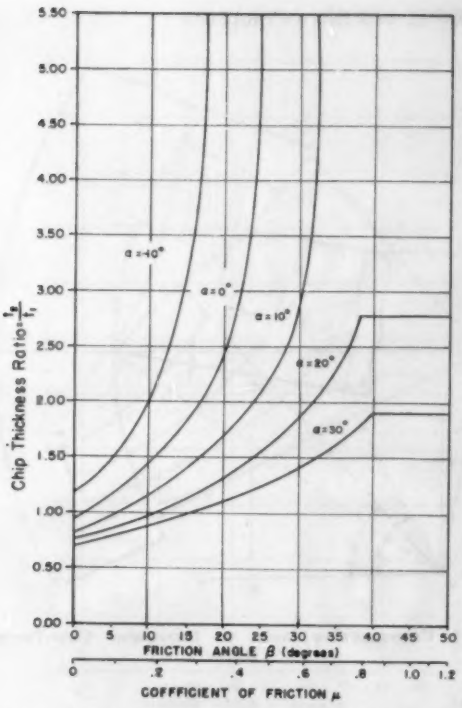

FIG. 10 CHIP-THICKNESS RATIO AS A FUNCTION OF FRICTION, $r_2/r_1 = 1.10$

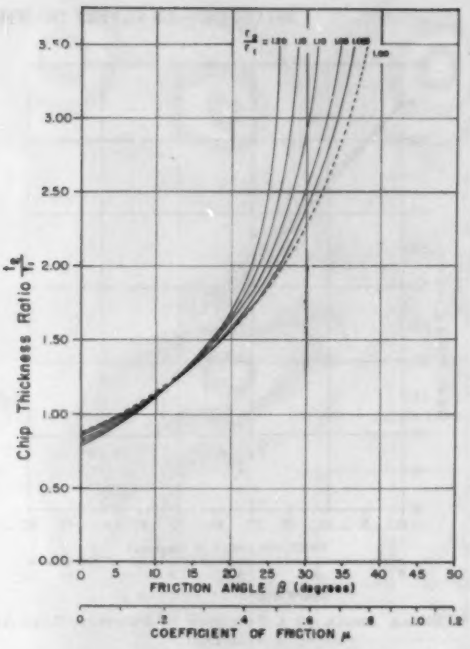

FIG. 11 CHIP-THICKNESS RATIO AS A FUNCTION OF FRICTION, RAKE ANGLE $\alpha = 10$ DEG

region and newly formed chip, moves as a rigid body. The uncut region rotates at a constant angular velocity ω while the newly formed chip translates at a constant linear velocity V_t. The two are related by Equation [8]. It is possible, therefore, to study the deformation of an initial grid engraved in the workpiece. This has been done, and is shown in Fig. 12 for the particular case: Rake angle equal to 10 deg, friction angle equal to 15 deg. It can be seen that initially straight radial lines become curved lines within the chip. Concentric circles become straight lines parallel to the face of the tool. The curved shear line separating the two rigid regions is also shown on this diagram.

CONCLUSION

It has been shown, in previous papers (3, 4), that the solution to the machining problem is given by that configuration which requires a minimum machining force and results in a satisfactory stress distribution within the chip. This principle, originally advanced as a solution to the planing or shaping operation, applies equally well to the boring operation.

From what we have seen, a complete analysis of the orthogonal boring operation will require more than the one solution considered here. If the orthogonal planing solution may be used as a guide toward what we might expect, there will be several solutions each of which applies over a limited range of variables. The present study, based on the idea that the element within the chip at the tip of the tool is most highly stressed, is but a step in that direction. It is felt, nevertheless, that even though this element may not always control, the solution presented here will play an important role in the over-all analysis of the orthogonal boring operation.

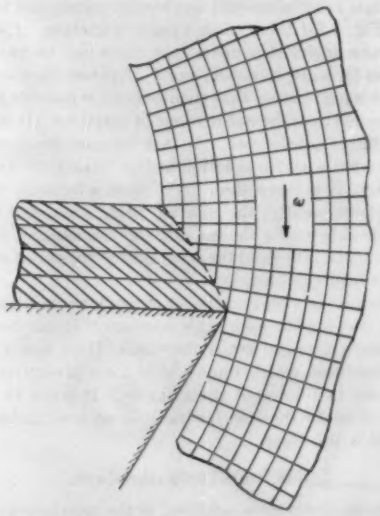

FIG. 12 DEFORMATION OF AN INITIAL GRID SYSTEM, RAKE ANGLE $\alpha = 10$ DEG, FRICTION ANGLE $\beta = 15$ DEG

BIBLIOGRAPHY

1 "The Effect of the Cutting Fluid Upon Chip-Tool Interface Temperature," by M. C. Shaw, J. D. Pigott, and L. P. Richardson, Trans. ASME, vol. 73, 1951, pp. 45–56.

2 "Basic Mechanics of the Metal-Cutting Process," by M. E. Merchant, *Journal of Applied Mechanics*, Trans. ASME, vol. 66, 1944, pp. A-168–175.

3 "The Theory of Plasticity Applied to a Problem of Machining," by E. H. Lee and B. W. Shaffer, *Journal of Applied Mechanics*, Trans. ASME, vol. 73, 1951, pp. 405–413.

4 "The Mechanics of the Simple Shearing Process During Orthogonal Machining," by B. W. Shaffer, Trans. ASME, vol. 77, April, 1955, pp. 331–336.

5 "Theory of Perfectly Plastic Solids," by W. Prager and P. G. Hodge, Jr., John Wiley & Sons, Inc., New York, N. Y., 1951, p. 126.

6 "Theory of Elasticity," by S. Timoshenko and J. N. Goodier, McGraw-Hill Book Company, Inc., New York, N. Y., 1951, pp. 13–17.

Discussion

E. K. Henriksen.[6] In the present paper, together with previous papers,[6] the author has shown that the shear line may take on three different shapes, differing from each other with respect to curvature.

One may say, with appropriate definitions, that the curvature of the shear line is positive, zero, or negative, depending upon whether the cut surface itself has positive, zero, or negative curvature (Fig. 13 of this discussion).

Another case of a curved shear line has been described by Merchant,[7] who observed that in orthogonal straight-line cutting the conventional rectilinear shear line is an approximation only, and that the real shear line in many cases showed a curvature (Fig. 14) although so small that the approximation is perfectly permissible. It is obvious that the curvature which Merchant refers to is of an origin and a nature different from the curvature in the author's cases.

However, it would be interesting if the plasticity theory developed by the author could be brought to explain the curvature in straight-line cutting observed by Merchant. Is there any possibility of doing this?

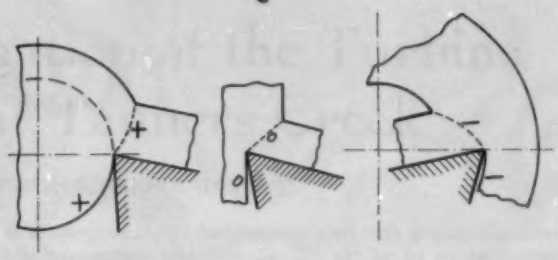

Fig. 13

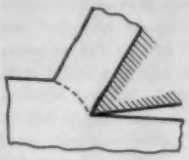

Fig. 14

Author's Closure

While it is true that a slightly curved shear line has been observed experimentally in orthogonal machining, the current theory which predicts a flat shear line does not offer an explanation for this phenomenon. It may be, as Professor Henriksen suggests, that an extension of the theory could be brought to explain the observed deviation.

[6] Professor of Mechanical Engineering, University of Missouri, Columbia, Mo. Mem. ASME.

[6] (a) "The Theory of Plasticity Applied to a Problem of Machining," by E. H. Lee and B. W. Shaffer, *Journal of Applied Mechanics*, Trans. ASME, vol. 73, 1951, pp. 405–413.

(b) "The Mechanics of the Simple Shearing Process During Orthogonal Machining," by B. W. Shaffer, Trans. ASME, vol. 77, 1955, pp. 331–336.

(c) "Analysis of Chip Formation in the Turning Operation," by B. W. Shaffer, Proceedings of the Second U. S. National Congress of Applied Mechanics, June 12–14, 1954.

[7] "Chip Formation, Friction and Finish," by Hans Ernst and M. E. Merchant, The Cincinnati Milling Machine Company, 1940.

Report of the Investigation of the Turbine Wheel Fracture at Tanners Creek

By A. W. RANKIN[1] and B. R. SEGUIN,[2] SCHENECTADY, N. Y.

In this paper the authors discuss the steam turbine wheel fracture which occurred at Tanners Creek early in 1953. The major parts of the investigation which was made to determine the cause of this fracture are presented together with the general conclusions.

Introduction

EARLY in January, 1953, the 1800-rpm low-pressure turbine of the No. 1 unit at the Tanners Creek Station of the Indiana and Michigan Electric Company suddenly went into violent vibration. The front standard—which contains the No. 1 bearing, the thrust bearing, hydraulic cylinder, and governing mechanism—cracked, and the resulting oil leakage caused a fire within the station. When the turbine was opened for inspection, it was found that a segment of approximately 100 deg had broken out of the first-stage (reheat) wheel of the intermediate-pressure turbine. The following is a report of the major investigations which have been conducted on this fracture, together with a summary of the significant conclusions.

Conclusions and Improvements

A review of the results of all the investigations conducted on this turbine rotor indicate that the most probable cause of this fracture was a combination of residual stresses which were not removed by the tempering and stress-relief heat-treatments, an unusually low long-time high-temperature ductility, and thermal stressing of the first-stage wheel resulting from admission into the first-stage wheel space of wet steam from the steam-seal regulator piping. Improved practices have been introduced to avoid the recurrence of difficulties due to any of these contributing causes: Specifically, residual stresses are now measured on all rotor forgings prior to machining; a modified heat-treatment has been introduced to give better long-time high-temperature ductility, although at some sacrifice in high-temperature strength; and the piping of steam-seal regulators has been modified to minimize the possibility of wet steam thermally stressing the rotor wheels. As is presented later in this paper, the modifications of the regulator piping were introduced a number of months before the Tanners Creek fracture when rapid temperature drops were observed in the leak-off pipes of the No. 1 packing of a duplicate unit during load-dump tests.

The fracture originated at the two holes in the wheel rim through which the notch bucket is attached to the wheel, and an improved notch assembly has been developed in which such pinning is not required. The developments and investigations aimed at producing a turbine-rotor steel with greatly improved high-temperature long-time ductility are by no means limited to the change in heat-treating temperatures; the effects of significant changes in alloy composition together with liquid quenching from the austenitizing temperature are also being investigated on full-size turbine rotors. In addition, the effects of vacuum pouring of the rotor ingot are also being investigated on a full-size turbine rotor to determine if this practice, in addition to the improvements in room-temperature properties expected from this innovation, will also produce an improved high-temperature ductility.

In the several months immediately following the Tanners Creek fracture, all duplicate units were inspected thoroughly; in particular, the notch buckets were removed from the first-stage wheels and a direct inspection made of the wheel rims in the vicinity of the notch opening. No signs of any incipient troubles whatsoever were found in these inspections. It should be noted that the No. 1 unit at the Philip Sporn station of the American Gas and Electric Company system, which unit is identical to the Tanners Creek No. 1 unit, had experienced an overspeed of between 40 and 50 per cent several months prior to the subject fracture, and later inspection of this unit showed no signs of trouble except for the loss of some bucket covers in one of the latter stages and rubbing of the root spill strips on the first-stage (reheat) buckets.

The presence of residual stresses seems to be one of the major contributing causes of this wheel fracture and, as previously stated, has resulted in the policy of measuring such stresses on all rotor forgings prior to machining. The results of such measurements on a number of rotors produced since the Tanners Creek fracture indicate that the residual stresses in the latter were unusually high and, in particular, are not representative of the results normally obtained with this alloy or its manufacturing practice.

General Description

The Tanners Creek unit No. 1 is rated at 125,000 kw, and is of the cross-compound 3600/1800-rpm type. The 3600-rpm high-pressure turbine receives steam at 2000 psig, 1050 F; the 1800-rpm low-pressure turbine receives reheated steam at 390 psig, 1000 F, and consists of an intermediate-pressure single-flow element followed by a low-pressure double-flow element. A cross section of the low-pressure turbine is shown in Fig. 1. This unit was one of seven identical General Electric turbine-generators purchased for the American Gas and Electric power system and put in service between July, 1949, and November, 1952; this particular unit was put in service in March, 1951. All these units had been designed and manufactured with conservative stresses, and with design and manufacturing practices proved on a large number of steam turbines. In particular, this is the first wheel fracture which has ever occurred on a General Electric turbine in which the wheels are integral with the shaft, and this type of construction has been used for approximately 26 years on a very large number of units.

A sketch of the line of fracture of the wheel is shown in Fig. 2 while a photograph of the broken wheel itself, after it was machined from the shaft, is shown in Fig. 3. In the latter figure the

[1] Structural Engineering Unit, Steam Turbine Engineering, Large Steam Turbine-Generator Department, General Electric Company. Mem. ASME.

[2] Structural Engineering Unit, Steam Turbine Engineering, Large Steam Turbine-Generator Department, General Electric Company.

Contributed by the Power Division and presented at a joint session of the Power and Metals Engineering Divisions at the Diamond Jubilee Annual Meeting, Chicago, Ill. November 13–18, 1955, of The American Society of Mechanical Engineers.

Note: Statements and opinions advanced in papers are to be understood as individual expressions of their authors and not those of the Society. Manuscript received at ASME Headquarters, October 18, 1955. Paper No. 55—A-210.

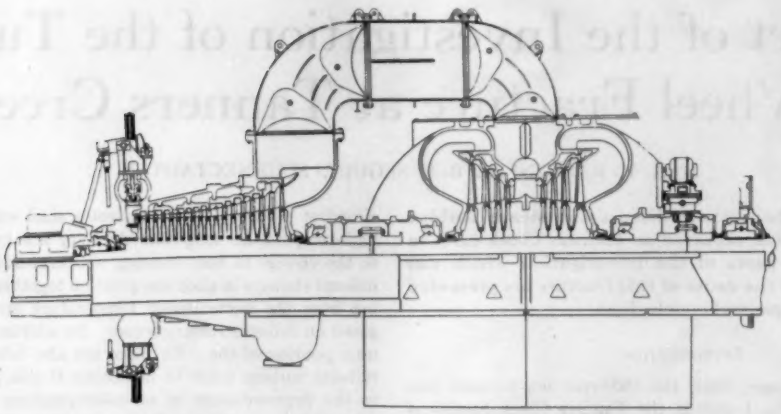

FIG. 1 CROSS SECTION OF TANNERS CREEK LOW-PRESSURE TURBINE SHOWING INTERMEDIATE AND LOW-PRESSURE ELEMENTS

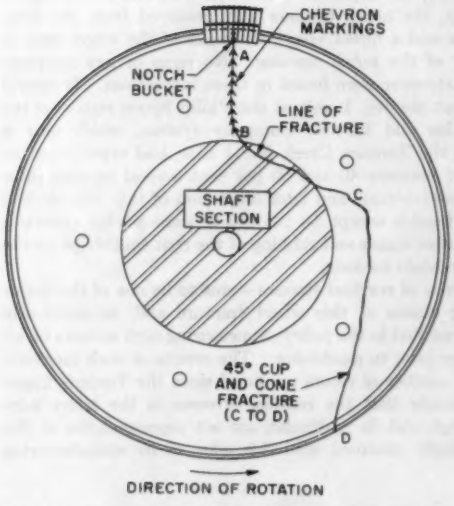

FIG. 2 SKETCH OF FIRST-STAGE WHEEL SHOWING LINE OF FRACTURE

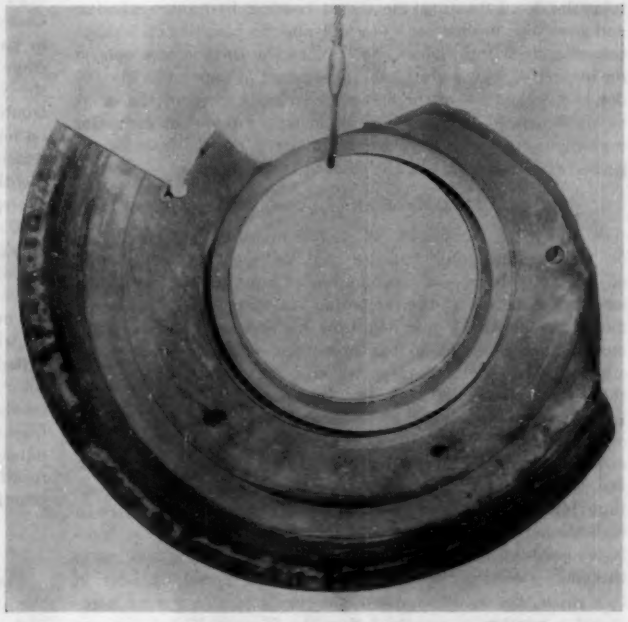

FIG. 3 VIEW OF BROKEN WHEEL AFTER MACHINING FROM SHAFT

outer periphery is the buckets which have been plugged and covered with metal melted from the buckets, covers, shell, and wheel fragment by the heat generated during rotation following the fracture. The notch opening of the wheel is located in the upper left of Fig. 3; it is missing in this figure because the rectangular section extending from the wheel rim and fracture surface down to the upper left steam-balance hole was cut from the wheel for initial investigations prior to removing the wheel from the shaft. It should be noted that the entire broken section of the wheel stayed within the turbine shell where it was essentially completely destroyed and melted by frictional impact while the shaft came to rest. The entire fracture surface was covered with a thin layer of this molten metal.

Referring to Fig. 2, the fracture consists of a radial break A-B from the two holes through which the notch bucket is pinned to the wheel down to the junction of the wheel and the integral shaft, thence B-C around the shaft between the high-pressure packing and the second-stage packing for about 60 deg, and then C-D outward along a spiral course terminating at the wheel rim about 160 deg from the notch opening. The radial portion A-B of the wheel fracture between the notch opening and the shaft section together with the shaft fracture B-C between the packings was flat and brittle with no evidence of distortion and no measurable reduction in thickness. Pronounced "chevron" markings, pointing toward the notch opening at the rim of the wheel, were present in the radial portion A-B of the fracture as shown in Fig. 4. The portion of the fracture C-D between the shaft and the wheel rim was a 45-deg shear break with a cup-and-cone appearance, but with no evidence of ductility or distortion. A distinct line of demarcation was visible at C between the flat brittle fracture and the 45-deg shear break; this is shown in Fig. 5.

Microexamination of sections perpendicular to the brittle-fracture surface A-B indicated that this was a high-temperature

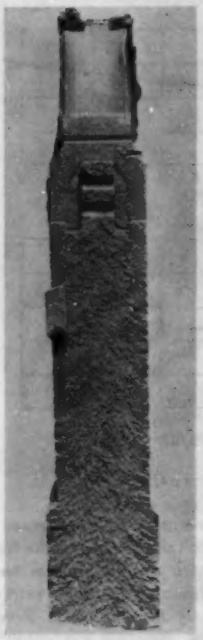

FIG. 4 PORTION OF RADIAL FRACTURE FACE OF FIG. 2 SHOWING CHEVRON MARKINGS

FIG. 5 VIEW OF POINT C OF FIG. 2 SHOWING DEMARKATION BETWEEN BRITTLE AND SHEAR FRACTURES

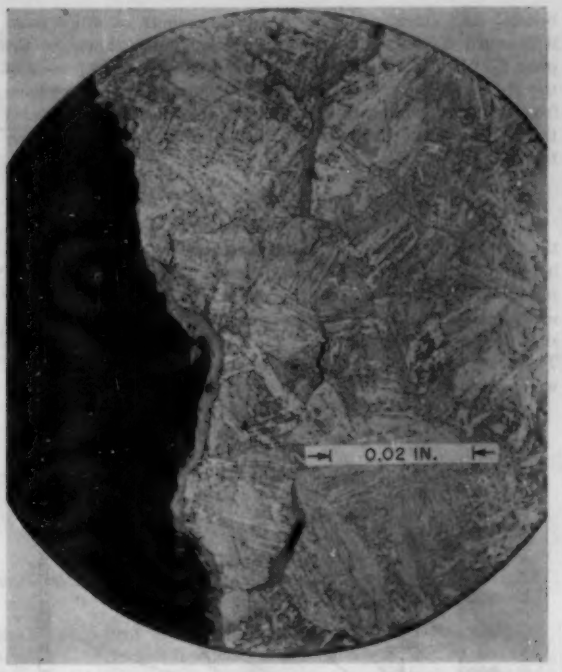

FIG. 6 PHOTOMICROGRAPH OF RADIAL FRACTURE

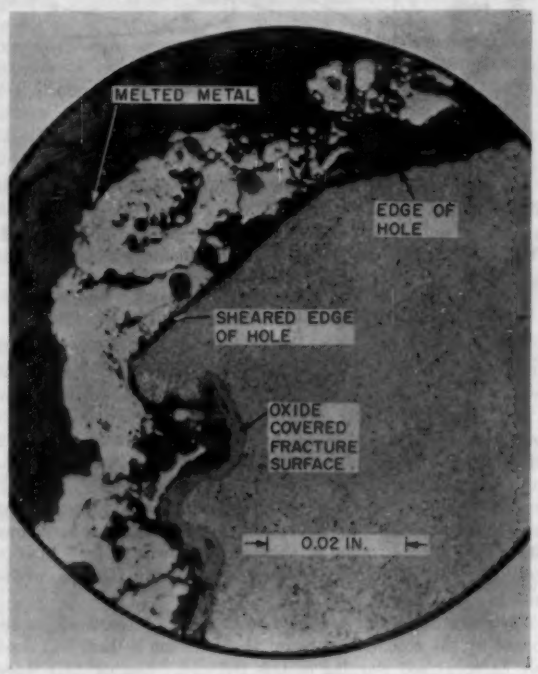

FIG. 7 PHOTOMICROGRAPH OF SHEARED PINHOLE

rupture break which progressed between grains along prior austenite grain boundaries, as shown in Fig. 6, with only a slight amount of intergranular secondary cracking. The general microstructure is bainitic, or acicular, as expected, with little variation from rim to shaft, and with carbides resolvable at X1000. The microstructure is normal for this alloy and heat-treatment, and there is no evidence of metallurgical defects or abnormal inclusion content. No evidence of fatigue could be found, either visually or by microscopic examination.

SEQUENCE OF FRACTURE

The chevrons shown in Fig. 4 indicate that the A-B portion of the wheel fracture originated in the region of the holes in the notch opening and progressed rapidly down to the shaft. The relatively heavy oxide coating indicated further that this portion of the fracture occurred some time before the final wheel fracture. That this oxide was caused by the operating temperature and not by the molten metal of the wheel fragment is shown by Fig. 7; this is a photomicrograph of a portion of the notch opening fracture showing the edge of a notch pinhole which was sheared over during the wheel fracture, thereby causing the oxide from previous service exposure to be removed. This sheared area was then covered with molten metal, and it can be seen that there is no oxide coating in this area as is present under the metal coating in the lower unsheared area. The uniform thickness of oxide coating found on the entire fracture surface A-B further indicated that this portion of the failure progressed rapidly some time before the final wheel fracture.

The oxide coating on the shaft fracture between the packings gradually diminished in thickness between points B and C indicating that here the fracture progressed much more slowly, although this portion of the fracture must also have occurred some time before the final wheel fracture. There was a complete absence of oxide on the fracture surface C-D, and the shear-fracture appearance indicated that this portion of the fracture occurred in a tearing manner.

The oxide coating thicknesses and chevron markings indicate that the fracture started in the notch opening and progressed

brittlely and quickly down to the integral shaft, at which point it changed direction and proceeded much more slowly to the point C. The A-B portion of the fracture together with most of the B-C portion occurred some time before the piece tore loose from the rest of the wheel. At point C bursting stresses equaled the 960 F rupture strength, at which time the entire wheel section tore loose.

Vibration Studies

Although no evidence of fatigue could be found at any point on the fracture surface, tests and analyses were made to determine if vibration could have contributed to this fracture. Vibration tests were conducted on the first-stage wheel of the spare rotor for these seven AG&E turbine sets, and the frequency curve shown in Fig. 8 was obtained. This rotor is a duplicate of the Tanners Creek, and no frequencies even close to running speed were obtained.

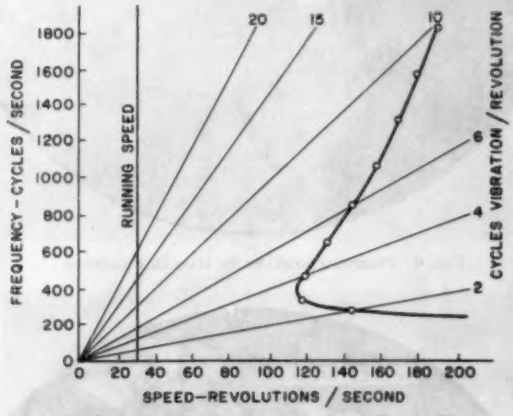

Fig. 8 Vibration Frequencies of First-Stage Wheel

Calculations were then made assuming an umbrella mode of vibration, but the calculated frequency was approximately 180 cycles per sec (cps), which is also well above running speed. The natural frequency for the mode in which the wheel vibrates radially inward and outward is approximately 1600 cps.

Review of Operating Records

As part of the general investigation to determine the cause of this fracture, a review was made of the supervisory-instrument records of both the high and low-pressure turbines to determine if any unusual operating conditions had been experienced. This review revealed that the unit had experienced 10 start-ups, 12 trip-outs, had been subjected to about 130 pressure perturbations caused by intercept-valve checking and boiler-slag removal, and in 46 instances the throttle temperature had changed at rates exceeding 300 deg F/hr, and in four instances exceeding 1000 deg F/hr. In none of these cases, however, were the operating conditions sufficiently severe to have caused damage to the unit.

Particular attention was paid to the shaft eccentricity as recorded by the eccentricity meter to determine if there had been any unrecognized warning of this fracture. During 1951 there was little variation in the shaft eccentricity but between January, 1952, and January, 1953, there was a gradual increase from 3 to 6 mils as is shown by the upper curve of Fig. 9. Thirty-five minutes before the fracture, there was a more rapid change in the eccentricity, with a decrease from 5.5 mils to 4.5 mils in twenty-five minutes, as is shown by the lower curve of Fig. 9. Ten

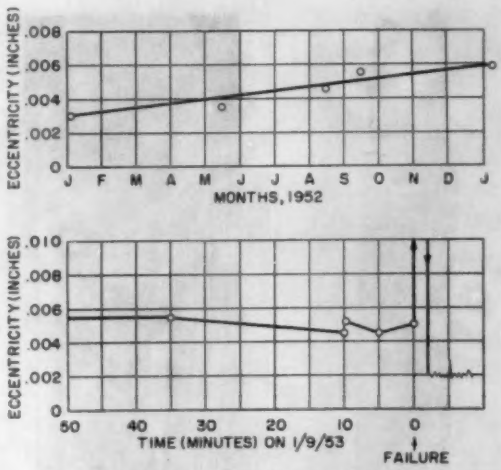

Fig. 9 Shaft Eccentricity Curves

minutes before the final fracture, there was a sudden increase to 5.2 mils, then a decrease to 4.5 mils five minutes before the fracture. During the last five minutes there was an increase back to 5 mils, and at the time of the final fracture the meter went off scale, returning to zero in approximately two minutes. Severe vibration of approximately two minutes' duration was noted at the same time on the high-pressure turbine.

Although this review of the eccentricity meter indicates that some changes were occurring in eccentricity approximately thirty-five minutes before the fracture, it should be noted that these changes were not of sufficient magnitude in themselves to justify tripping-out the turbine at the time they occurred since similar changes have been observed in other machines in which no trouble developed. It is possible, however, that in this particular instance the eccentricity changes were actually caused by the progression of the crack although it would have been impossible to so identify them before the final fracture because of their low magnitude.

Steam-Seal Regulator Piping

The function of the steam-seal regulator is to maintain a pressure of 1–3 psig at the gland leak-off of the high-pressure packing at all times. At start-up, the regulator furnishes steam to the packing to prevent air from entering the turbine, and, as the turbine builds up load, the steam regulator shuts off the high-pressure steam and unloads the increased flow of leak-off steam to maintain the pressure of 1–3 psig.

A particular feature of the steam-seal regulator piping and the possibility of its maloperation contributing to this fracture should be noted at this point. For approximately the first year of operation, the steam supply for the steam-seal regulator came from the intermediate superheater header, as shown in Fig. 10, and was drained by a trap. If this trap should fail, an appreciable quantity of water could build up in the line and would discharge through the steam-seal regulator on loss of load when the regulator opens to seal the turbine, unless the automatic valve for the steam jets opened first and drained the line. If the line is assumed to be drained adequately by the trap, the conditions would be less severe, but even in this case the steam temperature would drop rapidly because the temperature of the intermediate superheater header drops rapidly on loss of load. When 2000-psig saturated steam is throttled down to the required 5 psig, the steam temperature drops to 220 F and it becomes slightly wet. In either case, water or wet steam could have been

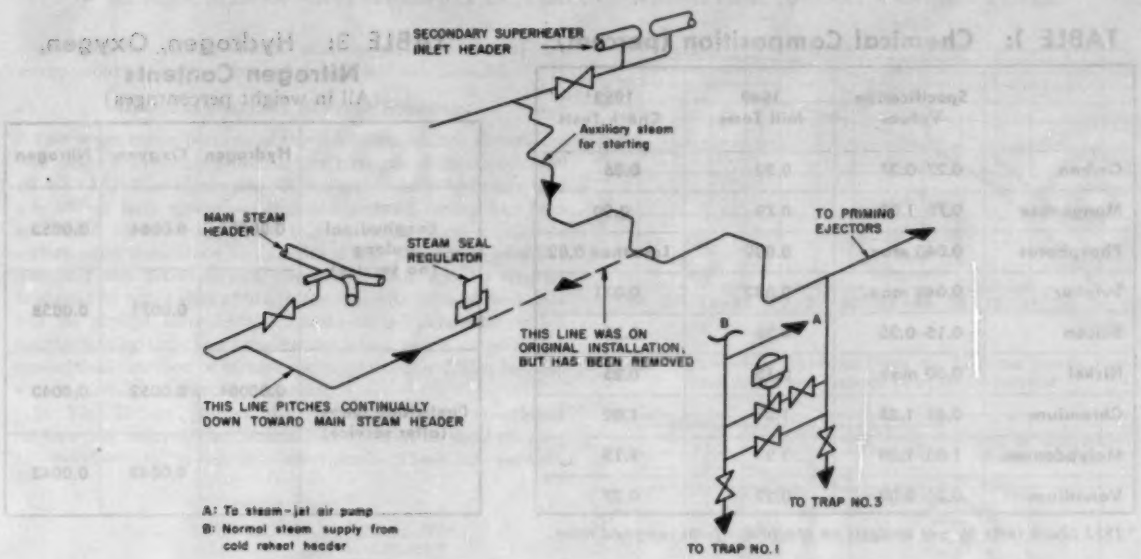
SECONDARY SUPERHEATER INLET HEADER
Auxiliary steam for starting
MAIN STEAM HEADER
STEAM SEAL REGULATOR
TO PRIMING EJECTORS
THIS LINE WAS ON ORIGINAL INSTALLATION, BUT HAS BEEN REMOVED
THIS LINE PITCHES CONTINUALLY DOWN TOWARD MAIN STEAM HEADER
B
A
TO TRAP NO. 3
TO TRAP NO. 1
A: To steam-jet air pump
B: Normal steam supply from cold reheat header

FIG. 10 INITIAL AND MODIFIED STEAM SUPPLY LINES FOR TURBINE STEAM SEALS

carried into the first-stage wheel space following trip-out, thereby causing severe thermal stresses in the wheel and reducing considerably the average wheel temperature.

Inspection of the Sporn No. 1 unit after its overspeeding revealed that the first-stage (reheat) covers were rubbed severely, and during subsequent load-dump tests a rapid drop in temperature was observed in the leak-off pipes from the No. 1 packing. This was attributed to the fact that the intermediate superheater header was used as the steam source for steam-seal regulator as discussed in the preceding paragraph. Following these load-dump tests, the steam-seal regulator piping of all units was changed, as shown in Fig. 10, so that the main steam line was used for the source of sealing steam, with the line sloped so as to be self-draining. This piping was changed on the Tanners Creek unit approximately a year before the wheel fracture, but for the entire preceding year the first-stage wheel could have been subjected to thermal shock following trip-out of the unit.

TURBINE-ROTOR FORGING

The ingot for the Tanners Creek rotor forging was cast in October, 1948, of acid open-hearth steel and the forging itself was accepted on physical properties early in 1949. Its chemical composition and final heat-treatment were in accordance with the General Electric specification which identifies a 0.3 C, 1 Cr, 1¼ Mo, ¼ V rotor alloy. With its rough-machined weight of 72,000 lb, length of 19 ft, and maximum diameter of 61 in., it was one of the largest forgings of this alloy ever produced for the General Electric Company. Fig. 11 shows the number and distribution by weight of all rotor forgings of this alloy which had been manufactured for the General Electric Company up to January, 1953.

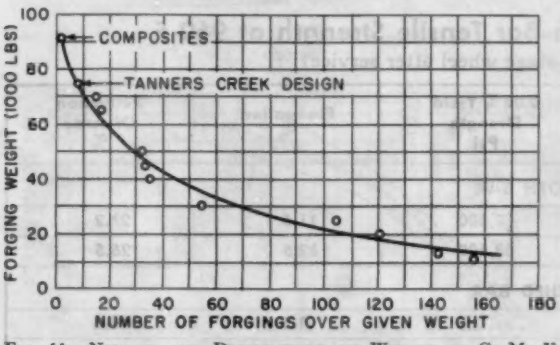

FIG. 11 NUMBER AND DISTRIBUTION BY WEIGHT OF CR-MO-V TURBINE ROTOR FORGINGS AS OF JANUARY, 1953

The specific heat-treatment for this Tanners Creek forging is shown in Fig. 12. The final solution treatment at 1850 F followed by tempering at 1250 F is in accordance with the General Electric specification for this steel. The chemical composition and room-temperature physical properties, as tested in 1949 and rechecked in 1953, are shown in Tables 1 and 2, respectively. All values are in accordance with the specification except for the elongation and reduction of area of the prolong specimen which are slightly under the expected values. This is not considered significant because of the difficulty of controlling the cooling on the small prolongation of a large forging. In addition, the elongation and reduction of area for the 1953 tangential-specimen tests are not considered unsatisfactory for specimens taken in this direction.

All of the normal quality-control tests were passed successfully, as is shown by the following tabulation:

Released on physicals, chemistry, microstructure	January 1949
Released on mill heat-indication test	February 1949
Released on ultrasonic examination	August 1949
Released on bore cleaning, inspection, and bore closure	September 1949
Released on magnetic-particle inspection	October 1949
Released on factory heat-indication test	November 1949

In addition to the elements detailed in Table 1, tests were made in 1953 to determine the hydrogen, nitrogen, and oxygen content, with the results as shown in Table 3. The tests marked "prolong" were taken from the rotor prolongation which was still available, while the tests marked "first stage" were taken from the first-stage wheel after the fracture. The hydrogen and nitrogen contents are representative for this class of forgings, as was

TABLE 1: Chemical Composition (percent)

	Specification Values	1949 Mill Tests	1953* Check Tests
Carbon	0.27–0.37	0.32	0.36
Manganese	0.70–1.00	0.79	0.90
Phosphorus	0.040 max.	0.031	Less than 0.02
Sulphur	0.045 max.	0.032	0.031
Silicon	0.15–0.35	0.26	0.26
Nickel	0.50 max.	0.15	0.25
Chromium	0.85–1.25	1.01	1.02
Molybdenum	1.00–1.50	1.23	1.13
Vanadium	0.20–0.30	0.22	0.27

** 1953 check tests by wet analysis on specimens from returned rotor.*

TABLE 3: Hydrogen, Oxygen, Nitrogen Contents

(All in weight percentages)

	Hydrogen	Oxgyen	Nitrogen
Longitudinal prolong (no service)	0.00005	0.0064	0.0053
	.....	0.0071	0.0058
First-stage wheel (after service)	0.00001	0.0052	0.0040
	.....	0.0042	0.0043

TABLE 2: Room Temperature Physical Properties

	Tensile Strength Psi	0.02% Yield Strength Psi	Elongation %	Reduction Of Area %
SPECIFICATION PROPERTIES				
Radial body	120,000	90,000	12.0	22.0
Longitudinal prolong	120,500	90,000	14.0	30.0
1949 ACCEPTANCE TESTS				
Radial body, at mill	130,500	99,000	13.0	29.2
Longitudinal prolong, at mill	136,000	104,500	12.5	29.2
Radial body, at GE	123,500	90,000	14.5	39.4
Longitudinal prolong, at GE	135,500	103,500	11.5	27.5
1953 CHECK TESTS (first-stage wheel)				
Radial body	133,900	101,700	12.0	22.3
Tangential	134,250	100,500	11.5	19.2

TABLE 4: Notched- and Smooth-Bar Tensile Strength at 960 F

(Specimens taken from first-stage wheel after service)

	Tensile Strength Psi	0.02% Yield Strength Psi	Elongation %	Reduction Of Area %
960 F SMOOTH BAR				
Radial	87,100	67,500	11.5	27.2
Tangential	86,600	63,500	12.5	26.5
960 F NOTCHED BAR				
Radial	126,000	.....	1.5	10.0
Tangential	126,000	.....	2.0	9.2

determined by making similar analyses on other rotors; the oxygen content appears somewhat high but not harmful.

High-Temperature Rupture Strength

One of the major portions of this investigation was the evaluation of the high-temperature rupture strength of this rotor steel after its 16,000 hr of service. It was particularly fortunate that a relatively large amount of high-temperature testing had been conducted on specimens from this particular forging prior to service since from these test results it was possible to establish definitely the before-service strength of this specific forging. It should be noted that although the majority of these test data will be plotted utilizing the Larson-Miller parameter which couples testing time and temperature into a single variable, the conventional method of stress-rupture plotting will also be used where possible or deemed necessary.

In Fig. 13 are plotted the high-temperature smooth-bar rupture data from all the General Electric tests on the 1 chrome, 1¼ molybdenum, ¼ vanadium rotor steel. These data were obtained from tests on 0.250-in-diam specimens conducted at temperatures ranging from 800 to 1350 F, and for test durations ranging from 1 to 16,442 hr. The two lines which encompass all the test points in Fig. 13 have been replotted in Fig. 14, and the points shown on this latter figure are the data from 20 rupture tests which were conducted on smooth-bar specimens taken from the Tanners Creek forging before its service installation. These 20 tests were conducted at temperatures ranging from 900 to 1300 F, and for times ranging from 26 to 7541 hr. Fig. 14 shows that the before-service strength of this rotor was well within the scatter band established for this material.

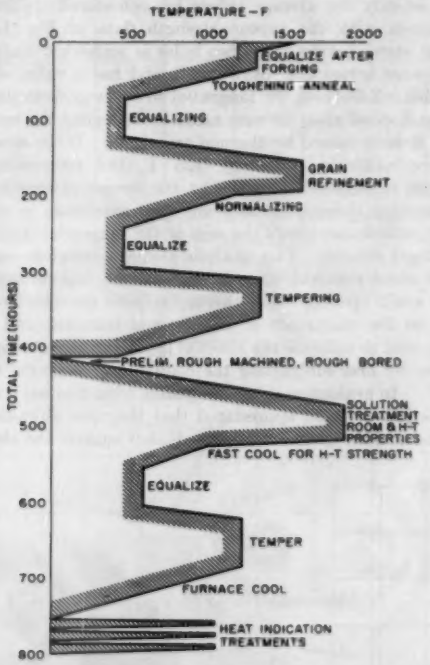

Fig. 12 Heat-Treating Cycle for Tanners Creek Rotor Forging

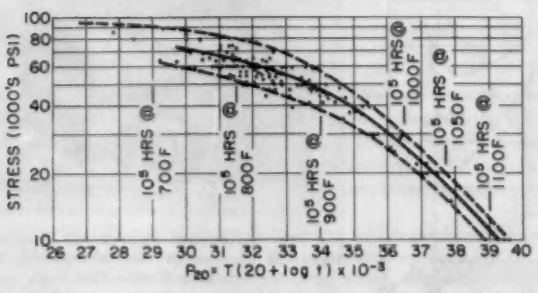

Fig. 13 High-Temperature Smooth-Bar Rupture Data on Cr-Mo-V Rotor Steel

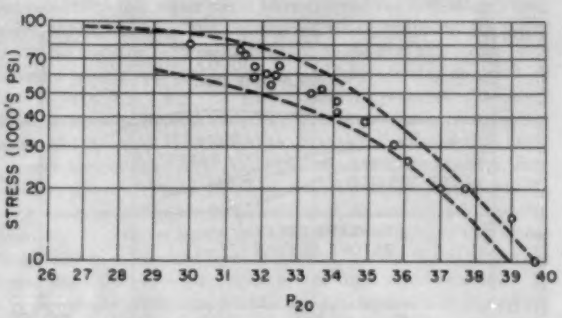

Fig. 14 Smooth-Bar Rupture Data on Tanners Creek Rotor Forging in the Before-Service Condition

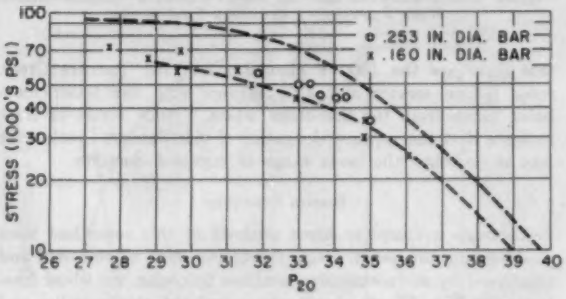

Fig. 15 Smooth-Bar Rupture Data on Tanners Creek Rotor Forging in the After-Service Condition

A number of rupture tests were conducted on smooth-bar specimens taken from the Tanners Creek rotor after the fracture, and the results of these tests are shown in Fig. 15 together with the range lines of Fig. 13. The circles are the results of tests on 0.250-in-diam specimens conducted at 1000 and 1050 F for times ranging from 71 to 9375 hr; the crosses are the results of tests on 0.160-in-diam specimens conducted at temperatures between 960 and 1175 F but for time ranging from 15 min to 173 hr. Although some of the crosses are slightly below the lower range lines, experience with parameter testing indicates that this is probably a result of the short testing times rather than an indication of material deterioration; this is substantiated by the long-time test results shown by the circles which are well within the range lines.

While the foregoing series of tests indicates that the before-service and after-service smooth-bar rupture strengths of this rotor agree with the values expected of this alloy, a similar unqualified conclusion could not be drawn with respect to the rupture elongation. A review was made of the long-time rupture tests conducted on specimens from six forgings of the same alloy as the Tanners Creek, and the spread in 1000 F rupture elongation obtained in these tests, of which some were conducted beyond 10,000 hr, is shown in Fig. 16 Also .shown in

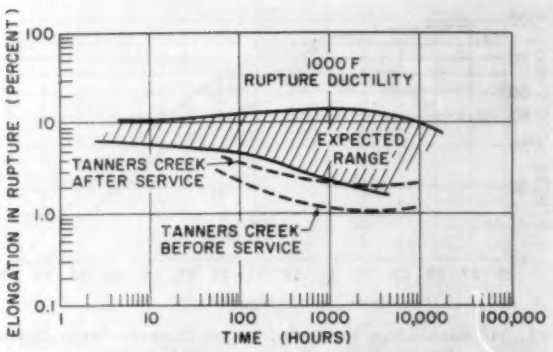

FIG. 16 1000 F RUPTURE ELONGATION OF TANNERS CREEK FORGING WITH EXPECTED RANGE FOR THIS ALLOY

this figure are the 1000 F elongations of the Tanners Creek rotor before service and after service with the latter tests being taken from the first-stage wheel. Both series of tests indicate that the rupture elongation of this Tanners Creek rotor was at or below the lower range of expected ductility.

ROTOR STRESSES

Although a complete stress analysis of this rotor had been made during the design stage, the figures were all reviewed and reinforced by more extensive analyses following the wheel fracture. In Fig. 17 are shown the calculated elastic radial and tangential stresses through the first-stage wheel caused by centrifugal forces, and comparison of these with the rupture-strength data of Fig. 14 shows quite conservative safety factors on these particular stresses. No local stress-concentration factors are included in this particular analysis, except for the effect of the central bore hole, because of the effect of creep in causing stress concentrations to relax at high temperature. The low value of average bursting stress should be noted particularly since previous publications have indicated that this is one of the major controlling factors in wheel bursting.

A section through the center of the notch opening, and through the holes which are drilled in the notch opening for pinning the notch bucket to the wheel, is shown in Fig. 18. Referring to the calculated stresses of Fig. 17, the tangential stress in the rim is 5500 psi, but this assumes complete continuity of the rim cross section through the notch opening, and accordingly must be increased to obtain the tangential stress at the notch opening where the rim cross section is reduced by the drilled holes and removal of the hooks. To determine the magnitude of this stress increase, recourse was had to photoelastic analysis to determine the complete stress configuration at the notch. A photograph of the photoelastic test specimen is shown in Fig. 19, while the tangential stresses through the notch opening (based on 5500-psi tangential rim stress at a distance from the notch) are shown in Fig. 20. The average tangential stress in the notch-opening region is approximately 2.0 times the tangential stress in the rim region away from the notch, and this corresponds to the reduction in rim area due to cutting away the hooks and drilling the two holes. Once again, it should be permissible to ignore local stress concentrations at the holes because of high-temperature creep, so only the average values are considered applicable for comparison with the rupture-strength data in Fig. 14. The average stress between the two holes is somewhat higher than the average across the entire notch, and has a value of 14,000 psi which is 2.54 times the tangential stress away from the notch.

Several stress analyses were made to determine the magnitude of the stresses caused by thermal transients. If the steam temperature suddenly drops by 125 F, the temperature distribution throughout the wheel at the instant of time at which the resulting thermal stresses are their maximum is shown in Fig. 21, which also shows the sum of the tangential thermal and centrifugal stresses. This analysis assumes complete continuity of the wheel rim and does not include the higher local stress at the notch opening. The thermal stresses are directly proportional to the magnitude of the thermal transient and Fig. 21 can be used to estimate the effect of greater or lesser temperature changes by first subtracting the centrifugal tangential stress of Fig. 17. In evaluating stresses resulting from thermal transients, however, it must be appreciated that they are short-time phenomena and as such must be evaluated against the short-time

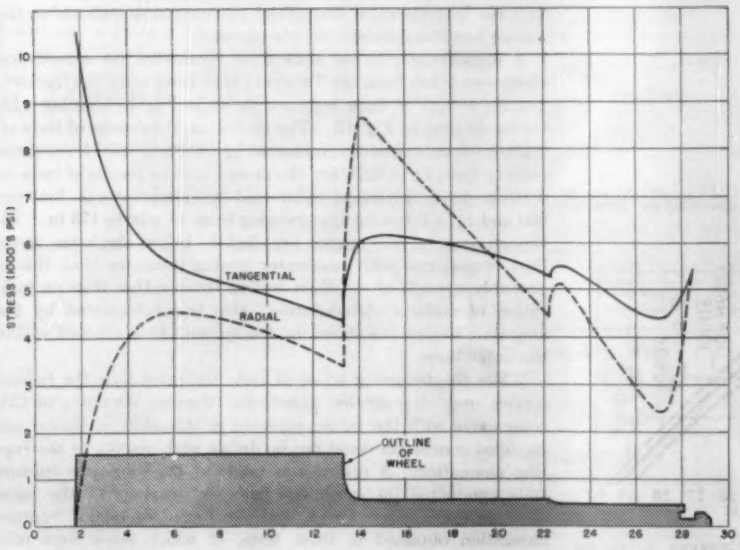

FIG. 17 CALCULATED CENTRIFUGAL STRESSES IN FIRST-STAGE WHEEL

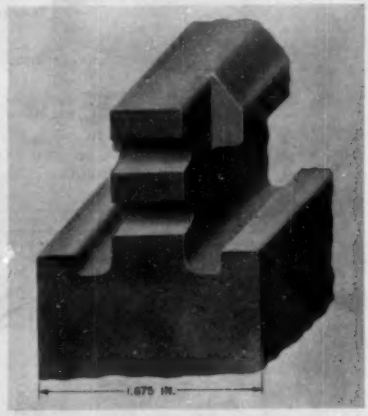

FIG. 18 ISOMETRIC SKETCH OF SECTION THROUGH CENTER OF NOTCH OPENING IN TURBINE-WHEEL RIM

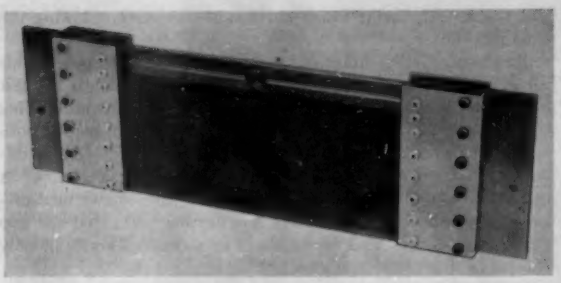

FIG. 19 VIEW OF PHOTOELASTIC TEST SPECIMEN OF WHEEL RIM

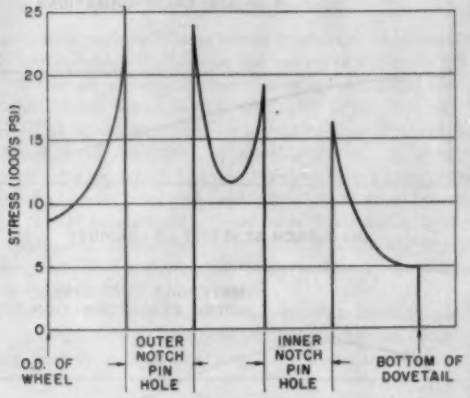

FIG. 20 TANGENTIAL STRESSES THROUGH CENTER OF NOTCH OPENING AS DETERMINED BY PHOTOELASTIC TESTS

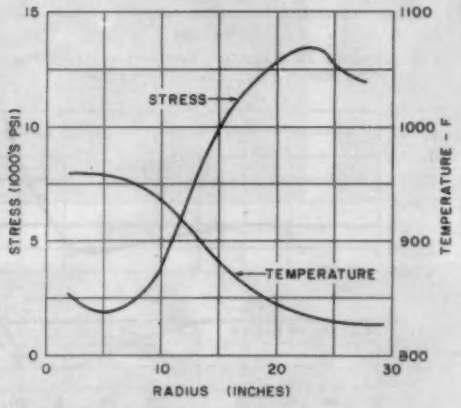

FIG. 21 TEMPERATURE AND STRESSES IN TURBINE WHEEL FOR 125 F DECREASE IN STEAM TEMPERATURE

strength of the rotor steel. Accordingly, Table 4 lists the results of 960 F tensile tests conducted on both smooth-bar and notched-bar specimens taken from the Tanners Creek rotor after the wheel fracture. These data indicate that the thermal stresses caused by a moderate drop in temperature are not sufficient to cause a wheel fracture.

A particular type of thermal transient which could result in relatively large stresses and at the same time appreciably cool the wheel could be caused by the water which might have condensed in the piping to the steam-seal regulator. During trip-out conditions this water could have entered the first-stage wheel space, through gaps in the packing segments created by the chilling of the packing, and calculations indicate that this could have caused a temperature difference through the wheel of as much as 560 F in 6 sec. Fig. 22 shows the temperature difference through the wheel under these conditions and the corresponding tangential stresses. In particular, it should be noted that such a severe temperature drop could conceivably carry the rim temperature down to a point at which a brittle fracture might result.

An analysis was made to determine if, in consideration of the relatively low stress levels employed in this design, the wheel could have been cracked from the notch opening down to the integral shaft for some time prior to the final wheel fracture. If it is assumed that no tangential stresses are present in the wheel itself, that is, that the centrifugal forces of the wheel and buckets are carried by radial restraints only, as would be the case if slotted radially, a radial stress of only 17,000 psi is obtained.

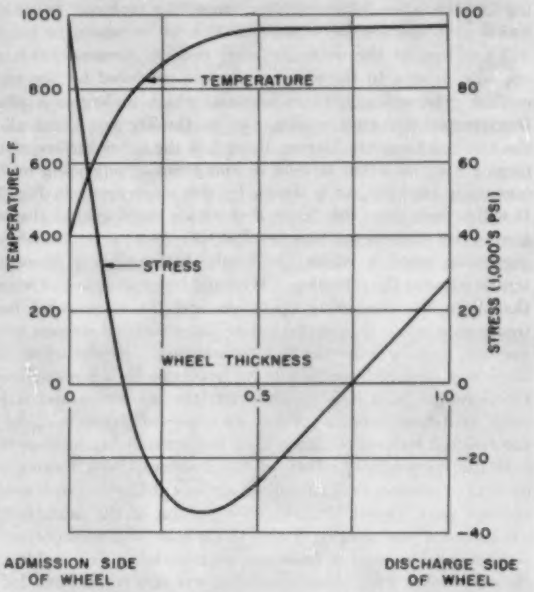

FIG. 22 CALCULATED TEMPERATURE AND STRESS DISTRIBUTION THROUGH FIRST-STAGE WHEEL UNDER ASSUMED TRIP-OUT CONDITIONS RESULTING IN WATER IN FIRST-STAGE WHEEL SPACE

Even if nominal stress concentrations exist at the root of the radial cuts, the foregoing calculated stresses indicate that the wheel could have operated satisfactorily for a reasonable length of time under such conditions. These results confirm the previously mentioned observations that the radial fracture from the notch opening down to the junction of the shaft existed for some time prior to the final wheel fracture.

Calculations also were made to determine if on a temperature increase the bucket temperature could lead the wheel temperature by an amount sufficient to cause the buckets to become arch-bound and thereby introduce an unexpected tensile stress in the wheel rim. Assuming no initial clearance between the buckets and wheel, a 100 F temperature difference between the buckets and wheel will increase the rim tangential stress only 10 per cent. It should be appreciated that the coefficient of thermal expansion of the 12 per cent chromium bucket material is slightly less than that of the ferritic wheel material, and accordingly it is difficult for the buckets to become arch-bound due to a temperature difference between the buckets and wheel.

Residual Stresses

The foregoing analysis of the centrifugal and possible thermal stresses indicates that, except for the severe thermal stresses which might have accompanied entrance of water through the packing following trip-out conditions, these are not sufficient to account for this wheel fracture. Accordingly, studies and investigations were initiated to determine if residual stresses could have been a contributing factor.

Rapid cooling, or quenching, of a cylinder from the outer surface may produce only residual tangential compression on the outer surface if the cylinder is made of a material which does not undergo a phase transformation. The magnitude of this residual compression is proportional to the quenching rapidity, as is shown schematically by the upper curve of Fig. 23. If the cylinder is made of a material which does undergo a phase transformation during cooling, the residual tangential stress at the outer surface may be either tension or compression depending on the quenching rapidity since the volume expansion which accompanies the transformation of austenite to bainite will produce, at the outer surfaces, residual stresses which are opposite in sign to the thermal stresses produced by the rapid cooling. Accordingly, for a material which undergoes a phase transformation during cooling, such as the Tanners Creek alloy, the residual tangential stress, if any, at the outer surface of the forging may be either tension or compression depending on the quenching rapidity, as is shown by the lower curve in Fig. 23. It will be seen from this figure that with a rapid quench the tangential rim stress is compressive, but there is a range of moderate quenching rapidity which can result in there being a residual tensile stress at the rotor rim. It should be appreciated, of course, that both the tempering operation and the stress-relief heat-treatments act to relieve and reduce these residual stresses which may be present following the normalizing. Nevertheless, this alloy was designed specifically to have excellent high-temperature strength, and it is possible that the tempering and stress-relief heat-treatments were not adequate to reduce sufficiently the residual stresses resulting from the normalizing treatment.

If the quenching rapidity of the Tanners Creek forging was such as to produce residual tensile stresses at the rim, or if similar stresses were caused by any other portion of the heat-treating cycle, and if the tempering and stress relief were insufficient to reduce these stresses to harmless magnitudes, it is possible that these, coupled with other operating stresses, could have led to this wheel fracture. Accordingly, several tests were conducted to determine the residual stresses in this rotor following the wheel fracture.

The first test, which was somewhat unplanned, occurred during the sectioning of the first-stage wheel for microscopic and physical studies. This first-stage wheel was parted from the rotor by cutting between the high-pressure packing and second-stage packing below the fractured surface, as was illustrated in Fig. 3. A radial cut was then made at the minimum remaining section, but before the saw had cut completely through the remaining area broke apart, presumably from the residual stress. The circumferential gap left by the break thereafter remained open by $^1/_{16}$ in. If this irregularly shaped wheel section were considered as a thin ring of 24-in. diam, which is the inner diameter after parting the wheel from the shaft, this $^1/_{16}$-in. gap would indicate a maximum residual stress of 24,500 psi. If the wheel section is considered as a thick ring of 24-in. ID and 60-in. OD, however, the residual stress would be 10,500 psi. The actual residual stress in this wheel section is probably intermediate between these two values, although it is obviously impossible to determine whether this residual stress is a consequence of the heat-treatment or was caused by the fracture itself and the molten metal which covered the buckets following the fracture.

To obtain further information on the residual stresses in this rotor, a 3-in. rim was cut from the 13th wheel, which is the last integral wheel on this rotor, with the five following wheels being shrunk on. The outside diameter of this rim was measured both before and after parting it from the wheel, with no detectable difference being found in these micrometer measurements. A radial cut was then made in this rim, and micrometer measurements over the cut showed that the cutting permitted the gap to open 0.078 in. This corresponds to a residual stress of only 630 psi in this 13th-stage wheel.

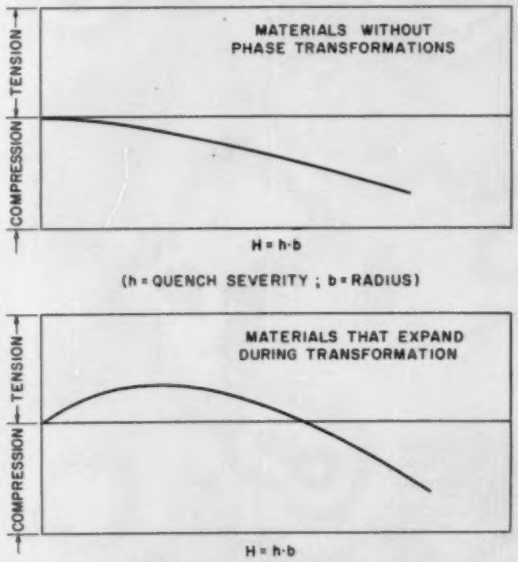

Fig. 23 Schematic Diagram of Tangential Rim Stresses in Cylinders Produced by Quenching

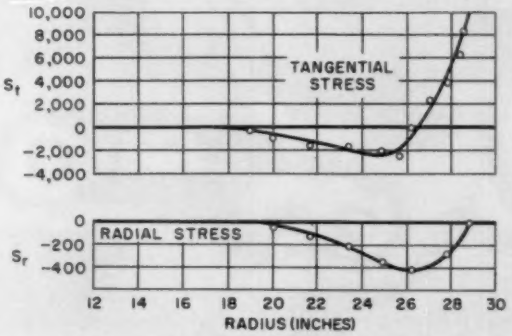

Fig. 24 Measured Residual Stresses in Tanners Creek Second-Stage Wheel

A much more precise measurement of residual stress was then conducted on the second-stage wheel. Twenty-six SR-4 strain gages were mounted at selected spots, and the wheel was then parted from the shaft and cut into nine concentric rings starting at the inner diameter. Diameter and circumference measurements together with strain-gage readings were taken before and after parting the wheel from the shaft, and before and after cutting each of the rings off. The nine concentric rings were subsequently parted by radial cuts with suitable measurements

being taken to detect the springing open of the rings from the radial cuts and the stress changes. Utilizing the diametral and circumferential measurements taken after cutting off the concentric rings, and assuming plane stress, the residual stresses were then calculated with the results shown in Fig. 24. A maximum residual tangential stress of 10,000 psi is obtained at the wheel rim, and when the centrifugal rim tension of 5500 psi is added to this and the 15,500 psi sum is multiplied by the notch-opening average concentration factor of 2.54, a stress is obtained, between the pinholes of the notch opening, of 39,400 psi. Referring to Fig. 15, it will be seen that this corresponds to the 16,000 hr 960 F rupture strength of the Tanners Creek rotor, which are, respectively, the service life and operating temperature of the fractured first-stage wheel.

Embrittlement Studies

The brittle portion of this wheel fracture was intergranular, which first focused attention on the nature of the grain boundaries. While no unusual features were noted when specimens from the broken wheel were etched with 2 per cent nital and examined at ×100, examination at higher magnification showed an almost continuous film of another phase. Etching with Zephrian chloride, which has been used to reveal temper brittleness in alloy steels, produced unusually distinct grain boundaries, and at ×1500 magnification these have finite width, due either to a continuous second phase or to a peculiar etching effect. Fig. 25 shows this grain-boundary distinction at three levels of magnification.

Specimens were then taken from another rotor (rotor 585), whose chemical composition and physical properties are given in Table 5, and these were examined metallographically, using the Zephrian-chloride etchant, after aging for up to 928 hr at 1000 F. The micrographs from these specimens are shown in Fig. 26 and they indicate that this grain-boundary film develops progressively with time; comparison with the right micrograph of Fig. 25 shows that the longer exposure time of the Tanners Creek specimen has resulted in a more pronounced grain-boundary film.

In continuation of the embrittlement investigations, the extracted carbides were studied by x-ray diffraction and chemical analysis. Identification of the carbide phases present was desired in order to determine if any unusual phase change occurred in service. The effect of prior heat-treatment and comparison of the phases in the Tanners Creek rotor with rotor 585 of the same alloy also was desired. Accordingly, samples were electrolytically digested to remove the metallic matrix and leave a residue of the carbide phase or phases. These carbides were then analyzed by x-ray diffraction with the following results:

Sample	Source and Treatment	Structure
A.....	Tanners Creek first-stage wheel	Fe_3C type
B.....	Prolong, rotor 585	Fe_3C type
C.....	Tanners Creek prolong	Fe_3C type

The x-ray diffraction patterns showed that the 16,000-hr 960-F service of the Tanners Creek rotor had not changed the carbide structures, and these were the same as those present in rotor 585.

Laboratory studies on the 1 Cr, 1¼ Mo, 0.2 V composition of the Tanners Creek rotor have shown that, when oil-quenched and tempered at 1300 F, what embrittlement did occur from further tempering would be a maximum around 1000 F which is close to the operating temperature of the Tanners Creek wheel.

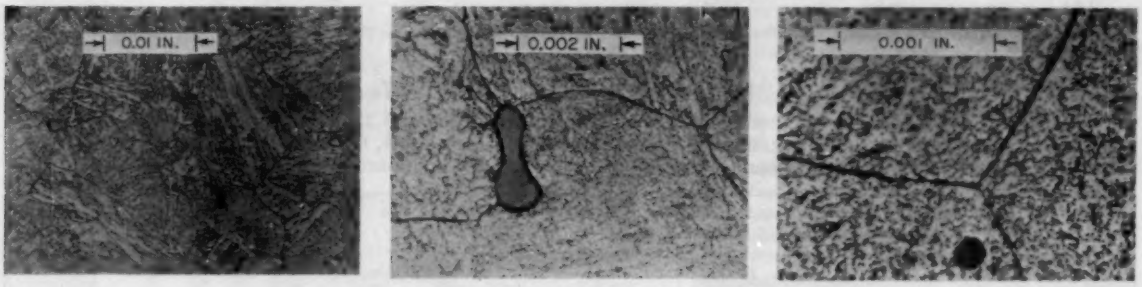

Fig. 25 Photomicrographs Showing Grain-Boundary Films in Tanners Creek Turbine Wheel

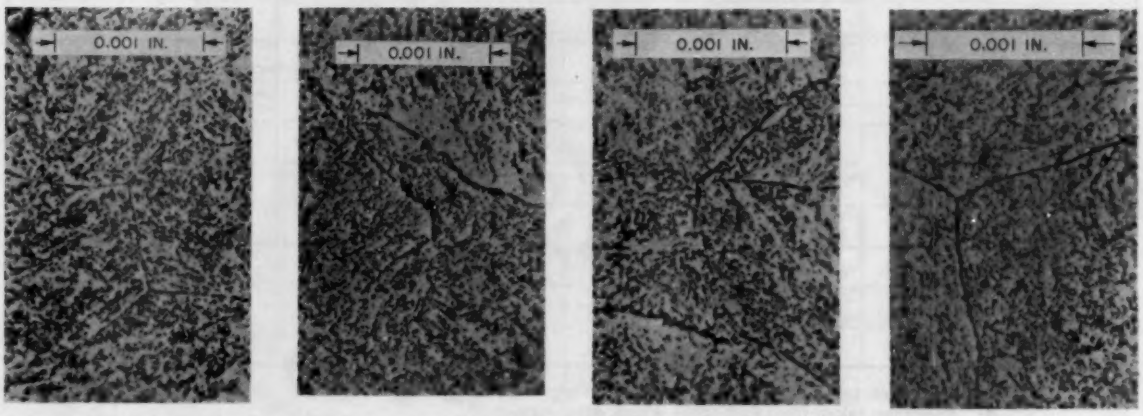

Fig. 26 Photomicrographs of Rotor 585 Showing Growth of Grain-Boundary Films After Various Exposure Times at 1000 F

TABLE 5: Rotor 585

CHEMICAL COMPOSITION (PERCENT)				ROOM-TEMPERATURE PHYSICAL PROPERTIES			
C	0.34	Si	0.31	Tensile Strength Psi	0.02% Yield Strength Psi	Elongation %	Reduction of Area %
Mn	0.80	Ni	0.24				
P	0.017	Cr	0.95				
S	0.014	Mo	1.25	127,000	98,500	16.5	47.7
V	0.25						

TABLE 6: Room-temperature Physical Properties

(Tests conducted on specimens from longitudinal prolong after flow rate and creep tests)

	Tensile Strength Psi	0.02% Yield Strength Psi	Elongation %	Reduction of Area %
	CONDITION			
A	131,000	100,000	10.7	15.1
B	137,200	109,200	12.0	18.9
C	135,200	107,200	7.0	8.0
D	134,500	105,800	2.5	4.5

A: After 2673 hours in flow-rate test at 1000 F
B: After 230 hours in creep test at 66,000 psi, 900 F
C: After 600 hours in creep test at 62,000 psi, 900 F
D: After 900 hours in creep test at 60,000 psi, 900 F

TABLE 7: Notched-bar Rupture Tests

(All tests were conducted at 1000 F with notch dimension of 0.357 in. major diameter, 0.253 in. minor diameter (50% notch), 60 degree notch angle, 0.005 in. notch radius, and 4.6 elastic stress concentration factor based on the minimum section.)

Condition	Stress Psi	Rupture Life Hours	P_{20}
A	70,000	20	31.1
A	62,000	46	31.6
A	50,000	262	32.7
A	40,000	252	32.7
A	40,000	382	32.9
A	35,000	214	32.6
A	30,000	716	34.2
B	50,000	94	32.1
B	40,000	378	32.9
B	30,000	1900	34.0
B	23,000	13403	35.2

A: Specimen taken from prolong, before service
B: Specimen taken from first-stage wheel, after service

This is shown by the iso-embrittlement diagram in Fig. 27 in which the co-ordinates are tempering temperature and time at that temperature. The numerical figures on this plot are the impact transition temperatures and the curves are lines of constant transition temperature. As is shown by this figure, tempering for 100 hr at 1000 F of this oil-quenched steel would raise the impact transition temperature from about —65 to —18 F. These data are not directly applicable to the air-cooled steel of the Tanners Creek rotor, whose transition temperature is around 200 F, although they do suggest that if embrittlement should occur it would be most severe around the 1000 F tempering level.

Another indication that service embrittlement might be a factor was found from the results of room-temperature tensile tests on specimens from the prolong of the Tanners Creek rotor after some high-stress creep tests. These data are shown in Table 6 from which it can be seen, by comparison with Table 2, that after 900 hr at 900 F in a 60,000-psi creep test, the room-temperature ductility had dropped from about 12 per cent elongation and 28 per cent reduction down to 2.5 per cent elongation and 4.5 per cent reduction. Such a severe loss in ductility was not found in the Tanners Creek rotor (as is shown in Table 2) since radial specimens taken from the first-stage wheel after the fracture gave ductility values of 12 per cent elongation and 22 per cent reduction as compared to the average before-service values of 14 per cent elongation and 34 per cent reduction. There was some loss in reduction of area, but this is by no means as serious as that shown in the high-load creep tests. In addition, notched-bar tests at 960 F gave a value of 10 per cent for reduction of area, which is quite satisfactory ductility for a notched-bar test.

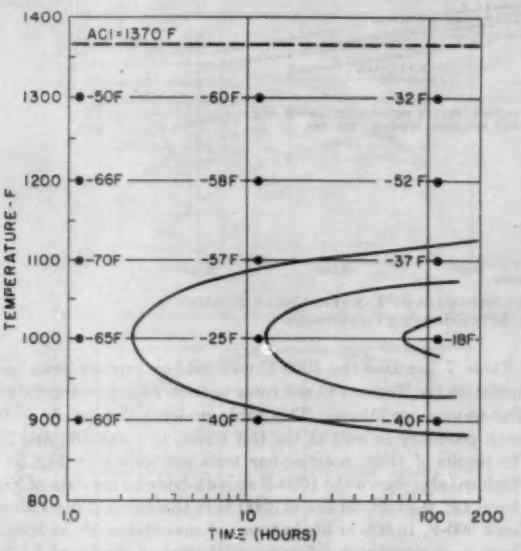

FIG. 27 ISOEMBRITTLEMENT DIAGRAM

A large number of Charpy impact tests were conducted on the Tanners Creek material with the results as shown in Fig. 28. As can be seen from this figure, these impact tests were conducted at temperatures ranging from 32 to 1200 F, on specimens of both the standard width of 0.394 in. (10 mm) and double width, and with both keyhole notches and 45-deg V-notches; all specimens were oriented in the tangential direction in both the first-stage wheel (after service) and the rotor prolong (before service). The curves in Fig. 28 indicate that exposure to the service conditions has not significantly modified the transition temperature, nor is any embrittlement shown by the comparison between the standard and double-width specimens. The transition temperature is above room temperature, but is well below the operating temperature.

In a further effort to determine if this rotor alloy would embrittle in service, material was taken from the prolong of rotor 585 and aged for various times at 1000 F. This latter temperature was selected because it is near the Tanners Creek 960 F operating temperature, and is at the point of severest embrittlement as shown in Fig. 27; and aging at 1000 F should be equivalent to accelerated prototype service at 960 F. Four series of V-notch Charpy impact tests were conducted on this aged material, with the results as plotted in Fig. 29 on which are also plotted V-notch Charpy impact data of specimens taken from the first, second, and thirteenth-stage wheels of the Tanners Creek rotor after service. This figure indicates that the 1000 F aging of rotor 585 produced no significant embrittlement, and that the impact strength of the Tanners Creek rotor agrees with that of rotor 585. In addition, comparison of the first, second, and thirteenth-stage wheels of the Tanners Creek rotor shows that the heating of the first-stage wheel during and following the fracture had not altered its impact strength.

A series of smooth-bar and notched-bar tensile tests at 70 and 960 F together with stress-rupture tests at 960 F for times out to 1000 hr were conducted on specimens from rotor 585 after aging at 1000 F for up to 1000 hr. No embrittlement due to this exposure at 1000 F could be detected in these tests.

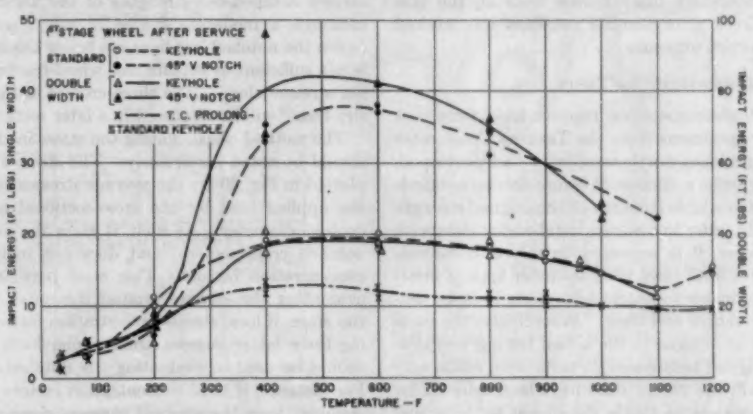

FIG. 28 CHARPY TRANSITION CURVES OF TANNERS CREEK ROTOR IN BEFORE-SERVICE AND AFTER-SERVICE CONDITIONS

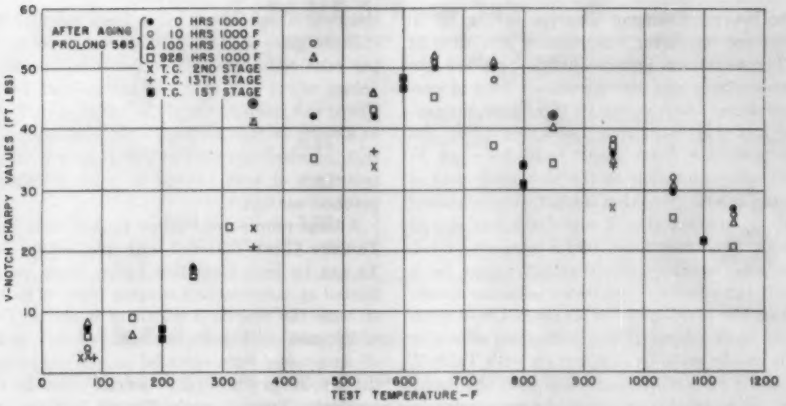

FIG. 29 EFFECT OF AGING ON CHARPY TRANSITION CURVES OF TANNERS CREEK ROTOR AND ROTOR 585

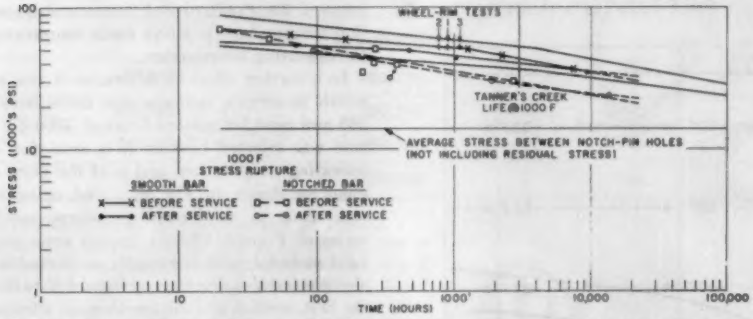

FIG. 30 SMOOTH-BAR AND NOTCHED-BAR RUPTURE STRENGTH OF TANNERS CREEK TURBINE ROTOR IN THE BEFORE-SERVICE AND AFTER-SERVICE CONDITIONS

Summarizing the results of the foregoing embrittlement studies, a grain-boundary film was noted on the Tanners Creek rotor, and experiments on rotor 585 showed that this developed progressively with time at temperature. The various physical tests, such as Charpy impact, smooth and notched tensile tests, and stress-rupture tests, did not reveal any effects of this film on the physical properties. The low ductility observed after the 900-hr, 60,000-psi, 900-F creep test probably resulted from the loss of total elongation incurred during the creep test and not as a result of the grain-boundary film; tensile tests on the first stage of the Tanners Creek rotor also did not show this marked loss in ductility after service exposure.

NOTCHED-RUPTURE TESTS

A large number of high-temperature rupture tests were conducted on notched-bar specimens from the Tanners Creek rotor to determine if any significant notch sensitivity had developed. As with the smooth-bar tests, a number of before-service notched-bar test specimens were available from which the original strength could be determined. In order to compare notched-bar data with smooth-bar data, however, it is necessary to resort to conventional log-log plotting for both since the parameter type of interpretation is not too applicable to notched-bar tests in large conversions between temperature and time. Accordingly, the comparisons must be made at or close to the actual testing temperatures and, since the original before-service tests were made only at 900, 1000, and 1100-F, the 1000-F data have been selected for the initial basis of comparison as this is the closest to the actual operating temperature of 960 F.

Table 7 itemizes the 1000-F notched-bar rupture tests conducted on the Tanners Creek rotor in both its before-service and after-service conditions. This table presents the details of the notch geometry as well as the test stress, temperature, and life. The results of these notched-bar tests are shown in Fig. 30 in which are also shown the 1000-F smooth-bar rupture data of Figs. 14 and 15; the vertical line at 3000 hr in this figure is the Tanners Creek 960-F, 16,000-hr life in terms of smooth-bar life at 1000 F. There is no significant difference in the before-service and after-service notched-bar strengths of the Tanners Creek rotor, and although a moderate degree of notch sensitivity is indicated (since the notched-bar lines are below the smooth-bar lines), this is not sufficient to explain this wheel fracture in terms of operating stresses alone. The three crosses in Fig. 30 marked "wheel-rim tests" will be discussed in a later section.

The method of calculating the stress in these notched-bar tests should be noted particularly. The stresses given in Table 7 and plotted in Fig. 30 are the average stresses as obtained by dividing the applied load by the cross-sectional area at the minimum (notch) diameter. As such, it gives the average stress over the notched cross section, and does not include any local stress-concentration factors. This is of particular importance when evaluating the stresses around the notch opening in the wheel rim since, if local stress-concentration factors are used in evaluating these latter stresses, then similar local concentration factors should be used in evaluating the notched-bar rupture strength. For instance, if local concentration factors are used at the notch opening, then the average stresses given in Table 7 should be multiplied by the local concentration factors of Table 7 to obtain

the comparable notched-bar rupture strength. It should be noted, however, that because of the creep which invariably occurs at high temperature, it is generally believed unnecessary to apply elastic stress-concentration factors to the design of high-temperature equipment.

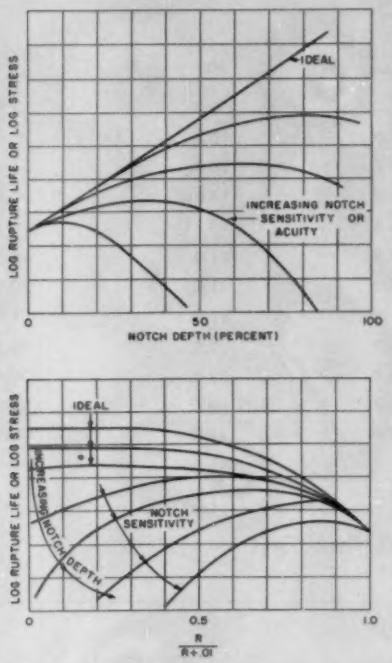

FIG. 31 SCHEMATIC DIAGRAMS ILLUSTRATING NOTCH SENSITIVITY

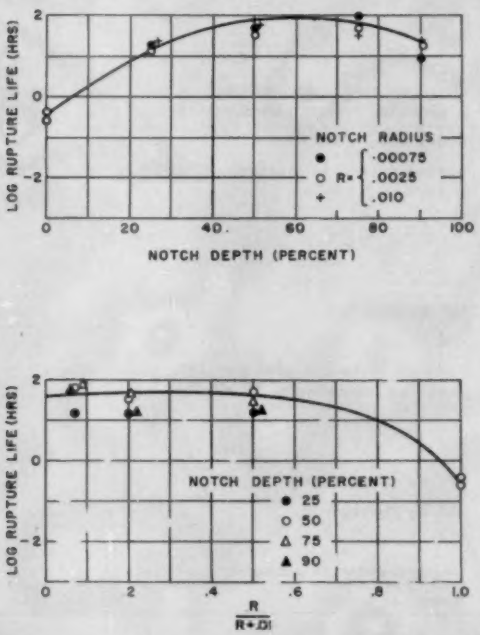

FIG. 32 EFFECT OF NOTCH RADIUS AND NOTCH DEPTH ON RUPTURE LIFE OF TANNERS CREEK TURBINE ROTOR

In Table 8 are given the pertinent data on a particular series of notched-bar tests designed to reveal any significant notch sensitivity of the Tanners Creek material which could be disclosed by short-time high-temperature testing; this test series is particularly interesting since it involves notch radii down to 0.00075 in. The behavior of materials ranging from fully notch-ductile to severely notch-sensitive is illustrated schematically in Fig. 31. The upper curves show how rupture life, or rupture strength, varies with notch depth as one progresses from a fully notch-ductile material to one which is severely notch-sensitive. Similarly, the lower curve illustrates how the rupture life, or rupture strength, varies with the fillet radius as the notch sensitivity increases. With such behavior established theoretically, the test series of Table 8 were planned to determine the degree of notch sensitivity of the Tanners Creek material. All these tests were conducted at a stress of 72,000 psi at 960 F corresponding to a P_{20} parameter value of 31.2 which, based on the middle of the range of test data from the smooth-bar tests, should give a life of 100 hr. In Fig. 32 have been plotted the results of this test series, and comparison of Figs. 31 and 32 shows that this material is only slightly notch-sensitive under these severe notch conditions.

SPECIAL PHYSICAL TESTS

In addition to the relatively classical physical tests, such as room and high-temperature tensile tests and stress-rupture tests of both smooth and notched bars, a number of special physical tests were conducted to more accurately evaluate the effects of either particular design features or possible service conditions.

To determine quickly whether the holes through which the notch bucket is pinned to the wheel could, by either their location or their size, appreciably reduce the high-temperature strength of this rotor, two tensile specimens were made in essential geometric similitude to the Tanners Creek first-stage wheel, particularly with respect to the holes in the wheel rim and their relation to the wheel diameter. A sketch of these specimens, together with the pertinent dimensional data, is shown in Fig. 33.

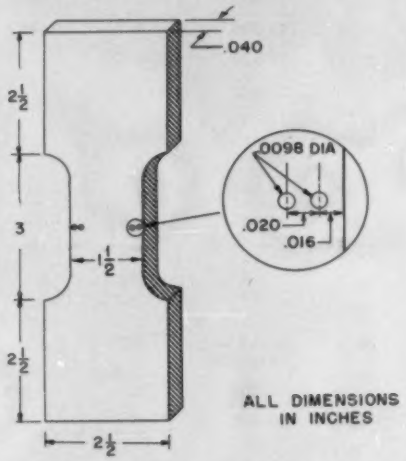

FIG. 33 HOT TENSILE-TEST SPECIMEN

Both these specimens were tested at 960 F; one specimen failed in 0.23 hr at 72,000 psi while the second failed in 71.6 hr at 58,000 psi. These holes had no significant effect on the strength of these specimens; both gave ductile fractures and lives and stresses correspond very well with what would be expected of smooth bars.

In an effort to duplicate the brittle fracture which occurred in

TABLE 8: Notched-bar Rupture Tests

All tests were conducted at 72,000 psi and 960 F, corresponding to a smooth-bar life at 960 F of 100 hours, on specimens taken from the first-stage wheel after service. All specimens were 0.160-in. major diameter notched to various depths with 60-degree V-notches of various radii. Elastic stress concentration factors are based on the minimum section.

Diameter	% Notch	Notch Radius	Stress Concen. Factor	Life Hours	P_{20}
0.160	0	.....	1.0	0.3	27.7
.160	0	.....	1.0	0.3	27.7
.138	25	0.010	2.7	20.0	30.2
.138	25	.0025	4.0	14.0	30.0
.138	25	.00075	6.6	17.2	30.1
.113	50	.010	2.8	51.0	30.8
.113	50	.0025	4.3	31.0	30.5
.113	50	.00075	7.2	61.8	30.9
.080	75	.010	2.5	30.5	30.5
.080	75	.0025	4.0	34.0	30.4
.080	75	.00075	6.7	89.5	31.2
.050	90	.010	2.0	21.5	30.3
.050	90	.0025	3.2	15.0	30.1
.050	90	.00075	5.4	61.0	30.9

TABLE 9: Tanners Creek Rim Test

(First-stage wheel material)

Test No.	Time Hours	960 F Longitudinal Load—Psi		960 F Pin Load—Psi		Comments
		Initial	Final	Initial	Final	
1	0	21,000	.....	9,600	.....	
	520	21,000	16,400	9,600	9,150	OK
	2812	21,000	16,800	.....	1,470	Disassembled—magnafluxed—crack found through pinholes—micro sample removed.
	3004	.....	.....	.....	.....	Crack into fillets.
	3672	.....	.....	.....	.....	Specimen broke—necked .007–.009 in. per side at edge of fracture.
2	0	21,000	.....	9,600	.....	
	500	21,000	16,000	9,600	8,060	OK
	1000	.....	.....	9,600	.....	OK by magnaflux.
	2000	.....	14,300	.....	6,200	OK by magnaflux.
	2504	.....	.....	.....	.....	OK visually.
	3004	Broke at 18,000 lb	17,000	...	0	Cracked between pinholes into body—X-ray. Broke on reloading at 18,000 lb.
3	0	21,000	.....	No pin load		
	500	21,000	17,000			OK
	1350	.....	.....	.....	.....	OK by magnaflux.
	2350	21,000	17,100	.....	.....	OK by magnaflux.
	2854	.....	.....	.....	.....	OK visually.
	3354	.....	17,900	.....	.....	Cracked between pinholes.
	4300	.....	.....	.....	.....	Specimen broke.

Cross-sectional area away from notch—.808 in.^{2}
Cross-sectional area at notch—.674 in.^{2}
Pinholes—.125 in. diameter
Center of gravity of unnotched section used as centerline of specimen

the Tanners Creek wheel, a large-specimen test was conducted with the dimensions restricted only to the largest solid section which could be obtained from the prolong of a rotor forging of the same specification as Tanners Creek, and the load capacity of the existing machines and fixtures. The test-specimen dimensions are as shown in Fig. 34 and a special furnace was built to accommodate this specimen. In order to introduce severe notched conditions, since brittle behavior of steel is also dependent on notch severity, the specimen was notched to one half of its unnotched area with the final notch root being cut by a jeweler's saw.

When subjected to a hot-tensile test at 960 F, failure occurred at 107,000 psi, which is sufficiently higher than the 87,000 psi (Table 4) at which smooth-bar specimens broke when tested at the same temperature to prove that no significant notch sensitivity was introduced by these severe size and notch conditions.

A particularly disturbing metallurgical feature of this Tanners Creek wheel fracture was the apparently rapid brittle progression of the radial portion of the fracture between the notch opening and the integral shaft. Accordingly, a series of bend tests were conducted to determine if this alloy showed any unusual tendency toward brittle-crack propagation. The specimens were standard V-notch Charpy bars machined out of material from the Tanners Creek first-stage wheel. These bars were placed in a tensile testing machine and bent away from the V-notch by the movement of the head of the testing machine. The head movement was held constant at 0.002 in/min, and applied force was plotted against the total travel as shown in Fig. 35. All the fractures, although intergranular, were accompanied by considerable distortion of the adjacent material. In particular, however, an increase in the energy was required to propagate the cracks as is shown by the slowly declining tails on the four curves of Fig. 35. A brittle-crack propagation, similar to that observed on Tanners Creek, would not have produced any gross distortion and, in particular, would have resulted in a sudden drop in the load-travel curves of Fig. 35.

Several tests were conducted on wedge-shaped samples to determine if cracking would be produced by repeated heat shocks of either moderate or extreme severity. Two wedge-shaped

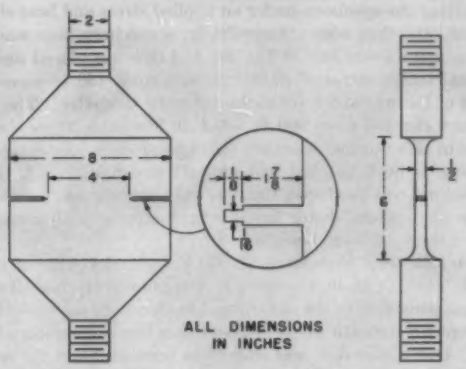

FIG. 34 LARGE NOTCHED HOT TENSILE-TEST SPECIMEN

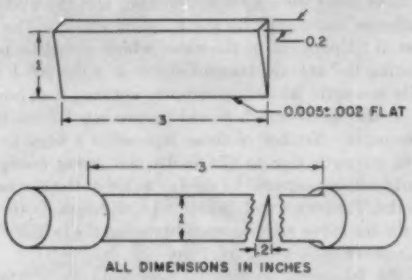

FIG. 36 SPECIMENS FOR HEAT-SHOCK TESTS

samples as shown in the upper half of Fig. 36 were constructed. One of these was cycled 50 times between lead baths at 960 and 830 F without producing any detectable cracking. The second such specimen was cycled 50 times between a lead bath at 960 F and a water bath at 70 F, and again no cracking could be detected. It was then postulated that cracking might be produced

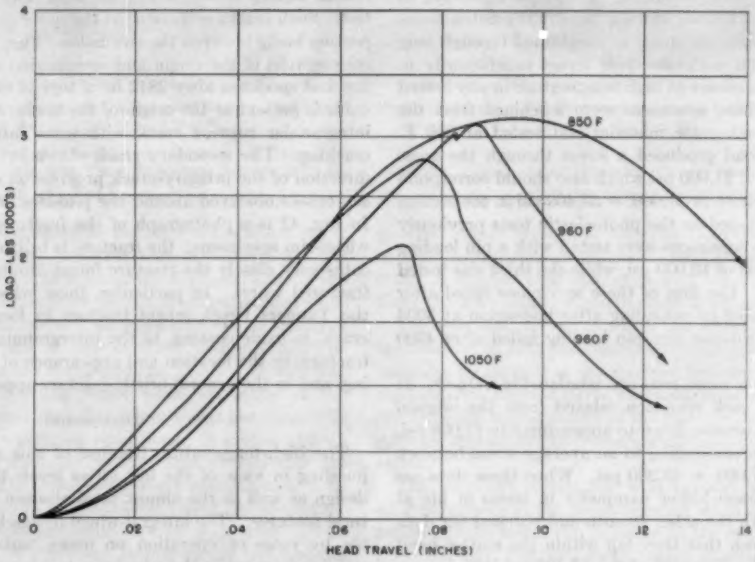

FIG. 35 LOAD VERSUS HEAD TRAVEL FOR SLOW-BEND TESTS ON CHARPY SPECIMENS FROM TANNERS CREEK ROTOR

by holding the specimen under an applied stress and heat-shocking only the thin edge. Accordingly, a specimen was made as shown in the lower half of Fig. 36, and this was placed under a nominal tensile stress of 50,000 psi and subjected to successive cycles of thermal shock by air-blasting the thin edge. The temperature changed from 960 to 830 F in less than 30 sec, but 50 cycles of this thermal shocking failed to produce any detectable cracking in both notched and unnotched condition. Although no cracking was produced, this thermal shocking was sufficiently severe to produce distortion of the specimen with convexity toward the thick edge being noted.

Two spin tests were made at 960 F on model disks of 10 in. OD, $1^1/_2$ in. ID, $^3/_8$ in. thickness to determine if the biaxial stress configuration due to the centrifugal loads would seriously lower the rupture strength below expectations based on uniaxial test data. One model disk was smooth in section, while the second was notched on one side to a depth of 0.67 in., at the base of which there was an 0.005-in-wide cut made by a jeweler's saw. Both of these disks were spun to bursting and the average tangential stresses calculated for the bursting speed. The smooth disk burst at 91 per cent of the speed which would be predicted by comparing the average tangential stress to the 960 F smooth-bar tensile strength, while the severely notched disk burst at 84 per cent of the speed which would be predicted from the same tensile strength. Neither of these represents a very serious reduction in strength due to the multiaxial stress configuration, particularly when compared to the low value of the corresponding stress in the Tanners Creek wheel. In addition, both of these were ductile fractures with no resemblance to the brittle character of the Tanners Creek wheel fracture.

All of the foregoing special physical tests were attempts to reproduce in short-time testing the brittle features of the Tanners Creek wheel fracture. None of these attempts was successful, and accordingly long-time tests were initiated using a test specimen designed to duplicate as closely as possible the wheel-rim configuration and applied centrifugal loads. Figs. 37 and 38 show the essential characteristics of this specimen. Physically, this specimen duplicates, at half scale, the wheel rim at the notch opening, not only in the holes through the notch opening, but also in the notching of the wheel-rim hooks. A load corresponding to the notch-bucket load is applied through pins in the notch-opening holes, while the tangential stress is maintained through long longitudinal bolts which maintain their stress satisfactorily in spite of the creep which occurs at high temperature in any bolted assembly. Three of these specimens were machined from the first-stage Tanners Creek rotor material and tested at 960 F. The initially applied load produced a stress through the gross unnotched rim section of 21,000 psi which also should correspond to an average stress of $2.54 \times 21{,}000 = 53{,}400$ psi in the section between the two holes based on the photoelastic tests previously discussed. Two of the specimens were tested with a pin loading to give a pin shear stress of 10,000 psi, while the third was tested without any pin load. The first of these specimens failed after 3672 hr, the second failed on reloading after inspection at 3004 hr, and the specimen without any pin loading failed after 4300 hr.

The complete data on these tests are tabulated in Table 9. It should be noted that each specimen relaxed from the original load of 21,000 psi rim tension down to approximately 17,000 psi, with this latter load corresponding to an average stress between the holes of $2.54 \times 17{,}000 = 43{,}200$ psi. When these data are interpreted by the Larson-Miller parameter in terms of life at 1000 F and plotted with the other smooth and notched-bar data in Fig. 30, it can be seen that they fall within the scatter band limits for this material. The plot of the 53,400-psi initial stress falls on the before-service smooth-bar rupture curve, while the plot of the average of the initial 53,400 psi and residual 43,200 psi falls on the after-service smooth-bar rupture curve; a similar correspondence with the smooth-bar data is obtained if the plotting is done at 960 F instead of at 1000 F.

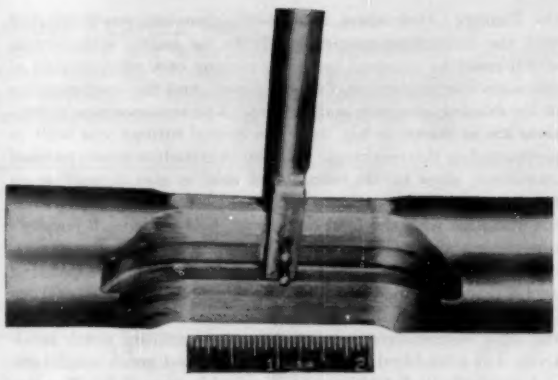

FIG. 37 VIEW OF TEST SPECIMEN SIMULATING WHEEL-RIM CONFIGURATION AND LOADING OF NOTCH OPENING

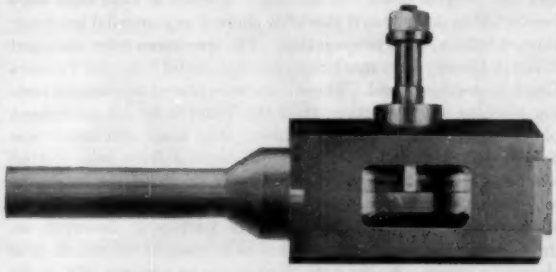

FIG. 38 VIEW OF ASSEMBLED WHEEL-RIM TEST SPECIMEN

A crack was found in each of the wheel-rim test specimens, similar to that shown in Fig. 39, after approximately 3000 hr of test. Such cracks originated at the outer pinhole with the longer portion being between the two holes. Figs. 40 and 41 are photomicrographs of the origin and termination of the crack found in the first specimen after 2812 hr of test at 960 F. A fairly heavy oxide is present at the origin of the crack, and the fracture is an integranular rupture crack with some intergranular secondary cracking. The secondary crack shown in Fig. 40 points in the direction of the primary-crack progression similar to the secondary cracks observed around the pinholes of the fractured wheel. In Fig. 42 is a photograph of the fracture face of one of these wheel-rim specimens; the fracture is brittle in nature and duplicates very closely the fracture found around the pinholes of the fractured wheel. In particular, these wheel-rim tests duplicate the Tanners Creek wheel fracture in location of the original crack, in oxide coating, in the intergranular nature of the main fracture, in the location and appearance of the secondary cracking, and in the general brittle-fracture appearance.

DISCUSSION

The high-temperature fracture of this unit was particularly puzzling in view of the low stress levels that were used in the design as well as the almost total absence of any untried structural features. The integral-wheel design had been proved reliable by years of operation on many turbines, and the notch-opening features at the wheel rim had been in use ever since the introduction of outside dovetails during the first world war.

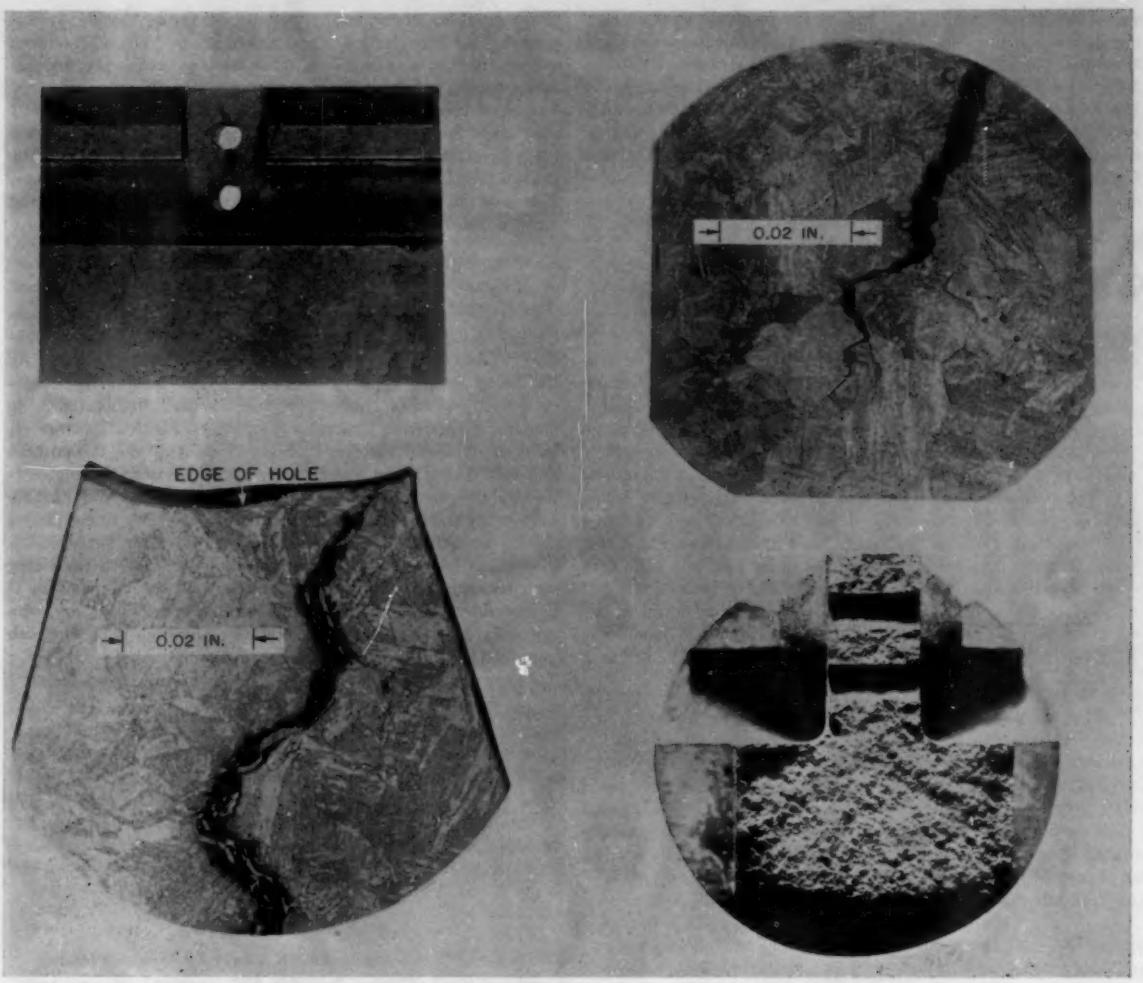

FIG. 39 (*Upper left*) VIEW SHOWING CRACK IN A WHEEL-RIM TEST SPECIMEN AFTER 3000 HR AT 960 F

FIG. 40 (*Lower left*) PHOTOMICROGRAPH OF ORIGIN OF CRACK AT NOTCH PINHOLE IN A WHEEL-RIM TEST SPECIMEN AFTER 2812 HR AT 960 F

FIG. 41 (*Upper right*) PHOTOMICROGRAPH OF TERMINATION OF CRACK OF FIG. 40

FIG. 42 (*Lower right*) VIEW OF FRACTURE FACE OF ONE OF THE WHEEL-RIM TEST SPECIMENS

The inadvertent overspeeding by 40 per cent of the Sporn No. 1 unit without serious damage indicated that the design was not marginal structurally, and inspection of the duplicate units of the Tanners Creek design subsequent to the fracture further indicated that the structural features were sound since no evidence of deterioration was found in any of these inspections. The vibration tests as well as the metallographic studies showed that fatigue was not a contributing factor while inspection of the operating records indicated that this fracture was not caused by any unusual or harmful operating conditions. A review of both the smooth-bar and notched-bar rupture data proved that the material was not lacking in high-temperature strength and, to be certain that this was no false conclusion based on short-time testing, the after-service smooth-bar rupture tests were carried out to 9375 hr at 1000 F while the corresponding notched-bar tests were carried out to 13,403 hr.

The brittle nature of the radial crack suggested that embrittlement had played a significant part but, although a distinct grain-boundary precipitate could be observed, it was not possible to demonstrate any significant embrittlement or notch sensitivity in any physical test, even with the severe notched conditions which were introduced in many of these tests.

The excellent degree in which the wheel-rim tests duplicated the fracture in both macroscopic and microscopic characteristics indicates strongly that the fracture was due primarily to a continuously maintained stress which ultimately equaled its rupture life, with the brittle nature of the fracture being due to the intergranular mechanism of fracture and the multiaxial stress configuration.

The excellent correlation with rupture strength of the calculated stresses at the notch opening when the observed residual tension in the wheel rim is added to the centrifugal stresses suggests strongly that this combination of residual and centrifugal stresses supplied the necessary "continuously maintained" stress. It should be noted at this point that, since the notch opening is only a small fraction of the wheel perimeter, creep or elongation

at the notch opening does not reduce the residual stress by any significant amount; in this respect, this configuration differs from those in which creep due to the residual stresses acts to alleviate the residual stresses themselves, as, for instance, in bolting, and thereby prevents the occurrence of rupture failure. In addition, recent tests on a number of rotors in which only minor, if any, residual stresses were observed indicate that the Tanners Creek rotor was somewhat unique in the magnitude of its observed residual stresses.

The relatively low long-time high-temperature elongation of the Tanners Creek rotor material should not be ignored. Although it would be difficult in a high-creep-strength material to supply sufficient elongation between the pinholes in the notch opening to relieve the residual stresses without fracture occurring at the notch opening, yet it is possible that a material with greater elongation would have prevented the progression of this crack down to the shaft. In addition, the fact that the rupture elongation available in this particular rotor is less than is usually expected of this alloy suggests that it was a contributing cause to the wheel fracture. In a similar manner, the high stresses which may have occurred due to the admission at trip-out of wet steam into the first-stage wheel space may have triggered the crack after most of the rupture strength and elongation were used up. The load dump tests on the Sporn No. 1 unit indicated that the temperature of the sealing steam was quite low, and that this could dish the wheel and thereby cause severe stresses was indicated when severe rubbing of the first-stage buckets was found on the Sporn No. 1, Sporn No. 2, and Twin Branch machines. All these units are duplicates of the Tanners Creek machine, and all operated for a considerable period with the sealing steam supplied by the intermediate superheater header. In addition, no serious rubbing was found on those units in which the sealing-steam supply was initially taken from the main steam line, nor was any additional serious rubbing observed on the Sporn No. 1 unit after the seal piping was modified. Although no bucket rubbing could be observed on the Tanners Creek unit when the molten metal was removed from the buckets after the fracture, it is possible that sufficient clearance was available so that the wheel deflection did not result in rubbing.

Acknowledgment

It is difficult for the authors to express properly their appreciation to the many persons who participated in this investigation. Tests, analyses, and other contributions were made by the Large Steam Turbine Engineering Sub-Section, the Materials and Processes Laboratory, the Thomson Laboratory, the General Engineering Laboratory, and the Research Laboratory, all of the General Electric Company. In addition, the authors and their Department express their appreciation to the engineering and operating personnel of the American Gas and Electric system for their co-operation and contributions in many phases of this investigation. It would take considerable space to acknowledge individually the authors' indebtedness to the many who contributed to this investigation, but special mention is deserved by Dr. R. P. Carreker of the Research Laboratory, who not only participated in many of the investigations, but also compiled the initial report on the many results.

Investigation of Large Steam-Turbine Spindle Failure

By H. D. EMMERT,[1] MILWAUKEE, WIS.

The low-pressure spindle of a 165,000-kw cross-compound steam turbine burst during a routine overspeed-trip test. An intensive investigation of the design, metallurgy, and manufacture of the spindle and of the operational history of the turbine was completed within four months of the date of the accident. The nickel-molybdenum-vanadium material currently being specified by the turbine industry for large turbine spindles and generator rotors is known to be susceptible to brittle failure in the presence of notches in heavy sections. It was determined that the initiating cause of the Ridgeland accident was flakes or thermal cracks developed in the shaft during heat-treatment. These flaws provided the notches necessary to trigger a catastrophic burst of the shaft. The incident and subsequent investigation focus attention on the metallurgy, production, and inspection of large turbine-spindle forgings.

Introduction

SHORTLY before midnight on December 19, 1954, the low-pressure turbine spindle of Unit No. 4 in the Ridgeland Station at Chicago of the Commonwealth Edison Company burst during a routine overspeed-trip test. Immediately following this tragic occurrence, a continuous and intensive investigation of its circumstances and cause was initiated and completed. This report has been prepared to present the story of the investigation and analysis of the accident. From its inception, the primary purpose of the investigation has been to increase the knowledge of the steam-turbine industry so as to minimize the possibility of similar occurrences in the future.

Description of Unit

General Design of Turbine. Ridgeland No. 4 is of conventional cross-compound design, with the high-pressure turbine turning at 3600 rpm and the intermediate-pressure and low-pressure turbines in tandem on the 1800-rpm shaft (1).[2] The unit is rated at 150/165 mw and was placed in commercial service on August 19, 1954. Fig. 1 shows the installation in the Ridgeland Station, the high-pressure turbine and generator being in the background and the 1800-rpm elements in the foreground.

The 1800-rpm low-pressure turbine is of double-flow construction. One end of the shaft is solidly coupled to the low-pressure end of the intermediate-pressure turbine spindle, and the other end is solidly coupled to the generator rotor. The cylinder is of conventional cast-iron construction, with two crossover pipes connected at the top.

Low-Pressure Turbine Spindle Design. Fig. 2 shows the general construction and principal dimensions of the low-pressure turbine spindle. The high-pressure blades are carried in grooves machined directly into the main spindle-shaft body. The last three rows of blades in each flow are mounted in heavy rings shrunk onto the spindle-shaft extensions. There is a circumferential groove at the center of the main body with an integral central ring for balance-plug holes. A center bore extends through the complete length of the shaft.

Five turbines, including the Ridgeland unit, have been built and placed into operation with low-pressure spindles of essentially identical construction. During the preliminary design phase on the first of these units, two types of spindle constructions were laid out. The first design contemplated the use of a central shaft with all blading carried on shrunk-on rings. Critical-speed considerations dictated the use of a large shaft diameter under all rings, resulting in ring stresses too high for the material with which we had the most experience at that time. The second design, which was the one finally selected, utilized a shaft with a large-diameter central body to carry the high-pressure blading and small-diameter extensions with shrunk-on rings for the last three stages of each flow. This design permitted low stress levels in the rings without undue increase in shaft flexibility.

Design Stresses and Factors of Safety. The stress analysis performed in the design of a highly loaded structure such as a turbine shaft includes the calculation of centrifugal, torsional, and bending stresses at many local points under varying conditions of operation. However, the basic criterion for acceptability is the average tangential stress. This criterion has been used for many years by most large-turbine designers (2), and it has since been adopted by both the U. S. Navy and the American Bureau of Shipping (3, 4).

The average tangential stress is the stress imposed on the radial cross-sectional area of the spindle by the centrifugal load of the blades and the spindle mass of the section. Burst tests of disks and small shafts have shown that the average tangential stress is an accurate measure of the actual bursting speed, and bursting speeds have been found to be relatively independent of any localized high stresses, provided there is a moderate amount of ductility in the material (5, 6).

The maximum value of the calculated average tangential stress in the Ridgeland low-pressure spindle shaft is 19,660 psi at 1800 rpm and exists in the portion of the main body toward the IP-turbine end. Our required factors of safety on these stresses are identical with those of the American Bureau of Shipping and are common with most large-turbine builders. At normal speed, the minimum factor of safety must be not less than four on ultimate strength and not less than three on yield strength. These factors of safety have been in use for many years, and their purpose is to cover overspeed requirements, normal variations in material properties, minor flaws and discontinuities, normal variations in quality of workmanship, and approximations in stress analysis.

Material Specifications. To meet the requirements of the calculated stresses and the specified factors of safety, the spindle shaft was made from a nickel-molybdenum-vanadium steel forging, ordered to Allis-Chalmers Material Specification ACM-

---

[1] Assistant Chief Engineer, Steam Turbine Department, Allis-Chalmers Manufacturing Company. Mem. ASME.

[2] Numbers in parentheses refer to the Bibliography at the end of the paper.

Contributed by the Power Division and presented at a joint session of the Power and Metals Engineering Divisions at the Diamond Jubilee Annual Meeting, Chicago, Ill., November 13–18, 1955, of The American Society of Mechanical Engineers.

Note: Statements and opinions advanced in papers are to be understood as individual expressions of their authors and not those of the Society. Manuscript received at ASME Headquarters, September 30, 1955. Paper No. 55—A-172.

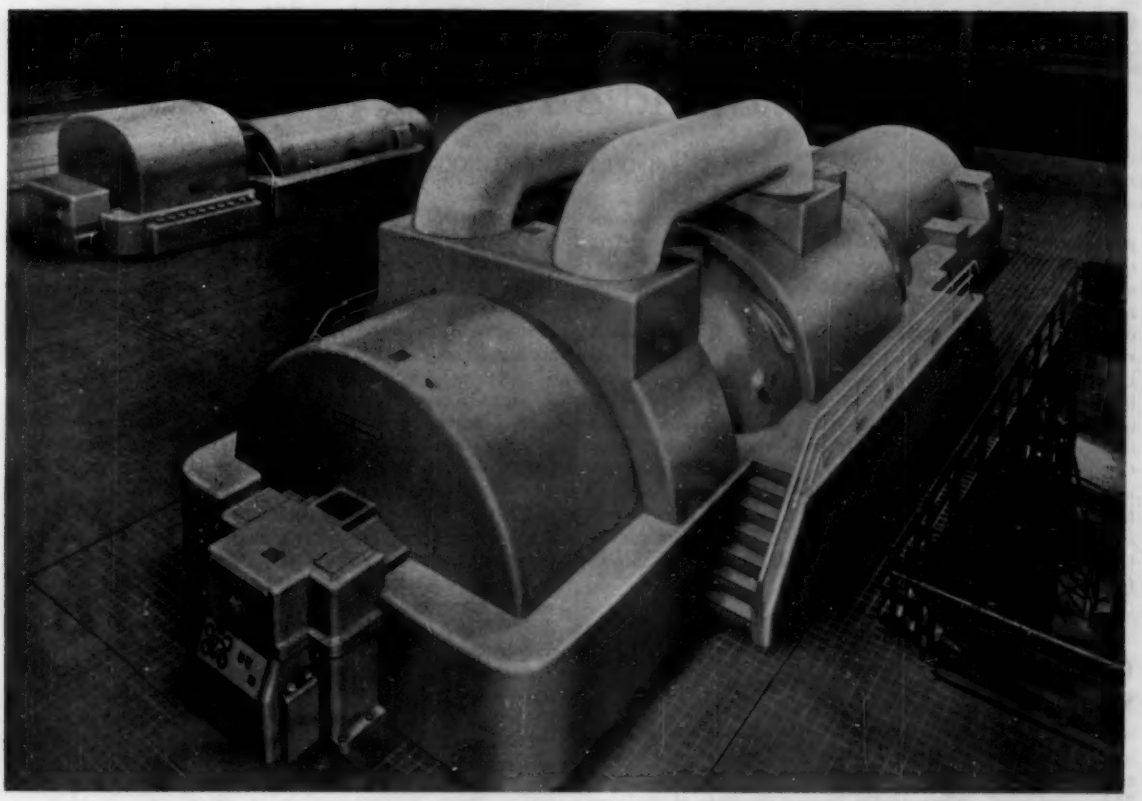

FIG. 1 165-MW CROSS-COMPOUND REHEAT UNIT
(Unit No. 4 at Ridgeland Station of Commonwealth Edison Company.)

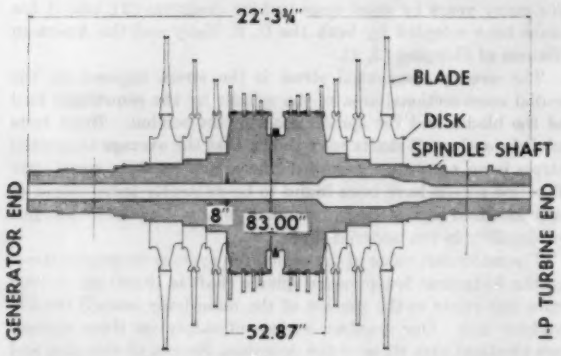

FIG. 2 LOW-PRESSURE TURBINE SPINDLE

11. This material is in general accordance with ASTM Specification A 293 Class 6 (Carbon and Alloy Steel Forgings for Turbine Rotors and Shafts). The specified chemical analysis and physical properties are given in Table 1.

The specification required that the ingot be reduced by forging in the ratio of 1.4 to 1 prior to upsetting. After forging, the ingot was to be given a flake or thermal-crack protection cycle. Physical properties were to be obtained by normalizing and tempering after rough machining. The last heat-treating temperature was to be not less than 1150 F.

Under Inspection and Tests, the specification included heat indication, dimensional inspection, and visual inspection of the bore. It was required that under careful inspection the forging should not exhibit injurious defects such as seams, flakes, holes, or flaws of any kind either on the outside or in the bore. Ultrasonic inspection was also specified, but by agreement with the forging manufacturer this test was to be for information purposes only and was not to be used as a basis for acceptance or rejection of the forging. This was normal procedure at the time the forging was ordered (1951), in view of the general lack of experience with the method at that time.

SPINDLE-SHAFT MANUFACTURE AND INSPECTION

Forging and Heat-Treatment. The low-pressure spindle-shaft forging for the Ridgeland unit was supplied by the forging manu-

TABLE 1 CHEMICAL ANALYSIS AND PHYSICAL PROPERTIES OF SPINDLE SHAFT

	Per cent
Chemical analysis:	
Carbon	0.25–0.35
Nickel	2.50–3.50
Chromium	0.25–0.75
Molybdenum	0.40–0.60
Vanadium	0.05 min.
Physical Properties:	
Tensile strength, psi	105000
Yield strength (0.02%), psi	85000
Elongation (in 2 in.), per cent:	
Longitudinal	16
Transverse or radial	12
Reduction of area, per cent:	
Longitudinal	30
Transverse or radial	23

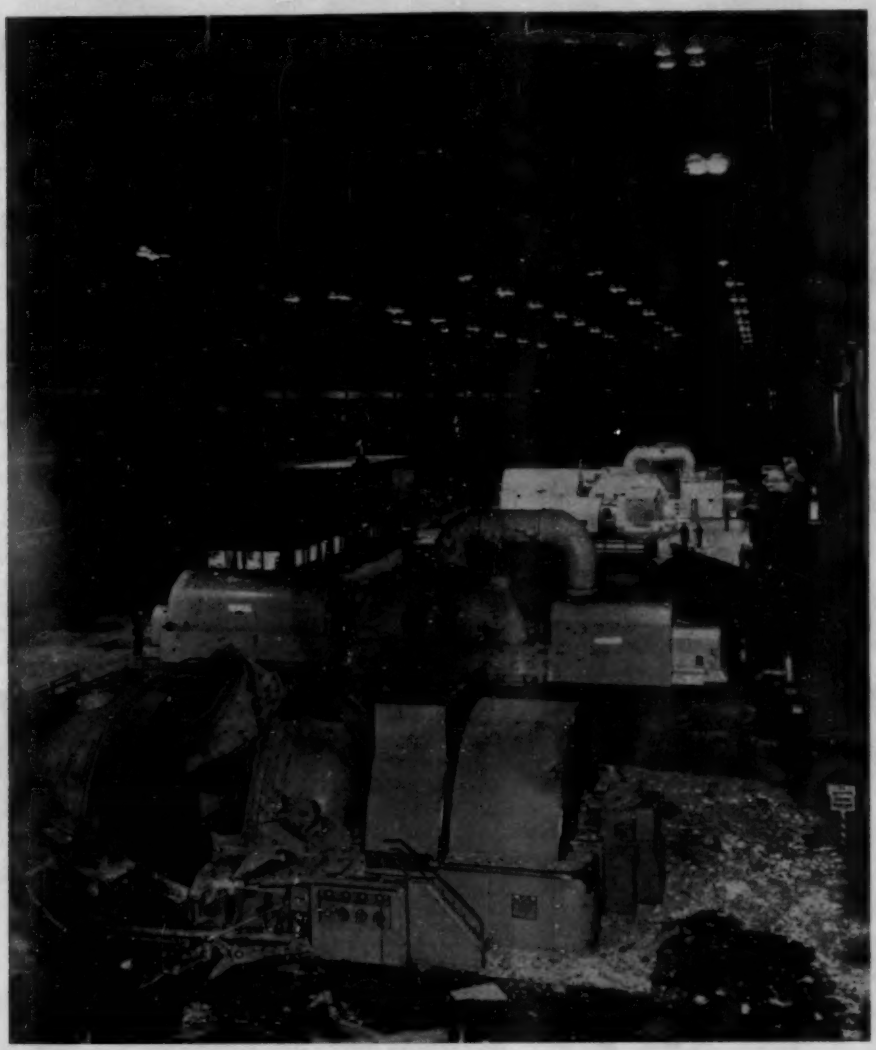

FIG. 3 VIEW OF RIDGELAND STATION AFTER ACCIDENT

facturer in a fully heat-treated and rough-machined condition. Processing was in accordance with the general requirements specified by Allis-Chalmers. Detailed procedures were established by the forging manufacturer based on his experience with alloy-steel forgings of this particular type and size.

The forging was made from a 108-in. ingot weighing 372,000 lb. Blocking, upsetting, and reblocking were done on a 7500-ton press, with a total reduction of 3.25 to 1. The forging was then given a 470-hr conditioning cycle followed by rough machining for preliminary inspection. In the preliminary inspection the center bore was inspected optically and the main body was sonic-tested both before and after boring. Sulphur prints were taken on the faces of the main body, and the fillets joining the main body and shaft ends were magnetic-particle tested.

Following preliminary inspection, the rough-machined forging was heat-treated for physical properties. This heat-treatment required 380 hr and consisted of double-normalizing at 1640 and 1600 F and tempering at 1180 F, followed by slow cooling. Four test bars were then taken and the tests witnessed and certified by Allis-Chalmers inspectors. Minimum properties from the bars met the specifications and were reported as follows:

Tensile strength, psi	111000
Yield strength, psi	85000
Elongation, per cent	19.0
Reduction of area, per cent	50.8

Borescope and Sonic Inspections. Following heat-treatment, the forging was given a final rough machining and annealing, and final optical borescope and sonic tests were completed. In the borescope inspection, discontinuities were observed in one of the shaft extensions adjacent to the main body. The original 8-in. bore at this point was increased in several successive steps to slightly over 16 in., at which diameter the bore was found to be free from visual defects.

The forging manufacturer's sonic tests disclosed a general area within the main body in which sonic indications were found,

varying from very small to somewhat over 100 per cent of the back reflection. In view of the satisfactory visual bore condition, it was decided to continue the processing of the forging.

Following sonic tests, the rough-machined forging was heat indicated for stability, the shaft being rotated slowly for about 11 hr at 1100 F and 20 hr at 950 F. The shaft was found to be very stable.

A second final sonic test of the forging was performed in the manufacturer's plant by Allis-Chalmers inspectors. This test confirmed those previously performed by the forging manufacturer. In view of the nature of the defects observed during visual inspection of the bore, it was considered by all concerned that the sonic indications in the main body were inclusions and stringers of a harmless nature.

Turbine Operating History

Initial Operation. Ridgeland No. 4 was first brought up to speed on July 17, 1954. Five overspeed runs were made on that date during various operational checks. The unit was placed in regular scheduled service on August 19, and there was a total of ten start-ups, including nine overspeed tests, prior to the start-up of December 19. The vibration history of the turbine during this period was excellent. Operation was smoother than average in the opinion of both our field engineers and the station operators.

Low-Pressure Turbine Failure. Unit No. 4 was taken off the line the evening of December 17, to clean the boiler. Both shafts were kept on turning gear until the evening of December 19, at which time the turbine was rolled with steam preparatory to being put back on the line. The speed was brought up to 3000 rpm, as measured on the high-speed shaft, in about an hour and a half, and the vacuum-trip setting was checked. Following this trip, the speed dropped to about 1500 rpm. The high-pressure shaft governor was then made inoperative and speed was increased until the low-pressure shaft overspeed governor tripped the unit at 7.8 per cent overspeed. The speed dropped to about 3000 rpm at which point the trip tester was placed in position to make the low-pressure overspeed trip inoperative during the anticipated succeeding high-pressure turbine trip. Speed was then again increased and at 3910 rpm, or 1955 rpm on the low-speed shaft, corresponding to 8.6 per cent overspeed, the low-pressure turbine spindle exploded. The accident occurred without warning, there being no noise or rubs or other abnormal indications up to the instant of failure.

Fig. 3 is a view of the interior of the station taken shortly after the accident, showing the condition of the low-pressure turbine and the general damage to the station. Units Nos. 1, 2, and 3 were tripped immediately following the accident, as a result of damage caused by flying parts.

Fig. 4 is a close-up of the low-pressure turbine taken shortly after the accident. It will be noted that the main body of the spindle is completely gone, with the shaft extensions and shrunk-on disks remaining overhung because of the solid couplings to the intermediate-pressure turbine shaft and the generator rotor. The crossover pipes and low-pressure turbine casing and cylinder rings were damaged beyond repair. There was miscellaneous

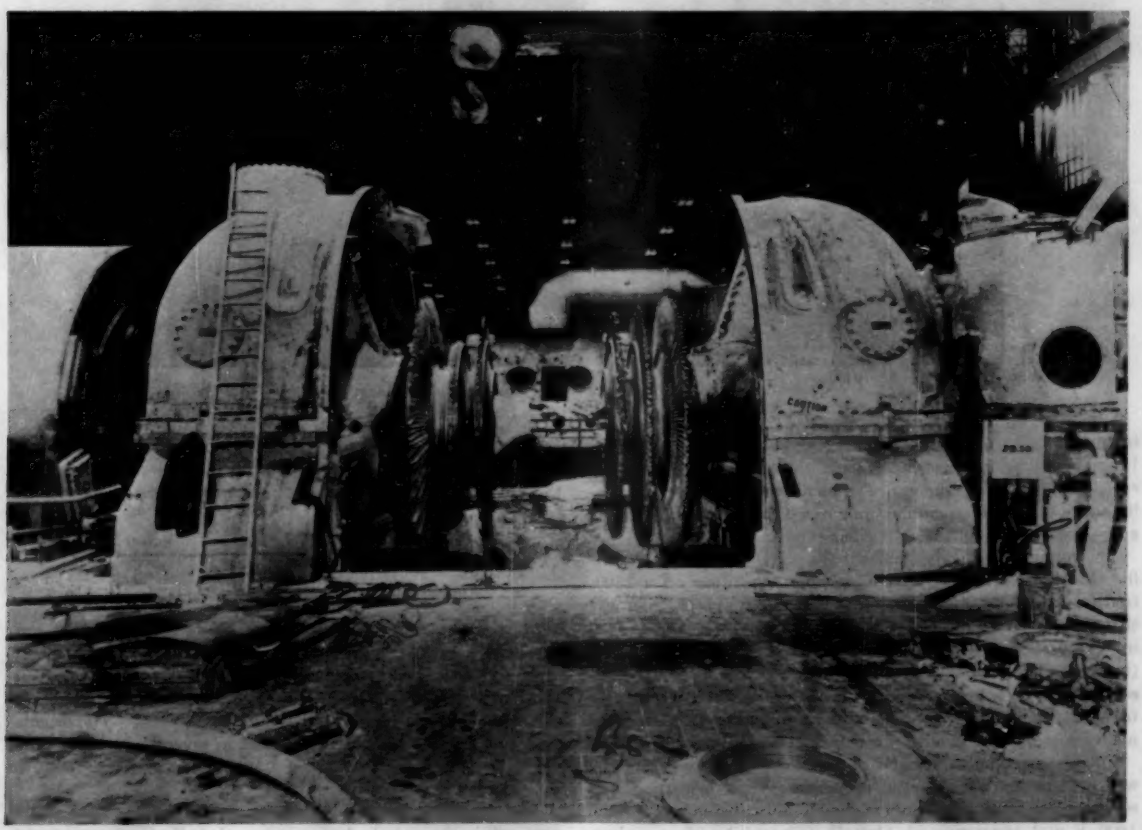

Fig. 4 Close-Up of Low-Pressure Turbine After Accident

damage to both the rotating and stationary elements of the intermediate-pressure turbine and generator, but not to such an extent that complete replacement of major parts has been required. Damage to the high-pressure turbine and generator was inconsequential.

Initial Investigations

Preliminary Survey. Although it was not possible to remove parts and fragments of the turbine from the station for some weeks following the accident, visual surveys of the spindle pieces were made immediately by our engineering and metallurgical staffs. It was found that the main body had burst into four main pieces. One piece was hurled through the air and fell into the basement adjacent to the condenser of Unit No. 1. Another piece flew in the opposite direction and eventually was located in the station coal pile. The remaining two pieces came to rest in the condenser of Unit No. 4. Fig. 5 shows one of these pieces, and it will be noted that it is almost a true 90-deg segment. The other three fragments are almost identical in appearance.

A preliminary assembly of spindle fragments at Ridgeland is shown in Fig. 6. The four quadrants of the main body are in the foreground. Some conical pieces mating with the quadrants were found as large separate pieces, but others were either shattered into a number of smaller fragments or remained with the shaft extensions. Of particular interest was a fatigue crack some 3 in. deep and 17 in. long in the fillet joining the shaft extension and main body at the generator end.

A preliminary estimate of the various factors which could have caused the accident was made during this initial period. Fig. 7 shows the pattern of the main-body burst, which was determined from detailed measurements of the four main quadrants. It was evident from this pattern that the failure extended in a main plane from end to end and was symmetrical to either side of the center of the main body. This failure pattern is typical of a simple overspeed burst, although there was positive evidence that the actual speed of the spindle at the time of failure was far below the estimated bursting speed.

Fig. 5 Quadrant of Main Body of Low-Pressure Spindle Shaft

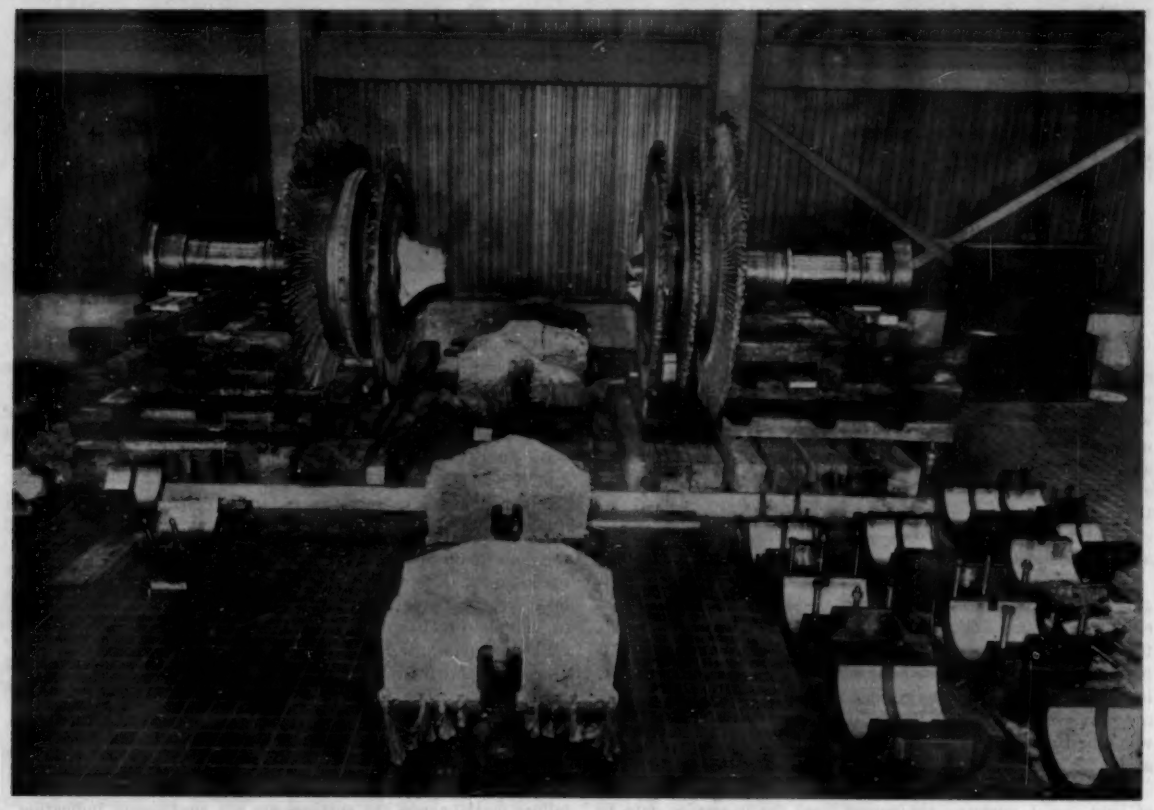

Fig. 6 Low-Pressure Spindle Fragments and Parts

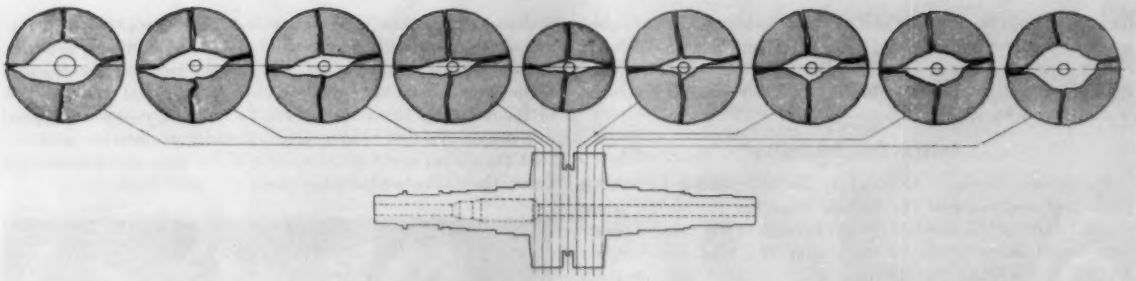

FIG. 7 GENERAL PATTERN OF SHAFT FAILURE

It was then conjectured that the same burst pattern could have resulted at a much lower speed if there were flaws or poor material near the center of the main body. In this case, the speed at which bursting would occur would depend largely upon the nature of the flaws or the extent of the inferior material.

A considerable amount of attention was given to the possibility of the failure originating with the fatigue crack, which in turn could have resulted from stress concentrations in the fillet joining the main body and shaft extensions or in the combination of fillet and adjacent shrink under the rings. These possibilities could not be ruled out, although it was our judgment at that time that the fatigue crack was not a major factor in the primary failure. It was considered that the crack had not progressed deep enough to cause complete destruction of the shaft, and in any case such a crack would be unlikely to cause a burst-type failure of the main body. In considering the effect of the adjacent shrink fit, it was noted that the fatigue crack originated high on the fillet, well away from the edge of the shrunk-on ring.

Spindle Design Analysis. As soon as possible following the accident, a reanalysis was completed of the stresses in the low-pressure turbine spindle shaft. This stress analysis included the following:

1 Complete survey of dynamic loads imposed on shaft.
2 Calculation of important local and average stresses.
3 Investigation of fatigue stresses in main fillet.
4 Investigation of shrink-fit stresses under rings.
5 Investigation of temperature gradients and thermal stresses.
6 Investigation of axial-stress effects.

In reviewing the results of this stress analysis, it was concluded that, while there were some unknowns and the calculations could perhaps be refined to some degree, the general stress level was very conservative and the margins of safety were adequate, given sound material. Computed stresses are mainly relative, and those in the Ridgeland shaft were, in general, lower than stresses in current 3600-rpm designs. It was considered that the unknown influences of size, material, and other variables were covered by adequate factors of safety when compared with available burst-test data.

Manufacturing and Inspection Records. A thorough investigation was made of the machining procedures and shop practices employed on the Ridgeland shaft, from initial receipt of materials through final completion of installation. Examination of all pertinent records disclosed nothing of significance. Visual inspection of turbine parts revealed no obvious defects such as machining errors, tool marks, or other fabrication damage. It was found that inspection records were adequate and in accordance with established practice.

Operation Records. An examination of the operating records of Unit No. 4, covering the period from the in-service date to immediately before the accident, revealed nothing abnormal. There was no difficulty of significance at any time in the operating history of the turbine.

At the start-up on December 19, the high-speed and low-speed generators were synchronized while the unit was still on turning gear. Fields were put on as the shafts came off the turning gear. The generators remained synchronized through the accident, and after the low-pressure turbine failure the drag of the low-speed generator brought the 3600-rpm elements to a stop in less than 1 min.

Steam temperature at the low-pressure turbine inlet was at a normal 300 F at the time of failure. Condenser vacuum was about $27^1/_2$ in. Starting time conformed to established operating procedure, and there were three independent checks of speed at all times until an instant or so before failure. During the preceding 25 min., the vibration at the low-pressure bearing pedestals did not exceed 0.3 mil, which is very good for a unit of this size.

METALLURGICAL INVESTIGATIONS

Reassembly of Spindle. As soon as all parts and fragments of the low-pressure turbine assembly were received in our plant, a reconstruction of the spindle from the fragments was started. The reconstructed spindle was reviewed in detail at a general meeting with Commonwealth Edison engineers and consultants, and a plan of metallurgical investigation was established. This plan called for the following specific investigations:

1 Detailed examination of parts for failure lines, hatch marks, and so on.
2 Magnetic-particle tests, acid etch, and sulphur prints of various slabs.
3 Photomicrographs.
4 Chemical analyses at various locations.
5 Determination of residual hydrogen.
6 Tensile and impact tests of bars from various locations.
7 Ultrasonic tests of large fragments.
8 Profilometer examination of fatigue crack.

Parts Examination. Fig. 8 shows a fracture surface of one of the four main-body quadrants. Detailed examination of the markings on these surfaces established two basic facts: (*a*) All main fractures progressed from the bore toward the outside, and (*b*) the main body split first into two halves and then each half split into quadrants. Fig. 9 shows the cradle reassembly of the quadrants and fragments composing one of the primary main-body halves. The failure marks are, in general, continuous across this entire surface, indicating that the complete half separated from the other half prior to breaking into smaller parts. A similar reassembly of one of the quadrants from this photograph with a quadrant from the opposite half shows that the failure marks across the surfaces are not continuous, indicating

FIG. 8 QUADRANT III OF MAIN BODY

FIG. 9 ASSEMBLY OF QUADRANTS I AND II

that splits in the smaller parts occurred prior to splits in the main segments.

Deductions from examinations of the cradle reassemblies were confirmed when all four main-body quadrants were assembled together. Fig. 10 is a view of one end of the reassembled main body. It is apparent from this picture that quadrants I and II were joined when they separated from quadrants III and IV, and the separation of quadrant I and quadrant II followed later.

The position of the fatigue crack is evident in Fig. 10, and it will be noted that it has no significant relation to the main planes of failure.

In summary, the detailed examination of the fracture surfaces clearly indicated that the spindle failure originated in the main body, spreading out both radially and longitudinally from the general vicinity of the center bore.

Macroexaminations. The most significant phase of the metallurgical investigation was the macroexamination of various slabs cut from the main-body segments. Fig. 11 shows the results of magnetic-particle test of a longitudinal slab. This picture clearly indicates the presence of a large number of cracks in an area extending from near the bore out to approximately mid-

FIG. 10 ASSEMBLY OF FOUR QUARTERS—GENERATOR END

radius. These cracks are several inches in length, and longitudinal in direction. They follow a definite pattern in the forging and are concentrated in the main body. Fig. 12 is a photograph of magnetic-particle indications in a transverse slab from one of the quadrants. In the transverse plane the cracks are generally radial in direction, although some appear at all angles. The average radial depth is of the order of 1 in.

Fig. 13 is a sulphur print of the same longitudinal slab as in Fig. 11. The dark areas are elongated sulphur segregates or sulphide stringers. This sulphide pattern is not particularly unusual, but the combination of stringers and cracks is abnormal. Comparison of Figs. 11 and 13 shows that in general the cracks detected by magnetic-particle tests are associated with sulphide stringers.

At this point in the investigation it became evident that the forging contained a typical flake or thermal-crack pattern (7, 8). This condition is characterized by cracks appearing in large numbers, fairly evenly distributed circumferentially from near the bore out to about mid-radius, and tending to lie in radial planes extending longitudinally.

Magnetic-particle tests of the fatigue-crack area, which caused concern throughout the investigation, showed the presence of numerous flakes in and around the fatigue crack, some lying at the fatigue-crack initiating points as determined from "beach marks" on the surfaces. Subsequent strain-gage tests by The Detroit Edison Company on a duplicate shaft and by Battelle Memorial Institute on a 12-in. model shaft showed that the actual fillet stresses were conservative and slightly less than predicted by the designers. It can only be concluded that the fatigue crack started from a flake and would not have appeared at all in the absence of this initiating crack.

Metallographic Examination. Fig. 14 is a photomicrograph at 100× of a typical crack near the mid-radius of the forging. The extreme tightness of these cracks is well demonstrated here. This is important in establishing the fact that the cracks were in the shaft prior to operation and were not secondary results of stresses imposed at the time of failure. This fact is corroborated by the absence of cracks near the bore, which is the most highly stressed area of the shaft.

Chemical Analysis. The chemical analysis of material from various sections was well within the original specifications. Sulphur content was greater in the vicinity of the segregates or stringers, but it was not as high as expected, probably owing to the difficulty of obtaining a true sample. Hydrogen checks made by Battelle showed only about 1 ppm. This is normally considered satisfactory. However, the hydrogen samples were

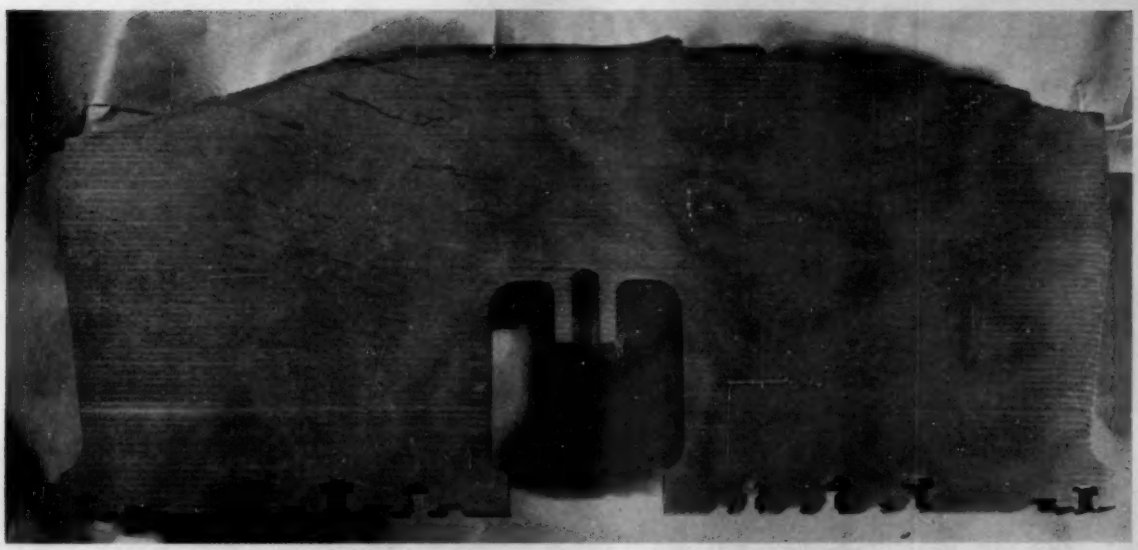

FIG. 11 MAGNETIC-PARTICLE INDICATIONS—LONGITUDINAL SLAB FROM QUADRANT III

FIG. 12 MAGNETIC-PARTICLE INDICATIONS—TRANSVERSE SLAB FROM QUADRANT III

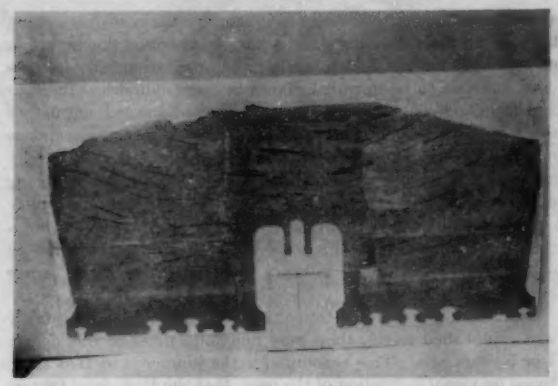

FIG. 13 SULPHUR PRINT—LONGITUDINAL SLAB FROM QUADRANT III

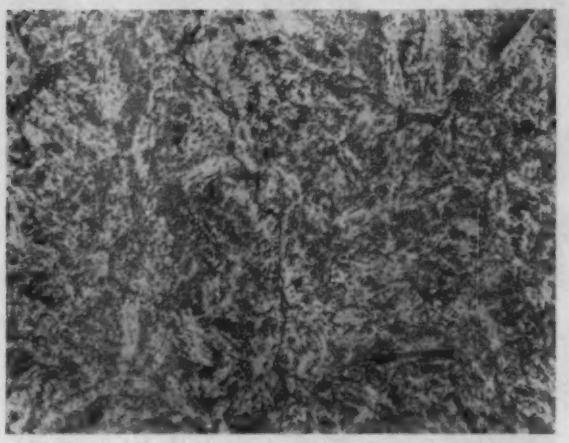

FIG. 14 MICROSTRUCTURE OF TYPICAL CRACK NEAR MID-RADIUS OF FORGING

taken from material adjacent to the stringers, and hydrogen content at these locations is likely to be quite low as a result of diffusion from the metal into the stringer volume.

Physical Tests. Tensile tests of bars taken from various areas of the shaft showed no alarming drop in physical properties at any point. In general, tensile strengths meet the original specifications, while yield strengths are slightly low toward the center. The most significant figures were low values for elongation and reduction of area near the bore, indicating a considerable loss in ductility. Some of the test-bar fractures exhibited "fish eyes," which are bright spots resulting from the presence of hydrogen, a strong reducing agent. Also significant is the fact that test bars from areas of low ductility showed fully restored ductility after baking for 2 hr at 400 F. This results from excess hydrogen in the metal which is removed by the baking.

Fig. 15 is a plot of the results of the Charpy V-notch impact tests. The transition temperature is high and probably above the average metal temperature during operation. This indicates a probability of high notch sensitivity and brittle rather than ductile failure under conditions of multiaxial stress.

Ultrasonic Tests. A complete sonic test of one of the quadrants showed the presence of numerous indications, with general pattern and magnitude very similar to those recorded in the

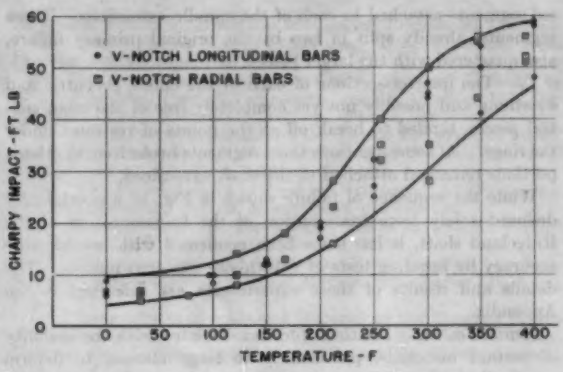

FIG. 15 CHARPY IMPACT TESTS FROM MID-RADIUS OF MAIN BODY

original sonic tests of the rough-machined forging. There was no indication of any significant change in sonic pattern.

ANALYSIS OF FAILURE

Sequence of Failure. A probable sequence of failure can be established with considerable accuracy from the examinations of fragments. While the failure was explosive in nature and occurred completely in only a very small fraction of a second, the sequence of events is believed to be shown in Fig. 16.

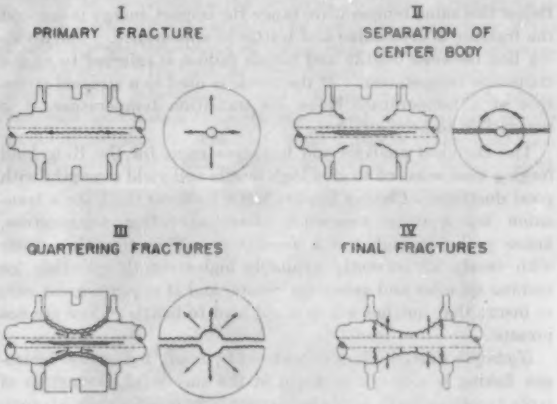

FIG. 16 SEQUENCE OF FAILURE

I Initial failure originated at the bore within the main body and progressed in a longitudinal plane both radially and toward the shaft ends, tending to split the main body into two halves. The actual pin point of origin cannot be determined positively, but a probable location has been identified as a granular area on one of the major cleavage surfaces adjacent to the bore.

II Extension of the primary failure into the shaft ends was limited by the clamping effect of the shrunk-on rings. These rings also restrained the two halves of the main body, and extremely high stresses were then set up at the fillet corners. Secondary failures from these corners immediately progressed in an inward direction toward the center of the main body.

III As cracks from the fillet corners progressed in a direction to free the halves of the main body, strong centrifugal forces in each of these halves almost simultaneously split them into quarters. At the same time the center portion of the material enclosing the bore in the main body fragmented, leaving coni-

cal segments attached to each of the spindle extensions. These segments, already split in two by the original primary failure, also quartered with the larger pieces.

IV The quarter-sections of each of the cones, eccentric and overhung and possibly not yet completely free of the main central pieces, tended to break off at the points of restraint under the rings. At some locations these segments broke free; at others, portions remained attached to the shaft extensions.

While the sequence of failure shown in Fig. 16 was originally deduced solely from examination of the fragmentation of the Ridgeland shaft, it has since been confirmed with considerable accuracy by bursting tests of 1/15th-size cast-iron models. The details and results of these experiments are described in the Appendix.

Brittle Failure. Brittle failure is associated with the inability of certain materials, particularly in large masses, to deform plastically in the presence of a stress at the root of a sharp notch (9). In such materials a moderate or low stress may be sufficient to initiate failure in the presence of notches or similar stress raisers, hence the classification of materials susceptible to brittle failure as having high notch sensitivity. Brittle failures are characterized by sudden catastrophic cleavages at extremely high rates of propagation, perhaps 6000 fps or more.

Susceptibility to brittle failure is not revealed in the conventional tensile test. The criterion in greatest use today is the Charpy impact test (10). For a specific material and heat-treatment, there is a narrow test-temperature range above which the impact energy absorbed is relatively high and the test-bar fracture exhibits ductile shear-type failure characteristics. Below this same temperature range the impact energy is low and the fracture is crystalline and brittle in appearance. The dividing line between ductile and brittle failure is referred to as the transition temperature. If the metal is used in a stressed structure at a temperature below its transition temperature, it is susceptible to brittle failure.

The chemical analysis and heat-treatment for the Ridgeland forging were selected to give high tensile and yield strengths with good ductility. Charpy impact tests, however, indicate a transition temperature somewhat above operating temperature, hence probable high notch sensitivity. This condition exists with nearly all currently available high-strength materials for turbine spindles and generator rotors, and it requires great care to insure that notches which could lead to brittle failure are not present.

Hydrogen Flakes. It is considered by many today that hydrogen flaking is a major problem in the successful production of large turbine-spindle forgings, particularly in sizes over approximately 50 in. diam.

The conditions leading to the formation of flakes are fairly well established (11, 12). Atomic hydrogen is highly soluble in molten steel and becomes available to a varying degree from the moisture present during melting. As the molten steel solidifies, hydrogen is evolved and forms molecular hydrogen gas in the microcavities and internal voids in the metal. As gas collects in these pockets, the resultant pressures may rise to extremely high values.

The effects produced by hydrogen pressure depend upon another important factor. During the transformation of steel in cooling from high temperature, high thermal stresses are set up in large ingots owing to the relative volume changes between core and rim. These transformation or cooling stresses, combined with the effect of entrapped hydrogen gas at points of already incipient weakness in the metal, may result in metallic separations or cracks variously identified as thermal cracks, segregation cracks, or hydrogen flakes.

Individual flakes vary considerably in size. Ultrasonic examination is therefore sometimes indeterminate in distinguishing between an individual flake and a harmless nonmetallic inclusion or shrinkage cavity. Also, while flake orientation may be random, it tends to be in radial planes in large cylindrical forgings and thus edge-on to sound waves projected inward normal to the forging circumference. The resultant ultrasonic response may be of low intensity. On the other hand, it is generally recognized today that flakes have the characteristic of being present in large numbers if they appear at all and of being fairly evenly distributed circumferentially in a band at about mid-radius in the forging. This band lies well inside the periphery of the forging and some distance out from the core or center bore.

Whereas the ultrasonic-test characteristics of flakes are fairly well established today, they were not understood to this degree 4 or 5 years ago. This accounts for the judgment at that time, based on visual inspection of the bore, that the Ridgeland forging contained harmless inclusions rather than the more dangerous flakes.

Cause of Failure. A study of the sequence of failure has indicated that it originated deep in the mass of the main body of the shaft. Metallurgical examinations have confirmed the fact that the metal was notch-sensitive and susceptible to brittle failure. Various inspection techniques have shown the presence of an overabundance of cracks in the form of flakes, providing the notches necessary to trigger a sudden and catastrophic failure of the shaft. The only point of uncertainty is the means by which the shaft maintained its integrity as long as it did. It is probable that failure started when one or more of the numerous flakes in the main body near the bore extended slowly and approached the bore surface, a region of high local stress. At this instant, the brittle nature of the material caused this surface crack to widen into a major separation at an extremely high rate of propagation.

Conclusion

It is evident from this investigation that the Ridgeland low-pressure turbine failure is primarily centered around the metallurgy of large forgings. This and other incidents have served to focus much attention on material specifications and on the general procedures for producing and inspecting these large pieces of metal.

The influence of the material in preventing shaft failures is of primary importance. The susceptibility to brittle failure of the standard nickel-molybdenum-vanadium analysis in common use today is of great concern to the industry. Unfortunately, available alternate materials at the same strength levels offer little improvement. Materials totally immune to brittle failure, such as austenitic steel or some nonferrous metals, have been proposed for turbine shafts, but their lower strength levels and other unfavorable characteristics make their use undesirable. The most logical attack on the problem seems to be in a continuing study of the factors influencing notch sensitivity, such as composition, heat-treatment, microstructure, and processing.

Much development work within the steel-making industry will be required so that techniques and controls are established to eliminate all possibility of flakes in large forgings. The allowable hydrogen content in an ingot is probably well under 2 ppm, and ladle metal generally runs 4 ppm or higher. Even partial control of hydrogen requires controlled heats and close attention to tapping and pouring procedures. Hydrogen-free steel could be produced if the steel-making process was isolated from all sources of hydrogen, but this is very difficult to accomplish in manufacturing large ingots. Most attempts at hydrogen control have been in the direction of removing the gas after it has already been introduced. One of the most promising current

developments is the vacuum-casting process, which has received considerable attention in Europe (13).

An equally important factor in large-forging development is the improvement of inspection methods. The Ridgeland forging was produced about 4 years ago, and in the intervening period much has been accomplished in this respect. As a matter of policy, all large turbine shafts are bored axially, since optical and magnetic-particle inspection of the bore surface gives a good indication of the general quality of the forging. However, some of the more dangerous types of discontinuities may lie away from the bore and hence not be detectable by bore inspection. Ultrasonic inspection has become our most important tool for the interior examination of metal masses (14), and intensive effort has been put into the development of improved sonic-inspection techniques. Forgings are now searched both radially and longitudinally at various frequencies, and techniques for searching radially outward from the bore are under development. Shear-wave crystals have been brought into use to improve the examination of areas formerly difficult to reach with straight crystals.

Even more important than the development of new sonic-inspection techniques is our continually increasing knowledge enabling better interpretation of test results. Sonic testing is very sensitive, and interpretation requires a considerable amount of background experience. The most common sonic indication is that of inclusions and segregations of inclusions found in nearly all large forgings. It is frequently difficult to distinguish between these harmless types of discontinuities and the more dangerous types of flaws such as flakes or thermal cracks. It is now considered that the determination of pattern and distribution of indications is as important as the measurement of the magnitude of any particular individual indication, and it is in this respect that a growing background of experience and information in interpretation is greatly improving the inspection situation.

Acknowledgments

The Allis-Chalmers Manufacturing Company gratefully acknowledges the excellent co-operation, advice, and assistance of the Commonwealth Edison Company and its consultants in the investigation of the Ridgeland accident. Within Allis-Chalmers, the contributions of the Research Division, the Manufacturing Department, the Inspection Department, and the Office of the Director of Engineering were all of vital importance in bringing the investigation to an early and successful conclusion. The author expresses his indebtedness to the many individuals in these departments who accomplished the work that has been outlined in this report.

BIBLIOGRAPHY

1 "Cross-Compound Steam Turbines for Large Capacity Installations," by C. D. Wilson, Proceedings of the American Power Conference, vol. 15, 1953, pp. 144–151.

2 "Steam Turbines and Engines," by A. G. Christie and W. Trinks, Section 8 of Power volume, Kent's Mechanical Engineers' Handbook, John Wiley & Sons, Inc., New York, N. Y., twelfth edition, 1950, pp. 8–38, 8–39.

3 Military Specification—Turbine, Steam, Propulsion (For Naval Shipboard Use), MIL-T-17600 (Ships), U. S. Navy, June 26, 1953, para. 3.4.17.4.1.

4 "Rules for the Classification and Construction of Steel Vessels," American Bureau of Shipping, New York, N. Y., 1954, pp. 131–132.

5 "Bursting Tests of Steam-Turbine Disk Wheels," by E. L. Robinson, Trans. ASME, vol. 66, 1944, pp. 373–386.

6 "Effect of Strength and Ductility on Burst Characteristics of Rotating Disks," by A. G. Holms and J. E. Jenkins, NACA TN 1667, July, 1948.

7 "Rotor Forgings for Turbo-Generators," by J. Novak, *Engineers' Digest*, vol. 11, March, 1950, pp. 72–74.

8 "Testing of Heavy Forgings for Steam Turbine Sets," by R. Schinn, Fourth International Mechanical Engineering Congress.

9 "Brittle Failure of Steel Structures," by M. E. Shank, *Metal Progress*, vol. 67, June, 1955, pp. 111–121.

10 "Important Considerations in Charpy and Izod Testing," by C. M. Schwitter, *Product Engineering*, vol. 18, October, 1947, pp. 106–109; vol. 18, November, 1947, pp. 159–162.

11 "The Effect of Hydrogen on the Tensile Properties of Steel," by J. D. Hobson and J. Hewitt, *Journal of the Iron and Steel Institute*, vol. 67, February, 1953, pp. 131–140.

12 "The Embrittlement of Steel by Hydrogen," by W. A. Bell, *Product Engineering*, vol. 26, March, 1955, pp. 189–192.

13 "Vacuum Cast 150-Ton Forging Ingots in German Plant," *Iron Age*, vol. 175, February 17, 1955, pp. 91–94.

14 "Ultrasonic Testing of Spindle and Rotor Forgings," by R. G. Matters, Allis-Chalmers Electrical Review, 4th quarter, 1953, pp. 4–8.

15 "Some Effects of Scale and Material on the Bursting Speeds of Turbine Discs," by A. Graham, T. M. Jones, and V. C. H. Bailey, National Gas Turbine Establishment Report No. R.166, January, 1955.

Appendix

Model Bursting Experiments

After the close of the formal engineering and metallurgical investigation into the Ridgeland accident, it was decided to conduct model bursting experiments to demonstrate the sequence and mode of failure which had been deduced previously.[8] In justification for such model testing, it has been shown that small disks of brittle materials tend to behave like large disks of more ductile material (15).

A series of spin tests was conducted on 1/15th-size model spindles to demonstrate the patterns of failure resulting from various initiating conditions. The principal dimensions of the main body and extensions of the original Ridgeland shaft were held to scale. The models were turned from cast-iron sticks after careful radiography, and longitudinal rim and center test bars were taken from the sticks with physical test results as shown in Table 2. The blade rings adjacent to the main body were simulated with small shrunk-on rings of high-strength steel.

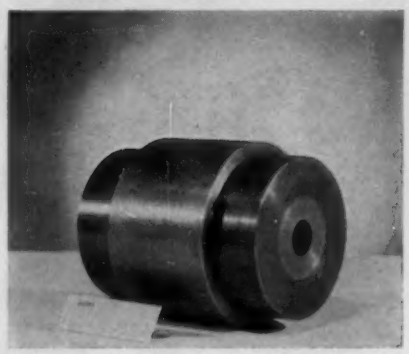

Fig. 17 Model Test Spindle

Main fillet radii and center-bore and overbore configurations and locations were maintained at their proper relative dimensions. A photograph of one of the models prior to test is shown in Fig. 17.

Using the calculated average tangential stress and the average of the rim and bore tensile strengths as criteria, an estimated bursting speed for each model was determined as shown in Table 2.

[8] Our sincere appreciation is due Mr. R. E. Peterson of the Westinghouse Mechanical Laboratories at East Pittsburgh, Pa., who first called our attention to the remarkable accuracy with which the Ridgeland failure pattern could be reproduced with spin tests of small cast-iron models.

TABLE 2 MODEL SPINDLE BURST TESTS

Model no.	1	2	3
Tensile strength, psi:			
Rim	23200	23500	23800
Center	18200	17400	17500
Average	20700	20450	20650
Bursting speed, rpm:			
Calculated	31550	31350	31500
Actual	29520	29820	29280
Bursting stress, psi:			
Actual	18120	18500	17820
Per cent of tensile strength	88	91	86

Model No. 1. The first model burst at a speed of 29,520 rpm, corresponding to a calculated average stress of 88 per cent of the average tensile strength. The resultant main-body fragments were very similar to the Ridgeland pieces, as was the general burst pattern. So far as could be determined from the fracture-surface directions and intersections, the sequence of failure was essentially the same as that previously deduced for the full-scale shaft.

Model No. 2. The second model had a configuration and dimensions identical with those of the first model, except that the fatigue crack found in the Ridgeland shaft was introduced as a thin saw-cut in one of the main fillets, as closely to scale as possible. When this model was spun to destruction, failure occurred at a calculated average stress of 91 per cent of the average tensile strength. The differences in bursting speeds and stresses between models Nos. 1 and 2 are insignificant. The fragments of model No. 2 are shown in Fig. 18. These are very similar to those of the first model, and the accuracy of duplication of the original full-scale fragmentation is very apparent. Fig. 19 is a reassembly of the model main-body fragments. The similarity between this photograph and Fig. 9 is rather striking.

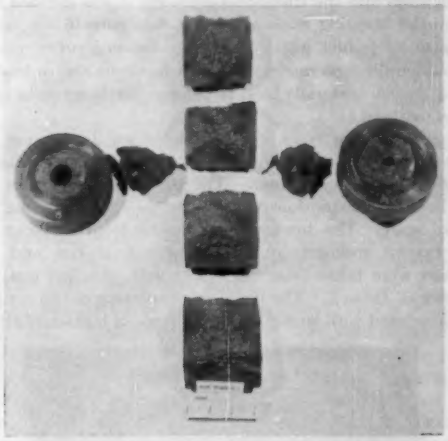

FIG. 18 TEST-SPINDLE FRAGMENTS

At this point in the model burst tests, it had to be concluded that the fillet crack had exerted no influence on the burst pattern, since the fragmentation and failure stress were identical whether the crack was present or not. Failure could not, therefore, have originated from the fillet crack.

Model No. 3. It was then decided to test a third model in which the fillet crack was exaggerated in depth to the point where it would of necessity influence the fragmentation and possibly the bursting stress. The crack was deepened until it intersected the center bore, thus reducing the cross-sectional area of the shaft extension by almost 50 per cent. Model 3 failed when the calculated average stress was 86 per cent of the average tensile strength, insignificantly different from models Nos. 1 and 2. However, the fragmentation pattern was affected in the vicinity of the crack. Whereas the main body still separated into four main pieces and the conical fragments were formed at the unaffected end, no cone was formed in the vicinity of the crack and the adjacent main-body quadrants included a substantial portion of the original center-bore surface. This pattern is evident in Fig. 20.

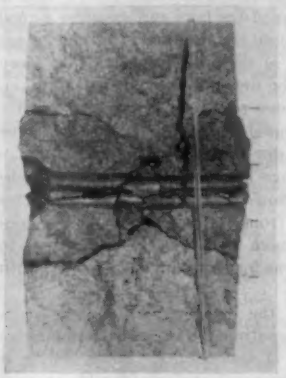

FIG. 19 ASSEMBLY OF TEST-SPINDLE FRAGMENTS

FIG. 20 MODEL NO. 3 MAIN-BODY QUADRANTS

This experiment confirmed the original conclusion that the fatigue crack in the Ridgeland shaft probably would never have caused a catastrophic bursting of the main body. Instead, in accordance with past experience on the effects of cracks in shafts, the crack would undoubtedly have continued to extend with time until it became deep enough to affect the running balance of the spindle. The turbine would have become inoperative due to roughness before a spindle burst could have occurred.

Discussion

M. K. DREWRY.[4] A valuable service has been rendered the power industry by the author, his company, and the Society, in publishing this comprehensive report.

Better-quality uniformity of all turbine and generator forgings is emphasized as a high need. Of four other forgings identical to the Ridgeland design and supplied by the same mill, one was essentially without any sonic indications. Two had a few minor indications and they were in regions indicating they were not cracks. The fourth forging required scrapping. All were made in a period of about two years, and their quality bore no relation to the order of manufacture. That important improvements in the making of consistently reliable forgings will occur as a result of this unfortunate experience seems a reasonable prediction.

Especially is quality vital in the notch-sensitive steel of usual

[4] Chief Engineer of Power Plants, Wisconsin Electric Power Company, Milwaukee, Wis. Mem. ASME.

turbine and generator forgings. The stress at the point of a crack that approaches zero width is almost infinite. Brittle fracture occurs at an over-all stress that is but a minor fraction of usual tensile strength. Behavior is like that of glass; not that of a ductile steel as usual elongation tests indicate. A less notch-sensitive steel is needed, especially until forgings of integrity can be consistently assured.

C. M. Laffoon.[5] The two companies responsible for the manufacture of the turbine-generators under discussion are to be commended for the thorough and painstaking investigations they have made to ascertain the causes of the failures. Likewise, the authors of the papers[6] also deserve commendation for the splendid preparation and presentation. It is always comforting and gratifying, in the case of such disasters, to be able to find the cause of the trouble so that adequate steps can be taken to avoid the occurrence of similar or related troubles on other units. In these instances of trouble, deficiencies in design and manufacturing practices and defects in materials are concluded to be responsible for the failures. Operating procedures and conditions were not judged to be factors contributing to the failures.

These papers and the three related papers presented at the meeting direct major emphasis on the material phase of the problem. It is surprising to note that these particular forgings had such great numbers of sonic indications, some of which were very large, and the rotors were judged usable. Of several hundred rotor forgings produced for turbine-generators for the Westinghouse company all of which were sonically inspected, none has had sonic indications that approached the number or size reported for these rotors. Another striking difference is the much smaller percentage of our rotors which had hydrogen flakes or thermal-crack type of defects. Our generator forgings were produced by the same forging suppliers using the same material composition, manufacturing equipment, methods, and processes to meet essentially the same specification requirements. The only apparent reason for this wide spread in sonic indications is that most of our forgings were probably smaller in diameter and weight than those covered by the papers under discussion. This is in conformity with our major design premise that smaller forgings can be obtained with a better relationship of strength and ductility, greater uniformity of properties throughout the entire section of the rotor, and greater freedom from internal defects in general and thermal cracks in particular.

In the case of one large generator-rotor forging, numerous sonic indications of appreciable magnitude were found randomly located in radial-longitudinal planes in the deep-seated sections of the body. The defects were diagnosed as cracks by our engineers and metallurgists, and the forging was considered unusable. However, the forging supplier was equally convinced that the indications were harmless inclusions. A subsequent sectioning of the forging definitely established the fact that they were cracks. It is quite probable that a rotor failure would have occurred if this forging had been used.

Reference is made in these and the related papers to several rotor-forging phenomena; namely, (*a*) delayed flaking in ingots and forgings, (*b*) transition temperatures, brittle-fracture susceptibility, and influence of "stress raisers," and (*c*) the effect of occluded hydrogen on ductility and crack formation. It is apparent from the limited knowledge and effects of these factors that the equipment-design engineers, and the metallurgists of both the equipment and forging suppliers have not been fully cognizant of their extent and significance for the alloy steels used for rotor forgings. Recently, the few cases of the delayed flaking in small billets and forgings that have been experienced have been rather disconcerting and raise the question in regard to the possibility of their occurring in turbine-generator forgings. There is some comfort in the fact that delayed flaking usually occurs within a short time (few weeks) after a billet or forging is completed, and thus should be detected if carefully checked ultrasonically at the time the unit is completed and ready for shipment. These items are being investigated by the forging suppliers and the equipment manufacturers.

During the past five years, design engineers and metallurgists of the writer's company have been working co-operatively with all of the United States forging suppliers with the goal of developing specifications covering the material composition, physical and performance characteristics, inspection techniques, and acceptance standards for turbine-generator-rotor forgings. The co-operative program includes (*a*) obtaining complete data of the characteristics for all sections of forgings on the basis of present material compositions, (*b*) review of melting, forging, and heat-treating practices in this country and Europe, (*c*) development of sonic-inspection techniques to locate and identify forging defects, (*d*) determine by spinning and stress-cycling tests on large pieces the effect of different types of defects on rotor performance, and (*e*) preparation of inspection techniques and acceptance standards. Although this is a long-range program, much work has been done and real progress accomplished. Significant improvements in the forging situation and in the quality of forgings are being obtained now as compared to those obtained in the period prior to 1950.

In one of the related papers reference is made to a 100,000-kw, 3600-rpm Westinghouse turbine-generator with a 40-in. rotor diameter which was inadvertently subjected to a rotation speed of 150 per cent or more. The mean and peak stresses in the main rotor parts were increased more than 125 per cent over those existing at normal speed. A complete examination of the generator rotor indicated that (*a*) the blower hubs had yielded plastically and had become elliptical in shape; (*b*) the retaining rings were still in alignment and in proper pressure contact with the rotor body but had yielded slightly at their outboard ends and were elliptical in shape; and (*c*) the material at the rotor bore had yielded plastically at several areas having minor inclusions. The shrink fits and truth of the respective parts were restored by machining and/or replacement of minor parts. The inclusions at the bore surface and immediately back of this surface, as found by sonic and magnetic-particle checks, were removed by enlarging the bore. The reconditioned rotors of the turbine and generator have been returned to service and are now in satisfactory operation. This accidental overspeed run demonstrated that the material of the highly stressed rotor components had good ductility, was free of cracks and stress-raiser defects, and had appreciable reserve strength for speeds much greater than 150 per cent.

Recently, a retaining ring of a 1500-rpm, 25-cycle, 20,000-kw turbine-generator failed during an overspeed check of the turbine governor after 42 years of operation. The rings had positioning rectangular-shaped notches cut in one end with relatively sharp fillets at the corners. The fractures started at the corners of the positioning notches and progressed rapidly in a longitudinal direction across the ring section. The fractures were of the brittle type with the surfaces following the grain boundaries. Subsequent checks of the material showed very low impact values, and a transition temperature in the range just below operating temperatures. It appears that for this particular day the combination of temperature and material characteristics was favorable to crack propagation when the overspeed run was made.

Although the forging reliability record of turbine-generators

---

[5] Consulting Engineer, Westinghouse Electric Corporation, El Cajon, Calif. Mem. ASME.

[6] This discussion also includes discussion of "Report of the Investigation of Two Generator Rotor Fractures," by C. Schabtach, A. W. Rankin, E. H. Fogelman, and D. H. Winne, published in this issue, pp. 1567–1584.

placed in service prior to the use of sonic testing has been good, the occasional failure and the lack of complete information on the rotor materials raises a question as to what consideration should be given to operating practices, inspection, and maintenance procedures. In view of the fact that some of these rotors may have design and machining features below present-day standards, and that rotor parts have been exposed to abnormal localized stresses from short circuits, overspeed, and cycling during starting and stopping, it is our recommendation that the user give consideration to a comprehensive program of inspection and maintenance at periodic intervals. All of the present-day inspection techniques can and should be used in all of the major parts of the rotor.

Company engineers have recently developed a method by which complete sonic indication can be made on the rotor body at any time. It involves machining crescent-shaped longitudinal grooves in the surface of the pole centers near the slotted sections, as shown in Fig. 21 of this discussion, and the use of circular crystals. In the future, all turbine-generators having rotors of 34-in. diam and above will be provided with such grooves so that complete sonic investigation can be made at any time after the unit is placed in service.

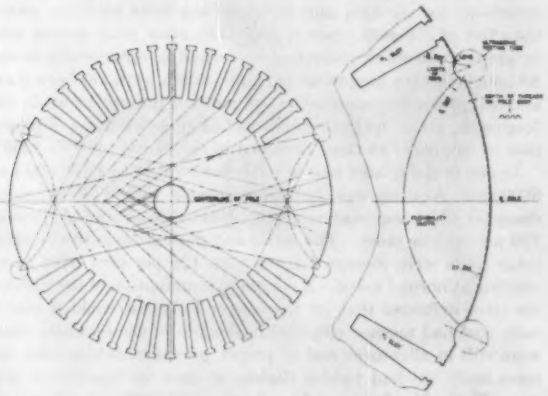

FIG. 21 FIELD ULTRASONIC INSPECTION FOR TURBINE-GENERATOR ROTORS

This method of sonic inspection is the most sensitive and searching of all present-day methods under consideration because the direct beam of the most favorable frequency with its maximum energy can be used and the defect can be viewed from all directions from two to four locations on the rotor surface. It consequently offers the greatest potential for determining the type and magnitude of defects. The crescent-shaped grooves can be cut in rotors in service at relatively small expense and time by means of portable tools and established procedures. Other parts such as retaining rings can be reliably checked for external surface cracks by means of surface-type crystals and recently developed techniques.

Although adequate data are not yet available on transition temperature and brittle-fracture susceptibilities of alloy steels, maximum protection against failures from this cause can be obtained by preheating the rotor body at low rotational speed during the starting-up period following prolonged shutdowns.

In fairness to the rotor-forging suppliers, it should be remembered that an adequate solution to the rotor-reliability problem necessitates that searching consideration be given to the equally important factors of mechanical design, manufacturing practices, and operating procedures. It is the inherent responsibility of the equipment manufacturer to make certain that design standards and manufacturing practices, and processes, and materials used in the construction of large high-speed turbine-generator units are compatible and commensurate with the highest state of the art at the time in question. Entry into an unexplored field such as large increments in size, should be made with caution and each step should be made only after having considered and evaluated all of the pertinent factors involved.

It is encumbent on the designer to realize and appreciate that forgings are not perfect and have inherent limitations as a result of variations in structure, and lack of uniformity in strength and ductility. The design must be tempered accordingly and first emphasis placed on mechanical reliability with cost and performance efficiency relegated to positions of lower order. The purchaser has a right to expect that the mechanical reliability of turbine-generators of large rating be equal or superior to that of smaller units. This objective cannot be readily accomplished by simply making them larger and larger, and working the materials harder and harder for the larger ratings. Curves showing desired mechanical reliability as a function of size and obtainable reliability are divergent as the size increases for a given type of design.

The approach of the writer's company to the solution of the problem of obtaining greater mechanical reliability for large turbine-generators can be divided in two steps. The first step was the development of the 3600-rpm units so that rotor forgings of smaller diameter and weight could be used. The gains apply to both the turbine and generator. The second step was the development of inner cooling which has made possible a further material reduction of the rotor diameter and approximately 50 per cent reduction in rotor weight for a given rating. Inner-cooled 3600-rpm turbine-generators can be built for ratings up to 350,000 kw with rotor diameters no larger than now used for 60,000-kw units of conventional design, and thus have the mechanical reliability of the smaller unit. The large reduction in rotor weight makes it possible to keep the ratio of rotor-body length to diameters well within the values now used for units of conventional design and smaller rating. Smaller forgings not only result in improvements in characteristics under the present state of the art but will accelerate the programs now under way for obtaining further improvements from changes in composition, melting and ingot casting methods and controls, forging techniques, and heat-treatment practices.

It is encouraging that so much work is being done by the equipment manufacturers, and the forging suppliers in this country and in different parts of Europe. Out of this determined effort will come better forgings, better designs, improved manufacturing procedures, and realistic operating practices.

F. E. REED.[7] When the failure of the Ridgeland low-pressure turbine spindle was discussed at the meeting, the writer had the feeling that although the material of the rotor was not as good as would be desired, the explanation of the failure in only metallurgical terms did not explain some of the characteristics of the failure. Brittle fracture caused by poor material should occur the first time an overspeed is reached, not after four months of service, ten start-ups, and nine overspeed tests. Slow progressive fracture is a characteristic of fatigue, not of brittle fracture. The paper does not indicate that there was fatigue crack initiating the brittle fracture.

If the tangential stress reported for the normal operating speed is stepped up to account for the 8.6 per cent overspeed, the resulting 23,000 psi is still a moderate stress for the material which is used. If this stress is given a stress-concentration factor of 3, the resulting stress is below the experimentally determined yield

[7] Technical Operations, Inc., Arlington, Mass.

point and well below the tensile strength. It is not indicated that the flakiness in the test samples removed from the rotor influenced either the tensile strength or the impact values enough to bring those properties significantly below the specification limits.

In searching for some additional reasons which might help to explain the failure, it appeared that the failure might arise from the thermal stress induced when warming up the turbine. This could differ from one start-up to another and, if significant as compared to the centrifugal stresses, might explain the failure occurring after considerable use. At first it was thought that this thermal stress might be intensified by the fact that the turbines were carrying no external load. The steam passing through them would therefore be doing no external work and might therefore be highly superheated when it reached the low-pressure turbine. However, it was noted in the paper that the steam temperature at this point was 300 F so that the flow must have been so low that the structure absorbed the temperature.

To check the thermal-stress hypothesis, calculations were made of the stresses resulting from heating of the exterior of the spindle. These calculations are presented in a later part of this discussion. Since they are somewhat complicated and since detailed information on the construction and operation of the turbine was not available, they have been simplified and should be considered to indicate about what might occur. These calculations indicate:

(*a*) The transient thermal stresses in the spindle may be considerably greater than the centrifugal stresses.

(*b*) The maximum transient thermal stress occurs about 2½ hr after the heating is initiated.

It would appear from this approximate calculation that thermal stresses might be significant in the design of large-diameter spindles, even built-up units, and that thermal stress may have been the major contribution to the Ridgeland turbine failure.

In connection with the general experience of poor-quality material in the center of ingots because of the late solidification, the question might be raised as to the practicability of moving this area of inferior material into the outer portions of the ingot by cooling the center. A concentric tube cooling lance, which could be inserted into the center of the molten ingot and cooled at a suitable rate by the use of steam or air, might be effective in controlling this cooling. This lance would be removed in machining the central bore hole.

Calculations: The differential equation for transient heat flow in a cylinder, assuming no heat flow from the ends is

$$\frac{\partial^2 T}{\partial r^2} + \frac{1}{r}\frac{\partial T}{\partial r} - \frac{1}{\kappa}\frac{\partial T}{\partial \theta} = 0$$

The solution for this equation as applied to a hollow cylinder is given by Carslow and Jaeger.[8]

The equations for thermal stress in a hollow cylinder are developed by Timoshenko.[9] If it is assumed that the cylinder is unrestrained at the ends, it can be shown that the stresses in the inner surface will be

$$\sigma_r = 0$$

$$\sigma_\theta = \sigma_z = \frac{\alpha E}{1-\mu}\left(\frac{2}{b^2-a^2}\int_a^b Tr\,dr - T\right) \quad \ldots\ldots [1]$$

If, now, it is assumed that there is no heat flow across the inner surface of the cylinder, it will be found by inserting the theoretical temperature distribution in the stress relationships that the thermal stresses at the inner radius are given by

$$\sigma_\theta = \sigma_z = \frac{\pi \alpha E}{1-\mu}\sum_{n=1}^{\infty} e^{-\kappa \alpha_n^2 \theta}$$
$$\left\{\frac{[K\alpha_n J_1(b\alpha_n) - k_2' J_0(b\alpha_n)][-k_2' \alpha_n J(a\alpha_n)]}{F(\alpha_n)}\right\}$$
$$\left\{J_0(a\alpha_n)\alpha_n Y_1(a\alpha_n) - Y_0(a\alpha_n)\alpha_n J_1(a\alpha_n) - \frac{2b}{(b^2-a^2)}[Y_1(a\alpha_n)J_1(b\alpha_n) - J_1(a\alpha_n)Y_1(b\alpha_n)]\right\} \quad \ldots\ldots [2]$$

where

α = coefficient of linear expansion of rotor material; taken as 6.67×10^{-6} per 1 deg F
E = elastic modulus of rotor material; taken as 30×10^6 psi
μ = Poisson's ratio; taken as 0.33
κ = diffusivity of the material = $K/c\rho$
K = thermal conductivity of rotor material; taken as 1.818 Btu/hr sq in. deg F/in.
C = specific heat of rotor material; taken as 0.12 Btu/lb deg F
ρ = density of rotor material; taken as 0.284 pci
α_n = eigenvalues obtained by the solution of Equation [3]
θ = time, hr
k_2' = surface conductivity of the rotor; taken as 50 Btu/hr sq ft deg F or 0.347 Btu/hr sq in. deg F.
k_2' = product of surface conductivity and difference between external temperature and initial uniform rotor temperature
a = inside radius of rotor, taken as 4 in.
b = outside radius of rotor, taken as 40 in.
$J_0(\ )$, $J_1(\ )$, $Y_0(\ )$, and $Y_1(\ )$, are Bessel functions

$$F(\alpha_n) = (K^2\alpha_n^2 + k_2'^2)[\alpha_n J_1(a\alpha_n)]^2 - \alpha_n^2[K\alpha_n J_1(b\alpha_n) - k_2' J_0(b\alpha_n)]^2$$

α_n are the roots of

$$\alpha J_1(a\alpha)[K\alpha Y_1(b\alpha) - k_2' Y_0(b\alpha)] - \alpha Y_1(a\alpha)[K\alpha J_1(b\alpha) - k_2' J_0(b\alpha)] = 0 \quad \ldots\ldots [3]$$

When these relationships are solved the stress is found to be given by the equation

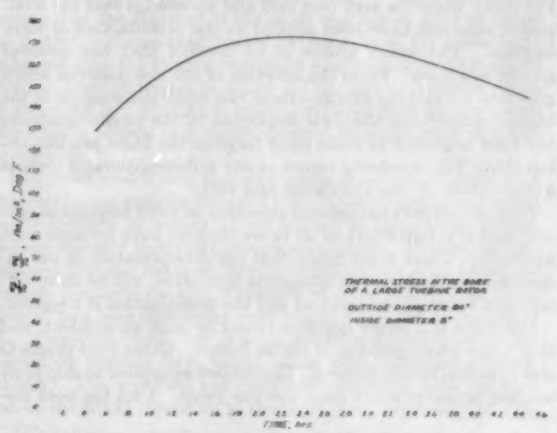

FIG. 22

[8] "Conduction of Heat in Solids," by H. S. Carslow and J. C. Jaeger, Oxford University Press, London, England, first edition, 1947, pp. 278–279.

[9] "Theory of Elasticity," by S. Timoshenko, McGraw-Hill Publishing Company, New York, N. Y., 1934, p. 371.

$$\sigma_\theta = \sigma_z = T_0 [303.6e^{-0.1351\theta} - 290.6e^{-0.2611\theta} + 140.9e^{-2.2\theta} - 91.2e^{-4.221\theta} + 57.6e^{-7.24\theta} - 42.4e^{-10.25\theta} + \ldots\ldots]$$

The plot of this stress is given in Fig. 22 of this discussion.

If it is assumed that the mean temperature of the rotor is 150 F when 300 F steam is introduced to the outside, a maximum stress of 25,850 psi would be set up in the bore about 2½ hr after the steam is introduced to the exterior.

A. O. SCHAEFER.[10] The author is to be congratulated upon his very clear presentation of a very well-designed and planned examination of a rotor forging. The results and the conclusions are indisputable and little more can be added to the paper. In the years to come, however, there will be much more to be said on ultrasonic testing and its interpretation, hydrogen flakes, brittle failure, segregation, transition temperatures, and all of the other aspects of the use of steel (or of any engineering metal, for that matter) which have again been brought into the limelight by this tragic accident.

Many of these subjects are considered controversial; at least it can be said that metallurgists and engineers do not always agree upon them. Some say that flakes are caused by hydrogen alone, many do not agree and can present data to show that other stresses are necessary. Certainly we cannot say what level of hydrogen content is necessary to cause or contribute to the cause of flakes. We know positively that flakes have occurred in steels with very low hydrogen concentration, and that they have been avoided by very careful heat-treatment of steels with quite high hydrogen concentrations.

Segregation accounts for many of the ills of steel. It is a result of natural laws operating during the solidification of a complex solution, and is unavoidable in the casting of ingots by conventional means. Furthermore, it is undoubtedly exaggerated in large ingots. The degree of segregation permissible in ingots of a size (and of a given material) is again approaching a point on which we might have disagreement.

Certainly we have designed and made many fine rotor forgings, which are proving themselves by giving excellent service. Some of them may be performing satisfactorily even in spite of the presence of flakes, because we are just now beginning to feel certain that we can find flakes if they are present by ultrasonic equipment. Whether or not some of these rotors are flaked, it is certain that all of them contain segregated metal to a degree, and that all of them contain hydrogen.

There is another very important thing that we may be sure of. For many years the very best skill and knowledge that the steelmaker possesses have been applied to the manufacture of rotor forgings. The writer knows of no product that has received greater attention. From the selection of the raw material which goes into the melting charge—these raw materials must be of the highest quality—to the final inspection of the product, nothing has been neglected to make rotor forgings the finest product obtainable. The wonderful record of our turbine-generator units is a verification of this knowledge and care.

Now an accident has focused attention on rotor forgings in general, and it is important to all to see that we have no more such accidents. There is no doubt that our interpretation of our inspection, particularly the ultrasonic inspection, will be more certain as a result of the accident and the investigation it triggered.

But there is a larger question raised by such an accident, and that is the whole problem of brittle failure. Other steel products also have had brittle failures. The subject as applied to ship plate has had intensive study since the war years. A lot has been discovered, but a lot remains to be done until we fully understand why cracks originate in materials. When we understand this, we must also know something about how they propagate. Knowledge of the intricate relationship of design and structure and the unavoidable irregularities in metal objects will benefit by research and development prompted by our recent experience.

A failure such as that here reported is a horrible thing, and it is most unfortunate that it had to happen. Since it did happen, we can be thankful that its cause was not so obscure as to leave doubts in the minds of those who investigated it. Ways of inspection have been suggested which make it probable we will correctly appraise such conditions in the future. This is good. It is also good that we can hope for needed fundamental information on the propagation of cracks, so that we can fully understand how material as ductile as this can fracture in a brittle manner.

V. L. STONE.[11] This paper covers the accident, the investigations, and the findings on the cause of the failure so completely there is little that can be added. However, we feel that for the benefit of the industry, certain facts should be emphasized.

In order to obtain a completely unbiased opinion as to the causes of the accident, the Commonwealth Edison Company employed Battelle Memorial Institute, Dr. A. E. White, formerly of the University of Michigan, and Sargent & Lundy to conduct independent investigations.

The fatigue surface in the fillet area, which the author discusses, became a point of intensive investigation because of its critical location, the fact it conceivably could have been caused by high stresses due to design, and because it was clearly evident to all who viewed the debris. Without going into detail, the writer is pleased to report that, as a result of tests on models and an extensive stress analysis made by our consultants, it has been definitely concluded that the design was conservative and that the stresses, even at the fillets which are points of maximum stress concentrations, were well within the safe limits of the sound material and were not the cause of this fatigue crack or the failure.

Our consultants in their independent metallurgical tests found the thermal-crack condition described by the author and arrived at the same conclusion as Allis-Chalmers; that is, these cracks were unquestionably the primary cause of the failure and the cause of the fatigue crack.

Allis-Chalmers is to be commended for its energetic and objective search for the primary cause of the failure and for its complete co-operation with our consultants.

This failure has played an important role in focusing attention on the metallurgy of large forgings, on the general procedures for producing and inspecting such forgings, and has contributed to the advancement of the art of interpretation of sonic indications by providing a unique opportunity to evaluate test results against the actual discontinuities in a shaft which failed because of these causes. As a result, our confidence in the dependability of present and future large rotating elements has been substantially increased.

The reconstructed unit was returned to commercial operation on November 14, 1955, approximately 10½ months after the accident. Our thanks are extended to Allis-Chalmers for completely rebuilding the unit in such a short time after a disaster of this magnitude.

R. M. VAN DUZER.[12] The report on the Ridgeland disaster was received with concern on December 20, 1954, by the writer's company as two units, identical in all essential details, were in opera-

[10] Vice-President, The Midvale Company, Nicetown, Philadelphia, Pa.

[11] Manager of Production, Operating Division, Commonwealth Edison Company, Chicago, Ill. Mem. ASME.

[12] General Superintendent of Production, The Detroit Edison Company, Detroit, Mich. Mem. ASME.

tion in the St. Clair Power Plant of The Detroit Edison Company. One of these units was started in November, 1953, and the second in June, 1954.

As a result of the preliminary description of the Ridgeland failure, a load limit was immediately applied at 125 mw on the St. Clair units and periodic overspeed trials were eliminated. The plant personnel immediately were informed of known facts and subsequent information as it became available regarding the disaster.

After the manufacturer had an opportunity to examine the inspection and engineering design records of the St. Clair units, consultations were held regarding inspection thought necessary at St. Clair.

As a result of these conferences, it was decided to open and examine the low-pressure rotor of St. Clair No. 2. The low-pressure spindle forging during manufacture had disclosed some porosities in the bore of the forging. As a result, the original 8-in. hole was enlarged to 12 in. for approximately 75 per cent of the forging length. In contrast, the forging for St. Clair No. 3 had disclosed no defects upon examination of the original 8-in. bore.

The rotor was removed, bore plugs taken out, blade rings on each side of the main body were removed, and the forging was inspected thoroughly. This consisted of visual examination, magnetic particle, and ultrasonic testing. Prior to testing, the fillet areas and the interior bore were cleaned and polished thoroughly.

All tests indicated the absence of any defects. Accordingly, load limitations on St. Clair No. 3 were removed and the St. Clair No. 2 unit was reassembled. At that time, inspection of No. 3 was deferred until the cause of the Ridgeland failure was determined. These results have, of course, been presented by the author.

The Ridgeland results, together with the field examination of No. 2 St. Clair, reconfirm that the two St. Clair forgings are sound. The No. 3 St. Clair low-pressure spindle will not be stripped during the inspection of this unit in 1956.

In view of the Ridgeland failure and those of other large turbine and generator forgings, the most recent early in November, 1955, a reliable and simple inspecting method should be developed. There are a great number of turbine and generator forgings in service that did not have the benefit of thorough sonic testing at the time of their manufacture, nor an intelligent interpretation of sonic results where such testing was done.

The author and his company must be complimented for the active part they have taken in the industry to prevent the recurrence of such failures as that experienced at Ridgeland. This paper represents only a portion of that very worth-while endeavor.

Author's Closure

The reception by the power-generation industry and its associated engineers of the Allis-Chalmers report on its investigation of the Ridgeland failure has been very gratifying to the author and his co-workers. The most important objective in an investigation of this type is the determination beyond any reasonable doubt of the cause of failure. The general acceptance of the conclusions of our investigation strengthens the conviction that the basic cause of the accident has been found and that our efforts in developing preventive measures are properly directed.

Mr. Drewry has mentioned the other machines which were put into service with low-pressure spindle designs identical to that of Ridgeland. Immediately following the accident in Chicago, an extensive resurvey was made of the records of the remaining four forgings. Three machines eventually were taken out of service and their low-pressure shafts thoroughly retested with ultrasonic, magnetic particle, and borescope inspection equipment, taking full advantage of the technical knowledge developing from the Ridgeland investigation. One shaft was scrapped, and subsequent destructive examinations have shown that the forging contained a crack pattern very similar to that of the Ridgeland shaft. Fortunately, a duplicate unit was being processed through our shops at the time, and the scrapped shaft was replaced and the unit was quickly returned to service.

The inspections of the other two disassembled units indicated basic soundness of the low-pressure shafts, and the units were therefore reassembled and returned to service. The fifth unit was not shut down, since the integrity of its low-pressure shaft was beyond question.

Mr. Laffoon's comments reflect much of the present general thinking of the turbine industry on large forgings. The use of increasingly bigger forgings, as a consequence of demands for more turbine capability by the power generation industry, has been of concern to turbine designers for some time. The paper presented by Messrs. Mochel, Peterson, Conrad, and Gunther[12] at this meeting points out that Westinghouse placed into service during the period 1947–1951 six units with low-pressure turbine shafts similar in both configuration and size to the Ridgeland shaft. Westinghouse engineers apparently decided in favor of large forgings, even though adequate means were not available at the time for inspecting the interiors of these large masses of metal.

Allis-Chalmers retained until 1951 the principle of constructing large low-pressure turbine spindles by shrinking disks onto a central shaft. After this date, for reasons outlined in the paper, the five machines of the Ridgeland design incorporated low-pressure shafts with large-diameter central bodies. When a sixth machine of the series was ordered in late 1952, prior to the Ridgeland accident, a high-strength disk material, meeting ASTM Specification A294-52T Class B3, was adopted. This permitted reverting back to a central shaft with all blading carried on shrunk-on rings. This all-disk design was preferred from the standpoint of both cost and production time, and it has relieved to some extent the problem of procurement of sound shaft forgings. Fig. 23 is a cross section through the modified low-pressure turbine design as it appears in Unit 3 at the Oak Creek Station of the Wisconsin Electric Power Company. The spindle construction of the rebuilt Ridgeland low-pressure turbine is identical.

Mr. Reed's discussion covers several points which were not included in the paper in the interest of brevity. He is generous in stating that the material of the shaft was not so good as would be desired. Macro-examination of slabs from the main body indicated that the forging contained approximately 5000 cracks with an average length of about 1.7 in. and an average depth of about 0.8 in. Putting it mildly, material such as this leaves much to be desired in a highly stressed structure such as a turbine spindle.

Mr. Reed points out that the paper does not indicate that flakiness in test samples removed from the shaft influenced either tensile strength or impact values enough to bring those properties significantly below the specification limit. It must be emphasized that the flakes or thermal cracks which were found are actually complete metallic cleavages of considerable area. Obviously, test bars containing such cracks could not be pulled at all. Therefore, each bar was carefully magnetic-particle inspected for freedom from cracks before being subjected to physical test. The reported test results consequently bear no relation to the flaked condition of the shaft; they serve only to indi-

[12] "Large Rotor Forgings for Turbines and Generators," by R. E. Peterson, N. L. Mochel, J. D. Conrad, and D. W. Gunther, Published in this issue, pp. 1585–1600.

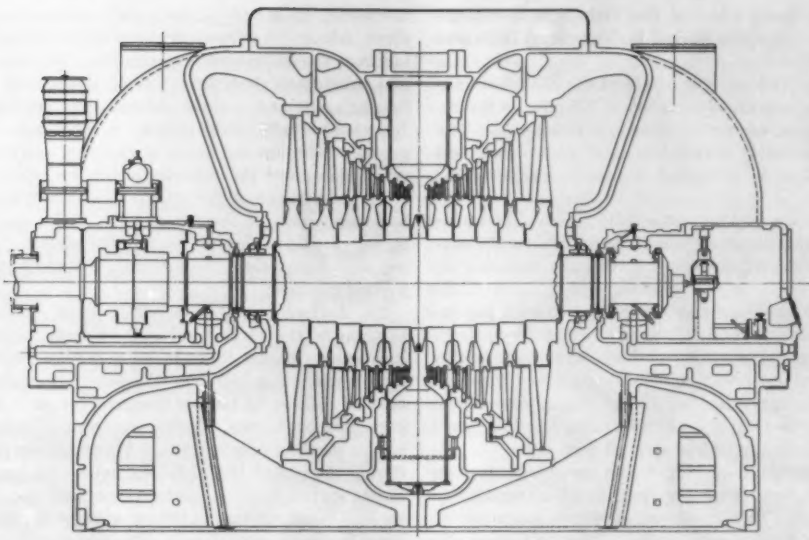

FIG. 23 CROSS SECTION OF LOW-PRESSURE TURBINE WITH MODIFIED SPINDLE DESIGN—OAK CREEK UNIT 3 OF WISCONSIN ELECTRIC POWER COMPANY

cate the general strength and ductility levels of unflaked areas.

Mr. Reed states that brittle fracture caused by poor material should occur the first time an overspeed is reached and that slow progressive fracture is a characteristic of fatigue, not of brittle fracture. It is stated in the paper that the bursting speed of a sound and ductile shaft is governed by the level of the average tangential stress. Unfortunately, the average tangential stress loses significance in a shaft of notch-sensitive material containing cracks. The local elastic stress at the bore of the Ridgeland shaft at nominal overspeed is of the order of 48,000 psi. This stress is well below the yield strength, and in sound material it will not affect bursting speed. But in the presence of discontinuities such as sharp cracks and consequent plastic constraint, such a stress is quite sufficient to cause crack extensions. It is thought that there were ductile crack extensions near the bore to some degree each time the turbine was overspeeded. Since these extensions were in the interior of the metal, demarkation lines normally associated with fatigue did not appear. In accordance with present concepts of brittle failure, the cracks continued to extend under periodic overstress until at a critical crack size and stress they became unstable and ran catastrophically.

Mr. Reed's thermal-stress analysis closely parallels normal turbine design practice in general approach. The only significant differences are the designer's use of actual operating temperatures, experimentally determined film coefficients, and estimated isothermals for each specific spindle configuration.

Normal turbine operating procedure is of significance in considering the possible effects of thermal gradients and stresses in large shafts. In shutting down a large cross-compound machine, load is generally reduced gradually and the machine tripped off the line. Both shafts decelerate independently to a standstill and are then immediately placed on their turning gears. At Ridgeland, the turning gears rotate the high-speed shafts at 40 rpm and the low-speed shafts at 20 rpm. For a two-day shutdown the shafts are kept rotating continuously, and after some hours the low-pressure shaft main body attains a fairly uniform temperature of about 175 F.

When the machine is to be started again, the stop valves and No. 1 inlet valve are opened and the shafts are rolled off the turning gear with steam. Fig. 24 shows a typical temperature

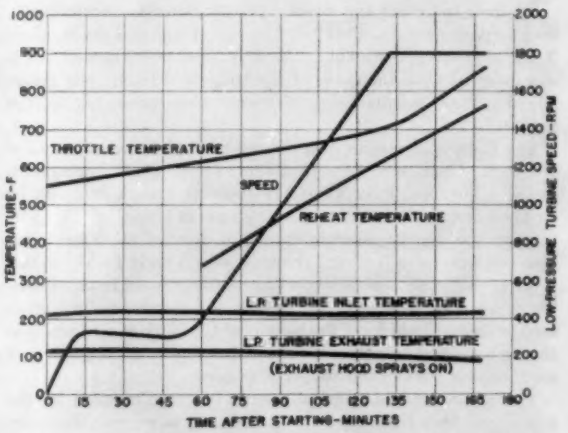

FIG. 24 TYPICAL START-UP CURVES—RIDGELAND UNIT 4 OF COMMONWEALTH EDISON COMPANY

variation curve for the Ridgeland unit on start-up following a two-day shutdown. These data are representative of the start-up on December 19, following which failure occurred. As the shafts come off turning gear the throttle temperature is between 500 and 600 F, the low-pressure turbine inlet temperature is slightly over 200 F, and the low-pressure turbine exhaust temperature is slightly over 100 F. The temperature differential between steam entering the low-pressure turbine and the adjacent spindle surface metal is less than 50 F. Thermal gradients within the spindle are much smaller.

Turbine speed is brought up rapidly to about 325 rpm on the low-pressure shaft and held for 30 to 40 minutes. During this time vacuum is improved and throttle temperature is increased about 50 F. The turbine is then accelerated uniformly to rated speed over a time interval of approximately one and one-half hours. Fig. 24 shows that throttle and reheat temperatures are gradually increased during this period, but low-pressure turbine inlet temperature remains essentially constant. Cylinder and

spindle metal temperatures in the vicinity of the low-pressure turbine inlet gradually approach 200 F during this period.

If the turbine is to be oversped after attaining rated speed, the inlet valve is opened further to accelerate the machine and the low-pressure turbine inlet temperature tends to rise. This rise is not great and is for only a brief period. As soon as the machine trips out, the temperature drops back down to the 200 F level. The change in spindle metal temperature during this short interval is insignificant.

Our reasons for considering that thermal stresses did not play a dominant part in the Ridgeland low-pressure turbine failure will be evident from the foregoing data. Analyses of thermal effects are an important phase of modern turbine engineering, and the results on any specific machine not only dictate much of the design, but they also establish recommended operating procedures and schedules such as shown in Fig. 24. That the thermal-stress level permitted by such operation is not dangerous in the absence of abnormal discontinuities or stress raisers is well evidenced by the successful long-time operation of many machines under similar and frequently more strenuous conditions. The basic test for any theory of failure is whether it satisfactorily separates the unsuccessful from the successful. The assumption that thermal stresses were a primary cause of the Ridgeland failure does not meet this test.

As chairman of the ASTM Task Group on Brittle Failure of Steel Forgings, Mr. Schaefer has a broad picture of the circumstances and subsequent investigations of all of the failures which have recently disturbed the industry. He is correct in pointing out that many of the metallurgical factors surrounding brittle failure, hydrogen flakes, and ultrasonic testing and interpretation are considered controversial. The author's company has participated fully in the work of Mr. Schaefer's Task Group, and we believe that the calm and methodical approach of this group to its assignment is contributing greatly toward resolving many of the present controversies and developing additional fundamental information.

Mr. Stone's statements regarding the independent investigations conducted by consultants to the Commonwealth Edison Company are very valuable in judging the merit of the conclusions from our investigation as reported in the paper. The fact that the unbiased opinions of the Commonwealth Edison consultants were in essential agreement with ours is of itself strong supporting evidence that the basic cause of failure was found. Tragic as the accident was, it furnished the incentive for these many parallel investigations and afforded an opportunity to evaluate causes and effects that would never have been available under less drastic circumstances.

The inspection of the No. 2 unit in the St. Clair Power Plant of The Detroit Edison Company, as described by Mr. Van Duser, emphasized to us the necessity of developing improved methods of examining large forgings in the field. The experiences in 1955 with this turbine and others, under widely varying conditions, have enabled us to draw a number of practical conclusions regarding both techniques and probable value of results using equipment available today. In particular, we have found that ultrasonic inspection in the field is not presently developed to the point where completely satisfactory examinations can be made.

A basic part of any field inspection of a forging must therefore be a thorough check of the bore surface using modern high-power borescope and magnetic-particle equipment. Even though this requires removal of bore plugs, any less complete inspection is presently so inconclusive as to be worthless. To assist in bore inspection, design changes have recently been put into effect to facilitate plug removal. Also, all turbine-shaft center bores are now charged with nitrogen after final plugging, to resist rusting and corrosion in service.

Report of the Investigation of Two Generator Rotor Fractures

By C. SCHABTACH,[1] E. L. FOGLEMAN,[2] A. W. RANKIN,[3] and D. H. WINNE,[4] SCHENECTADY, N. Y.

The recent fractures of two large generator rotors led to the initiation of an extensive investigation to clarify the causes of the trouble. This paper describes the various phases of the investigation, which included a thorough study of features of design and manufacture and the characteristics of the rotor materials, together with a presentation of the results.

Introduction

TWO large 3600-rpm generator rotors burst during 1954, while rotating near rated speed. In both cases, the fractures were of a brittle nature and occurred suddenly and without warning. The materials were ductile by common standards and of a type widely used in this country for generator rotors. Although the rotors were relatively large—one was of the largest size built thus far for 3600 rpm—all of the many others of the same sizes have operated satisfactorily. The design stresses in relation to the mechanical strength of the materials provide for adequate margins of safety. The exceptional nature of these accidents, coupled with the great importance of reliability in central-station generating apparatus, called for a complete and careful investigation of all features of the design and manufacture and of the characteristics of the materials of the rotors all of which might clarify the cause of the trouble. This investigation was initiated promptly and is being carried out energetically with all of the resources available. This paper is a summary report of the results to date.

The investigations presented in this paper have established that these rotors burst because of particular differences between them and others of the same size and design. These investigations have confirmed the soundness of the normal design features and the adequacy of the materials specified and, with the improved practices which will henceforth eliminate the particular differences which were the major causes of the two bursts discussed here, there is no reason to believe that reliable units of still larger capacity cannot be built in the future. Beyond this, these studies have improved our general knowledge of the behavior of steel in these large rotor masses. This knowledge, coupled with the alloy and steel making modifications now being intensively investigated, should result in steels with properties even superior to those of the rotor alloys for which past records of successful operation have been established.

[1] Manager-Engineering, Large Steam Turbine-Generator Department, General Electric Company. Mem. ASME.

[2] Large Steam Turbine-Generator Department, General Electric Company.

[3] Large Steam Turbine-Generator Department, General Electric Company. Mem. ASME.

[4] Large Steam Turbine-Generator Department, General Electric Company. Assoc. Mem. ASME.

Contributed by the Power Division and presented at a joint session of the Power and Metals Engineering Divisions at the Diamond Jubilee Annual Meeting, Chicago, Ill., November 13–18, 1955, of The American Society of Mechanical Engineers.

Note: Statements and opinions advanced in papers are to be understood as individual expressions of their authors and not those of the Society. Manuscript received at ASME Headquarters, November 9, 1955. Paper No. 55—A-208.

Arizona Rotor

Nature and Circumstances of the Burst

On March 4, 1954 the rotor of a 147,000-kva, 3600-rpm generator being manufactured for the Arizona Public Service Company burst while being balanced in the factory. The balancing was being done in the "precision balance pit," a below-floor-level trench in which the rotor was driven by a small steam turbine. It had been run intermittently at speeds below 2000 rpm as part of the normal balancing procedure and was being brought slowly up to full speed when it burst suddenly at about 3400 rpm.

The body dimensions of this rotor were 39 in. diam by 15 ft long. Several dozen others of the same or larger size are in service. The Arizona rotor, however, was unique in two major respects: (1) The number of large indications observed during ultrasonic testing of the rotor forging was greater than in any other forging accepted since sonic testing of rotors was begun in 1947. (2) A series of plugs had been shrunk into the bore of the rotor to increase its magnetic capacity.

Sonic tests of the rough forging at the steel mill showed numerous large indications throughout the entire length of the body and extending 10 or 11 in. radially outward from the axis. Consequently, the center was bored out to 3 in. diam, and the bore surface was examined with a borescope and a magnetic-particle test. Porosity was found, so the bore was enlarged to $3^1/_2$ in. and reexamined. Porosity was still evident. Greater enlargement of the bore hole would reduce the magnetic capacity of the rotor below excitation requirements, unless the bore hole could be filled with magnetic steel plugs. After careful consideration, it was decided to enlarge the bore further to gain additional information concerning the condition of material near the bore.

The bore was enlarged successively to $4^1/_2$, 5, and finally $5^1/_8$ in. and carefully examined at each step with the magnetic-particle test and borescope. No cracks were observed in the bore surface during any of these examinations. It was, therefore, concluded that the numerous sonic indications of imperfections remaining in the body outside the bore were dirt or slag inclusions which were believed to be harmless on the basis of our past experience. This conclusion was based on past practice that defects ranging outward from the bore could be identified by examination of the bore surface. At $5^1/_8$ in. in diam, the bore surface showed a few small spots of slag or dirt but no porosity. It was decided that the quality of the forging was acceptable and that, after inserting plugs in the oversize bore to restore the magnetic capacity, the forging could be used.

After the rotor burst, it was evident from the large number of fragments and examination of the fracture surfaces that the burst occurred in a brittle manner. No single origin of fracture could be found. However, there were numerous flat circular areas of about $1^1/_4$ in. diam on the primary fracture surfaces, noticeably different in color and texture from their surroundings. One of these marks is shown in Fig. 1. Their significance is discussed later.

Forging Manufacture and Properties

The forging as received from the mill weighed about 80,000 lb and was 30 ft long with a body $39^1/_2$ in. diam and 15 ft long. It was made from a 75-in. octagonal ingot weighing 212,000 lb.

TABLE 1 ARIZONA ROTOR CHEMICAL COMPOSITION

Element	Specification	Percentage composition: Ladle analysis	Bore surface	8-in. radius	Outer surface
C	0.32 max	0.29	0.32	0.31	0.29
Mn	0.90 max	0.90	0.99	0.97	0.97
P	0.050 max	0.013	0.014	0.013	0.013
S	0.050 max	0.024	0.020	0.020	0.020
Si	0.15–0.35	0.25	0.28	0.27	0.28
Ni	2.50 min	2.53	2.55	2.54	2.49
Mo	0.40 min	0.55	0.56	0.55	0.54
V	0.03 min	0.05	0.06	0.06	0.08
Cr	0.25 max	0.05	0.05	0.05	0.05
Sb	Not specified	...	0.005	...	...
As	Not specified	...	0.011	...	...

The ladle analysis of the basic open-hearth heat used to cast the ingot is given in Table 1. Supplementary analyses taken at several radial locations in a main-body fragment after bursting are also shown in the table. The chemical analyses indicate conformance to the specification and excellent correspondence between ladle and check analysis, with uniformity of composition from the bore to the surface of the forging.

The operations used to produce the rough forging were surface conditioning, upsetting, two operations to consolidate the center, rough shaping, rounding up, and two finishing operations. All forging operations were performed under a 3000-ton press, and the forging temperature range was 2250 to 1750 F. The ingot was reduced approximately 3:1 in cross-sectional area in forging to final size.

Prior to forging, the ingot received a preliminary annealing treatment to minimize the possibility of cracking during forging. Heat-treatment of the finished forging consisted of two normalizing cycles from 1650 F followed by 1100 F and 1200 F tempering treatments to produce the specified mechanical properties. It was stress-relieved at 980 F after rough machining and boring. The complete thermal treatment of the ingot and forging is given in Fig. 2.

The mechanical-property requirements of the specification and the results of acceptance tests are listed in Table 2. In accordance with standard procedure, the radial body specimens were taken near the outer periphery of the forging. Additional results of tests made on specimens from fragments of the burst rotor presented in Table 3 show little variation in tensile and yield strength from the acceptance-test values. However, specimens located within 6 in. of the bore generally exhibited lower ductility than those near the surface.

Preparatory to inserting plugs in the bore, the bore diameter was measured carefully throughout its length, and 16 plugs, each 1 ft long, were made to fit into it with 10 to 12-mils interference on the diameter. The plug material was a modified AISI-4140 composition. The rotor was heated to 980 F, equalized, and held for 48 hr. The plugs, at room temperature, were slid into the bore from the turbine end at half-hour intervals to permit each plug to come up to temperature and expand before inserting the next. After all the plugs were inserted, the forging was held at temperature for 4 more hours and furnace cooled.

Ultrasonic inspection of the forging following insertion of the plugs in the bore revealed no change in the number and magnitude of the indications found previously. The general level of magnitude of these indications ranged from 5 to 75 per cent of the bore reflection. Several indications as high as 225 per cent magnitude were noted.

Metallurgical Examination of Rotor Material

Ultrasonic examination of some of the larger fragments of the rotor located numerous internal defects which, when broken open, exhibited the same distinctive appearance as the circular marks observed on the primary fracture surfaces, Fig. 1. No large concentrations of porosity or nonmetallic inclusions were found of sufficient size to account for the indications found during ultra-

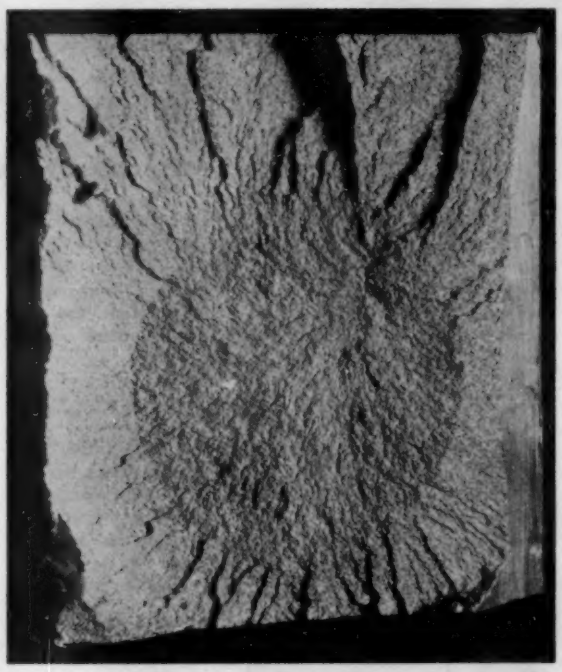

Fig. 1 Distinctive Circular Mark on Primary Fracture Surface
(Actual size shown here.)

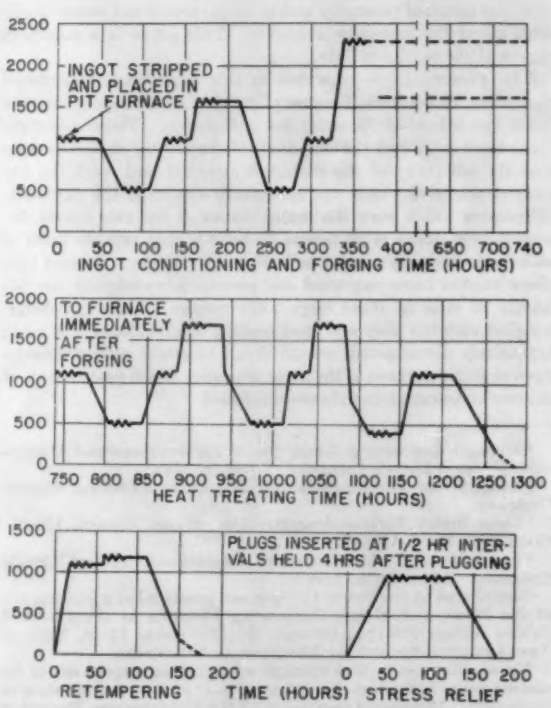

Fig. 2 Complete Heat-Treating Cycle

TABLE 2 ARIZONA ROTOR ACCEPTANCE TESTS FOR MECHANICAL PROPERTIES

	Location	Test direction	Tensile strength, psi	0.02 per cent yield strength, psi	Per cent elongation	Per cent reduction of area	Keyhole Charpy, ft-lb
Specification (minimum values)	Prolong	Longitudinal	100000	75000	17.0	32.0	...
	Body	Radial	100000	75000	13.0	22.0	...
Acceptance-test results	Prolong	Longitudinal	113000	85000	20.0	54.6	12, 14
	Mid-body	Radial	109500	80000	16.5	49.1	...
	End-body	Radial	114000	87500	15.0	39.4	...

TABLE 3 VARIATION OF TENSILE PROPERTIES IN ARIZONA ROTOR

Location rum bore, in.	Test direction	Tensile strength, psi	0.02 per cent yield strength, psi	Per cent elongation	Per cent reduction of area
10–14	Radial	108400	81700	15.5	34.7
		108500	82300	18.0	46.3
0–6	Radial	109600	82700	16.5	17.7
		110200	84000	..[a]	15.2
0–6	Radial	110500	86000	7.0	6.6
		104800	81500	5.0	4.1
6	Tangential	108400	81200	10.5	14.5
		107500	83000	8.0	10.4
1/2	Longitudinal	111300	82500	14.0	27.2
		112000	86000	13.5	26 1

[a] Not measured.

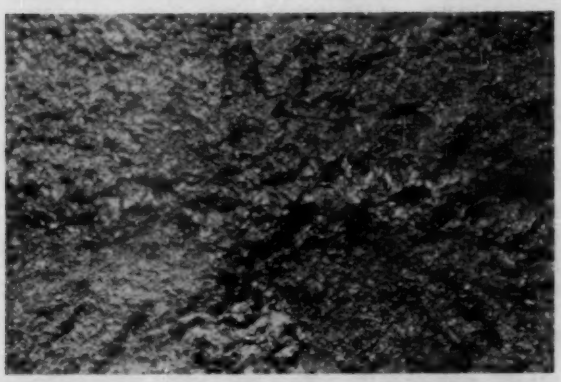

FIG. 3 PHOTOMICROGRAPH OF NUCLEUS OF CIRCULAR AREA OF FIG. 1 SHOWING COARSE GRAIN STRUCTURE; ×5

FIG. 4 SECTION OF ETCHED SPECIMEN SHOWING CRACKING ASSOCIATED WITH SEGREGATION LINES; HALF SIZE

sonic examination of the rotor. It must be concluded, therefore, that these indications came from disk-shaped cracks or areas of ruptured metal present in the forging before it burst, not from inclusions or dirt as the sonic-inspection data were originally interpreted.

Referring to Fig. 1, the fracture markings within the circular area appear to emanate from a definite nucleus. Metallographic examination at this location revealed abnormally coarse grains. The coarse-grained nucleus is shown enlarged in Fig. 3. In longitudinal and transverse etch test sections, these coarse-grained areas were found to lie in streaks of segregations oriented more or less parallel to the axis of the rotor. A photograph of a macro-etched section, Fig. 4, shows cracks originating at the segregation streaks and extending into the matrix.

The microstructure of the coarse-grained regions may be compared with the coarse bainite comprising the general microstructure of the forging in Fig. 5. The structure in the segregated areas appears to be martensite or fine bainite that formed after the transformation of the surrounding material. The hardness of the coarse-grained areas was found to range from Rockwell A62 to 66 (Brinell 243 to 297) as compared with 60.5 to 62.5 (Brinell 226 to 249) for the normal material.

Metallographic examination of the fractures indicated that they were predominantly transcrystalline, except at the circular marks

FIG. 5 PHOTOMICROGRAPH SHOWING COARSE GRAIN STRUCTURE OF SEGREGATION REGION TOGETHER WITH ADJACENT HOMOGENEOUS STRUCTURE; ×25

and in the disk-shaped cracks, where they were mostly intergranular, indicating a difference in origin.

The numerous experts who have examined these circular marks and cracks do not agree on what they are. However, we believe they are thermal cracks formed as a result of strains set up by volumetric changes during transformation, probably coupled with the embrittling effects of hydrogen dissolved in, or coming out of, solution in the metal.

Effects of Plugs in Bore

The plugs were shrink-fitted in the bore to keep them tight at speeds up to 25 per cent above normal. The resulting moderate increases in the tangential stress at the bore and in the average bursting stress at rated speed are shown in Table 4.

TABLE 4 CALCULATED ARIZONA ROTOR STRESSES

	Psi at		
	0 rpm	3400 rpm	3600 rpm
Average tangential bore stress (with plugs)	33500	50900	53200
(without plugs)	0	36500	41000
Radial bore stress (with plugs)	31000	13300	11300
Average bursting stress (with plugs)	8000	24300	26300
(without plugs)	0	20800	23400
Maximum tooth-root stress	0	22300	25000

These stress calculations ignore the effects of temperature gradients and friction as the cold plugs were heated and expanded in the hot bore. Therefore, in co-operation with the forging supplier, the plugging operation was repeated on a second forging suitably instrumented to measure strains, dimensional changes, and temperatures. This experimental rotor was of the same chemical composition as the Arizona rotor and was heat-treated to obtain the same mechanical properties and microstructure. It was machined to the same body and bore dimensions, but was only 10 ft long with a 7-ft body length as compared to the 15-ft body length of the Arizona rotor. Eight plugs, each 1 ft long, were assembled in the body portion of the bore.

Before assembling the bore plugs in the experimental rotor, the rotor was balanced statically, the rotor and plug dimensions were measured carefully, and the rotor was inspected by ultrasonic, magnetic-particle, and visual means. The ultrasonic test showed sonic indications ranging in magnitude from 5 to 15 per cent of the bore reflection, and in this respect the rotor was significantly different from the Arizona rotor.

After the plugs were assembled and the rotor had cooled to room temperature, no change in the ultrasonic indications could be found and the balance was found to have changed only slightly. The diameter and length at the outside of the body had not changed, the over-all length at the bore had increased 27 mils, and the total length of the plugs had shortened 54 mils, assuming their ends were all tight together.

The rotor was parted into eight disks each containing one plug. The plugs were removed from the disks by either sectioning the disk or boring out the plug. After removing the plugs in this manner, it was found that the bore had increased in diameter 0.8 mil per in., and the plugs had shortened 0.25 mil per in. and had increased slightly in diameter as compared to their original dimensions.

This change in dimensions of the plug and rotor bore probably was caused by strains due to temperature gradients set up following insertion of the cold plugs into the hot bore. The material near the surface of the plugs was heated quickly and yielded in compression while the material near the bore surface was chilled and yielded in tension. Some additional minor permanent deformation may have resulted from creep after the plugs heated up and expanded sufficiently to seize in the bore and then were restrained from expanding freely both radially and axially.

Strain gages were attached to two of the eight disks and their respective plugs and used to measure the changes in strain produced when the disks were parted from the rotor, when the plugs were bored out of the disks, and when the disks were sectioned. It was found that the stresses relieved by boring out the plugs were 16,000-psi compression axially in the plugs and 23,000-psi tension circumferentially and 22,000-psi compression radially in the disks at the bore. The elastic stresses in the complete rotor before it was parted into disks were probably somewhat higher because some axial strain was relieved when the disks were cut from the rotor. The difference between these measured elastic stresses and those calculated, Table 4, is probably due to yielding of the plugs and rotor at the bore.

After the plugs were removed from the bore, the residual stress remaining at the bore of the disks was determined, by sectioning the disks, to average 15,000-psi compression circumferentially. Hence the net circumferential stress at the bore of the disks with the plugs in place was 8000-psi tension. The strain-gage data from the two disks were averaged to obtain these stresses.

Results of this investigation indicate that the stress condition induced in the rotor by plugging was moderate and should have been largely relieved by rotation at normal speed. However, during the plugging process, temporarily higher stresses resulting in permanent set were developed in the plugs and rotor material near the bore. In the Arizona rotor, which had lower tensile ductility and numerous thermal cracks in the region near the bore, these temporary stresses may have caused propagation of the cracks, although evidence of this was not found by the ultrasonic tests.

Material Fracture Characteristics

Hydrogen Embrittlement. The hydrogen content of some ferritic materials has been found to have a large influence on tensile ductility. To determine the effect of hydrogen on the ductility of the Arizona rotor material, a comparison was made between aged and unaged tensile specimens. The aging treatment consisted of heating the specimens for 2 hr at 212 F. Results of tests on these specimens are shown in Table 5. The marked increase in ductility upon aging is similar to that observed in other steels where the effect has been attributed to the removal of hydrogen. To investigate this further, specimens were machined from another fragment under a stream of refrigerated coolant to minimize the loss of hydrogen by diffusion. The ductility of these specimens, also shown in Table 5, is very low.

TABLE 5 EFFECT OF AGING ON DUCTILITY OF ARIZONA ROTOR

Condition	Location from bore, in.	Test direction	Tensile strength, psi	0.02 per cent yield strength, psi	Per cent elongation	Per cent reduction of area
Unaged	0–6	Radial	108000	81700	13.5	14.5
			108500	80000	14.5	23.4
Aged	0–6	Radial	108400	80500	18.0	37.9
			108500	81000	17.0	34.0
Unaged	6	Tangential	91200	82700	3.0	1.9
			109000	82000	12.5	18.0
Aged	6	Tangential	109000	80000	15.5	33.1
			109000	80000	15.0	25.5
Refrigerated	0–6	Radial	104000	82000	3.0	1.9[a]
			107000	88000	3.5	2.7

[a] Segregation observed at fracture surface.

The hydrogen content of specimens core-drilled from a large fragment ranged from 2.8 to 3.2 parts per million at locations 3 to 6 in. from the bore. This level of hydrogen is known to have a deleterious effect on tensile ductility. This subject has been under study by an ASTM task force for several years.

Temper Embrittlement. To assess the possibility that temper embrittlement of the rotor material resulted from holding it at 980 F for installation of the plugs, three sets of V-notch Charpy specimens were tested—one set as removed from a large fragment, one set tempered 1 hr at 1200 F, and water quenched to eliminate any possible embrittlement, and one set tempered 1 hr at 1200 F, held 65 hr at 980 F to reintroduce any embrittlement, then air-cooled. The results showed no evidence of temper embrittlement due to the 980 F treatment.

Notch Sensitivity. Notched-bar tensile strengths of six 0.505-in-diam specimens from a rotor-body fragment are listed in Table 6. The notched-strength ratio (notched-bar strength/smooth-bar strength) is 1.25 to 1.3 indicating little sensitivity to stress concentrations.

TABLE 6 NOTCHED TENSILE STRENGTH OF ARIZONA ROTOR

Location from bore, in.	Test direction	Tensile strength,[a] psi	Notched-strength ratio[b]
0–6	Radial	143000	1.30
0–6		135800	
1½	Longitudinal	142000	1.25
1½		136500	
6	Tangential	138750	1.25
6		131500	

[a] Test-specimen dimensions—0.505-in. minimum diam at notch, 60-deg V-notch, 0.005-in. root radius, 50 per cent reduction in cross-sectional area.

[b] Calculated from average notched and unnotched strengths of specimens from same location.

The impact strength of the rotor forging as determined originally from tests on two standard keyhole Charpy specimens taken from the end prolongation was 12 to 14 ft-lb at room temperature. This is at the lower end of the range for rotors of this material. Standard V-notch Charpy specimens taken in different directions from fragments near the bore were tested at a range of temperatures with the results shown in Fig. 6. The "fracture-appearance impact transition temperature," defined as the temperature at which half of the fracture surface of an impact specimen shows a ductile (fibrous) fracture and half shows a brittle (cleavage) type fracture, was found to be about 150 C. In the 25 to 40 C temperature range where the rotor burst, the notched impact strength in the region of the bore was 4 to 12 ft-lb. Under these conditions brittle fracture predominates with only a narrow shear lip under the notch. Most of the impact energy is absorbed in initiating the fracture, with little required to propagate the crack.

Smooth and notched-bar fatigue tests were made on longitudinal bars taken 2 to 6 in. from the bore. The minimum cross section of these specimens was 0.625 in. × 0.343 in., and the notched specimens had two opposed 60-deg notches 0.075 in. deep with 0.020 in. root radii on the 0.625-in. surface. The elastic stress-concentration factor for this notch geometry is 2.6. The results, Fig. 7, show that the strength of the notched bars is reduced fully in proportion to the stress-concentration factor.

Disk-Bursting Tests. To study the behavior of the rotor ma-

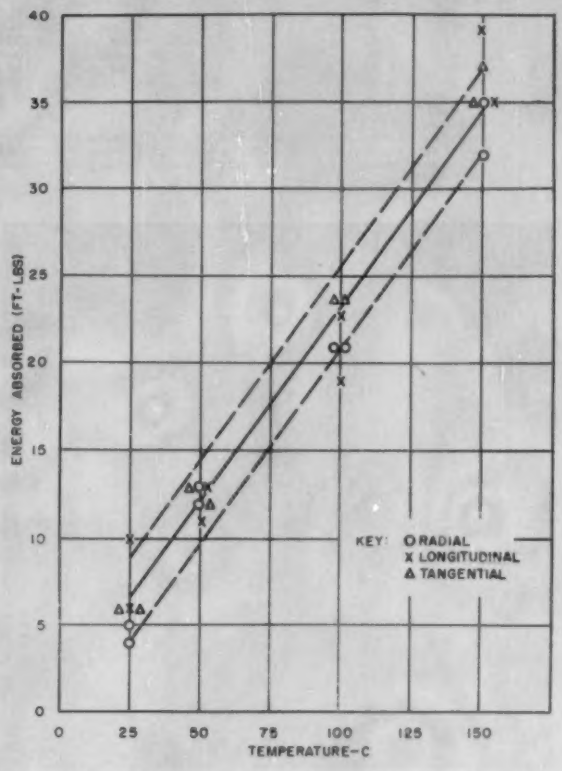

FIG. 6 CHARPY V-NOTCH IMPACT ENERGY TRANSITION CURVE FOR MATERIAL NEAR BORE

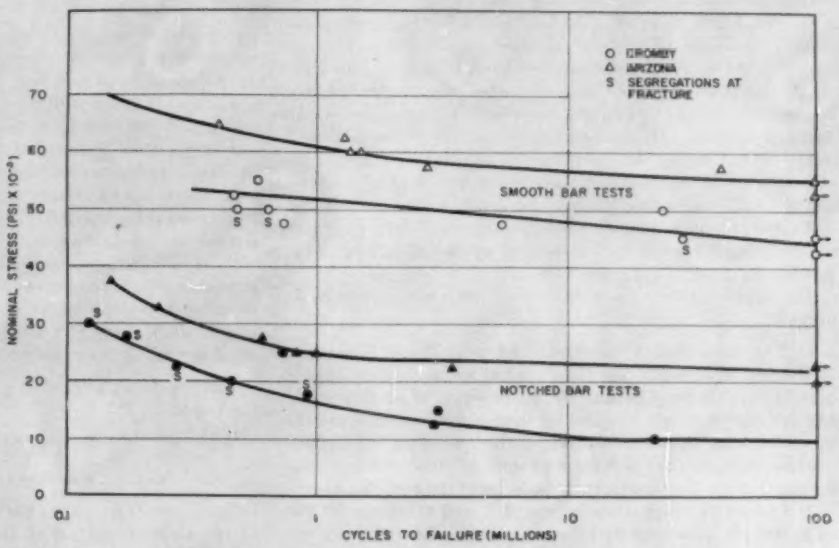

FIG. 7 SMOOTH AND NOTCHED-BAR FATIGUE STRENGTH

TABLE 7 DISK-BURSTING TESTS OF ARIZONA ROTOR MATERIAL

Disk no.	Outer diam, in.	Bore diam, in.	Thickness, in.	Condition	Soundness	Tensile strength, psi	0.02 per cent yield strength, psi	Per cent elongation	Per cent reduction of area	V-notch Charpy, ft-lb	Average burst stress, psi
1	8.20	1.928	3/8	(1)	Sound	115000	87500	9.5	11.5	4	87400
2	8.00	1.65	3/8	(1)	Cracked	109000	80000	15.2	29.3	6	47000
3	8.00	1.65	3/8	(1)	Cracked	109000	80000	15.2	29.3	6	54000
4	8.00	1.656	3/8	(1)	Cracked	111500	85000	15.0	22.3	4	44200
5	8.00	1.656	3/8	(2)	Cracked	111500	85000	15.0	22.3	4	47400
6	8.23	2.00	3/8	(3)	Sound	105800	82500	21.0	53.3	39	82200
7	8.00	1.656	3/8	(3)	Cracked	105800	82500	21.0	53.3	39	65100
8	9.00	1.00	3/8	(1)	Sound (4)	110000[a]	82500[a]	15.0[a]	25.0[a]	5[a]	32400
9	9.00	1.00	3/8	(1)	Sound (5)	110000[a]	82500[a]	15.0[a]	25.0[a]	5[a]	47900

(1) As received.
(2) Aged 4 hr at 392 F.
(3) Heat-treated (1550 F, 4 hr, air-cooled; 1200 F, 20 hr, air-cooled).
(4) Two saw cuts at bore, diametrically opposite, 0.8 in. deep with 0.005-in. radius at V-bottom.
(5) Four saw cuts, two at bore diametrically opposite, two at OD diametrically opposite spaced 90 deg from saw cuts at bore; all 0.8 in. deep with 0.005 in. radius at V-bottom.
[a] Estimated values.

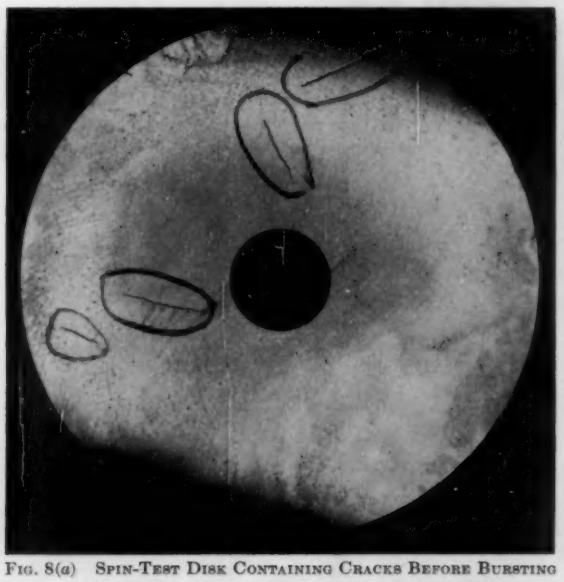

FIG. 8(*a*) SPIN-TEST DISK CONTAINING CRACKS BEFORE BURSTING

FIG. 8(*b*) SPIN-TEST DISK CONTAINING CRACKS AFTER BURSTING

terial under loading conditions more nearly approximating those in the rotor, a number of disks cut from large fragments were spun to bursting. The tests included the effects of internal cracks in the material and heat-treatment to improve the ductility. One of the cracked disks is shown before and after bursting in Figs. 8(*a* and *b*) to indicate the effect of the cracks on the paths of fracture. Dimensions and properties of the disks and results of the bursting tests are presented in Table 7. The strength values were calculated on the basis of net cross section of sound metal, i.e., not counting notches and cracks. For the cracked disks, the average bursting stress was calculated by dividing half the centrifugal force on half of the disk by the radial area of the side having the smaller net cross section.

The significant features of the results are considered to be as follows:

1 The sound disk (1) burst at 87,400 psi. This is 76 per cent of the tensile strength, less than normal for material of similar ductility. This may be due to the presence of small internal cracks which were not revealed by the magnetic-particle tests of the disks before they were tested and which were not found in the fracture surfaces after test because some of these surfaces were damaged when the pieces struck the sides of the test chamber.

2 Disks with internal cracks (nos. 2, 3, and 4) burst at 44,000 to 54,000 psi, substantially below the sound disk but twice the average stress in the Arizona rotor.

3 The disk aged at 392 F (5) had about the same bursting strength as the unaged disks. The aging treatment was intended to drive out hydrogen. However, the hydrogen content of the unaged disks is not known.

4 Heat-treating, which nearly doubled the tensile ductility and greatly increased the impact strength, produced a sizable improvement in the bursting strength of the cracked disk (7) but produced no improvement in the sound disk (6).

5 Reductions in bursting strength equal to, or greater than, those caused by internal cracks can be produced by mechanical notches as in disks 8 and 9.

6 Although the reduction in disk-bursting strength caused by internal cracks is not big enough to account fully for the Arizona rotor burst, it suggests that under the more severe state of stress present in a rotor (triaxiality as compared to biaxiality) the effect of such stress concentrations would be even greater.

Notched-Bend Tests. These are presented in a later section of the paper.

CROMBY ROTOR

NATURE AND CIRCUMSTANCES OF THE BURST

On September 27, 1954 the rotor of the 216,000-kva generator at the Cromby Station of the Philadelphia Electric Company burst while running at 3780 rpm to check the overspeed trip pre-

paratory to putting the machine on the line following a week-end shutdown. The unit had been put in service about three months earlier and had previously satisfactorily undergone two overspeed trip tests to 3950 rpm. It had been started and stopped 21 times.

Except for an oil and hydrogen fire which was quickly extinguished and minor damage to the turbine due to vibration plus a sudden forward movement of the rotor, the damage was contained within the casing of the generator. Preliminary observation of the generator following the accident showed that the generator field had burst in about the same manner as the Arizona rotor. A view of the broken rotor after the upper half of the stator had been cut away is shown in Fig. 9. Subsequent examination of the broken pieces showed that the main fracture in the rotor passed through a row of holes drilled and tapped into the rotor body to hold studs used to repair damage caused by the breaking of a milling cutter during machining of the coil slots.

From the striations on the fracture surface, it appears that the fracture may have started at the third stud hole from the right in Fig. 10 (third from the left in the row of eleven shown in Fig. 11), at the intersection of the conical and cylindrical sections of the drilled hole. The fracture then progressed inward, although not along a radial path, and intersected the bore at an oblique angle. There was no evidence of a fatigue or progressive-type fracture. The general appearance of the fracture surface and the characteristic chevron markings indicated the fracture had spread almost instantaneously across the diameter and along the length, more or less splitting the rotor in half before it broke up into many smaller pieces.

FIG. 9 VIEW OF BURST FIELD AFTER REMOVAL OF UPPER HALF OF STATOR FRAME AND CORE

The arrangement and location of studs used for reconstructing the damaged portions of the teeth is shown in Fig. 11. Two adjacent teeth were damaged. To rebuild them, one row of eleven studs and an adjacent row of two studs, all interlocked, were used. The stud holes were drilled to a depth about $4^1/_2$ in. below the bottom of the coil slots. A shoulder to seat the stud was provided at the top and the holes were threaded for about $3^1/_4$ in. below this shoulder. The bottom of the hole was of a conical shape corresponding to the end of the drill with a corner left at the intersection of the sides and the bottom of the hole. After the rotor burst, the radius at this corner was measured to be 8.6 mils. This method of repair has been used during the past 20 years and about two dozen rotors have been so repaired in the past 10 years.

The Arizona rotor had been repaired similarly but less extensively with two rows of three studs each, diametrically opposite. In that rotor one of the fractures intersected one of these rows of holes diagonally to their axes, and examination indicated that it had not originated at the holes; there was no fracture through the opposite row of holes.

We always have recognized that this method of repair caused an increase in the stress in the vicinity of the stud hole. In evaluating its significance and that of bore holes, winding slots, and other irregularities in cross-sectional configuration, we have relied upon numerous disk-bursting tests on a wide variety of materials, shapes, and sizes. These tests, which have included bursting of 3-in-thick sections of 36-in-diam generator rotors of the normal cross-sectional configuration, have shown that in rotor materials with ductility equivalent to the Cromby rotor, the bursting strength is not seriously reduced by the presence of localized regions where the elastic stresses are several times the average. Center holes in disks, for example, have been found to have little influence on the bursting strength although the elastic stress near the center of a disk is nearly doubled by the presence of a small hole.

FORGING MANUFACTURE AND PROPERTIES

The forging which was used for the Cromby rotor is one of the

FIG. 10 FRACTURE SURFACE AT BASE OF REPAIR STUD HOLES

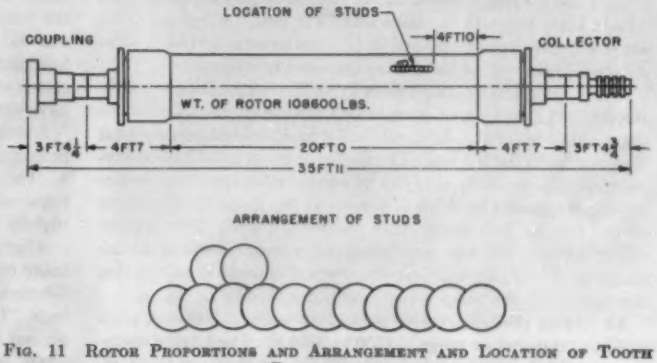

FIG. 11 ROTOR PROPORTIONS AND ARRANGEMENT AND LOCATION OF TOOTH REPAIR STUDS

TABLE 8 CROMBY ROTOR CHEMICAL COMPOSITION

		Percentage composition						
		Ladle analysis			Main body			
Element	Specification	Acid heat	Basic heat	Base of coil slots	6 in. below coil slots	1 in. from bore	Collector end Surface	Bore
C	0.32 max	0.27	0.31	0.23	0.24	0.27	0.23	0.28
Mn	0.90 max	0.58	0.53	0.59	0.60	0.60	0.60	0.60
P	0.05 max	0.037	0.017	0.028	<0.02	0.040	0.02	0.036
S	0.05 max	0.030	0.009	0.030	0.035	0.036	0.026	0.031
Si	0.15–0.35	0.13	0.22	0.13	0.14	0.14	...	0.13
Ni	2.50 min	2.55	2.84	2.54	2.56	2.59	...	2.68
Mo	0.40 min	0.52	0.52	0.51	0.51	0.52	0.42	0.50
V	0.03 min	0.06	0.06	0.10	0.09	0.10	0.08	0.04
Cr	0.25 max	0.09	0.19	0.09	0.10	0.10	0.12	0.15
Sb	Not specified	...	...	<0.005	<0.005	<0.005	...	...
As	Not specified	...	...	0.012	0.014	0.015	...	...

TABLE 9 CROMBY ROTOR ACCEPTANCE TESTS FOR MECHANICAL PROPERTIES

	Location	Test direction	Tensile strength, psi	0.02 per cent yield strength, psi	Per cent elongation	Per cent reduction of area	Keyhole Charpy, ft-lb
Specification (minimum values)	Prolong	Longitudinal	105000	85000	15	30	
	Body	Radial	105000	85000	10	20	
Acceptance-test results	Prolong	Longitudinal	122000	88500	18.2	56.8	17, 18
	Mid-body	Radial	119000	86500	14.0	26.5	
	End-body	Radial	119500	87500	13.7	27.5	

TABLE 10 VARIATION OF TENSILE PROPERTIES IN CROMBY ROTOR

Location in forging	Test direction	Radial location	Tensile strength, psi	0.02 per cent yield strength, psi	Per cent elongation	Per cent reduction of area
End-body	Longitudinal	Surface	117000	84000	16.5	39.1
	Longitudinal	Surface	117100	83800	18.0	43.4
	Longitudinal	Mid-radius	124000	89000	12.5	22.3
	Longitudinal	Mid-radius	122300	87500	13.0	28.8
	Longitudinal	Bore	128000	67000	7.0	8.1
	Longitudinal	Bore	127500	85500	14.5	29.5
	Radial	Surface	116000	83500	12.0	17.9
	Radial	Surface	115000	83800	9.0	12.0
	Radial	Bore	125000	91500	6.5	6.6
	Radial	Bore	126300	90000	6.5	4.7
	Tangential	Surface	115100	84000	8.0	12.2
	Tangential	Surface	116900	84000	11.0	15.9
	Tangential	Bore	119600	87000	8.0	13.0
	Tangential	Bore	119800	87300	8.5	11.5
In vicinity of repair studs	Radial	Surface	115200	86000	14.0	27.9
	Radial	Bore	120500	88000	5.0	3.5[a]
	Radial	Mid-radius	128500	90000	9.0	8.5

[a] Segregation observed on fracture surface.

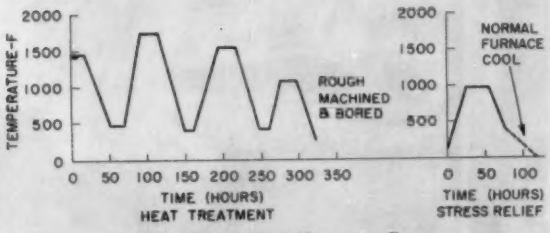

FIG. 12 FINAL HEAT-TREATING CYCLE

largest employed for 3600-rpm machines. As received from the vendor the forging weighed about 118,000 lb and was 36 ft long with a main body 43 in. diam and 20 ft long. Forgings of the same size have been employed in 16 other generators put in service since 1953. All of these have operated satisfactorily.

This forging was produced from an 82-in. octagonal ingot weighing 269,000 lb. An acid open-hearth heat filled the body of the ingot plus 3 in. of the sinkhead, and a basic electric-furnace heat was used to fill the hot top. The results of the original ladle analysis and supplementary analyses of several main body and collector-end fragments in Table 8 show that the general composition of the forging is uniform from surface to bore. The slightly higher carbon, sulphur, and phosphorus concentrations at the center of the forging represent the normal amount of segregation accompanying the progressive solidification of large ingots.

All forging operations were performed under a 7000-ton press within a temperature range of 1750 to 2250 F. The forging operations included initial reduction to 73 in., upset, forge to 58 in. diam, forge body and ends, and finish forge all over. The collector end of the forging corresponded to the bottom of the original ingot.

The final heat-treatment of the forging is shown graphically in Fig. 12. After stripping the ingot from the mold it was directly charged into a furnace to heat for forging. The finished forging was double normalized from 1750 F and 1550 F, respectively, and tempered for mechanical properties at 1080 F. After rough machining and boring, the forging was stress-relieved at 980 F.

Nondestructive testing of the forging included ultrasonic test and visual and magnetic-particle examinations. Bore explorations showed it to be free of visible defects, and magnetic-particle checks of the outside surface showed no indications. Ultrasonic inspection revealed fifteen to twenty 5 to 10 per cent indications in the body. These were scattered 360 deg circumferentially, and out to 3 in. from the bore. Indications of this magnitude have generally been found to be associated with the normal segregation of nonmetallic inclusions at the center of a large ingot, and have not been a cause for concern.

Specimens taken from the forging met all the mechanical-property requirements of the specification, as indicated in Table 9. The specified tensile and yield-strength levels are above those required for the Arizona rotor because of the larger size and slightly increased working stress levels of the Cromby rotor.

After the rotor burst, a series of smooth-bar tensile tests were made on specimens taken from various large rotor fragments to determine the uniformity of tensile properties from surface to bore. The specimens were machined at room temperature using normal cutting lubricants. No special precautions were taken to retain or remove dissolved hydrogen. Results of these tensile

tests, Table 10, show a slight increase in the tensile and yield strengths at the mid-radius and bore with some ductilities substantially lower than at the surface. These variations in tensile ductility, which are somewhat beyond the variations usually found between surface and bore in large forgings, are believed to be due to a combination of segregation and hydrogen content.

Metallurgical Examination of Rotor Material

Metallographic examination of specimens from the end-body, mid-body, and collector-end fragments disclosed that the general microstructure of the forging was uniform from surface to bore. The structure was composed of acicular ferrite and bainite and is considered normal for large forgings of similar composition and heat-treatment. Representative photomicrographs of the main-body structure at the surface and bore are shown in Fig. 13. The ASTM grain size of the steel was approximately no. 7 and did not vary over the cross section.

Sections of several fragments of the rotor were surface-ground and macroetched to study the homogeneity of the steel. Segregation bands running in the axial direction, similar to those shown in Fig. 14, were found in all sections tested. Metallographically, these segregated bands were found to be associated with concentrations of sulphide inclusions generally surrounded by ferrite islands in a matrix of higher carbon bainite. A transverse view of a typical segregation line is shown in Fig. 15. In several places adjacent to the fracture surface extending from the row of stud holes, small cracks were found to have started in the segregated regions. Upon careful microexaminantion of specimens taken as close as possible to the point where the primary fracture appeared to have originated, a segregation region was found which extended to within a few thousandths of an inch of this point.

The proximity of these segregations to the stud holes is believed to have contributed to the initial crack formation, since the ductility of the material in the segregations was found to be low. By bending small specimens containing segregate bands, it was shown by J. R. Low that the ductility was drastically lowered when the bands were oriented transverse to the direction of applied stress as they were in the rotor, although the ductility was not much affected when the segregate bands were parallel to the direction of bending.

To check the chemical nature of the segregated areas, x-ray emission techniques were employed. The use of normal spectrographic methods was unsuccessful. The x-ray emission analyses indicated significant segregation of the strong carbide-forming elements Mo and V. For elements below Ti in the periodic chart, segregated material was isolated and the analysis of C, S, P, and Si performed by standard chemical methods. Table 11 lists the results of the analyses in terms of ratios of segregated to normal area concentrations of the elements. These results confirmed the conclusions reached from metallographic examination. The gross carbon content of the segregated area appears to be lower than in the normal area because the sampling technique for chemical analysis did not permit the degree of isolation of higher carbon areas indicated metallographically.

TABLE 11 CONCENTRATION OF ELEMENTS IN SEGREGATED AREAS OF CROMBY ROTOR

Element	Method of analysis	Concentration ratio[a]
Mo	x-ray emission	1.6
V		1.7
Cr		1.1
Mn		1.0
Ni		1.1
C	chemical	0.9
S		1.6
P		1.9
Si		1.4

[a] Ratio of segregated to normal area compositions.

Several hardness tests were made to compare the hardness of the segregated areas to that of the homogeneous material. The Rockwell A hardness was found to vary from 61 to 68 (Brinell 231 to 329) along the lengths of several segregation bands. The hardness in the homogeneous matrix was significantly lower and ranged from Rockwell A 61 to 63 (Brinell 231 to 255). Knoop hardness tests made in the area adjacent to the stud hole where the fracture originated and where segregation bands were found showed high hardness. The higher hardness level in the segre-

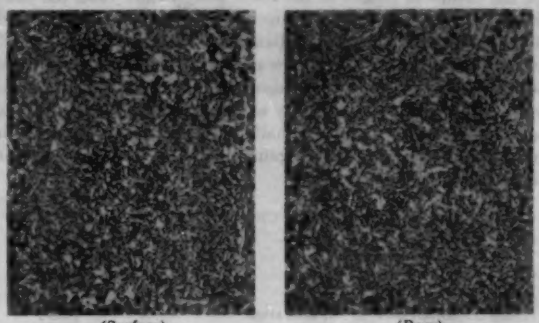

(Surface) (Bore)

Fig. 13 Microstructure Near Outer Surface and Near Bore; ×40

Fig. 14 Etched Section Showing Segregation Lines; One-Fourth Size

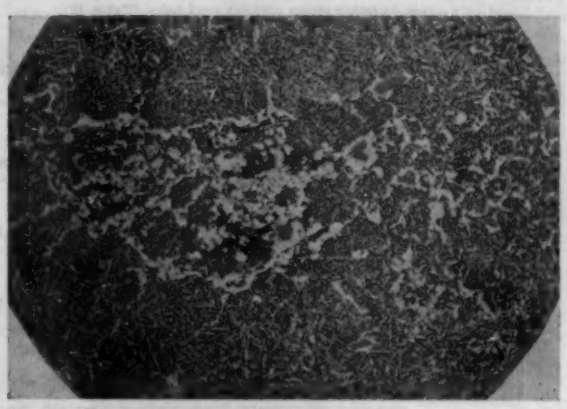

Fig. 15 Photomicrograph of Structure in and Around Segregation Line (Transverse Section); ×50

gated areas is consistent with the higher concentration of Mo and V found by the x-ray emission analysis.

Rotor Stresses and Effect of Repair Studs

Original design stress calculations indicated conservative values of rotor stresses within normal design limits. The significant stresses are tabulated in Table 12. In an attempt to include the effect of the repair stud holes on the calculated stresses, a pessimistic assumption was made that the row of holes extended for the complete length of the rotor body rather than the relatively short distance actually occupied by the repair studs and that there was a similar row diametrically opposite. Values of average bursting stress and average tangential bore stress computed on this basis are shown also in Table 12. Although somewhat higher than the originally calculated stresses, the average bore stress is only about one half the material tensile strength and a factor of safety of 3:1 against bursting exists at the speed at which fracture occurred.

TABLE 12 CALCULATED CROMBY ROTOR STRESSES

	Psi at 3600 rpm	Psi at 3780 rpm
Average tangential bore stress	44500	49100
Average bursting stress	24800	27300
Maximum tooth-root stress	27500	30300
Average tangential bore stress, with studs	56300[a]	62100[a]
Average bursting stress, with studs	33800[a]	37300[a]

[a] Calculated assuming two diametrically opposite rows of studs extend the full length of the rotor.

Photoelasticity was used to evaluate the stress concentrations in the rotor and also to study possible ways to improve the stress distribution in a rotor by modifying its cross-sectional configuration. Disks of photoelastic material, slotted to simulate rotor cross sections, were spun in an oven at constant speed to develop the stress patterns. Then the disks were cooled while still spinning to freeze in the stress patterns for photoelastic analysis.

Analysis of a disk slotted to simulate the normal Cromby rotor cross section yielded results shown in Table 13. The calculated average bursting stress in the rotor is used as a reference stress upon which all stress-concentration factors are based, although it is recognized that the fillet stresses at the bottoms of the rotor teeth are more closely related to the radial stresses in the teeth. The measured value of average bore stress checks closely with the calculated value (Table 12).

TABLE 13 CROMBY ROTOR STRESS-CONCENTRATION FACTORS—NORMAL DESIGN

Location	Stress-concentration factor[a]
Bore hole, maximum	2.48
Bore hole, average	1.77
Fillet of slot 1 (pole side)[b]	2.66
Fillet of slot 2 (pole side)[b]	3.95
Fillet of typical interior slot[b]	1.77

[a] Based on average bursting stress without stud holes (Table 12).
[b] Slot 1 is 7 in. deep, all other slots are 8$^3/_{16}$ in. deep.

Another disk was machined with two deeper slots, simulating rows of repair stud holes. One slot, having a drill-pointed bottom, represented the Cromby repair stud holes and the other had a semicircular bottom for comparison. The disk was run with the slots empty and also with teeth doweled in place to simulate the actual repair studs. Table 14 shows the measured stress concentrations, here referred to the calculated average bursting stress in the rotor assuming two diametrically opposite rows of stud holes, exist.

The highest stress-concentration factor was measured at the bottom of the slot representing the repair stud holes rather than at the shoulder where the rotor fracture initiated. However, since the discrete pointed bottoms of the stud holes are not truly simulated by the slot in the disk, the actual stress-concentration factor at this location will be somewhat less than that obtained in the photoelastic tests. Also the presence of a region of low-ductility segregation at the shoulder was conducive to cracking at this location.

Since the fillets in the photoelastic disk could not be machined proportionally as sharp as those in the repair stud holes, the measured stresses are too low. Stress-concentration factors calculated for the fillet sizes used in the photoelastic tests showed excellent agreement with the corresponding factors determined photoelastically, Table 14, and when these calculations are extended to the fillet radii of the actual rotor a further fourfold increase in the concentration factor was obtained.

Additional tests were made to determine the effect of round-bottoming the coil slots, and to find the reduction in stress that could be attained by adjusting the depth of slot number 2 (second slot from the pole face). It was found that the stress-concentration factor at slot 2 was reduced 12 per cent by round-bottoming the slots. Then by adjusting the depth of slot 2 to the optimum value intermediate between the depths of slots 1 and 3, an additional 20 per cent reduction was obtained.

The investigation of stresses due to slot repair also included an evaluation of the small interference fit (0.002 in. maximum, 0.000 in. minimum) between the repair studs and the holes in the rotor body used to insure that the studs remained tight in operation. A large steel block was drilled with holes like those in the rotor, and studs chilled with dry ice were inserted in essentially the same manner as in the rotor, using the maximum interference fit of the tolerance range. Stresses resulting from insertion of the studs were determined from strain-gage measurements.

The holes were drilled and plugged consecutively, with suf-

TABLE 14 CROMBY ROTOR STRESS-CONCENTRATION FACTORS AT REPAIR STUD HOLES

Type of Slot	Inserted Tooth	Location	Stress Concentration Factor*		
			Photoelastic r = 0.25 inch	Calculated r = 0.25 inch	Calculated r = 0.0086 inch
P		Root (A)	7.6		
P		Shoulder (B)	5.1	5.2	21.7
P		Root (A)	7.8		
P		Shoulder (B)	5.9		
R		Root (C)	2.7		
R		Root (C)	2.7		

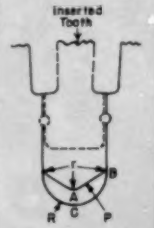

* Based on average bursting stress assuming two diametrically opposite rows of stud holes (Table 12).

TABLE 15 NOTCHED TENSILE STRENGTH OF CROMBY ROTOR

Test direction	Radial location	Diameter at notch, in.	Notch[a] root radius, in.	Stress-concentration factor (Timoshenko)	Tensile strength, psi	Notched-strength ratio[b]
Longitudinal	Surface	0.505	0.005	7.2	167200	1.42
Longitudinal	Surface	0.505	0.005	7.2	165200	
Longitudinal	Mid-radius	0.505	0.005	7.2	156800	1.33
Longitudinal	Mid-radius	0.505	0.005	7.2	171000	
Longitudinal	Bore	0.505	0.005	7.2	176600	1.35
Longitudinal	Bore	0.505	0.005	7.2	168200	
Radial	Surface	0.505	0.005	7.2	143200	1.36
Radial	Surface	0.505	0.005	7.2	169500	
Radial	Bore	0.505	0.005	7.2	133800	0.84
Radial	Bore	0.505	0.005	7.2	77300[c]	
Tangential	Surface	0.505	0.005	7.2	163800	1.41
Tangential	Surface	0.505	0.005	7.2	162900	
Tangential	Bore	0.505	0.005	7.2	162000	1.35
Tangential	Bore	0.505	0.005	7.2	162100	
Radial	Mid-radius	0.225	0.0017	8.3	164000	1.44
Radial	Mid-radius	0.225	0.0017	8.3	164100	
Radial	Mid-radius	0.294	0.0016	9.7	166200	1.46
Radial	Mid-radius	0.294	0.0016	9.7	166500	
Radial	Mid-radius	0.505	0.005	7.2	160000	1.41
Radial	Mid-radius	0.505	0.005	7.2	162000	
Radial	Mid-radius	1.130	0.005	10.8	103800[c]	0.80
Radial	Mid-radius	1.130	0.005	10.8	76900[c]	
Radial	Mid-radius	1.470	0.005	14.2	116000[c]	1.07
Radial	Mid-radius	1.470	0.005	14.2	126600[c]	

[a] 60-deg V-notch, 50 per cent reduction in cross-sectional area.
[b] Calculated from average notched strength of duplicate specimens.
[c] Segregation bands intersected root of notch.

ficient time being allowed after stud assembly for temperatures to equalize before drilling the next hole. The holes were finished with flatbottoms having $^1/_4$-in. fillet radii to permit the installation of strain gages at the fillets after drilling each hole.

The highest stress measured at the fillet at the bottom of a hole due to installing a stud in that hole was 12,300 psi. The insertion of all the studs produced a 9000-psi tensile stress in the material immediately adjacent to the ends of the row of studs. In the rotor, these stresses would be considerably relieved during operation by elastic stretching of the material around the row of studs. Also, the average interference fit in the rotor was only half that employed in the model test. Thus it is concluded that the standard interference fit between the repair studs and holes would produce only a small stress increase in the rotor.

Material-Fracture Characteristics

Hydrogen Embrittlement. The radial distribution of hydrogen in the main body was found to vary from one part per million at the bore and at the bottom of the coil slots to two parts per million at the root of the repair stud holes. Considerable variation was observed in the ductility of tensile specimens which had been refrigerated during machining to prevent escape of hydrogen before test. Examination of the fractured bars indicated that much of this variation was probably due to the effect of segregation in the material, but after allowing for this there was still a significant reduction in ductility attributable to hydrogen. This may have been a factor in the formation of an initial small crack at the stud hole in the Cromby rotor. However, it is believed that hydrogen was not a factor in the rapid propagation of fracture through the rotor because tests at high strain rates show that neither strength nor ductility is affected by the presence of two parts per million of hydrogen.

Notch Sensitivity. The results of notched tensile tests taken from different radial locations in the rotor body are listed in Table 15 with the corresponding notched-bar/smooth-bar strength ratios. In general, these data indicate a small decrease in notched strength from the surface to the bore and slight sensitivity to stress concentrations. The specimens which broke at low stresses were all found to have portions of the segregation bands previously described intersecting the root of the notch at the point where fracture originated.

The room-temperature impact strength of the forging as determined originally from two keyhole specimens taken from the end prolongation was 17 and 18 ft-lb. Although this is about

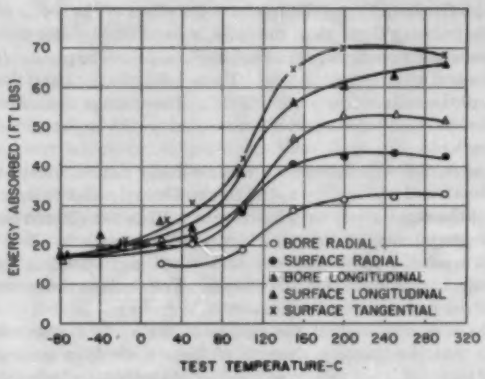

Fig. 16 Charpy V-Notch Impact Energy-Transition Curves

5 ft-lb higher than the Arizona material, it is somewhat below the average for rotors of this material. Standard keyhole and V-notch Charpy impact values at several locations within the rotor body were generally about the same as the prolong values. A few specimens, however, had unusually low impact strength. As in the case of the notched tensile tests, the low impact strengths were found to be attributable to segregated areas in the region of the notch. The low strength associated with segregations at the notch in certain of the notched tensile and impact specimens supports the conclusion mentioned earlier that the segregations at, or near, the stud holes in the Cromby rotor were an important factor in causing the primary fracture.

The V-notch Charpy impact strength of the material near the surface and bore over a range of temperatures is shown in Fig. 16. The fracture-appearance transition temperature was found to be about 100 C for material near the body surface and about 120 C for material at the bore. At the estimated temperature of the rotor when it burst the notched impact strength in the region of the bore is 18 to 26 ft-lb and at the surface 24 to 34 ft-lb. This level of impact strength usually has been considered high enough to preclude brittle fracture.

Smooth and notched-bar fatigue tests were made at room temperature on radial bars from a large main-body fragment. The notches were located approximately at the same radial distance from the bore as the bottom of the repair stud holes and

were oriented circumferentially. The geometry of the test specimens was similar to that described previously under the Arizona rotor.

The results are shown in Fig. 7 with similar data on the Arizona material. The 100-million-cycle smooth-bar fatigue strength is only 37 per cent of the tensile strength. The corresponding figure for the Arizona material is 50 per cent. In addition to its low smooth-bar strength, the Cromby material is unusually sensitive to stress concentrations; the strength of the notched bars is reduced substantially more than in proportion to the stress-concentration factor.

To determine whether the fractures in these tests were related to the segregation bands, the specimens were macroetched after testing. Segregations were observed on the fracture surfaces in five of the nine notched and three of the ten unnotched specimens tested. These specimens are indicated in Fig. 7 by the letter "S" adjacent to the data points. It appears that the presence of the segregation has a small effect on the fatigue strength but does not account for the high notch sensitivity of the material in fatigue.

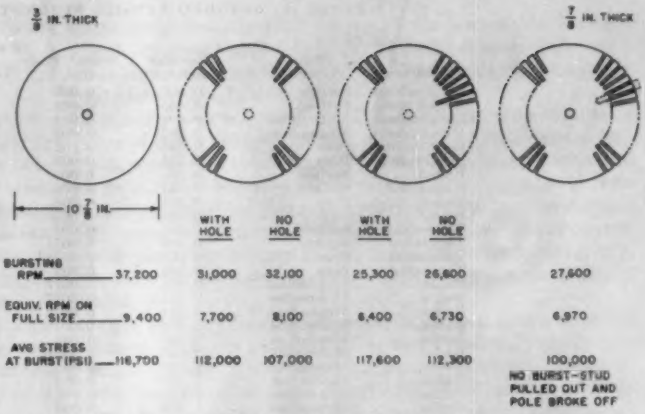
3/8 IN. THICK
7/8 IN. THICK
10 7/8 IN.
WITH HOLE
NO HOLE
WITH HOLE
NO HOLE
BURSTING RPM 37,200 31,000 32,100 25,300 26,800 27,600
EQUIV. RPM ON FULL SIZE 9,400 7,700 8,100 6,400 6,730 6,970
AVG STRESS AT BURST (PSI) 116,700 112,000 107,000 117,600 112,300 100,000
NO BURST—STUD PULLED OUT AND POLE BROKE OFF

FIG. 17 SUMMARY OF DISK-BURSTING TESTS

Disk-Bursting Tests. To evaluate the effect of the repair studs on the bursting strength of the rotor, several quarter-size disks of representative configurations were machined from large rotor fragments and spun to destruction. These configurations and the results of the tests are shown in Fig. 17. The average stress for five of the disks at bursting is almost equal to the material tensile strength.

A sixth disk with a borehole was normally slotted, except that one tooth was replaced by a stud screwed into the disk to simulate one of the repair studs used in the rotor. This disk did not burst; the material around the stud hole yielded enough to allow the fine-threaded stud to pull out at a speed corresponding to an average bursting stress of 100,000 psi. The studs in the rotor did not come out until the rotor burst.

These results confirm the results of earlier spin tests which show that the bursting strength of disks made from generator-rotor material is not greatly reduced by center holes, winding slots, and similar irregularities in cross section. The difference between these results and those reported for the Arizona rotor is probably due to the more severe stress concentrations caused by the thermal cracks in the Arizona disks than by the simulated repair stud holes in the Cromby disks, and to the lower ductility of the Arizona material.

NOTCHED-BEND TESTS

ARIZONA AND CROMBY MATERIALS

In a notched-bend specimen where the notch radius is very small compared to the width of the specimen, the triaxiality of the stresses around the root of the notch may closely approximate that around internal cracks or deep, sharp, mechanical notches in a large rotor. A notched-bend test, therefore, appears to afford a way to simulate, under controlled conditions, the operating stresses near such stress concentations in a large rotor. Many such tests have been made in connection with the Arizona and Cromby investigations, and some of the results are shown in Fig. 18, taken from the work of Lubahn and Yukawa who are expected to publish the results of their investigations in greater detail soon.

The specimens are bars of square cross section with a 45-deg V-notch across one side perpendicular to the length of the bar. They are loaded slowly in simple bending to break them open at the notch. The nominal bending strength at fracture is the calculated simple bending stress in the net section at the root of the notch.

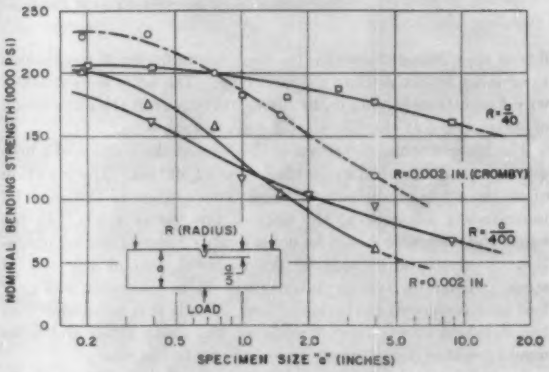

FIG. 18 NOTCHED-BEND STRENGTH ARIZONA ROTOR MATERIAL

Fig. 18 shows that the bending strength of notched bars decreases with size and notch severity. The bending strength of unnotched bars of Arizona rotor material is about 220,000 psi. No effect of size was found.

Tests of a series of geometrically similar specimens, each with a notch radius equal to $1/400$ of the bar thickness, show that the strength of small bars is close to that of unnotched bars, but the strength of larger notched bars falls off to only a third or less of the smooth-bar strength. These bars have an elastic stress-concentration factor of $K = 12$ at the root of the notch. The strength of a 9-in. sq bar with a 0.001-in. notch radius was only about 40,000 psi.

With less severe notches, the reduction in strength with size is relatively small. Tests of geometrically similar specimens, each with a notch radius equal to $1/40$ of the bar thickness and with an elastic stress-concentration factor of $K = 5$ at the root of the notch, show that the strength of the large notched bars is about 75 per cent of the smooth-bar strength.

Fig. 18 shows the results of tests on a series of notched bars of the Cromby material in which the notch radius was held constant at 0.002 in. for sizes up to 4 in. and similar data on the Arizona material for comparison. These results include the effects of both size and notch severity; consequently, the strength decreases more sharply with size than is the case when geometrical similarity is maintained. In these tests the bending strength of the Cromby material is 30,000 to 40,000 psi higher than that of the Arizona material, but the effect of size and notch severity is about the same on both.

In all of these tests the larger notched bars broke suddenly and with almost no plastic deformation. Only in the case of the smallest bars was there any evidence (and only very little) of a tough break in which the load had to be applied continuously to force the crack across the specimen.

These notched-bend tests show that the rotor material fractures rather than yields to relieve intense localized stresses under certain conditions. It is believed that the conditions near the root of the notch in the larger specimens simulate those at the internal cracks in the Arizona rotor or at the bottoms of the stud holes in the Cromby rotor better than a spinning-disk test of the rotor cross-sectional configuration with respect to the state of stress (triaxiality), presence, and effect (if any) of hydrogen dissolved in the metal and size effect. Considering the size of the rotors as compared to the largest of the notched-bend specimens, the trend of the notched-bend strength with size and notch severity, the severity of the stress concentrations caused by the internal cracks in the Arizona rotor and the stud holes in the Cromby rotor, and the segregations in the Cromby rotor, it is believed that these notched-bend test results provide an understandable explanation of the bursting of the rotors at relatively low levels of average stress.

On the other hand, the tests show also that in spite of the unsatisfactory behavior of this rotor material when it is severely notched, it may safely be used for rotors like Cromby and Arizona provided intense stress concentrations due to internal cracks or mechanical notches are avoided. The severity of the stress concentrations caused by the configuration of the winding slots, ventilation holes, and other details of normal design are kept within the range where the fracture strength of large-size specimens or components is not drastically lowered by them.

Beyond elucidating the cause of the Arizona and Cromby rotor bursts, these notched-bend tests have led to an improved understanding of the relationship between the behavior of steel in large masses and its behavior in laboratory tests and of the relationship between the behavior of steel in different kinds of tests. These afford guidance for mechanical design within the limitations of available materials and for the development of better materials.

Relationship of Notched-Bend and Impact Tests

The phenomenon of brittle fracture of materials has long been the subject of intensive study. It has been shown repeatedly that the fracture behavior—that is to say, the strength developed and the ductility exhibited before complete fracture—is dependent on the state of stress, temperature, speed of loading, and microstructure of the steel. Generally, the tendency to fracture in a brittle manner is increased by increasing the triaxiality of the stresses, lowering the temperature, or increasing the strain rate. This suggests that the effect of notch severity on fracture behavior in notched-bend tests may be analogous to the effect of strain rate on fracture behavior in the Charpy test and that the effect of temperature is similar in both types of test. This appears in fact to be the case. It was found, for example, during the course of these investigations that identical notched-bend test specimens broke at a nominal bending stress of 116,500 psi at room temperature and at 192,000 psi when tested at 200 F. Further, there is excellent correlation between the Charpy fracture-appearance transition temperatures and the room-temperature slow-notched-bend strengths of a number of steels of similar tensile strengths, as shown in Table 16.

These results support the hypothesis that there is a correlation between the fracture behavior of steels in the notched-bend and Charpy V-notch impact tests and that a material will not show a marked loss in strength in the notch-bend test provided it is above its transition temperature as determined in the V-notch impact test. Thus the impact transition temperature appears to afford guidance for judging the susceptibility of steels to brittle fracture. Further investigation in this direction is continuing actively.

TABLE 16 FRACTURE-APPEARANCE TRANSITION TEMPERATURES AND NOTCHED-BEND STRENGTHS

Impact fracture-appearance transition temperature, deg F	Notched-bend strength 3-in. specimen size, 0.003-in. radius, psi
275	75000
220	86000
210	132000
150	165000
40	200000

Effect of Microstructure. The problem of finding steels with lower-impact transition temperature can be attacked on a straightforward metallurgical basis. It has long been known that maximum toughness is obtained by quenching a fully hardenable steel to obtain a martensitic structure and then tempering to the desired hardness. The increase in the notched-bend strength of the Arizona rotor material obtainable in this way is shown by the comparison in Table 17.

TABLE 17 NOTCHED-BEND STRENGTH COMPARISON

Condition	Notched-bend strength 1¼-in. specimen size, 0.003-in. radius, psi
Original	105000
Reheat-treated to better microstructure	208000

Obtaining a martensitic structure in 40-in-diam rotors is probably out of the question, but intermediate-type structures with lower transition temperatures than those now obtained in air-cooled Ni-Mo-V and Cr-Mo-V rotors undoubtedly can be obtained by faster quenching. Further reductions in transition temperature can be gained by changes in composition to improve hardenability. We believe that a higher alloy content for greater hardenability, and a faster quenching rate for a lower transformation product, coupled with steel of the highest cleanliness to reduce the effect of nonmetallic inclusions, will result in rotor steels having substantially greater toughness. This is the basis of our extensive rotor-development program described more fully in the following section of the paper.

IMPROVEMENTS

Design and Manufacture

Extensive improvements in the machining of turbine-generator rotors have been introduced which essentially should eliminate damage to the rotor teeth. The breakage of cutters is being reduced through improvements in slot and cutter design and greater attention to keeping cutters sharp and tight on the spindle. In the unusual case in which damage does occur, the rotor will be scrapped rather than resorting to repair studs.

Sonic test acceptance levels have been defined more precisely and tightened substantially. This is covered in a companion paper by Rankin and Moriarty.[5]

The sonic-test data and the records of repairs with studs screwed into the rotor body have been reviewed and evaluated for all rotors. In no other rotor have the magnitude and number of sonic-test indications equaled those in the Arizona rotor. However, there were nine rotors in which the magnitude of the localized stresses at the repair studs was equal to, or of, the same order of magnitude as that in the Cromby rotor and these rotors have been replaced. A number of others in which conditions are more favorable so that there is no question of their continued safe and reliable operation are not being replaced.

Numerous details of rotor design are being improved to minimize stress concentrations with the largest possible fillets at tooth

[5] Published in this issue, pp. 1603–1622.

slots, ventilation slots, balance slots, cross slots, and so on. All closed-end holes, such as balance plug, ventilation, and coupon holes, drilled in a rotor are now finished with hemispherical ends after drilling. Semicircular fillets are now being employed at the bottom of the first one or two coil slots or subslots adjacent to the poles. The photoelastic tests previously described show that the highest stresses in a rotor of normal cross section exist at these locations and that the semicircular fillets reduce the stress-concentration factor from 3.95 to 3.47.

Materials

Eleven full-size rotor forgings, some generator and some turbine, have been ordered from the four heavy-forging producers in this country and one in Germany to evaluate the effect of modifications in composition, melting, and pouring practice, and heat-treatment on soundness, cleanliness, and mechanical properties. Six of these are composition modifications of our present standard grades. The others are intended to evaluate the benefits of duplex melting, vacuum pouring, and several quenching media. One of the forgings has been instrumented to determine cooling rates throughout the body of the forging when quenching in air, oil, and water.

In addition, laboratory studies are being conducted on small heats of several new compositions. Certain of these show promising property improvements with commercially feasible melting and heat-treating practice.

Immediate improvement of present rotor materials is being obtained through revision of our forging specifications to include requirements for higher tensile ductility and Charpy impact strength; provisions for additional tests to determine transition data, hydrogen content, segregation pattern, and property uniformity; and continued refinement of the ultrasonic inspection techniques and tightening of the acceptance limits.

At our suggestion, the American Society for Testing Materials has formed a task force under its forgings committee, with representation from the three large turbine-generator manufacturers and the five heavy-forging manufacturers to pool all available technical knowledge pertinent to the improvement of rotor forgings. A report[6] of the work of this task force to date was made at the 1955 Annual ASME Diamond Jubilee Meeting.

SUMMARY AND CONCLUSIONS

1 The Arizona and Cromby rotor bursts were caused primarily by unusual and severe stress concentrations combined with the characteristics of the materials from which these rotors were made. In the Arizona rotor, these stress concentrations were created by numerous internal cracks in the body of the forging. Although the best methods of nondestructive examination known at the time were used to determine the soundness of the forging, ultrasonic indications in the body were interpreted as caused by harmless dirt and slag similar to that found in the bore. In the Cromby rotor, these stress concentrations were created by a row of holes drilled and tapped in the rotor body for the attachment of studs used to repair portions of the teeth damaged when milling the coil slots.

2 The shrink fit of the plugs in the bore of the Arizona rotor and the interference fit between the studs and the holes in the Cromby rotor caused some increase in the critical stress levels at operating speed but are not believed to have been the primary cause of the bursts. Since both rotors were below normal operating temperature and were being heated from the outside by windage when they burst, the lower resistance of the material to brittle fracture at low temperatures along with some additional stress induced in the center portion by thermal expansion of the outside may have contributed to causing the bursts and suggest the desirability of warming generator rotors slowly to normal operating temperature before they are brought to full speed.

3 Alloy segregation, in stringlike regions of above-average alloy content, contributed to the cause of both bursts. The strength and ductility of the metal in these segregations have been found to be low. In the Arizona rotor, the segregations appear to have been the nuclei of the internal cracks formed during manufacture of the forging. In the Cromby rotor, the corner of the stud hole at which the primary fracture originated was in one of these segregation regions. This coincidence seems to explain the bursting of this particular rotor when spin tests of models and the successful operation of other identical rotors indicate that it should not have burst.

4 The hydrogen content of both rotors caused the ductility of the material, as measured in tensile tests, to be lowered significantly. However, the hydrogen is believed not to have been the cause of the brittle nature and rapid propagation of the fractures throughout the rotors. It may have contributed to the starting of a small crack at the corner of the stud hole in the Cromby rotor, but no evidence of such a small crack, different in character from the rest of the primary fracture, could be found. In the Arizona rotor, the hydrogen may have contributed to the formation of the internal cracks during manufacture of the forging, although the amount of hydrogen present was at the lower end of the range normally associated with hydrogen flaking.

5 This investigation has led to a better understanding of the relationship between the behavior of steel in massive rotors and its behavior in laboratory tests and of the relationship between its behavior in different kinds of tests, which afford guidance for mechanical design within the limitations of available materials and for the development of better materials. It appears, however, that bursting tests of essentially full-size models or of complete rotors may be necessary to a full understanding of these relationships and to prove the real margins of safety against bursting of such rotors. Accordingly, a facility in which to make such tests is being designed.

6 The kind of material used for the Arizona and Cromby rotors may fracture in a brittle manner under certain conditions, as in these two cases and in bend tests of large severely notched bars. Nevertheless, it can be used safely for such rotors provided severe stress concentrations are avoided, as demonstrated by (1) the successful and reliable operation of dozens of rotors in which the normal design stresses are equal to, or of, the same order of magnitude as those in Arizona and Cromby, and (2) the relatively moderate reduction in the bending strength of large notched bars with stress concentrations at the notch comparable to those in rotors of normal design.

7 Material suitable for rotors and having greater resistance to brittle-crack propagation can be obtained by alterations in composition and heat-treatment coupled with improved melting practice to improve cleanliness and reduce the effect of nonmetallic inclusions. Accordingly, extensive laboratory studies and full-scale trials of such alterations and improvements are being carried out. Successful culmination of these will permit added margins of safety against the unknown and unforeseeable to be built into our machines. In the meantime, use of more stringent ultrasonic acceptance standards, discontinuance of tooth repair with studs, and introduction of improved design, manufacture, and inspection techniques will prevent the recurrence of the conditions responsible for the Arizona and Cromby bursts.

Acknowledgment

Space is too limited for the authors to express their appreciation individually to the many persons who contributed to this investigation. Tests, analyses, and other contributions were made by many members of Large Steam Turbine-Generator

[6] Published in this issue, pp. 1623–1626.

Engineering, Analytical Engineering, the Materials and Processes Laboratory, as well as by the Thomson Laboratory, the General Engineering Laboratory, and the Research Laboratory, all of the General Electric Company. The authors take this means of expressing their appreciation to the many members of these organizations for their initiative, originality, and wholehearted assistance. In addition, the authors express their appreciation to the engineering and operating personnel of the Arizona Public Service Company and the Philadelphia Electric Company for their co-operation and assistance.

Discussion

E. L. Layland.[7] The authors have conducted a most thorough and exhaustive study of the conditions leading to these two unfortunate mishaps. They refer to "fracture-appearance transition temperatures" of 150 C and 100–120 C for the Arizona and Cromby rotors, respectively, based on Charpy V-notch impact tests. The writer's company also has been doing a great deal of work on determining the transition temperature of rotor steels by means of both Charpy V-notch and Drop-Weight Tests (DWT). This latter test was developed by W. S. Pellini and associates of the Naval Research Laboratories.

Extensive investigations of the brittle fracture of welded ships by the Naval Research Laboratories during and after World War II established the Drop-Weight Test as having excellent correlation to service failures. In every case where the Drop-Weight Test has been performed on steels which failed in service by brittle fracture, it has been found that the failure occurred at a temperature below the transition temperature as determined by the DWT. This perfect correlation has not been restricted to ship-plate failures but has been extended to the brittle fractures of other steels such as an annealed alloy-steel pressure vessel, a normalized and tempered alloy-steel pressure vessel, and a quenched and tempered alloy-steel retaining ring.

All of these investigations have shown that three conditions are necessary and sufficient for brittle fracture:

1 A stress raiser resulting from design or fabrication.

2 A stress sufficiently great to cause localized yielding in the vicinity of the stress raiser.

3 A service temperature below the ductile-to-brittle transition temperature of the material with the given stress raiser.

When all three conditions are present, a brittle fracture occurs; when any of these conditions is absent, a brittle fracture does not occur.

Fig. 19 of this discussion shows the pertinent features of the Drop-Weight Test. The specimen is approximately 14 in. long × 3½ in. wide × ½ to 1 in. thick. The sharpest possible notch, a cleavage crack, enters the sample from a brittle hard-facing weld deposit. When the specimen is loaded as a simple beam with the previously notched hard-facing bead on the tension side, a cleavage crack is formed in the weld as soon as incipient yielding of the steel specimen occurs. Specimens are tested over a range of temperatures to find the transition temperature. This is the temperature below which the steel, in the presence of this cleavage crack, will not deform plastically prior to fracturing and above which the steel possesses considerable ductility prior to fracturing.

The Drop-Weight Test is relatively inexpensive and simple to perform. After the specimen has been heated or cooled to the desired testing temperature, it is quickly transferred to the anvil of the testing machine. A 60-lb weight is then dropped on the specimen from a height of 10 to 14 ft which is sufficient to deflect the sample about 5 deg. Deflection is limited by a stop. The specimen begins to take a permanent set and the weld cracks after about 3-deg deflection. The remaining 2-deg deflection is arbitrarily, but realistically, chosen to determine whether the steel can deform plastically in the presence of a crack. This test is therefore a "go—no-go" type of test; either the specimen breaks or it doesn't break.

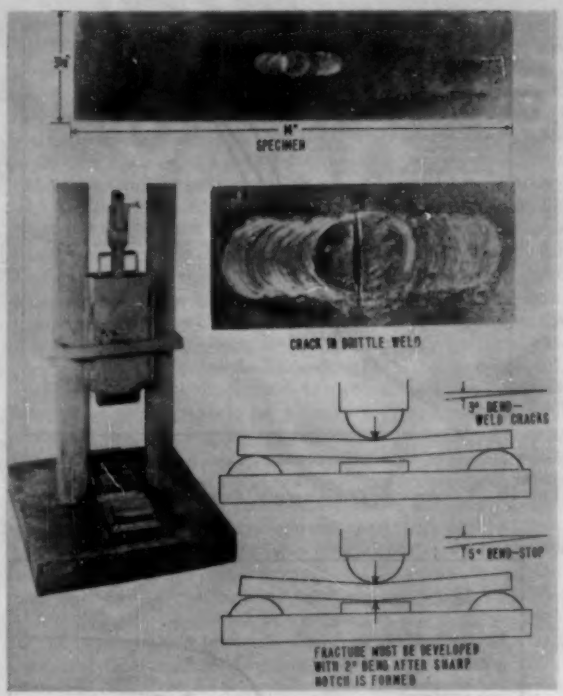

Fig. 19 Drop-Weight Apparatus, Test Specimen, and Test Procedures

To date, the transition-temperature studies have been completed on two 37-in-diam high-strength normalized and tempered Ni-Mo-V rotor forgings. Results from the first rotor are shown in Fig. 20. The average tensile properties on radial core bars were 118,000 psi TS, 100,500 psi YS (0.2 per cent offset), 15.5 per cent elongation, and 34.5 per cent reduction of area. Charpy V-notch and drop-weight specimens were machined from the surface, mid-radius, and center positions with radial notches in all samples. Drop-Weight Tests showed that the nil-ductility transition temperature was between 120 and 130 F (49–54 C). The Charpy energy level at the nil-ductility transition temperature was between 14 and 17 ft-lb. Note that this transition temperature corresponds to the lower part of the curve relating Charpy energy to testing temperature whereas the fracture-appearance transition temperature (50 per cent shear—50 per cent cleavage) is usually near the point of maximum slope in the curve.

The second rotor, as shown in Fig. 21, had a lower carbon content and slightly lower alloy content as well as lower strength combined with better ductility as shown. The Drop-Weight Tests indicated that the nil-ductility transition temperature was 54 F (12 C) for both mid-radius and center positions and 84 F (29 C) at the surface. Nevertheless, the Charpy V-notch energy levels were approximately the same at the three locations and ranged between 11 and 14 ft-lb.

The results of tests on many different steels conducted both at

[7] Materials Engineering Department, Westinghouse Electric Corporation, East Pittsburgh, Pa.

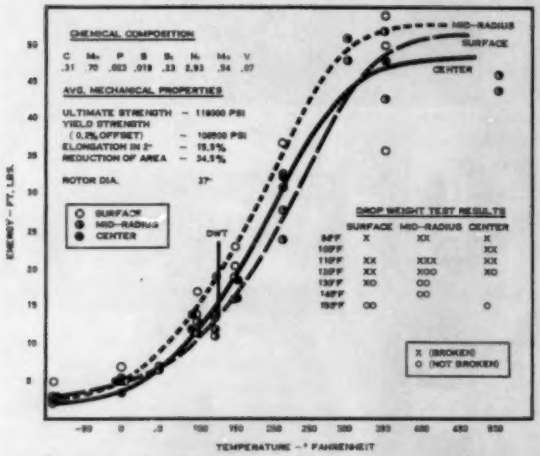

FIG. 20 TRANSITION TEMPERATURE STUDIES OF A ROTOR STEEL

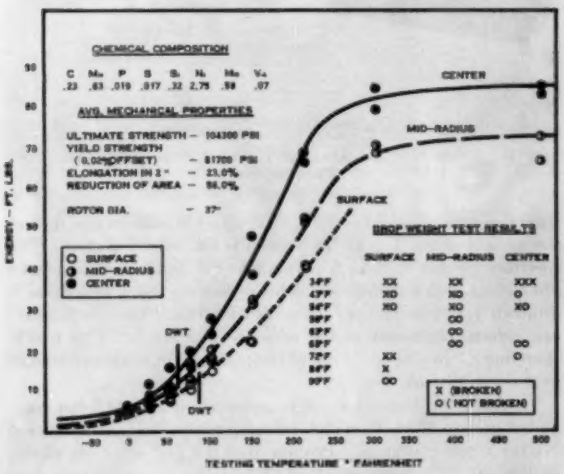

FIG. 21 TRANSITION TEMPERATURE STUDIES OF A ROTOR STEEL

the writer's laboratory and the Naval Research Laboratories have shown that the Drop-Weight Test can be correlated with the Charpy V-notch impact test; i.e., in testing different lots of steel having the same chemical composition and heat-treatment, approximately the same Charpy value (ft-lb of absorbed energy) is obtained for each lot at its respective drop-weight nil-ductility transition temperature.

We have been collecting room-temperature Charpy V-notch impact-test data on all of our rotor forgings for several years; this has been done not as an inspection test but merely for information purposes. As stated earlier in this discussion, we have data showing the correlation between the drop-weight nil-ductility transition temperature and Charpy V-notch energy levels on only two rotors at present, but the over-all program will include testing of many additional high-strength Ni-Mo-V rotors to establish definitely the existing correlation between the two tests. We then hope to specify a minimum acceptable Charpy V-notch value for impact tests conducted at the minimum operating temperature of our generators. This requirement, we believe, will insure our rotors against susceptibility to brittle fracture.

A. O. SCHAEFER.[8] This paper is so comprehensive and thorough that one hesitates to comment on it except after careful study. The authors are to be congratulated on the open-minded approach they obviously have brought to their problem as well as for their excellent presentation of the great amount of work that has been performed in their laboratories on these two particular rotors.

The writer wishes only to point out several aspects of the problem which occur to a manufacturer of these large and important forgings.

It has been repeated several times and it is well worth emphasizing, that a great many rotors have been made and placed in service and are performing satisfactorily.

The problems that have been discussed in this paper and in others are magnified by the size of the rotors as well as by the required strength levels of the materials. In other words, it becomes more difficult to manufacture rotor forgings as their size is increased and also as the required tensile properties are increased. Segregation and shrinkage in a steel ingot do not cause us too great concern in small ingots of mild carbon steel. They cause increasing trouble as the carbon and alloy contents of the steel are increased, and also as the size of the ingot is increased.

In recent years there has been a trend in demand for larger rotor forgings of higher tensile properties. We can say, in general, that the needs of the designing engineers have been met, but we also can say that we have experienced losses in our attempts to do this.

As we look into the future we know that we have all benefited by the investigation reported in this and other papers. We also know that there are many problems to be faced and much work to be done.

Hardenability is increased by adding carbon and alloy content. Such steels are being made as part of the program here reported. They will be cast in large ingots, and the forgings made from them will be liquid-quenched. We will be interested to see to what extent the increased alloy content contributes to the severity of the segregation in the large ingots, and to what extent such increased segregation may be safely permitted in rotors.

Liquid quenching introduces stress patterns that we decided to avoid some years ago.

In all of this work, as a steelmaker, the writer must point out the fact that heats of steel vary considerably. It will not be enough to prove superiority of one forging, of one chemistry, and of one heat-treatment. We can follow the lead of one forging if results from it are favorable, but practice must be established only on the basis of experience with a number of forgings.

It will take time and the continuing efforts of a group such as that represented in the program of which this paper is a part to accomplish the improvement we want and need.

J. M. HODGE.[9] In the first place the discusser wants to congratulate the authors and their company on their realization of the far-reaching significance of these two fractures, and on their acceptance of the challenge which they present, as exemplified not only by this extremely thorough and comprehensive investigation, but also by the vigorous and well-conceived improvement program which they have embarked upon, based on the findings of this investigation.

---

[8] Vice-President and Executive Assistant, The Midvale Company, Nicetown, Philadelphia, Pa.

[9] Chief Research Engineer, Alloy, Forgings and Railroad Materials, Applied Research Laboratory, United States Steel Corporation, Monroeville, Pa.

Although the specific major factors involved in each of these fractures are well established by this investigation, the scope of their program extends well beyond the establishment of these specific answers into studies of the basic factors involved in the production of forgings of much greater notch toughness, so that the probability of the catastrophic brittle fracture, which occurred in both of these accidents, would be minimized.

This discusser would like to comment briefly on only one of the many factors which are involved in this problem; the segregation streaks which played a prominent part in both of these fractures. In this connection it should be pointed out that the Arizona rotor was 39½ in. in diameter and was forged from a 73-inch ingot, the Cromby rotor was 43 in. in diameter and was forged from an 82-inch ingot, and that many of the forgings currently being produced are even larger in diameter and require the use of still larger ingots. For example, ingots 95 in. and even 110 in. in diameter are in current use for the production of such forgings.

With these large ingots and the consequent very slow solidification, segregation of the type exemplified by these streaks cannot be entirely avoided, although they can admittedly be minimized by proper control of the melting and forging practices. We have, as General Electric did, evaluated by spectrochemical and microanalytical methods, the chemical segregation associated with these streaks and have found very similar answers to those reported in this paper. We have also studied the effects of this segregation on the transformation behavior of the austenite, both isothermally and on continuous cooling at cooling rates similar to those used in the heat-treatment of these forgings, and have found these streaks to be much more sluggish in transformation than the matrix unsegregated material. For example, samples of nickel-moly-vanadium steel, cut from an area in a forging which contained these segregation streaks, showed up to 20 per cent untransformed austenite in the streaks and complete transformation in the matrix material, after cooling from an austenitizing temperature of 1475 F to a temperature of 600 F at a rate corresponding to a location 3 inches below the surface of an air-cooled 45-inch-diameter forging. The marked concentration of molybdenum in segregated streaks is undoubtedly a significant factor in the differences in transformation behavior in the bainite transformation temperature range. Effects of this magnitude must be given serious consideration in planning the heat-treatment of these large forgings and also in the design of new compositions for these applications.

Authors' Closure

The comments offered by Messrs. Layland, Schaefer, and Hodge are greatly appreciated by the authors. These two rotor bursts, coupled with the results of the extensive laboratory investigations which were conducted, revealed a metallurgical problem of far-reaching significance, toward the complete solution of which a very large program of investigation and development is continuing. As part of this program, the authors' company has on order about thirty full-size rotor forgings with modified compositions, steel-making practices, and heat-treatments, all designed to produce a forging with greatly improved toughness characteristics. The discussers have called attention to a number of factors of importance in the evaluation of these developmental rotors, some of which are already arriving at the authors' plant.

Mr. Layland's comments are especially applicable at this time with respect to the warming of generator rotors prior to rated speed or overspeed operation as recommended both in the conclusions of this paper and in the companion paper[10] by Messrs. Mochel, Peterson, Conrad, and Gunther, which practice is now being followed by most turbine-generator owners. Although it is generally recognized that a transition temperature does exist which apparently separates brittle fractures from ductile fractures, the quantitative definition of this transition temperature depends markedly on the type of test used and the interpretation of the results. For instance, in a simple V-notch Charpy test, the specific transition temperature depends on whether one uses an energy criterion or a fracture-appearance criterion. The Pellini Drop-Weight Test described by Mr. Layland furnishes another transition temperature which is 50 F to 100 F below that defined by the V-notch Charpy energy criterion. Similarly, slow bend tests give transition temperatures different from, and generally lower than, those obtained from Charpy impact tests and, in addition, the magnitude of the difference is dependent on the specimen size. Mr. Layland's results are also interesting in that, as he points out, the DWT transition temperature of material from two Ni-Mo-V rotor forgings corresponds to a V-notch Charpy energy level around 15 foot-pounds which agrees well with results of tests at the Naval Research Laboratories, mostly on carbon steels, which also gave 15 foot-pounds as the distinguishing level between brittle and ductile fractures. This, of course, raises the question as to whether a minimum Charpy impact energy (such as 15 foot-pounds) or a maximum transition temperature is the better criterion of resistance to brittle fracture. At the estimated temperature of the Cromby rotor when it burst, the V-notch Charpy value of the material exceeded 15 foot-pounds, as shown in Fig. 16.

The relationship between the operating temperature of a large rotor and the transition temperature or impact energy as determined from Charpy or other tests of small samples of the material, necessary to preclude the possibility of brittle fracture of the rotor is unknown. Generally speaking, however, the higher the temperature, the higher the impact energy and the smaller the likelihood of brittle fracture. It appears highly desirable, therefore, to maintain rotor temperatures, particularly during start-ups and overspeed testing, as high as is practicable, and specifically to refrain from such operation when the rotors are around 80 F or lower. Some spin tests recently conducted in our Product Development Laboratory bursting chamber also seem to substantiate the benefits obtained by warming below the transition temperature. In these tests, three disks, each 24-in. OD, 4-in ID, 6 in. thick, severely notched at the bore and mid-radius points were spun to bursting at various temperatures. The V-notch Charpy energy transition temperature of this material was 275 F. A disk spun at —50 F burst at 15 per cent of the tensile strength; one spun at 200 F burst at 25 per cent of the tensile strength; and one spun at 400 F went to 40 per cent of the tensile strength before bursting. It should be emphasized that these relatively low bursting strengths were due to the severely notched conditions which were used; nevertheless, the benefits of warming even below the Charpy transition temperature are evident. More extensive tests of this type are now under way to determine transition temperature under the specific stress conditions which occur in rotating turbine and generator rotors.

Mr. Schaefer's comments pointing out the difficulty the steelmakers face in producing the required large forgings are also appreciated. The large ingots required for these forgings present their own problems in regard to solidification patterns and segregation, and it is regrettable that more is not known in this field. Mr. Schaefer's company and other forging manufacturers are participating in the rotor development programs of the authors' company, and we are mutually interested in the extent to which increased alloy content contributes to segregation severity. We are also concerned with the stresses introduced by liquid quenching, and all of our development rotors scheduled to be so treated have a long extension beyond the coupling for complete evalua-

[10] "Large Rotor Forgings for Turbines and Generators" by N. L. Mochel, R. E. Peterson, J. D. Conrad, and D. W. Gunther, published in this issue, pp. 1585–1601.

tion of residual stresses. In addition, Mr. Schaefer's comments regarding the variability between successive heats of the same alloy will be evaluated by producing several forgings of any promising alloy.

We appreciate that we have embarked on a program of considerable scope in our rotor development activities, and we require the considered technical advice of the steel producers to carry this program to a successful conclusion. We have maintained continuous contacts with the personnel of the contributing mills and appreciate their advice and suggestions. In particular, the points raised by Mr. Schaefer illustrate the type of problems on which the steel mill personnel are most expert, and on which their advice is needed.

Mr. Hodge also points out the difficulty of avoiding segregation in large ingots, and his comments as to the possible degree of retained austenite emphasize the need for control of melting and forging practices so as to keep such segregation down to absolute minimum values. If alloy segregation occurs such that any significant amount of retained austenite is present after the tempering treatment, it is possible that this austenite will transform slowly during service to unwanted structures with both high residual stresses and brittle fracture characteristics. In developing new rotor alloys, this phenomenon must be given serious consideration, as Mr. Hodge points out, but it is equally important that the mills themselves consider and quantitatively evaluate these effects in the rotor alloys now in almost continuous production.

Large Rotor Forgings for Turbines and Generators

By N. L. MOCHEL,[1] R. E. PETERSON,[2] J. D. CONRAD,[3] AND D. W. GUNTHER[4]

The paper discusses turbine-generator rotor forgings. It includes a brief history of the development of present designs, materials used, manufacturing methods, and the various testing practices employed. Special reference is made to low-pressure rotor construction. A discussion on types of instability encountered in turbine rotors is included. The paper includes a section on design criteria dealing with static considerations, fatigue considerations, and reports the results of several model bursting tests. The importance of proper alignment of rotor shafts is covered.

AT every stage during our 60 years of experience in this country in the building of steam turbines and steam-turbine-driven generators, one of the most important considerations has been the development of the design, of the materials, and of the manufacturing skills, necessary for making reliable rotors for both turbine and generator.

Perhaps at this point, we should note the remarkable progress that has been made in these 60 years of steam-turbine-generator experience. Inlet steam temperatures have been raised at a rate of 12 or 13 deg F per year. Turbines are in operation at 1100 F; others are now building to operate at 1150 and 1200 F. Pressures have advanced from around 150 psi to the level of 5000 psi. Capacities have progressed from 400 to 325,000 kw and even higher. Single-shaft generators may develop 275,000 kw. Great reductions in the weight of metals required and in floor space involved have been reported elsewhere (1).[5]

These accomplishments were hardly possible without the continued advances that have been made in the design of the major rotating elements, advances in metallurgy and evaluating practices, and in our being able to secure bigger and better steel forgings from those skilled in their manufacture. The rotor forging is the very heart of the turbine-generator.

Perhaps, too, in passing, we should note that the installed capacity in this country of steam turbine-generators is over 100 millions of kilowatts, and this means that there are a great many turbine and generator rotors in successful operations.

Rotor designs have developed gradually from built-up types using many parts that were pressed, shrunk, keyed, or bolted together in various ways, to fewer and fewer parts, finally to those employing essentially a single forging, for each turbine and generator component Figs. 1 and 2.

Originally, reaction or impulse-reaction turbine rotors consisted of a hollow shell body, with shaft ends fitted thereto, and a number of rings shrunk thereon. There was a gradual reduction in the number of parts, this being especially observed during the period from about 1912 to 1923. At that time designs were so modified that rarely were there more than two forgings per rotor, and whenever possible, the rotor then followed a definite trend toward single-piece construction.

Impulse turbine designs have long used a central shaft on which are fitted a number of disks, with each disk as a rule carrying a single row of blades. This design is still used extensively where temperatures of operation permit, especially in industrial turbines and in large 1800-rpm low-pressure turbine rotors.

But as temperatures advanced to higher levels, these built-up shaft-and-disk rotors also turned to a single-piece forging, the disks being carved to the desired shape from a solid forging; thus disks and shaft are integral.

Often low-pressure rotors and complete expansion rotors, of both 1800 and 3600-rpm designs, employ a combination of the two general practices, in that the main body and shaft ends of the rotor may be a single forging, and one or more disks may be used at one end or both ends.

Also, as will be discussed later, large low-pressure reaction-turbine rotors of the 1800-rpm type are built up of a large central shaft, with a number of blade rings and disks shrunk thereon, for reasons that will be given.

Somewhat similar changes have taken place in generator-rotor construction. Rotors were at one time built up of many comparatively thin steel plates, stacked together, and secured to stub shafts by through-bolts. Then thicker steel disks of specially heat-treated steel forgings replaced the thinner plates. And then came the move to the present single-forging construction. Of course, when we refer to single-forging rotor construction, we must remember that there are retaining rings, an important matter also, blower-hub forgings, and coupling-hub forgings, produced as separate forgings and secured to the main member.

From the turbine standpoint, these gradual changes were largely initiated in the smaller industrial turbines, and as experience grew, they moved over into the larger units. Also, we should not overlook the many contributions to our developments, and experiences, made by the many steam turbines for marine propulsion built both before and during World War II, which invariably made use of the single-forging construction, and the forgings were quite comparable in size and materials to many used for central-station applications.

Fig. 3 shows a collection of rotor forgings for central station, industrial and marine turbines. Fig. 4 shows a typical single-piece generator rotor, nearing completion of its machining operations. Figs. 5 and 6 show typical turbine rotors of the single-piece construction, in the nearly finish-machined condition.

Our experience with what we may term large rotor forgings goes back to the 1913–1914 period, when we secured some large rotor end forgings, for 20,000 and 30,000-kw turbines, from Fried Krupp, at Essen, Germany. As received, these weighed ap-

[1] Manager, Metallurgical Engineering, Steam Division, Westinghouse Electric Corporation, Lester Branch Post Office, Philadelphia, Pa. Mem. ASME.

[2] Manager, Mechanics Department, Westinghouse Research Laboratories, East Pittsburgh, Pa. Mem. ASME.

[3] Manager, Engineering Services Division, Steam Division, Westinghouse Electric Corporation, Lester Branch Post Office, Philadelphia, Pa. Mem. ASME.

[4] Manager, Materials Engineering Department, Westinghouse Electric Corporation, East Pittsburgh, Pa.

[5] Numbers in parentheses refer to the Bibliography at the end of the paper.

Contributed by the Power Division and presented at a joint session of the Power and Metals Engineering Divisions at the Diamond Jubilee Annual Meeting, Chicago, Ill., November 13–18, 1955, of THE AMERICAN SOCIETY OF MECHANICAL ENGINEERS.

NOTE: Statements and opinions advanced in papers are to be understood as individual expressions of their authors and not those of the Society. Manuscript received at ASME Headquarters, November 13, 1955. Paper No. 55—A-215.

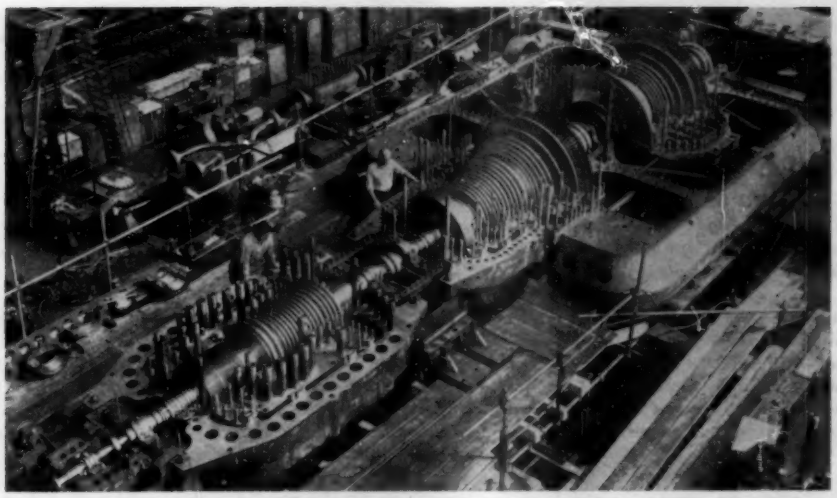

FIG. 1 THREE-CYLINDER TURBINE CONSTRUCTION SHOWING HP, IP, AND LP ROTORS

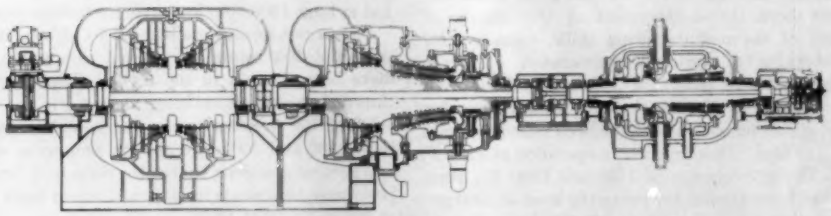

FIG. 2 CROSS-SECTIONAL THREE-CYLINDER TURBINE SHOWING HP, IP, AND LP, ROTOTO
(185,000-kw-capability, 3600-rpm reheat turbine; 2350 psig—1100/1050 F total temperature, 15 in. Hg abs.)

proximately 30,000 lb. They were roughly 8 ft long, with a main body about 23 in. long and 60 in. diam. They were not machined closely to size, requiring considerable further machining, heat-treating, and testing on our own part. Very shortly thereafter, we secured similar forgings from the Midvale and the Bethlehem companies.

We had long ago attempted to simplify matters by pointing out that there were two fundamental considerations that must control the selection of material and the heat-treatment of turbine-rotor parts (2):

1 The material must have general physical characteristics to withstand rotation and transmit load.

2 The rotor must be possessed of such general stability as to operate smoothly over many years.

Originally, we more or less assumed the responsibility for both considerations, and as a result gained much experience with forgings of several compositions, and of varying sizes. The use of round vertical furnaces, now considered quite necessary in the heat-treatment of rotor forgings, goes back to the 1915 period. Hanging such forgings in these round vertical furnaces, and other types of support, during heat-treatment, were practices of that time. Liquid quenching of carbon-steel and low-alloy-steel forgings was a matter of experience then, as well. Gradually, our policy changed until in the early 1920's we worked out practices with our suppliers that placed in their hands the supply of forgings that would have all heat-treatment, testing, and machining closely to size and shape, completed in their shops. We desired the forgings to be ready for our finish-machining lathes upon delivery to our gates. Fig. 3, therefore, shows the condition of the forgings as received by us. Depending upon their size, they have stock left on them of $^1/_8$ or $^1/_4$ in. on the main body and $^1/_4$ or $^1/_2$ in. on the shaft ends. They are ready to finish-machine. Fig. 3 does not show any impulse-type rotors, but these, too, are machined closely to size, and the carving out of the integral disks is performed at the forging plant before final heat-treatments.

FIG. 3 ROTOR FORGINGS FOR CENTRAL STATION, INDUSTRIAL AND MARINE STEAM TURBINES

Throughout the years there has been much variation in the

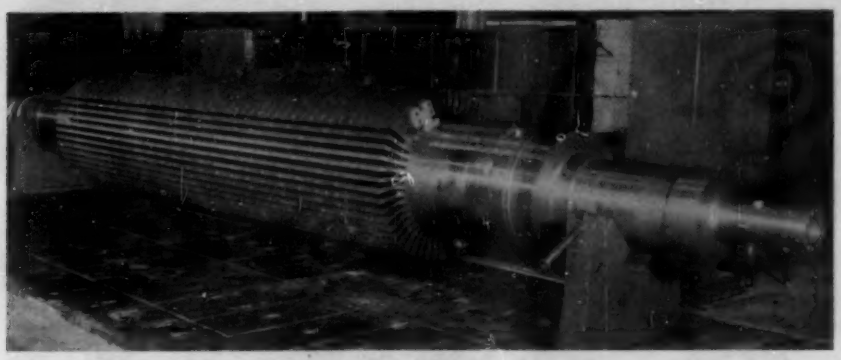

FIG. 4 TYPICAL GENERATOR ROTOR

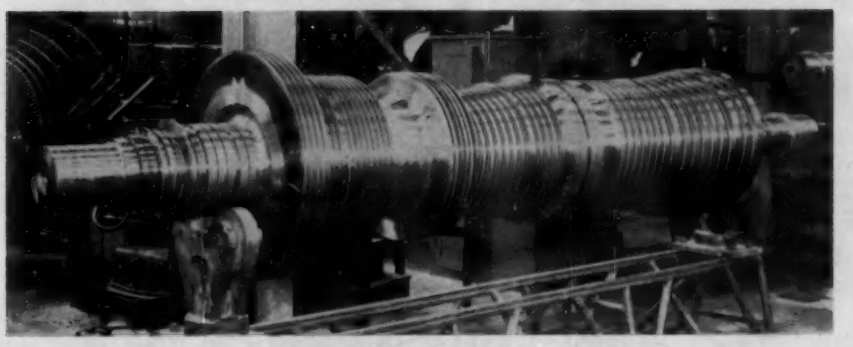

FIG. 5 HP-IP TURBINE ROTOR

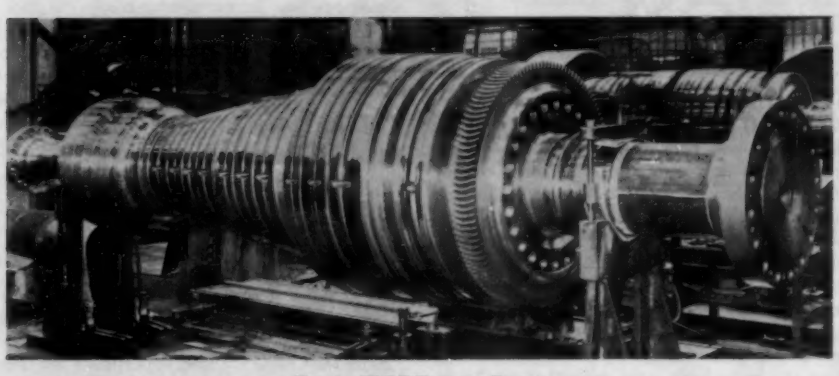

FIG. 6 IP-LP TURBINE ROTOR

size and shape of the rotor forgings for the turbine. Some of this variation has already been illustrated. As capacities increased in the 1800-rpm fields, such forgings became quite large, taxing the very limits of ingot sizes and facilities available. Many required the use of large 108-in. ingots, sometimes weighing over a half-million pounds, and requiring as many as three heats of steel. One such rotor, made from a 108-in. ingot weighing 405,000 lb is illustrated in Fig. 7. In the condition shown, it weighs but 144,000 lb. This serves to indicate the amount of excess metal that must be provided and handled in order to secure a sound forging of this type.

From the standpoint of the rotor forgings, the development of the 3600-rpm turbine-generator into larger capacity units has been very important. In general, it has permitted the use of smaller forgings, made from smaller ingots, and with less trouble in manufacture.

High-speed generator forgings have been discussed in some detail by Laffoon (3). He has shown the advantages of the smaller 3600-rpm rotors over the larger 1800-rpm rotors. He also deals with the very important contribution of inner cooling in making possible the use of smaller-sized forged rotors.

As regards the turbine, of the 3600-rpm types, the dividing up of the unit into two, or three, or four separate casings, and likewise the same number of rotating elements, has permitted a general reduction in the sizes of the forgings required. We feel this is a very important development in securing sound forgings and in the development of alloy-steel rotors of high strength.

Earlier reference was made to large 1800-rpm low-pressure tur-

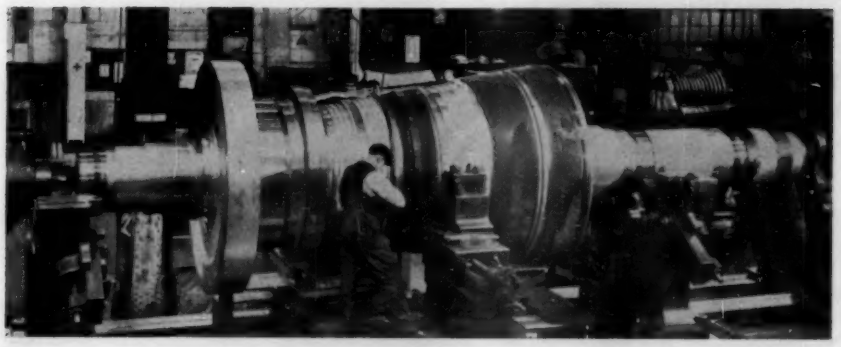

FIG. 7 LARGE 1800-RPM TURBINE ROTOR

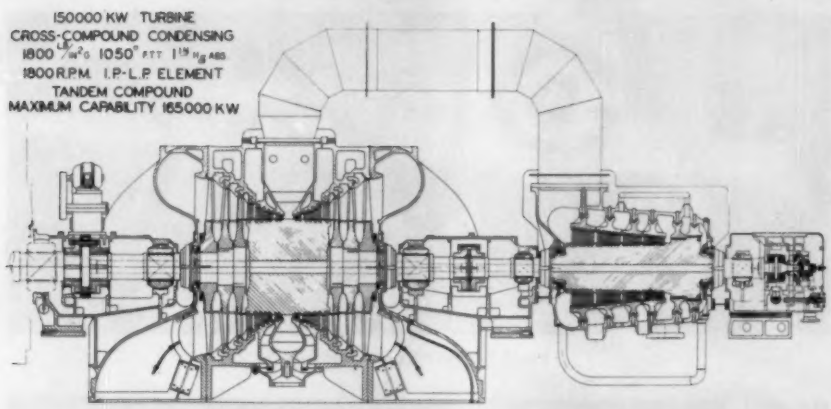

FIG. 8 MAIN BODY FORGING AND DISK DESIGN OF LP ROTOR

bine rotors and to the several types of construction used in recent years. A current paper (4) deals with the failure of one such rotor at the Ridgeland Station here in Chicago in December, 1954. The general construction consisted of a large central cylindrical rotor body with integral shaft ends, and with three disks shrunk on the shaft portion, at each end.

At the time, the authors' company had some six low-pressure turbine rotors in operation, having a somewhat similar design to that which failed. Fig. 8 illustrates the design that had been employed. The main body in the company designs was slightly smaller, being 76½ or 77 in. diam. The length of the main body was somewhat greater than in the failed rotor, and the shaft diameters adjacent to the main body were somewhat smaller in diameter. Three of our forgings had been produced from 82-in. ingots, three from 108-in. ingots. A 3 per cent nickel steel requiring but 55,000-psi yield strength and 85,000-psi tensile strength, offered a much more ductile material than that described in the paper (4).

Under the circumstances, it may be of interest to record our experiences with these six units, the subsequent examinations made on three of the rotors, and changes in design that had been effected long before the incident at Chicago.

The six units were placed in regular service at the following times:

Unit A	July 19, 1947
B	September 3, 1947
C	January 14, 1948
D	March 16, 1951
E	October 4, 1950
F	August 1, 1951

The large central forgings for the first five units listed were produced by one forging manufacturer; the sixth one was produced by a second supplier.

Ultrasonic testing had not been employed at the time the rotors for units A, B, and C were produced. Limited application was employed with the forging for unit E. The forgings for units D and F were examined by ultrasonic means during forging manufacture, and again after finish-machining. The record was excellent.

Since the Chicago failure, opportunity has been presented owing to work of other nature on these units, to examine carefully the rotors from units A, C, and E. Center plugs were removed to examine the bores, and ultrasonic methods were employed working from all available exterior surfaces, examining both radially, longitudinally, and in angular directions. A very few minor irregularities were observed. All the rotors were returned to service. When opportunity presents, it is expected that the other three rotors likewise will be examined.

There was particular interest in the rotor in unit E, since the bore in this rotor had been enlarged under the main body to as much as 24 in. diam, in order to remove unsoundness found in the bore. (To compensate for this bore enlargement the mid-portion of the outside diameter, between the first rows of blades, had been reduced to 65 in. diam for a length of 11½ in., and the average tangential stress at the areas involved was actually below the designed stress. The yield strength in this particular forging was

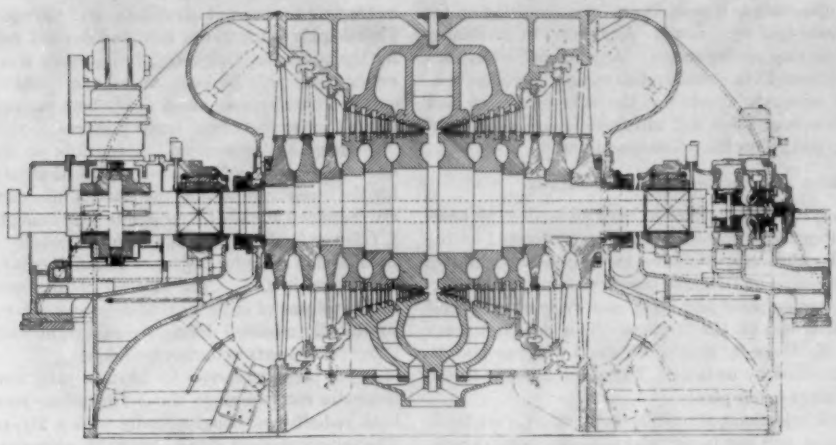

FIG. 9 ALL DISK AND SHAFT DESIGN OF LP ROTOR
(165,000-kw-capability, 1800-rpm LP element, reheat cross-compound turbine; 1800 psig—1050/1000 F total temperature, 10 in. Hg abs.)

also well above that specified.) The four small irregularities observed, in the re-examination referred to, were not at the point of major counterbore.

To secure the five large rotor forgings, made by the one supplier, actually seven forgings were made. Two were rejected. One was rejected because of instability. Numerous heat-treatments failed to pass it through the heat-indication test. The other rejection was due to serious unsoundness in the bore. Counterboring revealed the presence of a large crack, and the forging was therefore rejected. If we add to this record the necessity to greatly enlarge the bore from 10 to 24 in., in the case of the forging in unit E previously referred to, and appreciate what these retreatments, and reborings, and final rejections would do to a production schedule, the situation was one that required re-examination of our design approach. In 1935 we had placed in operation in Philadelphia a 165,000-kw unit, in which the low-pressure turbine rotor had been built up of a large central shaft, with ten blade rings and disks shrunk thereon. This design has given splendid service.

After weighing advantages and disadvantages, we returned to this design approach for our large 1800-rpm rotors, and some seven such rotors have since been constructed. Fig. 9 illustrates this design, in which six blade rings and six disks are shrunk on the shaft member. It is a more costly design, involving a great deal more initial cost, more machining, and great deal more assembly time and expense. However, it is a more trouble-free production item. Smaller forgings are used, and they may be critically examined more readily than the larger mass. The parts in general may be made from smaller ingots, and better worked all over.

MATERIALS

The years have witnessed a constant development in materials; from cast carbon steels originally, to forged carbon and nickel steels, to nickel-chromium steels, to nickel-molybdenum, and nickel-chromium-molybdenum, and additions of vanadium and then to chromium-molybdenum-vanadium steels for higher temperatures. And in the immediate future, there will be several installations where austenitic steels of several compositions will be employed for high-temperature rotors, and likewise modified 12 per cent chromium steels will probably enter the field.

In our present general practices, we may summarize by saying that three types of steel are employed for turbine rotors, carbon steel, nickel-chromium-molybdenum-vanadium steel, and chromium-molybdenum-vanadium steel. Of the two alloy groups, and speaking very broadly, the chemical analyses employed will fall within the over-all ranges given in Table 1.

TABLE 1 CHEMICAL COMPOSITIONS

	Ni-Cr-Mo-V steel	Cr-Mo-V steel
Nickel, per cent.....	2.50 min	0.50 max
Chromium, per cent..	0.30–1.00	0.85–1.25
Molybdenum, per cent	0.20–1.00	1.00–1.50
Vanadium, per cent..	0.08–0.30	0.20–0.30

TABLE 2 TENSILE PROPERTIES

	Longitudinal tests	Tangential tests
Yield strength, psi, min.....	100000	100000
Tensile strength, psi, min.....	120000	120000
Elongation in 2 in., per cent, min	16	14
Reduction of area, per cent, min	40	35

Tensile properties have advanced to the point where our strongest Ni-Cr-Mo-V grade requires acceptance tests as given in Table 2.

Reference should be made to the specifications for turbine-rotor forgings issued by the Bureau of Ships of the U. S. Navy (5), and to those prepared and issued by the American Society for Testing Materials, (6–8). Those issued by the ASTM are constantly under study by the large forging manufacturers and the turbine-generator builders.

MANUFACTURE

In the procurement of our rotor forgings, we do not attempt to tell those skilled in the manufacture of forgings how to do their job, neither do we take the opposite extreme and just sit back and await results. Rather, we take a deep interest in every move. We want to know the kind of steel used, and the size of ingots employed, and the various steps in the forging operations, we specify the general nature of the heat-treatments employed, and set forth the testing practices. We have worked with the steel people as closely as possible. We note the ingot practices, and the facilities on hand, the attitudes as regards good heat-treating practices, and the placing of our orders for forgings depends on many such things. We discuss trends and troubles as quickly as possible. We are more than just interested in such new developments as vacuum pouring.

MACHINING

As suggested before, we do as little machining as possible on our turbine-rotor forgings after the final stress-relieving treat-

ment. We look upon this as a precision matter, requiring up-to-date rugged machine-tool equipment. Any errors in machining must be reported for engineering action. Any unusual conditions noted are likewise brought to metallurgical engineering attention. Good radii and adequate finish are the rule by design and practice. Complete magnaflux and ultrasonic examination and a further stability test follow the finish-machining.

Testing and Acceptance of Forgings

As stated earlier, it is our practice to have all testing, all heat-treatment, and acceptance so far as possible, performed at the forging plant. To that end we have metallurgical inspectors from both our generator and turbine plants who follow the forgings through the forging plant and verify and witness the several tests that are performed on the forgings. This does not mean that further examinations by magnaflux and by ultrasonic devices are not performed by us later. These are repeated in the finish-machined rotors in our plants.

The point is that rejections, almost in their entirety, are made in the forging plant and not in our plants. The metallurgists, at times, wonder if this is to their advantage, since it deprives them of "guinea pigs" to cut up for study.

Just as we have developed in so many ways in this matter of rotor forgings, so have we developed in our testing practices, to evaluate the acceptance or rejection of the forgings. A few general comments in passing will illustrate the point we are trying to make.

Chemical-Composition Analysis. The chemical composition has been more or less basic. At present thinking turns to more closely controlled analyses, especially lower phosphorus and sulphur, and other impurities.

It has been recognized for some time that hydrogen dissolved in steel may have a deleterious effect on its quality. Two conditions may prevail due to this condition, one is "flaking" or the creation of cracks in the body of the steel piece, the other is hydrogen "embrittlement" or a reduction in the ductility property of the material. Flaking, if it exists, generally occurs during the processing of the material and may be detected by ultrasonic testing. It is to be noted, however, that a few cases of delayed flaking have been reported.

The embrittling effect of hydrogen is much more insidious and difficult to determine since hydrogen is a very elusive element and is easily lost during sampling and testing if many precautions are not taken. The embrittling effect has been under study for several years and more recently has been recognized by the American Society for Testing Materials through the creation of a task force to investigate the effect of hydrogen in forgings. It should be noted that a much clearer understanding of this phenomenon has now been attained and forging suppliers are studying production techniques aimed at the reduction or elimination of this element in the materials produced.

Mechanical Properties. Tension tests in the longitudinal, tangential, and radial directions have long been a rather basic form of testing. Present thinking is in the direction of better ductility and several moves in that direction are in the making.

At times impact tests on notched specimens have been made. Impact tests, notched-bend tests, transition temperatures will be referred to in probably all the presentations today. This general subject is being closely studied by the forging makers and the turbine-generator builders.

Sulphur Prints. We have been a little old-fashioned, in a sense, in our continued use of the old sulphur print method in our turbine rotor inspection to check against serious ingot corner segregation at the larger diameters of our forgings.

Bore Inspection. Since the early 1920's we have employed the axial hole or bore for borescope examination. When suitable instruments were not available, Dr. George S. Crampton of Philadelphia came to our help and devised excellent borescopes for the purpose. Originally, the purpose was to guard against major ruptures, "clinks," fissures, etc. But with the hole present, and the increased stress at the bore surface, precautions had to be taken against much smaller defects.

Magnaflux Examination. Magnaflux or similar type of examination has long been used. Critical areas are examined during the acceptance tests at the place of manufacture. The rotors are examined all over in our plants after being finish-machined.

Ultrasonic Examination. The ultrasonic reflectoscope has been used in rotor-forging examination since it first became available for use in 1947. The method of ultrasonically testing the entire volume of large turbine-generator rotor forgings has been continually modified during the past eight years so as to include many refinements in testing technique.

In the present practice for ultrasonically testing large turbine-generator rotor forgings, the entire surface area is first traversed both radially and longitudinally with a $2^1/_4$-mc searching unit. The minimum-sized defect detectable ultrasonically is a function of the frequency and length of the transmitted wave. Inasmuch as defects not favorably oriented to the direction of the wave present a very small reflecting surface to the wave, it is possible to miss these discontinuities when testing with relatively low frequencies; for this reason, $2^1/_4$-mc has been adopted as the standard testing frequency. Each individual indication of a discontinuity is carefully investigated and its exact position is plotted on a chart which is subsequently filed as a permanent record. This chart not only contains the position of the discontinuity, but also its relative size in proportion to the back reflection; any changes in the size of the back reflection are also noted. All indications of discontinuities found with a $2^1/_4$-mc searching unit are further investigated with a 1-mc searching unit; the results of this test are also carefully plotted. All of these tests are performed by company metallurgists at the suppliers' plants. Engineers, rather than inspectors, conduct the ultrasonic investigation of rotor forgings because it is felt they are best suited to consider the effects of metallurgical variables such as melting practice, forging, and heat-treatment.

Turbine-rotor forgings likewise are examined by the ultrasonic means at the place of manufacture by our metallurgical inspectors, a part of our metallurgical engineering organization, following the same general practice just outlined. After all finish turning has been completed at the turbine shop, they are again examined all over, in both radial, longitudinal, and, in some cases, in an angular direction.

Considerable progress has been made in the past eight years toward the positive identification of discontinuities found in ultrasonic testing. Forgings showing various types of ultrasonic indications have been sectioned or trepanned so that the type of indication can be correlated with observed defects. One cannot hope to list the results of years of experience in a short paper such as this, but typical findings are:

1 Many sharp indications (pips) found near the center of the section and having pronounced effect on the back reflection are caused by thermal ruptures or flakes.

2 Sharp pips found in a definite pattern equidistant from the bore and close to it which show a pronounced effect on the back reflection are indicative of large amounts of segregation or pipe usually caused by insufficient working of the center of the ingot.

3 Isolated indications having no noticeable effect on the back reflection are usually associated with porosity or inclusions and are of little concern unless they are close to the bore.

4 Isolated indications following a pattern 5 to 10 in. from the surface and having little effect on the back reflection are usually caused by interdendritic or intergranular segregation of inclusions

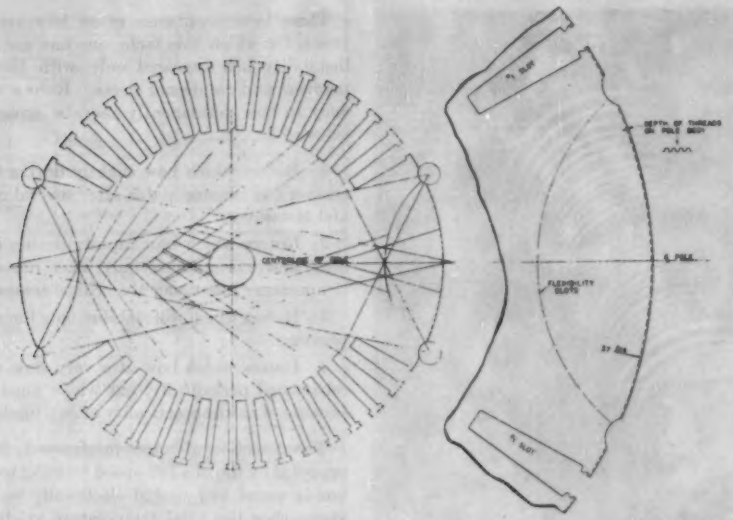

FIG. 10 FIELD ULTRASONIC INSPECTION OF GENERATOR FORGINGS

(from the original columnar grain structure). They are of concern if they fall in the same plane as the bottom of the slots.

5 Small bulbous indications next to the back reflection are usually caused by porosity near the bore. Sharp indications in the same location which travel with movement of the searching unit are usually associated with pipe or shrinkage. In either case the discontinuities are carefully investigated with the crystal tuned to a high sensitivity in order to pin point the amount of overboring necessary to obtain a clean, sound bore. In some cases, this investigation of defects close to the bore is supplemented by further tests with a variable angle crystal.

Company engineers are not primarily concerned with the average number of size of discontinuities found in a rotor forging; their major concern is with the location of the defect and its positive identification. In some cases, a core bar is trepanned from the defective area and subjected to metallurgical investigation. The results of both ultrasonic testing and tensile tests of each rotor forging are thoroughly discussed in a meeting of the engineers who performed the ultrasonic test, other metallurgists concerned with forgings, and the mechanical engineers responsible for the design of the generator. At this meeting the final disposition of the rotor forging is made.

As previously mentioned in this report, interpretations of ultrasonic test results are sometimes confusing. To this, one must add that some types of defects, particularly radial cracks near the bore, are extremely difficult to detect during the usual ultrasonic inspection. When the crystal is held directly over the radial crack, no pips are seen on the screen and there is no loss of back reflection; however, when the crystal is moved to a position 90 deg from the radial crack a small pip may be found behind the back reflection. This indication is obtained because of fanning out of the longitudinal wave so that although most of the wave is returned to the searching unit when it hits the bore, some of it continues around the bore and is reflected from the radial crack. Pips from radial cracks are very small and may be missed if the reflectoscope is not tuned to give a perfectly sharp back reflection from the bore. For this reason, a modification of the standard test is being adopted on generator rotors.

Two shallow, crescent-shaped axial grooves (2 in. diam and $^5/_8$ in. deep) can be machined in each pole of a two-pole machine or one in the center of each pole of a four-pole machine. By moving a specially ground curved crystal ($1\frac{5}{8}$ in. long, $^1/_2$ in. wide, and accurately ground to a 2-in. diam) both axially and circumferentially along the axial grooves, it is possible to test almost the entire body of a rotor ultrasonically. These grooves with resulting wave patterns are shown in Fig. 10. By moving the searching unit over an arc of about 10 deg, the direction of the wave can be changed from one in which the major part of the wave is reflected from the bore to one which just misses the bore and scans the bore surface. All cracks, including radial ones, near the bore result in a definite pip behind the back reflection when the rotor is being tested from at least one of the four axial grooves. This pip travels to and from the back reflection with movement of the searching unit; the amount of travel is useful in determining the severity of the discontinuity.

Heretofore, standard methods of inspecting rotor bodies were not applicable to finish-machined rotors due to small, closely spaced grooves which are machined around rotor bodies to reduce losses. By means of these shallow grooves, it is now possible to test finished rotors and even to explore the bottom of each slot. Rotors are tested prior to shipment. All indication of discontinuities are plotted and these records can be checked against subsequent ultrasonic tests at customers' plants. Present plans call for periodic ultrasonic inspection of generator rotors at installations in the field.

The question has been raised as to re-examination of steam-turbine rotors in service. Most of our turbine designs are such that fairly good ultrasonic coverage is possible by applying the crystal between blade rows and from end faces. Studies are under way to examine from the bore outward, as well.

Heat-Indication Test. The so-called heat-indication test or stability test, as described in reference (7), has long been employed in verifying turbine rotors for use. More recently, we have experienced other instability of such rotors, after the forging has successfully passed the usual acceptance test. A discussion of this added instability will be of interest.

ROTOR STABILITY

An occasional large rotor forging will bow at elevated temperature and speed. This bowing takes place despite the fact the forging has passed all required tests, including the heat-indication test described previously. The bowing may be either of two dis-

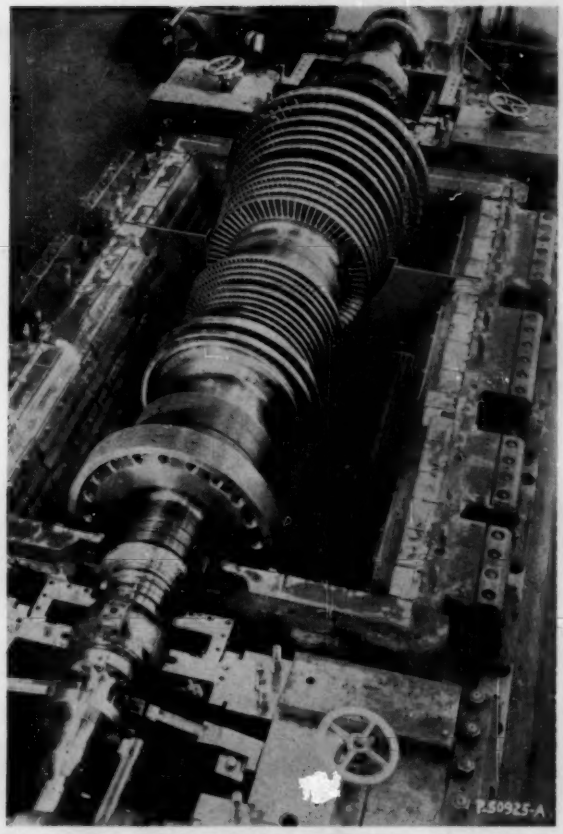

FIG. 11 HEATER BOX FOR TESTING AND CONDITIONING TURBINE ROTORS

tinct types. The first type is of the nature that no permanent deformation takes place. It has the same magnitude for any state of speed, or temperature, and always returns to same outage cold on slow roll of the machine. The second type is a permanent bowing and increases with time.

Type I—Transient Bowing. One cause for this condition was established recently, as a nonuniform coefficient of thermal expansion (9). Another cause is a circumferential temperature gradient, caused by a nonuniform rate of heat flow. The latter actually has been established in generators (10), and has been suspected, but not actually proven in turbines. This condition often is aggravated during transients, such as starting, stopping, changing steam-inlet temperature, and so on.

Resulting unbalance and vibration at any given steady-state condition may be reduced by a compromise in the mechanical balance correction. For example, the compromise may be between a part load and full load, starting temperatures and operating temperature, and so on. It is of course more desirable to remove the basic fault when such is possible. As an example, circumferential temperature gradients in generator rotors have been removed by controlling the ventilation on selected passages.

Type II—Permanent Bowing. This second type of bowing is more serious and must be corrected or the rotor replaced. Again, the heat-indication test, performed at the place of forging, has served to detect most rotors having this characteristic and enabled correction or rejection early in the production schedule.

There have been some cases, however, particularly in recent years, for which this technique has not proved infallible. The instability has appeared only with the combination of temperature and rotational stress. Rotors which display this tendency to bow permanently may be grouped into one of several classes:

1 Rotors which bow slightly during the initial stages of operation but become stable after several cycles of normal heating and stressing.

2 Rotors which bow rapidly during initial heating and running, and will stabilize only after reheating and soaking at a temperature just under the critical temperature for the material.

3 Rotors which will stabilize only for a reduced operating temperature.

4 Rotors which bow at a very slow rate and are operable if rebalanced periodically, but which must be replaced eventually because of the impracticality of any further balance correction.

The detection of rotors in classes 1, 2, and 3 has been found practical by use of a full-speed rotating test in a heater box. The box is zoned and heated electrically to give a condition which approaches the axial temperature gradient encountered in operation. The rotor being tested is driven by another turbine, Fig. 11. The slightest bowing of the rotor is reflected by a change in vibration. Modern vibration instruments will detect a change in amplitude as small as 0.1 mil or a change in location of the high spot as small as 0.1 radian. A test of 12-hr duration is sufficient to determine if a rotor is in class 1, 2, or 3.

During the past two years approximately 80 rotors, with operating metal temperatures of 900 F or higher, have beent ested in this heater box with the following results: Class 1, 6; class 2, 3; class 3, 1.

Figs. 12, 13, and 14 show typical vibration records for rotors in each of these classes.

Prior to the introduction of the stability test just described, more than 25 rotors, with metal temperatures of 900 F or higher were put into operation. It has been reasonably well established that 2 or 3 of these rotors were in class 1. In fact the field-balance experience with one of these rotors led directly to the initiation of the factory stability test.

About six years ago another rotor of class 3 had to be replaced. Also during the past decade two rotors of class 4 have been replaced. The rotors class 3 and class 4 are still available for further investigation.

Cause of Instability. The cause of the instabilities has not been determined. It is suspected that classes 3 and 4 are associated with nonuniform creep. New facilities in the authors' factory will make it possible to study running characteristics of these rotors after which they will be cut up for various metallurgical tests including creep tests.

It is possible that nonuniform creep in the primary stage also might be the cause in classes 1 and 2. Other possible causes in these two classes include:

1 Incomplete metallurgical transformation.

2 Relaxation of setup stresses caused by machining of the rotor.

3 Relaxation of nonuniform stresses caused by calking of the blades.

It will be more difficult to determine the cause in these classes. Regardless of the cause, however, the correction is relatively easy by use of the stress and temperature-cycling technique in a heater box. With the use of such a facility, final balance can be accomplished before attempting to put the machine into operation in its own casing.

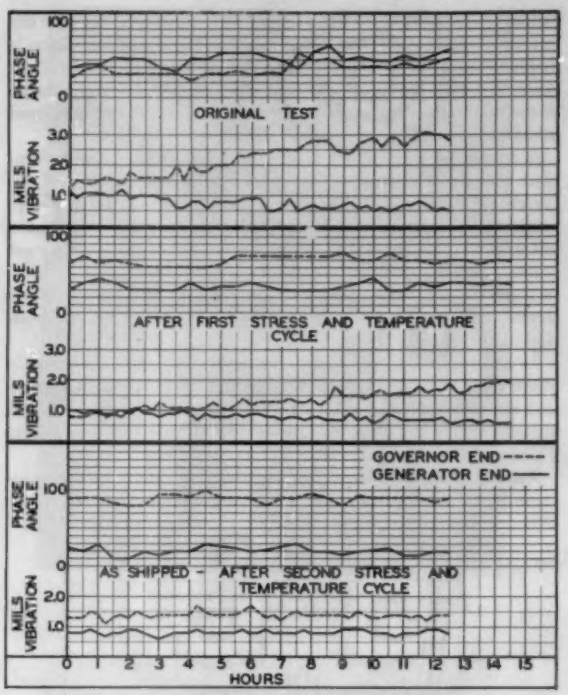

FIG. 12 VIBRATION RECORD OF A TYPICAL ROTOR IN CLASS 1

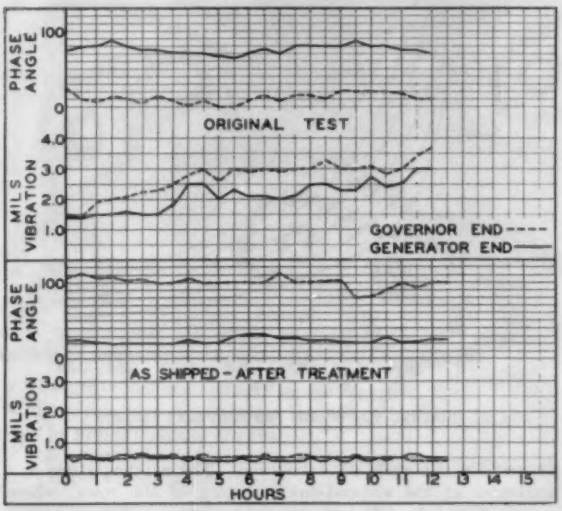

FIG. 13 VIBRATION RECORD OF A TYPICAL ROTOR IN CLASS 2

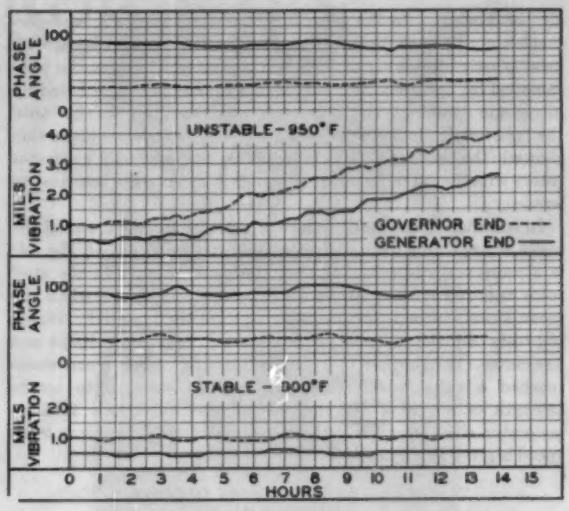

FIG. 14 VIBRATION RECORD OF A TYPICAL ROTOR IN CLASS 3

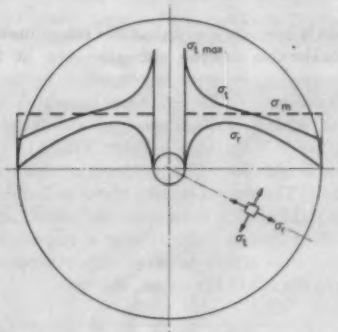

FIG. 15 STRESS DISTRIBUTION IN ROTATING CYLINDER

ROTOR DESIGN CRITERIA

Static Considerations. The stresses due to rotation (centrifugal force) are, of course, constant at operating speed, Fig. 15. Rotors are designed so that at normal operating speed the peak stress at the bore is 50–60 per cent of the yield strength; which at 10 per cent overspeed corresponds to 60–72 per cent and at 20 per cent overspeed corresponds to 72–86 per cent. Should higher speeds occur accidentally in a rotor the following would be expected: At approximately 35 per cent overspeed the bore stress would become equal to the yield strength and at higher speed the material at the bore should yield and redistribute the stress provided the material possesses adequate ductility and does not contain harmful defects or severe stress concentrations at critical regions.

An instance of such redistribution under conditions of excessive speed was provided recently by the accidental overspeeding of a 100,000-kw 3600-rpm turbine-generator to 5400 rpm, or 50 per cent overspeed. The stress at the bore would thereby be multiplied by the square of the speed ratio, $(1.5)^2 = 2.25$, if elastic conditions prevailed. The peak stress at the LP turbine-rotor bore at normal speed for this particular rotor is 49,000 psi, and multiplying by 2.25 gives 110,000; since this exceeds the yield strength of 85,000 psi,[6] the bore surface had obviously undergone plastic deformation. The corresponding figure for the generator at overspeed was 104,000 and the yield strength was 89,000 psi.[7] Examination of the turbine bore revealed no

[6] Average of two tests: Yield strength—87,500; 82,000 psi. Tensile strength—102,000; 107,000 psi.

[7] Average of four tests: Yield strength—88,500; 89,500; 89,000; 90,500 psi. Tensile strength—114,000; 113,000; 113,500; 111,500 psi.

sign of damage. In the generator bore a number of axial deformation marks were found which appeared to be associated with local plastic stretching of inclusion regions. These marks were removed by light reboring but further indications were found by ultrasonic examination. The bore was machined locally until the ultrasonic indications disappeared; borescope inspection showed the bore to be clean. The turbine and generator rotors were found to be entirely satisfactory so were returned to service.

In considering the static failure of a sound, ductile material the mean stress acting over a diametral cross section (σ_m in Fig. 15) is a more realistic criterion than the peak stress. In the steel rotor test reported in Appendix 2 failure took place when the mean stress reached the tensile strength of the material. Bursting tests of disks reported by Robinson (11) and by Holms and associates (12) showed that failure occurred when mean stress reached a value which varied from yield strength to tensile strength of material. In the case of the 100,000-kw turbine-generator cited previously the mean stress at 50 per cent overspeed is given in Table 3.

TABLE 3 MEAN STRESS AT OVERSPEED

	LP turbine	Generator
Mean stress	55000	51000
Per cent of tensile strength	53	45
Per cent of yield strength	65	57

On this basis it appears likely that the rotors under discussion possessed considerable reserve strength even at 50 per cent overspeed.

Some mention should be made of transition temperature. This is a broad subject and has received wide attention in connection with the ship-fracture problem (13, 14). Briefly, the general concept is as follows: Impact tests are made as a function of temperature. The resultant data curve or band, Fig. 16, has a region to the right of high values (ductile failure), a region to the left of low values (brittle failure), and a transition region. It has been found that cracks in structures propagate readily at temperatures to the left of the transition region.

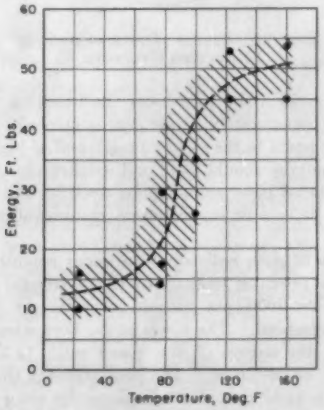

FIG. 16 CHARPY V-NOTCH IMPACT VALUES VERSUS TEMPERATURE FOR LOW C STEEL AND IN ROTOR MODELS

In many instances the band is a very flat S which makes it difficult to pin point a transition range or temperature. A number of definitions of transition temperature have been proposed, such as, temperature corresponding to (*a*) 15 ft-lb Charpy V-value, (*b*) mid-point of Charpy V-values, (*c*) fracture area half fibrous and half crystalline in appearance. Regardless of definition, it can be said that it is desirable to have available for use in critical applications, materials in which the transition region is displaced to the left with respect to the lowest temperature of the stressed metal. Since this is a relative matter the temperature of the bore region under stressed conditions should be considered in this connection.

It should be pointed out that if one could be certain of complete absence of high stress concentrations (primarily flaws of unfavorable shape and orientation) then transition temperature would not be an important factor in this application. As pointed out in the early part of the paper, every effort is made to detect harmful flaws and either to remove these or not use the rotor. It is our belief that as an added factor of safety concerted efforts should also be made to provide large forgings with lower transition temperature.

In addition to defects, other factors which might conceivably affect rotor strength, such as segregation, residual stresses, thermal stresses, hydrogen content, etc., have been considered and are covered by the Chairman of the ASTM Task Force on Brittle Failure of Steel Forgings (18).

Fatigue Considerations. Because of the weight of the rotor there is at the rotor surface a bending stress which alternates

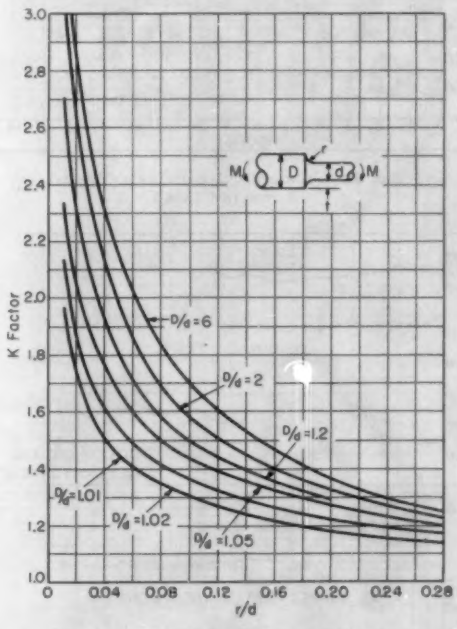

FIG. 17 K-FACTORS FOR SHOULDER FILLETS

sinusoidally one cycle per revolution. The bending stress is a maximum at the stepped-down portion of the rotor, where $\sigma_{max} = K_t \sigma_b$, where K_t is the stress-concentration factor due to a shoulder fillet (15) (Fig. 17). It will be seen that by judicious choice of the fillet radius, the K_t-factor can be kept relatively low. However, it turns out that the nominal bending stress σ_b is only of the order 1000–3000 psi; even if we multiply this by a K_t of 3 the maximum stress is so low that failure from this source is not to be expected in sound material and has not to our knowledge been experienced. However, if there are external bending moments (misalignment is an example of a possible source of bending) then it is possible to experience larger stresses than those due to the rotor weight. Two examples of failure due to

FIG. 18 FATIGUE CRACK DUE TO MISALIGNMENT
(Generator solid coupling 8-in. shaft diameter.)

FIG. 19 SAME SHAFT AS FIG. 18, OPENED BY CUTTING APART

FIG. 20 FATIGUE CRACK DUE TO MISALIGNMENT (TURBINE ROTOR) CRACK HAS PENETRATED HALFWAY THROUGH 9-IN-DIAM SECTION

FIG. 21 SAME ROTOR AS FIG. 20, OPENED BY CUTTING APART

severe misalignment are shown in Figs. 18 to 21. Possible bending-moment sources which should be kept in mind are:

1 Failure or malfunctioning of supporting parts.

2 Excessive pipe or condenser reactions which can be controlled by proper design or erection.

3 Differential thermal expansion of supporting structure.

4 Uneven foundation settlement.

It is often desirable to determine the amount of misalignment which will cause failure to a given machine. Bending moments at critical points due to misalignment of any particular journal are readily determined. Effect of steady torsional stress on fatigue strength is known. Small specimen fatigue strength of a given material is usually known or may be established readily. However, it is still difficult to determine just what amount of alternating stress the shaft will take.

Two shaft failures where the amount of misalignment was afterward determined give important information on the subject (Table 4).

If we divide σ_{fs} which is the endurance limit adjusted for steady torque by σ_b, which is the nominal alternating bending stress determined from known misalignments, we obtain the ratio given in the last column of Table 4. This ratio combines several factors: Stress concentration, plate bending of coupling flange, surface roughness, and possible size effect. Some work is under way to attempt to separate and evaluate these factors. For example, fatigue tests are being made on shafts up to 9 in. diam with and without notches. These shafts are made of material generally used in large turbine rotors.

A cyclic variation of another type is the O-$\sigma_{t\ max}$ variation (Fig. 15) due to starting and stopping. In a base-load machine the number of stops and starts is small, but a peak-load machine may have two such cycles per day, approximately 700 per year,

TABLE 4 DATA FROM SHAFT FAILURES

	Case material	Shaft diam	Steady torque	Alternating bending(σ_b)	Endurance limit small specimen, psi	Endurance limit adjusted for steady torque (σ_{fs}), psi	σ_{fs}/σ_b
A	Nickel steel.....	8.25	2500	8000	45000	42000	5.25
B	Nickel-chrome-moly	9.00	4500	9000	56000	50400	5.60

7000 in ten years. One also should take account of periodic test runs to 10 per cent overspeed. If we consider a bore element and no defects in the material, calculations (15) for a rotor stressed to 50–60 per cent of the yield strength indicate that it is likely that an unlimited number of stops and starts could be made without fatigue failure. If we consider the effect of a small round hole or an axially aligned ellipsoidal cavity (inclusion shape), $K_t = 3$, at the bore region, a rough estimate (16) of fatigue life is approximately 150,000 cycles or 200 years at two cycles per day.[8] This means that fatigue failure of the type described requires defects which are either cracks of some depth or are in effect thin plate-shaped ellipsoids oriented radially. In recent years attention has been focused on detecting these particular kinds of defects. It is of prime importance to emphasize the shape and orientation of defects. The size and number are also important, but perhaps to a somewhat lesser degree.

Model Tests

In another paper (4) the failure of Ridgeland No. 4 LP turbine rotor is discussed. The Nos. 2 and 4 LP units initially installed at Ridgeland Station were of essentially the same rotor design, namely, enlarged central portion and reduced end sections carrying shrunk-on disks. Because of this similarity the authors were particularly interested in the No. 4 rotor failure (4) and an intensive investigation of its cause was undertaken by the Research Laboratories. The first report regarding Ridgeland No. 4 was that failure was due to fatigue at the fillet at the juncture of the central and end portions of the rotor. Since complete fracture of the type experienced would not be expected with a relatively shallow and nearly transverse fatigue crack, it was thought that by considering various sequences of failure and comparing these with the main fracture characteristics a decisive answer as to the source might be deduced. Such an analysis was made (Appendix 1) and led to the definite conclusion that initial failure occurred in the bore region, not at the fillet.

It was decided to check this by means of a spin test to destruction of a brittle rotor model (cast iron). This is not to imply that turbine-generator rotors are made of cast iron or anything approaching such material but rather was a choice to insure failure in the test rig available and also was a choice influenced by the absence of gross deformation in the prototype failure. The spin-test apparatus has been discussed previously (17). The fractured cast-iron model (Fig. 22) duplicated the main features of the prototype failure remarkably well (Appendix 2). Additional tests (Appendix 2) including a recent test of a steel rotor (Fig. 23) have added further confirmation regarding fracture characteristics.

The theory as given in Appendix 1 has been deduced independently by the manufacturer, but it is our understanding that the fatigue theory is still being advocated by other interested groups. It is obviously important to resolve this and it is perhaps of some significance, as noted, that independent investigations by turbine builders have resulted in essentially the same conclusions, namely, initial failure at the bore region.

The steel-rotor model did not fail until the mean stress reached the tensile strength of the material, which may be regarded as a par value for large rotors if all factors introduced by size are eliminated or controlled. In this connection it is interesting to note that the maximum mean stress in a typical turbine-generator at operating speed is only about $^1/_4$ of the tensile strength and even at 20 per cent overspeed is only about $^1/_3$ of the tensile strength. Or to put this in another way, the condition of mean stress equal to tensile strength corresponds to about 100 per cent overspeed.

[8] This does not mean that gross inclusions are acceptable. As previously discussed, the "overspeed" strength could be affected in a material of high transition temperature.

Fig. 22 Fractured Cast-Iron Rotor Model No. 1

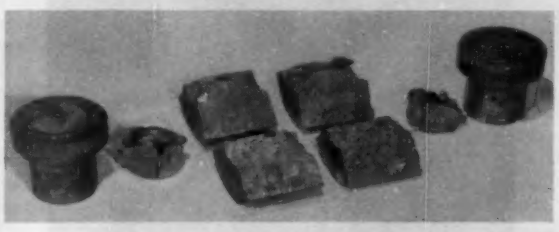

Fig. 23 Fractured Steel Rotor Model No. 7

Summary

The materials used for turbine and generator forgings have been described, together with precautions taken with respect to soundness and high quality. Although important progress has been made in recent years, it is recommended that the following directions be pursued: (*a*) Continue advances in ultrasonic detection and evaluation; (*b*) strive for lower transition temperature in rotor materials as an added margin of safety; (*c*) consider starting procedure which assures a bore temperature near that of normal operating conditions when the rotor is brought to speed. This would provide an added margin of safety and might involve a longer starting period for a turbine after a prolonged shutdown, or preheating of a generator rotor. In this connection it should be mentioned that it is our belief, based on all available evidence, that a sound ductile rotor, free of severe stress concentrations, possesses a large margin of safety.

Some tests of cast-iron and steel model rotors have been described. Tests of model cast-iron rotors gave results in agreement with a theory regarding a mode and sequence of failure at Ridgeland. The steel model did not fail until the mean stress reached the tensile strength. It should be noted that the mean stress in a typical turbine-generator rotor is only about $^1/_3$ of the tensile strength at 20 per cent overspeed. Differences, other than defects, which can occur in large rotors as compared to model rotors, and which might conceivably affect the strength have been studied and should continue to receive careful consideration. Some of these factors have been mentioned in the foregoing.

An instance is cited wherein a 100,000-kw turbine-generator was accidentally overspeeded 50 per cent without failure; at this overspeed the mean stress was about $^1/_2$ of the tensile strength.

A discussion is given of turbine-rotor stability since in some instances failure to meet rigid requirements in this connection have resulted in rejection of a forging.

The fatigue problem is discussed and the role of careful alignment emphasized. Since starting and stopping may be regarded as cycling, this is discussed as a fatigue problem and the indications based on calculations are that only a very severe defect, unfavorably oriented, would be expected to behave as a source of a fatigue crack. Such defects are quite rare and readily detected by modern methods; under no circumstances, as prevously indicated, would defects of this type be acceptable.

All aspects of turbine and generator rotors—material, inspec-

tion methods, design—are being continuously reviewed, to assure that reliable rotors will be reproduced to satisfy the growing requirements of the electric-power industry.

Acknowledgments

Reporting on such a large subject as turbine and generator reactors must necessarily be a team effort. The following have contributed notably, although many others also have been helpful: J. R. Carlson, Engineering Manager, C. B. Campbell, Chief Engineer, and F. C. Eaton, of the Steam Division; A. M. Harrison, Engineering Manager, and R. A. Baudry of the Transportation and Generator Division; A. C. Hagg and A. M. Wahl of the Research Laboratories; and E. T. Hughes of the Materials Engineering Department, Westinghouse Electric Corporation.

BIBLIOGRAPHY

1 "Man, Metals and Power," by N. L. Mochel, Gillett Memorial Lecture, Proceedings ASTM, vol. 52, 1952, p. 691.

2 "Steels for Turbine Rotor Forgings and Their Heat Treatment," by N. L. Mochel, *Metals and Alloys*, vol. 8, 1937, p. 265.

3 "High-Speed Generator Forgings," by C. M. Laffoon, *Westinghouse Engineer*, vol. 15, May, 1955, p. 94.

4 "Investigation of Large Steam-Turbine Spindle Failure," by H. D. Emmert, published in this issue, pp. 1547–1565.

5 "Military Specification—Steel Forgings for Steam Turbine Rotors," Mil-S-860A (Ships), March 28, 1955.

6 "Standard Specification for Carbon and Alloy Steel Forgings for Turbine Generator Rotors and Shafts," ASTM Designation A-292-54.

7 "Tentative Specification for Carbon and Steel Forgings for Turbine Rotors and Shafts," ASTM Designation A-293-52T.

8 "Standard Specifications for Carbon and Alloy Steel Forgings for Turbine Bucket Wheels," ASTM Designation A-294-54.

9 "The Reversible Bending of Turbine Shafts With Temperature," by A. Barker and F. W. Jones, paper presented before The Institution of Mechanical Engineers, London, England, May 6, 1955.

10 "The Balancing of Large Turbine-Generator Rotors," by C. M. Laffoon, A. C. Hagg, C. H. Janthey, and P. R. Heller, Trans. AIEE, vol. 70, part 3, 1951, p. 593.

11 "Bursting Tests of Steam-Turbine Disk Wheels," by Ernest L. Robinson, Trans. ASME, vol. 66, 1944, pp. 373–386.

12 "Effect of Strength and Ductility on Burst Characteristics of Rotating Disks," by A. G. Holms and J. E. Jenkins, NACA TN 1667, 1948.

"Correlation of Tensile Strength, Tensile Ductility and Notch Strength With the Strength of Rotating Disks of Several Designs in the Range of Low and Intermediate Ductility," by A. G. Holms and A. J. Repko, NACA TN 2791, 1952.

13 "Investigation of Fractured Steel Plates Removed From Welded Ships," by M. L. Williams, Ship Structure Committee Report, Series No. NBS-3, June, 1951.

14 "Evaluation of the Significance of Charpy Tests," by W. S. Pellini, ASTM, Symposium on Metallic Materials at Low Temperatures, Atlantic City, N. J., June 23–30, 1953.

"Crack-Starter Tests of Ship Fracture and Project Steels," by P. P. Puzak, M. E. Schuster, and W. S. Pellini, AWS, Chicago, Ill., November 1–5, 1954.

15 "Stress Concentration Design Factors," by R. E. Peterson, John Wiley & Sons, Inc., New York, N. Y., 1953.

16 "Fatigue and Fracture of Metals," by W. M. Murray, John Wiley & Sons, Inc., New York, N. Y., 1952.

17 "A High-Speed, High-Temperature Precision Test Machine for Gas Turbine Disk Research," by A. C. Hagg, B. Cametti, and G. O. Sankey, Proceedings SESA, vol. 8, no. 2, 1951, p. 17.

18 "The Work of the ASTM Task Forces on Hydrogen and on Brittle Fracture of Large Forgings," by A. O. Schaefer, published in this issue, pp. 1623–1626.

Appendix 1

Proposed Theory of Failure Sequence of Bored Rotor With Enlarged Central Portion

Step 1. Referring to Fig. 24, it is proposed that failure starts at the bore and proceeds in an axial plane to the outside of the rotor.

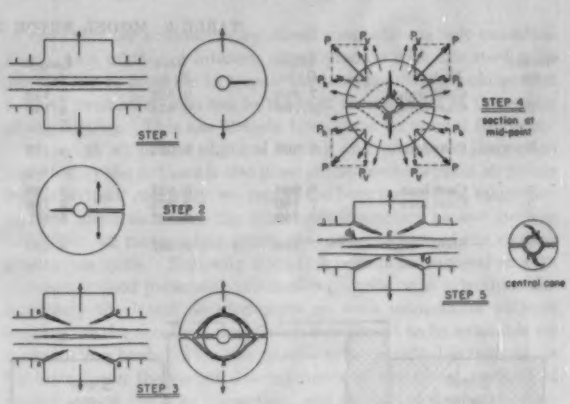

Fig. 24 Failure Sequence of Rotor

Step 2. As a result of the centrifugal force (CF) components indicated, the "C ring" splits into two halves, as shown in Fig. 24. These halves, however, are not yet free at the ends, since the axial cracks stop under the disks, which do not fail.

Step 3. Large CF components are exerted on the two halves of the split central portion. This results in tension at fillet regions *a* (Fig. 24—step 3) and failure starts at these four places. The cracks start in an inclined direction in accordance with the stress field.

Step 4. The two halves which are rotating are acted on by CF forces having components P_h which cause cracks to start at *b*, resulting in splitting into a total of four segments (Fig. 24—step 4). Step 4 begins before the conical cracks of step 3 reach the bore.

Step 5. The central portion is acted on by radial forces and moments which cause axial splitting failures as at *c* and cantilever failures as at *d*. The final primary result is therefore separation into four outer quadrant pieces and eight inner conical quadrants (4 at each end). Secondary failures can be expected as a consequence of impacts involved.[9]

The "steps" would be expected to occur in microseconds and, as indicated, would overlap to some extent. To an observer it would seem like a single "explosive" failure.

Appendix 2

Spin Tests of Model Rotors

Model dimensions and test data are shown in Table 5 (see Fig. 25 for notations). The tests were run at the Westinghouse Research Laboratories by A. C. Hagg, G. O. Sankey, and J. H. Bitzer.

Cast Iron. Cast iron of tensile strength 28,000 psi was used for models Nos. 1–5. Rotor No. 1 was a scale model of the essential features of Ridgeland No. 4 LP turbine rotor. The fracture segments (Fig. 22) were of essentially similar geometry as the prototype. Rotor No. 2 (Fig. 26) was made initially split axially (see Appendix 1—step 2) and one of the fillet failures (presumed to be initial failure in this test) was the same as the prototype. It could not be expected that all details would be checked in this instance since with the initial split the failure speed (Table 5) was much lower. Model No. 3 (Fig. 27) had a sharp V-groove turned in the fillet to cause failure to start there and as can be seen the fracture is entirely different. Model No. 4 differed from Model No. 1 only in some minor details and again duplicated the main features of the prototype failure. Model No. 5 was made some-

[9] In the model tests (Appendix 2) secondary damage was minimized by intercepting the pieces in a sandbag barrier.

TABLE 5 MODEL ROTOR DIMENSIONS AND TEST DATA

Rotor no.	Material	Diam D, in.	Bore B, in.	Length L, in.	Fillet radius R, in.	Date of test	Speed at fracture, rpm	Test temp, deg F	Remarks
1	Cast iron	7.250	0.625	4.140	0.0625	2/10/55	24500	80–90	
2	Cast iron	6.750	0.625	4.140	0.078	2/16/55	11400	80–90	Rotor body initially split in longitudinal plane
3	Cast iron	6.900	0.625	4.140	Sharp "Vee" 1/2 in. deep axially	2/22/55	18500	80–90	
4	Cast iron	6.900	0.625	4.140	0.078	3/4/55	26250	80–90	
5	Cast iron	7.180	0.875	5.780	0.131	9/16/55		80–90	
6	Steel	7.750	0.687	4.650	0.087	6/2/55	31150	80	No fracture, cracks in bore
7	Steel	7.750	0.687	4.650	0.087	8/25/55	31750	25	First run; no fracture, cracks in bore
						8/29/55	33205	20	Second run; fracture

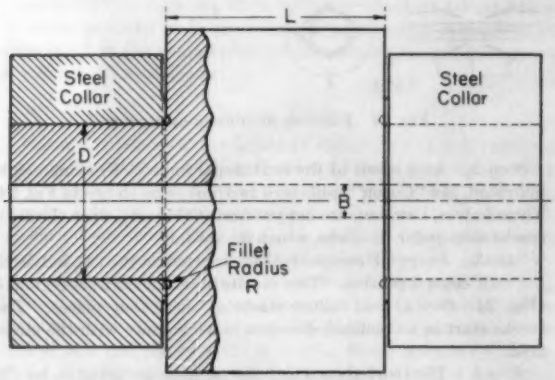

FIG. 25 TEST ROTOR

TABLE 6 SAE 1015 STEEL FOR MODELS NOS. 6 AND 7

Chemical analysis, per cent

C	Mn	Si	P	S	Fe
0.17	0.53	0.16	0.019	0.019	remainder

Tensile properties

Yield str, psi	Tensile str, psi	Elong, per cent	RA, per cent
28000	48000	14	21

what longer in the body portion, to correspond to certain existing designs, but again the failure characteristics were similar to Model No. 1.

Steel. Owing to speed limitation of the existing spin-test apparatus (17) a weak steel was selected for the initial test. Later on some tests will be made with rotor steel. Data concerning the SAE 1015 steel used in the tests reported in this paper are given in Table 6. Model No. 6 was taken up to 31,150 rpm (mean stress 42,500 psi) without failure. From the operation of the machine there was evidence of something happening to the rotor (thought to be discontinuous yielding) and since the stated speed was thought to be near the capacity of the machine, it was shut down. The bore of the model showed evidence of considerable plastic deformation (bore enlarged about 9 per cent at midsection) and some axial tears were present. It was thought the reason that the tears did not propagate was that the transition temperature of the material was favorable. To pursue this, impact tests were made and a transition-temperature curve was obtained (Fig. 16). Model No. 7 was a duplicate of No. 6, but the test was run with a temperature of 25 F at the bore. This model was run to about the same speed (31,750 rpm) and after shutdown showed plastic deformation and had tears in the bore surface. In view of the low temperature it would have been expected that the tears would propagate. It was decided to rerun again (at low temperature, 20 F) to the full capacity of the machine and failure

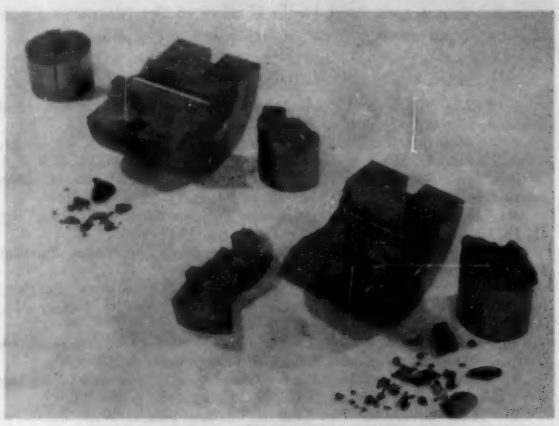

FIG. 26 FRACTURED CAST-IRON ROTOR MODEL NO. 2

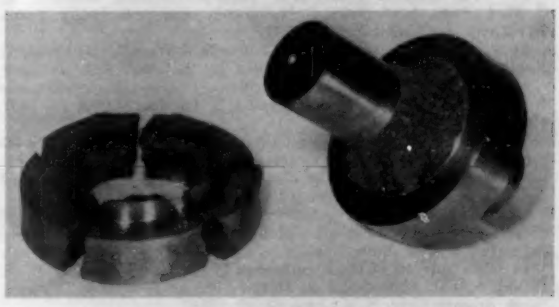

FIG. 27 FRACTURED CAST-IRON ROTOR MODEL NO. 3

was obtained at 33,205 rpm. The mean stress was 48,400 psi which agrees closely with the tensile strength reported in Table 6, namely, 48,000 psi. This, as has been previously indicated, is about what one might expect in sound material. The tears apparently behave quite differently from cracks present in a material before stressing. The ends of the tears in section are rather rounded and show evidence of plastic flow. The following additional tests are scheduled:

Model No. 8—same as Model No. 6—Test to destruction at 20 F (except with sharp stress raiser in bore)
Model No. 9—same as Model No. 8—Test to destruction at room temperature
Model No. 10—same as Model No. 6—Test to destruction at room temperature

Discussion

J. M. Lessells.[10] It has been very enlightening and a very rare experience to read the six papers which were presented at the two sessions of the Annual Meeting on "material failures of large turbine and generator rotors." Engineering knowledge will be advanced by the publication of such histories and it is surely fitting that on the occasion of the Diamond Jubilee Meeting of the ASME such information be given the engineering profession. It is true that failures of these large units are rare which continues to justify the late H. G. Wells' expressed belief that "the ability of man to handle large masses of metal successfully has been one of his greatest achievements since he stepped from the cave." The companies which have come forward to present such information on their failures, usually buried in their files, deserve the thanks of the engineering profession, and it is to be hoped that this practice will be continued on some future occasion.

Each of the papers tells an important story. It is only possible to refer to a few of the many points which are suggested.

The value of model testing in providing useful design data, as shown by Mr. Peterson's contribution to two of the papers[11, 12] and as discussed in a previous paper,[13] cannot be overemphasized.

Referring to the matter of instability of large rotors, since this has recently been receiving attention in England, possibly reference should be made to the paper by F. Dollin[14] of C. A. Parsons & Co. Ltd. and the paper by A. Barker and F. W. Jones[15] of Brown-Firth Research Laboratories. In these papers the influence of different metallurgical structures arising from faulty heat-treatment on the coefficient of expansion and hence on the dynamic characteristics of rotors is discussed.

A. W. Rankin[16] and C. D. Moriarty.[17] The general review presented by the authors of the developments which have taken place in the manufacture of turbine and generator rotors is of interest to all concerned in that it is representative of the efforts of all the large turbine and generator manufacturers to maintain the utmost in the reliability of these components. The practices used by the writers' company, however, differ in some respects from those outlined by the authors. For instance, we have utilized the wheel construction of Fig. 9 of the paper for all 1800-rpm low-pressure rotors for many years, and with a generally lighter wheel construction because of the lower number of stages involved. A similar construction, although with the wheels integral with the shaft, is used for all 3600-rpm high-pressure and low-pressure turbine rotors, and this construction enables the physical properties to be determined from radially trepanned bars taken from between the integral wheels, at which point the properties are more truly representative of the rotor forging itself. In addition, machining of the integral-wheel construction exposes much more of the rotor for evaluation by direct magnetic-particle examination. As a matter of interest, developments with the steel mills are already in progress to trepan the bore inspection hole so that a direct evaluation also can be made of the material at the center of the forging. This has already been done on several forgings.

Although all of the physical testing and ultrasonic inspection reported by the authors is also done at the vendor's plant on rotors for the writers' company, we repeat the bore inspection, magnetic-particle inspection, and the ultrasonic inspection at our turbine factory on all turbine and generator rotors as part of the routine production cycle. Not only does this permit an inspection with our own trained personnel, but it also permits us to introduce immediately the latest developments on such inspections without waiting for the necessary inspection equipment to be available on a production basis. This has proved to be a valuable feature, as for instance in the recent developments of the direct method of magnetization for bore inspection, and the use of double crystals for ultrasonic inspection.

The matter of identification of the causes of ultrasonic reflections from discontinuities within the forging body is of deep concern to all manufacturers and users of these rotors, and in this respect the writers cannot agree with the general conclusions presented by the authors. The authors have not furnished any direct evidence to substantiate these conclusions, and it is doubtful if such evidence can be obtained to the degree required for the evaluation of forging soundness on the generalized basis propounded by the authors. Although any single forging might be trepanned or destructively examined to substantiate any particular conclusion, such evidence cannot be used to evaluate soundness on forgings with a similar ultrasonic pattern until a quantitative relation is available between reflection characteristics and defect identification.

It is doubtful if this relation will ever be obtained satisfactorily when relying on a "pip" on an A-screen presentation as now used. Radar using the A-screen method is incapable of giving more information on a detected airplane than its distance from the detector and the speed at which it is moving.

Attempts to correlate defects by their depth location in a rotor forging are predicated on a metallurgical expectancy. The fact that cracks have been found at all angles and at all depths in large rotor forgings is sufficient proof of the existence of the unexpected—and it is the unexpected that the writers are concerned about.

A survey of actual findings on large rotor forgings reveals numerous cases wherein positive metallurgical identification did not agree with the expected results predicted in the guides listed by the authors. Five of these cases in the writers' experience are illustrated, each in relation to one of the authors' guides (Figs. 28–32 of this discussion).

The authors place considerable weight on the decrease in bore reflection when defects are giving ultrasonic reflections. This can be very misleading. In the average large rotor forging the effective circumferential width of the convex bore surface that reflects sound back to the crystals is of the order of $^1/_{16}$ in., while the effective width of a 1-mc sound beam in the region of the bore is of the order of 10 in. Maximum reflecting ability of a defect within the 10-in-wide beam is not likely to coincide with its maximum absorption ability when passing in front of the $^1/_{16}$-in-wide bore reflecting surface. In fact many of the defects that were trepanned had maximum reflecting magnitude up to 90-deg radial displacement from the position where they created maximum loss of bore reflection. There even have been instances wherein a maximum magnitude from a defect has been accompanied by a simultaneous increase in bore reflection. The loss of bore reflection has its greatest significance in the absence of definite defect reflections.

---

[10] President, Lessells and Associates Inc., Boston, Mass. Fellow and Hon. Mem. ASME.

[11] "Investigation of Large Steam-Turbine Spindle Failure," by H. D. Emmert, published in this issue, pp. 1547–1566.

[12] "Large Rotor Forgings for Turbines and Generators," by N. L. Mochel, R. E. Peterson, J. D. Conrad, and D. W. Gunther.

[13] "Model Testing as Applied to Strength of Materials," by R. E. Peterson, Trans. ASME, vol. 55, 1933, paper APM—55-11.

[14] "Factors Influencing the Continuing Development of the Steam Turbine," by F. Dollin, Nineteenth Parsons Memorial Lecture, *The Chartered Mechanical Engineer, Jr., of The Institution of Mechanical Engineers*, vol. 1, no. 9, Nov., 1954, p. 429.

[15] "The Reversible Bending of Turbine Shafts With Temperature," by A. Barker and F. W. Jones, *The Chartered Mechanical Engineer, Jr., of The Institution of Mechanical Engineers*, vol. 2, April, 1955, p. 192.

[16] Supervisor, Turbine Structural Engineering, General Electric Company, Schenectady, N. Y. Mem. ASME.

[17] Supervisor, General Electric Company, Schenectady, N. Y. Mem. ASME.

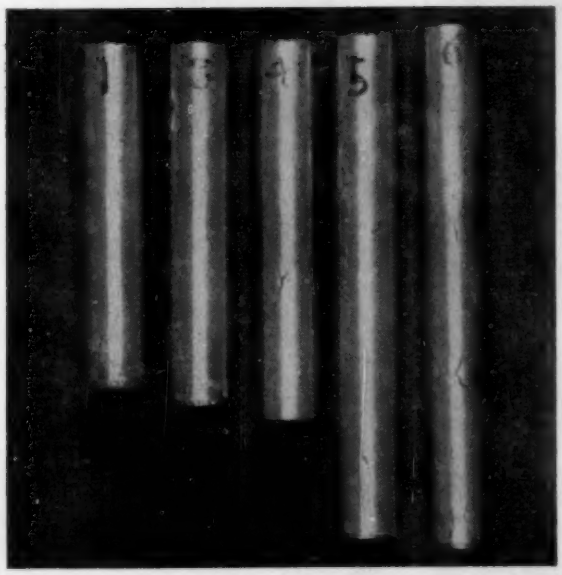

FIG. 28 TREPANNING REVEALED INCLUSIONS INSTEAD OF PREDICTED THERMAL RUPTURES OF GUIDE NO. 1

FIG. 29 TREPANNING REVEALED THERMAL RUPTURES INSTEAD OF PREDICTED SEGREGATION OF GUIDE NO. 2

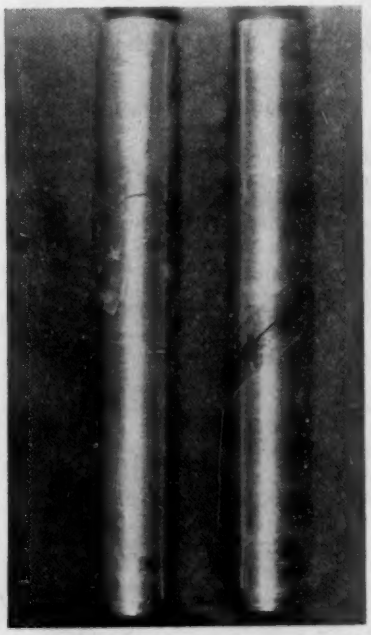

FIG. 31 TREPANNING REVEALED A CRACK 8 IN. FROM THE OUTSIDE SURFACE INSTEAD OF PREDICTED INTERGRANULAR SEGREGATION OF INCLUSIONS OF GUIDE NO. 4

FIG. 30 TREPANNING REVEALED THERMAL RUPTURES INSTEAD OF PREDICTED POROSITY OR INCLUSIONS OF GUIDE NO. 3

FIG. 32 TREPANNING REVEALED A THERMAL RUPTURE INSTEAD OF PREDICTED PIPE OR SHRINKAGE OF GUIDE NO. 5

The authors state that they trepan for positive metallurgical identification "in some cases." The use of number and magnitude lines is one way of defining when trepanning for positive metallurgical identification is advisable, even if it is only to confirm the predicted harmless nature of the defect.

The grooves on the generator-pole faces as described in Fig. 10 of the paper represent an interesting and valuable addition to ultrasonic inspection techniques. In the writers' opinions, however, a more thorough inspection, and one applicable to generators already in service, is the use of a wide-beam 1-megacycle crystal directly over the pole-face grooving. The 1-megacycle wide beam will not only pick up reflections from all defects, as they will be favorably oriented with respect to the wide beam at some point in the circumferential movement of the crystal over the pole face, but, in addition, will continuously furnish a bore reflection for quantitative evaluation of the defect reflection. As a matter of interest, this system has already been used successfully on a slotted rotor in which defects were known to be present; the defects were revealed and by using a 5-megacycle pin-pointing

beam, four out of five defects were successfully trepanned for further identification.

Authors' Closure

The paper mentions a few uncompleted tests. These have now been completed with the results given in Table 7 of this closure.

TABLE 7 RESULTS OF ADDITIONAL TESTS

Rotor No.	Material	Rotor dimensions	Speed at fracture rpm	Test temp, deg F	Remarks
8	Same as No. 7	Same as No. 7	33025	15	With 45-deg V-groove 1/8 in. deep, approx-1 mil radius
9	Alloy steel	Same as No. 7	42850	17	Same but 0.08-in-deep V-groove

Rotor No. 8 contained a sharp V-groove in the bore and was tested at 15 F. Even under these severe conditions, the average stress at bursting was approximately equal to the tensile strength of the material.

Rotor No. 9 was made of alloy steel of the following composition and properties: 0.25 C, 0.58 Mn, 2.75 Ni, 0.64 Mo, 0.09 V, 0.11 Cr, 0.12 Si, 0.02 P, 0.012 S. Yield strength, 76,000 psi; tensile strength, 95,000 psi; 24 per cent elongation; 63 per cent reduction in area.

In this instance the average stress at failure was 83,000 psi or about 87 per cent of the tensile strength of the alloy steel.

The authors appreciate the comments and the added references by Mr. J. M. Lessells.

The discussion by Messrs. Rankin and Moriarty is much appreciated. They make reference to the fact that magnetic particle inspection and ultrasonic inspection are repeated at the turbine factory as a matter of routine. This was brought out in the paper as being standard practice at the authors' plants as well.

Every manufacturer of equipment of this kind is very anxious to learn all that he can about the internal conditions of the forging he uses. For this reason, ultrasonic testing is used to develop information concerning the interior condition of the forging but is certainly not relied upon as an absolute and final test. The ultrasonic test provides only "indications" of internal conditions, not specific information concerning specific defects. Operator skill and ability are important in evaluating these indications at the present state of the art.

For these reasons, there are differences of fundamental philosophy concerning the ultrasonic test. As stated in this paper, the authors consider each forging to be an individual case and are primarily concerned with the locations and identification of discontinuities rather than only their number and magnitudes. We believe it is important that all possible discontinuities be located so we use the highest practical operating frequency for the first examination. Our forgings, therefore, are initially tested at a frequency of $2^1/_4$ mc, which is more sensitive than 1 mc and provides better definition of discontinuities. All indications of discontinuities are further checked at a testing frequency of 1 mc and sometimes 5 mc for additional information.

Messrs. Rankin and Moriarty seem to have misunderstood our method of interpreting results. Loss of back reflection and depth of discontinuities are important only in so far as they help to identify the discontinuities. The examples of metallurgical interpretation of ultrasonic indications listed in the paper were not meant to be "guides" but were merely illustrations of typical findings. The fact that the defects shown in Figs. 28–32 of the discussion were misinterpreted is not surprising when one considers that the ultrasonic testing of these forgings was performed at a frequency of 1 mc. The authors have contended in this paper and elsewhere that accurate interpretation of ultrasonic indications requires an over-all test at a frequency of at least $2^1/_4$ mc, that all discontinuities be investigated with at least one additional testing frequency, and that height of back reflection be taken into consideration.

The axial crescent-shaped-groove technique for testing finish-machined rotors in the field has proved to be very satisfactory and gives wide coverage of a $2^1/_4$-mc ultrasonic beam. The beam can be directed to scan the surface of the bore, to pick up the edges of each slot, and to test the metal not only under the pole face but under the slots as well. We have tried holding a 1-mc searching unit directly over the pole-face grooves and have found this method of inspection to be very limited and insensitive.

Acceptance Guides for Ultrasonic Inspection of Large Rotor Forgings

By A. W. RANKIN[1] and C. D. MORIARTY,[2] SCHENECTADY, N. Y.

This paper discusses the problem of establishing criteria, based on ultrasonic examination, for the acceptance or rejection of large rotor forgings. From the results of trepanning and cutting up a number of such forgings, guide lines are established for determining when trepanning should be used for identification of the ultrasonic discontinuities.

Introduction

EARLY in 1950, the authors, together with two of their colleagues, presented a paper[3] on the ultrasonic inspection of large turbine- and generator-rotor forgings. In that paper, it was pointed out that the ultrasonic method of inspection furnished an unequalled tool for the detection of subsurface discontinuities in heavy forgings, but that this tool had the disadvantage of being unable to identify conclusively the discontinuity as being harmless or potentially harmful. Eight years of experience in the ultrasonic testing of large rotor forgings have verified conclusively the original statements regarding the ability of ultrasonic inspection to detect subsurface discontinuities, but, while a number of improvements have been made in the techniques of ultrasonic inspection during this period, there have been no basic developments by which these subsurface discontinuities could be identified conclusively as harmless or potentially harmful short of destructive, or semidestructive, examination.

The most commonly suggested method to circumvent the inability of ultrasonic inspection to identify the causes of ultrasonic reflections is to reject all rotor forgings on which reflections of any magnitude whatsoever have been found but cannot be identified. This policy would be impracticable, however, since, based on the authors' experience with a very large number of rotor forgings, ultrasonic indications can be found on almost any large rotor forging if the sensitivity of the ultrasonic inspection equipment is sufficiently high. In addition, such a policy, which is counter to the established and accepted methods of inspection and acceptance on such equally important parts such as castings and weldments, would result in the rejection of a large number of forgings containing the harmless nonmetallic inclusions so difficult to eliminate in the pouring of the large ingots needed for these forgings. Similar to the casting and weldment acceptance standards, guides for the acceptance of rotor forgings containing ultrasonic reflections which cannot be identified short of destructive or semidestructive examination should be based on the experience derived by such examinations of rotors in the past.

Studies along these lines have been in progress for some time in the Large Steam Turbine-Generator Department of the authors' company, and these studies have culminated in a set of acceptance guides which appears both practical and conservative. Experience with these guides is now sufficient that the time seems appropriate to present to the industry not only these guides but also the details of the destructive and semidestructive examinations on which they are based. It should be noted that these guides have been established on the basis of ultrasonic inspection of 1500 large turbine and generator rotors reinforced by frequent destructive and semidestructive examination. These guides are applicable only to those rotors, containing a limited number of ultrasonic defect reflections, on which no other method has revealed harmful defects; where other inspection means have demonstrated that a single reflection is caused by cracking, the forging is to be rejected.

Interpretation Techniques

Before proceeding to the establishment of acceptance guides based on number and magnitude of ultrasonic reflections, the advantages and limitations of the available identification means deserve clarification; specifically, the magnetic-particle examination of the bore and outer forging surfaces and trepanning of some of the discontinuities. If the discontinuities are all located close to the bore or external surfaces, magnetic-particle inspection can be used to identify those which break through to the surface. In most cases, however, the discontinuities are located an appreciable distance from the bore and external surfaces, in this case, a magnetic-particle examination can give, at best, only circumstantial evidence regarding the identity of the subsurface discontinuities. If nothing is revealed by the magnetic-particle examinations—neither cracks, open metal, slag, inclusions, nor porosity—then not even circumstantial evidence has been obtained to aid in the identification of the subsurface discontinuities. If, however, the magnetic-particle examination has disclosed some further information, as for instance slag and inclusions in the bore surface, this may be interpreted as circumstantial evidence that the subsurface discontinuities are likewise slag and nonmetallic inclusions. It should be emphasized that, although in most cases this conclusion is valid, destructive examination of some forgings has proved that it is not always correct.

Identification by trepanning is also fraught with complications, and, to a lesser degree, sometimes furnishes only circumstantial evidence. If the discontinuity is located in a highly stressed region, then trepanning is itself a destructive examination because of the stress concentrations which will exist around the trepan hole. In this case, except for the specific information obtained by the trepanned specimen, trepanning is a waste of time and effort since, no matter what information is so obtained, the forging is not usable because of the location of the trepan hole. In addition, precise "pinpointing" of a deep-seated discontinuity is necessary if the trepanned specimen is to enclose the discontinuity. Several years ago, such pinpointing was not sufficiently accurate, and the trepanned specimen when removed was often found to have missed the discontinuity completely. Further de-

[1] Supervisor, Structural Engineering Unit, Steam Turbine Engineering, Large Steam Turbine-Generator Department, General Electric Company. Mem. ASME.

[2] Manager, Nondestructive Testing Unit, Materials and Processes Laboratory, Large Steam Turbine-Generator Department, General Electric Company. Mem. ASME.

[3] "Thermal Cracks in Turbine and Generator Rotor Forgings," by A. W. Rankin, C. J. Boyle, C. D. Moriarty, and B. R. Seguin, *Mechanical Engineering*, vol. 72, 1950, pp. 559–566.

Contributed by the Power Division and presented at a joint session of the Power and Metals Engineering Divisions at the Diamond Jubilee Annual Meeting, Chicago, Ill., November 13–18, 1955, of The American Society of Mechanical Engineers.

Note: Statements and opinions advanced in papers are to be understood as individual expressions of their authors and not those of the Society. Manuscript received at ASME Headquarters, October 5, 1955. Paper No. 55—A-194.

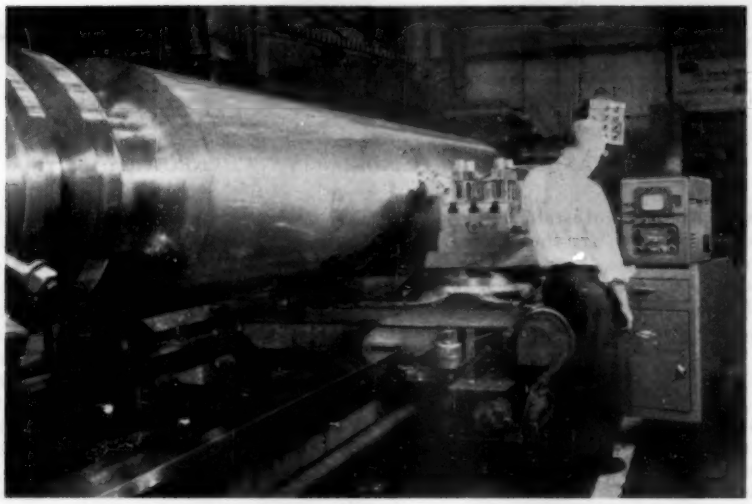

FIG. 1 ULTRASONIC INSPECTION OF GENERATOR-ROTOR FORGING
(Crystals are held in toolholder of lathe and moved along forging at about 1 in. per revolution while forging is rotated continuously at 3 to 4 rpm.)

velopments in ultrasonic inspection, however, have refined the pin-pointing techniques to the degree that, out of the last 59 trepanned specimens removed, 57 of them have enclosed the discontinuity being investigated.

Somewhat of a statistical analysis is also needed in trepanning identification. If a forging contains a large number of discontinuities, and the first trepanned specimen reveals nonmetallic inclusions, direct evidence for identification has been found for the trepanned specimen, but only circumstantial evidence is available for identification of the remaining reflections. Specifically, the question arises as to how many trepanned specimens from a single forging, all free of harmful defects, are necessary to establish a reasonable degree of assurance that all the ultrasonic reflections in that particular forging are caused by harmless defects. In addition, the question arises as to how many trepanned specimens may be removed from a forging without rendering the forging unacceptable on the basis of trepanned holes alone.

It is accordingly evident from the foregoing that trepanning, to some degree, is itself never completely conclusive. If any trepanned specimen reveals harmful or potentially harmful defects, the forging is immediately rejected, but where trepanning is not advisable because of stress considerations, or even where trepanning has revealed only harmless forging defects, some form of policy or guide is needed to determine if the forging is satisfactory for use or not.

ULTRASONIC INSPECTION TECHNIQUE AND NOMENCLATURE

Fundamental to the establishment of referee methods or operating guides is the standardization of techniques and nomenclature; this is not intended to stifle the development and introduction of improved techniques and nomenclature, but rather to establish a common basis for current discussions and interpretations.

All of the ultrasonic inspection results presented in this paper are based on a frequency of one megacycle using either the single-crystal or double-crystal reflection technique. One-megacycle frequency is used for the inspection of these large rotor forgings because it provides the widest beam divergence (for the detection of "traveling" defects discussed later) consistent with adequate sensitivity to detect defects with a minimum size of $^1/_8$ in. diam. It is a moot question as to whether 1.00 megacycle or 2.25 megacycles is more sensitive in disclosing particular forging defects; in the authors' experience the higher frequency has given lower sensitivity as often as it has improved the sensitivity. In particular, however, the narrow beam of 2.25-megacycle frequency reduces sensitivity to radial defects.

The single-crystal technique is the reflection method in most common use in this country although the double-crystal technique is somewhat easier to handle in routine ultrasonic inspection, and is superior in the inspection of small-diameter forgings since the initial pulse is eliminated. For most defects, however, the single-crystal method is superior in sensitivity, and is also superior in pinpointing defects for trepanning.

The most important common denominator in this survey of ultrasonic inspection of large rotor forgings was that all tests were made while the forgings were being rotated slowly in a lathe as shown in Fig. 1. Moving the ultrasonic crystal slowly along the entire length of the rotating forging at approximately 1 in. per revolution (ipr) assures complete inspection coverage of the entire forging.

The magnitude of the ultrasonic reflection from a defect (defect magnitude) is given in per cent of the reflection from the bore in a defect-free area. For instance, a "25 per cent defect" defines a defect whose reflection gives a pip on the oscilloscope screen which rises to a maximum of 25 per cent of that caused by the normal reflection from the bore surface; such a defect reflection is shown in Fig. 2. It should be noted that since only a small percentage of the beam is normally reflected from the convex surface of the bore, it is possible to have a defect of such size and/or orientation that the defect reflection is several hundred per cent of the normal bore reflection, even though the defect itself is much smaller than the bore. Changes in the bore reflection caused by the presence of the defect and its partial masking of the bore have not been considered of primary importance in this survey since the bore reflection also can vary depending on the attenuation constant, grain structure of the rotor material, and surface roughness. In addition, for those few cases in which no bore hole was present in the rotor, the defect has been defined

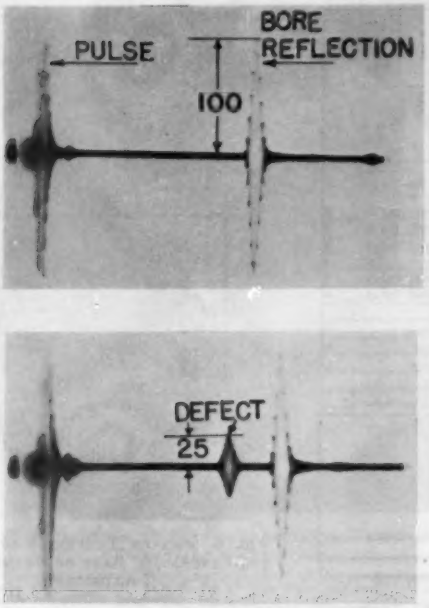

FIG. 2 ILLUSTRATION OF A "25 PER CENT DEFECT"
(Upper photograph shows reflection from bore in a sound portion of forging; lower photograph shows reflection from a defect as well as bore reflection. Reflection from defect in lower photograph is 25 per cent of bore reflection in upper photograph.)

with respect to the reflection from the diametrically opposite side of the forging in a defect-free area.

The number of ultrasonic defect reflections is counted and recorded with respect to the magnitude of the reflection, as, for instance, 40 defects at 10 per cent magnitude, 20 defects at 25 per cent magnitude, and so on. Where the number of defects runs into several hundred or more, a reasonably accurate estimate is made of the number.

In addition to recording the number and magnitude of the defect reflections, it is also necessary to note whether the indication on the screen rises to a maximum while staying in one spot relative to the distance from the bore reflection, or whether the indication travels to the right or left with respect to the bore reflection while varying in magnitude. The first type is termed a "stationary" indication, while the second type is termed a "traveling" indication. The stationary indication is easier to visualize, it is the most common type of pip observed in ultrasonic inspection, and would show up equally well whether the crystal is moving or the forging is rotating. A stationary indication implies that the defect is predominantly tangential, and no traveling of the pip is seen on the oscilloscope screen because the defect presents an adequate reflecting surface to the ultrasonic beam for only a short travel of the forging as shown in Fig. 3.

A traveling indication implies that the defect causing the reflection is predominantly radial, and the pip on the oscilloscope screen moves (or travels) from right to left with respect to the bore reflection as the defect-reflecting surface, during the rotation of the forging, moves toward the sound source; subsequently, the pip travels from left to right as the defect moves away from the sound source during further forging rotation. This is illustrated in Fig. 4, and the net effect on the oscilloscope screen is a pip that starts at the right of the screen, travels to the left while it first increases and then decreases in magnitude, and then reverses its direction and travels to the right while repeating the rise and fall

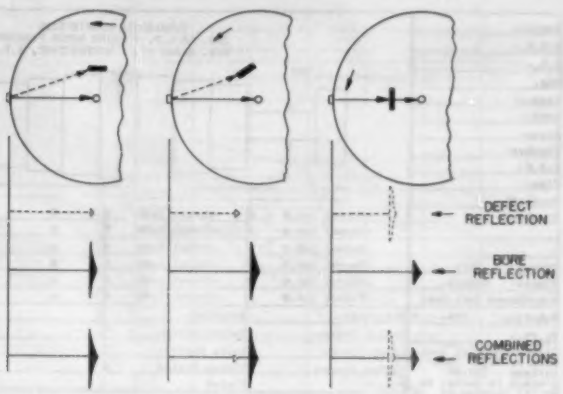

FIG. 3 SCHEMATIC ILLUSTRATION OF A STATIONARY INDICATION
(Note that defect is predominantly tangential and defect reflection on oscilloscope screen does not travel appreciably with respect to bore reflection as forging is rotated.)

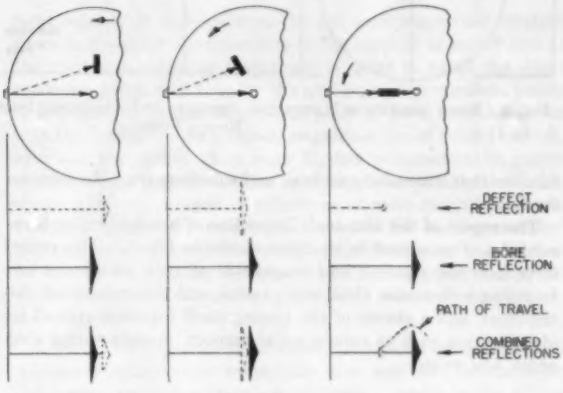

FIG. 4 SCHEMATIC ILLUSTRATION OF A TRAVELING INDICATION
(Note that defect is predominantly radial and defect reflection travels appreciably with respect to bore reflection as forging is rotated.)

in magnitude. The maximum magnitude reached by the traveling indication is the one reported in the inspection results.

If the defect causing a traveling indication had its most favorable orientation while passing through the strongest part of the sound beam, a much higher reflection magnitude could be obtained. An angular beam for scanning would result in increased magnitude from these radial defects, but at a sacrifice of reflection magnitude from both the bore and the tangential defects; in addition, it would not be possible to see the indication traveling in both directions. This latter phenomenon is important when a radial defect is curved such that it presents alternately its concave and convex surfaces to the sound source. One method of obtaining maximum magnitude from a radial defect regardless of its lateral displacement from the forging center line is to modify the sound beam so that uniform sound-energy distribution is obtained over the affected forging area. This and other methods of increasing detection sensitivity are being studied.

Another effect of a traveling indication which is occasionally observed is "bore whipping." This is a violent increase and decrease of the bore reflection caused by a traveling indication of high magnitude creating wave interference with the bore reflection at the instant when both are equidistant from the crystal although not on the same line. The result is an in-and-out phase

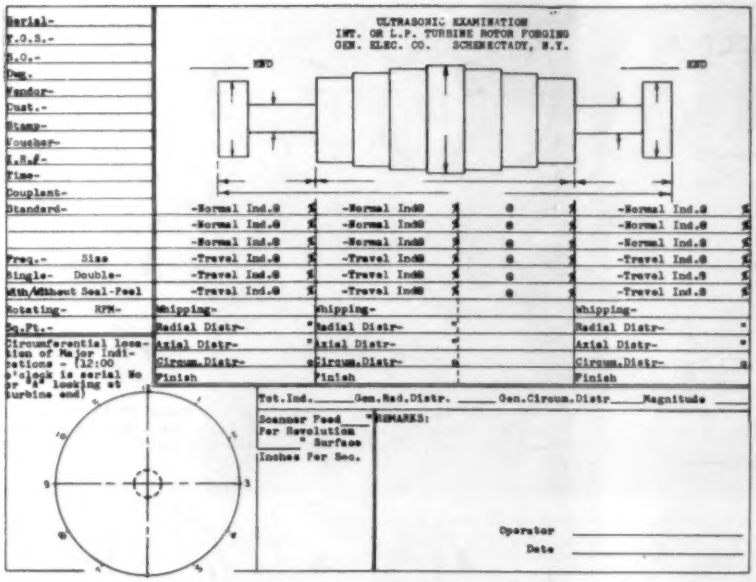

FIG. 5 FORM SHEET FOR REPORTING RESULTS OF ULTRASONIC INSPECTION OF A TURBINE-ROTOR FORGING

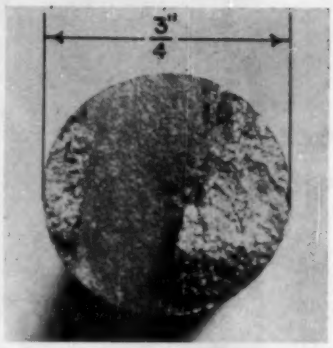

FIG. 6 BROKEN TREPAN CORE SHOWING TANGENTIAL BAND OF NONMETALLIC INCLUSIONS

(This defect gave a stationary reflection of 300 per cent and was the only indication in the entire forging.)

relation that alternately adds to and subtracts from the bore reflection.

The report of the ultrasonic inspection of a rotor forging is recorded and presented in the form shown in Fig. 5. This report form lists the number and magnitude of both stationary and traveling indications, their axial, radial, and circumferential distribution, and a sketch of the forging itself together with all its identification such as vendor serial number, manufacturing shop order, and so on.

FORMATION AND CALIBRATION OF ACCEPTANCE GUIDES

The basic information obtained from the ultrasonic examination is the number of defect reflections, their magnitude with respect to the bore reflection in a defect-free area, and their identification as either stationary or traveling indications. In particular, the reflection magnitude alone cannot be used as a criterion of the nature of the defect since some stationary indications of 300 per cent magnitude have been proved by trepanning to be nonmetallic inclusions as shown in Fig. 6, while other indications ranging from 25 per cent to 225 per cent magnitude have been proven by trepanning to be actual cracks as shown in Fig. 7 for the 225 per cent defect. Similarly, certain traveling indications of 20 per cent maximum magnitude have been proven to be nonmetallic inclusions as shown in Fig. 8, while others of only 15 per cent magnitude have been proven by trepanning to be cracks as shown in Fig. 9.

While the reflection magnitude alone is not indicative of the nature of the defects, as seen from Figs. 6 to 9, inclusive, the combination of reflection magnitude and number of defect reflections seems to afford some index of quality, and has been chosen here as a starting point for establishing the acceptance guides. The choice of these two variables as the starting point is supported by the inspection results on the forgings from which the previous examples were taken. In the two examples in which nonmetallic inclusions were obtained (Figs. 6 and 8), only a small number of defects were present, while in the two examples in which cracks

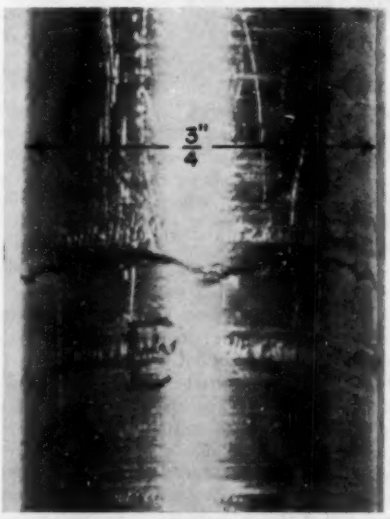

FIG. 7 TREPAN CORE SHOWING A TANGENTIAL CRACK

(This defect gave a stationary reflection of 225 per cent, but there were approximately 3000 indications of various reflection magnitudes up to 225 per cent in this forging.)

were found (Figs. 7 and 9), a relatively large number of defects were present. This suggests that plotting the number of defect reflections against their magnitude, as is illustrated for five rotor forgings in Fig. 10, would provide a direct visual method of relating the number of defects with their magnitude, and accordingly would furnish a first step in evaluating the ultrasonic soundness of a forging. Experience has shown, however, that this direct method of plotting has certain disadvantages, and must be modified as follows in order to get a clear appraisal of quality.

1 The point farthest to the left on the plot of number of de-

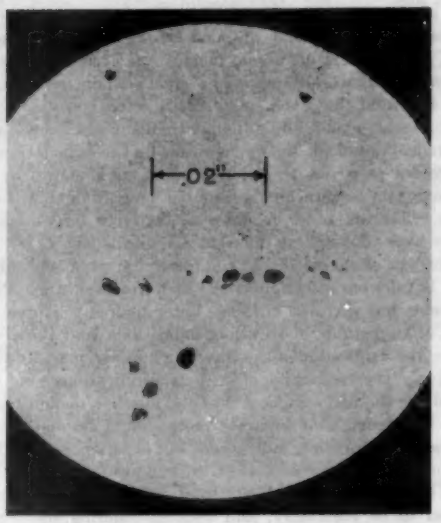

FIG. 8 PHOTOMICROGRAPH OF A CROSS-SECTIONED TREPAN SHOWING NONMETALLIC INCLUSIONS

(These inclusions gave a traveling indication of 20 per cent magnitude which was the maximum magnitude of five traveling indications. There were a total of thirty indications in this forging.)

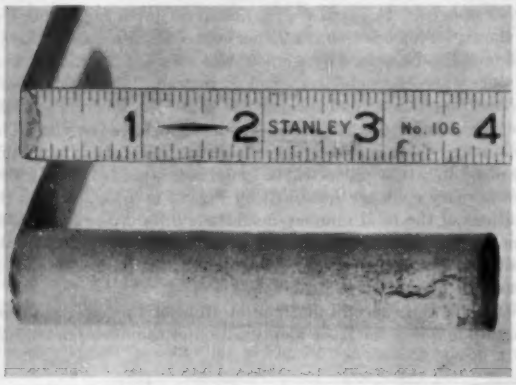

FIG. 9 TREPAN CORE SHOWING A RADIAL CRACK NEAR BORE

(This defect gave a traveling reflection of 15 per cent magnitude, but there were approximately 500 traveling indications of up to 100 per cent magnitude in this forging.)

fects versus their magnitude, hereafter termed the "number/magnitude" line, should be placed at the point corresponding to the total number of defect reflections since, if the observer reports the reflections in sufficiently small increments of bore-reflection magnitude, a forging may give a number/magnitude line which appears better than is justified by the actual inspection results, as is shown by comparing rotor A of Fig. 10, with a total of 54 reflections, with rotor B which has 64 reflections.

2 This left end of the number/magnitude line, which now corresponds to the total number of reflections, should be plotted at the 15 per cent bore-reflection magnitude since it is difficult for the operator to estimate accurately at lower magnitudes; it is self-evident that, if the left end corresponds to the total number of indications, it is relatively unimportant if this point is placed at the 5, 10, or 15 per cent magnitude so long as the same minimum reflection magnitude is used for all rotor forgings.

3 The number/magnitude line should go directly from the

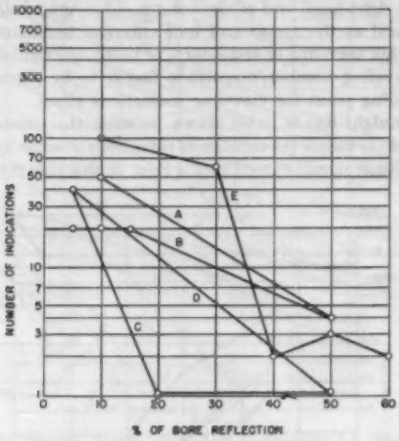

FIG. 10 DIRECT PLOTTING OF NUMBER OF DEFECTS AGAINST REFLECTION MAGNITUDE

total number of indications at 15 per cent magnitude straight down to the point corresponding to the number of indications at the maximum reflection magnitude in order to avoid the slight confusion which may arise by the plotting of intermediate points as is illustrated by the 20 per cent point of rotor C as compared with the corresponding number/magnitude line of rotor D which, with one less defect than rotor C, has a considerably poorer number/magnitude line. The only exception to this third rule occurs when the number of reflections at some magnitude intermediate between 15 per cent minimum and the maximum reflection magnitudes exceeds the straight line drawn between the latter two, as is illustrated by rotor E of Fig. 10, in which case the number/magnitude line must be broken to include the intermediate magnitudes.

It should be appreciated, however, that plotting of number of reflections against their magnitude does not take into account the possibility that a traveling indication, which in its purest form would be a reflection from a radial defect, is potentially more harmful than a stationary indication which in its purest form would be a reflection from a tangential defect. While the relative weight factors which should be assigned to this theoretical distinction are debatable, the possibility that such a distinction is valid makes it imperative that a separate number/magnitude plot be made for the traveling indications. Two plots are necessary; namely, the first is to include all reflections, whether stationary or traveling, and the second is to include traveling indications alone.

Summarizing the foregoing comments, experience with a large number of forgings indicates that the best evaluation of the ultrasonic soundness can be obtained if the following rules are utilized in drawing number/magnitude lines:

1 A number/magnitude line is to be drawn corresponding to all reflections whether stationary or traveling; this will be termed the total number/magnitude line.

2 A number/magnitude line is to be drawn corresponding to the traveling indications alone; this will be termed the traveling number/magnitude line.

3 The left point of the total number/magnitude line is to be placed on the 15 per cent magnitude line at the level corresponding to the total number of stationary and traveling indications; the left point of the traveling number/magnitude line is to be placed on the 15 per cent magnitude line at the level corresponding to the total number of traveling indications alone.

4 The right-hand end of the total number/magnitude line is to be placed at the number of indications of maximum amplitude whether traveling or stationary, or both; the right-hand end of the traveling number/magnitude line is to be placed at the corresponding point for traveling indications alone.

5 A straight line is to be drawn between the points defined by (3) and (4) unless the number of reflections at some intermediate magnitude should exceed such a line; in this case the straight line is to be broken so as to also enclose the number of reflections at these intermediate magnitudes.

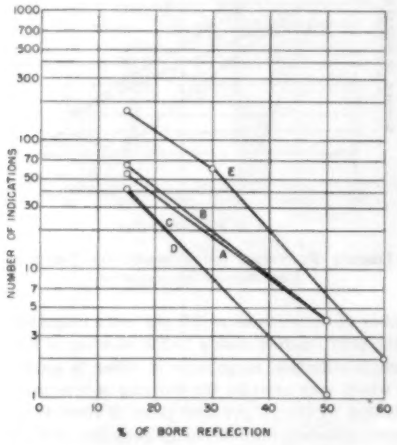

FIG. 11 MODIFIED PLOTTING OF NUMBER OF DEFECTS AGAINST REFLECTION MAGNITUDE; THESE ARE THE "NUMBER/MAGNITUDE" LINES

The number/magnitude lines of Fig. 10 have been redrawn in Fig. 11, as total number/magnitude lines alone, corresponding to the foregoing rules. It is evident that the foregoing rules provide a clearer picture for the evaluation of the relative ultrasonic soundness of these five forgings than was available from Fig. 10.

While plotting of number of defects versus their magnitude for both total and traveling indications, similar to Fig. 11, can be used for quality comparisons between forgings, further data are required to fix quantitative limits within which rotor forgings can be deemed acceptable, and such data are available from turbine- and generator-rotor forgings which have been either trepanned to identify the causes of ultrasonic reflections, or destructively examined. Specifically, we have cut up nine turbine- and generator-rotor forgings and have removed 85 trepans for identification of the cause of ultrasonic reflections from an additional 39 rotors. Trepanning proved that in 48 instances the ultrasonic reflections were caused by nonmetallic inclusions, while in the remaining 37 cases the ultrasonic reflections were caused by cracks, and these data can be used as follows to fix on the total and traveling number/magnitude plots the quantitative limits needed to establish the ultrasonic soundness of rotor forgings.

Total number/magnitude plots were made, as shown on Fig. 12, of all rotors on which trepanning of stationary indications had revealed cracks. The small squares in Fig. 12 show the ultrasonic magnitudes of the stationary indications which were found to be cracks when trepanned. It should be noted that each small square refers to a single trepan at the indicated magnitude although there may have been a number of reflections of the same magnitude on the same forging. On some rotors only one trepan was taken, as is shown by there being only one square on the number/magnitude line for that forging, while on other forgings a relatively large number of trepans were removed at different magnitude levels.

It must be emphasized that the total number/magnitude lines in Fig. 12 refer only to forgings on which trepanning of stationary indications has revealed cracks. Later figures will present the results of trepanning of traveling indications, and these will be used for the calibration of the traveling number/magnitude lines; accordingly, the trepanning of stationary indications alone should be used for the calibration of the total number/magnitude lines. It can be argued that separate plots should be made of both stationary and traveling indications, but experience has indicated that the best evaluation of the ultrasonic soundness can be obtained by considering first the total number of reflections, all assumed to be stationary, and then considering the traveling reflections alone.

Having established the positions on the total number/magnitude charts of the stationary reflections which were found to be cracks when trepanned, it is necessary to consider the total number/magnitude lines of the forgings from which these trepans were removed. In particular, it should be noted that while Fig. 12 shows, for instance, that a 25 per cent reflection was trepanned and found to be caused by a crack, this does not indicate that all 25 per cent reflections are cracks; instead, this chart merely implies that if a second forging has a total number/magnitude line similar in location to one on which cracks have been found by trepanning, there is evidence available from this chart indicating the possibility that cracks will be found in this second forging also. The primary evidence furnished by Fig. 12 is to be found in the positions of the total number/magnitude lines of the forgings on which cracking at any point has been found rather than in the positions of the squares which define only the particular indications which were trepanned.

Utilizing the concept that the location of the total number/magnitude line is the basic identification of the ultrasonic sound-

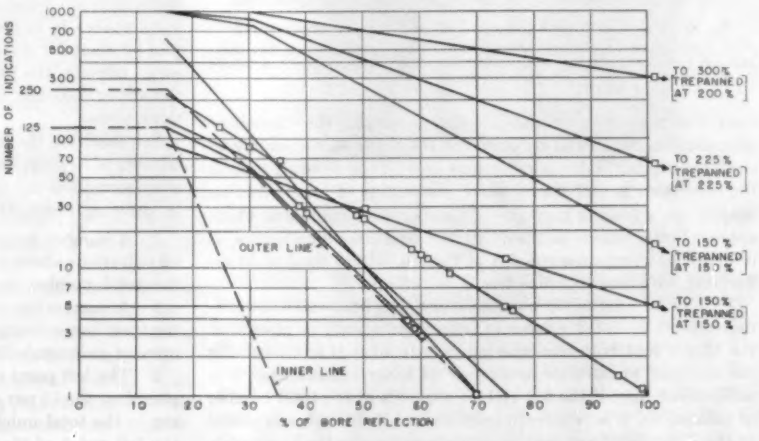

FIG. 12 TOTAL NUMBER/MAGNITUDE PLOTS OF ROTOR FORGINGS ON WHICH TREPANNING OF STATIONARY INDICATIONS DISCLOSED CRACKS; REFLECTION MAGNITUDES OF TREPANNED CRACKS SHOWN BY SMALL SQUARES

ness of a rotor forging, a hypothetical, but representative, total number/magnitude line can be drawn beyond which the results of the trepanning identification of stationary indications imply that cracking may be found. This line, hereafter called the "outer" line, is shown in Fig. 12 and is so drawn that it is simply representative of the several minimum total number/magnitude lines of the rotors on which cracking has been found by trepanning. It should be noted that this (representative) outer line has not been drawn so as to lie to the left of all reflection magnitudes on which trepanning has revealed cracks (and this will be more evident in later discussions of traveling indications). Instead this outer line is drawn solely as representative of the minimum total number/magnitude lines on which trepanning has revealed cracks. This is in accordance with the fundamental concept that it is the entire number/magnitude line which defines ultrasonic soundness rather than the results of specific trepans.

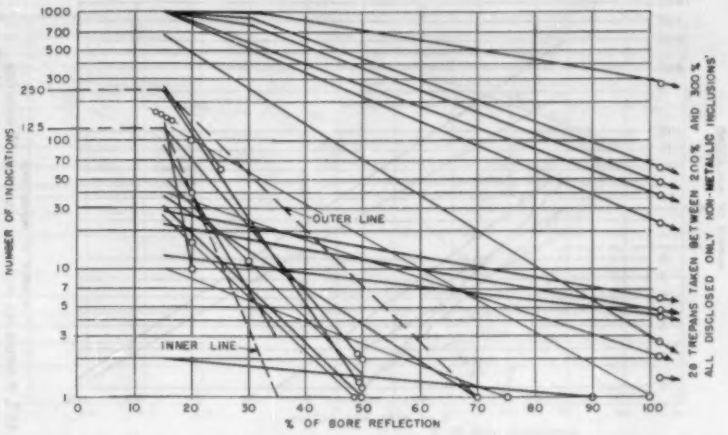

FIG. 13 TOTAL NUMBER/MAGNITUDE PLOTS OF ROTOR FORGINGS ON WHICH TREPANNING OF STATIONARY INDICATIONS DISCLOSED ONLY NONMETALLIC INCLUSIONS; REFLECTION MAGNITUDES OF TREPANNED INCLUSIONS SHOWN BY SMALL CIRCLES

It must be recognized, of course, that the outer line merely establishes the representative lower limit at which cracked forgings have been found, but without establishing definitely that cracking will be found in all rotors whose total number/magnitude lines exceed the outer line. This is illustrated in Fig. 13 in which the total number/magnitude lines are presented of rotors on which trepanning revealed only slag inclusions. This illustrates that it is not possible to make the statement that rotor forgings whose total number/magnitude lines extend beyond the outer line are necessarily cracked. Specifically, a rotor with harmless nonmetallic inclusions can give a total number/magnitude line extending beyond the outer line, and ultrasonic inspection alone cannot differentiate this rotor from one having a duplicate total number/magnitude line, but containing potentially harmful cracks.

In a similar fashion, however, it is not possible to state definitely that rotor forgings whose total number/magnitude lines lie completely within the outer line will always contain only harmless nonmetallic inclusions; continuous policing through further trepanning is required to establish such a conclusion. Pending this conclusion, the outer line of Fig. 12 was used to establish the "inner" line shown on the same figure. The lower point of this inner line is set at 35 per cent magnitude, which is one half the 70 per cent magnitude of the lower point of the outer line, while the upper point of the inner line is set at 125 indications of 15 per cent magnitude with the value of 125 being one half of the 250 indications of the same reflection magnitude as taken from the upper end of the outer line. These reduction factors of $^1/_2$ on both the number of indications and the maximum reflection magnitude were selected on the basis of engineering judgment and conservatism similar to the selection of safety factors on stress levels. However, with the establishment of the inner line on this basis, the following policy was formulated for the acceptance procedure for the ultrasonic examination of rotor forgings with respect to the total number of indications:

1 Rotor forgings whose total number/magnitude lines are completely within the inner line are acceptable without trepanning provided that magnetic-particle and visual examination of the bore and outside surfaces reveal no harmful defects.

2 Rotor forgings whose total number/magnitude lines are partly within the inner line and partly between the inner and outer lines are rejected unless at least two trepans are taken in representative areas and all reveal only harmless nonmetallic inclusions, and provided that magnetic-particle and visual examination of the bore and outside surfaces reveal no harmful defects.

3 Rotors whose total number/magnitude lines are completely between the inner and outer lines are rejected unless at least four trepans are taken in representative areas and all reveal only harmless nonmetallic inclusions, and provided that magnetic-particle and visual examination of the bore and outside surfaces reveal no harmful defects.

4 Rotors whose total number/magnitude lines at any point are outside the outer line are rejected unless at least six trepans are taken in representative areas and all reveal only harmless nonmetallic inclusions, and provided that magnetic-particle and visual examination of the bore and outside surfaces reveal no harmful defects; in addition, such rotors are acceptable only for relatively low-stressed applications.

(*a*) If all the ultrasonic defects are in localized areas and are not widely distributed, or if the maximum reflection magnitude does not exceed 15 per cent, the number of trepans may be reduced from six to four.

Experience has indicated that the minor modifications of item 4(*a*) are justified since, if the ultrasonic reflections are in localized areas, then four trepans are representative of the conditions causing the reflections, while if all the reflections are within the limit of 15 per cent magnitude the presence of slag inclusions only is strongly indicated.

Outer and inner lines were established for traveling indications in a similar manner, and are shown in Fig. 14 together with the trepanning points and traveling number/magnitude lines of the rotor forgings on which such trepanning revealed cracks. It should be noted, however, that while the survey of stationary indications was carried back to the initiation of ultrasonic inspection in 1948, the survey of traveling indications was carried back only to 1954 since this was the first period at which the traveling indications were measured and reported separately from the stationary indications. It will be noted in Fig. 14 that cracking has been found at ultrasonic magnitudes within the outer line, but in this case it occurred on a rotor whose traveling number/magnitude line extended beyond the outer line. This is in further agreement with the concept that the ultrasonic soundness of a forging is defined by the complete number/magnitude line

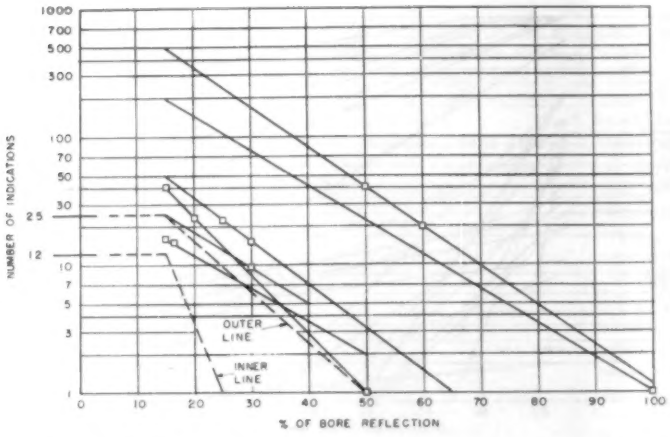

FIG. 14 TRAVELING NUMBER/MAGNITUDE PLOTS OF ROTOR FORGINGS ON WHICH TREPANNING OF TRAVELING INDICATIONS DISCLOSED CRACKS; REFLECTION MAGNITUDES OF TREPANNED CRACKS SHOWN BY SMALL SQUARES

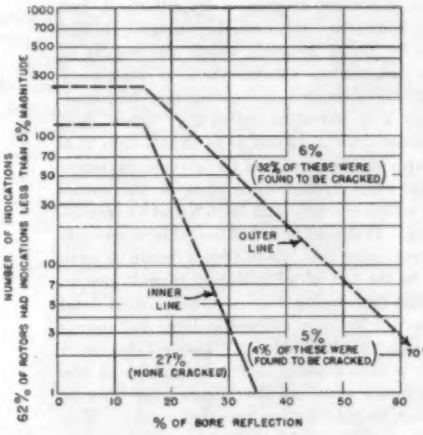

FIG. 15 DISTRIBUTION WITH RESPECT TO TOTAL INDICATIONS OF ROTOR FORGINGS RECEIVED BETWEEN 1948 AND 1955, INCLUSIVE

(Rotors found cracked in region between inner and outer lines had traveling number/magnitude lines beyond outer line for traveling indications, and cracks were found by trepanning traveling indications.)

rather than by the ultrasonic magnitude of any specific reflection.

A policy on acceptance procedure for ultrasonic examination of rotor forgings was then established for traveling number/magnitude lines duplicating that itemized previously for the total number/magnitude lines, but with the additional provision that a rotor must be acceptable on both total and traveling number/magnitude plots before being released for production. It should be noted that the inner and outer lines for the traveling indications are considerably lower in both number of defects and defect magnitude than the corresponding lines on the total number/magnitude charts, which substantiates the original conclusion that the traveling indications should be considered separately.

REVIEW OF PAST RECORDS ON 1500 ROTOR FORGINGS

Having established an acceptance policy based on inner and outer lines, a survey was made of all rotor forgings on which ultrasonic-inspection reports were available to determine if past decisions on forgings with ultrasonic defects were compatible with the newly developed acceptance policies, or, if this were not so, to determine the impact on forging production of the more rigorous acceptance standards. Specifically, if the proposed standards would result in a greatly increased rejection rate on rotor forgings, then the ordering of back-up forgings must be increased. Since ultrasonic records for large turbine and generator production of the authors' company are available back to the introduction of ultrasonic inspection in 1948, a total of 1500 large rotor forgings was available to establish a reasonable basis for conclusions on the proposed acceptance policies. Such records were incomplete in two respects, however, since the traveling indications were not measured and reported separately until late 1953, and the number of stationary defects of the lower magnitudes were not reported, except as "few," "numerous," or "many," until early 1954. Fortunately, however, the company personnel who had made the ultrasonic inspections at Schenectady had sufficient personal notes in the files which, together with their log-book records, were adequate to supply rough numerical values to these otherwise indeterminate terms.

Of all the rotors covered in this survey, 62 per cent had no ultrasonic defects, while the remaining 38 per cent had stationary and/or traveling indications of various magnitudes, with the traveling indications being restricted to rotors inspected after late 1953. Total number/magnitude lines were plotted for all rotors containing such defects, with the results as indicated in

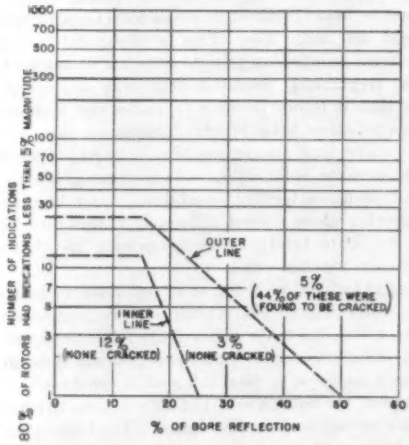

FIG. 16 DISTRIBUTION WITH RESPECT TO TRAVELING INDICATIONS OF ROTOR FORGINGS RECEIVED IN 1954 AND 1955; TRAVELING INDICATIONS NOT MEASURED AND REPORTED SEPARATELY FROM STATIONARY INDICATIONS PRIOR TO THIS DATE

Fig. 15. Twenty-seven per cent of the rotors remained within the inner line (in addition, of course, to the 62 per cent on which no defect reflections were found), and, of this 27 per cent, none was found to be cracked. Five per cent fell within the outer line but wholly or partly outside the inner line, and 4 per cent of these (0.2 per cent of all rotors reviewed) were found to be cracked. It should be noted, however, that the traveling number/magnitude lines of this entire 4 per cent lay beyond the outer line of traveling indications, and the cracks were found by trepanning traveling indications. The number/magnitude lines of 6 per cent of the rotors fell wholly or partly outside the outer line, and 32 per cent of these were proved to contain cracks.

Number/magnitude plots were then made for the traveling indications with the results as shown in Fig. 16; only 331 forgings were considered in this part of the study since, as stated previously, the traveling-indication records are limited to the period

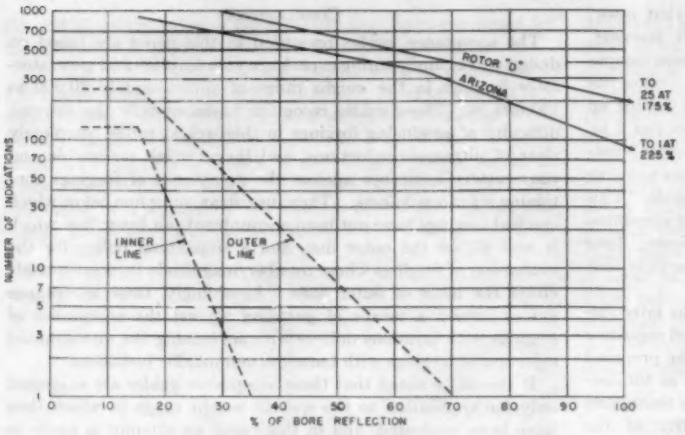

FIG. 17 TOTAL NUMBER/MAGNITUDE PLOTS OF ROTOR D AND ARIZONA ROTOR

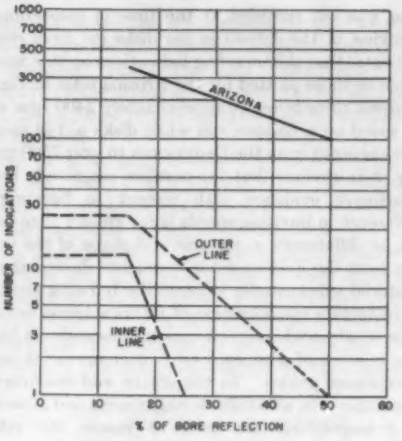

FIG. 18 TRAVELING NUMBER/MAGNITUDE PLOT OF ARIZONA ROTOR

following late 1953. On 80 per cent of these rotors, the traveling indications were less than 5 per cent in reflection magnitude, which is essentially within the noise level of the inspection equipment. Twelve per cent remained within the inner line, and none of these was cracked. The traveling number/magnitude lines of 3 per cent of the rotors fell within the outer line and wholly or partly outside the inner line, and in this range also, none was found to be cracked. The number/magnitude lines of 5 per cent of the rotors fell wholly or partly outside the outer line, and 44 per cent of these were found to contain cracks.

The foregoing review of 1500 rotor forgings indicates that the proposed acceptance policy will not result in an impracticable situation with regard to forging rejections or the maintenance of sufficient back-up forgings. These acceptance guides will not result in excessive rejections, but will require more careful investigation of those whose number/magnitude lines are beyond the limits established by past destructive and semi-destructive examination. In particular, forgings whose number/magnitude lines are well outside the outer line will require a relatively large number of trepans to establish the harmless nature of all defects even when, as in the case of the Arizona[4,5] rotor whose number/magnitude plots are shown in Figs. 17 and 18, continued examination of the bore reveals only minor porosity and nonmetallic inclusions.

DISCUSSION

The review of 1500 rotor forgings as discussed in the preceding section was followed immediately by a close scrutiny of those rotor forgings already in service whose number/magnitude lines were outside the currently proposed acceptance guides. This scrutiny involved a consideration of the position of the number/magnitude line of each such forging together with its physical properties, operating stresses, years of operating service, and the means which were used before release of the forging to identify the cause of the ultrasonic reflections. In none of these cases was any cause found for questioning the continued safe operation of these rotors; specifically, no case was found in which the combination of number/magnitude line, operating stresses, and material ductility approached that present in the Arizona rotor.[5] In the interests of obtaining further basic knowledge, however, it is planned to replace, and cut up, one large 1800-rpm generator rotor which had a number of ultrasonic reflections. Although even in this case there was no question about its continued safe operation, since it had excellent physical properties and was designed with low stress levels, this was a spare field built in 1949, which could be replaced without involving any shutdown; accordingly, it was agreed to take advantage of this opportunity to obtain further experimental data.

It is, of course, self-evident that during the review of the rotors on which complete ultrasonic inspection reports were available, some questions should arise concerning the status of rotors shipped before the introduction of ultrasonic inspection; it should be noted, incidentally, that most turbine and generator rotors now in service were never subjected to a complete ultrasonic inspection since the latter is a relatively recent introduction. Accordingly, on most rotors now in service no ultrasonic records are available for comparison with the proposed acceptance guides, and none will be available until more advanced ultrasonic-inspection techniques, usable in the field, have been developed. Accordingly, it seems advisable at this point to delineate more carefully the purposes and limitations of the proposed acceptance guides. Specifically, these are only guides for determining when it is advisable to obtain direct evidence for the interpretation of ultrasonic reflections; they do not imply that all forgings with number/magnitude lines outside the outer line contain harmful defects, nor, in particular, should they be interpreted to mean that such rotors will not give reliable service.

The propagation of internal defects into a general fracture is determined most importantly by the notch sensitivity or crack-propagating propensity of the rotor material. This characteristic, not yet thoroughly understood, is receiving intensive study on many fronts. The degree by which this characteristic affects bursting strength can be illustrated by the results obtained on two rotors with comparable number/magnitude lines but with widely different bursting speeds. These two rotors are the D-rotor[3] and the Arizona rotor.[4] Number/magnitude plots of these two rotors are shown in Figs. 17 and 18, together with the inner and outer lines proposed in this paper. No traveling number/magnitude line is shown for the D-rotor since such informa-

[4] This particular rotor had been constructed for Arizona Public Service Company, but burst while on a balance run in the manufacturer's plant. It was never shipped to the intended purchaser, but, since it is generally referred to throughout the power-generation industry as the "Arizona" rotor, this identification is continued both in this paper and in the companion paper.[5]

[5] "Report of the Investigation of Two Generator Rotor Fractures," by C. Schabtach, D. H. Winne, E. H. Fogleman, and A. W. Rankin, published in this issue, pp. 1567–1584.

tion was not recorded at the time of inspection of that rotor; a review of the defects in the disks cut from rotor D, however, indicates that the traveling indications on this rotor were comparable to those plotted for the Arizona rotor in Fig. 18. Since the Arizona rotor burst at approximately 3400 rpm while coming up to speed on a balance run while disks of full diameter and 2 in. thickness cut from the D-rotor ran to over 7500 rpm before bursting, it is obvious that the number/magnitude line does not give conclusive evidence with respect to bursting speeds. This difference in bursting speeds is far greater than can be accounted for by differences in the size and shape of the test pieces; disks cut from the Arizona rotor fragments showed that cracks in that material substantially lowered the bursting strength.

In further consideration of rotors shipped before the introduction of ultrasonic inspection, some discussion is justified regarding the relation of past successful rotor operation and the proposed acceptance guides. In the design and construction of turbine-generator sets, all available engineering and laboratory techniques and inspections are used to insure the reliability of the equipment, and operating experience has demonstrated that such means have been applied correctly in all but a very few cases. No rotors are released for production if there is any question concerning their ability to operate reliably, and such a policy is followed for the protection of the manufacturer as well as the purchaser. All rotors are initially run at overspeed by the manufacturer. It must be recognized, however, that operation of the unit is the ultimate test of all the factors involved; successful operation is convincing evidence of the adequacy of the design, quality controls, safety margins, and other provisions against the unknown and unforeseeable. The basic function of the proposed acceptance guides is to furnish the maximum assurance possible with the present knowledge, prior to the initial operation, that no harmful defects are present which might propagate into a forging burst. Equal or greater assurance is afforded by several years of successful operation; in particular, such service operation is superior to laboratory testing since the latter, at best, can furnish only an approximation to service conditions.

The consideration of rotors shipped before the introduction of ultrasonic inspection and their possible relation to the proposed acceptance guides does not present the industry with any basically new questions since this situation has arisen with every introduction of a new technique for insuring the quality of large rotor forgings. The continuous endeavors of the steel mills and turbine-generator manufacturers to improve and inspect these large rotor forgings resulted in the introduction in 1921 of bore inspection holes through which the center quality could be established, the introduction in 1933 of magnetic-particle inspection to reveal surface defects, the introduction in 1948 of ultrasonic testing through which, for the first time, the entire forging could be inspected, the recognition of traveling ultrasonic reflections in late 1953, and the introduction of residual-stress measurements in 1954.

The introduction of each of these techniques has always resulted in questions concerning the quality of the forgings manufactured and inspected prior to the introduction of the latest inspection technique. In each case, the prior successful operation of the rotors was used, consciously or unconsciously, to answer such questions, and continued successful operation through the years has demonstrated the validity of such reasoning. It should be noted, of course, that on the basis of the review of the 1500 rotor forgings on which ultrasonic inspections were made, only a small percentage fall outside the proposed acceptance guides, and the number of forgings considered in this review was sufficiently large that the results are also undoubtedly indicative of the results which would be obtained from a similar survey of rotors placed in service prior to ultrasonic inspection.

Conclusions

The acceptance guides presented in this paper are based on design and manufacturing experience with turbine- and generator-rotor forgings in the weight range of approximately 20,000 to 150,000 lb. These guides recognize fundamentally the extreme difficulty of producing forgings in this weight range completely clear of ultrasonic reflections, and they furnish reasonable and conservative assurance against the acceptance of forgings containing injurious defects. They furnish an outer line below which cracked forgings have not been encountered, an inner line which is well within the outer line, and a trepanning policy for the evaluation of forgings whose number/magnitude lines are outside either the inner or outer lines. Accordingly, these acceptance guides furnish a means of guarding against the acceptance of forgings with injurious defects without causing the unwarranted rejection of forgings with harmless nonmetallic inclusions.

It should be noted that these acceptance guides are suggested only for application to the specific weight range in which they have been evaluated, and in this range no attempt is made to distinguish between individual weights and diameters; specifically, these guides are used directly for either a 20,000-lb or a 150,000-lb forging. Although the defect-reflection magnitude has no direct relation to the forging weight or diameter, being based solely on the bore reflection, there is some evidence that the number of defects increases with both forging weight and diameter. Accordingly, it is possible that using the number of indications as a criterion penalizes the larger forgings, and it might be more logical to use instead the number of indications per unit volume. Since other qualifications of equal validity also can be considered, as, for instance, the axial and radial distribution of defects within a given unit volume or even the operating stress levels, it appears more conservative to consider primarily the defect magnitude and number of defects alone. In particular, it should be noted that the penalty of this simplification is only that further evaluation, in the form of trepanning, may be more frequent than necessary on the larger forgings, but in view of the recognized difficulty of producing the larger forgings to the high quality standards desired by both the vendor and user, the possible additional trepanning to insure freedom from injurious defects is not unwarranted.

It is fully appreciated that the available data for establishing these acceptance guides are rather limited, although the authors believe that these are the best and most extended data available. Further trepanning will be done in the future on an almost continuous basis, and the positions of the inner and outer lines will be revised whenever the results of the trepanning indicate that such revision is necessary. The authors' company believes, however, that this publication of the current acceptance guides together with the limitations of the data on which such guides have been based is to the best interests of the power-generation industry. It is planned to publish in the future in a similar fashion any modifications of the inner and outer lines if trepanning should show that such modification is necessary.

Acknowledgments

The authors take pleasure in acknowledging their indebtedness to the many members of the Department's laboratory and engineering organizations who participated in this development. In particular, they express their indebtedness to Messrs. R. A. Fitzgerald and G. Lockyer for many important contributions.

Discussion

R. A. Baudry.[6] The authors must be congratulated for a very

[6] Manager, Mechanical Development Section, Transportation and Generator Engineering Department, Westinghouse Electric Corporation, East Pittsburgh, Pa. Mem. ASME.

interesting presentation of the methods they have developed for the ultrasonic inspection and evaluation of large forgings.

The detection of radial defects by means of the traveling indications is of particular interest. However, it appears that the magnitude of the traveling indication should be a function of the radial location of the defect; it is even possible that a radial defect traveling mostly outside of the effective part of the beam would be difficult to detect. Therefore it appears that any evaluation of a forging by the number of traveling indications should make allowance for the relative location of the radial

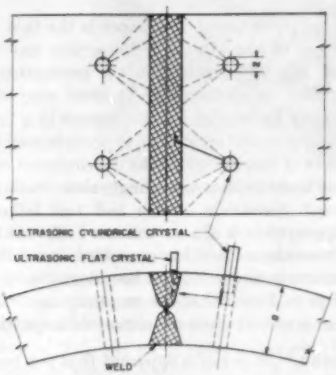

FIG. 19 ULTRASONIC INSPECTION OF WELDED ROTOR RIM

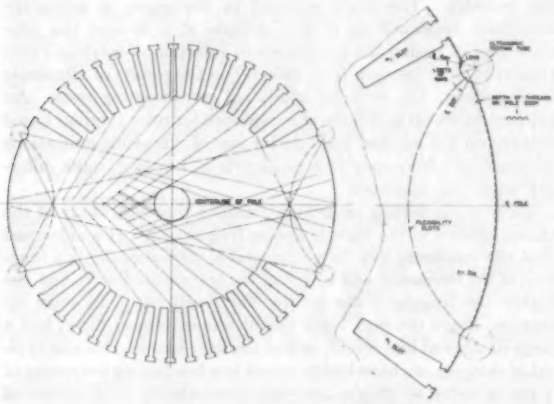

FIG. 20 FIELD ULTRASONIC INSPECTION FOR TURBINE-GENERATOR ROTORS

defects in the divergent ultrasonic beam and in the forging. Data giving the magnitude of a traveling indication for a given radial defect at various locations would be very valuable.

Since the early use of ultrasonic inspection, it has been appreciated that it is difficult to detect defects parallel to the ultrasonic beam. The need for a more sensitive method to detect flaws in the very thick butt-weld joint of large salient-pole rotor rings led to the development, several years ago, of the circular crystal described in a companion paper.[7]

As shown in Fig. 19 of this discussion, the cylindrical crystal was used in radial holes to survey the entire welded joint and to have the maximum sensitivity for detection of radial flaws in the plane normal to the hoop stresses. The possibility of being able to survey from two planes at right angle made it possible to pinpoint exactly the location of any flaw by using the maximum intensity of the ultrasonic beam. The same cylindrical crystal is also used (Fig. 20) to make ultrasonic inspection of a completed rotor forging from longitudinal crescent-shaped grooves machined in the surface of the rotor.

As shown in Fig. 21, these grooves make it possible to make a complete and accurate survey of a forging before slotting to obtain a positive sonic indication and evaluation of any defect. A radial defect will show only a very small indication with the radial beam and a large indication with the cylindrical crystal. A small cavity would give large indications on both crystals. These indications are produced by the maximum intensity of the ultrasonic beam and therefore can be used to determine the shape of a defect and its proper identification by the metallurgist who is inspecting the forging A further advantage of this method

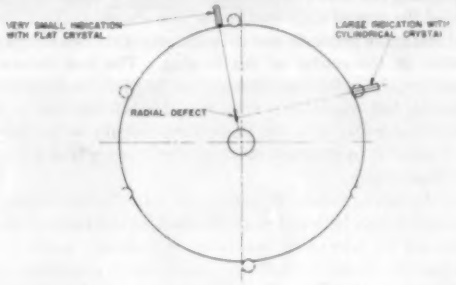

FIG. 21 ULTRASONIC INSPECTION OF TURBINE-GENERATOR ROTOR
(Use of cylindrical crystal for precise detection of radial defect.)

is that it permits a precise evaluation of a defect at any radial location.

The concept of evaluating the quality of a forging by the number and magnitude of ultrasonic indications proposed by the authors is a radical departure from the present practice of carefully investigating the nature of any ultrasonic indication and its possible effect on the strength of the forging in any particular location. While the formulation of precise standards of acceptance of forgings is very attractive they must always be used with caution.

In the case of turbine-generator rotors the failure of which has disastrous consequences, all the most positive methods of evaluating the quality of the forging must be used. A forging with ultrasonic indications cannot be used unless there is a very positive proof that ultrasonic indications in any particular location are shown to be harmless.

The most critical part of the rotor is the material surrounding the bore where the centrifugal stresses are at their maximum value and where ultrasonic indications are usually found.

It has been an established practice for many years not to use a forging unless the bore was found perfectly clean by visual examination with a boroscope or by inspection with magnetic particles. Local overboring is sometimes used to remove small inclusions or cavities. The use of the cylindrical ultrasonic crystal makes it possible to determine very accurately the nature and location of any indication near the bore and the extent of the necessary overboring.

Any zone of the forging which has a large number of indications must be investigated thoroughly. The forging cannot be used unless the indications are found to be harmless inclusions by means of trepanning.

If a cluster of indications is found in the highly stressed zone near the bore where no trepanning can be done, it is not believed

[7] "Large Rotor Forgings for Turbines and Generators," by N. L. Mochel, R. E. Peterson, J. D. Conrad, and D. W. Gunther, published in this issue, pp. 1585–1601.

that with the present status of the art such a cluster of indications can be judged harmless and, therefore, such a forging cannot be used. Only very few forgings of this type have been found and this conservative practice has so far not resulted in an unbearable burden on the production of generating equipment.

The physical tests used for acceptance of the rotor are usually taken at the center of the poles which are the only parts of the rotor body where holes can be trepanned. It is, therefore, very desirable to locate zones having numbers of ultrasonic indications in or under the poles of the rotor to make possible further evaluation of the ultrasonic indications by trepanning. This makes it also desirable to make an early ultrasonic survey of the forging before it is bored or trepanned for acceptance tests. This practice would permit locating the poles, and taking an axial trepan from the bore in the location which is the most favorable for the evaluation of the observed ultrasonic indications. The practice of trepanning the bore of the forging to make it possible to have a sample of the core of appreciable size also should make it possible to evaluate more precisely not only the structure but the physical properties at the center of the forging. The test values thus obtained could not for the present time be used for acceptance of the forging, but would give very valuable information as to the nature of the material in the immediate vicinity of the bore and make it possible to evaluate more precisely any ultrasonic indication in that region.

Several years ago when the ultrasonic inspection of forgings was introduced it was believed that this tool would make it possible to eliminate the bore at the center of the forging. A few forgings which had no ultrasonic indications were thus produced. However, later investigations showed that the normal hydrogen content of rotor forgings is sufficient to lower very appreciably the ductility of the material. As a result it was felt that a bore at the center of a forging would be beneficial in permitting the slow escape of occluded hydrogen and ultimately result in a higher ductility of the material at this critical part of the rotor. As a result all our forgings are now provided with a bore hole.

The comments of the authors would be appreciated on this practice since they have also, in a few cases, used rotors in which no bore hole was present.

The use of the traveling-indication technique described by the authors should make possible the early detection of harmful defects in forgings. However, a forging cannot be considered as usable on the basis of a minimum number of indications alone but only when the number of indications per unit volume of a highly stressed part of the rotor has been evaluated by "all available engineering and laboratory techniques and inspections" as mentioned by the authors.

It is hoped that the authors will be successful in their endeavor to increase the accuracy of the traveling indications by the development of the ultrasonic beams of uniform energy that they are investigating. It also would be of interest to the industry if they could extend their survey of ultrasonic indications in rotors to show a relation between the nature of defects and the density of indications in highly stressed zones rather than for the complete rotor.

It is encouraging to hear reports of the progress made in the art of using ultrasonic inspection to procure rotor forgings of continuously improved reliability.

R. C. FITZGERALD.[8] The authors have proposed standards for acceptance or rejection of large rotor forgings based on ultrasonic examination alone. This is a bold forward step in the field of ultrasonic inspection.

As the authors mention, the ultrasonic method will not distinguish between harmful cracks and harmless nonmetallic inclusions and there is a natural reluctance to reject materials with this essential question unanswered.

The scheme of evaluation the authors propose is certainly empirical and arbitrary but it is based on wide experience and it appears to this reader that there is no other way to accomplish the necessary and desirable end of elimination of service failures of these forgings. Whether or not the acceptance limits the authors propose are exactly where they belong is unimportant at the present time. These matters can be settled more accurately later.

The important point about this paper is the fact that a basis for intelligent use of the ultrasonic inspection tool is proposed. It behooves all who are involved in the production and use of large rotor forgings to consider this proposal very seriously and to contribute their knowledge and experience in a joint effort to refine the present proposal or, in turn, to provide something better.

To many users of large forgings the development of ultrasonics as an inspection tool has been exceedingly slow—too slow when we recall the recent disastrous service and test failures of these parts. The apparent lack of a co-ordinated effort in the development of an ultrasonic method has gone far beyond the bounds of proprietary interests and scientific boondoggling.

It is indeed to be hoped that the present paper will provide at least a basis for a specification on ultrasonic inspection.

H. GREENBERG.[9] It is quite apparent that the paper contains a great deal of useful data and the authors are to be commended for making the results of years of experimental work available to the industry. The work outlined in the paper is extremely important inasmuch as it is a definite step toward the ultimate goal of basing the acceptance or rejection of forgings (with respect to their freedom from defects) on the results of ultrasonic testing alone; i.e., without additional corroborating tests. An attempt to set up standards of acceptance for rotor forgings based entirely on the number and relative size of ultrasonic indications obtained at a frequency of 1 megacycle is, however, quite different from our approach.

Early in our testing program we made a thorough study of the characteristics of the various testing frequencies. It was learned that the minimum size defect detectable ultrasonically is a function of the frequency and length of the transmitted wave and the higher the frequency the greater the sensitivity. In some instances, where the part being tested was extremely dirty, had a large number of fine cracks, or had the very coarse grain size typical of castings, we have had to resort to a low testing frequency of 1 mc in order to obtain adequate detectability or definition of gross defects.

The relative sensitivities of $2^1/_4$ and 1 megacycle testing frequencies were established by a testing program performed on an aluminum test block furnished by ASTM Committee E7, Subcommittee VI, to a few laboratories for evaluation. This reference block was 15 in. long, $1^5/_8$ in. wide, 6 in. deep, and had eight 1-in-deep flat-bottomed holes drilled in the bottom face of the block. The holes were of diameters ranging from $^1/_{64}$ to $^5/_8$ in. A composite photograph of the ultrasonic indications from these holes tested at frequencies of 1 and $2^1/_4$ megacycles is shown in Fig. 22 of this discussion. At $2\ ^1/_4$ megacycles, the $^1/_{64}$-in-diam hole was barely detectable, the $^1/_{32}$-in-diam hole showed a $^3/_{16}$-in. pip, and the heights of the rest of the indications increased proportionately to the diameters of the test holes. Fig. 22 also shows that one does not obtain indications from test holes less than $^3/_{32}$ in. diam while testing at a frequency of 1 mc. As a result of this, we decided that the higher testing frequency of

[8] Senior Engineer, Power Production Stations, Baltimore Gas & Electric Company, Baltimore, Md. Mem. ASME.

[9] Materials Engineering Department, Westinghouse Electric Corporation, East Pittsburgh, Pa.

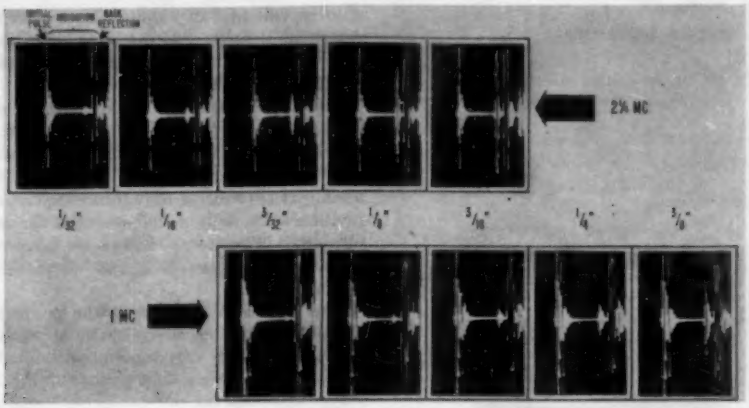

FIG. 22 ULTRASONIC INDICATIONS FROM TEST HOLES OF VARIOUS DIAMETERS AT TESTING FREQUENCIES OF 2¼ AND 1 MC

2¼ mc was necessary for the detection and positive identification of the very fine defects sometimes found in rotor forgings.

To cite a specific example of the relative merits of testing rotor forgings at 2¼ and 1 megacycles: The rotor forging in question was 40 in. diam and was tested solid; i.e., without a bore hole. At a frequency of 2¼ mc, many indications were found concentrated in a section approximately 7½ to 8 in. diam near the center of the forging; some of the indications were much larger than others. It was noted further that with movement of the searching unit many of the indications moved to an extent which indicated considerable change in depth of the discontinuities. To complete the sonic investigation, the forging was tested at 1 mc. The same questionable section of the forging yielded only a relatively few small isolated indications; furthermore, there was no movement of the indications with movement of the crystal. Typical reflectograms taken at 2¼ and 1 mc are shown in Fig. 23 herewith. An analysis of the defects in this forging based solely on the testing at a frequency of 1 mc would probably have been "small isolated defects, probably nonmetallics." The actual conclusion drawn from the investigation at 2¼ mc was "interdendritic shrinkage which had not been completely consolidated by the forging process." Investigation by destructive means confirmed this analysis and a photograph of the macroetched section is shown in Fig. 24. The two encircled

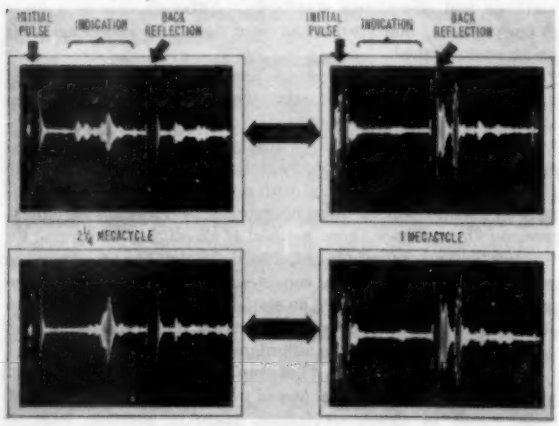

FIG. 23 COMPARISON OF ULTRASONIC INDICATIONS AT TESTING FREQUENCIES OF 2¼ AND 1 MC OF CENTERLINE SHRINKAGE IN A 40-IN-DIAM ROTOR FORGING

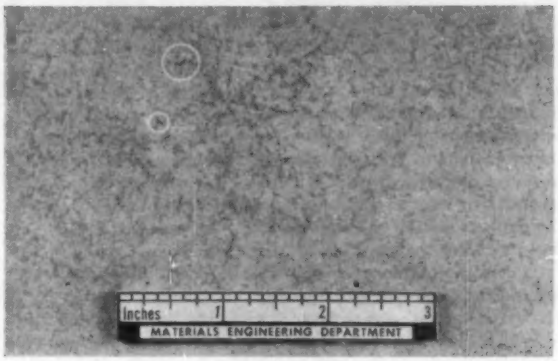

FIG. 24 MACROETCHED SECTION SHOWING INTERDENDRITIC SHRINKAGE IN THE CENTER OF A 40-IN-DIAM ROTOR

areas were felt to be the type of discontinuity causing the 1-mc indications.

An almost identical ultrasonic pattern occurred on a 31-in-diam rotor forging. This time, however, the routine 2¼-mc inspection revealed many small to medium-size indications near one end of the body of the forging in a circumferential band approximately 1 in. thick and 4 to 5 in. below the testing surface. These indications would have been dismissed as merely the pattern of nonmetallic inclusions which sometimes segregate themselves in the ingot between the outer layer of columnar grains and the equiaxed center grains, excepting that there were several indications of markedly greater magnitude interspersed among these many smaller indications. This led us to believe that there were fine hairline cracks connecting some of the inclusions; this diagnosis proved to be correct as shown in Fig. 25. When this same section of the forging was then checked at 1 mc, as specified in all of our ultrasonic investigations, only the larger indications found at the higher frequency were detectable. Since these small isolated indications at 1 mc occurred in an area where one normally would expect to find inclusions, they probably would have been considered inconsequential if the testing had been performed at 1 mc alone.

It is our understanding that, in spite of the increased sensitivity and better definition generally acknowledged for 2¼ mc, 1 mc was chosen as the testing frequency in the authors' inspection practice because it provided a wider beam divergence which would be desirable for the detection of radial flaws. Data found

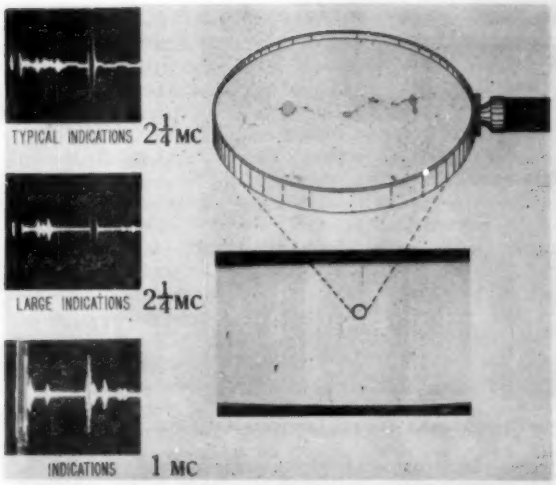

FIG. 25 TYPICAL REFLECTOGRAMS AT 2¼ AND 1 MC OF A FINE HAIRLINE CRACK CONNECTING THE INCLUSIONS

in the literature indicate that the angle of divergence for a 1-in-diam, 1-mc crystal is 9.5 deg which means that, in a testing distance of 18 in., the distance between the surface and bore of a 40-in-diam rotor, the wave would spread over a cone 6 in. diam. If the rotor is rotated and tested at a constant speed of ¾ in. per revolution, would not the same deep-seated discontinuity be counted as many as nine times?

A great deal of importance has been placed on the relative size of indications in the authors' inspection method and yet depth below the testing surface does not appear to have been taken into consideration in the proposed acceptance charts. Is it not true that a given size defect will result in a larger ultrasonic indication as the testing distance is decreased and, therefore, more weight would be given to less serious defects close to the surface?

G. T. JONES[10] AND C. W. GRATER.[10] The authors have presented an excellent paper describing their use of ultrasonic equipment to evaluate the internal quality of large rotor forgings. It represents a most significant advance in this type of inspection and, undoubtedly, will be a basis upon which a further increase in the effectiveness of this inspection will be attained.

To us as a forging producer, we should like to stress the authors' introductory remarks concerning the difficulty in eliminating harmless nonmetallics in the casting of large forging ingots. In our production, there are many occasions when ingots 95 in. diam and weighing 350,000 lb are used. The problems involved in melting and casting of these large ingots are many.

The technique employed by the authors seems to contain three very significant factors; namely, the use of a double crystal, the rotation of the forging during inspection particularly to detect traveling indications, and the mechanical holding of the crystal during rotation. While the authors have mentioned the background of these factors, it would be interesting to know in some detail their experience regarding the effect of double versus single-crystal practices on the indication size.

There has been no mention of the use of a crystal shield, such as seal peel or alumimum foil. Here again the question arises as to whether or not indication size is affected by the use of a shield.

The authors' success in pin-pointing internal discontinuities is of great value for it permits accurate trepanning of samples to determine the nature of the sonic indications. Mention is made that the trepanning of a sample at a location which destroys the usability of a forging is a waste of time. However, to a forging producer it is essential that the exact nature of the indication be identified.

It is realized that the acceptance guides described in this paper have been arbitrarily established and should be recognized on that basis. It is probable that future experience may result in their revision. There is a definite need for establishing a uniform ultrasonic inspection technique for large rotor forgings in order that consistent evaluation of ultrasonic indications may be obtained.

The industries involved in the production and use of these large rotor forgings should well appreciate the efforts of the authors to employ ultrasonic inspection effectively as a measure of internal soundness.

C. M. LAFFOON.[11] The authors deserve much credit for the great amount of work done in sonic inspecting rotor forgings, analyzing the data obtained, improving sonic systems and inspection techniques, and attempting to rationalize and classify the data into forms which can be useful to industry for forging acceptance.

The approach of the writer's company to the solution of steam turbine-driven generator forging problems differs from that used by the author's company in that our complete rotor inspection is made at the supplier's plant prior to acceptance. This procedure is in conformity with an over-all program in which our design engineers and metallurgists have been working co-operatively with all the forging suppliers in the United States on all phases of rotor-forging problems. We are firmly convinced that the best interest of forging suppliers, equipment manufacturers, equipment users, and the industry as a whole can be served best by maintaining a close and harmonious working relationship between the equipment manufacturer and the forging suppliers. This co-operative program includes (*a*) obtaining complete data covering the material characteristics at all sections of the forging, (*b*) obtaining data on transition temperatures, (*c*) review of the forging-manufacturing practices used in this country and Europe with respect to composition, melting, casting, forging, and heat-treating, (*d*) development of sonic-inspection systems and techniques to locate and identify forging defects, (*e*) determine by spinning and stress-cycling tests on large pieces the effects of different types of defects, and (*f*) the preparation of inspection methods and acceptance standards. Although this is a long-range program, much work has been done and real progress is being accomplished.

The sonic-scanning technique presented by the authors is interesting and offers some attractive possibilities. It appears that after the inspection setup is made for a rotor, the sonic equipment tuned to the required sensitivity and calibrated for indication magnitude, the number, magnitude, and location of defects can be observed and recorded with a reasonable degree of accuracy by a skilled nontechnical operator or by recording the indications on film. The authors' method of classifying the forging by the number and magnitude of defect indication has an advantage with respect to maintaining consistency in evaluating and interpreting routine test data. The statistical approach by which an arbitrarily selected number of trepanning test pieces is used to determine acceptability is in accordance with considerable inspection practices in industry. However, when used for the acceptance of forging with defects, one of which may be of a type that could result in disastrous failure, there is question whether

[10] U. S. Steel Corporation, Pittsburgh, Pa.

[11] Consulting Engineer, Westinghouse Electric Corporation, El Cajon, Calif. Mem. ASME.

reasonable assurance based solely on limited experience is sufficient guarantee against failure for the manufacturer and the generator user. The authors apparently recognize this condition as they state that rotor forgings in the most unfavorable class and which pass all the acceptance requirements, are "acceptable only for relatively low-stressed applications." This offers protection to the customer on whose machine the rotor is to be used, but does not offer an economic solution for the utilization of the forging since in most instances other relatively low-stressed applications are not available. As a result, such forgings accepted from the supplier but unusable for the intended application would add to the inactive-materials inventory for the equipment manufacturer.

There are several references in the paper to harmless nonmetallic inclusions and an inference may be drawn that nonmetallic inclusions and defects other than cracks are harmless. There is rather general agreement that small inclusions, and cavities of spheroidal shape with smooth contours are harmless if they are randomly located at uncritical sections. The degree of potential harmfulness of large inclusions, or clusters of small inclusions located at critical sections remains to be evaluated. These and inclusions or cavities which are interconnected by hairline cracks or film-type bands must be considered questionable until proved otherwise. The authors, in arriving at the conclusion that the number and magnitude of sonic indications in a rotor forging can be used as the basis for determining the acceptability of forgings, state that during the period after 1950 "there have been no basic developments by which these subsurface discontinuities could be identified conclusively as harmless or potentially harmful short of destructive or semidestructive examination." Although this statement is true, we have not given up hope nor lost confidence that sonic equipment, sonic systems, and inspection techniques can, and will be, developed to identify types of defects and classify them with respect to harmfulness. One part of our program on forgings covers the evaluation of this type of defect on rotor performance from spinning and cycling tests on large pieces.

Our sonic inspection of turbine-driven generator-rotor forgings has been based on the use of the single crystal with force waves of 1 and $2^1/_4$ megacycles projected into the forging in longitudinal, radial, and off-radial directions.[12] With this approach, the forging has to be proved good before it is considered usable, whereas with sonic scanning and forging classification with respect to number and magnitude of indications and their relative evaluation, the forging is considered acceptable provided external surface examination, and a statistically determined number of trepanned sections, do not disclose a crack.

In our judgment this latter approach is not sufficient to give the economical maximum determinable assurance that the rotor forging has not potential material-failure hazards for its application. A review of the entire paper indicates that the authors share in this conclusion, and state: "In the design and construction of turbine-generator sets, all available engineering and laboratory techniques and inspections are used to insure the reliability of the equipment. . . . . No rotors are released for production if there is any question concerning their ability to operate reliably, and such a policy is followed for the protection of the manufacturer as well as the purchaser."

In our opinion, it would have been more appropriate if the authors had titled this paper as a progress report on the application of the new sonic techniques and forging-classification methods for equipment of their manufacture. The term "acceptance guides" is too suggestive of "acceptance standards" and thus may wrongly imply that they can be used for acceptance standards purposes at the present time.

The proposals outlined by the authors deserve consideration by the forging suppliers and the other equipment manufacturers. They will be investigated thoroughly by engineers and metallurgists of the writer's company to determine their usefulness and applicability as a component of our broader sonic inspection and interpretation program for rotor forgings now in progress.

J. Mowat.[13] Acceptance or rejection of rotor forgings by the ultrasonic method of testing is now more or less recognized as a standard procedure, the acceptance or rejection being established on a percentage basis of the height of the flaw signals against the height of the received back-wall signal, coupled with the number of discontinuities present in the forging under examination.

This acceptance or rejection method has been in operation at our works for a considerable time, the only difference being that we consider that all defects which give flaw signals greater than 10 per cent of the back-wall echo should be regarded as having their origin in defects which we consider are worthy of further investigation. Some of the arguments for and against this standard we shall attempt to explain, but we are in agreement with the authors that an acceptance or rejection standard can only be set by a flaw signal against the back-wall-signal method.

Since the orientation of the defects in a rotor have a very important bearing on the returned flaw signals we should like to draw attention to some of the authors' statements. In the introduction the following passage appears: "It should be noted that these guides have been established on the basis of ultrasonic inspection of 1500 large turbine and generator rotors, reinforced by frequent destructive and semidestructive examination. These guides are applicable only to those rotors containing a limited number of ultrasonic defect reflections, on which no other method has revealed harmful defects; where other inspection means have demonstrated that a single reflection is caused by cracking, the forging is to be rejected."

The authors claim quite correctly that the presence of a single crack in a forging should result in the rejection of the forging, but it is an opinion that many rotors containing cracks are in service at the present time, having passed an ultrasonic examination which failed to reveal their presence. Should a rotor forging contain cracks of a purely radial nature, it is possible when using, say, a straight probe, to receive no flaw signals whatever. In a forging having a 38-in. body and employing a frequency of $2^1/_2$ megacycles, radial cracks contained within a radius of approximately 3 in. from the longitudinal axis can be determined, since circumferential scanning of the rotor will prove that the radial cracks in this zone offer some part of their surfaces parallel to the scanning probe; i.e., at right angles to the beam.

At a frequency of $1^1/_4$ megacycles, when testing a rotor of the same diameter (38 in.), it will be found that within a radius of approximately 5.9 in. from the longitudinal axis any radial crack present in this zone must offer some part of its surfaces parallel to the scanning probe. The locating of radial cracks as such in a rotor outside the zone for the given frequency can never be established unless angle probes are used. Since a radial crack, when testing in a radial direction, will always be in the plane of the sound beam outside the foregoing zones, total reflection is not possible, but it is possible to have a stationary indication from a certain position on a radial crack. In other words, we could receive a flaw signal whose height is perhaps 5 per cent of the returned back-wall signal which we must assume to be from a small defect, but which is in actual fact coming from a point on a radial crack. Fig. 26 of this discussion shows such a possibility. As the authors claim, the use of angle probes are limited because the absence of the usual back-wall signal is a disadvantage, since no measure of the flaw signal versus the back-wall signal can be obtained.

[12] Details given in discussion by Greenberg, p. 1614.

[13] Director, William Beardmore & Co., Ltd., Glasgow, Scotland.

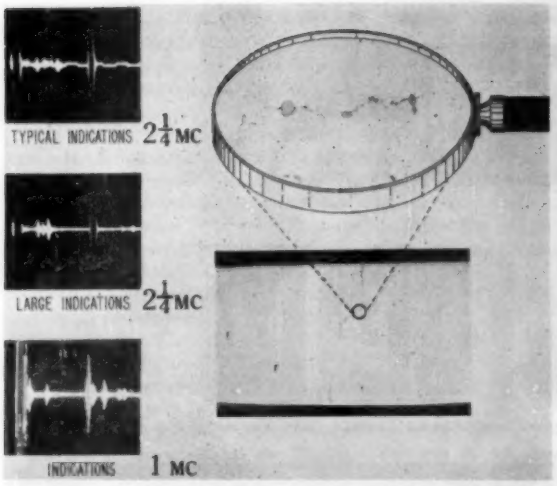

FIG. 25 TYPICAL REFLECTOGRAMS AT 2¼ AND 1 MC OF A FINE HAIRLINE CRACK CONNECTING THE INCLUSIONS

in the literature indicate that the angle of divergence for a 1-in-diam, 1-mc crystal is 9.5 deg which means that, in a testing distance of 18 in., the distance between the surface and bore of a 40-in-diam rotor, the wave would spread over a cone 6 in. diam. If the rotor is rotated and tested at a constant speed of ¾ in. per revolution, would not the same deep-seated discontinuity be counted as many as nine times?

A great deal of importance has been placed on the relative size of indications in the authors' inspection method and yet depth below the testing surface does not appear to have been taken into consideration in the proposed acceptance charts. Is it not true that a given size defect will result in a larger ultrasonic indication as the testing distance is decreased and, therefore, more weight would be given to less serious defects close to the surface?

G. T. JONES[10] AND C. W. GRATER.[10] The authors have presented an excellent paper describing their use of ultrasonic equipment to evaluate the internal quality of large rotor forgings. It represents a most significant advance in this type of inspection and, undoubtedly, will be a basis upon which a further increase in the effectiveness of this inspection will be attained.

To us as a forging producer, we should like to stress the authors' introductory remarks concerning the difficulty in eliminating harmless nonmetallics in the casting of large forging ingots. In our production, there are many occasions when ingots 95 in. diam and weighing 350,000 lb are used. The problems involved in melting and casting of these large ingots are many.

The technique employed by the authors seems to contain three very significant factors; namely, the use of a double crystal, the rotation of the forging during inspection particularly to detect traveling indications, and the mechanical holding of the crystal during rotation. While the authors have mentioned the background of these factors, it would be interesting to know in some detail their experience regarding the effect of double versus single-crystal practices on the indication size.

There has been no mention of the use of a crystal shield, such as seal peel or alumimum foil. Here again the question arises as to whether or not indication size is affected by the use of a shield.

The authors' success in pin-pointing internal discontinuities is of great value for it permits accurate trepanning of samples to determine the nature of the sonic indications. Mention is made that the trepanning of a sample at a location which destroys the usability of a forging is a waste of time. However, to a forging producer it is essential that the exact nature of the indication be identified.

It is realized that the acceptance guides described in this paper have been arbitrarily established and should be recognized on that basis. It is probable that future experience may result in their revision. There is a definite need for establishing a uniform ultrasonic inspection technique for large rotor forgings in order that consistent evaluation of ultrasonic indications may be obtained.

The industries involved in the production and use of these large rotor forgings should well appreciate the efforts of the authors to employ ultrasonic inspection effectively as a measure of internal soundness.

C. M. LAFFOON.[11] The authors deserve much credit for the great amount of work done in sonic inspecting rotor forgings, analyzing the data obtained, improving sonic systems and inspection techniques, and attempting to rationalize and classify the data into forms which can be useful to industry for forging acceptance.

The approach of the writer's company to the solution of steam turbine-driven generator forging problems differs from that used by the author's company in that our complete rotor inspection is made at the supplier's plant prior to acceptance. This procedure is in conformity with an over-all program in which our design engineers and metallurgists have been working co-operatively with all the forging suppliers in the United States on all phases of rotor-forging problems. We are firmly convinced that the best interest of forging suppliers, equipment manufacturers, equipment users, and the industry as a whole can be served best by maintaining a close and harmonious working relationship between the equipment manufacturer and the forging suppliers. This co-operative program includes (*a*) obtaining complete data covering the material characteristics at all sections of the forging, (*b*) obtaining data on transition temperatures, (*c*) review of the forging-manufacturing practices used in this country and Europe with respect to composition, melting, casting, forging, and heat-treating, (*d*) development of sonic-inspection systems and techniques to locate and identify forging defects, (*e*) determine by spinning and stress-cycling tests on large pieces the effects of different types of defects, and (*f*) the preparation of inspection methods and acceptance standards. Although this is a long-range program, much work has been done and real progress is being accomplished.

The sonic-scanning technique presented by the authors is interesting and offers some attractive possibilities. It appears that after the inspection setup is made for a rotor, the sonic equipment tuned to the required sensitivity and calibrated for indication magnitude, the number, magnitude, and location of defects can be observed and recorded with a reasonable degree of accuracy by a skilled nontechnical operator or by recording the indications on film. The authors' method of classifying the forging by the number and magnitude of defect indication has an advantage with respect to maintaining consistency in evaluating and interpreting routine test data. The statistical approach by which an arbitrarily selected number of trepanning test pieces is used to determine acceptability is in accordance with considerable inspection practices in industry. However, when used for the acceptance of forging with defects, one of which may be of a type that could result in disastrous failure, there is question whether

[10] U. S. Steel Corporation, Pittsburgh, Pa.

[11] Consulting Engineer, Westinghouse Electric Corporation, El Cajon, Calif. Mem. ASME.

reasonable assurance based solely on limited experience is sufficient guarantee against failure for the manufacturer and the generator user. The authors apparently recognize this condition as they state that rotor forgings in the most unfavorable class and which pass all the acceptance requirements, are "acceptable only for relatively low-stressed applications." This offers protection to the customer on whose machine the rotor is to be used, but does not offer an economic solution for the utilization of the forging since in most instances other relatively low-stressed applications are not available. As a result, such forgings accepted from the supplier but unusable for the intended application would add to the inactive-materials inventory for the equipment manufacturer.

There are several references in the paper to harmless nonmetallic inclusions and an inference may be drawn that nonmetallic inclusions and defects other than cracks are harmless. There is rather general agreement that small inclusions, and cavities of spheroidal shape with smooth contours are harmless if they are randomly located at uncritical sections. The degree of potential harmfulness of large inclusions, or clusters of small inclusions located at critical sections remains to be evaluated. These and inclusions or cavities which are interconnected by hairline cracks or film-type bands must be considered questionable until proved otherwise. The authors, in arriving at the conclusion that the number and magnitude of sonic indications in a rotor forging can be used as the basis for determining the acceptability of forgings, state that during the period after 1950 "there have been no basic developments by which these subsurface discontinuities could be identified conclusively as harmless or potentially harmful short of destructive or semidestructive examination." Although this statement is true, we have not given up hope nor lost confidence that sonic equipment, sonic systems, and inspection techniques can, and will be, developed to identify types of defects and classify them with respect to harmfulness. One part of our program on forgings covers the evaluation of this type of defect on rotor performance from spinning and cycling tests on large pieces.

Our sonic inspection of turbine-driven generator-rotor forgings has been based on the use of the single crystal with force waves of 1 and $2^1/_4$ megacycles projected into the forging in longitudinal, radial, and off-radial directions.[12] With this approach, the forging has to be proved good before it is considered usable, whereas with sonic scanning and forging classification with respect to number and magnitude of indications and their relative evaluation, the forging is considered acceptable provided external surface examination, and a statistically determined number of trepanned sections, do not disclose a crack.

In our judgment this latter approach is not sufficient to give the economical maximum determinable assurance that the rotor forging has not potential material-failure hazards for its application. A review of the entire paper indicates that the authors share in this conclusion, and state: "In the design and construction of turbine-generator sets, all available engineering and laboratory techniques and inspections are used to insure the reliability of the equipment. . . . . No rotors are released for production if there is any question concerning their ability to operate reliably, and such a policy is followed for the protection of the manufacturer as well as the purchaser."

In our opinion, it would have been more appropriate if the authors had titled this paper as a progress report on the application of the new sonic techniques and forging-classification methods for equipment of their manufacture. The term "acceptance guides" is too suggestive of "acceptance standards" and thus may wrongly imply that they can be used for acceptance standards purposes at the present time.

The proposals outlined by the authors deserve consideration by the forging suppliers and the other equipment manufacturers. They will be investigated thoroughly by engineers and metallurgists of the writer's company to determine their usefulness and applicability as a component of our broader sonic inspection and interpretation program for rotor forgings now in progress.

J. Mowat.[13] Acceptance or rejection of rotor forgings by the ultrasonic method of testing is now more or less recognized as a standard procedure, the acceptance or rejection being established on a percentage basis of the height of the flaw signals against the height of the received back-wall signal, coupled with the number of discontinuities present in the forging under examination.

This acceptance or rejection method has been in operation at our works for a considerable time, the only difference being that we consider that all defects which give flaw signals greater than 10 per cent of the back-wall echo should be regarded as having their origin in defects which we consider are worthy of further investigation. Some of the arguments for and against this standard we shall attempt to explain, but we are in agreement with the authors that an acceptance or rejection standard can only be set by a flaw signal against the back-wall-signal method.

Since the orientation of the defects in a rotor have a very important bearing on the returned flaw signals we should like to draw attention to some of the authors' statements. In the introduction the following passage appears: "It should be noted that these guides have been established on the basis of ultrasonic inspection of 1500 large turbine and generator rotors, reinforced by frequent destructive and semidestructive examination. These guides are applicable only to those rotors containing a limited number of ultrasonic defect reflections, on which no other method has revealed harmful defects; where other inspection means have demonstrated that a single reflection is caused by cracking, the forging is to be rejected."

The authors claim quite correctly that the presence of a single crack in a forging should result in the rejection of the forging, but it is an opinion that many rotors containing cracks are in service at the present time, having passed an ultrasonic examination which failed to reveal their presence. Should a rotor forging contain cracks of a purely radial nature, it is possible when using, say, a straight probe, to receive no flaw signals whatever. In a forging having a 38-in. body and employing a frequency of $2^1/_2$ megacycles, radial cracks contained within a radius of approximately 3 in. from the longitudinal axis can be determined, since circumferential scanning of the rotor will prove that the radial cracks in this zone offer some part of their surfaces parallel to the scanning probe; i.e., at right angles to the beam.

At a frequency of $1^1/_4$ megacycles, when testing a rotor of the same diameter (38 in.), it will be found that within a radius of approximately 5.9 in. from the longitudinal axis any radial crack present in this zone must offer some part of its surfaces parallel to the scanning probe. The locating of radial cracks as such in a rotor outside the zone for the given frequency can never be established unless angle probes are used. Since a radial crack, when testing in a radial direction, will always be in the plane of the sound beam outside the foregoing zones, total reflection is not possible, but it is possible to have a stationary indication from a certain position on a radial crack. In other words, we could receive a flaw signal whose height is perhaps 5 per cent of the returned back-wall signal which we must assume to be from a small defect, but which is in actual fact coming from a point on a radial crack. Fig. 26 of this discussion shows such a possibility. As the authors claim, the use of angle probes are limited because the absence of the usual back-wall signal is a disadvantage, since no measure of the flaw signal versus the back-wall signal can be obtained.

[12] Details given in discussion by Greenberg, p. 1614.

[13] Director, William Beardmore & Co., Ltd., Glasgow, Scotland.

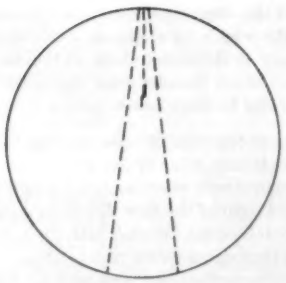

FIG. 26 POSSIBILITY OF PART REFLECTION FROM A RADIAL CRACK
(Flaw indication will be small in relationship to back-wall signal.)

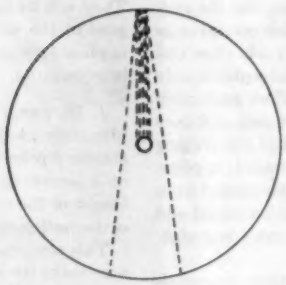

FIG. 27 SMALL BORE OFFERING SMALL AREA TO ULTRASONIC BEAM

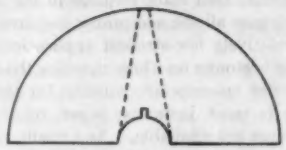

FIG. 28 LARGE BORE AND DRILLED HOLE IN A TEST BLOCK

We do feel that the best possible test of a rotor forging is obtained after the heat-treatment stage prior to boring, since the examination will result in the reception of a much greater height of a back-wall signal from the diametrically opposite concave surface than will result from the convex surface of the rotor bore. Since a small bore will offer less reflecting area than a larger bore, there is a tendency when testing a rotor with a small bore to amplify the back-wall signal to a given height of, say, 50 mm with the result that returned flaw signals are amplified out of all proportion. Cases have arisen wherein operators have recorded the presence of what were thought to be large discontinuities, with the result that the forging was rejected, but cutting up of the rotor revealed only harmless nonmetallics of a very small nature. Going to the opposite extreme, cases have arisen whereby operators have dismissed smaller signals as coming from flaws of a minor nature, but due to the orientation of the defects, total reflection was not possible, with the result that major defects in a rotor remained undetected.

In Fig. 2 of the paper, the authors show an illustration of a "25 per cent defect." Let us assume that the illustration shows a flaw signal and back-wall signal from a 38-in-diam rotor with a 3-in. bore.

To receive such signals the amplifier may have been set with the gain at full sensitivity, in order that the back-wall echo height could be maintained at 50 mm. Let us now assume that we have increased the bore to 5 in. diam, with the result that we have offered a larger reflecting surface to the ultrasonic waves. The back-wall echo height will increase so that reduction of the amplifier to record the back-wall signal at 50 mm means a decrease in the height of the flaw signal, with the result that the measurement of the flaw signal against the back-wall signal will be less than the original 25 per cent.

Bored rotors which have been rejected could be used as test blocks to set standards of acceptance for future inspection. These should be split and flat-nosed drilled holes machined to various depths in from the bore. The heights of the signals could be used for correlating the sensitivity of the test block with the rotor under examination.

The question of the lower frequency versus the higher frequency, in so far as sensitivity is concerned, is a matter for conjecture, but we do believe that employing a frequency of 2 megacycles gives much better definition of the smaller defects lying at or about the bore wall. The authors further state that the 2.25-megacycle frequency reduces sensitivity to radial defects and that they prefer the use of the wider beam at 1.00 megacycle. We think that this idea is not entirely true, since it is not wholly a matter of beam spread but more a question of orientation. We have carried out tests at frequencies of 1, 2, 3, and 4 megacycles from visible radial cracks and are of the opinion that determination of radial cracks constitutes one of the biggest problems of ultrasonic testing.

Figs. 27 and 28 show examples supporting statements made in the foregoing.

In conclusion, we should like to add that the authors are to be commended for their attempts at a standard of acceptance satisfactory to both customer and supplier.

A. O. SCHAEFER.[14] From its very first appearance as a method of inspecting the interior of steel (and other) objects, ultrasonic testing has been considered to have great promise. It was early regarded as being the tool we have long wished for to enable us to look into the interior of solid objects and know just what we have there for our encouragement or otherwise.

Because of this potential, the method has found increasing application in the last decade; until now, in the forging industry, it is in general use.

The value of the test has been hindered in reaching its maximum usefulness for two reasons.

Ultrasonic testing can be extremely sensitive. It reveals many conditions, called, for want of better terms, irregularities. These may be variously injurious or not injurious, avoidable or unavoidable.

Then, too, ultrasonic testing reveals conditions in solid sections heretofore impossible for us to be aware of. Now that we know definitely when and where they exist, we need standards to evaluate them.

Progress has been continuous in both of these phases, but it is understandable that our strong desire to make positive use of this new tool has made it appear to be slow.

The present paper takes us far along the road in both cases. Based on extensive experience and data with one product, it offers us a means of standardization upon results; which, in turn are based on information as to what the indications of the test mean. So it represents an extremely valuable contribution to the use of ultrasonic testing; and, in a larger sense, to the use of large steel forgings.

However, it is well to point out some of the problems this paper presents to us, along with its unquestioned benefits.

The authors have used equipment which differs somewhat from that generally used in the industry. Their examining "head" utilizes two crystals, one for sending and one for receiving, rather than the one crystal which is now in widespread use. Clearer indications are reported to be found by the use of two crystals. Industry is just now rapidly equipping itself with the two-crystal searching units, and will proceed to acquire experience with them.

[14] Vice-President, The Midvale Company, Nicetown, Philadelphia, Pa.

The method is proposed specifically for the examination of rotor forgings. It relies upon application of the test while the rotor is revolving, preferably with the scanner held in a mechanical device with an automatic feed. While some testing has been carried out in other shops on rotating shafts, this has not yet become general. The use of mechanical scanning is still further restricted at the present time. There is no doubt that industry will have to equip itself for such testing. Whether or not it will be economical to carry out the test in the large lathes in which they are machined, or in simpler devices designed primarily merely to rotate the shafts, will have to be developed. With this, we will have to work out the problem of a satisfactory couple to use under these conditions.

The rotors used by the authors' company are practically always composed of cylindrical sections. Those used by other manufacturers often contain conical sections. Further work must be done to apply this method to such conical sections.

It also should be pointed out that there may remain a small residue of rotor forgings so designed that ultrasonic examination may reveal areas which should be examined by core drilling, but on which design may not permit such drilling. In such cases, we may have to fall back on the old destructive test of cutting up the piece, and placing the responsibility where subsequent examination indicates it should be.

The method described in this paper has been worked out with great care on one product. It should be extended to other products only with comparable care and experience. The same standards charts will certainly not apply in all cases.

The authors have displayed great ingenuity, and vision, and courage, in developing the first real system of examination and appraisal of a product by ultrasonic methods. It is certain that this paper will inspire further work in a field where such work is needed. It will be read and used for many years.

J. A. Succop.[15] We, in the forging industry, who have been attempting to manufacture turbine shafting to a very exacting specification, can very well appreciate just what this excellent contribution of the authors will mean to our efforts. These guides represent the first real effort of a consumer to put on paper the basis of acceptance or rejection of a forging by ultrasonic inspection. We have all been waiting for this type of a "yardstick" to judge the quality of our forgings. The work is a serious effort by the authors to put together the records of inspection and service of 1500 turbine shafts. This in itself would indicate the true significance of the work done and the value it will render to both the manufacturer and the consumer.

Since the guides proposed have not been in the hands of the forging manufacturer prior to the past several weeks, we have not had the time to apply the guides and to judge their true value and accuracy. As we develop the opportunity to apply them against production forgings, we will learn the significance of their limitations, and the severity of their requirements.

Some minor points of confusion exist and these points will be clarified as experience in the application of the guides is obtained. However, there is one point that should be cleared when the guides are made effective and that is the responsibility of a forging that passes all other inspection but is destroyed by trepanning into the forging and the indication is not found to be objectionable.

However, as the guides are now offered, we welcome them in our plant inspection of turbine forgings and we sincerely hope that they will lead to a better understanding of the true interpretation of the ever-present indications which are exposed by ultrasonic inspection.

[15] Vice-President—Metallurgy, Happenstall Company, Pittsburgh, Pa.

We thank the authors for a very significant contribution to the art of the inspection of large turbine forgings.

Authors' Closure

The authors are pleased that this paper evoked so much constructive comment and express their appreciation to the many discussers. Throughout all these discussions there is an unmistakable desire to assure the highest quality rotors, and it is only in the method used in pursuit of this desire that there are differences of opinion. That these differences do exist, however, does emphasize the need in this field of ultrasonic inspection for a paper such as this containing the results of inspection and interpretation techniques on many rotors, and the comments of the discussers are valuable in the degree to which they broaden the paper's applicability. It is regrettable, however, that the discussers have furnished relatively little, if any, quantitative information, as obtained from direct defect identification, to support their comments on interpretation techniques; the authors have found through cutting up rotors and trepanning that isolated examples are traps for the unwary in identifying deep-seated indications within a large rotor.

With regard to interpretation studies, the authors wish to take the liberty at this time of reporting on the development of an ultrasonic rotor-inspection simulator as shown in Fig. 29. The

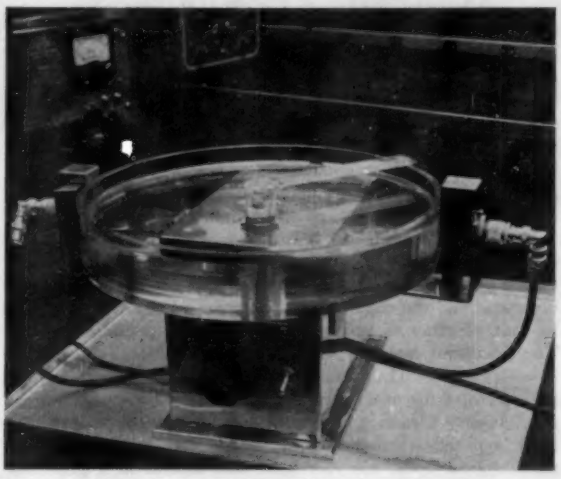

Fig. 29 Ultrasonic Rotor-Inspection Simulator

portion of the rotor seen by the inspection crystal is simulated by a lucite container filled with glycerine. The glycerine together with smaller testing crystals reproduces, on a smaller scale, the conditions existing in an actual rotor during inspection; in addition, the lucite container is rotated by a motor to duplicate the forging rotation. Simulated defects can then be placed in the glycerine so that qualitative and quantitative evaluations can be made of defect position, orientation, size, shape, and so on. In addition, the effects of beam frequency and divergence and the effects of bore-hole diameter, and the like, can be studied. Fig. 30 shows a similar arrangement for studying the inspection of slotted and wound generator rotors.

Mr. Baudry's comments are appreciated, particularly his discussion of the cylindrical crystal used for weld inspection on salient-pole machines, and its use in crescent-shaped grooves for rotor inspection. It should be appreciated, of course, that with these crescent-shaped grooves the back reflection is no longer uniform, and accordingly it is difficult to assign a specific per

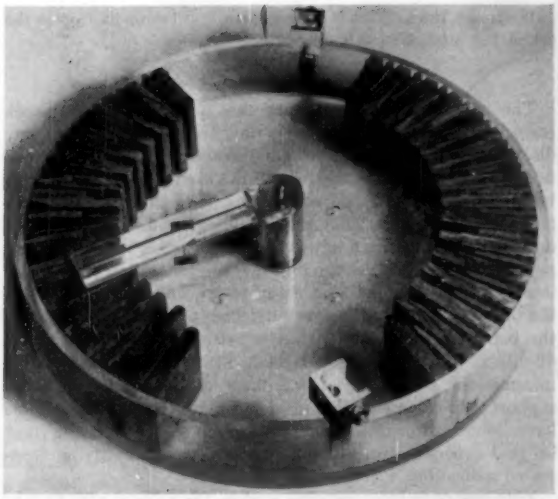

FIG. 30 SIMULATOR USED FOR SLOTTED GENERATOR ROTORS

cent magnitude to the defect reflection since the latter will now vary with both the defect orientation and the angle between the beam and the back-reflecting surface. The detection of radial (traveling) defects is difficult, and their magnitude does depend on their distance from the bore. It should be noted, however, that the inner and outer lines for traveling indications, which are based on direct evidence from trepanning, are significantly lower than the corresponding lines for total indications. It also should be noted that when an angular defect is so located radially that its traveling reflection is low, its reflection when directly under the beam is usually higher as a result of coming closer to the crystals.

Mr. Baudry's comments that the authors' concept of evaluating a forging by the number and magnitude of ultrasonic indications is a radical departure from the present practice of "carefully investigating" the nature of any ultrasonic indication is similar to that of other discussers and deserves a considered reply. The significant question here is: What is meant by "carefully investigating"? The ultrasonic inspection can reveal only the presence of a discontinuity, its magnitude, its location, and its orientation; it cannot reveal its nature any more than radar alone can tell whether a plane is friendly or hostile. On a metallurgical basis, one can state that defects in a particular location and with a particular pattern can be caused by specific steelmaking practices or forging operations, but to use such information alone in defect interpretation is to leap to the conclusion that harmful defects cannot cause a similar pattern. It would have been especially interesting if Mr. Baudry had elaborated on his "positive methods of evaluating" so that their experimental verifications could have been compared with all the trepanning results obtained by the authors. Specifically, the authors' experience indicates that positive identification of the cause of a reflection can be obtained only by trepanning, and, as stated in the paper, if such trepanning should reveal cracking between the inner and outer lines, it is intended then to move these lines closer to the origin so as to maintain the region between the inner and outer lines free of cracking.

We also are using the practice outlined by Mr. Baudry of having an ultrasonic inspection of the rotor prior to testing for physical properties so that the test coupons and identification trepans, if necessary, can be located in the pole regions. We also have trepanned the bores of several forgings and hope to extend this process further when sufficient trepanning equipment is available at the mills. Our experience with bore holes duplicates that of Mr. Baudry; some forgings were left unbored if the ultrasonic inspection revealed essentially no defects in the bore region, but this practice was discontinued as the effects of hydrogen content on ductility were clarified. For several years now, we have been boring all forgings independent of the results of the ultrasonic inspection.

Mr. Greenberg's discussion of the relative merits of 2.25 and 1.00-megacycle frequency on test blocks covers one of the many factors the authors considered during the introduction of ultrasonic inspection of rotor forgings. The authors agree that the frequency of 2.25 megacycles has superior sensitivity when examining artificial defects oriented normal to the ultrasonic beam as shown in Fig. 22. Defects within a rotor forging, however, are randomly oriented, and this establishes the need for the more divergent 1.0-megacycle beam. The more divergent beam is needed to increase the probability that the randomly oriented forging defects will reflect a detectable amount of the ultrasonic beam.

A directly applicable illustration of the inspection merits of 2.25 and 1.0 megacycles is furnished by Fig. 31 which shows the results obtained in a number of actual forging inspections using

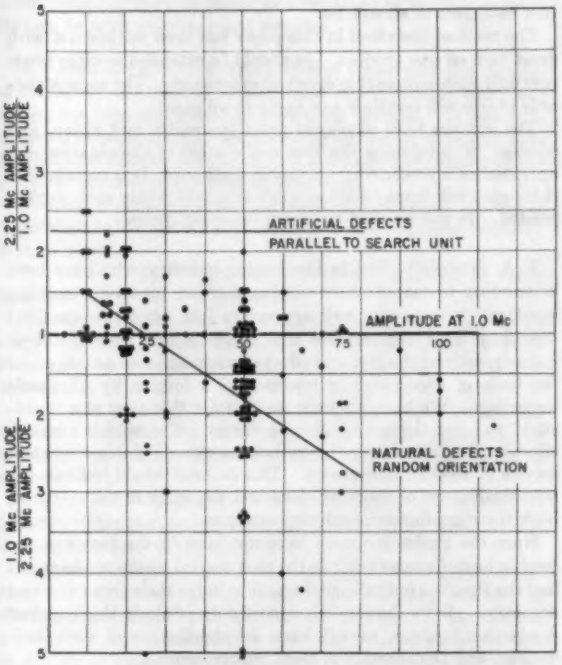

FIG. 31 DETECTING ABILITY—1.0 MEGACYCLE VERSUS 2.25 MEGACYCLES

both frequencies. A total of 150 randomly oriented defects within rotors were detected, and their relative reflection amplitudes at each frequency are shown on this figure. At the lower magnitudes, the 2.25 megacycles give larger values than the 1.0 megacycle, but this is reversed above the 25 per cent magnitude line, and thereafter the 1.0-megacycle frequency is superior. The advantage of the 2.25 megacycles on small defects is overbalanced by its disadvantage on the larger angular defects; it is particularly interesting to note how many indications with a reflection magnitude of 50 per cent with the 1.00-megacycle beam had reflection magnitudes of 25 per cent and less with the 2.25-

megacycle beam, which practical result contradicts the laboratory results obtained with the 2.25-megacycle beam and artificial defects oriented normal to the beam. The authors prefer to retain the advantages of 1.0 megacycle on angular defects, and compensate for its lower sensitivity at the smaller magnitudes by plotting all 5 and 10 per cent reflections at the 15 per cent point as described in the paper.

Mr. Greenberg's two illustrations of defect identification are welcomed by the authors, but, as in our reply to Mr. Baudry's discussion, it would have been interesting if a larger number of such illustrations could be furnished. Specifically, it would be worth while if a broad experimental basis could be established from which identification of the cause of reflections could be made solely on the basis of the ultrasonic-inspection pattern as implied by Mr. Greenberg. On the basis of the many trepans we have taken, the authors do not believe this can be done with any reasonable assurance of the reliability of the results.

Mr. Greenberg's reference to the 9.5-deg angle of divergence for a 1-in-diam 1-megacycle crystal must be an error in the literature to which he refers since the divergence formula for such a beam will give a 16.3-deg angle. With reference to the multiple counting of a single defect, the crystal location on the forging is marked whenever an indication shows on the screen. Any proximity of such marks is then explored, with the forging stationary, after completion of the initial test with the forging rotating. In this way, multiple counting of a single defect is avoided.

Messrs. Jones and Grater have raised some very practical questions and the authors appreciate their reference to the ingot sizes involved in the production of these heavy forgings. The spring-mounted double crystals have been found more convenient to use on rotating forgings, but our own tests do not indicate their sensitivity to be significantly different from that of the single crystals. We do appreciate that the results obtained at some of the steel mills indicate that the double crystals have greater detecting sensitivity and this is being investigated further. Rotation of the forging during test is assurance that any given defect will have an opportunity over 360 deg to assume its most favorable orientation for reflection; its progress in arriving at this position is also important. The mechanical holding of the crystal during rotation, where it is feasible, allows the operator more freedom to concentrate on viewing the screen and marking locations of indications. A shield over the crystal is not necessary on a satisfactory surface finish and may cause inaccuracies in defect reflection. As Messrs. Jones and Grater are aware, progress has been made recently on the adoption of a uniform ultrasonic-inspection technique through the activities of the ASTM Committee A1, Subcommittee VI, Brittle Fracture Task Force.

With respect to Mr. Laffoon's comments, we also maintain close and harmonious relations with the forging suppliers, and a complete ultrasonic inspection of our forgings is made at the steel mill before shipment. However, we repeat the quality inspections at our own factory and this system has advantages since it enables us to introduce immediately any improvements or developments without waiting for the necessary equipment to be made available at the mills. An illustration of this is our recent development of magnetic-particle inspection of the bore using continuous rather than residual magnetism; this is now being used on all forgings even though such equipment is not yet available for steel-mill use.

Mr. Laffoon also comments on the "limited experience" on which our acceptance guides have been established, but without furnishing any quantitative data to support his own suggestions. He states that in his inspection techniques both 2.25 and 1.0 megacycles are used and "the forging has to be proved good before it is considered usable" without giving any specific comments on how the forging is then "proved good." In any discussion of defect identification short of trepanning, it is always interesting to determine how much actual experimental evidence was used to establish the basis for the discussion itself.

It is particularly interesting that Mr. Laffoon agrees our statement is true that "there have been no basic developments by which these subsurface discontinuities could be identified conclusively as harmless or potentially harmful short of destructive or semidestructive examination," while at the same time he alleges that through the 2.25 and 1.0-megacycle examinations he can "prove" the forging good. This implies that Mr. Laffoon has used destructive and semidestructive examinations on a great number of defects, and it would be interesting to see the results published.

Mr. Mowat's comments are especially welcome since, to some extent, they reflect the British approach to ultrasonic inspection of rotors. Mr. Mowat also points out that any defects of greater than 10 per cent reflection magnitude are considered "worthy of further investigation." Once again the authors must ask what is this further investigation, and on what experimental grounds is

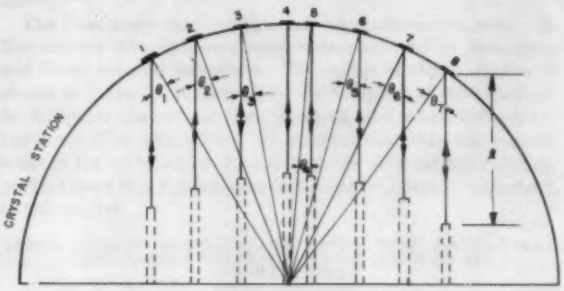

FIG. 32 FORGING SECTION USED FOR BEAM DISPERSION MEASUREMENTS

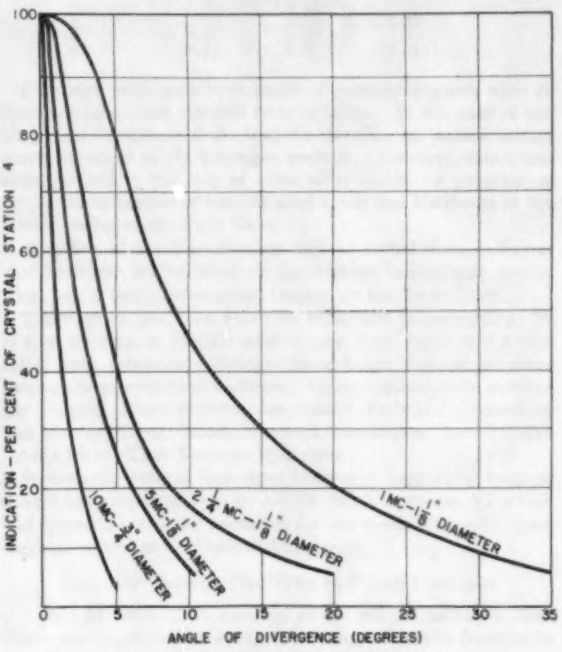

FIG. 33 BEAM DISPERSION PATTERNS

it based? Mr. Mowat's reference to the limitation in divergence of the beam in detecting radial defects is based on the conventional divergence formula wherein ideal coupling conditions are assumed, but the actual conditions present in a rotor forging give significantly different results.

In order to get an experimental evaluation of the beam divergence, a series of tests was conducted on a rotor section using artificial defects as shown in Fig. 32. The defect distances were taken well outside the Fresnel zone and held constant to eliminate attenuation effects. The results are given on Fig. 33 which shows that, with a 1.0-megacycle beam using a $1^1/_8$-in-diam crystal, detection is still practicable within a 60-deg cone (30-deg divergence angle) although the magnitude has been reduced to 10 per cent of that obtainable from the beam center line. In Mr. Mowat's example, this would include radial defects 11 in. off the center line rather than the 5.9 in. predicted by the formula.

We must point out that examination of a rotor in the unbored condition does not necessarily give a higher back reflection than testing in the bored condition. We have examined several rotors in the unbored condition and the effects of attenuation in the central section frequently can overbalance the beneficial effects of the opposite concave surface.

The authors appreciate the comments of Messrs. Schaefer and Succop on the difficulties that undoubtedly will arise in attempting to put these acceptance guides into practice. Many of these already have been overcome through the co-operative efforts of the steel mills and the turbine-generator manufacturers. The continuing efforts of the forging producers to meet and surmount these application difficulties is another encouraging indication of the sincerity of their efforts to produce rotor forgings to the highest quality standards.

Mr. Fitzgerald's comments are of particular interest since they come from a user of the ultrasonically inspected product. It is hoped that the present paper will provide an impetus to a more co-ordinated effort on reflection identification and forging evaluation, and that in subsequent years an even more satisfactory acceptance procedure can be developed. The authors believe that this paper presents the best evaluation of the currently available information, but they also would be pleased if a better procedure could be developed through future evaluations.

Work of the Task Group on Brittle Failure of Steel Forgings

By A. O. SCHAEFER,[1] PHILADELPHIA, PA.

Specifications for steel products as well as the methods of testing and inspecting steel products are entrusted by the American Society for Testing Materials to Committee A-1. This is the oldest and one of the largest technical committees of the Society. The work of the committee is, in turn, delegated to a number of subcommittees covering various products such as sheet, plate, pipe, bars, etc. Steel forgings are the responsibility of Sub-Committee VI. The current yearbook of the Society indicates that Sub-Committee VI has 65 members. This paper covers the activities of Sub-Committee-VI Task Force on Brittle Failure of Steel Forgings.

Introduction

THE foundation for the work now being done by the ASTM Task Force on Brittle Failure of Forgings was laid during the last war. The problem of conservation of alloys in forgings for steam turbines, generators, and related equipment became of extreme importance. All purchasing of these forgings was done by means of company specifications. These were characterized by many special features, the work of a number of individuals working separately. It was thought to be difficult or impossible to expect all manufacturers of electrical equipment, and all suppliers of forgings for such equipment, to reach agreement on material specifications.

The miracle was performed, however, at the urgent request of the National Emergency Steel Specifications Project, after much hard labor, and with the utmost co-operation between equipment and forging manufacturers. The resulting "Emergency" specifications were published by ASTM, and found their way as such into the Book of Standards.

At the close of the war consideration was given to discontinuing the whole group of specifications covering turbine, generator, and related forgings. They were retained largely because they represented so much work. They have been kept up to date by frequent revision. There is no suggestion now of deleting them from the Book of Standards. Forgings, made to these specifications, are in successful service in thousands of power units throughout the country.

Several years ago the steel committees of ASTM revised the stated methods of making mechanical or physical tests for their products. A new "Method" (Designation A370) was prepared for the Book of Standards incorporating all current methods of testing. The formulation of this method brought to light a misunderstanding. A large segment of the forging industry considered it to be normal practice to stress-relieve tension test specimens after they had been removed from the forgings they represented. This practice was challenged by others, and it was stated that the low-temperature heat-treatments given the specimens couldn't possibly remove stresses, but did accomplish the removal of hydrogen, with consequent improvement in ductility. Present interest in hydrogen in steel forgings originated from this discussion.

Hydrogen in Steel Forgings

Sub-Committee VI recognized the importance of this subject at its regular meeting in January, 1953, by appointing a Task Group on Hydrogen charged specifically with "studying the problem of hydrogen in steel forgings" and with "advising Sub-Committee VI when it should become advisable to take cognizance of the effects of hydrogen by suitable alterations in specifications."

The Task Force on Hydrogen has been extremely active. It first studied various laboratories' determinations of hydrogen, and found extreme variations. The extent of that variation is shown in Table 1. A method for the sampling of steel forgings for hydrogen content has been prepared, and is now being processed in ASTM committees. It is hoped that this will remove some of the variations in results between different laboratories, as it is known that the sampling technique is extremely important in this respect.

TABLE 1 ASTM HYDROGEN IN STEEL TEST DATA—FIRST COMPARATIVE DETERMINATIONS MADE BY SIX LABORATORIES

Laboratory	Relative volumes Hydrogen content			
1	0.57	0.50	0.46	
2	0.94	0.91	1.03	0.73
3	0.46	0.48		
4	0.63	0.62	0.62	
5	0.66	0.67		
6	0.61	0.67	0.58	

Extensive tests have been made of specimens which were or were not aged after removal from forgings. In the case of one alloy steel the data indicate that the ductility on tension testing varies inversely as the hydrogen content. However, this is not substantiated in the case of other alloy steels. A program of further investigation of various alloy steels was instituted at the latest meeting of the Task Force.

A review of the literature, as well as actual data, indicates that hydrogen has no effect on notched-bar impact-test results. This, too, is being investigated further by the Task Force.

The work of the Task Force on Hydrogen is continuing. It is now working in parallel with a new Task Force which was called into existence following three tragic failures of rotor forgings in generators or turbines. Other organizations, notably the Forging Manufacturers Association Technical Committee and the Acid Open Hearth Research Association, have collaborated with the Task Force on Hydrogen.

It was only natural that three failures of large rotor forgings should have repercussions in ASTM Sub-Committee VI which had prepared and was responsible for the specifications for these forgings current in the Book of Standards.

Study of Brittle Fracture in Steel Forgings

At the January, 1955, meeting of the subcommittee, a Task Force was appointed to study the "cause of brittle fracture in steel forgings with the aim of establishing a criterion by means

[1] Vice-President and Executive Assistant, The Midvale Company.

Contributed by the Power Division and presented at a joint session of the Power and Metals Engineering Divisions at the Diamond Jubilee Annual Meeting, Chicago, Ill., November 13–18, 1955, of The American Society of Mechanical Engineers.

Note: Statements and opinions advanced in papers are to be understood as individual expressions of their authors and not those of the Society. Manuscript received at ASME Headquarters, October 18, 1955. Paper No. 55—A-209.

it based? Mr. Mowat's reference to the limitation in divergence of the beam in detecting radial defects is based on the conventional divergence formula wherein ideal coupling conditions are assumed, but the actual conditions present in a rotor forging give significantly different results.

In order to get an experimental evaluation of the beam divergence, a series of tests was conducted on a rotor section using artificial defects as shown in Fig. 32. The defect distances were taken well outside the Fresnel zone and held constant to eliminate attenuation effects. The results are given on Fig. 33 which shows that, with a 1.0-megacycle beam using a $1^1/_8$-in-diam crystal, detection is still practicable within a 60-deg cone (30-deg divergence angle) although the magnitude has been reduced to 10 per cent of that obtainable from the beam center line. In Mr. Mowat's example, this would include radial defects 11 in. off the center line rather than the 5.9 in. predicted by the formula.

We must point out that examination of a rotor in the unbored condition does not necessarily give a higher back reflection than testing in the bored condition. We have examined several rotors in the unbored condition and the effects of attenuation in the central section frequently can overbalance the beneficial effects of the opposite concave surface.

The authors appreciate the comments of Messrs. Schaefer and Succop on the difficulties that undoubtedly will arise in attempting to put these acceptance guides into practice. Many of these already have been overcome through the co-operative efforts of the steel mills and the turbine-generator manufacturers. The continuing efforts of the forging producers to meet and surmount these application difficulties is another encouraging indication of the sincerity of their efforts to produce rotor forgings to the highest quality standards.

Mr. Fitzgerald's comments are of particular interest since they come from a user of the ultrasonically inspected product. It is hoped that the present paper will provide an impetus to a more co-ordinated effort on reflection identification and forging evaluation, and that in subsequent years an even more satisfactory acceptance procedure can be developed. The authors believe that this paper presents the best evaluation of the currently available information, but they also would be pleased if a better procedure could be developed through future evaluations.

Work of the Task Group on Brittle Failure of Steel Forgings

By A. O. SCHAEFER,[1] PHILADELPHIA, PA.

Specifications for steel products as well as the methods of testing and inspecting steel products are entrusted by the American Society for Testing Materials to Committee A-1. This is the oldest and one of the largest technical committees of the Society. The work of the committee is, in turn, delegated to a number of subcommittees covering various products such as sheet, plate, pipe, bars, etc. Steel forgings are the responsibility of Sub-Committee VI. The current yearbook of the Society indicates that Sub-Committee VI has 65 members. This paper covers the activities of Sub-Committee-VI Task Force on Brittle Failure of Steel Forgings.

Introduction

THE foundation for the work now being done by the ASTM Task Force on Brittle Failure of Forgings was laid during the last war. The problem of conservation of alloys in forgings for steam turbines, generators, and related equipment became of extreme importance. All purchasing of these forgings was done by means of company specifications. These were characterized by many special features, the work of a number of individuals working separately. It was thought to be difficult or impossible to expect all manufacturers of electrical equipment, and all suppliers of forgings for such equipment, to reach agreement on material specifications.

The miracle was performed, however, at the urgent request of the National Emergency Steel Specifications Project, after much hard labor, and with the utmost co-operation between equipment and forging manufacturers. The resulting "Emergency" specifications were published by ASTM, and found their way as such into the Book of Standards.

At the close of the war consideration was given to discontinuing the whole group of specifications covering turbine, generator, and related forgings. They were retained largely because they represented so much work. They have been kept up to date by frequent revision. There is no suggestion now of deleting them from the Book of Standards. Forgings, made to these specifications, are in successful service in thousands of power units throughout the country.

Several years ago the steel committees of ASTM revised the stated methods of making mechanical or physical tests for their products. A new "Method" (Designation A370) was prepared for the Book of Standards incorporating all current methods of testing. The formulation of this method brought to light a misunderstanding. A large segment of the forging industry considered it to be normal practice to stress-relieve tension test specimens after they had been removed from the forgings they represented. This practice was challenged by others, and it was stated that the low-temperature heat-treatments given the specimens couldn't possibly remove stresses, but did accomplish the removal of hydrogen, with consequent improvement in ductility. Present interest in hydrogen in steel forgings originated from this discussion.

Hydrogen in Steel Forgings

Sub-Committee VI recognized the importance of this subject at its regular meeting in January, 1953, by appointing a Task Group on Hydrogen charged specifically with "studying the problem of hydrogen in steel forgings" and with "advising Sub-Committee VI when it should become advisable to take cognizance of the effects of hydrogen by suitable alterations in specifications."

The Task Force on Hydrogen has been extremely active. It first studied various laboratories' determinations of hydrogen, and found extreme variations. The extent of that variation is shown in Table 1. A method for the sampling of steel forgings for hydrogen content has been prepared, and is now being processed in ASTM committees. It is hoped that this will remove some of the variations in results between different laboratories, as it is known that the sampling technique is extremely important in this respect.

TABLE 1 ASTM HYDROGEN IN STEEL TEST DATA—FIRST COMPARATIVE DETERMINATIONS MADE BY SIX LABORATORIES

Laboratory	Relative volumes—Hydrogen content			
1	0.57	0.50	0.46	
2	0.94	0.91	1.03	0.73
3	0.46	0.48		
4	0.63	0.62	0.62	
5	0.66	0.67		
6	0.61	0.67	0.58	

Extensive tests have been made of specimens which were or were not aged after removal from forgings. In the case of one alloy steel the data indicate that the ductility on tension testing varies inversely as the hydrogen content. However, this is not substantiated in the case of other alloy steels. A program of further investigation of various alloy steels was instituted at the latest meeting of the Task Force.

A review of the literature, as well as actual data, indicates that hydrogen has no effect on notched-bar impact-test results. This, too, is being investigated further by the Task Force.

The work of the Task Force on Hydrogen is continuing. It is now working in parallel with a new Task Force which was called into existence following three tragic failures of rotor forgings in generators or turbines. Other organizations, notably the Forging Manufacturers Association Technical Committee and the Acid Open Hearth Research Association, have collaborated with the Task Force on Hydrogen.

It was only natural that three failures of large rotor forgings should have repercussions in ASTM Sub-Committee VI which had prepared and was responsible for the specifications for these forgings current in the Book of Standards.

Study of Brittle Fracture in Steel Forgings

At the January, 1955, meeting of the subcommittee, a Task Force was appointed to study the "cause of brittle fracture in steel forgings with the aim of establishing a criterion by means

[1] Vice-President and Executive Assistant, The Midvale Company.

Contributed by the Power Division and presented at a joint session of the Power and Metals Engineering Divisions at the Diamond Jubilee Annual Meeting, Chicago, Ill., November 13–18, 1955, of The American Society of Mechanical Engineers.

Note: Statements and opinions advanced in papers are to be understood as individual expressions of their authors and not those of the Society. Manuscript received at ASME Headquarters, October 18, 1955. Paper No. 55—A-200.

of which the tendency of a material to fracture in a brittle manner may be appraised, and also to discover the causes of brittle fracture and its cure."

This Task Force comprises representatives of eight companies—three manufacturers of electrical equipment, five manufacturers of large forgings for turbines and generators. This represents all of the makers and the users of large forgings of this type in the United States. The Task Force has met monthly since it was formed. Partial meetings were held in Europe during the recent World Metals Congress.

It began its work by reviewing the failures being currently discussed. These were described in detail, and the comments of the Task Force guided the testing programs so that test data were obtained which could be correlated to the greatest extent.

It has next sought to rationalize the rather broad charter under which it came into existence. The work it has had to do subdivides itself naturally into three main headings:

1 To discover a test to determine whether or not a steel is subject to brittle failure, or its relative susceptibility to brittle failure.

2 To attempt to make rotors less susceptible to brittle failure:

(*a*) By heat-treatment.

(*b*) By chemistry.

(*c*) By vacuum-pouring techniques.

3 To develop methods of inspection and of interpretation to avoid brittle failure of forgings in service.

It is important to realize that the manufacture of turbine- and generator-rotor forgings has, throughout the years, been subject to constant review, and has been changed and improved with the growth of metallurgical and engineering knowledge and experience. It is safe to say that this product has commanded the attention of our best talent, and represents the finest practice of which the industry knows. The excellent record of our units substantiates this. The new factor, introduced by the Task Group, is the correlation of thinking and experience to the end that our development may be more rapid.

The remainder of this discussion will be divided into reports of the progress of the Task Force in three fields of activity.

A Test to Appraise the Tendency of a Forging to Fail in a Brittle Manner

At the outset it was realized that it is possible to set up a stress pattern in any piece of steel that will cause it to fail in a brittle manner. The importance of design cannot be overemphasized. However, design is outside of the scope of this Task Force, and the importance of this factor is pointed out solely that it may be recognized.

The best of steelmaking practice goes into the manufacture of turbine- and generator-rotor forgings. However, metallurgical and mechanical irregularities become of increasing importance at higher strength levels, and the utmost in resistance to brittle failure is required when irregularities exist at such high levels.

It is obvious that the usual tension tests, and notched-bar impact tests, do not give sufficient information to appraise entirely the tendency of a steel forging to brittle failure. Poor ductility and low impact values are indicative of brittleness, but good ductility and high impact values do not necessarily mean that the material cannot fail in a brittle manner under certain conditions.

The problem is somewhat analogous to that faced by the forging industry in the manufacture of highly stressed gun barrels during the last war. All barrels show incipient cracks in the form of heat checks in the bores on initial rounds. The problem is to find a steel, or a condition of the steel, in which these incipient cracks will not progress too rapidly.

The Task Force is collecting data at the present time on two methods of testing with the hope that they may provide information indicative of the tendency of forgings to brittle failure.

It has been found that the transition temperature range, in which the results of notched bar-impact tests fall off rapidly, is a possible answer to this question. Rotors now in process have been tested to determine what this range is, or should be. Other papers report results of this test. The type of data obtained is illustrated in Fig. 1.

Data also are being obtained on notched-bar bend tests. Such tests are made on specimens removed from the forgings, machined in several sizes, notched, and bent to fracture as simple beams. In all cases the unit breaking load decreases as the cross section of the specimen increases. If the results of such tests are plotted, using a log scale for the specimen size only, approximately straight lines result. Fig. 2 illustrates the type of data obtained. Others have reported results of this test in specific cases. On the basis of the tests made to date there is a possibility that the slope of this line may be correlated with the property we are trying to measure. The more nearly horizontal such a line is, the less sensitive the steel is to stress concentrations, and the lower is its transition-temperature range for notched-bar impact tests.

Both of these tests (the transition-temperature range for notched-bar impact tests and the multiple-size notched bend test) involve the machining of a number of specimens, and require considerable test metal. It is not considered that either one gives us the whole answer we are looking for.

So the Task Force is looking for other and better criteria. Among those that have been mentioned are brittle-to-ductile transition-temperature tests along the lines developed by Pellini, the development of true grain outline by etching technique, tear tests of specimens with incipient cracks, and so on.

The Attempt to Make Rotors Less Susceptible to Brittle Failure

(*a*) *By Heat-Treatment.* It has long been known that European practice in the manufacture of turbine and generator rotors sometimes employs liquid-quenching in heat-treatment. Practice in this country was based on cooling in air only, with liquid-quenching definitely forbidden because of the danger of cracking, instability, and residual stresses. This was substantiated by the failure of a quenched rotor at Canton, about 25 years ago.

The Task Group is re-examining its position with regard to liquid-quenching. Liquid-quenching, if it can be done properly, is known to benefit the metal structurally, and in resistance to brittle failure. Fortunately, the forging industry in the United States is equipped to liquid-quench rotors should it be found to be beneficial.

Initial experiments with quenched rotors have been carried out with forgings which have been rejected for one reason or another. Preliminary reports indicate some beneficial effects on properties measured in the conventional way. There are also indications that the benefits are to be found only in the surface metal, and that they will not extend to sufficient depth to be of real advantage. Rotors are now being quenched with buried thermocouples in all sections to record the actual rates of cooling at these points. Rotors which have been quenched are being sectioned for extensive testing. Some rotors which have been liquid-quenched are now being processed.

Meetings of members of the Task Group at the World Metals Congress developed the possibility that the liquid-quenching of rotors is not as widespread in Europe as we had been led to believe. Manufacturers there usually express a limitation in willingness to quench on the basis of diameter, or total mass, or total alloy content, etc.

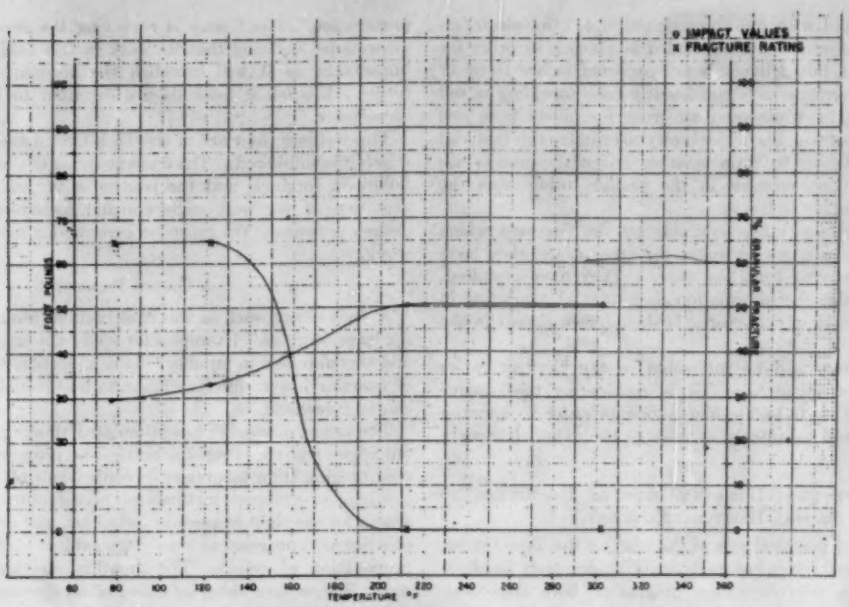

FIG. 1 TEMPERATURE TRANSITION CURVE OF A NICKEL-MOLY-VANADIUM ROTOR STEEL
(Plotting by Bethlehem Steel Company. V-notch Charpy test.)

(*b*) *By Chemistry.* The most common alloy steel used in rotor manufacture in the United States is the nickel-molybdenum grade containing about 2.75 per cent nickel, 0.50 per cent molybdenum, and 0.05 to 0.10 per cent vanadium. This alloy commonly contains less than 0.20 per cent chromium.

A similar steel with a higher chromium content has been used for the higher-strength grades.

An entirely different steel containing chromium, molybdenum, and vanadium is used in a number of cases for steam-turbine rotors operating at moderately high temperatures. The Task Group has to date devoted its attention to the larger rotors, for low-pressure units or for the generators. Grades other than those mentioned have been used for the smaller forgings used for high-pressure steam units.

A greater variety of steel is used in Europe. Rotors are not stressed as highly as ours, and they still find extensive use for carbon steel and carbon-molybdenum steel grades. In England there are several who champion a higher chromium steel on the basis that it has great uniformity of properties in large sections.

Rotors requiring the highest level of tensile properties are usually made of a modified nickel-molybdenum steel, but European grades almost invariably contain lower nickel and quite definitely higher chromium content than ours. Typical steel contains about 2 per cent nickel, 1.25 per cent chromium, 0.40 per cent molybdenum with or without vanadium.

In planning the rotors that will be liquid-quenched on a development program, it has been arranged that some forgings will be made of the European chemistry just reported, and some of an alloy with still higher hardenability which might be worth while if larger sections can be quenched effectively. Such forgings are currently in manufacture.

(*c*) *By Vacuum-Pouring Technique.* Vacuum melting of steel has been a tremendous aid in obtaining desired quality in the super alloys used for gas turbines and jet engines. The forgings required have been quite small in comparison with those under review by the Task Force.

In December, 1954, it became known that one German steelmaker was equipped to pour large ingots in vacuum. An article appeared in *Iron Age* describing in a general way what was being done at Bochumer Verein in Germany's Ruhr Valley.

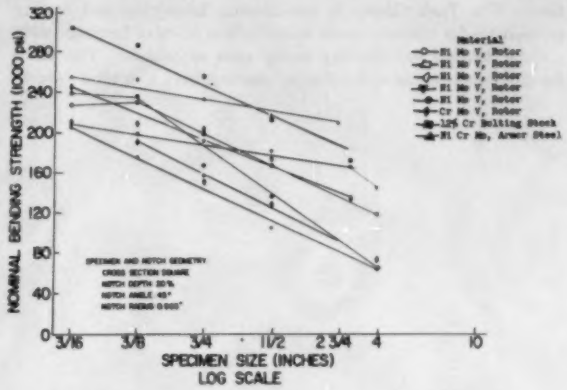

FIG. 2 INFLUENCE OF SIZE ON NOTCHED BENDING STRENGTH
(Plotting by General Electric Company.)

The idea of pouring heats in vacuum was described first as a means of avoiding the occurrence of flakes. The basic open-hearth and basic electric-furnace steel made in Germany is more susceptible to flakes than acid open-hearth steel. It is stated that Bochumer Verein has succeeded in markedly decreasing the incidence of flakes by its pouring technique.

This in itself is a worth-while achievement. However, if we note that the Hydrogen Task Group was started on its course because of the difference in test results obtained after hydrogen removal, we will realize that consideration must be given to the value of vacuum-pouring technique as a possible means of improving inherent ductility and toughness.

Efforts were made by both forging manufacturers and users to purchase material poured in vacuum at Bochum, so that it

might be compared with our domestic product. One electrical-equipment manufacturer has succeeded in placing an order for rotors with them, but delivery is not expected before 10 or 11 months. The Germans have consistently been unwilling to sell ingots, but they have accepted an order for billets from one forging manufacturer. The opportunity to examine this material is important if we are to know whether or not the process has resulted in any improvement in the product other than the reduced susceptibility to flakes.

No data have been made available by the Germans which would indicate how much hydrogen (or other gases) they have succeeded in removing from the metal. They have promised, however, to divulge the information they have at a meeting in Germany in October of this year. It should then appear in the technical press.

The Task Group will be interested in the German rotors when they are received here. It is considering the relative merits of a pilot or full-scale installation in order to appraise in this country and as quickly as possible the value of vacuum pouring.

Means of Inspection, Interpretation of Inspection, to Avoid Brittle Failures

This is the very practical side of the work of the Task Group.

The inspection of rotors has made use of tension tests, notched-bar impact tests, microstructure, magnaflux, bore inspection, heat indication, and ultrasonic inspection.

There is no doubt that we have not yet reached either a full understanding of, or the limit of usefulness of, ultrasonic inspection. The Task Group is formulating inspection and testing procedures for the ultrasonic examination of rotor forgings, with a view toward establishing acceptance standards. The basis for this has been agreed upon in meeting, and a draft is now in preparation. The Group is reviewing the results of tests and inspections, realizing that its work in this field will be of great importance as it will establish the acceptance level for the future. Ultrasonic methods are expected to be of increasing importance.

This outlines the work of the Task Group and the program on which it is embarked. The understanding of the causes of brittle failure in forgings, and the control of it, are being given the attention of our best engineers and metallurgists. Everyone desires progress. We must be sure of our materials as we go along.

A Group Project

A Task Group such as this is of peculiar importance in studying large forgings. Examples for study are large and expensive, and therefore few in number. It is important that the methods of examination in different laboratories be similar so that data can be correlated.

The group discussion has stimulated thinking, it has brought out ideas, and encouraged action. The program is a very large one, ranging from laboratory investigations of test methods, to the trial of different methods of manufacture, to an intensive search for the right inspection technique, and to the formulation of a research program to clarify the subject of the initiation and propagation of cracks. The monthly meetings of the group result in everyone being informed of all developments.

It is only reasonable to point out the fine record of American turbines and generators and the steel forgings that are in them. For many years we have been practically free of major accidents. The spirit of co-operation that has and does exist in this industry between steelmaker and equipment manufacturer has established a fine record. The Task Group is a concentrated manifestation of this spirit.

Important Dimensional Standards and Construction Codes Published by the ASME

BOLTS, NUTS, RIVETS, AND SCREWS

In these American Standards will be found the proportions and dimensions, the tolerances, recommendations for material, and other pertinent data.

Large Rivets (½ Inch Nominal Diameter and Larger), B18.4—1950. $1.50
Small Solid Rivets, B18.1—1955. $1.50
Plow Bolts, B18.9—1950. $1.50
Round Head Bolts, B18.5—1952. $1.50
High - Strength, High - Temperature Internal Wrenching Bolts, B18.8—1950. $1.00
Slotted and Recessed Head Wood Screws, B18.6.1—1956. $1.00
Hexagon and Slotted Head Cap Screws, Square Head Set Screws, Slotted Headless Set Screws, B18.6.2—1956. $1.50
Socket Head Cap Screws and Socket Set Screws, B18.3—1954. $1.50
Square and Hexagon Bolts and Nuts and Lag Bolts, B18.2—1955. $2.00
Track Bolts and Nuts, B18.10—1952. $1.50

PIPE, PIPE FITTINGS, AND THREADS

These American Standards cover dimensions and tolerances, pressure ratings, size, marking, material, and threading.

Brass or Bronze Flanges and Flanged Fittings—150 & 300 Lb, B16.24—1953. $1.00
Brass or Bronze Screwed Fittings 125 Lb, B16.15—1947 (Reaffirmed 1952). $1.50
Brass or Bronze Screwed Fittings 250 Lb, B16.17—1949 (Reaffirmed 1953). $1.00
Cast-Brass Solder-Joint Fittings, B16.18—1950. $1.50
Cast-Brass Solder Joint Drainage Fittings, B16.23—1953. $1.50
C I Pipe Flanges and Flanged Fittings for 25 Lb Psi, B16b2—1931 (Reaffirmed 1952). $1.00
CLASS 125, B16.1—1948. $1.50
CLASS 250, B16b—1944 (Reaffirmed 1953). $1.50
800 Lb Hydraulic Pressure, B16b—1931 (Reaffirmed 1952). $1.00
Class 300 Lb Refrigerant Piping, B16.16—1948 (Reaffirmed 1952). $1.00
C I Screwed Drainage Fittings, B16.12—1953. $1.00
C I Screwed Fittings, 125 & 250 Lb, B16.4—1949 (Reaffirmed 1953). $1.50
Malleable-Iron Screwed Fittings 150 Lb, B16.3—1951. $1.50
Malleable-Iron Screwed Fittings 300 Lb, B16.19—1951. $1.00
Steel Pipe Flanges and Flanged Fittings 150, 300, 400, 600, 900, 1500, and 2500 Lb, B16.5—1953. $3.00
Ferrous Plugs, Bushings, and Locknuts With Pipe Threads, B16.14—1949 (Reaffirmed 1953). $1.00
Nonmetallic Gaskets for Pipe Flanges, B16.21—1951. $1.00
Ring-Joint Gaskets and Grooves for Steel Pipe Flanges, B16.20—1956. $1.00
Butt-Welding Ends, B16.25—1955. $1.00
Steel Butt-Welding Fittings, B16.9—1951. $1.50
Steel-Socket Welding Fittings, B16.11—1946 (Reaffirmed 1952). $1.00
Wrought-Copper and Wrought-Brass Solder-Joint Fittings, B16.22—1951. $1.00
Wrought-Steel and Wrought-Iron Pipe, B36.13—1950. $1.00
Pipe Threads, B2.1—1945. $2.50
Scheme for the Identification of Piping Systems, A13.1—1956. $1.00

SMALL TOOLS AND MACHINE TOOL ELEMENTS

These American Standards give the approved dimensions, permissible tolerances, and other specifications.

Accuracy of Engine and Tool Room Lathes, B5.16—1952. $1.00
Chucks and Chuck Jaws, B5.8—1954. $1.50
Circular and Dovetailed Forming Tool Blanks B5.7—1954. $1.50
Drill Drivers (Split-Sleeve, Collet-Type), B5.27—1951. $1.00
Involute Splines, B5.15—1950. $3.00
Involute Serrations, B5.26—1950. $2.00
Involute Spline and Serration Gages and Gaging, B5.31—1953. $1.50
Jig Bushings, B5.6—1941 (Reaffirmed 1949). $1.00
Knurling, B5.30—1953. $1.50
Machine Pins, B5.20—1954. $1.00
Punch and Die Sets for Two-Post Punch Press Tools, B5.25—1950. $1.50
Rotating Air Cylinders and Adapters, B5.5—1954. $1.00
Single-Point Tools and Tool Posts, B5.22—1950. $2.00
Spindle Noses for Tool Room Lathes, Engine Lathes, Turret Lathes, and Automatic Lathes, B5.9—1954. $2.50
Spindle Noses and Adjustable Adapters for Multiple Spindle Drilling Heads, B5.11—1954. $1.00
Spindle Noses and Arbors for Milling Machines, B5.18—1953. $1.00
Straight Cut-Off Blades for Lathes and Screw Machines, B5.21—1949. $1.00
T-Slots, Their Bolts, Nuts, Tongues, and Cutters, B5.1—1949. $1.50
Life Tests of Single-Point Tools, B5.19—1946 (Reaffirmed 1953). $1.00
Life Tests for Single Point Tools of Sintered Carbide, B5.34—1956. $1.00
Twist Drills, B5.12—1950. $1.50
Machine Tapers, B5.10—1953. $1.50
Milling Cutters, B5.3—1950. $3.00
Nomenclature for Milling Cutter Teeth, B5d—1947. $1.50
Reamers, B5.14—1949. $2.00
Taps—Cut and Ground Threads, B5.4—1948. $2.00
Markings for Grinding Wheels, B5.17—1949 (Reaffirmed 1953). $1.00
Mounting Dimensions of Lubricating and Coolant Pumps for Machine Tools, B5.28—1952. $1.00
Designation and Working Ranges of Grinding Machines, B5.32 & 33—1953. $1.00

GEARING STANDARDS

Here will be found the preferred tooth proportions, dimensions of gear blanks, data on instrument gears and on checking pressures of gear teeth, method of putting gear dimensions on drawings, formulas for calculating the values of the various tables, nomenclature, and symbols.

Spur Gear Tooth Form, B6.1—1932. $1.00
Letter Symbols for Gear Engineering, B6.5—1954. $1.50
Gear Tolerances and Inspection, B6.6—1946. $1.50
20-Degree Involute Fine-Pitch System for Spur and Helical Gears, B6.7—1956. $1.50
Fine-Pitch Straight Bevel Gears, B6.8—1930 $1.00
Design for Fine-Pitch Worm Gearing, B6.9—1956. $1.50
Inspection of Fine-Pitch Gears, B6.11—1956. $2.50
System for Straight Bevel Gears, B6.13—1955. $1.00
Gear Nomenclature, B6.10—1954. $1.50
Nomenclature for Gear Tooth Wear and Failure, B6.12—1954. $1.50

SAFETY CODES

In each of these documents will be found the minimum requirements for construction, rules for installation and maintenance along with a considerable amount of other useful information.

Power Boilers, 1956 Edition. $4.50
Material Specifications, 1956 Edition. $10.00
Boilers of Locomotives, 1952 Edition. $1.25
Low-Pressure Heating Boilers, 1956 Edition. $1.25
Miniature Boilers, 1952 Edition. $1.00
Suggested Rules for Care of Power Boilers, 1954 edition. $3.00
Unfired Pressure Vessels, 1956 Edition. $5.00
Welding Qualifications, 1956 Edition. $1.50
Price of these eight sections of the ASME Boiler and Pressure Vessel Code and binder— $27.50
Code for Pressure Piping, B31.1—1955 $3.50
(Requirements cover power, industrial gas and air, refinery and oil transportation, district heating, and refrigerating piping systems.)
Gas Transmission and Distribution Piping Systems, B31.1.8—1955. $2.50
Cranes, Hoists, Derricks, B30.2—1943 (Reaffirmed 1952). $2.50
Industrial Power Trucks, B56.1—1955. $1.50
Elevators, Dumbwaiters, and Escalators, A17.1—1953. $3.50
Manlifts, A90.1—1949 (Reaffirmed 1956) $1.00
Mechanical Power Transmission Apparatus, B15.1—1953. $2.00

20% discount to ASME members

THE AMERICAN SOCIETY OF MECHANICAL ENGINEERS
29 W. 39 St., N. Y. 18, N. Y.